THE COLD UNIVERSE

Cover illustration : *The "Nautilus" pierces the ice near the South Pole.*
(From Jules Verne's '20,000 Leagues Under the Sea', original French edition by Hetzel, 1870)

XXVIIIth Rencontre de Moriond
XIIIth Moriond Astrophysics Meetings
Les Arcs, Savoie, France - March 13-20, 1993

THE COLD UNIVERSE
Series : Moriond Astrophysics Meetings

ISBN 2-86332-150-1

EDITIONS FRONTIERES
B. P. 33
91192 Gif-sur-Yvette Cedex - France

Printed in Singapore

Proceedings of the XXVIIIth RENCONTRE DE MORIOND
XIIIth Moriond Astrophysics Meetings
Les Arcs, Savoie, France March 13-20, 1993

THE COLD UNIVERSE

edited by

Th. Montmerle
Ch. J. Lada
I. F. Mirabel
J. Trân Thanh Vân

EDITIONS FRONTIERES

The Astrophysics Session of the XXVIIIth Rencontre de Moriond

The Cold Universe

International Advisory Committee

C. Bertout	*(Grenoble)*
Y. Fukui	*(Nagoya)*
R. Güsten	*(Bonn)*
M. Hauser	*(Goddard)*
R. Hills	*(Cambridge, GB)*
E. Khachikian	*(Byurakan)*
C.J. Lada	*(Cambridge-USA)*
P. Léna	*(Meudon)*
T. Montmerle	*(Saclay)*
A. Natta	*(Florence)*
P. Planesas	*(Yebes)*
J.-P. Puget	*(Orsay)*
L.-F. Rodriguez	*(Mexico)*
D. Sanders	*(Hawaii)*
S. Stahler	*(Berkeley)*
R. Terlevitch	*(Cambridge-GB)*

Program Committee

Ph. André	*(Saclay)*
C. Césarsky	*(Saclay)*
J.-P. Chièze	*(Bruyères-le-Châtel)*
F. Genova	*(CNES, Paris)*
C.J. Lada	*(Cambridge-USA)*
P.-O. Lagage	*(Saclay)*
F. Mirabel	*(Saclay)*
T. Montmerle	*(Saclay)*
A. Omont	*(Paris)*
D. Rouan	*(Meudon)*
J. Trân Thanh Vân	*(Orsay)*
S. Volonté	*(ESA, Paris)*

TABLE OF CONTENTS

THE COLD UNIVERSE

FOREWORD

The "cold universe" is a present-day universe. In contrast to the high-energy "hot universe", it is a universe of birth, in which essential formation processes take place: moleculars clouds, stars, planets, even (perhaps) galaxies. It is mostly observable in the infrared and millimeter wavelentgh domains, and is therefore at the crossroads between space and ground-based astronomy. The study of our own galaxy provides many clues to understanding the chemical and physical processes that govern the structure and evolution of gas and dust, star formation, etc., while other galaxies often display extreme examples of these processes, such as starburst galaxies.

The aim of the meeting was to bring together observers and theoreticians from different, but complementary, fields, such as interstellar gas and dust, molecular clouds, stellar evolution, or galaxies, adopting a synthetic approach to the program. The meeting was also timely, since observational techniques are making spectacular progress (adaptive optics, interferometry, detector arrays; ongoing or proposed space missions, like COBE, ISO, SWAS, FIRST, etc.).

This means that the "Cold Universe" meeting was planned as a complement to specialized colloquia, which usually concern only part of the interested community. The program reflects this approach, which turned out to be particularly appreciated by the numerous students or post-docs attending.

The introductory chapter describes some of the current frontiers of the "Cold Universe": millimeter and submillimeter projects in Antarctica (cold indeed !), hypothetical low-mass, cold stars known as "brown dwarfs", which will be actively searched by a new generation of instruments, and the cosmological horizon itself, with the background structure at recombination first revealed by COBE. (The talk on "Brown dwarfs" was presented at a joint session with particle physicists attending a parallel "Rencontres de Moriond" conference.) The following chapters focus on current problems in interstellar gas and dust, molecular clouds and star-forming regions, protostars and young stellar objects, circumstellar disks and giant planets. The next two chapters are devoted to the cold components of galaxies up to high redshifts, and the last chapter gives a short overview of some of the current instrumental developments or projects in the IR and millimeter ranges, on the ground and in space.

The meeting took place from March 13 to 20, 1993, in the beautiful setting of the ski resort of Les Arcs (Savoie, France). It drew an audience of over 110, unprecedented in the "Moriond Astrophysics Meeting" series, and causing some last-minute housing problems. This audience would have been even larger but for a giant snowstorm which paralyzed the east coast of the US just before the scheduled start of the conference ! Fortunately, nobody had to build an igloo, even if this would have been particularly appropriate for a "Cold Universe" meeting ! (Igloos are needed in Antarctica, however...) The participants, coming from 16 countries, were mostly in the PhD-young senior age range, which testified to the attraction of the field and the emergence of a new generation. This is particularly reassuring when one realizes that some of the projects discussed during the meeting will not be operating before at least a decade !

The program comprised 43 review papers and 48 posters, out of which 16 were selected for oral presentation. The selection criterion was mainly to give participants the possibility to talk about topics not discussed in the reviews, or about recent hot (cold ?) topics. All the posters presented orally are included in these proceedings, but unfortunately a few review papers could not make it. We feel confident that in spite of this the book will remain a valuable tool both for specialists and students for some time. Also, the program included three round table discussions on controversial topics: "Dust in various astrophysical environments", "Turbulence in molecular clouds", and "The distant ultraluminous object IRAS10214+4724". These discussions, which drew a large audience, were very open and lively, too much so to be transcripted in written form (but there were no "expletives" to be deleted !).

The success of the meeting, and in particular the important participation of our younger colleagues, was made possible by the generous financial help of the European Community "Euroconference" series, of the European Space Agency, and of various French Institutions: the Space Agency (CNES), the Center for Scientific Research (CNRS), and the Atomic Energy Commission (CEA).

Last, but not least, we would like to thank several people without whom the organization of the meeting would not have been possible: Geneviève Thiéry and Joëlle Raguideau, as well as Jean Tran Thanh Van, Director of the "Rencontres de Moriond" and indefatigable promotor of an all-nation approach to particle physics and astrophysics.

Thierry Montmerle
Charles J. Lada
I. Félix Mirabel

L'UNIVERS FROID

AVANT-PROPOS

"L'Univers froid" est un univers contemporain. Au contraire de "l'Univers chaud" des hautes énergies, il s'agit d'un univers de naissance, dans lequel des processus de formation essentiels se déroulent: nuages moléculaires, étoiles, planètes, et même (peut-être) galaxies. On peut l'observer principalement dans les longueurs d'onde infrarouges et millimétriques; il s'agit donc d'un domaine au carrefour de l'astronomie au sol et de l'astronomie spatiale. L'étude de notre propre galaxie nous fournit de nombreux exemples pour comprendre les processus physiques et chimiques qui régissent la structure et l'évolution du gaz et de la poussière, la formation des étoiles, etc., tandis que les autres galaxies nous offrent des cas extrêmes, comme les galaxies à flambée d'étoiles.

Le but du colloque était de faire se rencontrer des observateurs et des théoriciens de domaines différents mais complémentaires: gaz et poussière interstellaire, nuages moléculaires, évolution stellaire, galaxies, etc., en adoptant une démarche synthétique. Le moment choisi était également opportun, puisque les techniques d'observation font chaque jour des progrès spectaculaires (optique adaptative, interférométrie, mosaïques de détecteurs, etc.; missions spatiales en cours ou proposées: COBE, ISO, SWAS, FIRST...).

Cela signifie que le colloque sur "l'Univers froid" a été conçu comme un complément aux colloques spécialisés, qui ne s'adressent d'habitude qu'à une partie seulement de la communauté concernée. Le programme reflète cette approche, qui a été jugée très favorablement par les nombreux étudiants et post-docs présents.

Le chapitre introductif décrit quelques-unes des frontières de "l'Univers froid": les projets millimétriques et submillimétriques en Antarctique (très froid !), les hypothétiques étoiles froides de petite masse appelées "naines brunes", qui sont activement recherchées, et l'horizon cosmologique lui-même, avec la structure du fond du ciel à l'époque de la recombinaison, révélée pour la première fois par COBE. (L'exposé sur les naines brunes a été présenté lors d'une session organisée conjointement avec les physiciens des particules qui assistaient en parallèle à une autre "Rencontre de Moriond".) Les chapitres suivants décrivent les problèmes actuels à propos du gaz et de la poussière interstellaires, les nuages moléculaires et les régions de formation d'étoiles, les proto-étoiles et autres "objets stellaires jeunes", les disques circumstellaires et les planètes géantes.

Les deux chapitres suivants sont consacrés à la composante froide des galaxies jusqu'à des décalages vers le rouge élevés, et le dernier chapitre donne un aperçu de quelques projets instrumentaux dans les domaines IR et millimétrique, tant au sol que dans l'espace.

Le colloque s'est déroulé du 13 au 20 mars 1993, dans le splendide site de la station des Arcs (Savoie). Il a attiré plus de 110 participants, ce qui est un record pour la série des "Rencontres de Moriond en astrophysique" —et qui a causé un certain nombre de problèmes d'intendance. L'auditoire aurait été encore plus nombreux si une énorme tempête de neige ne s'était abattue sur l'est des Etats-Unis juste avant le colloque. Heureusement, il ne fut pas nécessaire de construire des iglous, même si celà n'aurait pas paru déplacé dans le cadre d'un colloque sur "l'Univers froid" ! (Des iglous sont cependant nécessaires en Antarctique...) Les participants, originaires de seize pays différents, étaient en majorité des étudiants de doctorat ou de jeunes chercheurs, ce qui a démontré l'attrait du domaine et l'émergence d'une nouvelle génération. Ceci est particulièrement rassurant si l'on songe que certains des projets discutés pendant le colloque ne verront pas le jour avant une décennie !

Le programme comprenait 43 exposés de synthèse et 48 contributions affichées, dont 16 ont été sélectionnées pour être présentées oralement. Le critère de sélection reposait essentiellement sur l'occasion offerte de parler de sujets non abordés dans les exposés de synthèse, ou de sujets "chauds" (ou froids ?). Tous les exposés ainsi sélectionnés se retrouvent dans le présent volume, mais il faut déplorer que quelques exposés de synthèse manquent à l'appel. Nous pensons cependant que ce livre restera utile pendant un certain temps, tant pour les spécialistes que pour les étudiants. Egalement, le programme a inclus trois tables rondes sur des sujets controversés: "La poussière dans différents environnements", "La turbulence dans les nuages moléculaires", "Le lointain objet superlumineux IRAS10214+4724". Ces discussions, qui attirèrent un public nombreux, furent très ouvertes et animées, en fait trop pour être transcrites par écrit (mais aucun "nom d'oiseau" ne fut échangé...)

Le succès du colloque, et en particulier la participation importante de jeunes collègues, fut rendu possible par l'aide financière généreuse du fonds pour les "Euroconférences" de la CEE, de l'ESA, du CNES, du CNRS, et du CEA.

Enfin, nos remerciements, et non des moindres, vont à ceux sans qui le colloque n'aurait pu être organisé: Geneviève Thiéry et Joëlle Raguideau, ainsi que Jean Tran Thanh Van, Directeur des "Rencontres de Moriond" et promoteur infatigable d'une approche "toutes-nations" de la physique des particules et de l'astrophysique.

Thierry Montmerle
Charles J. Lada
I. Félix Mirabel

COLD FRONTIERS

ASTRONOMY IN ANTARCTICA

John Bally
Center for Astrophysical Research in Antarctica
Center for Astrophysics and Space Astronomy
Campus Box 389, University of Colorado, Boulder, CO 80309

ABSTRACT

The interior plateau of Antarctica may be the best place on Earth to perform observations in the infrared to mm-wavelength region of the spectrum. Recent results obtained at the South Pole indicate that the mm and sub-mm wavelength transparency of the atmosphere is substantially better than at any other known site. An effort to build a permanent astrophysics research facility at the South Pole is underway. The goals include searching for small angular scale (10 arcminutes to a several degrees) structure in the 2.7°K cosmic microwave background, a survey of the interstellar medium in the 492 GHz fine-structure line of atomic carbon (C I), and ultra-deep imaging of galaxies and star forming regions in the near-infrared. The feasibility of a large (7-m class) sub-mm to mid-IR telescope and a 2.5-m near-IR telescope are being evaluated.

1. Characteristics of Sub-Millimeter And Infrared Sites

In the infrared to mm-wavelength region of the spectrum ($\lambda = 1.0\mu$m to 3.0mm), water vapor is the primary source of atmospheric opacity. The complex symmetries of the H_2O molecule result in over 10^6 individual spectral lines which cover the spectrum. In addition to attenuating the signal, thermal emission from water dominates the emissivity of the atmosphere, producing a flux of radiation which can mask the flux received from sources above the atmosphere.

The primary characteristic of a good site usable at infrared to mm-wavelengths is a low overburden of precipitable water vapor. The total amount of water vapor that the atmosphere above a given site can hold is a strong function of the atmospheric temperature. Cold gas holds much less water than warm gas. In general, the average temperature of the atmosphere above a given site is a strong function of elevation and geographic latitude. The coldest, and therefore dryest, atmospheric conditions are found at high latitude, high elevations sites. Thus, infrared and sub-mm wavelength telescopes are usually located on high and dry mountaintops.

Although deserts are characterized by dry surface conditions, the warm atmosphere above them can contain large amounts of precipitable water vapor since the dew point of warm air is relatively high. Thus IR to mm-wave transmission (and emissivity) over temperate latitude deserts is not expected to be as good as over *cold* high latitude sites.

Evaporation and tropospheric convection injects water into the atmosphere. Distance from sources of evaporation can influence precipitable water vapor over a site. Water vapor can be pushed above coastal or islands sites by convection and prevailing winds. In sites such as Chile, the local topography forces the prevailing westerly winds to push water vapor over the Andean range, resulting in relatively high precipitable water content, even at high elevations. Isolated peaks or island mountains such as Hawaii are better since moist air can move around the mountain rather than over it. However, inland sites located far from the nearest large body of water in the prevailing wind direction have the dryest conditions. As moist air masses move overland, condensation and precipitation removes water from the air. Thus, high elevation inland sites tend to have the lowest overburden of precipitable water vapor.

The above considerations indicate that in general, the best infrared to mm-wavelength sites are to be found at high elevation, high latitude, inland parts of continents. Inspection of a map of the world indicates that the interior of the Antarctic Plateau best satisfies these site criteria. Less ideal sites may be found in the interior of Asia, in the Alps in Europe, on Greenland, in the Rocky Mountains in North America, and in the Andes in South America.

2. Antarctica As A Sub-Millimeter And Infrared Site

The primary considerations for selecting an infrared to mm-wavelength site are:

(1) *Low temperature.* At near-IR wavelengths on the Wien side of the blackbody spectrum, the thermal emission from the atmosphere decreases very rapidly with decreasing temperature. South Pole surface temperatures range from -10°C to -80°C. Figure 1 shows the temperature statistics for the South Pole.

(2) *High altitude.* At sub-mm and mid-IR wavelengths, pressure broadening dominates the line-width of atmospheric lines. For a given column density, the optical depth in the line wings decreases rapidly with decreasing pressure. The optical depth in most long-wavelength windows is determined by the far-wings of the most opaque lines, and therefore is very sensitive to the pressure. The altitude of the South Pole is 2,800 m. However, the pressure altitude is frequently closer to 3,500 m.

(3) *Low precipitable water vapor.* Low temperatures and high altitude imply low precipitable water vapor which results in lower optical depth in the water lines. At the south Pole, the precipitable water vapor is almost always less than 1 mm. Figure 2 shows the month-to month averages of precipitable water vapor over the South Pole and Vostok (located 800 miles from the Pole) along with the extreme high and low values observed during each month.

Several other factors should be considered in selecting a site:

(1) *Accessibility.* Most good sites are hard to get to. The South Pole is accessed by ski-equipped C-130 cargo planes.

(2) *Minimum Cloud cover.* Although this is a primary consideration for optical and near-IR sites, frozen clouds are relatively transparent at sub-mm and mm wavelengths. Visual and satellite observations indicate that the sky over the South Pole is clear about 40% to 50% of the time (see Figure 3). Due to the low environmental and atmospheric temperature, the sky is expected to be so much darker at near-IR wavelengths (near 2μm) from the Pole than at temperate latitude sites (when clear), that a much higher average data rate is expected despite a lower number of "photometric" quality hours.

(3) *"Dark" skies.* The South Pole is one of the most remote sites on Earth. All future telescopes will be located in the so called "Dark Sector" about a kilometer from the main South Pole base where artificial illumination and RF interference are expected to be at a minimum. OH airglow and auroral lines produce narrow band, time variable emission in the near-IR and optical windows. These emission lines can be avoided with active filtering (pass the light through a disperser, mask the unwanted frequencies, and recombine the light), or by choosing observation bands that avoid these lines. Spectroscopic observations naturally subtract these features. As shown below, Antarctica may provide the darkest sky on Earth at near-IR wavelengths.

(4) *Low atmospheric turbulence.* This is also a prime consideration for an optical or near-IR observatory. At mid-IR to mm wavelengths, the diffraction limit for single dish telescopes is usually larger that the seeing disk. However, the 20 to 30°C deep thermal inversion that develops over the Antarctic ice sheet during the night may be stable to convective overturning. This may result is very stable optical and near-IR seeing at times.

(5) *Long-baseline phase stability.* High angular resolution (1" or less) mid-IR to mm wavelength observations require large aperture synthesis arrays. Coherent combination of signals from different elements of such an array requires that the phase of the incoming electromagnetic wave remain stable to a fraction of a radian in an integration time. The refractive index variations that dominate sub-mm phase fluctuations are generally produced by water vapor. The extremely dry conditions and lack of convection over the Antarctic ice are expected to result in a high degree of phase stability. However, no measurements of phase stability are available yet.

(6) *Low average and peak wind.* Many high elevation sites occasionally suffer very high winds. Although the Antarctic coast suffers fierce winds, the interior Plateau has relatively mild winds. Figure 4 shows the average wind speed and surface temperature at the South Pole on a month by month basis.

Several geographic and meteorological factors conspire to make the interior of Antarctica an ideal place for near-IR to mm-wave observations. The continental mass is nearly centered on the geographic Pole. The global circulation pattern drives storms *around* the continental mass, frequently lashing the shores of Antarctica with fierce storms. However, this pattern forms a permanent high pressure zone in the continental interior. During most of the year, dry stratospheric air descends over the middle of the continent. Moist marine air masses rarely intrude over the interior plateau. These conditions result in less than 10cm of annual precipitation, low winds, and dry conditions.

During the 1980s several groups recognized the potential value of the South Pole for sensitive sub-mm and mm-wave measurements. Several experiments to search for structure in the 3^{o}K cosmic microwave background radiation (CMBR) started to operate at the South Pole during the late 1980s. These efforts led to a proposal to the US National Science Foundation to form a Science and Technologies Center to develop the South Pole for its unique astrophysical capabilities.

3. CARA

The Center for Astrophysical Research in Antarctica (**CARA**), a consortium of university and industrial research groups, was established to develop the first permanent observatory in Antarctica. Three groups of telescopes are nearing completion and will be deployed at the South Pole in the near future.

COBRA (COsmic Background Radiation Anisotropy), was designed to measure small angular scale fluctuations in the cosmic microwave background. Several 1-m class telescopes operating between 0.5 and 3mm, equipped with cooled bolometric detectors, have been deployed by Jeff Peterson and Mark Dragovan's group (Princeton University). These ground-based studies will compliment the large scale ($> 7^{o}$) studies of CMBR anisotropy with the COBE satellite. The larger aperture of ground-based telescopes can be used to measure the CMBR anisotropy on scales between 10' and 10^{o}. So far, COBRA experiments have operated only during the Austral summer when the South Pole station is accessible by air (from mid-October to mid-February). As CARA buildings and facilities are erected in the "Dark Sector", COBRA experiments will be operated as "winter-over" experiments, taking advantage of the dryer and colder conditions of the 6 month long Austral night.

AST/RO (Antarctic Sub-millimeter Telescope and Remote Observatory) is a 1.7 meter diameter telescope whose primary mission is to perform the first survey of the 492 GHz fine-structure line of neutral atomic carbon (C I) and high-lying (J=4-3) CO lines in the interstellar medium. Antony A. Stark (CfA) leads a group that is building this heterodyne system using state-of-the art SIS mixers for sub-mm observations. The carbon fiber primary has better than 10 μm rms surface accuracy that will permit observations throughout the sub-mm portion of the spectrum. The ATR/RO system will be the first general purpose year-round astrophysics facility in Antarctica. AST/RO will also be used for continuum studies of sub-mm dust emission, emission line studies of the Milky Way, the Galactic Center, nearby galaxies such as the LMC and SMC, heterodyne spectroscopy and profiling of atmospheric trace gasses that may play a role in the "greenhouse effect", global climate change, and ozone destruction. AST/RO will be used to obtain test measurements in the mid-IR spectral windows between 20 and 60 μm that are predicted by atmospheric modeling. AST/RO will be deployed in December 1994.

SPIREX (South Pole Infra-Red EXplorer) is a 50 cm class telescope being built by Mark Hereld's group (University of Chicago) for ultra-deep imaging in the 2μm region. The low temperature of the air over the South Pole during the polar night results in a flux of atmospheric radiation about 200 times lower than from the atmosphere above a temperate latitude observatory. Thus, in windows devoid of OH airglow and auroral lines, a given telescope/camera combination may reach about 5 magnitudes deeper in a given exposure time than the same equipment used at a site such as Mauna Kea. Atmospheric emission models (Harper 1989) indicate that observations confined to the upper portion of the K-window (between 2.25 and 2.45 μm) will be limited the background produced by the Zodiacal light and not the Earth's atmosphere. A 50-cm telescope and a 128 by 128 NICMOS2 camera will be deployed in December 1993 to obtain low dispersion spectra of the atmosphere, and to perform preliminary imaging experiments. An InSb photometer may also be deployed by the the Anglo-Australian Observatory infrared group to measure the sky brightness between 1 and 5 μm.

Preliminary results from the COBRA experiments and site testing performed by the **ATP** (Advanced Telescope Project - led by John Bally, University of Colorado) experiments indicate that the South Pole is the best site on Earth tested so far for astrophysical measurements in the infrared to sub-mm (1 μm to 1-mm) spectral region. During 1992, a 230GHz atmospheric brightness temperature monitor (tipper), borrowed from the National Radio Astronomy Observatory (NRAO), was deployed at the South Pole. Preliminary results of measurements made with this instrument are shown in Figure 5. During fall 1992, a 12" telescope equipped with a CCD camera was deployed to measure "seeing" (atmospheric turbulence) at optical wavelengths. In 1993, a Differential Image Motion Monitor (DIMM) will be deployed to measure the atmospheric turbulence parameter r_0.

4. Dome-A: A 4,200 meter Plateau at Latitude -82°

Lynch (1989) has pointed out that the high elevation plateau at latitude -82° near the middle of the Antarctic continent is potentially the best site for infrared to sub-mm wavelength observations. A 200 mile diameter flat region is located at an altitude in excess of 4,000 meters directly beneath the centroid of the permanent high pressure zone which develops over the Antarctic Plateau. Due to the low atmospheric temperature, the barometric pressure at the surface is equivalent to what is found near 5,000 meters altitude at temperate latitudes (pressure altitude of dome-A is thus 5,000 meters).

Dome-A may be the best IR to sub-mm site for 4 important reasons:

- Low water vapor. Atmospheric model calculations indicate that water vapor overburdens as low as 50μm are to be expected. Figure 6 shows a model calculation of the expected transmission over Dome-A (Bally 1989).
- The high pressure altitude implies less broadening of atmospheric lines. This implies that atmospheric windows are broader and more transparent than at lower altitudes.
- Average and peak wind velocities are expected to be very low because Dome-A is located near mean position of the permanent Antarctic high pressure zone where dry stratospheric air descends from above.
- Surface temperatures are very low (under 200K at times), resulting in very low thermal backgrounds, especially in the near infrared. The total amount of precipitation is less than 10 cm equivalent of liquid water.

Lynch (1989) has proposed that an international base be established at this site to take advantage of the exceptional conditions found there.

Dome-A may be a unique place for the development and testing of advanced infrared and sub-mm instrumentation. The flat ice surface is ideal for the deployment of long baseline interferometric arrays such as is required for the search for extra-solar planets. The remoteness, high altitude, and low temperature of Dome-A makes it the best analog to space on Earth. Many of the techniques required for operation of a Lunar base are required for operations at dome-A, including pressurized and heated working environments and long logistical supply lines. However, experience indicates that the cost of developing an Antarctic base is more than 3-orders of magnitude cheaper than accomplishing the same task in space.

5. Future Plans and Potential for Antarctic Astrophysics

5.1. The Next 10 Years

The immediate goal of CARA is to make the initial compliment of experiments at the South Pole operational. During the next few years, we hope to perform a sub-mm survey of CO (J=4-3) and CI (J=1-0) emission from the interstellar medium with AST/RO, obtain images of the small angular scale CMBR anisotropy with COBRA, demonstrate the utility of the South Pole for near-infrared imaging in the 2μm K^+ window, quantify the optical and near-IR seeing and sky brightness, and measure the mid-IR and sub-mm transmission spectrum with ATP experiments.

CARA is starting to plan for projects which may become operational during the next 5 to 10 year period. At the present time, the sub-mm characteristics of the South Pole have been demonstrated most convincingly. The next major step towards an Antarctic Observatory may be the design, construction, and deployment of a 7-m class sub-mm to mid-IR telescope. CARA laboratory facilities are being erected that will be capable of supporting the construction and operation of such a telecope. A 7-meter class large Antarctic sub-mm telescope might be designed with Ritchey-Cretien optics in an unobstructed, off-axis configuration that minimizes spill-over and scattering, and maximizes the field-of view (needed for large future focal plane arrays) and beam efficiency. A surface accuracy of several μm rms may be possible, which would permit mid-IR operations in the 10 to 60 μm windows accessible from the South Pole.

If the near-IR seeing and sky-brightness measurements indicate good conditions, a larger near-IR telescope with a 2.5-m glass primary may be considered. Such an instrument may be capable of reaching the faintest limiting magnitude in the K^+ window of any telescope in the world.

5.2. Far Future Potential

The basic reason for considering major astrophysics facilities in Antarctica is that it may be considerably cheaper to deploy large structures in Antarctica than in space. A variety of fundamental problems, such as the origin of stars and planets, the formation and evolution of galaxies, and the origins of structure in the early universe require both high sensitivity and high angular resolution. Antarctica may be the first place where very large aperture and/or long baseline mid-IR interferometers may be developed that are capable of searching for extra-Solar planets and imaging distant galaxies with sub-arc-second resolution at IR and sub-mm wavelengths.

Ultimately, it may be desirable to develop Dome-A as a manned astrophysics station. Such an endevour will almost certainly be international in scope. Either Dome-A or the South Pole may be ideal environments in which to test the technology needed for highly ambitious future space missions such as the establishment of a Lunar base, or an expedition to Mars. On the way, exciting new observations of the Cold Universe may become possible.

6. Conclusions

Preliminary measurements conducted under the CARA South-Pole site testing program indicate that the high, cold, and dry conditions which prevail in the interior of Antarctica provides the best place on Earth for the future deployment of large instruments in the infrared to mm-wavelength spectral range. High angular resolution, high sensitivity, and high spectral resolution observations can be performed throughout the mid-IR and sub-mm bands from high sites in the interior of Antarctica. Developing large telescopes that can operate in Antarctica is a logical step towards the development and eventual deployment of this technology in large space or Lunar observatories in the far future.

7. References

Bally, J. (1989) in "Astrophysics in Antarctica" ed. D. J. Mullan, M. A Pomerantz, and T. Stanev, AIP Conference Proceedings 198, AIP Press, New York, pg. 100.

Bromwich , D. H., Reviews of Geophysics, 26, 149, 1988.

Burova, L.P., Gromov, V.D., Lukyanchikova, N.I., and Sholomitskii, G. B., Soviet Astron. Lett., 12, 339, 1986.

Chamberlin, R. and Bally, J. (1993) Applied Optics (in press).

Lynch, J., T. (1989) in "Astrophysics in Antarctica" ed. D. J. Mullan, M. A. Pomerantz, and T. Stanev, AIP Conference Proceedings 198, AIP Press, New York, .pg. 249.

Harper, D. A. (1989) in "Astrophysics in Antarctica" ed. D. J. Mullan, M. A. Pomerantz, and T. Stanev, AIP Conference Proceedings 198, AIP Press, New York, .pg. 123.

Smythe, W. W, and Jackson, B. V. Applied Optics 16, 2041, 1977.

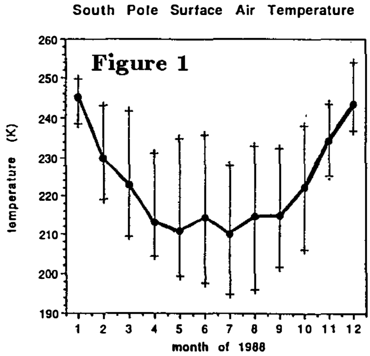

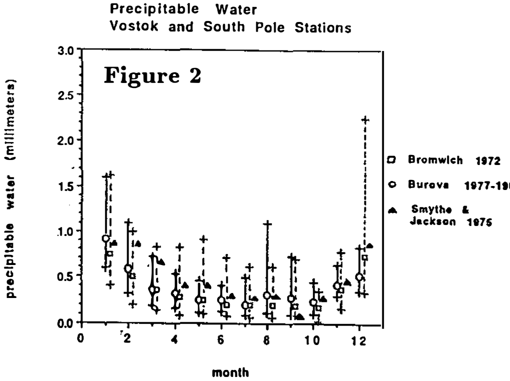

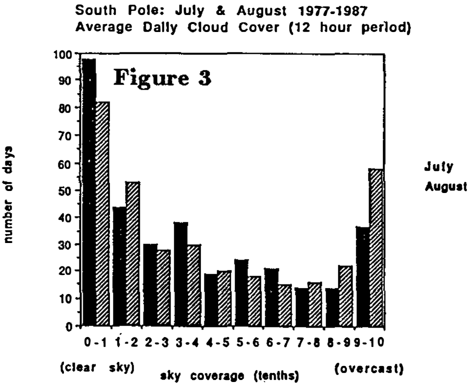

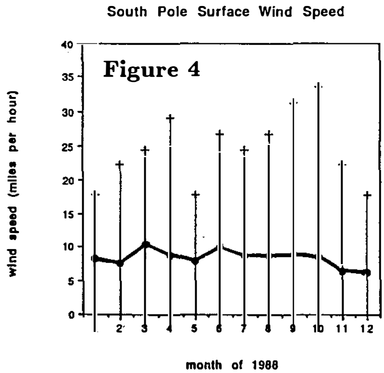

Figure 1. Surface air temperature statistics over South Pole.

Figure 2. Average precipitable water vapor over the South Pole and over Vostok. The highest and lowest values measured in each month are also shown. Taken from Bromwich (1988), Burova et al. (1986), and Smythe and Jackson (1977) for the years indicated in the figure.

Figure 3. Cloud cover statistics over the South Pole from visual observations by South Pole personnel.

Figure 4. Wind speed statistics at the South Pole.

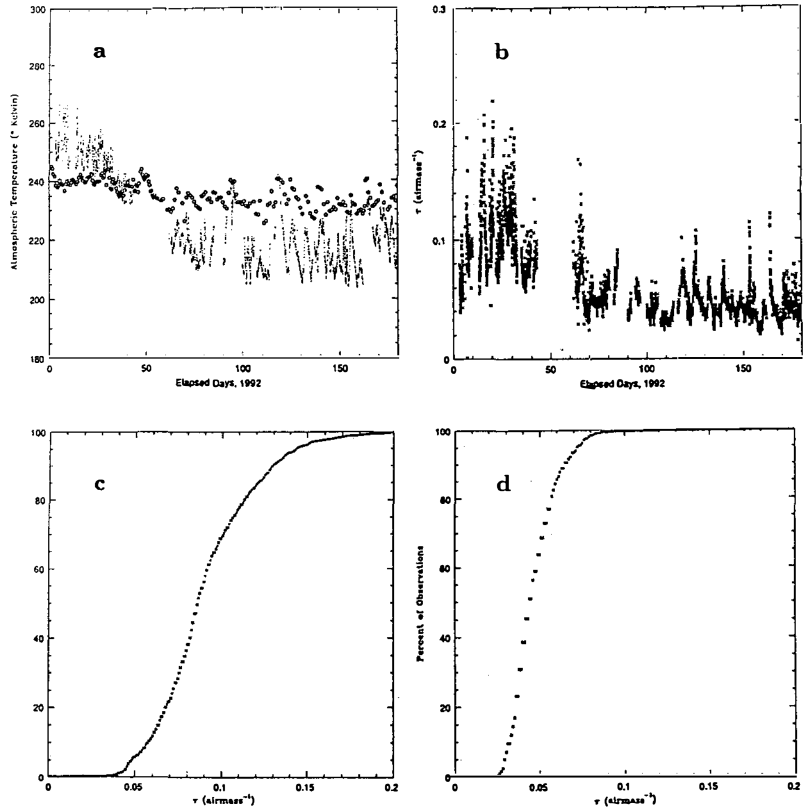

Figure 5. (a) Atmospheric temperature determined from a 230 GHz radiometric measurement (dotted curve). Surface temperature at the radiometer site at the South Pole (open circles). Taken from Chamberlin and Bally (1993).

(b) Atmospheric optical depth at 230 GHz determined by fitting a model atmosphere to the measurements of the sky brightness as a function of zenith angle at 230 GHz. Taken from Chamberlin and Bally (1993) .

(c) The percentage of measurements for which τ(225 GHz) was less than a given value between day 1 and day 70 in 1992. Quartiles are 0.068, 0.080., 0.103, 0.186. Taken from Chamberlin and Bally (1993) .

(d) The percentage of measurements for which τ(225 GHz) was less than a given value between day 71 and day 180 in 1992. Quartiles are 0.036, 0.042., 0.051, 0.083. Taken from Chamberlin and Bally (1993) .

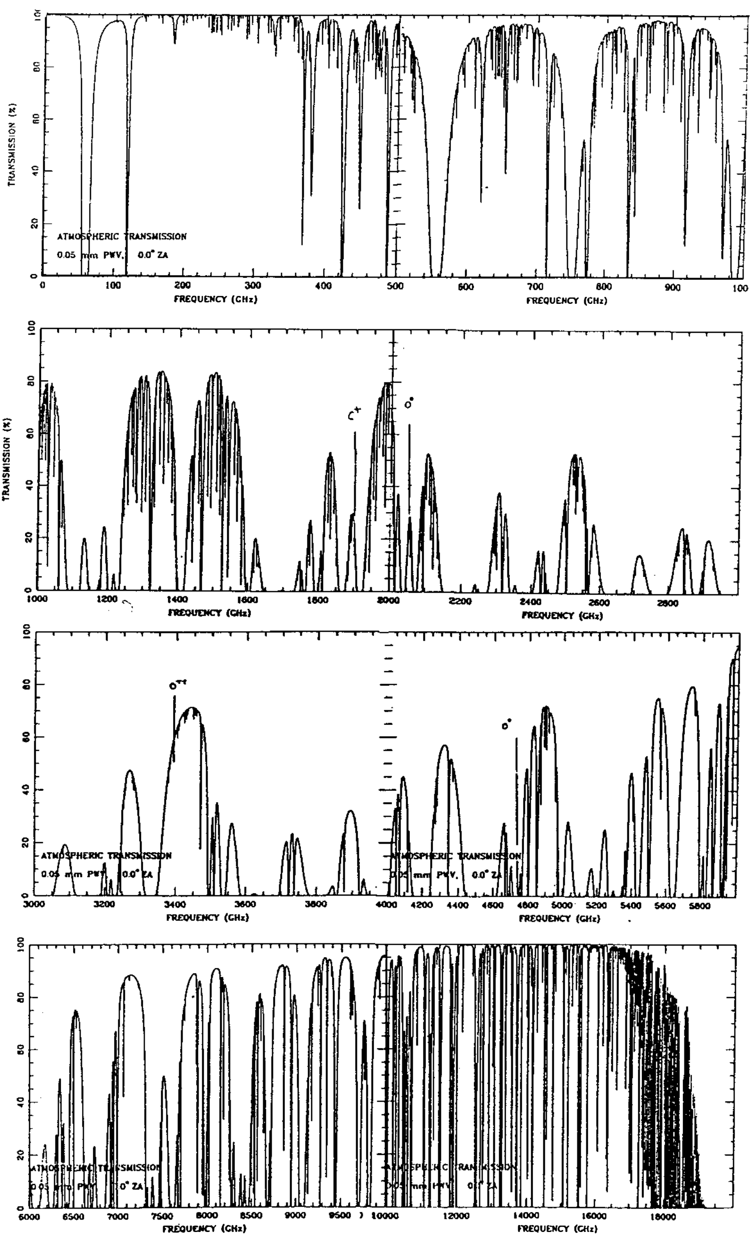

Figure 6. Model atmospheric transmission computed for Dome-A for 50 μm of precipitable water vapor.

BROWN DWARFS

William J. Forrest
Department of Physics and Astronomy
University of Rochester
Rochester, NY 14627
USA

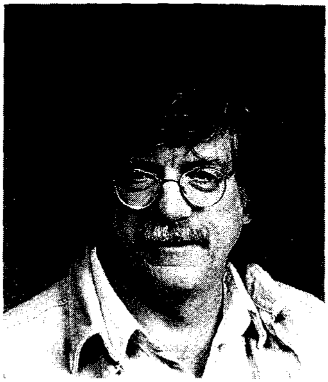

ABSTRACT
The term brown dwarf was introduced by Jill Tarter to describe self-gravitating bodies which are not sufficiently massive to sustain hydrogen fusion, but are more massive, or form in a different way, than planets. Their masses would range from roughly 0.001 to 0.08 $M_{\odot}$. It is known from extensive observations that stars with masses just above the hydrogen burning limit, 0.08 $M_{\odot}$, are quite numerous in our neighborhood of the galaxy. Since a body, when in the process of formation, is not aware of the mass limit, it is believed that objects should form rather readily below the stellar mass cutoff. Such objects lack a nuclear energy source and will cool throughout their lifetimes. This implies that older brown dwarfs will be dim and will radiate primarily at longer wavelengths, in the infrared. Thus, even though the current evidence for even one bona-fide brown dwarf is not conclusive, these objects could still be quite numerous, and perhaps even important sources of baryonic matter in the universe. Past searches for brown dwarfs are reviewed and future searches discussed. Of special interest are the planned cooled infrared space telescopes ISO and SIRTF, which will for the first time permit detection and investigation of older brown dwarfs in the solar neighborhood. Also interesting is the possibility of detecting such objects far from the solar system via their gravitational lensing effect.

I. NATURE OF BROWN DWARFS

Most of the (known) baryonic matter in the universe is in the form of stars or stellar remnants. Initially diffuse gaseous material is concentrated through gravitational attraction, leading to bound objects which eventually contract to form stars. Throughout the latter stages of the contraction, the contracting clouds are in hydrostatic equilibrium, whereby the inward gravitational attraction is exactly balanced by the pressure gradient. Under these conditions, the virial theorem applied to an ideal gas implies that the temperature in the interior will scale with radius R and mass M as $T \sim M/R$. Thus, contraction will continue until the interior temperature is high enough to generate nuclear fusion reactions sufficient to power the observed stellar luminosity. This is the point at which a star is born, and corresponds to a well defined luminosity and effective surface temperature (the zero age main sequence) which depends primarily on the stellar mass.

Kumar[1)] and Hayashi and Nakano[2)] showed that the above scenario would only apply to stars above a characteristic minimum mass, 0.07-0.08 $M_\odot$. Below this mass, electron degeneracy pressure becomes dominant and prevents further contraction. This limits the central temperatures below the characteristic value required for hydrogen fusion, about 2×10^6 K. Thus these objects would never reach stable thermal equilibrium. Their only source of energy is the heat stored in the interior. As this energy is radiated away, they will cool and become less luminous. Hence older brown dwarfs will be very inconspicuous and best detected in the infrared spectral region. An excellent review of the astrophysics of Brown Dwarfs is given by Burrows and Liebert[3)].

II. SIGNIFICANCE OF BROWN DWARFS

There are a number of reasons for the interest in brown dwarfs. Studies of the mass spectrum of stars which have formed clearly show that low mass stars are the most numerous. The observed masses range right down to the hydrogen burning limit[3),4)]. Since there is no known mechanism which constrains collapsing clouds to just the mass that will eventually burn hydrogen, it is commonly believed that a fair number of substellar objects have also formed. The mechanisms which govern the stellar mass spectrum (Initial

Mass Function) are not well understood, and a knowledge of this spectrum is important in guiding our understanding of star formation.

The lowest mass stars and the brown dwarfs will have very low surface temperatures. Below about 3000 K, molecules such as TiO, CO, H_2O dominate the opacity and the spectrum is decidedly non-Planckian [5]. Below 2000 K, dust grains are expected to condense[6]. The nature and structure of the resulting atmospheric dust clouds is quite uncertain and observations of the stellar spectra for these low temperature bodies are necessary for clarification. Recall the complex structure seen in the atmosphere of Jupiter, which can be considered a brown dwarf which has cooled to *circa* 135K. It would be extremely difficult to predict such complex structure theoretically.

A third reason for the interest in brown dwarfs is they are directly related, through physics, with the giant planets. In fact, the distinction between low mass brown dwarfs and giant planets is by the mode of formation: planets form in the circumstellar disk remaining after a star has formed. The physics governing these objects is the same, and therefore the appearance (temperature, luminosity, spectrum, etc.) should be the same at the same age and mass. The study of brown dwarfs will therefore illuminate planetary evolution and vice-versa.

Finally, the brown dwarfs may supply some of the considerable amount of "missing mass" in the universe. It has become clear in recent years that at least 90% of the mass in typical galaxies is not accounted for. It cannot be conventional stars, gas, or dust. It must be "cold", i.e. non-zero rest mass, because the mass concentrates around galaxies. One possibility for this mass is brown dwarfs. These objects would rapidly become very dim and cool, and could easily have escaped attempts to detect them. One expects that if brown dwarfs are so numerous, at least a few should be near the sun where they could be studied. The problem is to locate them.

III. SEARCHES FOR BROWN DWARFS

An excellent summary of the numerous searches for brown dwarfs is given in the review by Burrows and Liebert[3]. Here I only highlight a few examples. One tack taken in the search for brown dwarfs is to look in the vicinity of nearby stars for dim, red, "companions". If true companionship can be established, the primary component can be used to calibrate the age and distance of the candidate brown dwarf. The distance gives the luminosity. From the colors or spectra, the temperature may be estimated, though this is quite uncertain for temperatures below 3000K. The luminosity, temperature, and age may now be compared to theoretical values and known very low mass stars to assess the likelihood that the object is a brown dwarf. With current technology, the most sensitive searches have been carried out in the K band (2.2 μm), and, hence, are only sensitive to the younger, hotter, brown dwarfs. Proof of an undeniable brown dwarf would follow if the object is significantly less luminous and cooler than the lowest mass star possible[7)] (about 10^{-4} $L_{\odot}$, 1750K). No such objects have been discovered. Failing this, one must argue based on the age of the object; the many theoretical studies of sub-stellar evolution are in fairly good agreement on the decrease in luminosity with age for a given mass object. Unfortunately, precise ages are not easily determined and the range of possible ages will imply a range of possible masses. Two examples of this are the companions to GD 165 and Gliese 569. For GD 165B, the minimum mass of 0.06 $M_{\odot}$ is derived based on the minimum age of the white dwarf primary, 6x10^8 years. If it were this young, it would be a bona-fide, though rather high mass, brown dwarf. However, it could be much older and be, rather, a .08-.09 $M_{\odot}$ very low mass star. Similarly, the age of the Gl 569 primary has been estimated[8)] as between the age of the Pleiades (7×10^7 years) and the Hyades (6×10^8 years). Based on its luminosity, this implies masses between 0.05 and 0.1 $M_{\odot}$ for Gl 569B. Again, the object is either a young brown dwarf or an older very low mass star. Lack of lithium[9)] indicates a mass greater than 0.06 $M_{\odot}$ while the extremely late spectral type of M8.5[10)] probably rules out a mass greater than 0.09 $M_{\odot}$. More precise age determinations are not likely in the near future. More precise masses may be measured through analysis of the binary orbit. However, the orbital periods are many hundreds of years.

The above paragraph suggests one strategy in the search for brown dwarfs: find them when they're young, hot, and luminous[11),12)]. The up-side of this strategy is that such objects will be readily detectable. The down-side is that such objects will be similar to ordinary stars in luminosity and temperature. Proof of brown dwarf nature will require accurate assesment of the age and luminosity of the object. Good hunting grounds include the Taurus and ρ Oph star-forming regions ($10^6 - 10^7$ y, 140-160 pc), and the Pleiades (10^8 y, 120 pc) and Hyades (10^9 y, 45 pc) star clusters. For example, a 0.01-0.02 $M_{\odot}$ brown dwarf in Taurus or ρ Oph would appear at K = 14-16 mag, which is quite easy to detect with modern detectors. A key in this type of search is establishing cluster membership. The danger is that reddened background stars may masquerade as brown dwarfs.

Brown dwarf candidates have been located in the Pleiades[13),14)] and the Hyades[15)]. However, even if these candidates can be confirmed as true cluster members, they are positioned near the brown dwarf/low mass star border on the Luminosity *vs.* Age theoretical diagrams. Therefore, they are ambiguous and at best high mass brown dwarfs. In fact, enough studies have been carried out to show that high mass brown dwarfs, $> 0.05M_\odot$, are not numerous enough to supply interesting amounts of mass in the disk population of the solar neighborhood. This is not to disparage the effort: the discovery of even one true-blue brown dwarf would be extremely interesting.

The above noted confusion, i.e. young brown dwarfs have spectra similar to late-type stars and reddened background stars, can be overcome if we allow them to cool far enough. The lowest mass stars will have effective temperatures not much less than 1800K. Brown dwarfs of sufficiently low mass in the Hyades and Pleiades will cool well below this limit. Such cool objects will probably require cooled space telescopes, such as ISO, SIRTF or EDISON, for detection and characterization. In the tables below are given the predicted characteristics of brown dwarfs in the Pleiades (assumed age 10^8 y, distance 120 pc) and Hyades (assumed age 10^9 y, distance 45 pc) using typical evolutionary results[7),16)] and assuming black-body spectra.

Table 1. Fluxes and Magnitudes for Pleiades Brown Dwarfs

$M/M_\odot$	T(K)	1 μm mag	2.5 μm mag	3.5 μm μJy	7 μm mag	μJy
0.01	774	31.1	20.4	11	16.5	21
0.02	1271	23.5	17.5	74	15.4	56
0.04	2245	18.3	15.5	288	14.5	126
0.06	2829	16.6	14.6	563	13.9	216

Table 2. Fluxes and Magnitudes for Hyades Brown Dwarfs

$M/M_\odot$	T(K)	1 μm	2.5 μm	3.5 μm	7 μm	
		mag	mag	μJy	mag	μJy
0.01	425	46.0	25.0	4	17.0	12
0.02	661	33.0	20.0	19	15.4	57
0.04	1068	24.0	16.9	159	14.3	156
0.06	1482	20.4	15.4	405	13.8	253

The ISOCAM sensitivity in a broad band at 7 μm is 5 sigma of 25 μJy in 1 hour of integration. Thus the mass limit is similar in each cluster, about 0.015 $M_\odot$. The Hyades is attractive because all the brown dwarfs below about 0.06 $M_\odot$ will have cooled sufficiently to be easily distinguished from stars. The Pleiades is favored because of its greater star density (38 stars/sq. deg. *vs.* only 3 for the Hyades). Therefore a survey of about 50 fields near each cluster would probably locate bona-fide brown dwarfs, even if they are no more numerous than stars. SIRTF and EDISON would be considerably more sensitive than ISO. These experiments would be needed to do follow-up spectroscopy of brown dwarf candidates and make a more accurate assesment of the overall brown dwarf population.

IV. GRAVITATIONAL MICRO-LENSING

Compact objects will form multiple images of a background point source. For objects of 1 $M_\odot$, the typical deviations will be 10^{-6} arcsec, hence the name micro-lensing. These small angles will not be observable, but the attendent amplification in brightness will be. Such amplification will be detectable in the macro-lensed images of background QSO's lensed by an intervening galaxy. In this manner objects down to the QSO-size limited resolution (about 0.001 $M_\odot$) may be detected, well into the brown dwarf regime.

Micro-lensing of the "A" image of the quasar Q2237+0305 was clearly observed in 1988[17),18),19)]. The event was very short, and indicates a low-mass object in the intervening galaxy, probably $< 0.1 M_\odot$. Because of the high probability of micro-lensing in this system, a long series of photometric monitoring will be required to permit reasonable estimates of the number of brown dwarfs, compared to more massive objects, in the intervening galaxy. Nevertheless, it is astonishing that a bona-fide brown dwarf may have been first seen in a galaxy approximately 200 Mpc distant using this technique.

Micro lensing of individual background stars by foreground compact objects also will result in significant amplification[20]. Recently, 2 independent groups have reported 3 candidate MACHO (Massive Compact Halo Object) gravitational lensing events using background stars in the LMC. An Australian-American team[21] reports one very well observed event. A French team[22] reports 2 other candidate events and confirms the Australian-American event in the red (it was too dim for them in the blue). In each of these cases, the brightening is not repeated, equal in the blue and red, and time symmetric. These are 3 of the tests to distinguish between gravitational lensing and stellar variability. The Australian-American event is especially impressive in that the 414 high-quality data points could be fit by the most simple gravitational lensing model, with 4 free parameters[20]. With time, both groups plan to apply 2 further tests to these brightening events: independence of spectral type and the frequency of events as a function of peak amplification (high amplification events being less frequent). The French group reports that one of their stars was on the main sequence and the other above the main sequence. The Australian-American star was a giant.

The mass of the lensing object is indicated by the time-scale of the event. Since lensing cross section is proportional to mass, the time scale will be proportional to the square root of mass and inversely proportional to the transverse velocity. All three reported events were of short time scale (about 1 month), indicating a low mass. The Australian-American group reports a most likely mass of 0.12 $M_\odot$ with masses of 0.03 and 0.5 $M_\odot$ being half as probable. The mass estimates are based on detailed modelling of the Milky Way's dark halo[23]. The French group infer masses of a few % to 1 $M_\odot$ for their events. Interestingly, the French have another data set which suggests the dark halo can't consist of 10^{-7} to 10^{-5} $M_\odot$ objects.

The French group has reported an analysis of the frequency of events seen and find that the results to date are consistent with the entire dark halo consiting of such low mass objects. They note that if the halo objects had mass 10^{-2} $M_\odot$, they would expect 6 events while if they were all 1 $M_\odot$ they would expect 1 event in the data which showed 2 events. This gives the likely mass range and indicates low mass objects comprise a significant large part of the dark halo. The halo we are imagining provides a flat rotation curve out to the

LMC at 55 kpc. The density is about 8×10^{-3} $M_\odot/\mathrm{pc}^3$ in the solar vicinity. This density is about 10% the previously known density near the sun (stars, gas, dust, and white dwarfs).

V. DETECTING HALO BROWN DWARFS

It is likely that the dark halo objects really are substellar. Stars in such abundance should have been noticed in deep surveys[24)]. The masses are too low for neutron stars or black holes. White dwarfs are a possibility at this time but it seems unlikely that the required narrow range of masses would have been produced in the halo. If substellar objects predominate, then the gravitational lensing events will be predominantly of short duration and **this** will become clear as more of the lensing data is analyzed and more data is gathered.

The mass limit for brown dwarfs depends on the metallicity. It is approximately 0.077 $M_\odot$ for solar metallicity and 0.092 $M_\odot$ for zero metallicity[7)]. Objects in the halo are likely to be low to very-low metallicity so we should be prepared for this.

If the MACHOs are brown dwarfs, then we have a good chance of detecting them with cooled space telescopes such as SIRTF and ISO, but not from the ground. Using typical evolutionary results[7),16)] and assuming a black-body spectrum and an age of 10^{10} years, the expected fluxes at a distance of 10 pc are given in Table 3 and compared to the sensitivities of various telescopes.

Table 3: Brown Dwarf Fluxes (10 pc, 10^{10} y) *vs.* Telescope Sensitivities

$M/M_\odot$	$R/R_\odot$	T(K)	2.2 μm mag	2.2 μm μJy	4.5 μm μJy	7.5 μm μJy	12.5 μm μJy
0.01	0.12	225	38.7	...	0.07	4.5	32
0.03	0.10	450	23.3	0.3	65	230	300
0.06	.083	750	17.4	70	750	950	600
Point-source Sensitivities of various telescopes, 5 sigma in 1 hour:							
8m IRO Mauna Kea			23	0.4	...	...	...
0.85m SIRTF, EDISON			...	...	0.5	5	12
0.6m ISOcam			...	...	45	25	...

From Table 3, it can be seen that a 0.03 $M_\odot$ halo brown dwarf could be detected to a distance of 9 pc using an infrared-optimized 8 m ground based telescope. ISOcam could detect that object at 30 pc and an 0.85 m SIRTF to a distance of 110 pc. The likely presence of large H_2 opacity, and hence small fluxes, in the ground-based K-band near 2.2 μm, makes a search from the ground even less favorable[25].

REFERENCES

[1]Kumar, S.S. 1963, *ApJ*, **137**, 1121.
[2]Hayashi, C. and Nakano, T. 1963, *Prog.Theor.Phys.*, **30**, 460.
[3]Burrows, A. and Liebert, J. 1993, *Rev.Mod.Phys.*, **65**, 301.
[4]Liebert, J. and Probst, R.G. 1987, *Ann.Rev.Astron.Ap.*, **25**, 473.
[5]Kirkpatrick, J.D., Kelly, D.M., Rieke, G.H., Liebert, J., Allard, F., and Wehrse, R. 1993, *Ap.J.*, **402**, 643.
[6]Lunine, J.L., Hubbard, W.B., Burrows, A., Wang, Y.P., and Garlow, K. 1989, *Ap.J.*, **338**, 314.
[7]Burrows, A., Hubbard, W.B., Saumon, D., and Lunine, J.I. 1993, *Ap.J.*, **406**, 158.
[8]Forrest, W.J., Skrutskie, M.F. and Shure, M. 1988, *Ap.J.(Letters)*, **330**, L119.
[9]Magazzu, A., Martin, E.L. and Rebolo, R. 1993, *Ap.J.(Letters)*, **404**, L17.
[10]Henry, T.J. and Kirkpatrick, J.D. 1990, *Ap.J.(Letters)*, **354**, L29.
[11]Forrest, W.J., Ninkov, Z., Garnett, J.D., Skrutskie, M.F., and Shure, M. 1990, in *Strongly Coupled Plasma Physics*, edited by S. Ichimaru (Elsevier Science Publishers B.V./Yamada Science Foundation) p. 33.
[12]Stringfellow, G.S. 1991, *Ap.J.(Letters)*, **375**, L21.
[13]Stauffer, J.R., Hamilton, D., Probst, R., Rieke, G., and Mateo, M. 1989, *ApJ(Letters)*, **344**, L21.
[14]Simons, D.A. and Becklin, E.E. 1992, *Ap.J.*, **390**, 431.
[15]Bryja, C., Jones, T.J., Humphreys, R.M., Lawrence, G., Pennington, R.L., and Zumach, W. 1992, *Ap.J.(Letters)*, **388**, L23.
[16]Nelson, L.A., Rappaport, S.A. and Joss P.C. 1986, *Ap.J.*, **311**, 226.
[17]Irwin, M.J., Webster, R.L., Hewett, P.C., Corrigan, R.T., and Jedrzejewski, R.I. 1989, *A.J.*, **98**, 1989.
[18]Nadeau, D., Yee, H.K.C., Forrest, W.J., Garnett, J.D., Ninkov, Z., and Pipher, J.L. 1991, *Ap.J.*, **376**, 430.
[19]Corrigan, R.T *et al.* 1991, *A.J.*, **102**, 34.
[20]Paczynski, B. 1986, *Ap.J.*, **304**, 1.
[21]Alcock, C. *et al.* 1993, *Nature*, **365**, 621.
[22]Aubourg, E. *et al.* 1993, *Nature*, **365**, 623.
[23]Griest, K. 1991, *Ap.J.*, **366**, 412.
[24]Hogan, C.J. 1993, *Nature*, **365**, 602.
[25]Saumon, D., Bergeron, P., Lunine, J.I., Hubbard, W.B., and Burrows, A. 1993, *Ap.J.* in press.

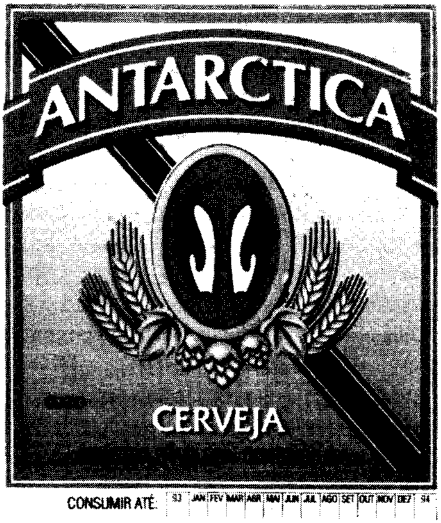

The way they see the cold universe in Brazil...
(Famous beer, courtesy J. Lépine, IAG, São Paulo)

COBE VIEWS THE COLD UNIVERSE

C. L. Bennett
Code 685, Infrared Astrophysics
NASA Goddard Space Flight Center
Greenbelt, MD 20771 USA

ABSTRACT

NASA's Cosmic Background Explorer (*COBE*[1]) has made precise measurements of the spectrum and anisotropy of the cosmic microwave background radiation on angular scales greater than 7°, and has set new conservative upper limits on the infrared sky brightness and thus on any diffuse cosmic infrared background radiation. The cosmic microwave background spectrum is that of a blackbody of temperature $T = 2.726 \pm 0.01$ K, with no deviation from a blackbody spectrum greater than 0.03% of its peak brightness. Statistically significant cosmic microwave background anisotropy has been detected with an effective quadrupole amplitude of 17 μK, and a pattern consistent with a scale invariant primordial density fluctuation spectrum. Galactic results from the *COBE* mission include an unbiased far infrared survey of the strength and distribution of atomic and molecular cooling lines from the Galactic interstellar medium, and a large scale infrared continuum emission survey that gives insight into the morphology of the Galaxy.

[1] The National Aeronautics and Space Administration Goddard Space Flight Center (NASA/GSFC) is responsible for the design, development, and operation of the *COBE* . Scientific guidance is provided by the *COBE* Science Working Group. GSFC is also responsible for the development of the analysis software and for the production of the mission data sets.

1. INTRODUCTION

Since 99% of the radiant energy in the Universe is in the cosmic microwave background (CMB) radiation at a temperature below 3 Kelvin, *COBE*'s view of "The Cold Universe" is highly appropriate for this book. Many experiments have been performed to measure the CMB spectrum and spatial anisotropies over a wide range of wavelengths and angular scales. Fewer attempts have been made to conduct a sensitive search for a cosmic infrared background (CIB) radiation, expected to result from the cumulative emissions of luminous objects formed after the universe cooled sufficiently to permit the first stars and galaxies to form. The purpose of the *COBE* mission is to make definitive measurements of these two cosmological fossils.

The three scientific instruments on *COBE* are the Far Infrared Absolute Spectrophotometer (FIRAS), the Differential Microwave Radiometers (DMR), and the Diffuse Infrared Background Experiment (DIRBE). The FIRAS instrument has met its major objective: to make a precision measurement of the spectrum of the CMB from 1 cm to 100 μm. The DMR's major objective has also been met: CMB anisotropies have been detected on angular scales larger than 7° at frequencies of 31.5, 53, and 90 GHz. The DIRBE objective is to search for a CIB by making absolute brightness measurements of diffuse infrared radiation in 10 photometric bands from 1 to 240 μm and polarimetric measurements from 1 to 3.5 μm. Preliminary upper limits have been placed on the CIB, but considerable analysis effort will be required to model and remove the strong astrophysical foreground emission for the high quality DIRBE data to produce more stringent limits or result in a detection of the CIB. Many papers giving overviews, implications, and additional detailed information about the *COBE* have been presented[1-13].

2. THE SPECTRUM OF THE PRIMEVAL RADIATION

The discovery of the CMB radiation[14] provided strong evidence for the Big Bang cosmology. Radiation produced in the very early universe was frequently scattered until about 300,000 years after the Big Bang. At this point the characteristic energy in the universe fell to the point where previously free electrons could combine with nuclei to form neutral atoms, the "recombination". The 2.7 K radiation we see today has been traveling to us unimpeded since that time. The rapid production and destruction of photons within the first year after the Big Bang forced the radiation to have a Planck (blackbody) spectrum. Any mechanism that injected energy into the Universe (e.g. a particle decay) between a year after the Big Bang and $\sim$ 2000 years after the Big Bang would give rise to a radiation spectrum characterized by a non-zero chemical potential. Thus there would be a Bose-Einstein spectral distortion with the photon occupation number $N(\epsilon) \sim 1/[e^{(\epsilon+\mu)/kT} - 1]$ where μ is the chemical potential and ϵ is the photon energy. A Compton distortion is usually parameterized in terms of a Compton y-parameter, $y = (\sigma_T/m_e c^2) \int n_e k(T_e - T_{CMB}) c dt$, where σ_T is the Thomson scattering cross-section and the integral is the electron pressure along the line of sight. A Compton distortion of the spectrum can become important when $(1+z)dy/dz > 1$, where this y is computed with T_{CMB} set to zero, which occurs $\sim$ 2000 years after the Big Bang. The thermodynamic temperature distortion observed at frequency ν is $\delta T/T \approx y\,[x(e^x+1)/(e^x-1) - 4]$ where

$x = h\nu/kT_{CMB}$, h is Planck's constant, and k is Boltzmann's constant. After recombination it becomes nearly impossible to distort the CMB spectrum short of reionizing the universe or through an intense early burst of star formation that produces both starlight and interstellar dust. Thus a perfect Planck CMB spectrum would support the prediction of the simplest Big Bang model of the universe, while spectral distortions would indicate the existence of more complicated releases of energy.

Initial results of analysis of the FIRAS data to date[15–18] confirm the prediction of the simplest Big Bang model that the CMB must have a thermal spectrum. In 1993, a new calibration model[19] for the FIRAS enabled Mather et al.[20] to use six weeks of interleaved sky and calibration data to determine the extragalactic background spectrum. They modeled the Galactic spectrum and fitted it by geometrical and spectral methods to remove it and find the mean CMB spectrum. The mean temperature is 2.726 ± 0.010 K, over the frequency range from 2 to 20 cm^{-1}. Over this range the maximum deviation from the blackbody form is less than 0.03%, with a weighted rms value of 0.01%. Fits to the dimensionless cosmic distortion parameters give 95% confidence limits of $|\mu/kT| < 3.3 \times 10^{-4}$ and $|y| < 2.5 \times 10^{-5}$ respectively.

The implications of these limits are summarized by Wright et al.[21]. Less than 0.03% of the energy in the CMB could have been added to it after the first year of the expansion. Less than 10^{-4} of the diffuse X-ray background can be produced by a smooth hot interGalactic medium. Less than 1% of the mass of hydrogen could be burned by Population III stars after a redshift of 80, and less than 1% of the hydrogen could be burned by an evolving population of galaxies like those seen by the *IRAS*. These limits are based on $\Omega_{baryon} = 0.0125h^2$. The Steady State theory is conclusively ruled out, as are theories of a Cold Big Bang with needle-shaped dust to thermalize stellar radiation.

The dipole anisotropy of the CMB, presumed due to our peculiar motion relative to the Hubble flow, is seen clearly in the FIRAS data, and is consistent with previous results[22]. These data show that the spectrum of the dipole is that expected from the Doppler shift acting on a blackbody spectrum[23]. The dipole amplitude is 3.343 ± 0.016 mK in the direction $(\alpha, \delta) = (168.9° \pm 0.5°, -7.5° \pm 0.5°)$, epoch $J2000.0$, or (l,b)=$(265.6°, 48.3°)$. The color temperature of the dipole is 2.714 ± 0.014 K, and the maximum deviation of the dipole spectrum from the expected form is 0.005% of the peak intensity of the CMB.

3. SPATIAL ANISOTROPY OF THE PRIMEVAL RADIATION

Primordial gravitational potential fluctuations at the surface of last scattering give rise to the distribution and motions of galaxies and to large angular scale fluctuations in the CMB[24]. In inflationary models of cosmology[25–27] the gravitational energy fluctuations arise from quantum mechanical fluctuations from 10^{-35} seconds after the Big Bang that inflate to become classical fluctuations with a nearly scale invariant power spectrum[28–29]. The large angular scale CMB temperature anisotropy ΔT and gravitational potential fluctuations at the surface of last scattering $\Delta\Phi$ are simply related by $3\Delta T/T = \Delta\Phi/c^2$ for adiabatic fluctuations in a universe with no cosmological constant (Λ=0).

Measurements of the abundances of the light elements together with nucleosynthesis calculations[30–31] imply that $0.01 \leq \Omega_B h^2 \leq 0.015$, where Ω_B is the fraction of the critical mass density ($\rho_c = 3H_\circ^2/8\pi G = 1.88h^2 \times 10^{-29}$ gm cm^{-3}) in baryons and $h = H_\circ/100$ km s^{-1} Mpc^{-1}, where $H_\circ$ is the Hubble constant and G is the gravitation constant. Inflation requires that $\Omega_\circ + \Lambda_\circ/3H_\circ^2 = 1$ so that either $\Lambda_\circ \neq 0$, or inflation theory is incorrect, or most of the mass in the universe is yet to be detected nonbaryonic material. It is useful to assume that this nonbaryonic material does not interact with light. This simultaneously explains why it is not seen, and allows it to begin clustering while the universe was radiation-dominated, earlier than is possible for the baryonic matter. The nonbaryonic material is broadly categorized as "hot" or "cold" dark matter, depending on whether it was or was not relativistic when the universe became matter-dominated. A neutrino with mass is a favorite hot dark matter candidate. A successful model of cosmology and the evolution of structure must match the amplitude and spectrum of density fluctuations from the galaxy scale to the horizon scale. Several observables have been derived from galaxy surveys, including the two-point correlation function, the amplitude of its integral, the rms mass fluctuation in a fixed radius sphere, and rms galaxy streaming velocities. Measurements of large scale (i.e. primordial) CMB anisotropies can provide the observational link between the production of gravitational potential fluctuations in the early universe and the observed galaxy distributions and velocities today. There are several excellent reviews of CMB anisotropy and cosmological perturbation theory[32–37].

DMR results have been reported based on six months of data[38] and based upon the first year of DMR data[39]. Bennett et al.[40] describe the calibration procedures, Kogut et al.[41] discuss the treatment of systematic errors, and Bennett et al.[42] discuss the separation of cosmic and Galactic signals. Wright et al.[43] compare these data to other measurements and to models of structure formation through gravitational instability. The first year DMR maps are dominated by the dipole anisotropy and emission from the Galactic plane. The dipole anisotropy is seen consistently in all channels with a thermodynamic temperature amplitude 3.365 ± 0.027 mK in the direction $l = 264.4° \pm 0.3°$, $b = 48.4° \pm 0.5°$, consistent with the FIRAS results, above[44]. Our motion with respect to the CMB (a blackbody radiation field) is assumed to produce the dipole anisotropy, so the dipole and associated ≈ 1.2 μK rms kinematic quadrupole are removed from the maps.

The DMR instrument noise and the intrinsic fluctuations on the sky are independent and thus add in quadrature to give the total observed signal variance $\sigma_{obs}^2 = \sigma_{DMR}^2 + \sigma_{Sky}^2$. The σ_{obs} is estimated from the two channel (A+B)/2 sum maps, and the (A-B)/2 difference maps provide an estimate of σ_{DMR}, yielding the sky variance $\sigma_{Sky}(10°) = 30\pm5$ μK for $|b| > 20°$. The observations are made with a 7° beam, and the resulting maps are smoothed with an additional 7° Gaussian function, resulting in the effective 10° angular resolution.

The correlation function, C(α), is the average product of temperatures separated by angle α. It is calculated for each map by rejecting all pixels within the Galactic latitude band $|b| < 20°$, removing the mean, dipole, and quadrupole from the remaining pixels by a least squares fit, multiplying all possible pixel pair temperatures, and averaging the results into 2.6° bins. The Galactic contribution to the correlation signal is small for $|b| > 15°$ [42]. This is consistent with the fact that the correlation function and rms sky fluctuation are insensitive to the Galactic latitude cut angles so long as $|b| < 15°$ is excluded. The DMR correlation functions exhibit temperature anisotropy on all scales greater than the beam size (7°) and differ significantly ($> 7\sigma$) from the flat correlation function due to receiver noise alone.

The detected signals expressed in thermodynamic temperature are nearly constant amplitude: the rms fluctuations on a 10° scale are proportional to $\nu^{-0.3\pm1}$ and the quadrupole and correlation functions $\propto \nu^{-0.2\pm1}$. The flat spectral index of the DMR anisotropy, without correction for Galactic emissions, is consistent with a cosmic origin and inconsistent with an origin from a single Galactic component. However, from this fact alone we are unable to rule out a correlated superposition of dust, synchrotron, and free-free emission and thus more detailed Galactic emission models are required. Bennett et al.[42)] constructed models of microwave emission from our Galaxy. CMB anisotropies are assumed to produce differences in the measured antenna temperature according to $\Delta T_A = \Delta T\ x^2 e^x/(e^x - 1)^2$, where $x = h\nu/kT$ and T is thermodynamic temperature. Synchrotron emission, free-free emission, and thermal emission from dust are important at microwave wavelengths. DMR maps, with the modeled Galactic emission removed, are fit for a quadrupole distribution. A cosmic quadrupole, corrected for the expected kinematic quadrupole, is $Q_{rms} = 13 \pm 4\ \mu$K, $(\Delta T/T)_Q = (4.8 \pm 1.5) \times 10^{-6}$, for $|b| > 10°$. When Galactic emission is removed from the DMR data, the residual fluctuations are virtually unaffected and therefore they are not dominated by any known Galactic emission component(s).

The anisotropy detected by the DMR is interpreted as being a direct result of primordial fluctuations in the gravitational potential. Assuming a power spectral density of density fluctuations of the form $P(k) = Ak^n$, the best-fit result is $n = 1.1 \pm 0.5$ with $Q_{rms-PS} = 16 \pm 4$ μK. Q_{rms-PS} is the rms quadrupole amplitude resulting from this power spectrum fit, i.e. making use of fluctuation information from all observed angular scales, as opposed to the Q_{rms} derived from a direct quadrupole fit. Forcing the spectral index to $n = 1$ gives $Q_{rms-PS} = 16.7 \pm 4\ \mu$K . Interpreted as a power-law spectrum of primordial fluctuations with a Gaussian distribution, the amplitude squared of the l^{th} order spherical harmonic component, ΔT_l^2, in each horizon has a χ^2 distribution with $2l + 1$ degrees of freedom, giving a cosmic variance for observations within a single horizon volume of $2 < \Delta T_l^2 >^2 /(2l + 1)$. Best fit values are $n = 1.15^{+0.45}_{-0.65}$ and $Q_{rms-PS} = 16.3 \pm 4.6\ \mu$K including the cosmic variance. Cross-correlation of the 53 GHz and 90 GHz maps are consistent with a power law spectrum with index $n = 1 \pm 0.6$ and amplitude $Q_{rms-PS} = 17 \pm 5\mu$K, including cosmic variance.

The observed cosmic quadrupole from the maps, $Q_{rms} = 13 \pm 4\mu$K, is slightly below the mean value predicted by the higher-order moments deduced from the correlation function, $Q_{rms-PS} = 16 \pm 4\mu$K. This is a likely consequence of cosmic variance: the mode of the χ^2 distribution is lower than the mean. A map quadrupole value of 13 μK or lower would be expected to occur 35% of the time for an $n = 1$ universe with $Q_{rms-PS} = 16\ \mu$K. The results above exclude the quadrupole before computing C(α). Including the quadrupole when $C(\alpha)$ is computed increases the χ^2, raises n to 1.5, and decreases Q_{rms-PS} to 14 μK. The measured parameters [$\sigma_{Sky}(10°)$, Q_{rms}, Q_{rms-PS}, $C(\alpha)$, and n] are consistent with a Peebles-Harrison-Zel'dovich (scale invariant) spectrum of perturbations. The minimum Q_{rms} for models with an initial Peebles-Harrison-Zel'dovich perturbations, normalized to the local large-scale galaxy streaming velocities, is predicted to be 12 μK, independent of the Hubble constant and the nature of dark matter[45-46].

The most natural interpretation of the DMR signal is the observation of very large (presently $\gg$ 100 Mpc) structures in the Universe which are little changed from their primordial state ($t \ll 1$ sec). These structures are part of a power law spectrum of small amplitude gravitational potential fluctuations that on smaller length scales are sources of the large scale structure observed in the Universe today. The DMR data provide strong support for gravitational instability theories[43]. Wright et al.[55] compare the 94 cosmological models from Holtzman[47] with the DMR anisotropy results. Three Holtzman models fit the observational data (galaxy clustering, galaxy streaming velocity, and CMB quadrupole amplitude) reasonably well: (1) A model with fractional vacuum energy density $\Omega_{vac} = \Lambda/3H_\circ^2 = 0.8$, $H_\circ = 100$ km s^{-1} Mpc^{-1}, $\Omega_B = 0.02$, $\Omega_{CDM} = 0.18$ is an excellent fit to the observational data; (2) A "mixed dark matter" (MDM) model that fits the data uses both hot dark matter (a massive neutrino with $\Omega_{HDM} = 0.3$) and cold dark matter ($\Omega_{CDM} = 0.6$) with baryonic dark matter $\Omega_B = 0.1$ and $H_\circ = 50$ km s^{-1} Mpc^{-1}; and (3) An open universe model with $\Omega_\circ = 0.2$, $\Omega_B = 0.02$, and $\Omega_{CDM} = 0.18$ for $H_\circ = 100$ km s^{-1} Mpc^{-1} satisfies the observations, except perhaps for the galaxy streaming velocities, but is in conflict with the inflation model and theoretical prejudices for $\Omega_\circ = 1$.

4. THE COSMIC INFRARED BACKGROUND RADIATION

The Diffuse Infrared Background Experiment (DIRBE) is the first space experiment designed primarily to measure the CIB radiation. The aim of the DIRBE is to conduct a definitive search for an isotropic CIB radiation, within the constraints imposed by the local astrophysical foregrounds.

Cosmological motivations for searching for an extragalactic infrared background have been discussed for several decades[48-52]. Both the cosmic redshift and reprocessing of short-wavelength radiation to longer wavelengths by dust act to shift the short-wavelength emissions of cosmic sources toward or into the infrared. Hence, the wide spectral range from 1 to 1000 μm is expected to contain much of the energy released since the formation of luminous objects, and could potentially contain a total radiant energy density comparable to that of the CMB. Measurement of the spectral intensity and anisotropy of the CIB radiation would provide important new insights into intriguing issues such as the amount of matter undergoing luminous episodes in the pregalactic Universe, the nature and evolution of such luminosity sources, the nature and distribution of cosmic dust, and the density and luminosity evolution of infrared-bright galaxies.

Preliminary results of the DIRBE experiment have been described previously [8-9),53-59]. Qualitatively, the initial DIRBE sky maps show the expected character of the infrared sky. For example, at 1.2 μm stellar emission from the Galactic plane and from isolated high latitude stars is prominent. Zodiacal scattered light from interplanetary dust is also prominent. These two components continue to dominate out to 3.4 μm, though both become fainter as wavelength increases. Because extinction at near infrared wavelengths is far less than in visible light, the disk and bulge stellar populations of the Milky Way are dramatically apparent at these wavelengths. At 12 and 25 μm, emission from the interplanetary dust dominates the sky brightness. As with the scattered zodiacal light, the sky brightness is strongly dependent upon ecliptic latitude and solar elongation angle. At wavelengths of 60 μm and longer, emission from the interstellar medium dominates the Galactic brightness, and the interplanetary dust emission becomes progressively less apparent. The patchy infrared cirrus noted in IRAS data[60] is evident at all wavelengths longer than 25 μm. False color all sky images prepared from DIRBE data have recently been presented by Hauser[54]. The DIRBE data will clearly be a valuable new resource for studies of the interplanetary medium and Galaxy (see §5, below) as well as the search for the CIB radiation.

In searching for the extragalactic infrared background, the most favorable conditions are directions and wavelengths of least foreground brightness. In general, because of the strong interplanetary dust foreground and the relatively modest gradient of that foreground over the sky, the infrared sky is faintest at high ecliptic latitude. A preliminary DIRBE spectrum of the sky brightness toward the south ecliptic pole was presented by Hauser et al.[53], and is reproduced in Table 1. This table shows the strong foreground from starlight and scattered sunlight at the shortest wavelengths, a relative minimum at 3.4 μm, emission dominated by interplanetary dust peaking around 12 μm, and generally falling brightness from there out to submillimeter wavelengths.

Table 1: Cosmic Infrared Background Limits

λ (μm)	λI_λ (10^{-7} W m^{-2} sr^{-1})	λ (μm)	λI_λ (10^{-7} W m^{-2} sr^{-1})
1.2	8.3 ± 3.3	22.	21. ± 8
2.3	3.5 ± 1.4	55.	2.3 ± 1
3.4	1.5 ± 0.6	96.	1.2 ± 0.5
4.9	3.7 ± 1.5	151.	1.3 ± 0.7
12.	29. ± 12	241.	0.7 ± 0.4

To meet the cosmological objective of measuring the CIB radiation, the foreground light from interplanetary and Galactic sources must be discriminated from the total observed infrared sky brightness. This task requires extensive careful correlation studies and modelling, which in the case of the DIRBE investigation is in progress. A conservative upper limit on extragalactic light is the total observed brightness in a relatively dark direction. The sky brightness at the south ecliptic pole is a fair representation of the best current limits from the DIRBE. The faintest foregrounds occur at 3.4 μm, in the minimum between interplanetary dust scattering of sunlight and re-emission of absorbed sunlight by the same dust, and longward of 100 μm, where interstellar dust emission begins to decrease. Through careful modelling, we hope to be able to discriminate isotropic residuals at a level as small as 1 percent of the foregrounds. These near-infrared and submillimeter windows will allow the most sensitive search for, or limits upon, the elusive cosmic infrared background.

These data are to be compared with the theoretical estimates of contributions to the CIB radiation from pregalactic and protogalactic sources in a dust free universe[6]. The present conservative observational limits are beginning to constrain some of the theoretical models at short infrared wavelengths, though in a dusty universe energy from these sources can be redistributed farther into the infrared. If the foreground components of emission can confidently be identified, the current *COBE* measurements will seriously constrain (or identify) the CIB radiation across the infrared spectrum. However, the spectral decade from about 6 to 60 μm will have relatively weak limits until measurements are made from outside the interplanetary dust cloud.

The CIB radiation promises to enhance our understanding of the epoch between decoupling and galaxy formation. The high quality and extensive new measurements of the absolute infrared sky brightness obtained with the DIRBE and FIRAS experiments on the *COBE* mission promise to allow a definitive search for this elusive background, limited primarily by the difficulty of distinguishing it from bright astrophysical foregrounds.

5. COBE GALACTIC STUDIES

COBE FIRAS results also include the first nearly all-sky, unbiased, far infrared survey of the Galactic emission at wavelengths greater than 120 μm [62]. Wright et al.[62] present a map of the dust emission across the sky from the FIRAS experiment. The total far infrared luminosity of the Galaxy is inferred to be $(1.8 \pm 0.6) \times 10^{10} L_{\odot}$. Spectral lines from interstellar [C I], [C II], [N II], and CO are detected in the mean Galactic spectrum. The lines of [C II] at 158 μm and [N II] at 205.3 μm were sufficiently strong to be mapped[62–63]. This was the first observation of the 205.3 μm line. Wright et al. interpret the [C II] line as coming largely from photodissociation regions and the [N II] lines as partially arising from a diffuse warm ionized medium and partially arising from dense H II regions. Petuchowski & Bennett[35] further elaborate on this conclusion by apportioning the [C II] and [N II] transition line intensities among various morphologies of the interstellar medium. Petuchowski & Bennett[64] have conducted observations on NASA's Kuiper Airborne Observatory to measure the scale height of the 205.3 μm [N II] line with a much higher angular resolution ($\sim$1 arcmin) than FIRAS. Bennett & Hinshaw[63] present the Galactic longitude ($|b| = 0°$) dependence of the *COBE* FIRAS line strengths. Significant portions of the emission can clearly be associated with the Galactic Center and the molecular ring. The [C II] intensity is closely correlated with the far IR continuum, $I(158\ \mu\mathrm{m}\ [\mathrm{C\ II}]) \propto I(FIR)$. The [N II] intensity is also correlated with the [C II] intensity, however with the surprising relation $I(205\ \mu\mathrm{m}\ [\mathrm{N\ II}]) \propto I(158\ \mu\mathrm{m}\ [\mathrm{C\ II}])^{\sim 1.5}$. Morphological models for the origin of these fine structure lines are presented by Petuchowski & Bennett[65].

Initial Galactic studies based on DIRBE data have been reported. A warp in the Galactic plane, similar to that seen in H I, is seen in the both the stellar and interstellar dust components of the *COBE* DIRBE data[56]. An examination of the color and extinction of integrated Galactic starlight[57] has been undertaken showing as much as $\sim 4^{\mathrm{m}}$ of extinction at 1.25 μm in the 0.7° beam, with the unreddened spectrum corresponding to that of K and M giants. The "peanut" shape of the bulge is an extinction effect. Also, a DIRBE study of asymmetries in the starlight from the bulge support the suggestion that the Galaxy has a stellar bar[58]. A study of physical conditions in the interstellar medium along the Galactic plane[59] indicates that most of the far infrared continuum emission arises from the neutral gas phase. The first results of polarization measurements with the DIRBE have also been presented[55], as have observations of comets[66].

The author gratefully acknowledge the contributions to this report by colleagues on the *COBE* Science Working Group and the other participants in the *COBE* Project. An earlier and longer version of this paper was previously presented[67]. Many people have made essential contributions to the success of *COBE* in all its stages, from conception and approval through hardware and software development, launch, flight operations, and data processing.

REFERENCES

1. Boggess, N. et al., *ApJ*, 397, 420 (1992)
2. Mather, J. C., et al., *IAU Colloq. 123, Observatories in Earth Orbit and Beyond*, ed. Y. Kondo, (Boston: Kluwer), 9 (1990)
3. Mather, J. C. et al., *Adv.Sp.Res.*, 11, 181 (1991)
4. Mather, J. C., *Highlights Astron.*, in press (1991)
5. Janssen, M. A. & Gulkis, S., *The Infrared and Submillimetre Sky After COBE*, eds. M. Signore & C. Dupraz, (Dordrecht: Kluwer), 391 (1992)
6. Wright, E. L., *Ann. NY Acad. Sci. Proc.*, 647, 190 (1990)
7. Wright, E. L., *The Infrared and Submillimetre Sky After COBE*, eds. M. Signore & C. Dupraz, (Dordrecht:Kluwer), 231 (1991)
8. Hauser, M. G., *Proc. Infrared Astronomy with ISO*, Les Houches series, eds. Th. Encrenaz & M. F. Kessler (New York: Nova Science), 479 (1992)
9. Hauser, M G., *Highlights Astron.*, in press (1991)
10. Smoot, G. F. et al., *After the First Three Minutes*, eds. S. S. Holt, C L. Bennett, & V. Trimble, (New York: AIP Conf. Proc. 222), 95 (1991c)
11. Smoot, G. F., *Highlights Astron*, in press (1991)
12. Bennett, C. L., *Highlights Astron.*, in press (1991)
13. Boggess, N. W., *Highlights Astron.*, in press (1991)
14. Penzias, A. A., & Wilson, R. W., *ApJ*, 142, 419 (1965)
15. Mather, J. C. et al., *After the First Three Minutes*, eds. S. S. Holt, C L. Bennett, & V. Trimble, (New York: AIP Conf Proc 222), 43 (1991)
16. Mather, J. C., et al., *ApJ*, 354, L37 (1990)
17. Shafer, R. A. et al., *Bull.Am.Phys.Soc.*, 36, 1398 (1991)
18. Cheng, E. S. et al., *BAAS*, 23, 896 (1991)
19. Fixsen, D. J. et al., submitted to *ApJ* (1993)
20. Mather, J. C. et al., submitted to *ApJ* (1993)
21. Wright, E. L. et al., submitted to *ApJ* (1993)
22. Cheng, E. S. et al., *Bull.Am.Phys.Soc.*, 35, 971 (1990)
23. Fixsen, D. J. et al., submitted to *ApJ* (1993)
24. Sachs, R. K. & Wolfe, A. M., *ApJ*, 147, 73 (1967)
25. Guth, A., *Phys.Rev. D*, 23, 347 (1981)
26. Linde, A., *Phys.Lett.*, 108B, 389 (1982)
27. Albrecht, A. & Steinhardt, P. J., *Phys.Rev.Lett.*, 48, 1220 (1982)
28. Hawking, S., *Phys.Lett.*, 115B, 295 (1982)
29. Starobinskii, A. A., *Phys.Lett.*, 117B, 175 (1982)
30. Walker, T. P., Steigman, G., Schramm, D. N., Olive, K. A., & Kang, H.-S., *ApJ*, 376, 51 (1991)
31. Olive, K. A., Schramm, D. N., Steigman, G., & Walker, T. P., *Phys. Lett. B*, 236, 454 (1990)
32. Bertschinger, E., in *Current Topics in Astrofundamental Physics*, eds. N. Sanchez & Z. Zichini, in press and in *New Insights Into The Universe*, eds. V. J. Martinez, M. Portilla & D. Saez, in press (1992)

33. Efstathiou, G., in *Physics of the Early Universe*, eds. J. A. Peacock, A. F. Heavens, & A. T. Davies (Edinburgh Univ. Press: Edinburgh, Scotland), p. 361 (1990)
34. Kolb, E., & Turner, M. S., *The Early Universe*, (Addison Wesley:Redwood City, CA) (1987)
35. Peebles, P. J. E., *Physical Cosmology*, (Princeton Univ. Press: Princeton, NJ) (1971)
36. Peebles, P. J. E., *The Large-Scale Structure of the Universe*, (Princeton Univ. Press: Princeton, NJ) (1980)
37. Wilkinson, D. T., *Science*, 232, 1517 (1986)
38. Smoot, G. F. et al., *ApJ*, 371, L1 (1991)
39. Smoot, G. F. et al., *ApJ*, 396, L1 (1992)
40. Bennett, C. L. et al., *ApJ*, 391, 466 (1992)
41. Kogut, A., et al., *ApJ*, in press (1992)
42. Bennett, C. L. et al., *ApJ*, 396, L7 (1992)
43. Wright, E. L. et al., *ApJ*, 396, L13 (1992)
44. Kogut et al. submitted to *ApJ* (1993)
45. Gorski, K., *ApJ*, 370, L5 (1991)
46. Schaefer, R. K., *After the First Three Minutes*, eds. S. S. Holt, C L. Bennett, & V. Trimble, (New York: AIP Conf. Proc. 222), 119 (1991)
47. Holtzman, J. A., *ApJS*, 71, 1 (1989)
48. Partridge, R. B. & Peebles, P. J. E., *ApJ*, 148, 377 (1967)
49. Low, F. J. & Tucker, W. H., *Phys.Rev.Lett.*, 22, 1538 (1968)
50. Peebles, P. J. E., *Phil.Trans.Royal Soc.London, A*, 264, 279 (1969)
51. Harwit, M.,*Rivista del Nuovo Cimento II*, 253 (1970)
52. Kaufman, M., *Ap.Sp.Sci.*, 40, 369 (1976)
53. Hauser, M. G. et al.,*After the First Three Minutes* eds. S. S. Holt, C. L. Bennett, & V. Trimble, (New York:AIP Conf. Proc. 222), 161 (1991)
54. Hauser, M. G., *Back to the Galaxy*, eds. S. S. Holt & F. Verter, (New York: AIP Conf. Proc), to be published (1993).
55. Berriman, G. B., et al. *Back to the Galaxy*, eds. S. S. Holt & F. Verter, (New York: AIP Conf. Proc), to be published (1993).
56. Freudenreich, H. T., et al., *Back to the Galaxy*, eds. S. S. Holt & F. Verter, (New York: AIP Conf. Proc), to be published (1993).
57. Arendt, R. G., et al., *Back to the Galaxy*, eds. S. S. Holt & F. Verter, (New York: AIP Conf. Proc), to be published (1993).
58. Weiland, J. L., et al., *Back to the Galaxy*, eds. S. S. Holt & F. Verter, (New York: AIP Conf. Proc), to be published (1993).
59. Sodroski, T. J., et al., *Back to the Galaxy*, eds. S. S. Holt & F. Verter, (New York: AIP Conf. Proc), to be published (1993).
60. Low, F. J. et al., *ApJ*, 278, L19 (1984)
61. Bond, J. R., Carr, B. J., & Hogan, C. J., *ApJ*, 306, 428 (1986)
62. Wright, E. L. et al., *ApJ*, 381, 200 (1991)
63. Bennett, C. L. & Hinshaw, G., *Back to the Galaxy*, eds. S. S. Holt & F. Verter, (New York: AIP Conf. Proc), to be published (1993).
64. Petuchowski, S. J. & Bennett, C. L., in preparation (1992)
65. Petuchowski, S. J. & Bennett, C. L., *ApJ*, 405, 591 (1993)
66. Lisse, C. et al., submitted to *ApJ* (1993)
67. Bennett, C. L., et al., *Grand Tetons Conference, July 1992*, ed. M. Shull & H. Thronson, to be published (1993).

INTERSTELLAR DUST AND GAS

INTERSTELLAR DUST – PHYSICAL PROCESSES

A.P.Jones[1,2] and A.G.G.M.Tielens[1]
1 NASA Ames Research Center, MS 245-3, Moffett Field, CA 94035
2 Department of Astronomy, University of California, Berkeley, CA 94720

ABSTRACT

Dust is formed in stellar environments, and destroyed by sputtering, shattering and vaporization in shock waves due to cloud-cloud collisions and supernova blast waves. Dust is also destroyed during star formation. We review the dust formation and destruction balance. The calculated destruction time-scale is ≤ 1 billion years and the star dust injection time-scale is ~ 2.5 billion years. Hence, the fractions of elemental carbon and silicon locked up in stardust are < 0.3 and < 0.15, respectively. An efficient ISM dust formation route is therefore implied. In particular, in dense clouds dust grows through the processes of coagulation and the accretion of gas phase molecules e.g. H_2O, CO, CH_4. These icy materials may then be photoprocessed to refractory materials in more diffuse regions. The resulting carbonaceous grain mantle may actually be the "glue" that holds the coagulated grains together.

1 Introduction

The observed depletions of the heavy elements in the interstellar medium (ISM) and the infrared absorption and emission features indicate that stardust consists primarily of silicates and carbons. Dust is formed in circumstellar shells through the processes of nucleation, condensation and coagulation, and is injected into the ISM through stellar winds and (super)nova explosions. Once in the ISM, dust is subject to destructive processing through shattering, sputtering and vaporisation in supernova (SN) blast waves in the intercloud medium. Constructive grain processing can take place in dense regions through the accretion of gas phase volatiles (ice mantles) and inter-grain coagulation. Ultraviolet (UV) photolysis by starlight of accreted ice mantles can lead to the formation of more refractory materials. Thus, dust is a dynamically evolving component of the ISM.

Modelling of the interstellar extinction curve and of the discrete emission features ($3\,\mu$m to $13\,\mu$m) indicate grain sizes ranging from a few tens of atoms (i.e. the Polycyclic Aromatic Hydrocarbon molecules, PAHs) to $\sim 10^{10}$ atoms (large grains, radius $\sim$ 2500Å). The implied dust size distribution (radius 5Å to 2500Å) is a power law[1] which appears to hold for the entire size range of interstellar dust down to the smallest PAH species. A power law size distribution is characteristic of many terrestrial aerosols and powders, and in the ISM may well be a product of the balance between the formation and destruction processes operating in circumstellar shells and in the ISM[2].

2 Stardust Injection

	Contribution (10^{-6} $M_\odot$ kpc^{-2} yr^{-1})		
Source	carbon	silicate	silicon carbide
C-giants	2	—	0.07
M-giants	—	3	—
novae	0.3	0.03	0.007
planetary nebulae	0.04	—	—
supergiants	—	0.2	—
WC stars	0.06	—	—
supernovae II	2	12	—
supernovae Ia	0.3	2	—

Table 1: Stardust Injection in the Galaxy

Table 1 summarizes the dominant sources for stardust formation averaged over the Galaxy[3),4)]. Late type giants dominate the mass injection (i.e. H and He) into the ISM.The heavy element (i.e. O, Si, Fe,...) budget of the ISM is however dominated by SN by a large margin. Carbon may be an exception to this, since helium burning is an efficient producer of carbon in low mass stars. In C-rich giants, the carbon is brought to the surface and reaches the ISM through gentle winds. Helium burning and mixing in massive stars also leads to the formation of C-rich stars, the WC Wolf-Rayet Stars. These objects also undergo mass loss and they are known observationally to inject as much carbon as C-rich giants. The SN injection rate of carbon is a theoretical estimate and is somewhat uncertain since it depends sensitively on the $^{12}C(\alpha,\gamma)^{16}O$ reaction rate. Our analysis is based upon the recent rather high rates for this reaction.

The dust injection rate depends sensitively on the nucleation and condensation efficiency in the outflows which are in general poorly known observationally or theoretically. Carbon stardust is known to be formed in the C-rich ejecta (i.e. $C/O > 1$) of C-giants. Type II SN may be an important source of carbon stardust as well, if mixing of the ejecta is precluded and if condensation is efficient. The dust condensation efficiency in WC stars is small ($\lesssim 2\%$) and hence they are unimportant in the dust balance (Table 1). For $C/O < 1$, silicate or metal grains are expected to condense, and M-giants and supergiants which show $10\,\mu$m and $20\,\mu$m emission or absorption features (SiO stretching and bending vibrations in amorphous silicates) are important contributors to the silicate stardust budget. Supernovae of types II and Ia are the dominant source of newly nucleo-synthesised silicon and could, in fact, be the dominant silicate dust producers (Table 1). Observations[5)] of SN1987a show conclusive evidence for newly condensed dust ($M_{dust} \geq 10^{-4}\,M_\odot$), although the absence of spectral features precludes a direct determination of the dust composition. From the SN composition, formation of Fe/Ni alloys, various oxides including silicates, as well as carbonaceous grains could be expected.

The minimum dust formation rate is $5 \times 10^{-6}\,M_\odot$ kpc^{-2} yr^{-1} averaged over the Galaxy and, assuming efficient dust formation in SN, the maximum dust formation rate is $2.1 \times 10^{-5}\,M_\odot$ kpc^{-2} yr^{-1}. Given the gas injection rate of $10^{-3}\,M_\odot$ kpc^{-2} yr^{-1}, then 0.5 – 2% of the total gas mass of $5 \times 10^9\,M_\odot$ is in dust. Thus, gas and dust cycle between stars and the ISM on a time-scale of 5×10^9 yr. With a 1% dust to gas mass ratio in the ISM, the interstellar dust is then replenished on a time-scale of 2.5×10^9 yr, if SN are efficient dust factories. Astration limits the lifetime of stardust to 2.5×10^9 yr. Finally, we emphasise that these numbers vary over the Galaxy due to, for example, the metallicity gradient. Also, the stellar population varies across the Galaxy; WC stars are more numerous in the inner Galaxy while C-stars are more populous in the outer parts.

3 Dust Destruction

In the three phase model of the ISM moderated by SN blast waves[6)] the destruction of IS dust occurs predominantly in the warm medium with $n_H \sim 0.25\,\mathrm{cm^{-3}}$ and $T_k \sim 10^4$ K. In the hot ionised medium, which has the largest filling factor, the density is too low to yield significant grain destruction, and the small filling factor (a few percent) for the cold neutral medium ensures little destruction in this medium also[6)]. Thus, in order to determine the lifetimes of

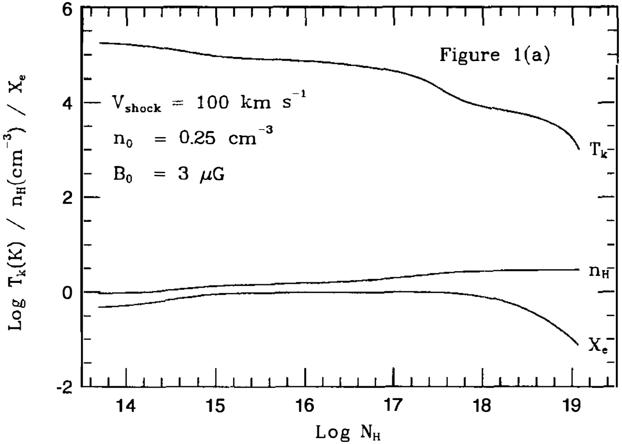

Figure 1(a)
V_{shock} = 100 km s^{-1}
n_0 = 0.25 cm^{-3}
B_0 = 3 μG
T_k
n_H
X_e
Log T_k(K) / n_H(cm^{-3}) / X_e
Log N_H

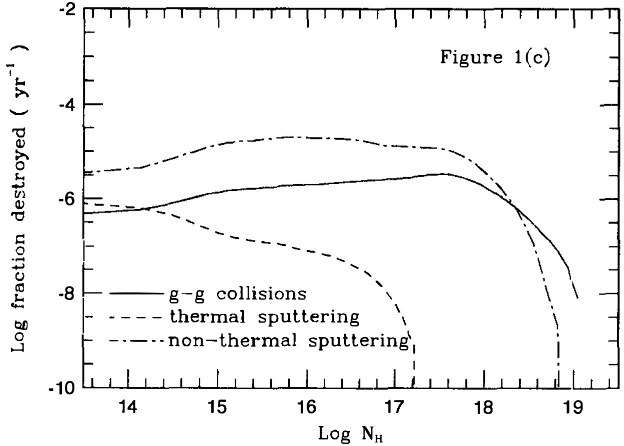

Figure 1(c)
g-g collisions
thermal sputtering
non-thermal sputtering
Log fraction destroyed (yr^{-1})
Log N_H

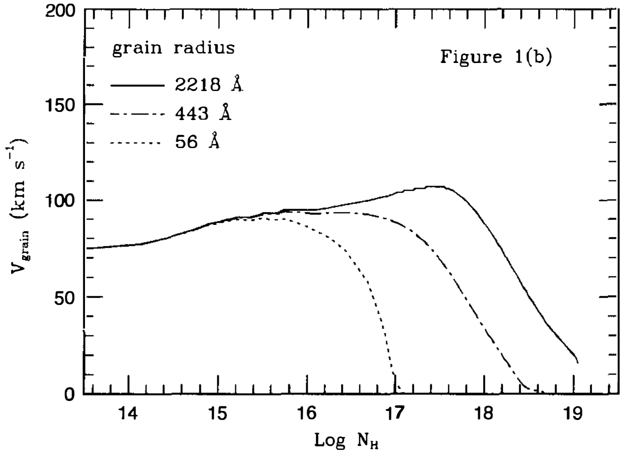

Figure 1(b)
grain radius
2218 Å
443 Å
56 Å
V_{grain} (km s^{-1})
Log N_H

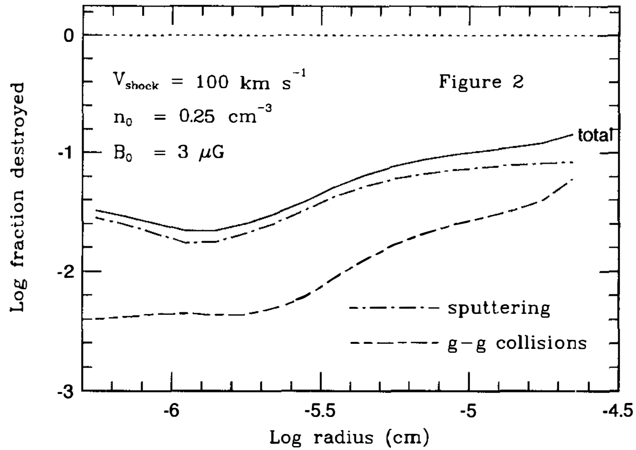

Figure 2
V_{shock} = 100 km s^{-1}
n_0 = 0.25 cm^{-3}
B_0 = 3 μG
total
sputtering
g-g collisions
Log fraction destroyed
Log radius (cm)

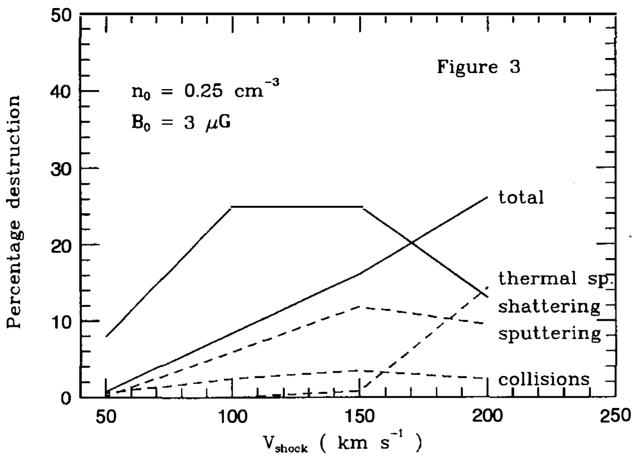

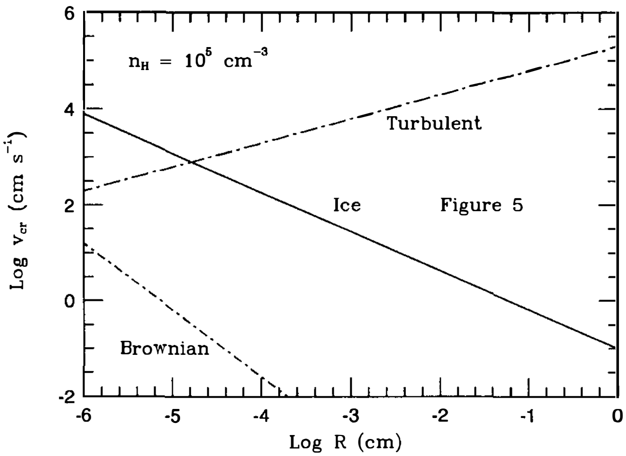

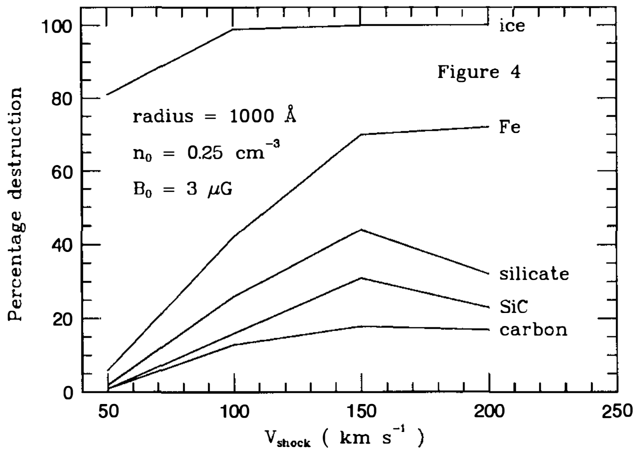

Figure 1

$N_H = n_0 \times V_{shock} \times \text{time}$

$\text{Log(time(yr))} = \text{Log } N_H(cm^{-2}) - 13.9$

Figures 1(b), 1(c), 2 and 3 – graphite grain calculations.

dust in the ISM we have modelled the destructive processes operating on interstellar grains subject to SN blast waves in the warm medium.

Our dust destruction calculations[7], based on an earlier theory[8], use new algorithms for the destructive processes of vaporisation, sputtering (thermal and non-thermal) and shattering[9], and for the first time fully treats the partial vaporisation of grains upon collision. The calculation assumes an initial power law mass distribution, $dn(a) = A_i\, n_H\, a^{-3.5}\, da$[1], and grain radii from 50Å to 2500Å. The numerical code integrates the simultaneous differential equations for silicate and carbon grain velocity and mass through a fixed shock profile[10], i.e. we do not concurrently solve the shock dynamics and grain physics. In Figure 1 we present the shock structure (temperature, T_k, density, n_H, and electron relative abundance, X_e) for a $100\,\mathrm{km\,s^{-1}}$ velocity shock, V_{shock}, the calculated graphite dust velocities (relative to the gas), V_{grain}, as a function of grain radius, and the fractional dust destruction for grain-grain (g–g) collisional vaporisation, non-thermal and thermal sputtering. The level of grain destruction in a shock is primarily determined by the grain velocity. In a shock wave, the gas is rapidly collisionally swept up and compressed by the shock, the density is enhanced by a factor of four and from conservation of momentum the gas velocity behind the shock is determined to be $0.25\times V_{shock}$. The grains, having greater inertia, are not immediately stopped behind the shock front and therefore have an initial post-shock velocity of $0.75\times V_{shock}$ relative to the gas. In the post-shock compression of the gas and the magnetic field, the charged grains are betatron accelerated until eventually brought to rest by the opposing plasma and collisional drag. These post-shock grain accelerations are evident in Figure 1(b). Silicate grains, of higher specific mass than carbon, are accelerated to higher post-shock velocities and therefore undergo enhanced destruction.

For $V_{shock} \leq 150\,\mathrm{km\,s^{-1}}$ the dominant grain destruction process is non-thermal sputtering i.e. the sputtering resulting from the impact of gas atoms and ions with the grains at the relative gas-grain velocity. For higher shock velocities thermal sputtering dominates. We find that grain-grain collisional vaporisation is only a significant destruction process, relative to sputtering, for the lowest shock velocities where sputtering is in any case unimportant. These trends are clearly shown in Figures 1(c) and 3. In high velocity shocks ($V_{shock} > 200\,\mathrm{km\,s^{-1}}$), thermal sputtering in the hot post-shock gas dominates grain destruction.

We have calculated the graphite and silicate grain destruction for steady-state shocks with velocities of 50, 100, 150 and $200\,\mathrm{km\,s^{-1}}$ for pre-shock density and pre-shock temperature of $n_0 = 0.25\,\mathrm{cm^{-3}}$ and $T_k = 10^4$ K, respectively, and pre-shock magnetic field of $B_0 = 3\,\mu$G perpendicular to the shock front. The results for graphite grains are presented in Figures 2 and 3 where the graphite grain destruction is given as a function of grain size ($V_{shock} = 100\,\mathrm{km\,s^{-1}}$) and shock velocity. The calculations for silicate grains indicate overall destruction rates that are about a factor of two higher than for graphite particles. For $V_{shock} \leq 150\,\mathrm{km\,s^{-1}}$ the dominant grain mass loss occurs for the largest particles through non-thermal sputtering (Figure 2). At higher shock velocities, grain mass is primarily lost through thermal sputtering of the smallest grains. The latter is a reflection of the fact that the small grains provide the bulk of the total grain surface area exposed to thermal sputtering. In Figure 3 we also show the fraction of the grain mass likely to be affected by shattering, calculated by assuming a shattering threshold of 100 k bar (*cf.* 5 M bar threshold for vaporisation). Clearly, dust shattering is likely to be the primary mass re-distribution process, and we are presently investigating this process in more detail.

In Figure 4 we show the results of test particle calculations for 1000Å radius carbon, silicate, silicon carbide, iron and ice grains. These data indicate that silicon carbide grains could co-exist with silicates and carbons, all being equally resilient to shocks. Whereas, icy materials, not surprisingly, and iron grains will be rapidly destroyed in the ISM. In the case of the iron particles the enhanced destruction is due to the high post-shock velocities achieved by these dense grains. Iron grains are therefore not expected to be a significant component of ISM dust.

4 Stardust Budget

Our results (§3) indicate that a significant fraction (≤ 0.5) of interstellar dust is destroyed in SN shocks in the warm medium. It is not possible to preserve grains in cold clouds which contain $\sim$ 90% of the mass because of the rapid cycling times between the phases. The time-scale to photo-ionise molecular clouds by massive star formation is on the order of 3×10^7 yr, and therefore in steady state the warm medium ($\sim$ 10% of the mass) must cycle through the cold medium on time-scales of the order of 3×10^6 yr.

In the three-phase model of the ISM[6)] the time-scale for SN shocks to destroy interstellar dust can be estimated[11)] and is $t_{SN} \sim 10^9$ yr for graphite and $\sim 5 \times 10^8$ yr for silicate. Adopting the maximum stardust injection rate estimated in §2, this indicates at most 30% of the available carbon in the form of stardust and < 15% of the heavy elements in silicate dust. Since the condensation efficiency may well be much less than one, these are really upper limits. For silicates, this is in direct conflict with the observed strength of the 10 μm silicate feature in the ISM and the observed silicon depletions which imply that $\sim$ 90% of the silicon is in the form of silicates.

Shattering of large dust grains is also an important process in the ISM. The lifetime of a large grain ($\geq$1000Å) against shattering is $\sim 2 \times 10^8$ yr and $\sim 10^8$ yr for graphite and silicate grains, respectively. Hence, the fraction of stardust mass in the form of large grains is expected to be ≤ 0.1 . Extinction studies show, however, that half of the dust mass is in grains larger than 1000Å. In order to explain the observed interstellar depletions, total dust mass, and grain size distribution, dust must grow *in situ* in the ISM. Hence, coagulation and grain mantle formation must be globally important dust processes.

5 Dust Growth In The ISM

Stardust can grow in the ISM through the accretion of ice mantles and also through inter-grain coagulation. These processes require high densities ($n_H \geq 10^5\ cm^{-3}$), and can therefore only occur in dense cold clouds. In Table 2 we show a typical dense cloud accreted ice mantle composition derived from infrared spectroscopy. The dominant component is H_2O ice with minor traces of other molecules such as CO, CH_3OH, NH_3 and CH_4. This is in reasonable agreement with theoretical studies of grain surface chemistry.

Species	Absorption features λ (μm)	Relative abundance (H_2O = 100)
H_2O	3.08/6.00	100
CO	4.67/4.68	0–25
CH_3OH	3.50/6.85	7–50
NH_3	2.95/6.10	<5
CH_4	7.70	2
H_2CO	3.53/5.80	< 0.2

Table 2: Composition of Interstellar Ice Grain Mantles

This material is relatively volatile and thus cannot be the source of grain growth in the general ISM where ice mantles are rapidly destroyed (see §3). However, in dense clouds the UV photolysis of this material by starlight can yield a refractory organic residue[12)] or ultimately a carbonaceous material[13)]. The idea of organic refractory carbonisation is derived from the extrapolation of laboratory data to interstellar conditions and suggests (optimistically) a solid carbon formation rate of $\sim 2 \times 10^{-5}\ M_\odot\ kpc^{-2}\ yr^{-1}$ [13)], i. e. about a factor of four larger than the carbon stardust injection rate (Table 1). However, it is not clear that an extrapolation of the laboratory UV processing fluxes, by more than two orders of magnitude, is valid. An alternative scheme has been proposed[14)] in which a hydrogen-rich amorphous or polymeric carbon accretes directly onto pre-existing silicate, and presumably carbon, grain cores. In a similar manner this material is UV photolysed and thermally processed to a more refractory amorphous carbon through dehydrogenation. This scheme does have its merits in that a solid carbon is formed directly in the ISM. However, the chemical processes involved in the direct deposition of a pure hydrocarbon solid from a gas also containing abundant oxygen and nitrogen atoms is unclear.

Whilst there are hypothesised routes to carbon grain formation and growth in the ISM, the analogous situation for silicate dust formation and growth is problematical. Firstly, the observed depletions indicate that almost all the silicate forming heavy elements in the ISM are in dust and, secondly, a plausible route to pure silicate dust formation in the ISM has to exist. There is now some experimental evidence for a silicate condensation route via SiH_n chemistry[15)].

Clearly, if silicate dust is indeed rapidly destroyed in SN shock waves, the SiH_n chemistry has to be an efficient route to its reformation in the ISM. Given the large dust destruction rates calculated, and the high observed silicate and carbonaceous dust abundances, the reformation of dust in the ISM requires that both carbonaceous and silicate materials condense independently of one another from the same cold interstellar gas. Under the generally accepted premise that accretion from the cold gas is indiscriminate it is therefore difficult to explain the (at least) bimodal interstellar grain composition. An attractive alternative explanation for the high silicate dust abundances observed in the ISM may be that silicate grains are protected against sputtering by carbonaceous grain mantles that can re-form on rapid time-scales ($\ll 5 \times 10^8$ yr).

In dense clouds grains may grow by coagulation, the efficient sticking of particles upon collision. Figure 5 shows the critical sticking velocity, v_{cr}, for ice grains as a function of radius[16]. For $v < v_{cr}$ colliding grains stick, for $v > v_{cr}$ they bounce. The curves labelled Brownian and Turbulent in Figure 5 refer to the random thermal motion and turbulent motion in interstellar clouds, respectively. Calculations indicate grain velocities in clouds are determined by their coupling to the gas turbulence and in general are much larger than the critical velocity. In dense cores ($> 10^4$ cm^{-3}), the gas turbulence has died down and coagulation can start. However, even under these conditions grain masses increase by only a factor of two over reasonable time-scales. Whereas, to reform large grains (a = 2500Å) from small, a = 500Åor 100Å, grain sub-units would require a mass increase of the order of 10^2 or 10^4, respectively.

Silicate grains and graphite grains do not stick as well as icy grains and little collisional growth of bare silicate and graphite grains is expected in molecular clouds[16]. However, accreted ice mantles will promote coagulation and this synergism between accretion and coagulation may play an important role in the reformation of large grains. The icy/silicate/graphitic conglomerates will be further processed in the ISM by UV photons and shocks. The UV production of organic grain mantles may actually be very important, not only in making the mantles more resistant to sputtering in shocks, but also to chemically bond the agglomerated grains across their contact surfaces. In that way, organic grain mantles could act as a "glue" which offers some protection against shattering in shocks.

6 Conclusions

On the basis of our calculations dust is relatively easily destroyed in the warm medium of the ISM in SN blast waves. Also, as shown in §2 stardust formation is < 100% efficient. Thus, dust must be formed and grow *in situ* in the ISM. The likely environment for dust growth is within dense clouds ($n_H \geq 10^5$ cm^{-3}) where dust can grow by the complimentary processes of accretion of gas phase volatiles to form ice mantles, and inter-grain coagulation. Ice mantles will subsequently be converted to a more refractory phase by UV photolysis, organic refractory, and may ultimately form a carbonaceous or graphitic material. While ice mantles are rapidly destroyed in the diffuse medium, the organic refractory grain mantles may be more resilient to destruction. In fact, they may act as a "glue" which keeps the coagulated grains together. The formation and growth of silicate grains in the ISM is somewhat more difficult to explain, given the almost complete depletion of the silicate forming elements that is observed. The condensation of pure silicate grains from the gas phase in a cold and relativity low density gas may proceed via SiH_n chemistry. Alternatively, silicate cores may be protected against sputtering by a carbonaceous coating.

We are indebted to J.Raymond for the shock profile data. This research was supported in part by NASA Consortium agreement NCA 2-637. Theoretical studies of interstellar dust at NASA Ames are supported through NASA grant 399-20-01-30 from the Theory Program.

REFERENCES

(1) Mathis,J.S., Rumpl,W., and Nordsieck,K.H. 1977, *Ap. J.*, **217**, 105.

(2) Bierman,P., and Harwit,M. 1980, *Ap.J. (Letters)*, **241**, L105.

(3) Gehrz,R., 1989, in *IAU Symposium 135, Interstellar Dust*, eds. L.J.Allamandola and A.G.G.M.Tielens, (Dordrecht, Kluwer), p.445.

(4) Tielens,A.G.G.M., 1990, in *Carbon in the Galaxy*, eds. J.C.Tarter, S.Chang and D.De Frees, NASA Conference Publication, 3061, p.59.

(5) Wooden,D.H., Rank,D.M., Bregman,J.D., Witteborn,F.C., Tielens,A.G.G.M., Cohen,M., Pinto,P.A., and Axelrod,T.S. 1993, *Ap. J.*Suppl., in press.

(6) McKee,C.F., and Ostriker,J.P. 1977, *Ap. J.*, **218**, 148.

(7) Jones,A.P., Tielens,A.G.G.M., Hollenbach,D., and McKee,C.F., 1993, in preparation.

(8) McKee,C.F., Hollenbach,D.H., Seab,C.G., and Tielens,A.G.G.M. 1987, *Ap. J.*, **318**, 674.

(9) Tielens,A.G.G.M., McKee,C.F., Hollenbach,D.H., and Seab,C.G. 1993, in preparation.

(10) Raymond,J. 1992, private communication.

(11) McKee,C.F. 1989, in *IAU Symposium 135, Interstellar Dust*, eds. L.J.Allamandola and A.G.G.M.Tielens, (Dordrecht, Kluwer), p.431.

(12) Greenberg,J.M. 1989, in *IAU Symposium 135, Interstellar Dust*, eds. L.J.Allamandola and A.G.G.M.Tielens, (Dordrecht, Kluwer), p.345.

(13) Jenniskens,P., Baratta,G.A., Kouchi,A., de Groot,M.S., Greenberg,J.M., and Strazzulla,G. 1993, *Astr. Ap.*, submitted.

(14) Jones,A.P., Duley,W.W., and Williams,D.A. 1990, *Q. Jl. R. astr. Soc.*, **31**, 567.

(15) Nuth,J.A., and Moore,M.A. 1988, *Ap.J. (Letters)*, **329**, L113.

(16) Chokshi,A., Tielens,A.G.G.M., and Hollenbach,D. 1993, *Ap. J.*, in press.

THE COAL MODEL FOR INTERSTELLAR DUST

Irène Nenner

CEA, Service des Photons, Atomes et Molécules, Bâtiment 522, Centre d'Etudes de Saclay, 91191 Gif sur Yvette cedex, France
and
LURE, laboratoire mixte CNRS, CEA, MENC, Bâtiment 209D, Centre Universitaire de Paris sud, 91191 Gif sur Yvette cedex, France

ABSTRACT

The main organic constituent of coal, kerogen, is shown to present a microstructure on a few nanometer scale, responsible of specific visible, ultra-violet and infra-red optical properties to fit various interstellar environments. Photoreflectance measurements using synchrotron radiation in the 300-4000 Å region, followed by Kramers-Kronig analysis have yielded the dielectric constants and refractive indices of polycristalline graphite and two high ranking coals. All three display two resonances which change regularly in shape and position with the extent of graphitization. Comparison of the deduced Q_{ext} with the extinction curve shows that anthracite is the closest fit to the λ2175 feature, while the carrier of the underlying continuum is probably due to low-rank, poorly graphitized coals. If coal is in the form of anthracite, 1/3 of the cosmic carbon is involved in the feature.

STRUCTURE AND PROPERTIES OF COAL

The coal model for interstellar dust has been introduced by Papoular et al (1989)[1)] because the mid infrared absorption spectrum of these materials resembles strikingly the sky observations towards carbon-rich nebulae, namely the unidentified infra-red bands (UIBs). This terrestrial material belongs to a family of carbonaceaous materials, which are classified in all countries according to their mining depth and depend only slightly on their birthplace. The main constituent of raw coal is a solid, insoluble, three dimensional, organic macromolecular skeleton, also called kerogen in dispersed form. It is mixed up with some minerals and free molecules. Note that most of the carbon content of primitive meteorites appears as kerogen[2]. Demineralized coal, is made up of the three most abundant (chemically active) elements in the universe. The atomic concentrations of carbon, hydrogen and oxygen are proportional to 1 : 0.5 : 0.02 respectively. The deeper is the mining seam, the more graphitized is the coal. Indeed, a large fraction of the carbon is arranged in graphite-like "bricks". These so-called basic structural units (BSUs) are oriented at random ; they are made of several layers of planar systems of polyaromatic rings packed together providing a medium-range order on a 10 to 20 Å scale. The carbon skeleton is aromatic and the hydrogen and oxygen atoms are attached to it under the form of functional groups like CH, CH_2, CH_3, OH etc.; other oxygen atoms form bridges between the bricks. Those bricks lie in an amorphous quasi-fluid phase in which the carbon is mostly aliphatic. The carbon skeleton of the bricks gives the π-π^* resonance near λ2200 Å (see below), the functional groups are responsible of the UIBs and the semi-conductor character of the solid material gives rise to a weak continuum starting in the infra-red and rising strongly towards the visible and ultra-violet[3,4]. Finally, coal is a material which evolves with time and temperature. Temperature rise favors the transformation of aliphatic carbon to aromatic ring structures, the introduction of medium range order and the decrease of the H/C abundance ratio. Therefore, one should consider coal as a class of materials with a continuous range of structural properties, which account for a large variety of interstellar medium observations.

THE VISIBLE/UV SPECTRUM OF COALS AND THE INTERSTELLAR EXTINCTION CURVE

The λ2175 Å bump in the interstellar extinction curve (ISEC) is extremely well documented in various celestial directions[5]. Although many models have been proposed[6-8], the interpretation is still a matter of discussion because of incomplete agreement with observations.

We have investigated the visible/UV spectrum of coals using photoreflectance measurements[9] using synchrotron radiation and a laboratory source. A *large* spectral region from 300 to 9000 Å is necessary to obtain after a Kramers-Kronig analysis, the complex and real part of the index of refraction. The spectral reflectances of polycristalline graphite and two high ranking coals "La Mûre" and "Escarpelle", (only La Mûre is shown in Fig. 1, see ref 9), exhibit two broad features with different shape and intensity. After the Kramers-Kronig analysis, one obtains the real n and imaginary k part of the refractive index. The k curve shows two resonances around 800 A and 2100 Å. They are due to $\sigma+\pi$ and π resonances. The $\sigma+\pi$ resonance does not change in position from graphite to coal but decreases in intensity ; in contrast, the π resonance is red shifted and extends a wing into the visible. Using the n and k value and the Rayleigh-Gans limit of Mie's theory, we have computed Q_{abs} only in the spectral region of relevance for the extinction curve. This region corresponds to the π resonance and the red wing of the $\sigma+\pi$ band. We show in Figure 1, the Q_{abs} results for "La Mûre" sample, and compare with the ISEC data after substraction of a smooth continuum of the form $\lambda^{-0.85}$ and a normalization of the two maxima. The agreement is quite satisfactory, although there is a 30 Å difference in the peak position. Notice also that a great part of the underlying continuum

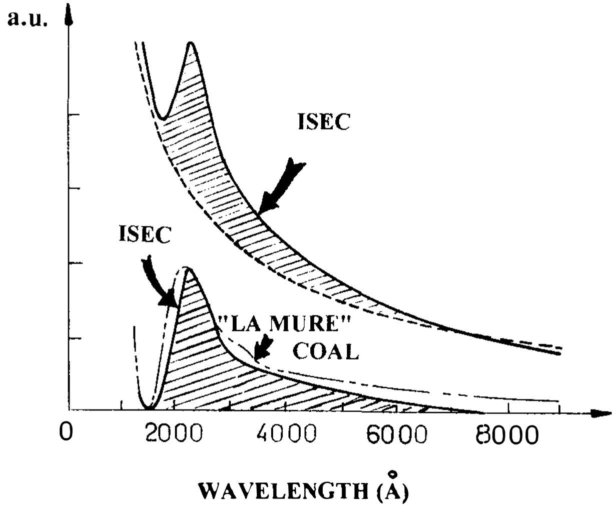

Figure 1 : *Relative extinction efficiency, Q_{abs} ($\sim Q_{ext}$) of "La Mure" coal as compared to the typical ISEC curve after substraction of a continuum (see text)*

of the ISEC may well be explained by low-ranking poorly graphitized coals[8] which do not exhibit the π resonance but only the $\sigma+\pi$ one (actually its red wing) which is always present in any carbonaceous materials. Considering the simple model of "La Mûre" extinction and the continuum, and $N(H_2) = 1.3\ 10^{21}\ A_V$, we obtain M(dust)/M(H) = 1/800, which is about 1/3 of the total C content of the galaxy.

In conclusion, coal is an attractive solid state model for the interstellar dust, since it accounts together for the ISEC bump in the UV and for the total UIBs (band and continuum). More work is in progress to refine the model in view of the (mild) discrepancies with the observations.

I am very grateful to R. Papoular for making me aware of this exciting problem and for developing our laboratory efforts. Thanks are due to my coworkers C. Reynaud, O. Guillois and K. Ellis for their essential contribution in the measurements.

REFERENCES

1 - R. Papoular, J. Conard, M. Giuliano, J. Kister and G. Mille, Astron. Astrophys. 217, 204 (1989)

2- J. Kerridge in *Carbon in the galaxy*, NASA Conf. Publ. 3061, p.10 Moffett Field, California USA (1990)

3 - R. Papoular, C. Reynaud and I. Nenner, Astron. Astrophys. 247, 215 (1991)

4 - R. Papoular, K. Ellis, O. Guillois, C. Reynaud and I. Nenner, J. Chem. Soc. Faraday Trans. 89, xxx (1993), in press.

5 - E. Fitzpatrick and D. Massa, Astrophys. J. 72, 163 (1990) ; ibid 307, 286 (1986)

6 - J. Hecht, Astrophys. J. 305, 817 (1986)

7 - J. Mathis and G. Whiffen, Astrophys. J. 341, 808 (1989)

8 - C. Joblin, A. Leger and P. Martin, Astrophys. J. 393, L79 (1992)

9 - R. Papoular, J. Breton, G. Gensterblum, I. Nenner, R.J. Papoular and J.-J. Pireaux, Astron. Astrophys., 270, L5-L8 (1993).

EXCITATION ANALYSES OF INTERSTELLAR CLOUDS

C.M. Walmsley
Max-Planck-Institut für Radioastronomie
Auf dem Hügel 69, 53121 Bonn, F.R.G.

ABSTRACT

A review is given of our present knowledge of the physical characteristics of interstellar clouds and the methods used to derive parameters such as temperature and density. In particular, I discuss what can be learnt from excitation analyses of molecular clouds and compare results obtained using different molecular tracers.

1. INTRODUCTION

The interstellar gas is in a highly unrelaxed state. In fact,maps made in the 21 cm line of atomic hydrogen or in a variety of molecular lines show that much of the gas is in clumps, filaments, sheets, and in other contorted structures. A consequence is that both the dense gas (mainly molecular) and the diffuse gas (mainly atomic) is highly inhomogeneous. Much of the material is clearly in structures with densities quite different from the average smoothed-out value that one obtains, for example, from the column density of hydrogen along a given line of sight. Estimating the *local* (as opposed to the mean) density in an interstellar cloud is usually therefore done by means of an excitation analysis. That is to say; one examines the balance between collisional excitation and radiative decay for some atom, molecule, or ion with observable spectral lines and predicts their relative intensities. The observed relative intensities are then used to put constraints upon the density of the colliders - usually but not always hydrogen. Simultaneously, such analyses normally allow an estimate of the temperature and hence also of the thermal pressure in the clouds of interest. A determination of these parameters is important from the point of view of the cloud dynamics . It additionally allows an estimate to be made of the gas cooling rate and hence of the dissipation rate of the "non-thermal turbulence" which is often present in both atomic and molecular clouds.

Many reviews of molecular cloud characteristics are available[3),43),56)]. Atomic hydrogen clouds are discussed by Kulkarni and Heiles[30)]. The basic properties of giant molecular clouds (GMC's) are summarised by Solomon et al.[48)] and the characteristics of the dense cores often found associated with GMC's are considered by Myers[39),40)]. Recently also, some useful theoretical insights have come from the work of McKee[37)], of Elmegreen[16)], of de Boisanger et al.[4),5)] and of Wolfire et al.[58)]. Both the observational work and the theoretical studies rely upon excitation analyses of one sort or another. In this article, I will thus confine myself to summarising the techniques used to analyse level excitation in a variety of situations in the interstellar medium ranging from diffuse atomic hydrogen clouds to their denser molecular counterparts. I will also briefly discuss the estimates of the thermal pressure which one make in diffuse and molecular clouds and their consequences for our understanding of the processes taking place within them. I begin with a short summary of results for diffuse clouds (section 2) which are atomic in the sense that CO is a minority species. In section 3, I consider in turn the methods used and the results obtained for the diffuse molecular material seen in CO and ^{13}CO; for molecular absorption lines seen along the few lines of sight where such measurements are possible; for the "dense cores" seen in ammonia, CS and other high density tracers; and for regions of high mass star formation. Finally, in section 4, I discuss some possibilities for future studies.

2. PARAMETERS OF DIFFUSE CLOUDS

An excellent description of the properties of diffuse atomic gas in the galaxy has been given by Kulkarni and Heiles[30),29)] and readers interested in more than a superficial understanding are invited to examine that article. Analyses of optical and ultraviolet absorption lines towards stars in the solar neighbourhood have yielded a lot of information about the characteristics of diffuse clouds. A good example is the study by Jenkins et al.[28)] of the lines at 1138-1328 Angstroms of neutral atomic carbon. These authors have utilised the fact that the excited fine structure levels of CI are appreciably populated at the densities of diffuse clouds and that the ratio of excited state to ground state population is a sensitive function of the product of density and temperature or equivalently of pressure. They found thermal pressures p/k between 1000 and $10^4 cm^{-3}$ K with a representative value being around 4000 cm^{-3} K. Kulkarni and Heiles[29)] also examined the possibility of using analogous data for ionized carbon (CII) for the same purpose and arrived at estimates for the thermal pressure a factor 2 higher than with CI. It seems in any case certain that the typical diffuse cloud pressure is below 10^4 cm^{-3} K.

It is worth noting that these estimates for the pressure are not greatly different from the thermal pressures found in the distributed ionized medium (sometimes known as WIM or Warm Ionized Medium) which is responsible for pulsar dispersion as well as the weak distributed Hα emission seen by Reynolds[42)]. Kulkarni and Heiles[29)] estimate for this component an electron density of 0.25cm^{-3} and a temperature of 8000 K corresponding to a pressure of 4000cm^{-3} K. This is close to the value derived for the cold clouds from CI data and suggests that rough pressure balance is maintained between the different phases in the diffuse atomic gas. On the other hand, this ignores the possible importance of magnetic and cosmic ray pressure. It also ignores pressure estimates based upon the scale height of local HI from 21 cm measurements (see Blitz's contribution) which suggest higher total pressures. Probably, the real truth is that all of the estimates discussed above have a factor of two uncertainty and, moreover, there are real pressure variations of this order also. In any case, these diffuse gas pressures are less than or of the same order as the molecular cloud pressures we discuss in the next section.

Before going on to this however, I note that at least *some* diffuse clouds appear to have relatively high thermal pressure (above $10^4 cm^{-3}K$) as evidenced by the detection of CS(2-1) emission at a very low level[14] towards 4 nearby stars. The interpretation is complicated by the fact that electron excitation becomes important in these regions but it is nevertheless interesting and a little surprising that CS emission is observable in this type of region. High thermal pressures are also estimated for the much studied cloud along the line of sight to ζOph[32]. Detailed models for this type of region have been computed by van Dishoeck and Black[51),52)].

3. MOLECULAR CLOUD PARAMETERS

The determination of densities and temperatures in molecular cloud regions has been reviewed by Walmsley[54] and by Cernicharo[8] among others. Briefly, one solves the statistical equilibrium equations for the level populations of a given molecule and uses an escape probability *ansatz* to correct for trapping in optically thick molecular lines. Rather doubtful assumptions about the geometry of the cloud, it's velocity field, and it's homogeneity are made in order to simplify the problem. A quick look at one of the many molecular line maps available in the literature suffices to see that the results of this procedure should be treated with some scepticism. On the other hand, more complex models are often not warranted.

In the following, we briefly review results from studies of this type for a variety of conditions. First, we consider observations of the "clumps" (for the purposes of this article, clumps are clouds with diameters of~ the order of roughly 1 parsec) which are commonly observed in regions such as Taurus and Ophiuchus.

3.1 Extended emission observed in CO isotopomers

Nature has decided that the most abundant interstellar molecule (apart from H_2) should have a small dipole moment which causes it to be excited in the relatively low density ($\sim 10^3 cm^{-3}$) parsec sized clumps out of which most molecular clouds appear to consist. This molecule is of course CO and it is interesting to speculate upon what masses might have been estimated for molecular clouds if CO had had a dipole moment of 1 rather than 0.1 debye. It is also of importance to realise that our estimates of the fraction of molecular cloud mass in structures with densities less than $10^3 cm^{-3}$ may be biased because in ^{13}CO and $C^{18}O$, even the J=1-0 transition is very sub-thermal.

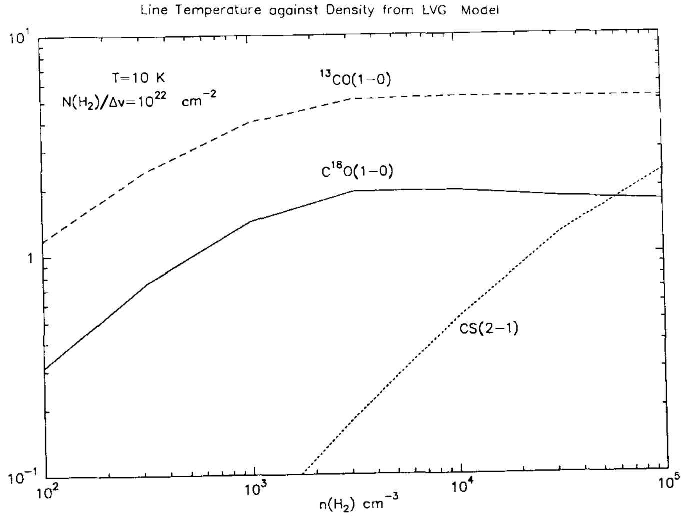

Figure 1: Predicted line temperatures of a model molecular clump of given hydrogen column density and temperature as a function of density for CS(2-1), $^{13}CO(1\text{-}0)$, and $C^{18}O(1\text{-}0)$. The temperature has been assumed to be 10K and the ratio of molecular hydrogen column density to linewidth has been taken to be $10^{22}cm^{-2}(kms^{-1})^{-1}$. The abundances relative to H_2 assumed for the various species are: 10^{-6} for ^{13}CO, 2 10^{-7} for $C^{18}O$, 3 10^{-9} for CS . Electron excitation is neglected.

In practise however, it turns out that ^{13}CO and $C^{18}O$ are excited at densities above $100cm^{-3}$ while high dipole moment species such as CS require much higher densities in order to produce observable emission. This is demonstrated in figure 1 which compares the results of statistical equilibrium calculations for the three species. The LVG computation carried out here assumes a molecular hydrogen column density of $10^{22}cm^{-2}$ and "typical" abundances (CS/H_2 =3 10^{-9}, $^{13}CO/H_2=10^{-6}$, $C^{18}O/H_2=2$ 10^{-7}). One sees that CS(2-1) becomes easily observable only above 10^4cm^{-3}. An implication of this is that one expects maps made in CS and in ^{13}CO (say) to look very different from one another as long as there is a considerable fraction of the molecular cloud material in low density gas (below 10^4cm^{-3}). In fact, the available observations[31)] do confirm this implying that the high density cores contain a small fraction of the total molecular cloud mass.

Can one make useful density estimates on the basis of the CO isotopcmer measurements alone? Figure 2 shows some sample results of an LVG calculation which has been carried out for $C^{18}O$. An abundance ratio $[C^{18}O]/[H_2]$ of 2 10^{-7} has been assumed and the calculations were carried out for temperatures of 10 and 20K.

One sees that the (2-1)/(1-0) ratio saturates above a density of $10^4 cm^{-3}$ and that it is most sensitive in the range 1000-10^4 . One sees also that a knowledge of or at least bounds upon the temperature are needed to use $C^{18}O$ (2-1)/(1-0) or $C^{18}O$ (3-2)/(2-1) as a density indicator.

Observationally, there has been rather little work studying the $C^{18}O$ (2-1)/(1-0) ratio. However, Young et al.[53)] have carried out a detailed study of the B5 cloud and use calculations similiar to those whose results are shown in figure 2 to derive a density of $4000 cm^{-3}$ for the central part of this cloud. Significantly, their study of ^{13}CO suggests smaller densities suggesting that density gradients are present. The "onion-skin" model of Gierens et al.[22)] offers one approach to solving such discrepancies. In the same spirit, large scale ^{13}CO and $C^{18}O$ maps[6)15)] towards the Orion A cloud have been used to "map" the local density. These authors find clumps with densities in the range 3000-1.5 $10^4 cm^{-3}$ and masses 1-20 solar masses. It will be interesting to compare these results with those from other tracers such as NH_3 and CS. Finally, Falgarone et al.[17] have examined the ^{13}CO (2-1)/(1-0) ratio in areas of low ^{13}CO brightness and conclude rather surprisingly that much of the matter is in rather high density clumps (above $10^4 cm^{-3}$). This however concerns regions which are non self-gravitating.

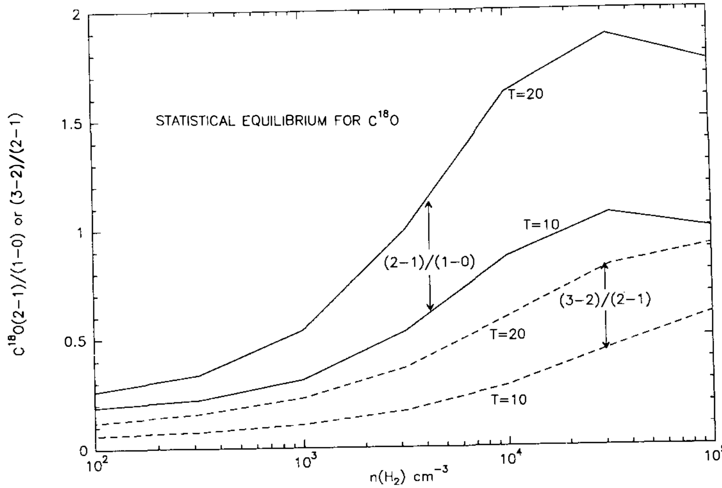

Figure 2: Results of LVG calculations similiar to those used for fig. 1 which show predictions for the $C^{18}O$ (2-1)/(1-0) line intensity ratio as a function of density. Calculations have been carried out for temperatures of 10 and 20K.

3.2 Low density gas seen in absorption

Centimeter wavelength molecular lines have been known for a long time to show absorption towards galactic continuum sources. It was rather more surprising to find absorption at millimeter wavelengths because continuum sources are relatively much weaker. However, it has been known for more than a decade that several ground state transitions can be observed in absorption towards sources such as SgrB2 and W49[33,41,24]. These lines are found to have excitation temperatures very close to that of the 3K microwave background suggesting densities of a few thousand cm^{-3} at most. It is significant that absorption is seen in transitions such as HCN(1-0) and HCO^+(1-0) but not in ^{13}CO or $C^{18}O$. The simplest conclusion is that the densities are such that $C^{18}O$ and ^{13}CO are excited whereas the high dipole moment species are not and, as one sees from figure 1, this implies densities in the range 10^3-$10^4 cm^{-3}$.

Some temperature estimates for the absorption features are available from ammonia measurements. For the Cas A clouds, Batrla et al. [1] find a temperature of 20K and a pressure of $10^5 cm^{-3}K$. This seems consistent with recent ^{13}CO measurements by Wilson et al.[57]. For the v=40 cloud towards W49, ammonia measurements by Mauersberger (priv.comm) suggest temperatures below 15K and the C_3H_2 measurements of Cox et al.[12] put an upper limit to the density of $5000 cm^{-3}$. This translates into an upper limit on the thermal pressure of 7.5 $10^4 cm^{-3}$. Thus the absorption line measurements ,which presumably sample random regions in molecular clouds, suggest that typical thermal pressures in molecular clouds are a factor of 20 at most above the diffuse cloud thermal pressures found in tracers such as CI.

Some work of this type has been carried out towards extragalactic continuum sources. These objects are in general at higher galactic latitudes than the regions mentioned above and hence relatively nearby clouds are observed. A recent survey by Liszt and Wilson[34] summarizes recent CO studies. One result of considerable interest is the detection of CO absorption towards BL Lac by Marscher et al.[36] using the Owens Valley Interferometer. Here, it is significant than the linewidth measured in *absorption* by the Interferometer is comparable to that measured in *emission* using a single dish. Thus the measured supersonic linewidth does not appear to be due to averaging velocity variations within the beam.

3.3 Parameters of dense cores

Many excitation analyses have been carried out of the dense "cores" found embedded in molecular clouds with densities of $10^4 cm^{-3}$ or more[8]. These cores are typically found using ammonia or CS as tracers of the dense gas. Figure 1 demonstrates why CS is appropriate for this purpose. Often, one finds associated with such cores infrared (IRAS) sources which appear to be young stars which are still embedded in a dust cocoon of stellar or interstellar nature.

Characteristics of the dense cores and their relevance for star formation are summarized in a series of articles by Myers and associates[39,40,20]. The basic conclusion is that these regions, which can easily be picked out in maps of the $NH_3(1,1)$ line, have typical dimensions 0.1 parsec and mass of the order of a few solar masses. There is strong evidence[11] for a correlation between ammonia cores and cool IRAS sources with color temperatures between 60 and 100 microns of order 40K. There is also a general correlation between ammonia cores and the positions of T.Tauri stars in well studied regions such as Taurus. Hence, there is good reason to believe that low mass star formation is taking place in dense cores.

The ammonia observations yield temperatures and limits upon the density[27,50,2]. Typical temperatures are in the range 10-20K if one restricts consideration to cores either without associated infrared sources or those associated with low luminosity IRAS sources. A curious feature of the data is that there appear to be differences between the cores embedded in different molecular clouds. Thus while Taurus dense cores have uniformly a temperature of around 10K, cores embedded in larger molecular clouds such as the Orion clouds (L1630 and L1641) have temperatures which average around 15K[10,25]. The cause of this difference is obscure. It seems to be related to the fact that measured line widths are also in general larger in the Orion clouds than in Taurus. This is also seen in the CS(1-0) survey of Tatematsu et al.[49]. One obvious difference between the Orion and Taurus regions is the presence of large OB associations in Orion. The supernova explosions and stellar winds associated with the presence of these young stars may be at the origin of the increased turbulence in the Orion cloud.

This difference in temperature is reflected in figure 3 which shows a comparison of the thermal pressures found in the nearby ($<$300pc) cores of the Benson Myers[2] sample(triangles) with the analogous results for the Orion cores of Harju et al.[25], open squares). While, for the reasons discussed below, the individual density determinations (and hence also pressure) are suspect, the trends seen in figure 3 are probably reliable. One can draw the general conclusion that, while there is no clear difference in density between Orion and local cores, the Orion GMC cores do have slightly higher pressure. One notes also that all of the cores have thermal pressures considerably in excess of the typical diffuse atomic clouds discussed in section 2.

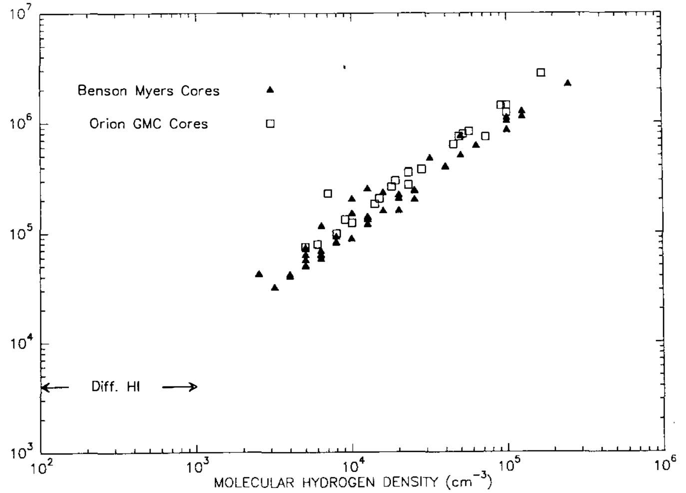

Figure 3: The thermal pressure and density derived from the ammonia data of Benson and Myers[2)] for nearby clouds (triangles) are compared with similiar results for cores in the Orion GMC obtained by Harju et al.[25)], open squares). For comparison, the typical density and pressure of interstellar HI clouds is shown at the lower left.

In the Orion cores, "turbulence" makes the main contribution to the observed line width. By contrast, in some of the nearby cores, the line widths are so small that the effects of thermal broadening are directly measurable. A recent multi-molecular study by Fiebig and Güsten[19,18)] examines the variation of linewidth as a function of molecular mass for three NH_3 cores (L1498, L1512, TMC1-C) and derives kinetic temperatures which (in two of the three cases) are completely consistent with the numbers obtained from the ammonia excitation analysis. The non-thermal line broadening in these objects has almost disappeared. A consequence of this is that thermal pressure plays an important role in the dynamics of the region and in fact thermal pressure and gravitation are roughly in balance in these cores. Magnetic field pressure and rotational energy seem incidentally to be negligible.

Comparisons of this sort often depend upon the density derived from the ammonia (1,1) excitation temperature. This method will be affected by clumping within the beam which causes one to underestimate the molecular hydrogen density. One clearly therefore needs to compare ammonia results with estimates based upon other molecules. A study of this type has been carried out by Zhou et al.[59)] who observed several CS and $C^{34}S$ transitions towards a sample of low mass cores. They derive higher densities from their CS measurements than from NH_3 which at first suggests that clumping is affecting the ammonia results. However, for the three sources studied by Fiebig[18], one can compare the 100-m NH_3 measurements taken with a 40" HPBW with the Haystack-Greenbank results of Benson and Myers[2] taken with beams roughly double the size. The results show that for one source (L1512), the density derived by Fiebig is a factor 8 smaller than by Benson and Myers whereas for L1498, the 100-m observations suggest a density 2 times larger than the results from Haystack and Greenbank. For TMC1-C, the different telescopes give results consistent within a factor 2. All of these sources have high NH_3 (1,1) optical depths and the above differences suggest that the combination of calibration errors together with the difficulty of making a precise trapping correction make densities derived from the estimated NH_3(1,1) excitation temperature very suspect. Probably, the only safe statement on the basis of the ammonia measurements is that the densities in all of these sources is above $10^4 cm^{-3}$.

On this basis, one might think that the CS results are preferable. However, one finds observationally[59] that the observed CS emission has typically larger linewidth and comes from a larger region than does NH_3. This suggests that chemical differences between the two species are confusing the issue with CS being relatively more abundant in the low density envelope surrounding the core with density above $10^4 cm^{-3}$. One can imagine then that the radiative transfer for CS is analogous to that for HCO^+ [7,23]. The scattering envelope redistributes the photons emitted by the core both spatially and in velocity. NH_3 (which seems to be thin in the envelope) gives a truer representation of the core characteristics. If this is generally true, one needs to measure an optically thin tracer such as $C^{34}S$ in order to derive reliable core densities. Another possibility is C_3H_2 [13].

The above discussion also suggests that homogeneous models are often not an appropriate approach to modelling dense cores. Some work has also been carried out assuming density distributions appropriate to star forming cores. Thus, Zhou et al.[60] suggest that their formaldehyde and CS data towards B335 can be explained by a model which, outside an inner core of radius 0.03 parsec, has an envelope with a $1/r^2$ density profile. In such a situation, higher angular resolution observations detect higher densities, which causes the simple LVG homogeneous models often used in this sort of analysis to be of doubtful value.

Nevertheless, the simple LVG models give an estimate of the density on the scale size of the beams used and hence of the local pressure. The Benson and Myers[2] ammonia data suggest that the pressure in their cores varies between $10^{4.7}$ and

$10^{6.1}$cm^{-3}K with a median value of $10^{5.2}$cm^{-3}K. In the smaller sample of Zhou et al.[59] observed in CS, the derived pressure varies between $10^{5.3}$ and $10^{6.7}$ with a median of $10^{6.1}$cm^{-3}K.

3.4 Physical Parameters of Regions of High Mass Star Formation

The techniques discussed earlier have found their greatest application in regions where O-B stars are currently forming. A pioneering work in this field was that of Snell et al.[47] who used CS observations to derive the molecular hydrogen density in the regions M17, S140, and NGC 2024. These authors observed CS(2-1),(3-2), (5-4), and (6-5) with an angular resolution of roughly 1 arc minute. They thus sampled a considerable range in "critical density " (i.e the density for which the collision rate $n(H_2)$, σv is equal to the transition Einstein A-value). They nevertheless managed to get single density solutions in a considerable number of positions and concluded that the CS emission arises in clumps of density between 4 and 9 10^5cm^{-3}. Their results were later confirmed by the subsequent $C^{34}S$ study of Mundy et al.[38]. More recent work with higher angular resolution (Ref.44) has directly demonstrated the existence of such clumps in the M17 cloud and confirmed that their densities are of order 10^6cm^{-3}. The most recent development is the extension of this work to the submm range with the CS(10-9) detections of Hauschildt et al.[26]. This transition has a critical density, above 10^7cm^{-3} and one would naively think it should trace extremely high density regions. This may be the case but it seems likely that in the sources where CS(10-9) has been detected, infrared pumping via the vibrational transition at 7.9μm is competitive with collisions.

Another possible tracer is formaldehyde. A very recent study by Mangum and Wootten[61] shows that one can exploit the fact that H_2CO is a slightly asymmetric top molecule in order to derive both density and temperature. The consequence of being slightly asymmetric is that there are several transitions at neighbouring frequencies whose intensity ratios are sensitive to temperature and relatively independent of density. Mangum and Wootten derive temperatures of 50-300K and densities of 10^5 to 10^7cm^{-3} for several regions of high mass star formation.

A number of detailed studies have also been made of the high density gas surrounding the Orion-KL region[35,45]. Over a region roughly 0.5 parsec in size, the 2cm ($2_{1,1}$-$2_{1,2}$) line of formaldehyde is found to be in emission (see Wilson and Johnston[55]) and this implies densities of at least 3 10^5cm^{-3}. In this case, the pressures are probably influenced by the nearby HII region and are probably above 10^7cm^{-3}K. The more distant regions in the inner galaxy studied by Cesaroni et al.[9] probably have similiar characteristics to the Orion ridge gas.

4. DISCUSSION

The molecular cloud physical parameters derived from excitation analyses are important in at least two respects. In the first place, they allow us to check cloud mass estimates and indeed mean densities derived from a tracer such as CO or dust. These latter estimates usually make an assumption (see Genzel[21]) for a discussion) about the abundance of the relevant tracer as well as about it's excitation temperature (temperature and emissivity in the case of dust). The excitation analyses do not require such assumptions and indeed provide a check upon their validity. It is thus only via excitation analyses that we are able to measure molecular hydrogen as opposed to something representing molecular hydrogen. On the other hand, the excitation analyses have also their weaknesses and one concludes that the two approaches to determining molecular cloud masses (from excitation and from column density) are complementary.

Secondly, the thermal pressure one derives from density and temperature measurements should also provide useful constraints upon molecular cloud models. Thermal pressure is certainly important dynamically in those dense "ammonia" cores where thermal broadening is larger than the non-thermal contribution to the linewidth. In this case, it appears that thermal pressure dominates magnetic and turbulent pressure. It seems reasonable to believe that these regions[46]) are a reasonable approximation to a hydrostatic isothermal sphere and the mass accretion rate of an embedded object is then simply a function of the temperature. Tests of this hypothesis on the lines of the study of Zhou et al.[60]) seem a reasonable way to go forward. In regions such as the Orion cloud cores where "non-thermal" turbulence dominates the line broadening, there is evidence[25]) that temperatures are higher than in the narrow line cores. Understanding the reason for this as well as understanding the nature of the non-thermal broadening is an important goal for the future. The proposals put forward by Chièze at this conference offer one approach to solving these problems theoretically.

The fraction of molecular cloud gas in high density material (above $10^4 cm^{-3}$) is still a controversial quantity. The excitation studies discussed in this article should be capable of providing a partial answer to this problem. In particular (see Fig.1), the comparison of maps of high density tracers such as CS with maps of ^{13}CO or $C^{18}O$ should allow crude estimates to be made. A start in this direction has been made by Lada et al.[31]) who have mapped a large fraction of the L1630 cloud in

CS(2-1). They detected CS emission over 10 percent of the region surveyed and conclude that less than 19 percent of the cloud mass is in cores with density above $10^4 cm^{-3}$. The absorption line measurements discussed earlier in this article (section 3.2) are broadly consistent with this result and suggest that the bulk of GMC material is in clumps with density of a few thousand per cubi centimeter or less. However, clearly the vastly improved data sets one can expect in the future (see Fukui's contribution) will provide new answers to this question.

As discussed in the Introduction, the origin of the non-thermal turbulence observed in most molecular clouds is not presently understood. One result which may help to find a resolution of this question is the observation (section 3.3 and fig.3) that there are marked differences between dense cores embedded in different molecular clouds. These differences appear to be in the sense that cores embedded in more massive clouds (10^5 solar masses or more) have higher pressure (both thermal and total) than cores associated with low mass aggregates such as Taurus[25)]. One possible explanation (see section II of Ref.37 and in particular equation 2.17) may be related to the higher pressures expected in massive clouds with high mean extinction. Here, the idea is that the pressure contrast between cloud edge and center should reflect the depth of the gravitational potential well.

Finally, I note that one fundamental problem with most of the excitation studies discussed in this article is that the clouds, clumps, and cores under consideration are far from being homogeneous entities. Hence, as with forbidden line studies of HII regions, one can have the problem that since each tracer is sensitive in a limited density range (for example $1000\text{-}10^4 cm^{-3}$ in the case of $C^{18}O$ - see fig.2), the result of excitation studies tends to be that one always derives a value corresponding to the critical density of the tracer under consideration. This criticism is certainly partially valid and in many cases, explains the discrepancies between density estimates derived using different tracers. However, one should also be aware that excitation studies using several molecular lines of differing critical densities have been carried out and one does often find an unique density within observational errors[38,61)]. Moreover, even when excitation studies do not yield unique densities, the derived limits can be significant. For example, the absorption line studies discussed in section 3.2 yield upper limits to the density whereas most emission line studies give lower limits. Combining the two can rather tightly constrain the density in the region under consideration. One should therefore not be too pessimistic about the possibility of learning something from excitation.

REFERENCES

1) Batrla W., Walmsley C.M., Wilson T.L. 1984 A&A 136,127.
2) Benson P.J., Myers P.C. 1989 ApJ Suppl. 71,89.
3) Blitz L. 1987 in *Physical Processes in Interstellar Clouds*, edited Morfill G.E., Scholer M., publ. D.Reidel, NATO ASI Series C, Vol 210.
4) de Boisanger C., Chièze J.P. 1991 A&A 241,581.
5) de Boisanger C.B. , Chièze J.P., Meltz B. 1992 ApJ 401,182.
6) Castets A. et al. 1990 A&A 234, 469.
7) Cernicharo J., Guélin M. 1987 A&A 176,299.
8) Cernicharo J. 1991 in *The Physics of Star Formation and Early Stellar Evolution*, edited by C.J.Lada and N.Kylafis, NATO ASI Vol 342, publ. Kluwer.
9) Cesaroni R., Walmsley C.M., Kömpe C., Churchwell E. 1991 A&A 252,278.
10) Cesaroni R., Wilson T.L. 1993 A&A (in press).
11) Clark F.O. 1987 A&A 180,L1.
12) Cox P., Güsten R., Henkel C. 1988 A&A 206,108.
13) Cox P., Walmsley C.M., Güsten R. 1989 A&A 209,382.
14) Drdla K., Knapp G.R., van Dishoeck E.F. 1989 ApJ 345,815.
15) Dutrey A. 1993 A&A (in press).
16) Elmegreen B.G. 1989 ApJ 338,178.
17) Falgarone E., Puget J.-L., Pérault M. 1992 A&A 257, 715.
18) Fiebig D., 1990. Doctoral Dissertation, Univ. of Bonn.
19) Fiebig D., Güsten R. 1993 (in preparation).
20) Fuller G.A., Myers P.C. 1987 in *Physical Processes in Interstellar Clouds*, edited Morfill G.E. and Scholer M., publ. D.Reidel, NATO ASI Series Vol. 210
21) Genzel R. 1992 Saas Fee advanced course 21, *The galactic interstellar medium*, (Burton W.B., Elmegreen B.G., Genzel R.; publ. Springer)
22) Gierens K.M., Stutzki J., Winnewisser G. 1992 A&A 259, 271.
23) Gonzalez-Alfonso E., Cernicharo J. 1993 A&A , in press.
24) Greaves J.S., White G.J., Ohishi M., Hasegawa T., Sunada K. 1992 A&A 260, 381.
25) Harju J., Walmsley C.M., Wouterloot J.G.A. 1993 A&A Suppl.98 51.
26) Hauschildt H. 1993 A&A (in press)
27) Ho P.T.P, Townes C.H. 1983 Ann.Rev.Astron.Astrophys. 21,239.
28) Jenkins E.B., Jura M., Loewenstein M. 1983 ApJ 270,88.
29) Kulkarni S.R., Heiles C. 1987 in *Interstellar Processes*, (ed. D.J.Hollenbach and H.A.Thronson Jr.) Reidel
30) Kulkarni S.R., Heiles C. 1988 in *Galactic and Extragalactic Radio Astronomy*, edited by G.L.Verschuur, K.I.Kellermann, publ. Springer-Verlag.
31) Lada E.A., Bally J., Stark A.A. 1991 ApJ 368,432.
32) Le Bourlot J., Gélin M., Pérault M. 1989 A&A 219,279.
33) Linke R.A., Stark A.A., Frerking M.A. 1981 ApJ 243,147.
34) Liszt H.S., Wilson R.W. 1993 ApJ 403,663.

35) Mangum J.G., Wootten A., Plambeck R.L. 1993 ApJ ,(in press)
36) Marscher A.P., Bania T.M., Wang Z. 1991 ApJ 371, L77.
37) McKee C.F. 1989 ApJ 345,782.
38) Mundy L.G. et al. 1986 ApJ 306, 670.
39) Myers P.C. 1987 in *Star Forming Regions*, edited by M.Peimbert and J.Jugaku, publ. D.Reidel, IAU Symposium 115.
40) Myers P.C. 1991 in *Fragmentation of Molecular Clouds and Star Formation*, (ed. E.Falgarone, F.Boulanger, G.Duvert ; publ. Kluwer) ; IAU 147.
41) Nyman L.A., Millar T.J. 1989 A&A 222, 231.
42) Reynolds R.J. 1984 ApJ 282,191.
43) Stutzki J. 1992 , *Reviews of Modern Astronomy*, vol. 6 (in press), publ. Springer.
44) Stutzki J., Güsten R. 1990 ApJ 356, 513.
45) Schilke P. et al. 1992 A&A 256, 595
46) Shu F., Adams F.C., Lizano S.1987 Ann.Rev.Astron.Astrophys. 25,23.
47) Snell R.L. 1984 ApJ 276, 625.
48) Solomon P.M., Rivolo A.R., Barrett J.W., Yahil A. 1987 ApJ 319, 730.
49) Tatematsu K. et al. 1993 ApJ 404, 643.
50) Ungerechts H., Walmsley C.M., Winnewisser G. 1986, A&A 157,207.
51) van Dishoeck E.F., Black J.H. 1986 ApJ Suppl. 62, 109.
52) van Dishoeck E.F., Black J.H. 1989 ApJ 340, 273.
53) Young J.S., Goldsmith P.F., Langer W.D., Wilson R.W., Carlson E.R. 1982 ApJ 261, 513.
54) Walmsley C.M. 1987 p.161 in *Physical Processes in Interstellar Clouds*, edited by G.E.Morfill and M.Scholer, NATO ASI Series, Vol 210, publ. Kluwer.
55) Wilson T.L., Johnston K.J. 1989 ApJ 340, 894.
56) Wilson T.L., Walmsley C.M. 1989 The A&A Review 1, 141.
57) Wilson T.L. et al. 1993 A&A (submitted)
58) Wolfire M.G., Hollenbach D., Tielens A.G.G.M. 1993 ApJ 402,195.
59) Zhou S., Wu Y., Evans N.J. II , Fuller G.A., Myers P.C. 1989 ApJ 346,168.
60) Zhou S., Evans N.J II, Kömpe C., Walmsley C.M. 1993 ApJ 404, 232.
61) Mangum J., Wootten A. 1993 ApJ Suppl.(in press)

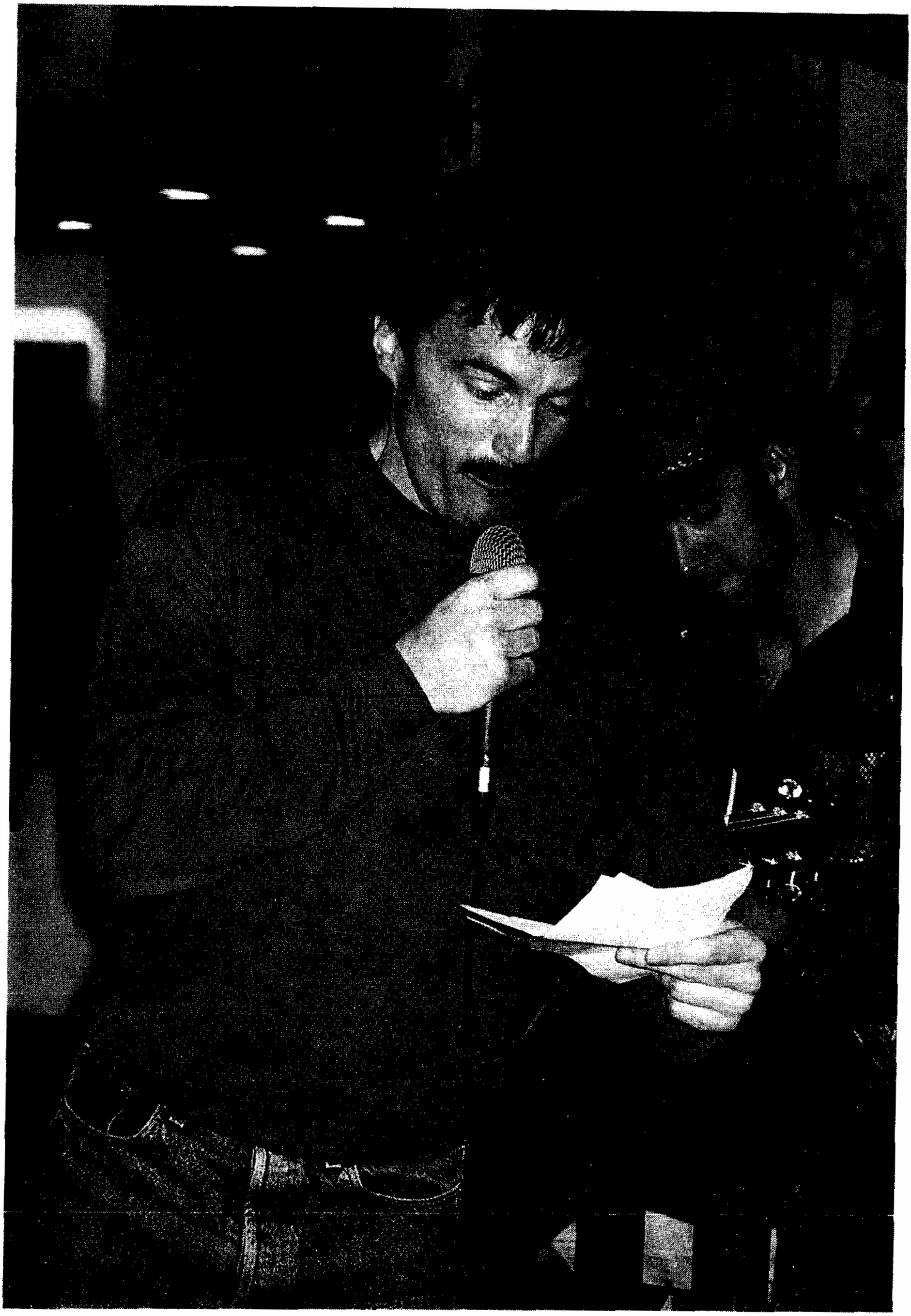

Pat Hartigan : Hot music !

RECENT PROGRESS IN INTERSTELLAR CHEMISTRY

T J Millar
Department of Mathematics, UMIST
P.O. Box 88, Manchester M60 1QD, U.K.

ABSTRACT

In this article I shall summarise recent applications of interstellar chemistry to a variety of astronomical scenarios. I shall look in detail at some of these, in particular at the chemistry of the polycyclic aromatic hydrocarbons (PAHs) and of the fullerenes (C_{60} and C_{70}). I shall also consider the chemistry that occurs in hot molecular cores and show how observations of these regions can be used to probe the chemical history of the material. Finally I shall make some remarks about the possible presence of H_2CO and SO^+ in oxygen-rich circumstellar envelopes.

1. INTRODUCTION

Our understanding of the chemical processes which occur in astronomy has greatly increased in the last few years. In part this has to with the great amount of data which has emanated from chemical kinetic laboratories,[1),2)] in part to the detailed molecular identifications and maps available from observers and in part to the application of astrochemical models to a wide range of astronomical objects including diffuse and dense interstellar clouds, carbon-rich and oxygen-rich circumstellar shells, shocked gas, photon-dominated regions, protostellar outflows, external galaxies and the early universe[3),4),5)].

To date, almost 100 molecules have been detected in interstellar and circumstellar clouds, comprising the elements H, C, N, O, Si, P, S, Cl and, most recently, Mg, although P and Mg are each detected in only one molecule and the identification of the only Cl-bearing molecule, HCl, remains insecure. The chemistries of most elements appear to be driven by ion-neutral reactions although neutral-neutral reactions make important contributions to the synthesis of molecules containing nitrogen and sulfur and the H_2 molecule, which is crucial to efficient molecular synthesis, is formed on grain surfaces. Ion-chemistry must be driven by ionisation; in diffuse clouds this is provided by the general interstellar ultraviolet radiation field, whilst in dense clouds it is provided by cosmic ray particles. In some regions, ionisation driven by X-rays might be important and lead to significantly different routes to molecule formation. In dense clouds, cosmic ray collisions with H_2 produce H_2^+ ions which, within about one day, are converted into H_3^+ ions. Because the proton affinity of H_2 is rather low, these ions transfer their protons to atoms such as C and O (but not N for which the proton transfer is slightly endothermic) to form ions such as OH^+ and CH^+. These ions react rapidly in a series of reactions with molecular hydrogen to form the terminating ions H_3O^+ and CH_5^+, respectively. These terminal ions then undergo dissociative recombination with electrons to form OH, H_2O and CH_4 among other possibilities. The H_3^+ ion is also crucial in the deuteration of interstellar molecules through its reaction with HD which, at low temperatures, is exothermic by about 220 K. The resulting H_2D^+ ion then transfers D through deuteron transfer reaction with neutrals such as CO, N_2, and H_2O, producing DCO^+, N_2D^+ and HDO. Once simple molecules are formed, reactive ions and radicals are produced through reaction with He^+ ions, which are formed by cosmic ray ionisation of He atoms, for example

$$He^+ + CO \dashrightarrow C^+ + O + He.$$

The C^+ ion can then react with methane to produce more complex hydrocarbon ions,

$$C^+ + CH_4 \dashrightarrow C_2H_2^+ + H_2$$

$$C^+ + CH_4 \dashrightarrow C_2H_3^+ + H.$$

Dissociative recombination of these ions with electrons can produce the observed interstellar molecules C_2, C_2H and C_2H_2.

Nitrogen bonds are formed through the reaction of N atoms with OH to produce NO which reacts with N atoms to form the N_2 molecule. N_2 takes a proton from H_3^+ to form the observed N_2H^+ ion and also reacts with He^+ to give kinetically excited N^+ ions. The reaction of N^+ with H_2 is slightly endothermic but the excess energy in the N^+ ions is sufficient to drive the reaction. The resulting NH^+ ion quickly undergoes a series of H-atom abstraction reactions with H_2 to form the terminating ion NH_4^+ which undergoes dissociative recombination to give NH_3. Reactions of this type are believed to form the bulk of interstellar molecules in dark clouds, although there is still a certain amount of doubt over the formation processes of some of the larger species, such as the cyanopolyynes - much of this is related to the lack of accurate laboratory studies on the reactivities of these species.

2. PAH/FULLERENE CHEMISTRY

In recent years, it has been suggested that a significant fraction of carbon is tied up in the form of small polycyclic aromatic hydrocarbon molecules. Such species appear to be required if a variety of observations, particularly those of the emission bands in the infrared are to be understood (see [6] for an up-to-date review of the subject). The influence of PAH, and fullerene, species on the chemistry of interstellar clouds has been discussed[7),8)]. It has been suggested that the majority of PAH molecules will be negatively charged even in diffuse clouds and that, since they will therefore carry the negative charge in these clouds, chemical models which incorporate dissociative recombination by free electrons in the gas phase may be seriously in error. In addition, PAH^+ ions have been suggested as the source of the diffuse interstellar absorption bands[9)]. The abundance of such molecules in the interstellar medium is uncertain. Although they are probably formed in the envelopes around late-type, carbon-rich stars,[10)] the mechanisms by which they are destroyed are unclear. It has been suggested that they are destroyed through being engulfed by supernova remnants[10)] on a time-scale of 10^8 years, while others[11)] have argued that they can be destroyed by oxygen atoms, although such a process may involve an appreciable activation energy barrier[12)].

More recently, there have been a number of experimental studies performed on the ion-neutral reactions of PAH and fullerene molecules, including C_{60} and C_{70} (see the review article [13)]). From these studies it is clear that doubly-charged PAH/fullerene cations are readily produced in the reaction of the neutrals with He^+ ions. The presence of such cations in interstellar clouds raises the possibility that their recombination with electrons may be dissociative rather than radiative, as is normally assumed for the singly-charged cations. The second ionisation potential of these neutrals is about 19 eV[14)] and the difference in energies between the first and second ionisation potentials - the energy released upon recombination - is about 12 eV. It is this large energy release which suggests that the recombination is dissociative rather than radiative. Note that since the energy difference is less than 13.6 eV, the general interstellar radiation field can produce doubly-charged PAH and fullerene cations in diffuse clouds[15)].

The influence of these new laboratory data on chemical models of diffuse and dense clouds has been investigated[16)]. In the particular case of dense clouds, if recombination is dissociative, and the molecules are not able to reform, a reasonable assumption,then all PAH/fullerene molecules are destroyed on a time-scale of $< 10^7$

years, while the time-scale in diffuse clouds is about 10^4 years because of the much larger electron abundance. This would suggest that PAH/fullerene species are not widespread in the interstellar medium. Although the thermodynamic properties of many PAH and fullerene molecules are remarkably similar, it is possible that the stability of the C_{60} sphere might ensure that the C_{60}^{++} + e reaction is radiative rather than dissociative. Thus C_{60} may be long-lived while PAHs, and particularly the smaller ones, are not. Laboratory studies are required to confirm this conjecture.

3. HOT MOLECULAR CORES

It has been become clear that an important component of molecular clouds in regions of star formation is contained in the so-called hot molecular cores (HMCs). These are small (0.01-0.1 pc), warm (100-300 K), dense (10^6-10^8 particles cm^{-3}) and opaque (N ~ 10^{23}-10^{24} cm^{-2}, A_V = 100-1000 mag) clumps of gas which contain unusual abundances of various types of molecule. In particular, small, saturated molecules such as NH_3, H_2S, CH_4 and CH_3OH are detected with fractional abundances enhanced over those in dark, dense clouds by factors of 100-1000; molecules containing deuterium, e.g. HDO, NH_2D, CH_3OD, and even a doubly-deuterated species, D_2CO,[17)] are readily detected and show deuterium enhancements of 100-1000 times the cosmic D/H ratio; and large, complex and relatively saturated molecules such as ethyl cyanide, CH_3CH_2CN, dimethyl ether, CH_3OCH_3, and methyl formate, $HCOOCH_3$, are detected[18)]. Since these observational facts are difficult to understand using conventional gas-phase chemistry,[19)] a consensus has emerged that the chemical composition of the hot gas is due to the evaporation of the icy mantles of dust grains due to the heating effects of nearby, newly-formed stars. In this type of picture there is an evolutionary sequence from cold, dark clouds with no embedded sources, such as TMC-1, in which molecules are observed in the gas phase, to cold regions, such as AFGL 2136, seen through infrared absorption toward protostars to contain dust having a rich molecular ice, to HMCs, such as the Hot Core and Compact Ridge regions in Orion, which have on-going star formation and anomalous gas-phase abundances. The chemistry of this type of sequence has been modelled[20),21),22)]. In this picture the hot core gas is chemically inert since it is largely composed of saturated, stable neutral molecules. For times up to 10^4 years after the mantle evaporation, little chemistry takes place because there is no ionisation from UV photons, and cosmic-ray ionisation is inefficient since the fractional ionisation produced by this means is inversely proportional to density. Radio observations of gas-phase species in hot cores may thus give important information on the physical and chemical processes occurring on the surfaces of cold dust particles; if this is so, radio observations are better able to detect the trace components of the mantles than direct IR measurements of the absorption bands due to the mantles themselves. As mentioned above, simple models appear to account reasonably successfully for the presence and amount of the smaller molecules and the degree of deuterium fractionation observed, providing that some molecular processing occurs in the grain mantle once material has been frozen out from the gas phase. However, these models are not able to account for the abundances of the larger molecules nor for the chemical differentiation observed between HMCs, including those which appear nearby in the sky. As examples of this, the Orion Hot Core, which has a density of 10^7 cm^{-3} and a temperature of 200 K is rich in nitrogen-bearing molecules, whilst the nearby Orion Compact Ridge, which has a density of 10^6 cm^{-3} and a temperature of 100 K, is rich in large, oxygen-bearing organic molecules. The chemistry of the Compact Ridge cloud has been modelled[19)] as due to the interaction of a wind containing H_2O and an ambient molecular cloud, following a previous suggestion,[23)] but the injected water is processed away from forming large oxygen-containing molecules. The evaporation of mantles rich in water ice was then studied[19)] but again poor agreement was found between calculated abundances and those observed. Finally, a model in which a methanol-rich mantle was evaporated was considered. In this case, good agreement between theory and observations was found, although there was no discussion as how different mantle compositions can arise in nearby regions - the Hot Core chemistry appears to be the result of the evaporation of ammonia-rich mantles[20]. Recent interferometric maps[24] of thermal CH_3OH, $HCOOCH_3$ and CH_3OCH_3 in Orion have shown that the spatial distribution of these molecules is consistent with the picture proposed in [19].

The hot gas-phase chemistry which occurs when simple molecules are released from the grain surfaces in hot core regions has been investigated in more detail[25] in an effort to see whether large complex molecules could be synthesised in the gas phase rather than on the grain mantles. It was shown that the evaporation of mantles which differed only in their NH_3/CH_3OH abundance ratio could account for the chemical differentiation observed in the Orion hot cores. In the Compact Ridge, release of CH_3OH drives the formation of methyl formate and dimethyl ether in the manner suggested by [19], namely that the released methanol takes a proton from H_3^+ and subsequently reacts with CH_3OH, to form CH_3OCH_3, or H_2CO, to form $HCOOCH_3$. The formation of other O-bearing molecules such as ketene, CH_2CO, and acetaldehyde, CH_3CHO, can be driven by the release of simple hydrocarbons such as ethene and ethane followed by protonation and reaction with oxygen atoms. Ethanol, CH_3CH_2OH, formation is slow in this model and gives a fractional abundance around 10^{-11}, in agreement with the upper limit of 5 10^{-10} derived by [23], but much less than the value of 10^{-6} derived by [18]. If correct, such an abundance would undoubtably imply a grain surface formation for ethanol. In any case, the gas-phase chemistry is unable to reproduce the fractional abundances of ethanol, ~ 10^{-8}, detected in other HMCs [26].

In the Orion Hot Core, which is denser and warmer, ion-molecule reactions play a less important role in driving the hot chemistry. NH_3 released from the grains is rapidly converted to the reactive CN radical which combines with the simple hydrocabons released to form complex, nitrogen-bearing species such as cyanoacetylene, HC_3N, and vinyl cyanide, CH_2CHCN. Ethyl cyanide, CH_3CH_2CN, is more difficult to form since the reaction of CN with C_2H_6 produces HCN and not ethyl cyanide[27]. A plausible scenario for the chemical differentiation between HMCs, involving both gas-phase and surface chemistry in a collapsing protostar, has been proposed[28]. The chemistry of two separated shells was followed for 10^5 years, at which time they are assumed to be impacted by a stellar wind from the protostar. The inner shell, which is dense, warm and molecular initially, was taken to represent the Orion Hot Core and the outer shell, less dense, colder and atomic initially, was taken to represent the Orion Compact Ridge. During the collapse phase, the surface chemistry of the two shells is different, molecules such as NH_3 and HC_3N dominating in the Hot Core and H_2O, CH_3OH and H_2CO dominating in the Compact Ridge. Important differences in the surface chemistry are related to the different grain temperatures which affect the evaporation rates of accreted material.

More recently, the hot gas-phase chemistry which results if alcohols more complex than methanol are evaporated from grains has been discussed[29]. Species such as methyl ethyl ether, $CH_3OC_2H_5$, and diethyl ether, $(C_2H_5)_2O$ can be formed with fractional abundances approaching 10^{-8} for an injected ethanol abundance of 10^{-6}. The abundances of these species scale with the adopted ethanol abundance.

4. OXYGEN-RICH CIRCUMSTELLAR SHELLS

Over the last few years, an increasing number of molecules containing carbon atoms have been detected in the circumstellar envelopes (CSEs) around late-type oxygen-rich stars. Since carbon should be entirely tied up in the stable CO molecule, the origin of the carbon in other molecules has been a matter of investigation. It has been suggested[30),31] that the photodissociation of methane, CH_4, provided the carbon even though there is no evidence for its presence from either observation or theory. Recently, the hypothesis that methane is the primary source of the reactive carbon has been tested by investigating its chemistry in more detail[32]. In particular it has been shown that H_2CO is a detectable molecule, since it is formed in the $CH_3 + O$ reaction, in which CH_3 and O are the photodissociation products of CH_4 and H_2O, respectively. Radial column densities and predicted antenna temperatures for a number of millimeter transitions have been tabulated for a number of likely sources[32]. The column densities of other molecules formed by the reactions of CH_3, namely H_2CN

and H_2CS, are at least an order of magnitude smaller than that of H_2CO and are therefore undetectable with current instruments. As a by-product of these calculations, column densities for the ion SO^+ have also been estimated. SO^+ has recently been detected toward the supernova remnant IC 443[33)] suggesting that it arises in chemistry driven by the interaction between the remnant and small clumps of molecular gas, although it is more likely a result of chemistry in a photon-dominated region[34)]. In O-rich CSEs, the SO^+ ion is formed readily by the reaction of S^+ and OH and lost by photodissociation and by dissociative recombination with electrons. Column densities fall in the range 2 10^{12} - 2 10^{13} cm^{-2} for mass-loss rates in the range 2 10^{-7} - 2 10^{-5} solar masses per year (see Figure 1). Although the dipole moment of SO^+ is relatively large, 2.2 Debye, the lines are expected to be weak but may be detectable with a large telescope.

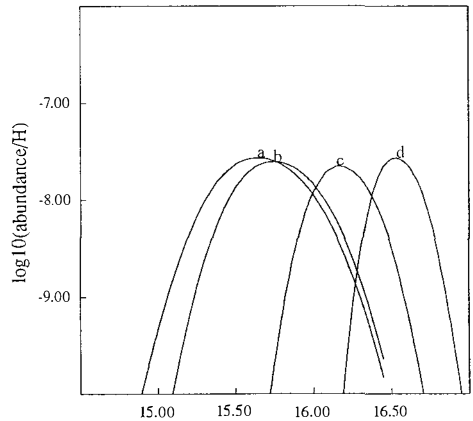

Figure1: The radial distribution of SO^+ is shown as a function of mass-loss rate: (a) 2 10^{-7}, (b) 5 10^{-7}, (c)5 10^{-6}, (d) 2 10^{-5} solar masses per year.

ACKNOWLEDGEMENT

Astrophysical research at UMIST is supported by a grant from the SERC. I am very grateful to Thierry Montmerle for his invitation to attend the meeting, his hospitality and for financial assistance.

REFERENCES

1. Millar T J & Williams D A 1988, *Rate Coefficients in Astrochemistry,* Kluwer:Dordrecht
2. Singh P D 1992, *The Astrochemistry of Cosmic Phenomena,* Kluwer:Dordrecht
3. Ikezoe Y, Matsuoka S, Takebe M & Viggiano A 1987, *Gas Phase Ion-Molecule Reaction Rate Coefficients Through 1986,* Maruzen Co. Ltd.:Tokyo
4. Anicich V G 1993, ApJS, in press
5. Herbst E & Millar T J 1991, in *Molecular Clouds,* eds. R A James & T J Millar, Cambridge University Press:Cambridge, p.209
6. Tielens A G G M 1993, in *Dust and Chemistry in Astronomy,* eds. T J Millar & D A Williams, IOP Publishing Ltd.:Bristol, p.99
7. Lepp S & Dalgarno A 1988, ApJ, 335, 769
8. Lepp S, Dalgarno A, van Dishoeck E F & Black J H 1988, ApJ, 329, 418
9. Leger A, d'Hendecourt L E B, Vestraete L & Schmidt W 1988, A&A, 203, 145
10. Latter W B 1991, ApJ, 377, 187
11. Duley W W & Williams D A 1986, MNRAS, 219, 89
12. Flower D R, Heck L & Pineau des Forets G 1989, MNRAS, 239, 741
13. Bohme D K 1992, Chem Rev, 92, 1487
14. Hrusak J & Schwarz H 1993, Chem Phys Lett, 205, 187
15. Leach S 1986, J Electron Spectrosc Relat Phenom, 41, 427
16. Millar T J 1992, MNRAS, 259, 35P
17. Turner B E 1990, ApJ, 362, L29
18. Turner B E 1991, ApJS, 76, 617
19. Millar T J, Herbst E & Charnley S B 1991, ApJ, 369, 147
20. Brown P D, Charnley, S B & Millar T J 1988, MNRAS, 231, 409
21. Brown P D & Millar T J 1989, MNRAS, 237, 661
22. Brown P D & Millar T J 1989, MNRAS, 240, 25P
23. Blake G A, Sutton E C, Masson C R & Phillips T G 1987, ApJ, 315, 621
24. Minh Y C, Ohishi M, Roh D G, Ishiguro M & Irvine W M 1993, ApJ, in press
25. Charnley S B, Tielens A G G M & Millar T J 1992, ApJ, 399, L71
26. Millar T J, Olofsson H, Hjalmarson A & Brown P D 1988, A&A, 205, L5
27. Lichtin D A & Lin M C 1985, Chem Phys, 96, 473
28. Caselli P, Hasegawa T I & Herbst E 1993, ApJ, in press
29. Charnley S B, Kress M E, Tielens A G G M & Millar T J 1993, ApJ, in preparation
30. Nejad L A M & Millar T J 1988, MNRAS, 230, 79
31. Nercessian E, Guilloteau S, Omont A & Benayoun J J 1989, A&A, 210, 225
32. Millar T J & Olofsson H 1993, MNRAS, in press
33. Turner B E 1992, ApJ, 396, L107
34. Sternberg A & Dalgarno A 1993, private communication

Molecular Emission of the Circumstellar Envelope IRC+10216

M. Guélin[1], R. Lucas[1], J. Cernicharo[2]

[1] IRAM, 300 rue de la Piscine, F-38406 St. Martin d'Hères, France
[2] Centro Astronomico de Yebes, Apartado 148, E-19080 Guadalajara, Spain

Abstract

Millimeter wave interferometers allow to study with arc second resolutions the molecular emission from opaque circumstellar envelopes. We present here recent data on IRC+10216, the prototypal C-rich envelope, obtained with the IRAM Plateau de Bure interferometer.

Claudine Kahane, J.C., M.G., and Jesus Gómez-González in 1985, during one of the very first observing runs with the 30-m telescope, discussing the discovery of an enigmatic new radical in IRC+10216. The radical was identified 8 years later with MgNC by K. Kawaguchi.

1 The IRC+10216 envelope

During the phase of high mass loss, red giants are surrounded by thick, dusty envelopes transparent only to far infrared and radio wavelengths. The gas in the envelopes is predominantly cold and molecular; it mainly radiates in the rotational lines of CO and of number of polar molecules. The rotational lines, many of which are readily detectable with large millimeter radiotelescopes, are the best tool for studying these objects. From their velocity profiles, one can derive a 3-D view of the envelopes and learn about the mass loss histories. From their brightness distributions, one can follow in time and space the ongoing chemistry; this latter, although similar in many respects to interstellar chemistry, is much easier to apprehend because of the simpler geometry and velocity field.

The most remarkable and (presumably) closest massive envelope is associated with the bright IR object IRC+10216 (CW Leo). IRC+10216 was first studied by Becklin *et al.* (1969) who observed intensity variations with a period of 2 yr and concluded it was a Mira-type variable enshrouded in a dusty shell. The distance D to IRC+10216 is poorly known. Becklin *et al.* (1969), from the lack of apparent motion of the fuzzy optical image over a period of 15 yr, derived a 'probable' lower limit of $D > 100$ pc (one arrives at a similar limit by considering the radio data presented by Lucas & Guilloteau 1992); Herbig & Zappala (1970), assuming a bolometric magnitude of -7, estimated a distance of 290 pc; recently, Winters *et al.* (1993), from a detailed modelling of the object luminosity, arrive at a distance $D = 170$ pc. For the sake of simplicity, we adopt below the commonly used value of 200 pc, for which $1''$ corresponds to $3\ 10^{15}$ cm. The radius of the central star ($\sim 1000 R_\odot$) is then $\simeq 0.02''$. The radius of the IR shell, the region where dust forms and the gas is accelerated, is 0.2–0.5$''$ (Bloemhof *et al.* 1988).

The outer envelope consists of a dense spherical core, of radius $R \simeq 20''$, and of an extended halo (Fig. 1). The 'core' is observed in the lines of 50 different molecules (Table 1); the halo is observed in the mm lines of CO and in the 492 GHz line of CI (Keene *et al.* 1993). ^{12}CO, which is after H_2 the most abundant molecule and the best shielded from dissociation by interstellar UV photons, extends up to a distance of $170''$ (or $5\ 10^{17}$ cm) from the star (see Fig. 1). The expansion velocity being 14.5 kms^{-1}, the gas from the outer layers of the envelope has been expelled some 11000 years ago.

The 'CO envelope' has been modeled by several authors (Kwan & Linke 1982, Sahai & Wannier, Truong-Bach *et al.* 1991). The results, rather discrepant, seem to indicate that the envelope density decreases more slowly than R^{-2}, i.e. that the mass loss has decreased in the last thousand years (from $8\ 10^{-5} M_\odot$ yr^{-1} 10^4 yr ago, to $2\ 10^{-5} M_\odot$ yr^{-1} a few hundred years ago. However, line opacity and temperature variations make this interpretation disputable.

The Bure interferometer is ideally suited to study IRC+10216's dense core. Its primary field has a FWHP of $50''$ at $\lambda = 3$ mm and its synthetized beam can be as small as $2''$. The large effective area of the instrument (460 m^2 since April 1993) makes it sensitive enough to map with a few arcsec resolution tens of molecular lines. The possibility to observe simultaneously two 500 MHz-wide IF bands with a good frequency resolution allows to study 5–10 lines in a single observing session.

A program of mapping the λ 3 mm lines of the chemically most significant molecules is under way at Bure (Lucas 1992, Lucas *et al.* 1992, Guélin *et al.* 1993, Lucas *et al. in*

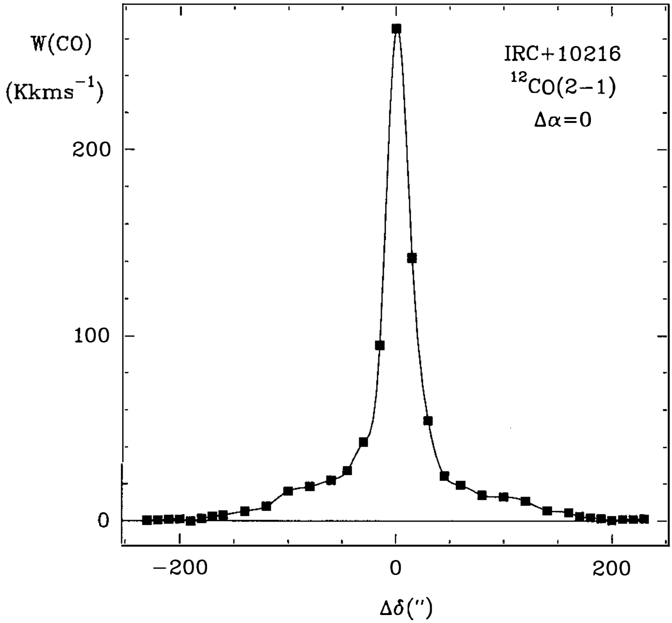

Figure 1: ^{12}CO J=2–1 line emission along a strip at constant **r.a.** passing through CW Leo. *Abscissa*: offset from central star (in arcsec); *ordinate*: intensity (in K.kms^{-1}) integrated over a 13 kms^{-1} velocity interval, centred on v_{sys} (-34 kms^{-1} $< v <$ -21 kms^{-1}). Note the halo component which extends from $R = 30''$ to $R = 170''$ (the contribution from the telescope error beam is negligible on this scale). The data were observed with the IRAM 30 m telescope and have an angular resolution of 12$''$ (Guélin & Cernicharo, *in preparation*).

Table 1: Molecules observed in IRC+10216 (as of Jan. 1st 1994)

– inorganic, stable molecules:		$\mathbf{CO}$	$\mathbf{NaCl}$	$\mathbf{H_2S}$	NH_3	SiH_4
		$\mathbf{CS}$	$\mathbf{KCl}$			
		$\mathbf{SiO}$	$\mathbf{AlF}$			
		$\mathbf{SiS}$	$\mathbf{AlCl}$			
			$\mathbf{NaCN}$			
– organic, stable molecules:		$\mathbf{HCN}$	$\mathbf{CH_3CN}$	$\mathbf{HC_3N}$	CH_4	C_2H_2 C_2H_4
– reactive molecules:	carbon chains	C_3	C_5	$\mathbf{SiC_4}$		
		$\mathbf{HC_5N}$	HC_7N	HC_9N	$HC_{11}N$	
		$\mathbf{H_2C_3}$,	$\mathbf{H_2C_4}$			
		$\mathbf{C_2S}$	$\mathbf{C_3S}$	C_5S		
	linear radicals	$\mathbf{C_2H}$	$\mathbf{l\text{-}C_3H}$	$\mathbf{C_4H}$	$\mathbf{C_5H}$	$\mathbf{C_6H}$
		$\mathbf{CN}$	$\mathbf{C_3N}$	$\mathbf{HCCN}$		
		$\mathbf{CP}$				
		$\mathbf{SiC}$	$\mathbf{SiN}$	$\mathbf{MgNC}$		
	isomers	$\mathbf{HNC}$				
	cycles	$\mathbf{c\text{-}C_3H}$	$\mathbf{c\text{-}C_3H_2}$	$\mathbf{SiCC}$		
	ion	$\mathbf{HCO^+}$				

(The molecules detected at millimeter wavelengths are in boldface character. The detections of HCO^+, H_2S and C_5S are based on only one transition)

preparation). 14 molecules have been observed to date: the carbon-chain radicals C_nH, n= 2–6, HC_5N, CO, CS and C_3S, SiO, SiS and SiC_2 and the metal compounds NaCl and MgNC. The synthetized beam sizes range from 10″ (for CCH and C_5H, two of the very first maps observed with the Bure interferometer) to 3″ (for the SiS map). In addition, vibrationally excited lines of C_4H and of HCN (Lucas & Guilloteau 1992) have been observed. Complementary programmes, with larger field of view, but a lower resolution and a poorer sensitivity, are also in progress with the BIMA (see Bieging & Tafalla 1993, Bieging 1993 and references herein) and the NMA (Takano *et al.* 1992) interferometers; these include maps of other transitions of C_4H, SiS, SiC_2 and HCN, as well as of 3 mm transitions of CN, C_3N, HNC and HC_3N. Finally, maps of 2 mm and 1.3 mm transitions of several species were observed with the IRAM 30-m telescope with 12–17″ angular resolutions (Kahane *et al. in preparation*).

Figure 2 shows four examples of the Bure maps: the emissions of the 95 GHz lines of MgNC and C_4H and of the 91 GHz lines of NaCl and SiS, integrated over a 13 kms^{-1}-wide band centered at $v_{sys}= -26.5$ kms^{-1}, the source systemic velocity. The spatial resolution is 5″ (3″ for SiS) and corresponds to 1.5 10^{16} cm.

2 What can we learn from Fig. 2?

The outer IRC+10216 envelope is known to expand with a fairly constant radial velocity (-14.5 kms^{-1}), so that the velocities close to v_{sys} plotted in Fig. 2 arise from a thin conical

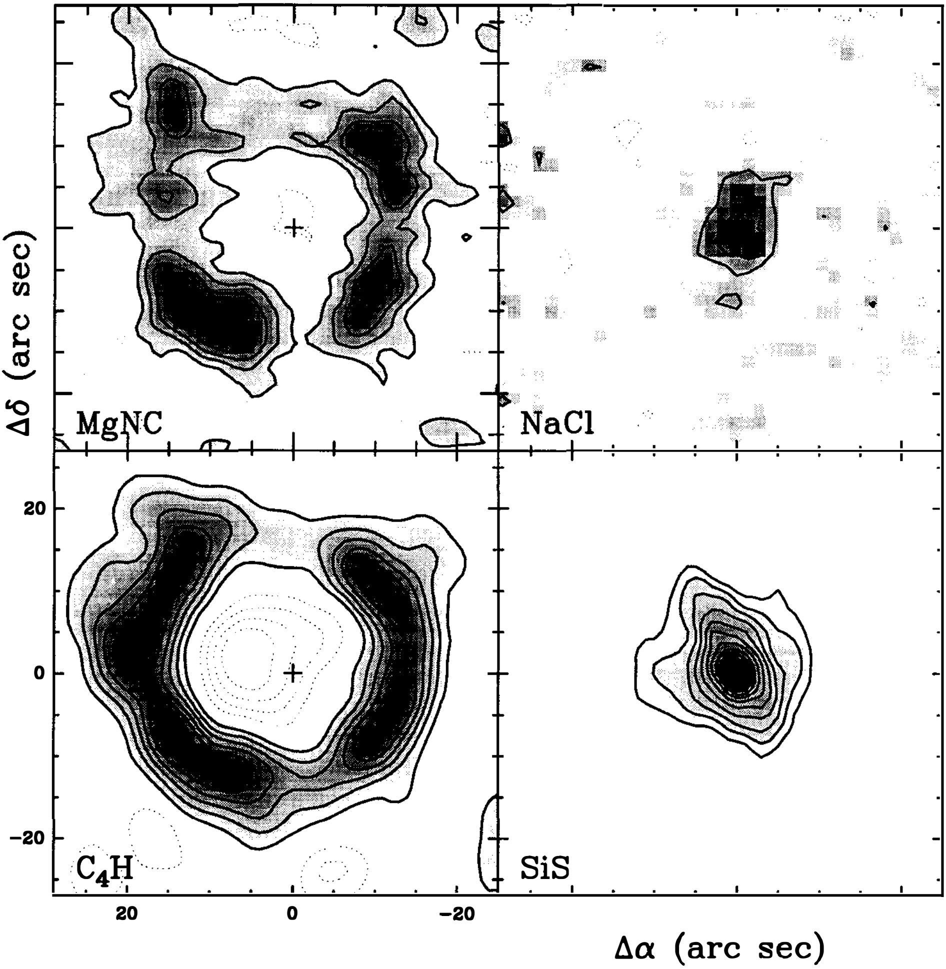

Figure 2: The intensity distributions in the 95 GHz lines of MgNC and C_4H (*left*) and in the 91 GHz lines of NaCl and SiS (*right*), integrated over the velocity interval -34 $kms^{-1} < v < -21$ kms^{-1}. The observations were made with IRAM interferometer; the angular resolution is $5'' \times 5''$, except for the SiS map where it is $3'' \times 2''$. The maps are not corrected for attenuation by the primary beam (HPBW 55″).

sector, axed on the line of sight and cutting through the envelope along the meridian plane. The contours represent roughly the line brightness distribution across this plane (the larger thickness of the conical sector at the edges is partly compensated by the primary beam attenuation).

The first thing which strikes in Fig. 2 is difference between the brightness distributions of the left and right maps: obviously, the MgNC and C_4H emissions arise mostly from a thin shell with a radius of $\simeq 15''$, whereas those of SiS and NaCl are much narrower and centrally peaked. The second is that despite their factor of 5 difference in the contour levels (note the higher noise in the MgNC map), the MgNC and C_4H brightness distributions are very similar. They show the same clumpy appearance (the bright clumps having almost exactly the same position on both maps) and the same intensity minima to the N and the SE. The central 'hole' seems more pronounced in C_4H than in MgNC (see the dotted negative contours), but this largely comes from the observing procedure. Whereas the MgNC map of Fig. 2 results from a combination of an interferometer map and of a single-dish map (made with the IRAM 30-m telescope), the C_4H map is the combination of the interferometer map with a *single* 30 m spectrum and lacks spacings $<$ 24m (see Guélin *et al.* 1993).

The NaCl and SiS sources are much more compact than the MgNC and C_4H sources and fit inside the central 'hole' of these latter. They are however well resolved and are elongated in the NS or NE-SW direction. North-NE to South-SW is also the direction of elongation of the infrared source and of the fuzzy optical picture published by Becklin *et al.* (1969).

The differences between the left and right maps in Fig. 2 cannot be explained only by the envelope structure and/or line excitation effects. Obviously, the 'central hole' is not due to lack of gas and the central peak is not just an excitation artifact: it is observed as well in the easy to excite CO molecule (dipole moment μ = 0.11 D – see Fig. 1), as in the hard to excite species SiS and NaCl (μ = 10 D), and not observed in C_4H (μ= 0.7 D), HC_5N (μ = 4 D) and MgNC (μ = 5 D). These differences must result from chemistry.

3 Chemistry in IRC+10216

The temperature, density and radiation in IRC+10216 are highly contrasted, laying the ground for a large variety of chemical processes. The atmosphere of the star ($R \leq 2R_*$) is dense and warm enough for exo- and endothermic 3-body reactions to proceed efficiently. It must be close to thermodynamical chemical equilibrium; the most abundant C- and Si-bearing molecules are CO, HCN, H_2C_2, SiO and SiS (Tsuji 1973, McCabe *et al.* 1979, Lafont *et al.* 1982). The temperature drops further out, in the inner envelope ($R \sim 10R_*$), where most 'heavy' atoms ($A \geq 12$ a.m.u.) and molecules condense onto grains.

The outer envelope ($R >> 20R_*$) is penetrated by the interstellar UV radiation which dissociates the 'parent' molecules (H_2C_2, HCN,..) still present in the gas phase. The radicals and ions produced by photodissociation fuel a rich gas phase chemistry (Glassgold *et al.* 1986, Millar 1990, Cherchneff *et al.* 1993). Finally, the grains transiting from the inner to the outer envelope are likely to be covered with mantles formed of adsorbed molecules. These mantles may partly evaporate in the outer envelope, when exposed to

UV radiation (photodesorption) or to shocks, releasing new molecules and radicals in the gas. At the outer edge of the envelope, the interstellar UV radiation dissociates even the most resistant species, CO and, finally, H_2.

In Cherchneff *et al.* (1993) model, SiS is a 'parent' molecule coming from the stellar atmosphere. Its distribution, is expected to peak on the star, as is observed in Fig. 3. In contrast, C_4H is formed from CCH by radical-radical reactions, in the outer envelope. It should thus have a shell-like distribution, as observed in Fig. 2. For a mass loss rate of 2 $10^{-5} M_{\odot} yr^{-1}$ and a 'normal' interstellar UV field, Cherchneff et al. predict a radius for the C_4H shell of 4-5 10^{16} cm, in perfect agreement with what is observed.

The observed maps are however much too detailed to be fully explained by simple chemical models. The C_4H and MgNC rings in Fig. 2 show bright patches which, remarkably, have nearly the same positions for both molecules (the small differences can be caused by the relatively high noise in the map of the weak MgNC emission). In fact, C_3H, another carbon chain molecule with relatively strong molecular lines, has almost exactly the same brightness distribution than C_4H. These similarities led Guélin *et al.* (1993) to suggest that photodissociation and gas phase reactions (radical-radical and ion-molecule reactions) may not be the whole story and that we may be observing at $R = 15''$ molecule desorption from dust grains.

4 Bipolar nebula and binary star?

The bright emission rings on Fig. 2 appear dimmer to the N and the SW. A similar pattern is observed for about all the molecules showing a shell-like brightness distribution. Very probably, these faint areas correspond to holes in the envelope. The holes define a N-SW axis more or less aligned with the major axis of the SiS source and with that of the IR source (P.A.= 20° according to Dyck *et al.* 1987). The outflow from the central star may not be as symmetrical as suggested by the fairly spherical CO outer envelope and may occur preferentially along a N-S axis, roughly perpendicular to the line of sight. The presence of a bipolar flow in IRC+10216 was already suggested by Serkowski (see Dyck *et al.* 1987) to explain the large intrinsic polarisation observed in the fuzzy optical source and by Dyck *et al.* (1987) to explain the shape of the IR source.

Finally, although the SiS and NaCl sources are centred right on the star (whose position, which coincides with the compact continuum source detected at λ 3 mm, is indicated by a cross in Fig. 2), the MgNC and C_4H sources are clearly shifted 2-3$''$ eastwards. This shift denotes that the outer shell has drifted by 10^6 cm with respect to the star in the last 10^4 yr; the most likely cause of this shift is that the central star is a long period binary system (Guélin *et al.* 1993).

References

Becklin, E.E., Frogel, J.A., Hyland, A.R., Kristian, J., Neugebauer, G. 1969 *Astrophys. J.* **158**, L133.
Bloemhof, E.E., Danchi, W.C., Townes, C.H. 1985 *Astrophys. J.* **299**, L37.
Bieging, J.H., Tafalla, M. 1993 *Astronomical J.* **105**, 576.

Bieging, J.H. 1993, in IAU Coll. 140, *Astronomy with Millimeter & Submillimeter Wave Interferometry*, Hakone, Japan Oct. 1992.
Cherchneff, I., Glassgold, A.E., Mamon, G.A. 1993 *Astrophys. J.* **410**, 188.
Cherchneff, I., Glassgold, A.E. 1994 *Astrophys. J. in press.*
Dyck, H.M., Zuckerman, B., Howell, R.R., Beckwith, S. 1987 *Publ. Astr. Soc. Pacific*, **99**, 99.
Glassgold, A.E., Lucas, R., Omont, A. 1986 *Astron. Astrophys.* **157**, 35.
Keene, J., Young, K., Phillips, T.G., Buttgenbach, H., Carlstrom, J.E. 1993 *Astrophys. J. in press.*
Kwan, J., Linke, R.A. 1982 *Astrophys. J.* **254**, 587.
Lafont, S., Lucas, R., Omont, A. 1982 *Astron. Astrophys.* **106**, 201.
Lucas, R. 1992 in *Astrochemistry of Cosmic Phenomena*, Ed. P.D. Singh, (publ. Kluwer: Dordrecht), p. 389.
Lucas, R., Guilloteau, S. 1992 *Astron. Astrophys.* **259**, L23.
Lucas, R. *et al.* 1992 *Astron. Astrophys.* **262**, 49.
McCabe, E.M., Smith, R.C., Clagg, R.E.S. 1979 *Nature*, **281**, 263.
Nejad, L.A.M, Millar, T.J. 1987 *Astron. Astrophys.* **183**, 279.
Sahai, R., Wannier, P.G. 1985 *Astrophys. J.* **299**, 424.
Takano, S., Saito, S., Tsuji, T. 1992 *Publ. Astr. Soc. Japan*, **44**, 469.
Truong-Bach, Morris, D., Nguyen Q. Rieu 1991 *Astron. Astrophys.* **249**, 435.
Tsuji, T. 1973 *Astron. Astrophys.* **23**, 411.
Winters, J.M., Dominik, C., Sedlmayr, E. 1994 *Astron. Astrophys. in press.*

THREE ASPECTS OF THE DYNAMICS OF MOLECULAR GAS

Jean - Pierre CHIEZE

Centre d'Etudes de Bruyères-le-Châtel, Service PTN
91680 Bruyères-le-Châtel, France

ABSTRACT

Morphology, dynamics and chemical abundances provide most of the informations one can obtain on cold molecular clouds. So far, these three aspects have been studied somewhat independently, but it becomes more and more evident that they are intimately coupled. We present some of the efforts made by different authors to make the transition from a static picture of interstellar clouds to that of dynamically and chemically evolving objects. It is a rather difficult task, which requires the calculation of the interplay between dynamics, thermal processes and time dependent chemistry. Noticeably, regarding clouds as dynamically evolving objects provides a new and promising approach of the interstellar chemistry.

1. INTRODUCTION

Informations on star forming clouds are obtained from three main sources : their morphology (mass distribution and fragmentation), their dynamical state (addressing the problem of supersonic turbulence) and their chemical content (the problem of anomalous abundances of various molecules). So far, these three aspects have been studied relatively independently. The morphology of molecular clouds is not, at the present time, completely aprehended. Even salient features, like Larson's relations, are not theoretically definitely well understood, or even not accepted. Noteworthing some computations of the interaction of (molecular) interstellar clouds with supernovae remnants, only very few calculations have been performed on their dynamical evolution, and when it has been done, it was by using oversimplified polytropic "equations of state". Interstellar chemistry has long been developed in the framework of "pseudo time dependent" models, that is under fixed density and temperature conditions. However, clouds are highly inhomogeneous and the physical conditions are evidently highly time dependent. It would be a formidable task to elaborate cloud models which would include self-consistently even the main features of their morphological, dynamical and chemical evolution.

The best one can do at present is to couple, step by step and in the most simple way, some of these different aspects. For exemple, a simplified chemical network can provide a good estimation of the thermal balance between heating and cooling processes, which can drive some of the dynamical evolution of molecular clouds. Once this is computed and accepted, the main features of the evolution – time scales, condensation ratios, etc ..., can serve as inputs for a calculation of the chemical history of a cloud parcell, on which the main effort is put on the quality of the chemical network, and so on. I present in the followings some attempts in this line.

One of the most vividely debated general property of molecular cloud complexes is perhaps the significance of observed scaling laws between the mass, the velocity dispersion and the size of different substructures in a cloud complex. Since their discovery by Larson (1981), their very existence and interpretation have been at the center of many discussions. This point is examined in Section 1.

The fragmentation of the molecular gas may have a profound incidence on the dynamical time scale of the evolution of a cloud complex, and also on the penetration of the ultraviolet radiation field in the depths of molecular clouds. Possible mass exchanges between gas phases of different densities may provide a radically new background to the problem of the molecular cloud chemistry. However, a lot of observations point to the existence of numerous clumps which are not confined by self–gravitation. The origin of these unbounds clumps, which may have a large density contrast with the ambient gas is presently unclear. However, we show in Section 2 that the ultraviolet interstellar radiation field may play some role in their formation.

The observation of the molecular abundances can also shed light on the dynamical state of cold interstellar gas. Section 3 sumarizes to which extent the consideration of dynamical phenomenons modifies the standard picture of interstellar chemistry.

2. CLOUD MORPHOLOGY

Molecular clouds and their clumps often appear to obey definite scaling laws, first noticed by Larson (1981). Since this original work, in which the data sample was inhomogeneous, the correlations between the mass, the radius and the velocity dispersion of various regions have been confirmed by many authors (for exemple : Tomita, Saito & Ohtani 1979, Leung, Kutner & Mead, 1982, Myers 1985, Dame et al. 1986, Falgarone & Pérault 1987, Scoville et al. 1987, Solomon et al. 1987, Fuller & Myers 1992).

But, following the point of view of Kegel (1989), one could argue that the basic scaling law, $M(L) \propto L^2$, is nothing but an observational bias, related to the sensitivity limit of the observations : this scaling implies a definite column density for all observed structure, which correponds to a visual extinction $A_v \sim 1\ mag$. But the velocity dispersion appears also to scale as $\sigma(L) \propto L^{1/4}$. This statement, which refers now to the dynamical state of the clouds, is independent of the evaluation of the $M - L$ relation, and is consitent, if virial equilibrium is assumed, with an actual mass distribution very close to the mass – radius scaling law.

Various tentative physical interpretations of Larson's relations have been proposed. Attempts based on the so–called Kolmogorov cascade turned soon to be unsatisfactory. A first class of models assumes that substructures can be regarded as virialized clouds in an ambiant contant pressure. It is the uniformity of this pressure which would be at the origin of the scaling laws. Chièze (1987), argued that it could be the result of fragmentation, at the threshold of gravitational instability, followed by the virialization of the fragments. The fragmentation process may be effective from a temperature of about 8000 K down to 100 K, where thermal stability is recovered, provided that at each fragmentation stage, the interclump gas pressure remains close to its constant and uniform interstellar value . The hierarchy would then cover the scales between 100 pc and 1 pc. However, the purely thermal interstellar pressure assumed in Chièze (1987) is too low if compared to the upper bound of the more commonly admitted value $\tilde{P} = P/k = 4000 - 20000\ Kcm^{-3}$. Similar approaches have been followed by Maloney (1988) and Elmegreen (1989).

Alternatively, a magnetic field of strength B can support clouds of mass less than the critical mass (see e.g. Mouschovias (1976)):

$$M_{cr} \approx 10^3 \left(\frac{B}{30\mu G}\right) \left(\frac{L}{2\text{pc}}\right)^2 M_{odot}$$

(Equ (2) of Shu, Adams and Lizano (1987)). But again, this would require that all clumps have the critical mass and that the magnetic field is practically uniform.

Another line of attack may be found in evaluating the momentum and energy tranfer in a clumpy medium. Consider the total momentum flux at any point of the medium where the density is ρ, thermal pressure p and velocity u. Let $\mathbf{g}$ and $\mathbf{B}$ be the local gravitational acceleration and magnetic field. Since gravity and magnetic fields are of prime importance, it is usefull to derive an exact expression of the momentum flux which include them. This can be achieved, using the Poisson equation for the gravitational field :

$$\nabla.\mathbf{g} \;=\; 4\pi G\rho \tag{1}$$

It turns out that the net momentum flux can be written as a two rank tensor of cartesian components :

$$\mathrm{P}_{ij} \;=\; \left(p - \frac{g^2}{8\pi G} + \frac{B^2}{8\pi}\right)\delta_{ij} + \rho u_i u_j + \frac{1}{4\pi G}g_i g_j - \frac{1}{4\pi}B_i B_j \tag{2}$$

Gravity has been explicitely introduced in the stress P_{ij}, and exhibits a formal equivalence with the magnetic field. A consequence of the Newton law is that the *total external force* exerted on the unit volume of gas by the pressure, the gravitation and magnetic fields, can be written as :

$$\mathbf{F} \;=-\nabla.\mathbf{\Phi} \tag{3}$$

where the cartesian components of $\mathbf{\Phi}$ are :

$$\Phi_{ij} \;=\; \left(p - \frac{g^2}{8\pi G} + \frac{B^2}{8\pi}\right)\delta_{ij} + \frac{1}{4\pi G}g_i g_j - \frac{1}{4\pi}B_i B_j \tag{4}$$

According to the preceding results, the variation of the kinetic energy $\mathcal{T} = \int \rho u^2/2\; dV$ of gas motions in a given mass of fluid can be written as :

$$\frac{d\mathcal{T}}{dt} = -\oint u_i \Phi_{ik} dS_k + \int \Phi_{ik}\frac{\partial u_i}{\partial x_k}dV \tag{5}$$

The total time derivative of the kinetic energy has been expressed as the sum of two terms. The first surface integral represents the work done per unit time by the stress $\mathbf{\Phi}$, flowing through the surface of the system; the second volume integral, the work done by the stress in the bulk of the system.

Consider now a fragmented sytem of mass M_L and scale L, in which matter is essentially concentrated in N_L fragments of scale l and mass m_l. The first surface integral in Equ (5) should then be taken over the total surface Σ of all the N_L fragments. Stationary states of the fragmented system are thus characterized by the equality :

$$\oint_\Sigma u_i \Phi_{ik} dS_k = \int \Phi_{ik}\frac{\partial u_i}{\partial x_k}dV \tag{6}$$

where the surface integral has been extended to the total surface of the clumps.

Since the mean velocity of a clump in the center of mass of the system is $< U >_L$, and approximating furthermore Σ by $4\pi N_L l^2$, the first surface integral scales as :

$$W_1 \sim < U >_L < \Phi >_L N_L l^2 \tag{7}$$

and the second volume integral as :

$$W_2 \sim < \Phi > \frac{< U >_L}{L} L^3 \tag{8}$$

If the mass of the interclump medium can be neglected (which is the case for L>1pc, where most of the mass is actually in the fragments), one has $N_L m_l = M_L$. The requirement that $W_1 = W_2$ implies the definite scaling :

$$\frac{M_L}{m_l}\frac{l^2}{L^2} = 1 \tag{9}$$

As it stands, the relation $M \propto L^2$ could be interpreted as the result of the energy exchanges in a system of scale L fragmented in $N_L = \left(\frac{L}{l}\right)^2$ sub–systems. In this way the effective area of the system as a whole remains proportional to the square of its linear extension. As long as dissipation of the kinetic energy can be ignored, the gravitational and magnetic energies stored in the bulk of a structure feeds up the internal kinetic energy of its substructure. Dissipation through gas cooling should take place at the scale where most of the gas is no more concentrated in clumps. According to Falgarone and Pérault (1987), this occurs typically at the scale of about 1 parsec. Note that calculations of hydrostatic clumps taking into account the relevant heating and cooling processes show that it is precisely the radius above which the *envelopes* of such clumps would become thermally unstable. Below the correponding mass of about $10^3 M_\odot$, the fragmentation hierarchy appears to break down, since then dense cores comprize only a small fraction of the mass of a cloud.

An alternative view can be the following. Equation (5) can also be written as :

$$\frac{d\mathcal{T}}{dt} = -\int u_i \frac{\partial \Phi_{ik}}{\partial x_j}\, dV \tag{10}$$

The stress $\mathbf{\Phi}$ can decomposed into its internal part $\mathbf{\Phi_i}$ and its external part $\mathbf{\Phi_e}$. Accordingly, a steady state requires :

$$\mathbf{\Phi}_i = \mathbf{\Phi}_e \tag{11}$$

The rate at which energy is flowing through the surface of the clumps (Eq. 7) can be written in a slightly different form. Introducing the clump number density n_L, one has : $W_1 \sim \Phi L^3 (n_l l^2 U_L) = \mathcal{E}/t_c$ since, to a factor about unity, $\mathcal{E} = \Phi L^3$ is the total gravitational plus magnetic energy of the system, while $(n_l l^2 U_L)$ is the inverse of the mean collision time t_c between clumps. Similarly, defining the dynamical time of the clump system as a whole as $t_d = U/L$, one has : $W_2 \sim \mathcal{E}/t_d$. This remark led Henriksen and Turner (1984) to postulate that a resonance should occur when $t_c = t_d$, from where a complete theory of the self similar evolution of cloud systems has been established (Henriksen 1986, Lattanzio and Henriksen 1988, Henriksen 1991).

Finally, a further consequence of Eq. (9) would be :

$$\mathrm{tr}\ \mathbf{P} = 3p + \rho u^2 - \frac{g^2}{8\pi G} + \frac{B^2}{8\pi} = \mathrm{Const.} \tag{12}$$

This may be a plausible generalization of the requirement of uniformity of the interstellar gas pressure, explicitely viewed as the sum of the thermal, kinetic, gravitational and magnetic pressures. It has been noticed by Larson (1989) that this "universal" value of this generalized pressure, with a magnetic field of about $30\mu G$ as observed in dense molecular gas (Myers and Goodman 1988), combined to a sound velocity of 0.2 km s^{-1} results precisely in a Jeans mass of 1 $M_\odot$

In fact, many clumps may not be in gravitational virial equilibrium, but more likely confined by the pressure of the ambient medium, in violation of the Larson's relations. This essential point has been examined by McKee (1989) and Bertoldi and McKee (1992). In this approach, ionization regulates the collapse of cloud fragments. Recent observations can be found in Falgarone, Puget and Pérault (1992). In the model propsed by McKee, the penetration of UV radiation regulates the collapse of clumps. We show in the followings that some of these unbound clumps could be in fact transient features arising from the thermodynamical properties of the molecular gas.

II. THERMAL PROCESSES AND THE GENERATION OF TRANSIENT CLUMPS AND TURBULENCE

Far from all clumps are really gravitationally bound. Some of them could be the result of the interaction of the molecular gas with the ultraviolet interstellar radiation field. In fact, in regions where the visual extinction is less than one magnitude, the UV field is a major energy input for the interstellar gas. This limit in magnitude is only indicative, and relevant for the *standard* value of the interstellar radiation field (IRF). In a fragmented medium, the shielding by already formed clumps can result in an inhomogeneous distribution of the UV intensity, pertubing the energy balance in the gas. Shielded gas will tend to be colder than the neighbouring unshielded regions. Since a general pressure equilibrium tends to be quickly restored, the density of shielded regions increases. An estimation of the

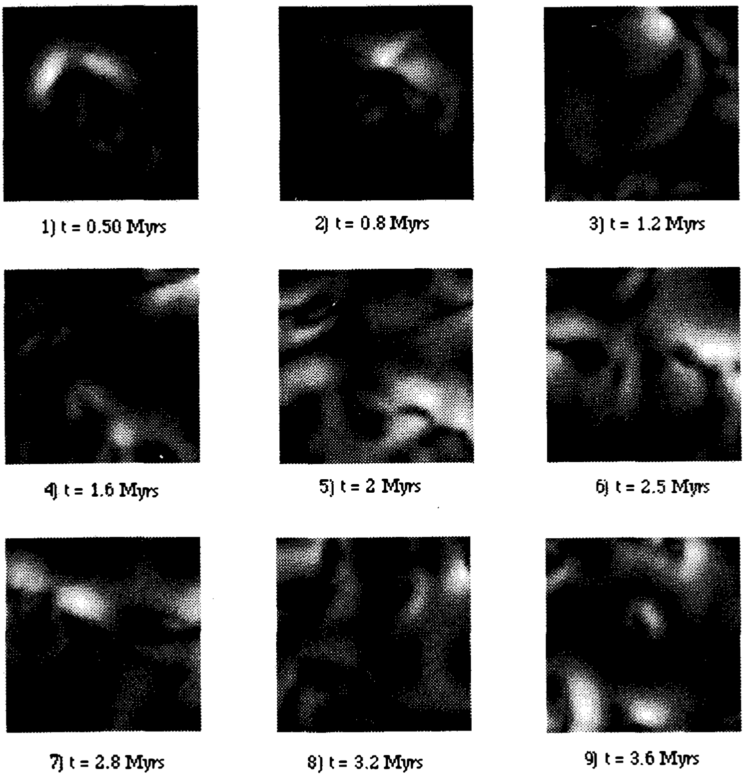

Figure 1 : *Shielding of ultaviolet radiation by moving clumps generates turbulent motions in cloud envelopes. The two dimensional velocity field calculated with an* **implicit** *2-D hydrodynamical code is shown here. Regions coded in black are virtually at rest, those coded in white are supersonic. In the present case, 80% of the surface is illuminated with a UV intensity corresponding to more than 90% of the Standard Interstellar Radiation Field, and only 2% with less than 20% of the IRF. The density varies from 10 to 370* cm^{-3}.

density contrasts which can be achieved has been proposed by de Boisanger and Chièze (1991) (see also the contribution of de Boisanger in this volume). Large values are indeed obtained, even for the standard value of the IRF.

Some dynamical aspects of this condensation process has been examined through 2D simulations, with naturally a special attention paid to heating and cooling processes (de Boisanger, Chièze & Meltz 1992). We have studied in particular the response of the interstellar gas to the shielding by a clump as a function of its velocity. We have generally adopted the standard UV field intensity, which is a minimum. Accordingly, the UV field affects the thermal balance of the gas lying at an optical depth less than about one : the following results concern only the envelopes of molecular clouds. No attention has been paid to the hydrodynamical interactions of the clump with the medium in which it moves, but only to its effect on the medium through the attenuation of the UV field. A velocity of the blockers subsonic relative to the unperturbed gas results essentially in the condensation of the gas in the shielded region, with small (subsonic) velocities. Supersonic velocities of the blockers are effective in the establishement of a sonic or weakly supersonic velocity field, but then, the condensation of the gas is only weak. We have extended this study to a collection of moving clumps, with a specified velocity dispersion. The cloud velocities where choosen between 0.3 km s^{-1} (subsonic) and 0.7 km s^{-1} (weakly supersonic). At anytime, about 80% of the surface remains essentially unshielded, shielding being effective over 2% of the surface, where the UV intensity is lowered below 20% of its *standard* value. For a mean density of $n_H \sim 50\ cm^{-3}$, the actual density varies typically between 10 cm^{-3} and 370 cm^{-3}. Much higher condensation factors can be easily obtained with a higher ($\times 10$) incident UV intensity. A second result of this study is that "turbulent motions" of the perturbed gas can be maintained in this manner (Fig. 1).

In this model, the turbulence has a double origin. It basically originates in the motions of the shielders, which, according to the discussion of Section I, is most likely of gravitational origin. When it is exposed to the UV field, the interstellar gas has in some sense a "potential energy" relative to the situation where the radiation field is switched off. The kinetic energy of the motions imparted to the shielded gas is then essentially extracted from this potential energy, which is proportional to the energy density of the incident UV radiation.

CO line profiles can be extracted from these hydrodynamical calculations. Figure 2 represents normalized CO line profiles, integrated through a 1 parsec line of sight in the simulation. The core line width sums up the termal velocity dispersion of the CO molecule in each cell, while the broad wings, at relatively low level, which extend to about 2 km s^{-1}

result from the chaotic velocity field generated by the time dependance of the UV field.

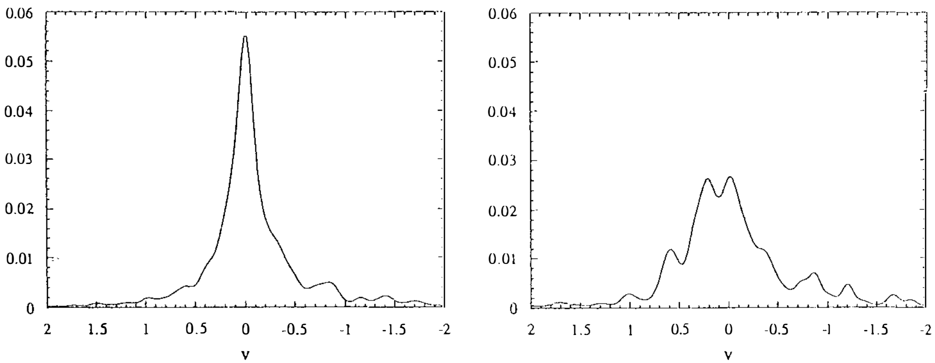

Figure 2 : *Two examples of the CO line profiles obtained in the simulation presented on Fig. 1, for t = 0.8 Myrs and t = 3.2 Myrs. Velocity is expressed in km/s.*

It is difficult to characterize turbulence in these two–dimensional simulations. However, Figure 3 represents the probability distribution of the velocity difference dv (projected on the line of sight) for two points separated by a distance of 0.1 parsec. The excess of large velocity differences relative to the gaussian law (solid line) is a measure of the intermittancy of the flow (see eg. Falgarone & Phillips 1990, and this volume). In each case, we have assumed an equilibrium abundance of CO in each hydrodynamical cell, calculated in terms of the density, temperature and extinction. Calculations of non–equilibrium chemistry in molecular gas show in fact that large departures from equilibrium values may be the rule.

In a one dimensional bi–fluid simulation, we have shown that large condensation factors can still be achieved, perpendicular to the magnetic field lines, if the radiation field is only ten times larger than the standard IRF. This process offers a natural context in which molecular gas experiences a succession of condensations and expansions, coupled to variations of the UV intensity. The characteristic times which are involved are of the order of a few 10^5 Myr. From a different point of view, the analysis of the molecular gas chemistry leads to a similar requirement : best agreement with observations is obtained in models which take explicitely into account cycling of the gas from intermediate to high densities in comparable time scales.

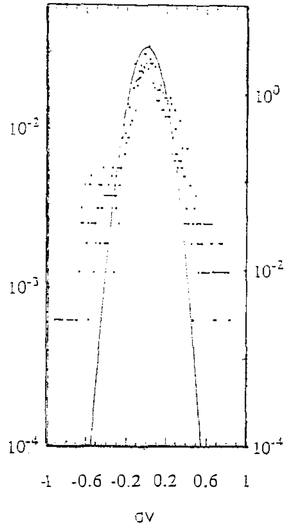

Figure 3 : *Representation of the intermitency of the velocity field according to the simulation presented on Fig. 1. The distribution of the velocity difference between points distant by 0.1 pc (dots) is compared to a gaussian distribution. The turbulent flow is characterized by a significant excess of large velocity differnces.*

III. OUT OF EQUILIBRIUM CHEMISTRY

Calculations of the gas phase chemistry in molecular gas in which the temperature and the density is maintained constant (or pseudo–time–dependent models) have shown that the abundances of organic molecules first increase, but soon, strongly deacrease. The maximum abundances are achieved after only 0.1–0.3 Myr. Large abundances of neutral atomic carbon (Phillips and Huggins 1981, Keene et al. 1985) are observed.

It was shown in the previous section that molecular gas could experience transient transitions between a diffuse phase, exposed to the ambient UV field and a more condensed, shielded phase. Furthermore, some effective turbulent mixing can take place during this continuous process. With a reduced but self–consistent chemical network connecting 50 species, Chièze and Pineau des Forêts (1989) showed that rapid mixing between two or more parcells of gas of increasing densities and extinctions strongly affect the abundances of C and C^+ in the densest regions, resulting in a steady state enhancement in polyatomic molecules such as C_3H_2. As is intuitively expected, mixing with a time scale less than 1

Myr effectively eliminates the time dependance of organic molecules observed in pseudo-time dependent models. An extension of this work to a much larger network (Chièze, Pineau des Forêts et Herbst, 1991), allowed for a better chemistry, so that the study has been extended to more complex molecules, as HC_9N. A carefull analysis of the chemical processes shows that the large amounts of C and C^+ flowing in the dense regions do not systematically result in the enhancement of the abundances of organic molecules. As noticed by Herbst and Leung (1989), this is because ion–molecule reactions between C^+ and neutral species tend to destroy complex molecules, and furthermore, high electron abundances deplete molecular ions which mediate their synthesis. It turns out that if the mixing process only is retained, the diffuse component should be rich in *neutral* rather than *ionized* carbon. This is not a conclusion reached by static models of diffuse clouds, in which the carbon is predominently in the form of C^+ or CO, depending on the optical depth (van Dishoeck and Black, 1988).

It turns out however that it is not a real difficulty if one considers the chemical evolution of *transient condensations* of the kind discussed in the preceding section, in which the matter flows in and out with calculated characteristic timescales of a few 0.1 Myr. In this context, ionized atomic carbon is actually rapidly converted to neutral as the extinction (and the density) increases, while the full conversion to CO requires considerably more time. For example, starting from the conditions $n_H = 40$ cm^{-3} and $A_v = 0.25$ mag, an increase in the extinction to $A_v = 2$ mag triggers a condensation to $n_H = 1100$ cm^{-3} after just 0.3 Myr. Carbon is by then essentially neutral with a ratio C/CO = 30, (de Boisanger and Chièze, 1990). On this basis, the gradual *compression followed by the decompression* of the gas as it passes through a condensation of that type has been introduced in the calculations of Chièze, Pineau des Forêts & Herbst, (1991). It turns out that it is in fact during the compression phase that C^+ recombines to large abundance of C while at the same time significant amounts of organic molecules are produced. This is a good point, because the strict "mixing scenario" (neglecting the compression stage) requires short mixing times scales, which may be in trouble with the theory of turbulent mixing (Williams & Hartquist, 1984). The basic conclusion of the study is that the introduction of the dynamics can, at the same time, remove the problem of the time dependence of organic molecules abundances and explain their large steady state abundances. The main requirement is that a large fraction of the molecular gas should be affected by that kind of cycling.

In an attempt to a more realistic coupling of hydrodynamics with time dependent chemistry, Prasad et al. (1991) reached similar conclusions. They followed the molecular abundances during the gravitational collapse of clouds with masses varied from 40 to 1000 solar masses. The basic feature of the model is that magnetic field is introduced to oppose to the gravitational force, so that the condensation is, here also, only ephemeral.

Furthermore, the initial densities are low (varying from 10 to 100 cm^{-3}). For the non-star forming cases, the collapse is reversed when the core density of about 10^5 cm^{-3}, and a sequence of contraction–expansion phases follws on a dynamical time scale (with a steadily decreasing maximum central density, however). The important point is that the life–time at a density greater than 10^4 cm^{-3} is, in most cases, only a few 0.1 Myr. The conclusion is that the short characteristic dynamical time scale of evolving cores actually limits the time available to chemistry to equilibrate, so that "early–time" molecular abundances are favored. Regardless some difficulties concerning the real dynamics of dense cores, this model provides the gravitational pendant of the compression–expansion process described previously.

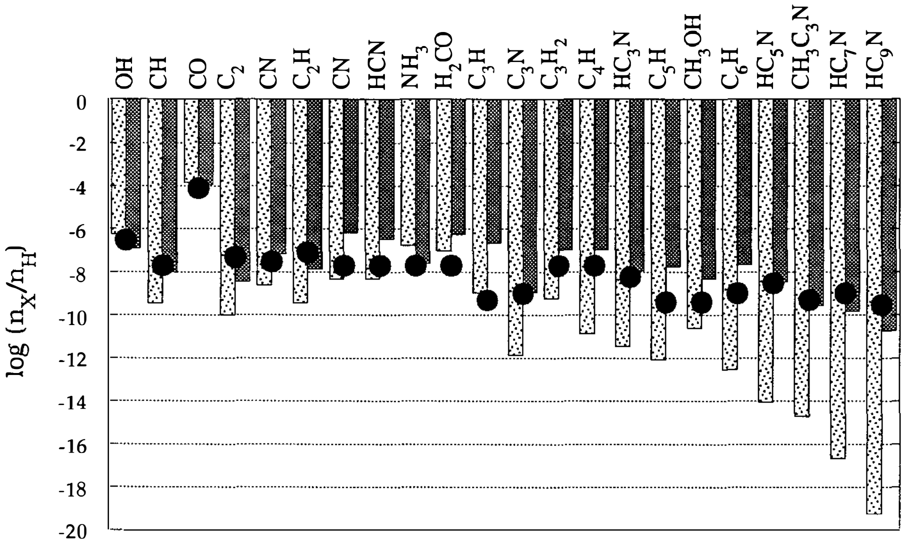

Fig. 4 : *Comparison of selected abundances, calculated at equilibrium (doted bins) and assuming a cycle of compressions and exansions (grey bins). In this case, the time dependent temperature is calculated self-consistently through the heating and cooling processes. Black dots represent the abundances observed in TMC-1.*

Other attempts to solve the problem raised by the agreement of the "early time" abundances with the observational data involve shocks and stellar winds, which both maintain chemical abundances far from their equilibrium values in star forming regions (Williams 1987, Charnley et al. 1988a,b, Nejad, Williams & Charnley 1990, Nejad & Williams 1992).

The non equilibrium energy balance in molecular gas can thus play quite a significant role not only on the dynamics of the gas, but also on its chemical hystory, through a continuous cycle of gas condensations and expansions. The observations of the abondances of organic molecules may, in this manner, provide valuable informations on the dynamical time scales which are actually involved.

REFERENCES

Bertoldi F. & McKee C.F. 1992, ApJ 395, 140

de Boisanger, C. & Chièze J.-P. 1991, A&A 241, 581

de Boisanger, C., Chièze J.-P. & Meltz B. 1992, ApJ 401, 182

Charnley, S. B., Dyson, J. E., Hartquist, T. W., & Williams, D. A. 1988a, MNRAS 231, 269

Charnley, S. B., Dyson, J. E., Hartquist, T. W., & Williams, D. A. 1988b, MNRAS 235, 1257

Charnley, S. B., Dyson, J. E., Hartquist, T. W., & Williams, D. A. 1990, MNRAS 243, 405

Chièze, J.-P. 1987, A&A 171, 225

Chièze, J.-P., Pineau des Forêts, G. 1987, A&A 183, 98

Chièze, J.-P., Pineau des Forêts, G. 1989, A&A 221, 89

Chièze, J.-P., Pineau des Forêts, G. & Herbst, E. 1991, ApJ 373, 110

Dame, T.M., Elmegreen, B.G., Cohen, R.S. & Thaddeus, P. 1986, ApJ 305, 892

Elmegreen, B.G. 1989, ApJ 338, 178

Falgarone, E. & Phillips, T.G. 1990, ApJ 359, 344

Falgarone, E., Pérault, M. 1987, in Physical Processes in Interstellar Clouds, ed. G.E. Morfill & M. Scholer (Dordrecht : Kluwer), 59

Falgarone E., Puget, J.-L. & Pérault, M. 1992, A&A 257, 715

Fuller, G.A., Myers, P.C. 1992, ApJ. 384, 523

Henriksen, R.N. & Turner, B.E. 1984, ApJ. 287, 200

Henriksen, R.N. 1986, ApJ 310, 189

Henriksen, R.N. 1991, in Fragmentation of Molecular Clouds and Star Formation, ed E. Falgarone, F. Boulanger & G. Duvert, IAU 147, (Kluwer Acad. Publ.), 83

Herbst, E. & Leung, C.M. 1989, ApJS, 69, 271
Herbst, E., Millar, T.J. 1991, in Molecular Clouds, ed. R. J. James & T. J. Millar (London : Cambridge Iniversity Press)
Larson, R.B. 1981, MNRAS, 194, 809
Larson, R.B. 1989, in Structure and Dynamics of the Interstellar Medium, ed. G. Tenorio-Tagle, M. Moles & J. Melnick, IAU 120 (Springer-Verlag)
Leung, C.M., Kutner, M.L. & Mead, K.N. 1982, ApJ. 262, 583
Lattanzio, J.C. & Henriksen, R.N. 1988, MNRAS, 232, 565
Maloney, P. 1988, ApJ. 334, 761
McKee, C.F. 1989, ApJ 345, 782
Keene, J., Blake, G.A., Phillips, T.G., Huggins, P.J. & Beichman, C.A. 1985, ApJ. 299, 967
Mouschovias, T. 1976, ApJ 207, 141
Myers, P. C. 1985, in Protostars and Planets II, ed. D. Black & M. Matthews, (Tucson : Univ. Arizona Press), 81
Myers, P.C. & Goodman, A.A 1988, ApJ. 329, 392
Nejad, L.A.M. Williams, D.A. 1992, MNRAS 255, 441
Nejad, L.A.M., Williams, D.A., Charnley, S.B. 1990, MNRAS 246, 183
Phillips, T.G. & Huggins, P.J. 1981, ApJ. 251, 533
Prasad, S.S., Heere, K.R., Tarafdar S. P. 1991, ApJ. 373, 123
Scoville, N.Z., Min, S.Y., Clemens, D.P. Sanders, D.B., & Waller, W.H. 1987, ApJS, 63, 821
Shu, F.H., Adams, F.C. & Lizano, S. 1987, Ann. Rev. Astr. Astrophys. 25, 23
Solomon, P.M., Rivolo, A.R., Barrett, J.W., & Yahil, A. 1987, ApJ 319, 730
Tomita, Y., Saito, T., Ohtani, H. 1979, Publ. Astron. Soc. Japan, 31, 407
van Dishoeck, E. F., & Black, J. H. 1988, ApJ, 334, 771
Williams, D.A. 1987, in Rate Coefficients in Astrochemistry, ed. T. J. Millar & D. A. Williams (Dordrecht : Kluwer Academic), p. 281
Williams, D.A. & Hartquist, T. W. 1984, MNRAS, 210, 141

MOLECULAR CLOUDS AND STAR-FORMING REGIONS

SIMPLE THINGS WE DON'T KNOW ABOUT MOLECULAR CLOUDS

LEO BLITZ
Astronomy Department, University of Maryland
College Park, MD 20742, USA

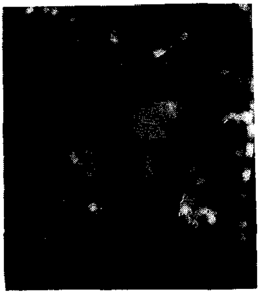

ABSTRACT

One of the ideas that most astronomers working in the interstellar medium take for granted is that Giant Molecular Clouds, as a whole, are gravitationally bound. In the following article this assertion is examined and it is concluded that the available evidence is surprisingly weak. Three arguments are discussed in detail: star formation, the virialization of clouds, and the internal pressures of clouds, all of which are found to be wanting. The importance of knowing whether GMCs are gravitationally bound is of fundamental importance in knowing whether gravity plays *any* role in their formation.

There are a number of fundamentally important things regarding Giant Molecular Clouds (GMCs) about which we are astonishingly ignorant. For example, we know very little about the distribution of angular momentum among the GMCs, and how this quantity varies as a funtion of galactic radius (see *e.g.* Blitz 1993). We are only beginning to get a detailed quantitative picture of the internal structure of GMCs. Surprisingly, as will be shown below, we really don't have any hard evidence that GMCs as a whole are bound by gravity.

That GMCs are gravitationally bound seems to have been taken as such a well established fact, that there is the only one work I am aware of that challenges the prevailing view (Maloney 1988). However, it is worth reexamining this question to see how well established the idea really is. Part of the motivation for looking at this question once again is to understand how clouds form and evolve. The detailed structure of a cloud is the result of the various forces that act on it, and it is important to know whether or not gravity is one them.

There are three fundamental arguments that GMCs are bound by gravity. Each of these is discussed below.

1. STAR FORMATION

The star formation argument goes as follows. Star formation is known to take place in GMCs. If the clouds form stars that are bound by gravity, then how could the stars form if the clouds themselves are not similarly bound? The basic flaw in this argument is that an entire cloud need not be bound for part of it to become self-gravitating and form stars. In fact, there is increasing evidence that at least some stars form in molecular clouds that are not themselves bound.

The star formation argument, invoked explicitly and implicitly for more than 20 years, gave rise to the realization that if GMCs are bound, the efficiency of star formation in GMCs must be low. If this were not the case, the mass of molecular gas in the Milky Way would imply a star formation rate much higher than observed (Zuckerman and Palmer 1974). This in turn led to the question, if molecular clouds are gravitationally bound, and if star formation is so inefficient, what prevents the clouds from collapsing; what holds GMCs up? Turbulence, it was realized, would dissipate too rapidly, and because there are no internal energy sources away from the sites of star formation, *something* has to be holding the clouds up if they are bound. This problem has never been solved to everyone's satisfaction.

Consider, on the other hand, the molecular clouds found at high galactic latitude (HLCs), most of which were shown by Magnani *et al.* (1985 - MBM) to be far from being gravitationally bound. The clouds have velocity dispersions far in excess of what is needed to bind them, a result confirmed by an independent study of Keto and Myers (1986). Observations of the molecular emission (MBM), the dust emission (Weiland *et al.* 1986), and the extinction (Magnani and de Vries 1986), confirm that the luminous masses are well enough known that given the observed velocity dispersions, they HLCs as a group cannot remain coherent entities for more than a few million years.

Nevertheless, some of the HLCs harbor star formation. For the most part, these are ones that have been previously classified as dark clouds by Lynds (1962). Examples are MBM MBM 12, the darkest part of which was catalogued as L1457/8, MBM 18, also catalogued as L1569, and MBM 20 also catalogued as L1642. There is known star formation in these clouds (MBM; Magnani personal communication), but MBM find that these clouds have insufficient mass to keep them bound by factors of 30 – 100. Apparently, star formation does occur in entities that are not in themselves bound, and an entire cloud need not be bound for a part of it to form a star.

In a study aimed at investigating the properties of the denser regions within the HLCs, Turner *et al.* (1989) found that many of the dense knots identified by Magnani *et al.* (1988) are sufficiently massive that the knots are gravitationally bound. Although there has been some controversy regarding this assertion (*e.g.* van Dishoeck 1992), molecules that are normally thought to be high density tracers are frequently found in molecular clouds where the mean extinction is considerably less than 1 mag (refs). In these regions, the expected H_2 column density implies extinctions considerably higher than what is inferrerd from star counts, suggesting that small dense regions can form which may be gravitationally bound even though the cloud as a whole is not. Therefore, not only is there star formation in clouds that do not appear to be bound, but bound clumps, a necessary precursor of star formation, also may have been detected in the HLCs.

2. THE VIRIAL THEOREM

That GMCs are gravitationally bound is implicit in the use of the virial theorem to determine the CO/H_2 conversion factor in the Milky Way. It is worth looking into the details of what is done in order to clarify how the results relate to the question of the boundedness of GMCs.

We start out with the ***assumption*** that GMCs obey the virial theorem. Thus:

$$2T = V.$$

which already introduces a factor of 2 uncertainty, because the clouds need not be virialized to be bound. Under the assumption that the clouds have an r^{-2} density profile,

$$\sigma_v{}^2 = GM/R.$$

where σ_v is the three dimensional velocity dispersion of the gas in a cloud. Now, $R = r\theta$, where r is the distance to the cloud, and θ is the mean angular radius of the cloud. M is obtained from the CO derived mass, M_{CO}. Observationally,

$$M_{CO} = \alpha < T_A > \sigma_v r^2 \theta^2$$

where

$$\alpha < T_A > \sigma_v = N(H_2).$$

Here, $< T_A >$ is the mean peak antenna temperature (corrected for atmospheric opacity and various antenna efficiencies) of the CO line in the cloud, and α is a constant in which the mean I(CO)/N(H_2) ratio is buried (I(CO) is the observed line strength of the J = 1-0 transition of CO).. Combining these terms, we obtain,

$$\sigma_v = \alpha T_A r \theta.$$

Because the variables on the right hand side as well as σ_v can all be obtained from observation, α can be obtained from a linear regression of the variable quantities. On the other hand, α, and hence the ratio I(CO)/N(H_2) may be obtained by other means, such as the extinction method (Dickman 1978), or from gamma-ray and CO surveys (Bloemen *et al.* 1986). All are fundamentally different methods of obtaining α, and the variation of published values has been more than a factor of 5. Although, the most extreme values are rejected by most observers, few would argue that α is known to better than a factor of 2 in the Milky Way, and probably exhibits a variation with radius at least that large. Another way of saying this is that if α as derived from application of the virial theorem is in error by only a factor of 2, a cloud, or an ensemble of clouds can be unbound even though it may appear to be gravitationally bound. For it to be *known* whether GMCs are gravitationally bound, the value of α needs to be known to better than a factor of two, an assertion with which many observers would feel uncomfortable.

It is worth noting that values derived from the application of the virial theorem tend to be higher than the others, suggesting that agreement can be obtained if one relaxes the assumption that $2T = V$. That is, if the clouds obey the relation $T = V$, the values of α derived from the three basic methods are in much closer agreement. The condition that the gravitational and kinetic energies are equal is one that may be characterized as gravitational neutrality. That is, clouds are gravitationally neutral if a small addition of kinetic energy will make them expand, but otherwise the clouds will neither expand, nor collapse with the energies they have. Note that gravitational neutrality is really an *average* condition over a molecular cloud, and need not be strictly true everywhere within a cloud. In other words, a clump within a cloud may be collapsing to form a star without violating the gravitational neutrality of the cloud as a whole. In that way, the cloud may be forming stars even if the cloud as a whole is not bound, or even expanding.

It seems that in the absence of some other arguments, the most commonly cited evidence that GMCs are gravitationally bound is in fact quite weak. Let us now examine what I have always believed to be the strongest argument in favor of molecular clouds being gravitationally bound.

3. THE INTERNAL PRESSURE

The structure of molecular clouds has long been known to be clumpy. From the work of Blitz *e.g.* (1978, 1980, 1993), we find that the volume averaged density of GMCs is one to two orders of magnitude less than the densities inferred from the CO emitting regions, implying that the volume filling fraction of the molecular emission is only a few percent of the volume of the cloud as a whole. This is confirmed by detailed maps of the GMCs which show numerous velocity components that correspond to the individual clumps within a cloud. Observations of the clumps can give a measure of both the density, temperature and velocity dispersion of the clumps, and therefore the pressure within a clump. It has long been known that the pressure within a typical clump of which a GMC is comprised is far larger than the pressure of the general interstellar medium as a whole. If the pressure within a typical GMC is an order of magnitude larger than the interstellar medium in which it is embedded, then it would seem that either all GMCs are expanding (an unpalatable conclusion), or that the pressure is due to the self gravity of the GMC, and the GMCs are therefore gravitationally bound.

Consider first the hydrostatic pressure of the ISM due to the gravity of the stars in the disk. This pressure can be written

$$P_{ISM} = 2\pi G {\Sigma'}_g \rho_* h_g$$

where Σ'_g is the gas surface density of the disk projected onto the plane, ρ_* is the density of stars in the midplane, and h_g is the gas scale height. Putting in the best values for these quantities gives a value of $P_{ISM}/k = 2 \times 10^4$ K cm^{-2}. For a GMC in hydrostatic equilibrium, the internal pressure is

$$P_{GMC} = 2\pi G {\Sigma_g}^2.$$

where Σ_g is the gas surface density of a GMC. Putting in the best values for the surface density from CO measurements one obtains that $P_{GMC}/k = 2 - 8 \times 10^5$ K cm^{-2}, at least an order of magnitude larger than the value for P_{ISM}. No error in the geometry of a cloud, or in the measured CO/H_2 ratio could make these two values agree.

Now let us look at the actual pressure within a clump. That pressure can be written

$$P_{CLUMP} = n m_{H_2} {\sigma_v}^2,$$

where n is the volume density of molecules, and σ_v is the three dimensional velocity dispersion of the gas. If we take a typical value of $n = 10^3$ (see *e.g.* Williams and Blitz 1994), and σ_v of 0.5 $\mathrm{km\,s^{-1}}$ in one dimension from measured line widths, we find that $P_{CLUMP}/k = 2 \times 10^5$ K cm^{-2}, a value commensurate with the hydrostatic pressure of the cloud as a whole. Apparently, the clumps are in pressure equilibrium with the with the hydrostatic pressure of the GMC in which it is found. On the other hand, the pressure is indeed at least an order of magnitude greater than that of the general interstellar medium.

But does this necessarily mean that the clouds are gravitationally bound? Consider the possibility that the reason we have clouds in the first place is that they only form in regions of enhanced interstellar pressure. Such regions are found in spiral arms, or in places where the there are large swept up volumes such as supershells (Heiles 1979). It is not difficult to imagine situations where the pressure is temporarily larger than the mean for the disk. Furthermore, because the GMCs take up such a small volume of the galactic disk (0.001 – Blitz 1978), these regions of higher pressure do not necessarily affect the overall pressure balance of the disk. Eventually, such high pressure regions will equalize their pressure on an acoustical timescale. Assuming that the pressure is carried primarily by the HI, a lower limit to this time scale is equal to a typical diameter of a cloud (which we may take as 50 pc), and an HI velocity dispersion of 3-5 $\mathrm{km\,s^{-1}}$. This gives a crossing time of 1-2 $\times 10^7$ y. HI envelopes arond clouds are typically much larger than the clouds themselves and contain similar masses (Blitz 1993). If the region of enhanced pressure is identified with the HI envelopes, the pressure equalization time is more in the range of 2-6 $\times 10^7$ y, a value quite close to the lifetime of GMCs estimated by Blitz and Shu (1980) and by Bash *et al.* (1977). That is, if GMCs form preferentially in high pressure regions and are gravitationally neutral, then the lifetime of the clouds is consistent with the star formation timescales of the clouds, and other measures of GMC ages. As long as gravitationally neutral clouds can form bound regions that give rise to OB associations, then the high pressures found in the clumps may simply be a remnant of the conditions under which the clouds formed, and need not be an indication that, as a whole, they are gravitationally bound.

Are we then to conclude that GMCs are *not* gravitationally bound? I think it is premature to draw that conclusion, but we should conclude, on the other hand that the evidence that GMCs are gravitationally bound is surprisingly weak. It will be important to look into this matter much more deeply and with much closer scrutiny.

4. THE RELEVANCE FOR CLOUD FORMATION

On the surface, it would seem that the discussion above is all about a factor of two, the difference between whether a cloud is gravitationally neutral, or whether a cloud is virialized and thus fairly tightly bound. While this is in some sense true, the consequences are actually far more fundamental. If all GMCs are gravitationally bound, then gravity *must* play an important role in how GMCs form in a galaxy. We must in turn look to gravitational instabilities such as the disk instability investigated by Toomre (1964) and applied by Kennicutt (1989) to understand both GMC formation and star formation in disks. On the other hand, if GMCs are gravitationally neutral, then clouds may form independently of any gravitational instability; it may be that what separates a GMC from the surrounding gas may simply be a matter of a phase transition. The process of star formation, or the formation of clusters is then reduced to a local one: we must look primarily for instabilities within a cloud rather than within a disk. The formation of individual stars is a very local process, but where stars form in a galaxy may in principle have nothing to do with gravity.

In any event, we must conclude that the argument that GMCs are bound because stars form within them is a very weak one. We must find evidence beyond that which is presently available to evaluate the boundedness of GMCs.

REFERENCES

Bash, F.N., Green, E., and Peters, W.L., 1977, *Ap. J.*, **217**, 464.

Blitz, L., 1978, Ph.D. Dissertation, Columbia University.

Blitz, L., 1980, in *Giant Molecular Clouds in the Galaxy*, Solomon and Edmunds, eds., Pergammon:Oxford, p.1.

Blitz, L., 1993, in *Protostars and Planets III*, eds. Levy and Lunine, University of Arizona Press:Tucson, p.125.

Blitz, L. and Shu, F.H., 1980, *Ap. J.*, **238**, 148.

Blitz, L, Bazell, D., and Desert, F.X., 1989, *Ap. J. (Letters)*, **352**, L13.

Bloemen, J.B.G.M., *et al.* , 1986, *Astron. Ap.*, **154**, 25.

Dickman, R.L., 1978, *Ap. J. Suppl.*, **37**, 407.

Heiles, C., 1985, *Ap. J.*, **229**, 533.

Kennicutt, R.C., 1989, *Ap. J.*, **344**, 685.

Keto, E.R., and Myers, P.C., 1986, *Ap. J.*, **304**, 466.

Lynds, B.T., 1962, *Ap. J. Suppl.*, , **7**, 1.

Magnani, L., Blitz, L., and Mundy, L., (MBM) 1985, *Ap. J.*, **295**, 402.

Magnani, L., and de Vries, C.P., 1986, *Astr. Ap*, **168**, 271.

Magnani, L., Blitz, L., and Wouterloot, J.G.A., 1988, *Ap. J.*, **326**, 909.

Maloney, P., 1988, *Ap. J.*, **334**, 761.

Toomre, A., 1964, *Ap. J.*, **139**, 1217.

Turner, B.E, Rickard, L. J, and Xu, L-P., 1989, *Ap. J.*, **344**, 292.

van Dishoeck, E.F., 1992, in *Astrochemistry of Cosmic Phenomena*, P.D. Singh, ed., Kluwer:Dordrecht, p. 143

Weiland, J., Blitz, L., Dwek, E., Hauser, M.G., Magnani, L., and Rickard, L.J, 1986, *Ap. J. (Letters)*, **306**, 463.

Williams, J. and Blitz, L., 1994, *Ap. J.*, in press.

Zuckerman, B. and Palmer P., 1974, *Ann. Rev. Astron. Ap.*, **12**, 279.

SMALL SCALE STRUCTURE IN THE COLD INTERSTELLAR MEDIUM

E. Falgarone

Radiastronomie Millimétrique, Ecole Normale Supérieure
24 rue Lhomond, 75005 Paris, France

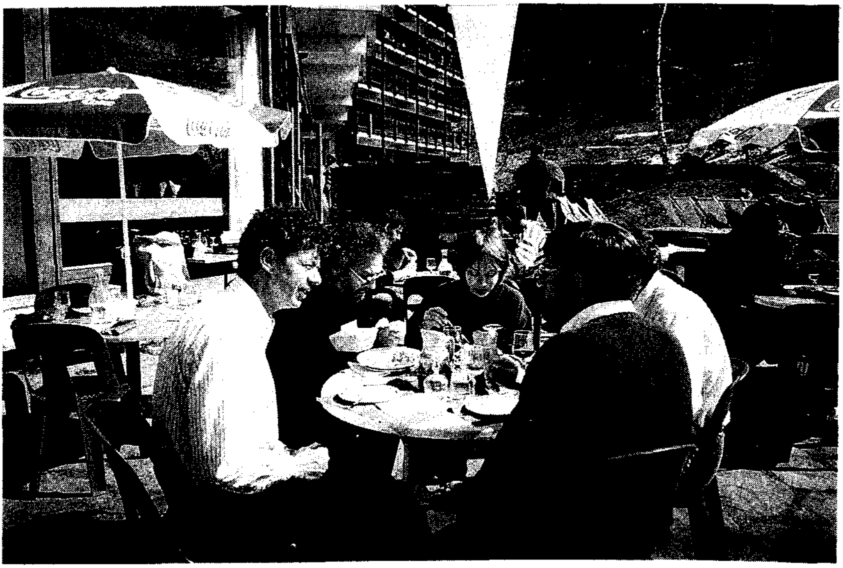

ABSTRACT

Away from active starforming regions, the various tracers of the cold interstellar medium, whether atomic or molecular, reveal its self-similar structure in space and in velocity space. No characteristic scale has yet been determined and self-similarity may extend to scales as small as a few 10 AU. Large local densities are inferred at the smallest scales from the observations of rotational transitions of polar molecules, but the actual gas mass distribution (*i.e.* the cloud mass fraction contained in these small scales) is still ill-determined. We show however that the observed small scale structure cannot be a mere artefact of the tracers used and reveals the existence of real density gradients at small scale. There are several possible origins for the self-similar structure of this medium, and we show why, among others, turbulence may play an important role at shaping the medium.

1 - Introduction

This paper reviews the observational grounds on which our knowledge of the structure of the cold interstellar medium prior to star formation is based. It is meant to clarify some confusing issues regarding the so-called *clumpy* structure of interstellar clouds, often viewed by theorists as a structure in which all (or most of) the mass is concentrated in the smallest dense units which thus have an extremely low volume filling factor. As will be seen, this is only a simplifying picture with little observational support. On the other hand, the small scale structure as observed in the rotational transitions of CO is not only apparent, as it has been also written. It traces actual gas density enhancements above a lower density medium, but, as long as high angular resolution maps over large cloud areas have not been performed, the gass mass distribution in the various density ranges remain unknown.

Why is it such an important issue? The mass (and therefore the dust) distribution controls the penetration of the radiation field into the gas (Boissé 1990) which in turn controls the gas heating processes, its ionization degree and its coupling to the magnetic field. It also modifies the dynamical evolution because kinetic energy dissipation of an ensemble of moving clumps at supersonic velocities of low volume filling factor is much smaller than if the mass is distributed (Scalo and Pumphrey, 1982). It also controls the mass accretion rate in the star forming process as discussed by Larson (1992). The rate not only depends on the distribution of clumps in space (uniform or sheet like or fractal, for instance) but on the cloud mass fraction contained in these clumps.

This paper is focused on gas structures with moderate column densities, up to $N_H \sim 10^{24}\,\mathrm{cm}^{-2}$ only. It includes low-mass dense cores in which star formation activity, if present, is lenient enough so that presumably it has not deeply modified the structure of placental matter, and clouds of low average column density $N_H < 10^{21}\,\mathrm{cm}^{-2}$, self-gravitating or not depending on the scale considered and their kinetic energy content. The review of Stutzki (1993) on a similar issue includes star-forming regions and is a useful complement to this one.

There is no definition, but observational, of a small scale in the interstellar medium. The determination of the existence of an ultimate building block of the cloud hierarchy would be an important step forward in the approach to the physics of interstellar matter. Yet, this lengthscale has never been found. Direct observations in the millimeter range for instance, with large telescopes or interferometers, provide a resolution of $\sim 0.005\,\mathrm{pc}$ or 1000 AU only in the nearest non star-forming clouds, almost five orders of magnitude smaller than the largest structures in the Galaxy but still orders of magnitude above the mean free path of an hydrogen molecule in a gas of density $100\,\mathrm{cm}^{-3}$ (~ 1 AU), and the dissipation scale of turbulence in atomic clouds which is about 10 AU.

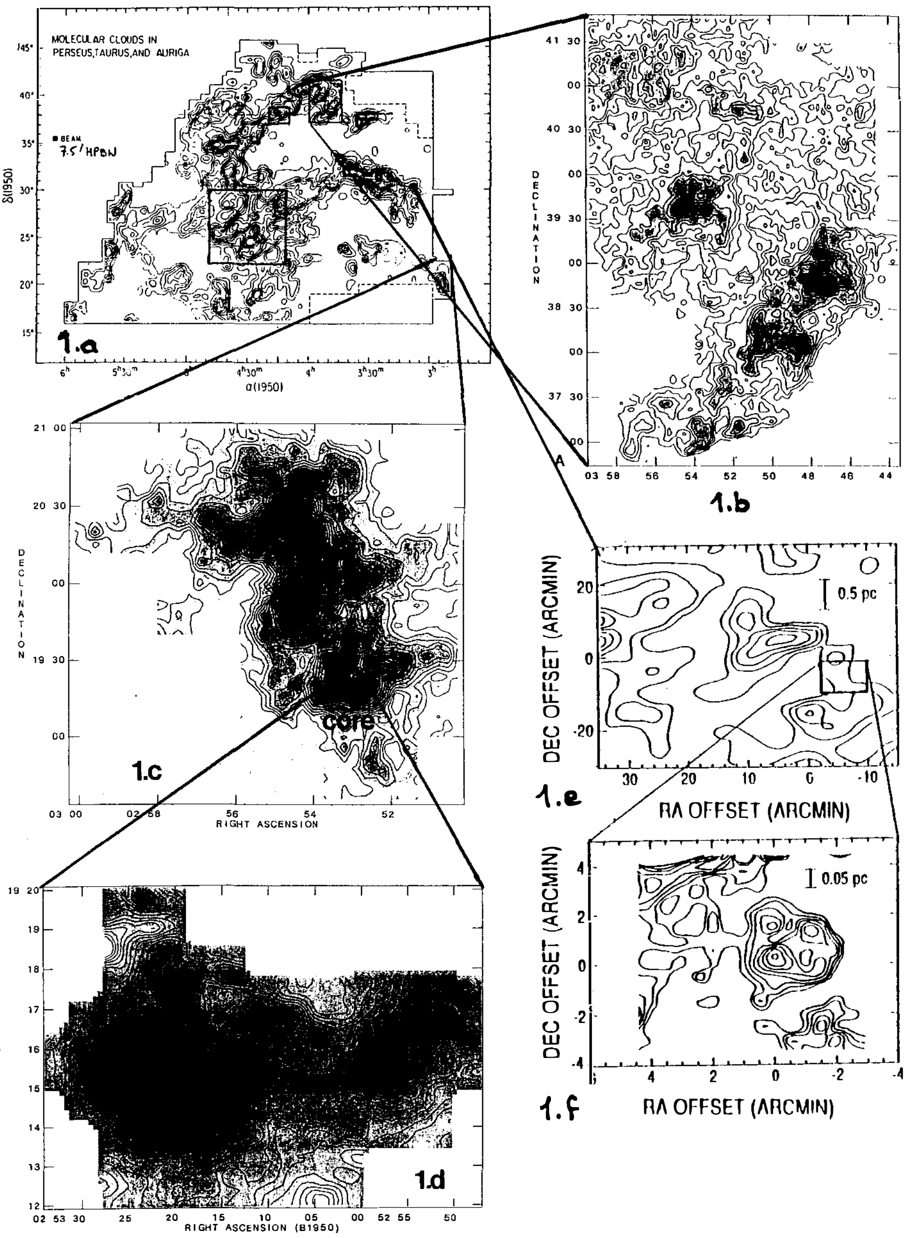

Figure 1 Illustration of the self-similar structure of molecular clouds observed in cores and in edges. Maps of ^{12}CO integrated emission in the Taurus–Auriga–Perseus complex *(a)* large scale map (Ungerechts & Thaddeus 1987), *(b)* NGC 1499 (Herbertz et al. 1990), *(c)* L1457 or MBM12 (Zimmermann & Ungerechts 1990), *(d)* core in L1457 (Zimmermann 1993), *(e)* undersampled and *(f)* fully sampled map of a small field in a cloud edge (Falgarone, Phillips & Walker 1991).

2 - The direct output of observations: brightness distributions

Molecular hydrogen being unobservable directly unless the vibrational transitions are excited, the knowledge of the molecular gas distribution relies on that of several tracers, like the rotational line emission of polar molecules such as CO, CS and C_3H_2, among many others, and the far-infrared thermal emission of the dust grains intimately mixed with the gas. The choice of the tracers of the cold molecular medium is limited because the gas and dust temperatures are low, thus many highly excited molecular levels are not populated, and column densities are often too small to allow detections of the dust emission in the millimeter range, for instance.

In the recent years, observations at many sizescales in several of these tracers have converged toward the idea that the structure of the cold interstellar medium is self-similar over an impressive range of sizescales. Beside several scaling laws which will be discussed below, self-similarity is inferred from the fractal dimension found for cloud contours in the above tracers (see references in Scalo, 1990; Falgarone & Phillips 1991). The unexpected and probably most meaningful result, is that the fractal dimension derived from the area-perimeter method is found to be the same whichever tracer is used, and is the same over the entire range of sizescales analysed, from 0.01 pc to about 50 pc (Falgarone, Phillips & Walker 1991; Zimmermann 1993). There is no evidence that any characteristic scale has yet been determined since unresolved structure is still present in the highest resolution maps whether in large column density cores or in low column density cloud edges, and the threshold of the hierarchy is still lying below 1000 AU (Figure I).

The existence of very small scale structure (down to a few 10 AU) is now observed or inferred from several data sets, in many kinds of cold clouds. Atomic clouds have long been considered as more or less homogeneous structures of a few pc with average densities of a few 10 cm^{-3}. Combinations of single dish telescopes and interferometric observations have revealed the existence of structure in the HI emission and absorption down to the resolution of the observations or 0.5 to 1 pc in Kalberla et al. (1985) and down to $\sim$ 0.3 pc in a nearby high latitude atomic cloud (Joncas, Dewdney & Boulanger 1991). Such a small scale structure had never been seen in emission in HI clouds before. It consists in the latter case of thin, very elongated filaments barely resolved in the transverse direction, intertwined with each other and which individually cover a broad velocity range compared to their small size. Still a smaller threshold in size is inferred by a few observations of another kind. In 1989, Diamond et al. have shown that the time variability of the VLBI visibility of several quasars was larger in the HI line than in the continuum. They inferred time variations of the HI λ=21cm optical depth which they ascribed to intervening structures in local cloud material. If located at about 100 pc from the Sun, the inferred density is $n_{HI} \sim 10^4$ to $10^5\,\mathrm{cm^{-3}}$ and sizes $\sim$ 25AU. The occultation of monitored quasars and the scattering of their radiation led also Fiedler et al. (1987) to invoke the existence of structures of that size in the electron density.

Unresolved structure is present in high angular resolution CO maps of all sorts of molecular media of low average column density, thus poorly shielded from the ambient UV field. It includes high latitude clouds (Falgarone & Pérault 1988; Zimmermann 1993), cloud edges (Falgarone, Phillips & Walker 1991), diffuse and translucent clouds (Gredel et al. 1992). Recently, Marscher, Moore & Bania (1994) have inferred the existence of structures even smaller than 10AU and denser than $n_{\mathrm{H_2}} \sim 10^6\,\mathrm{cm^{-3}}$ from secular changes in the formaldehyde absorption line profile toward two extragalactic sources whose lines of sight cross ordinary regions of molecular clouds.

Small scale and unresolved structure also exists in low mass dense cores traced by molecular line emission (Falgarone, Puget & Pérault 1992; Mauesberger et al. 1992; Schulz et al. 1992; Zimmermann, 1993; Fuller et al., 1994) or in the dust continuum submillimeter emission (André et al. 1990; Mezger et al. 1992*a*,*b*) down to scales of the order of 0.01 pc, one order of magnitude below the size of the observed cold dense cores which have been considered as the ultimate fragmentation stage out of which stars form (see Stahler, this conference). The knowledge of the actual mass distribution within these cores is essential to understand the trigger and development of the gravitational instability.

All the tracers of the cold interstellar medium reveal spatial structure down to scales even smaller than that directly observed. One of the major puzzle with such a picture is the following. There is *structure* visible in the tracers brightness distribution but does that mean that the bulk of the gas is actually *fragmented* down to these small scales? In other words, is all the mass in the smallest structures or is it also distributed in less dense components, and according to which distribution? How is the observed structure in the brightness maps related to the actual mass distribution? On the other hand, is it possible that this structure be only apparent, due for instance to small scale fluctuations of the abundance or optical properties of a tracer?

The next section is devoted to the limitations of the methods which have been devised to determine the local densities and gas mass distributions (and therefore the gravitational potential well) at all scales. These are the primary inputs in any description of the physics of the cold interstellar gas in its evolution toward star formation, and as will be seen, critically deserve improvements.

3 - The inferred densities.

There are essentially two methods used to determine densities. They have been described in several review papers (*e.g.* Wilson & Walmsley 1989; Stutzki 1993) and they will not be detailed here. The first, which consists in dividing the column density of a structure observed above a background emission, by its size l provides only an *average* density over the size l. The other which consists in measuring several line intensities in the rotational ladder of polar molecules and deriving the density from a study of collisional excitation provides a *local* gas density.

Each method has its limitations. The tracers mentioned above provide measures of the column density, but the uncertainties may be large. The $100\mu m$ brightness has been found to be a good tracer of the total gas column density (within a factor of a few) up to visual extinctions of the order of 1.5 mag only. This limit corresponds approximately to the domain for which the UV irradiation of the gas is uniform (see the discussion in Boulanger 1993). The line integrated emission of CO(J=1→0), I(CO), is also a tracer of H_2 but the calibration factor X = N(H_2)/I(CO) still being much debated (see the review of Combes 1991). CO surveys provide the range $10^{20} < X < 5 \times 10^{20}$ cm^{-2}/(K km s^{-1}) with a trend for the larger beam analyses to yield lower values (Sanders, 1994) . The range of values for X is indeed quite large since recent determinations of X in high latitude clouds give X $\sim 5 \times 10^{19}$ cm^{-2}/(K km s^{-1}) (de Vries et al. 1987; Heithausen et al. 1993) while in the Small Magellanic Clouds a value as large as X $\sim 6 \times 10^{21}$ cm^{-2}/(K km s^{-1}) is obtained (Rubio et al. 1991). The H_2 column densities, and therefore the average H_2 densities derived from CO and the calibration factor X may not be known better than within a factor of 10. The abundance of CO and its isotopic variants for instance is extremely sensitive to small fluctuations of the UV field intensity in the column density ranges relevant to interstellar clouds (van Dishoeck & Black 1988) but it may not be the only reason for such a large dispersion (see the discussion in van Dishoeck et al. 1992).

The limitations of the second method are mostly due to the difficulty in correctly treating the radiative trapping of the millimeter photons and the line excitation. None of the existing radiative transfer models is satisfactory (see Kegel, Piehler & Albrecht 1993). Additional processes may be important like collisional excitation by electrons for large dipole moment molecules (Drdla et al. 1988) and, in the vicinity of stars, radiative pumping of the excited vibrational levels by infra-red photons (Caroll & Goldsmith 1981). In addition, the density derived from the observation of a given pair of transitions seems always to provide a density value close to the critical density for these transitions. Higher densities cannot be derived because in that case both transitions are thermalized and their ratio stays the same. Much lower densities cannot be derived either, because the line intensities drop exponentially below the sensitivity limit. The detection of a given pair of lines just probes the existence of gas at about the critical densities of the transitions.

In spite of the above limitations, results of multiline analysis in emission seem to support the idea that the smallest observed structures correspond to dense gas. In the low average column density medium which contributes to most of the CO galactic emission, CO probably traces gas as dense as about $\sim 10^4$ cm^{-3}. The strongest support is the fact that the three lowest rotational transitions of CO have intensity ratios consistent with thermalized emission at low kinetic temperature. Not only is this ratio independent of the scale at which it is measured from small scale in dark clouds (Clemens & Barvainis 1988) or in cloud edges (Falgarone, Phillips & Walker 1991; Falgarone, Puget & Pérault 1992) to large scales from the Galactic survey of Sanders et al. (1992) but it is also independent of the velocity range across the CO line profiles and is therefore not affected by the degree of saturation of the emission. The line ratio being the same in the line cores where the opacity is much larger than 1 and in the line wings where it is much smaller supports the idea that all these transitions are (or close to) thermalized (Falgarone & Phillips, 1994). This however might be an artefact of the existence of turbulence in molecular clouds. The results of Albrecht & Kegel (1987) and Kegel et al. (1993) show that the existence of a correlation length in the velocity field of a cloud considerably modifies the variations of the CO(J=2-1) to J=1-0 ratio across a line profile. A large correlation length relative to the cloud size is even able to make this line ratio smaller than 1 in the linewings where it is expected to increase above 1. In this case, it is only for densities larger than 10^3 cm^{-3} that the line ratio is observed to be about constant across a lineprofile.

Recently, Lucas & Liszt (1993) have demonstrated that mm–wave absorption line studies in the direction of continuum sources occulted by molecular gas are powerful tools to determine the H_2 number density and temperature of intervening gas. In the direction of BL Lac, they derive H_2 densities close to $n_{H_2} \sim 7 \times 10^3$ cm^{-3} and temperatures sligthly below 10K.

Additional indirect constraints on the local density of CO structures are provided by their small size, when it is known. Small CO–rich regions in poorly shielded environments are very fragile against photodissociation and they have to be dense enough to allow the photodissociation front to cross them is a time longer than, say, their observed dynamical turnover time (*i.e.* the ratio of their size by their internal velocity dispersion δv). This provides the condition $v_\phi < \delta v$. The velocity of the photodissociation front depends on the external shielding from the ambient UV field through the photodissociation rate Γ_ϕ, on the local CO density $x_{CO} n_{H_2}$ and on the column density N^*_{CO} for which Γ_ϕ has decreased by a factor 2 (*i.e.* during the time $2/\Gamma_\phi$ N^*_{CO} molecules have been photodissociated and the front has progressed by $l \sim N^*_{CO}/x_{CO} n_{H_2}$). The front velocity is thus

$$v_\phi \sim \frac{N^*_{CO}\,\Gamma_\phi}{2\,x_{CO}\,n_{H_2}}$$

(Hartquist et al. 1992). The values computed by van Dishoeck and Black (1988) for various external shieldings, $\Gamma_\phi = 2 \times 10^{-12}$ and 2.5×10^{-14} s^{-1}, and $N^*_{CO} = 10^{15}$ and 10^{17} cm^{-2} for $A_v^{ext} = 0.5$ and 1 mag respectively, provide estimates of the front velocity in a gas of density $n_{H_2} = 10^3$ cm^{-3}, $v_\phi \sim 10$km s^{-1} in the former case where $x_{CO} = 10^{-6}$ and $v_\phi \sim 0.2$ km s^{-1} in the latter where $x_{CO} = 7 \times 10^{-5}$. Since $\delta v \sim 1$ km s^{-1}, the above constraint on the photodissociation front velocities implies that the H_2 densities be close to 10^4 cm^{-3} in the least shielded CO structures observed in the cloud edges. This of course is an estimate since v_ϕ depends as much on the density as on the CO abundance which precisely varies a lot in those transition regions. Furthermore, CO transition regions in cloud edges, when observed with large enough angular resolution, are found to be quite sharp, ~ 0.03 pc. Chemical models show that CO self–shielding is reached over such small pathlengths only for $n_{H_2} \sim 10^4$ cm^{-3} which is a further element to suggest that the densities are large (Le Bourlot et al. 1993).

In dense cores, density determinations rely on both the line excitation measurements and determinations of the total column density from dust millimeter emission (see examples in Mezger et al. 1992*a*,*b*; Schulz et al. 1991; Mauesberger et al. 1992). The determinations have long been in disagreement, in the sense that the column densities derived from the continuum mesaurements were in excess to that derived from molecular lines leading to the idea that molecules deplete onto grains. But in general the H_2 number densities derived from multiline analysis ($\sim$ a few 10^6 cm^{-3}) are larger than the core average density, suggesting small scale clumping.

The above discussion refers to gas actually detectable in the CO rotational transitions above the millimetric emission of the 2.7K cosmic background. In the regions where the star formation activity is reduced or non–existent, the lack of UV photons and cosmic rays may drive the gas kinetic temperature to values so close to that of the cosmic background that the line emission of even CO–rich components becomes undetectable. This is illustrated by the detection of very faint CO emission in the inner regions of M31 (Allen & Lequeux, 1993) and that, in absorption, of a CO–rich component difficult to detect in emission in the outer Galaxy (Lequeux, Allen & Guilloteau 1993). These authors argue that, if in virial balance between self–gravity and kinetic energy, the CO clouds are associated with amounts of molecular hydrogen which largely exceed the amounts of atomic HI.

Regardless of the existence of still denser and colder molecular components, which cannot be easily detected by the tracers discussed above, many molecular line observations of cold molecular clouds, (*i.e.* away from active star forming regions) suggest the existence of dense ($n_{H_2} \sim 5 \times 10^3$ to 10^4 cm^{-3}) and cold ($T_k < 10K$) gas at the smallest scales. This was already the results reported by Penzias et al. (1972) in their pioneering CO observations of molecular clouds. If a lower density CO gas exists, it does not in cloud edges or in poorly shielded clouds where it is photodissociated. We examine now the possibility that matter is divided, even in dense cores, into myriads of small fragments of mass $M \sim 2.5 \times 10^{-11}\, n_{\mathrm{H}_2}\, R^3_{100AU}\, \mathrm{M}_\odot$.

4 - The unknown density gradients

The inferred local densities being orders of magnitude larger than the average densities derived at much larger scales, molecular clouds are necessarily quite inhomogeneous everywhere, which raises the question: at which scale does the inhomogeneity appear or are the density gradients large or small?

It has been argued by Gredel et al. (1992) that the highly contrasted observed CO structures are only apparent. The argument which relies on a detailed knowledge of the photodissociation process of the CO molecule, is as follows. Small fluctuations of the local UV field, most likely provided by fluctuations of N_{H_2} by 20% to 50% around $N_{\mathrm{H}_2} \sim 10^{21}\,\mathrm{cm}^{-2}$ are sufficient in the transition region where $A_v \sim 0.5$ to 1 mag to increase significantly the CO abundance, and thus the CO column density by factors as large as 2 to 10. A small increase in N_{H_2}, not necessarily associated with a large increase in n_{H_2}, therefore amplifies the brightness contrast in the CO emission, by generating a local enrichment in CO. This amplification is probably real, but the structure seen in CO cannot be only apparent. Indeed, the CO structures are really small compared to the clouds large scale of several pc or tens of pc and a smooth density gradient across a large scale cloud would not produce the observed small scale structure, unless unlikely geometries are imagined. Because CO is structured at scales as small as 0.05 pc, the column density fluctuations $\Delta N_{\mathrm{H}_2} \sim 3 \times 10^{20}\,\mathrm{cm}^{-2}$ must be produced over similar pathlengths Δl, so that locally $n_{\mathrm{H}_2} > 2 \times 10^3/(\Delta l/0.05\,\mathrm{pc})\,\mathrm{cm}^{-3}$.

In summary, CO emission traces dense gas in molecular clouds but, because it has structure at very small scale, even in poorly shielded components, it also reveals the existence of large density contrasts, either between the CO–rich gas and the H_2 shielding layer or between the H_2 layer and the atomic gas. The internal thermal pressure of this gas is therefore of the order $P_{th}/k \sim 5 \times 10^4\,\mathrm{K\,cm}^{-3}$ which is far above the thermal pressure of all the known components of the atomic medium. This introduces a new question. Since the dense and cold structures are neither held by self–gravity because they are not massive enough nor by external thermal pressure, what is the mechanism for confining them? Or are they highly transient structures?

An element of answer comes from the measurements which exist now of the average kinetic energy density in clouds $P_{kin} = 1/2\, \rho\, \delta v^2$ where δv is the internal non–thermal velocity dispersion of a given structure (Myers & Goodman 1988 a,b; Falgarone, Puget & Pérault 1992). The kinetic pressure is found to fluctuate by two orders of magnitude from place to place about an average value independent of the scale or the cloud density, $\overline{P}_{kin}/k \sim 3 \times 10^4$ K cm^{-3} which is of the order of the pressure due to the weight of the HI layer in the disk of the Galaxy (Cox 1991). In addition, the kinetic pressure is comparable to the magnetic pressure derived from recent measurements of the field intensity in dark clouds $B^2/8\pi \sim 10^5\, k\, \mathrm{erg\,cm^{-3}}$ (Crutcher et al. 1993; Heiles et al. 1993; Goodman et al. 1994). Magneto–hydrodynamic turbulence is therefore an attractive frame to understand the evolution of the cold molecular clouds.

5 - What are the plausible physical processes at the origin of the self–similar structure of interstellar clouds?

Self–similarity manifests itself in the fractal structure of the cloud maps in several tracers and in the existence of power laws, among which the cloud mass spectra, the size–linewidth relation, and the mass–size relation. Yet, as the size of the samples of analysed clouds increases, it is no longer clear whether these power laws exist with a single exponent across four or five orders of magnitude. Recent determinations of the slope of the cloud mass spectra, $dN/dM \propto M^{-\alpha}$, span a broad range, from $\alpha \sim 1.7$ for three different nearby clouds (see the review of Stutzki 1993) and masses in the range $10^{-3} - 10^2$ $M_\odot$, to $\alpha \sim 1$ over a more reduced mass range (Williams & Blitz 1993). Early determinations from galactic surveys provided $1.5 < \alpha < 1.8$ for cloud masses in the range $10^4 - 10^6$ $M_\odot$. The exponent of the size–linewidth relation is not either the same depending on the cloud samples. In the samples of Larson (1981), Falgarone & Phillips (1990), Falgarone, Puget, Pérault (1992) it is close to 1/3, the value expected for incompressible turbulence while in those extracted from galactic surveys it is somewhat larger, ~ 0.5 (Dame et al. 1986; Solomon et al. 1987). When combined with the mass–size scaling law, $M \propto R^2$, the latter value means that large scale complexes are in virial balance between gravitational and internal kinetic energy, which may no longer be true at smaller scales where the cloud lifetimes are shorter.

These variations may reflect real changes in the physics of the hierarchy of clouds from the largest to the smallest structures. However, the self–similar structure of the entire medium, in space as well as in velocity–space, cannot be ignored. It reveals a coupling between the scales and an energy (and/or angular momentum) cascade, the question being now: what is the mechanism which drives the cascade.

Gravitational torques have been proposed long ago (Larson 1984; Henriksen & Turner 1984). It is an attractive scheme because it naturally connects the structure of the cold medium to the star formation process. However, it is in conflict with the fact that the scaling laws encompass the self–gravitating scales and include structures which are up to 10^4 times above virial balance (see the review of Falgarone 1994), if the gas mass determinations are correct (see the above sections). Another attractive possibility is a (magneto)hydrodynamic turbulent cascade. Interstellar turbulence is indeed quite different from turbulence studied experimentally or in numerical simulations. But there is some universality in turbulence, and as long as, in the equation of motion, no other force term dominates by one order of magnitude the non–linear $\mathrm{v} \cdot \nabla \mathrm{v}$ term, the dynamical evolution is controlled by this non–linear coupling.

Interstellar gas motions all have extremely large Reynolds numbers (see the review of Scalo, 1987), and this has been the basis of the turbulence hypothesis, which raises a vivid controversy (see the review of Elmegreen 1993). If the search for a correlation length of turbulence in molecular clouds has always been unsuccessful (Scalo 1984; Pérault, Falgarone & Puget 1986; Kitamura et al. 1993), it does not mean that turbulence is not present because, in a turbulent velocity field, correlations exist at all scales. A different approach to this question is the synthesis of molecular line spectra generated in the velocity field computed in numerical simulations of compressible turbulence (Porter, Pouquet and Woodward 1992; 1993 a and b). The unexpected result is the statistical resemblance of the synthetic spectra with those observed in molecular clouds, even in the optically thin approximation (Falgarone et al. 1994). These simulations show that shocks have a minor contribution to the non–Gaussian shapes of the line profiles and that turbulence generates velocity correlations in space which strikingly resemble the observations.

Another interesting aspect of the physics of turbulence is the fact that the velocity field cannot be described only as a random field, because it contains coherent structures (possibly at the origin of the phenomenon called intermittency, see Gagne 1987; Douady, Couder & Brachet 1991; Vincent & Meneguzzi 1991). These coherent structures are also those in which the dissipation of the turbulent kinetic energy is concentrated, giving rise to extremely localized regions in space and time where the kinetic temperature may reach very large values (Falgarone & Puget 1994). If detected in the interstellar medium, these regions would be a specific signature of the presence of turbulence.

6 - Concluding remarks.

The recent improvements in the receiver sensitivity, angular resolution and accessible wavelength ranges have permitted real observational breakthroughs, in the sense that our knowledge of the interstellar medium is no longer confined to the brightest regions (*i.e.* the star forming regions) but extend over the immense areas of placental gas. This allows a global approach to the self–similar structure of the cold interstellar medium which was not feasible ten years ago. Conspicuous enigma still exist, such as the value of the threshold in the hierarchy of the cold medium, the actual density and mass distribution at the smallest scales, or the reliability of the tracers of cold H_2. Furthermore, it becomes clear that, at small scale, clouds can no longer be described conveniently through their average properties and that the knowledge of the fluctuations of these properties may be as important as that of their average. Last, the processes at work in shaping the medium are the object of a vivid controversy and are presently unknown. Gravity, magnetic field and turbulence are all present but with time–varying relative importances in the history not only of a given cloud but of a piece of cloud, not to mention the additional contribution of all the thermal effects, driven or not by the UV irradiation... All the attempts at reproducing the complex structure of the interstellar clouds by considering one of these processes separately have failed. Turbulence is especially attractive given its ability to reproduce the observed molecular line profiles. Many observational tests, namely the possible signature of intermittency, are required before it can be assessed.

REFERENCES

Albrecht M.A. & Kegel W.H. 1987, *A&A*, **176**, 317.

Alllen, R.J. & Lequeux J. 1993, *ApJ*, **410**, L15.

André P., Montmerle T., Feigelson E.D., & Steppe H. 1990, *A&A*, **240**, 321.

Boissé P. 1990, *A&A*, **228**, 483.

Boulanger F. 1994 *First Symposium on infrared cirrus and diffuse interstellar clouds* eds. R. Cutri and W. Latter, The Arizona University Press.

Carroll T.J. & Goldsmith P.F. 1981, *ApJ*, **245**, 891.

Clemens D.P. & Barvainis R. 1988, *ApJS*, **68**, 257.

Combes F. 1991, *Ann. Rev. Astron. Astrophys.*, **29**, 195.

Cox, D. 1991 *Fragmentation of Molecular Clouds and Star Formation*, eds. E. Falgarone, F. Boulanger, & G. Duvert, Kluwer Acad. Pub..

Crutcher R.M., Troland T.H., Goodman A.A., Heiles C., Kazes I., Myers P.C. 1993, *ApJ*, **407**, 175.

Dame T. M. Elmegreen B.G. Cohen R.S. Thaddeus P. 1986, *ApJ*, **305**, 892.

de Vries, H.W., Heithausen, A., & Thaddeus, P. 1987, *ApJ*, **319**, 723.

Diamond P.J. et al. 1989, *ApJ*, **347**, 302.

Douady, S., Couder, Y. & Brachet, M.E. 1991, *Phys. Rev. Letters*, **67**, 983.

Drdla K., Knapp G.R. & van Dishoeck E.F. 1989, *ApJ*, **345**, 815.

Elmegreen B.G. 1993 in *Protostars and Planets III*, eds. E.H. Levy & J.I. Lunine, The university of Arizoña Press.

Falgarone, E. & Pérault 1988, *A&A*, **205**, L1.

Falgarone, E. & Phillips T.G. 1990, *ApJ*, **359**, 344.

Falgarone, E. & Phillips T.G. 1991 *Fragmentation of Molecular Clouds and Star Formation*, eds. E. Falgarone, F. Boulanger, & G. Duvert, Kluwer Acad. Pub..

Falgarone, E., Phillips, T. G., & Walker C. 1991, *ApJ*, **378**, 186.

Falgarone, E., Puget, J.-L., & Pérault, M. 1992, *A&A*, **257**, 715.

Falgarone E., Lis, D.C., Phillips, T.G., Pouquet A., Porter, D.H. & Woodward, P.R. 1994 in preparation.

Falgarone, E. & Puget J.-L. 1994 in preparation.

Falgarone E. 1994 *First Symposium on infrared cirrus and diffuse interstellar clouds* eds. R. Cutri and W. Latter, The Arizona University Press.

Fiedler R.L., Dennison, B. Johnston, K.J., Hewish A. 1987, *Nature*, **326**, 675.

Fuller G., Falgarone, E., Puget, J.-L. & Myers P.C. 1994, in preparation.

Gagne, Y. 1987, Thèse d'Etat, Université de Grenoble..

Goodman, A.A., Myers, P.C., Güsten, R., Heiles, C. 1994, *First Symposium on infrared cirrus and diffuse interstellar clouds* eds. R. Cutri and W. Latter, The Arizona University Press.

Gredel R., van Dishoeck, E.F., de Vries, C.P. & Black, J.H. 1992, *A&A*, **257**, 245.

Hartquist TW Dyson JE Williams DA 1992, *MNRAS*, **257**, 419.

Heiles, C., Goodman, A.A., McKee, C.F., Zweibel, E.G. 1993 in *Protostars and Planets III*, eds. E.H. Levy & J.I. Lunine, The university of Arizona Press.

Heithausen, A., Stacy, J.G., de Vries, H.W., Mebold, U. & Thaddeus, P. 1993, *A&A*, **268**, 265.

Henriksen R.N. & Turner B.E. 1984, *ApJ*, **287**, 200.

Herbertz, R., Ungerechts, H. & Winnewisser, G. 1991, *A&A*, **249**, 483.

Joncas, G., Boulanger, F. & Dewdney, P.E. 1992, *ApJ*, **397**, 165.

Kalberla P.M.W., Schwarz U.J. & Goss W.M. 1985, *A&A*, **144**, 27.

Kegel W.H., Piehler G., Albrecht M.A. 1993, *A&A*, **270**, 407.

Kitamura Y., Sunada K., Hayashi M., Hasegawa T. 1993, *ApJ*, **413**, 221.

Larson R.B. 1981, *MNRAS*, **194**, 809.

Larson R.B. 1984, *MNRAS*, **206**, 197.

Larson R.B. 1992, *MNRAS*, **256**, 641.

Le Bourlot J., Pineau des Forêts G., Roueff E., Flower D.R. 1993, *A&A*, **267**, 233.

Lequeux J., Allen R.J. & Guilloteau S. 1993, *A&A*, **280**, L23.

Lucas R. & Liszt H.S. 1993, *A&A*, **276**, L33.

Marscher A.P. Moore E.M. Bania T.M. 1994 *Astrophys. J. Letters* in press.

Mauesberger R. Wilson T.L. Mezger P. Gaume R. Johnston K.J. 1992, *A&A*, **256**, 640.

Mezger P. et al. 1992a, *A&A*, **256**, 631.

Mezger P. et al. 1992b, *A&A*, **265**, 743.

Myers, P.C., & Goodman A. 1988a, *ApJ*, **326**, L27.

Myers, P.C., & Goodman A. 1988b, *ApJ*, **329**, 392.

Penzias A.A., Solomon P.M., Jefferts K.B. & Wilson R.W. 1972, *ApJ*, **174**, L43.

Pérault, M., Falgarone, E., and Puget, J.L. 1986, *A&A*, **157**, 139.

Porter, D.H., Pouquet, A., & Woodward, P.R. 1992, *Phys. Rev. Lett.*, **68**, 3156.

Porter, D.H., Pouquet, A., & Woodward, P.R. 1993, *Theor. Comp. Fluid Dynamics* in press.

Porter, D.H., Pouquet, A., & Woodward, P.R. 1994, *Phys. Fluids A* in press.

Rubio M., Garay G., Montani J. & Thaddeus P. 1991, *ApJ*, **368**, 173.

Sanders D.B., Scoville N.Z., Tilanus R.P.J. Wang Z. & Zhou S. 1992 in *Back to the Galaxy* ed. F. Verter, (Dordrecht: Kluwer).

Sanders D.B. 1994 in *Sky Surveys: Protostars to Protogalaxies.*

Scalo J.M. 1984, *ApJ*, **277**, 556.

Scalo J.M. & Pumphrey W.A. 1982, *ApJ*, **258**, L26.

Scalo, J.M. 1987 in *Interstellar Processes* eds D.J. Hollenbach & H.A. Thronson, Reidel: Dordrecht.

Scalo, J.M. 1990 in *Physical Processes in Fragmentation and Star Formation*, eds R. Capuzzo-Dolcetta et al., Kluwer Academic Publ.: Dordrecht.

Schulz A., Güsten R., Zylka R., Serabyn E. 1991, *A&A*, **246**, 570.

Solomon P.M., Rivolo A.R., Barrett J., Yahil A. 1987, *ApJ*, **319**, 730.

Stutzki, J., 1993, in *Reviews of Modern Astronomy*, **6** 209, ed. G. Klare, The Astronomische Gesellschaft Pub..

Ungerechts, H. & Thaddeus, P. 1987, *ApJS*, **63**, 645.

van Dishoeck, E.F. & Black J.H. 1988, *ApJ*, **334**, 771.

van Dishoeck E.F. 1992, in *Astrochemistry of Cosmic Phenomena* ed. P.D. Singh, Dordrecht: Kluwer.

van Dishoeck E.F. et al. 1992 in *Astrochemistry of Cosmic Phenomena* ed. P.D. Singh, Dordrecht: Kluwer.

Vincent, A. & Meneguzzi, M. 1991, *J. Fluid Mech.*, **225**, 1.

Williams & Blitz L. 1993, *ApJ*, **405**, L75.

Wilson T.L. & Walmsley C.M. 1989, *A&A Review*, **1**, 141.

Zimmermann, T. 1993, PhD Thesis, University of Köln, Germany.

Zimmermann, T. & Ungerechts H. 1990, *A&A*, **238**, 337.

John Bally : An Astrophysicist beats the Particle Physicists !

MAGNETIC FIELD DISSIPATION AND CONTRACTION OF MOLECULAR CLOUDS

TAKENORI NAKANO†, RYOICHI NISHI‡, AND TOYOHARU UMEBAYASHI*
†Nobeyama Radio Observatory, National Astronomical Observatory
Nobeyama, Nagano 384-13, Japan
‡Department of Physics, Kyoto University, Kyoto 606, Japan
*Data Processing Center, Yamagata University, Yamagata 990, Japan

ABSTRACT

The magnetic flux Φ of a cloud or a cloud core is 0.1 to 1 times the critical flux $\Phi_{\rm cr}$ which is proportional to its mass M. The Φ/M (or equivalently $\Phi/\Phi_{\rm cr}$) ratio for a cloud or cloud core is several hundred to 10^5 times greater than the ratio for magnetic stars with mean surface field of 1 to 30kG. The dissipation of magnetic fields in clouds is complicated because they contain various kinds of charged particles (electrons, ions, and grains) whose degree of freezing to field lines is widely different and whose relative abundance changes drastically as the cloud contracts. With a quite general formalism applicable to such wide range of physical situation we investigate field dissipation in clouds containing ice-mantled grains, and find that there is a decoupling density $n_{\rm dec}$ such that the flux loss time t_B is less than the free-fall time $t_{\rm f}$ only at the cloud density $n_{\rm H} > n_{\rm dec}$ and that $t_B \simeq (10-500)t_{\rm f}(\Phi_{\rm cr}/\Phi)^2$ at $n_{\rm H} \ll n_{\rm dec}$ at least for $\Phi \simeq (1-0.1)\Phi_{\rm cr}$. The value of $n_{\rm dec}$ depends rather sensitively on the grain model and the minimum value we have found is $4 \times 10^9 {\rm cm}^{-3}$ including the cases of grains without ice mantles. Because a cloud with $\Phi < \Phi_{\rm cr}$ can begin dynamical contraction whose time scale is not much longer than $t_{\rm f}$, extensive flux loss down to far below $\Phi_{\rm cr}$ does not occur at least at $n_{\rm H} \ll 4 \times 10^9 {\rm cm}^{-3}$. In the past some numerical simulations were done on the quasistatic contraction of clouds induced by magnetic field dissipation by assuming that the gas moves only across field lines, and the results are quite different from the results on the realistic three-dimensional contraction. We summarize the essence and causes of this difference.

1. INTRODUCTION

Magnetic fields have various important effects on the processes of star formation. In this article we discuss the dissipation of magnetic fields and its effects on cloud contraction with some of our new results. We review in §2 the magnetic flux problem in star formation and in §3 the processes and the rate of magnetic field dissipation in molecular clouds. In §4 we discuss the effect of the cloud geometry on the cloud contraction.

2. THE MAGNETIC FLUX TO MASS RATIO OF INTERSTELLAR CLOUDS

Magnetic fields have significant effects on the contraction of interstellar clouds. An oblate cloud or cloud core, which has contracted somewhat along magnetic field lines, cannot contract dynamically when the magnetic flux through it, Φ, is greater than a critical flux

$$\Phi_{\rm cr} = b\ G^{1/2}M, \tag{1}$$

where M is the mass of the cloud or cloud core, G is the gravitational constant, and b is a constant of order unity[1), 2), 3)]. We take $b \simeq 2\pi$ in this paper. When the magnetic field outside the cloud is much weaker than in the cloud, the ratio of the mean magnetic force to the mean gravitational force in the cloud is nearly equal to $(\Phi/\Phi_{\rm cr})^2$. For a prolate cloud with the major axis parallel to field lines the magnetic force is stronger than the self-gravity even for some range of Φ less than $\Phi_{\rm cr}$. Therefore a cloud or a cloud core with $\Phi > \Phi_{\rm cr}$ must lose some magnetic flux before it can begin dynamical contraction.

If magnetic fields are nearly frozen to the gas during contraction of the cloud, the magnetic flux to mass (Φ/M) ratio, or equivalently $\Phi/\Phi_{\rm cr}$, of the cloud hardly changes. Nakano[4), 5)] showed that the $\Phi/\Phi_{\rm cr}$ ratio for molecular clouds takes values between about 0.1 and 1 and is 10^5 to several hundred times greater than the ratio for magnetic stars with mean surface field B_* of 1 to 30 kG. If we compare with nonpeculiar stars, the discrepancy in $\Phi/\Phi_{\rm cr}$ is even greater. Mouschovias[6)] asserts that Paleologou and Mouschovias[7)] first showed that the $\Phi/\Phi_{\rm cr}$ ratio for clouds is 10^2 to 10^5 times the ratio for stars. Although they wrote these values, they did not show how or by whom these values were derived. In addition to $B_* \simeq 1$kG Nakano[4)] writes on the comparison with a star of $B_* \simeq 30$kG. Substituting this value into Nakano's equation (6), one can easily find out that the lower bound to this ratio is several hundred. The value of several hundred to 10^5 has effectively been obtained by Nakano[4)]. Irrelevance of Mouschovias' remarks[6)] on Nakano has also been pointed out by Whitworth[8)]. Mouschovias[9)] writes that a cloud core of mass $\sim 1M_\odot$ has a flux 10 to 10^2 times $\Phi_{\rm cr}$ at least initially. For example, he considers that a spherical $1M_\odot$ blob of interstellar matter with the mean density ρ and magnetic field ($\simeq 3\mu$G) of the interstellar medium has $\Phi \simeq 10^2\Phi_{\rm cr}$. However, because the radius of this blob, $2.5(\rho/10^{-24}{\rm g\ cm^{-3}})^{-1/3}$ pc, is much smaller than the Jeans wavelength in this medium, $\lambda_{\rm J} \simeq 180(\rho/10^{-24}{\rm g\ cm^{-3}})^{-1/2}$ pc[4)], this part cannot contract by itself even along field lines, and then this part alone cannot become a star. Therefore it is of no use, or even misleading, to discuss the $\Phi/\Phi_{\rm cr}$ ratio of such a part. Only a part of the interstellar medium whose length along field lines is greater than $\lambda_{\rm J}$ can contract. The magnetic flux Φ of such a part is at most of the order of $\Phi_{\rm cr}$ as shown by Nakano[4)].

3. MAGNETIC FIELD DISSIPATION IN CLOUD CORES

The ohmic dissipation is quite inefficient in the ordinary interstellar clouds. Mestel and Spitzer[10)] showed that magnetic field dissipation in the ordinary interstellar clouds can be much more efficient than the ohmic dissipation because even if ions are nearly completely frozen to magnetic fields, ions and magnetic fields can drift in the sea of neutral particles because of very low ionization fraction. This process is called the ambipolar diffusion or plasma drift. The degree of freezing of a charged particle to magnetic fields is characterized by $\tau\omega$, the product of the cyclotron frequency ω of the particle and the viscous damping time τ of motion of the particle relative to the neutrals. When $\tau\omega \gg 1$, the particle is nearly completely frozen to magnetic fields. The molecular cloud contains various kinds of charged particles; electrons, many kinds of ions, and dust grains of various electric charge and size. The value of $\tau\omega$ is usually greater for a particle of smaller mass if the electric charge is the same. For example, $\tau\omega$ for an electron is about 30 times greater than for an ion HCO^+ and $\tau\omega$ for a grain of charge $\pm e$ with radius $a = 10^{-5}$ cm is 10^{-4} times that for this ion[5), 11)], where e is the unit electric charge. Because $\tau\omega \propto B/n_{\rm H}$, where B is magnetic field strength and $n_{\rm H}$ is the density of the gas by hydrogen number, and B increases more slowly than $n_{\rm H}$ even in flux-conserving contraction of the cloud, $\tau\omega$ for any particle decreases as the cloud contracts. Grains of $a \approx 10^{-5}$ cm are hardly frozen to magnetic fields in clouds of ordinary density. Even ions, which are frozen at such density, cannot be frozen at very high densities, *e.g.*, $n_{\rm H} \gtrsim 10^{10}\text{cm}^{-3}$. Moreover, while ions and electrons are dominant charged particles at low densities, grains of charge $\pm e$ are dominant at high densities and contribute most to preventing magnetic field dissipation even though they are not strongly coupled with magnetic fields. To investigate magnetic field dissipation in such wide range of the physical conditions of the cloud we need a general formalism on field dissipation. Nakano[5)] and Nakano and Umebayashi[11)] obtained such a formalism which can be summarized as follows.

Let us consider an arbitrary closed contour C in a cloud. When a point on C moves with a velocity $\mathbf{v}$ relative to the neutrals, the magnetic flux Φ through this contour changes with time according to

$$\frac{d\Phi}{dt} = -\oint_{\rm C} [(\mathbf{v} - \mathbf{v}_B) \times \mathbf{B}] d\mathbf{s}, \tag{2}$$

where $d\mathbf{s}$ is an infinitesimal line element along contour C. Because the magnetic flux Φ is conserved when every point on C moves with $\mathbf{v} = \mathbf{v}_B$, we call $\mathbf{v}_B$ the drift velocity of magnetic fields. Components of $\mathbf{v}_B$ parallel to magnetic force $\mathbf{j} \times \mathbf{B}/c$ (say the x-component) and perpendicular to both $\mathbf{B}$ and magnetic force (the y-component) are respectively given by

$$v_{Bx} = \frac{A_1}{A} \frac{1}{c} \mid \mathbf{j} \times \mathbf{B}|, \tag{3}$$

$$v_{By} = -\frac{A_2}{A} \frac{1}{c} \mid \mathbf{j} \times \mathbf{B}|, \tag{4}$$

where $\mathbf{j} = (c/4\pi)\nabla \times \mathbf{B}$ is the electric current density and

$$A_1 = \sum_\nu \frac{\rho_\nu \omega_\nu^2}{\tau_\nu \Omega_\nu^2}, \quad A_2 = \sum_\nu \frac{\rho_\nu \omega_\nu}{\tau_\nu^2 \Omega_\nu^2}, \quad A = A_1^2 + A_2^2, \quad \Omega_\nu^2 = \omega_\nu^2 + \frac{1}{\tau_\nu^2}. \tag{5}$$

Here c is the light velocity and ρ_ν, $\omega_\nu = q_\nu eB/m_\nu c$, τ_ν, m_ν, and $q_\nu e$ are the mass density, cyclotron frequency, viscous damping time, mass, and electric charge, respectively, of particle ν. To obtain simpler expression of the equations we have defined ω_ν so that it takes a negative value for a negatively charged particle. We need not define the component of $\mathbf{v}_B$ along $\mathbf{B}$ (or the z-component) because time variation of Φ is not related to this component as seen from equation (2). The dissipation rate of magnetic fields is determined only by v_{Bx} as shown by Nakano and Umebayashi[11]. This is self-evident for axisymmetric clouds because the drift in the azimuthal (y-)direction has nothing to do with magnetic flux loss of the cloud. The magnetic flux loss time, or the dissipation time of magnetic fields, can be given by $t_B = -\Phi/(d\Phi/dt) \simeq l/v_{Bx}$, where l is the length scale of magnetic fields.

From this general formalism we can derive formulae for some limiting cases. The first case is for $|\tau_\nu \omega_\nu| \gg 1$ at least for dominant charged particles. In this case we have $\Omega_\nu \simeq \omega_\nu$ and then $A_1 \simeq \sum_\nu \rho_\nu/\tau_\nu$ and $|A_2| \ll A_1$. Therefore we have from equations (3) and (5)

$$v_{Bx} \simeq \frac{1}{A_1}\,\frac{1}{c}\,|\,\mathbf{j}\times\mathbf{B}| \simeq \Big(\sum_\nu \frac{\rho_\nu}{\tau_\nu}\Big)^{-1}\,\frac{1}{c}\,|\,\mathbf{j}\times\mathbf{B}|. \tag{6}$$

The last expression of this equation is the terminal velocity of charged particles with which the magnetic force on them balances with the frictional force by the neutrals. Because the charged particles are nearly completely frozen to magnetic fields in this case, their drift velocity is the same as that of magnetic fields. Thus this is the drift velocity of fields by ambipolar diffusion. Equation (6) is a generalization of the drift velocity obtained by Mestel and Spitzer[10] which contains only the ion term in the summation.

The second limiting case is for $|\tau_\nu \omega_\nu| \ll 1$ at least for dominant charged particles. Because $\Omega_\nu \simeq 1/\tau_\nu$ in this case we have

$$A_1 \simeq \sum_\nu \rho_\nu \tau_\nu \omega_\nu^2 = \frac{B^2}{c^2}\sigma, \tag{7}$$

where $\sigma = \sum_\nu e^2 q_\nu^2 \tau_\nu n_\nu / m_\nu$ is the electrical conductivity with n_ν the number density of particle ν. We also have $A_2 \simeq \sum_\nu \rho_\nu \omega_\nu = (eB/c)\sum_\nu n_\nu q_\nu = 0$ because of charge neutrality of the gas. Therefore we have

$$v_{Bx} \simeq \frac{1}{A_1}\,\frac{1}{c}\,|\mathbf{j}\times\mathbf{B}| \simeq \frac{c^2}{4\pi\sigma l}, \tag{8}$$

The last expression of this equation has been obtained by taking $|\mathbf{j}\times\mathbf{B}|/c = |(\nabla\times\mathbf{B})\times\mathbf{B}|/4\pi \simeq B^2/4\pi l$. Finally we have

$$t_B \simeq \frac{l}{v_B} \simeq \frac{4\pi\sigma l^2}{c^2}. \tag{9}$$

This is nothing but the time scale of the ohmic dissipation which depends on the electric conductivity σ and the length scale of magnetic fields l but does not depend on the field strength B.

Thus equation (3) contains both the effects of ambipolar diffusion and ohmic dissipation. Magnetic field dissipation can be described by this equation for any situation as long as the fraction of charged particles is very small.

In addition to the interaction with magnetic fields and with the neutrals, grains have an important role in determining the ionization fraction through recombination of ions and electrons at grain surface. The dissipation rate of magnetic fields is rather sensitive to the grain model, especially to the size distribution[12), 13]. Here we consider ice-mantled grains.

Similar to the size distribution of grains without ice mantles as proposed by Mathis, Rumpl, and Nordsieck[14] we assume that grain cores have a power-law size distribution

$$\frac{dN}{da_c} = A a_c^{-3.5} \tag{10}$$

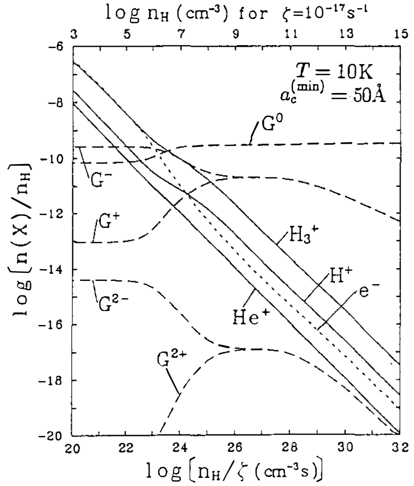

Fig. 1. The abundances of various particles relative to hydrogen in the gas with ice-mantled grains with $a_c^{(\min)} = 50\text{Å}$. Grains are denoted as G with a superscript representing their electric charge and ζ is the ionization rate of hydrogen by cosmic rays and radioactive elements.

for the core radius a_c between 2500Å and some minimum value $a_c^{(\min)}$, where $A = 1.5 \times 10^{-25}\text{cm}^{2}$ [5]. We assume that the ice mantle is composed of H_2O, CH_4, NH_3, and CO, that the mantle thickness b is independent of a_c because the growth rate of the mantle must be determined by the flux of condensable molecules on grains irrespective of a_c, and that there are no heavy elements in the gas phase. The value of b depends on $a_c^{(\min)}$ and the fraction of the condensable elements. Because of the uncertainty in $a_c^{(\min)}$ we consider the four cases of the combination $(a_c^{(\min)}, b)$=(30, 122), (50, 180), (100, 304), and (200, 520) in Å.

In molecular clouds shielded from ultraviolet radiation ions are first formed by ionization of H_2 and He by cosmic rays and radioactive elements and transformed into some sorts of molecular ions. Atomic ions can recombine radiatively and molecular ions can dissociatively with electrons. Both kinds of ions also recombine at grain surface and this process is more efficient than the other recombination processes at high densities. The gas in dense clouds is nearly in ionization-recombination equilibrium. Figure 1 shows the relative abundances of various particles as functions of the density n_H for the case of $a_c^{(\min)} = 50\text{Å}$ and the gas temperature $T = 10\text{K}$. In this figure ζ is the ionization rate of an H_2 molecule by cosmic rays and radioactive elements, and grains are represented as G with the superscript showing their electric charge. For the case of $\zeta = 10^{-17}\text{s}^{-1}$ ions and electrons are dominant charged particles only at $n_H < 10^6\text{cm}^{-3}$, and at $n_H > 10^8\text{cm}^{-3}$ grains are dominant and electrons are about 60 times less abundant than the ions (see Nakano[5] for the reason of this).

First we consider a cloud which is kept nearly in equilibrium by magnetic force across field lines, *i.e.*, $\Phi \simeq \Phi_{cr}$, and by the gas pressure along them. The contraction induced by magnetic flux loss is highly nonhomologous[15), 16), 17)], and only the central part of the cloud contracts rapidly. The time scale of such a nonhomologous process is nearly equal to the flux loss time in the central part of the cloud whose size across field lines is nearly equal to the size along them. This time scale is determined by the mean density of this part and is independent of the total mass of the cloud[12)]. Figure 2 shows this time scale t_B for the four models of the ice-mantled grains together with the case without ice mantles with $a^{(\min)} = 50\text{Å}$. The free-

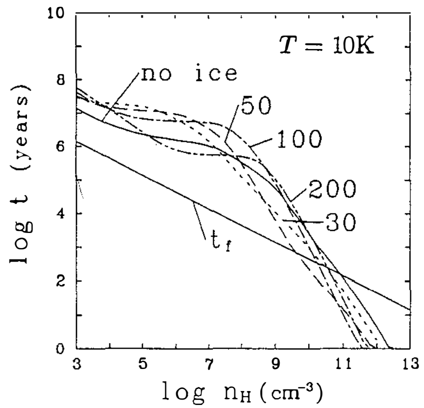

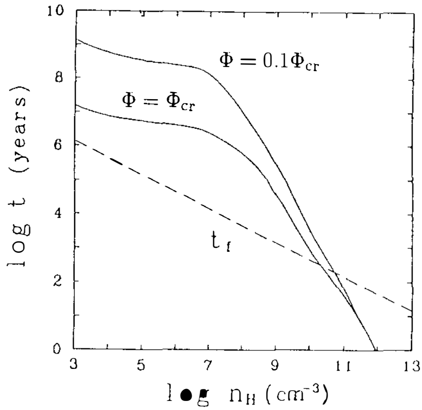

Fig. 2 (left). The time scale of magnetic flux loss, t_B, for the cloud core of $\Phi \simeq \Phi_{cr}$ with ice-mantled grains. Each curve is labeled with the value of $a_c^{(min)}$ in Å. For comparison t_B for the case of grains without ice mantles with the minimum radius $a^{(min)} = 50$Å is shown by the solid curve and the free-fall time t_f by the solid straight line.

Fig. 3 (right). The time scale t_B for the cloud core with $\Phi \simeq \Phi_{cr}$ and $\Phi \simeq 0.1\Phi_{cr}$ for grains without ice mantles (from Nishi *et al.*[13]).

fall time t_f is also shown for comparison. For all cases there is a critical density n_{dec} only above which $t_B < t_f$ holds. We find that t_B is 10 to 500 times t_f at $n_H \ll n_{dec}$ and decreases rapidly at higher densities. Because clouds usually cannot contract faster than free fall, magnetic fields are nearly completely decoupled from the gas at $n_H \gtrsim n_{dec}$. The value of n_{dec} is between 4×10^9 and 10^{11}cm^{-3} for the models in Fig. 2. For the other grain models investigated so far[11), 12), 13)] n_{dec} is between 10^{10} and 10^{12}cm^{-3}. Each curve for t_B in Fig. 2 has a nearly flat part in some density region. In this region the smallest grains are nearly frozen to magnetic fields ($\tau|\omega| \gtrsim 1$) and contribute to preventing field dissipation more efficiently than the other charged particles (*e.g.*, ions).

For $\Phi < \Phi_{cr}$, t_B is proportional to Φ^{-2} when dominant charged particles are frozen to magnetic fields because v_{Bx} is proportional to B^2 as seen from equation (6), while t_B is independent of Φ or B when dominant charged particles are not frozen as seen from equation (8). Transition from $t_B \propto \Phi^{-2}$ to $t_B \propto \Phi^0$ can be seen in Fig. 3 in which t_B for $\Phi = \Phi_{cr}$ and for $\Phi = 0.1\Phi_{cr}$ is shown as a function of the density for grains with no ice mantles[13]. Situation is the same for the other grain models.

The above results can be summarized as follows. At least for $\Phi \simeq (0.1-1)\Phi_{cr}$ we have

$$t_B \simeq (10-500)\left(\frac{\Phi_{cr}}{\Phi}\right)^2 t_f \qquad (11)$$

at $n_H \ll n_{dec}$, while t_B is almost independent of Φ at $n_H \gtrsim n_{dec}$.

The cloud core with $\Phi < \Phi_{cr}$ contracts dynamically if its mass is much smaller than the Jeans critical mass. Even if its mass is nearly equal to the Jeans mass, it easily begins dynamical contraction because a nearly isothermal cloud is unstable[18]. The dynamical contraction proceeds almost in a free-fall time t_f which is much shorter than t_B at the cloud density

$n_H \ll n_{dec}$. Therefore, extensive magnetic flux loss down to far below Φ_{cr} is impossible at $n_H \ll n_{dec}$ and then at least at $n_H \ll 4 \times 10^9 \mathrm{cm}^{-3}$.

4. CONTRACTION OF MAGNETIZED CLOUDS

Computer simulations have been made on quasistatic contraction of clouds induced by magnetic field dissipation for various cloud configurations: in chronological order, oblate clouds which contract along and across field lines[15), 16), 17)] (here we call this the 3D contraction), slab clouds with field lines parallel to the slab surfaces in which the gas is assumed to move only across field lines[19)] (the 1D contraction), and cylindrical clouds with field lines parallel to cylinder axes in which the gas is also assumed to move only across field lines[20), 21)] (the 2D contraction). The 1D and 2D contractions shown by these simulations are quite different from the 3D contraction on some important points. In the 3D contraction the quasistatic contraction ends (shifts to dynamical contraction) when the magnetic flux Φ of the cloud core decreases close to the critical flux Φ_{cr} even if the density of the core is much lower than n_{dec}, the amount of the magnetic flux lost at $n_H < n_{dec}$ is not large, and the contraction is highly nonhomologous. In the 1D and 2D contractions the magnetic flux of the clouds can decrease by several orders of magnitude even at $n_H \ll n_{dec}$, and contraction is quasistatic up to $n_H \simeq n_{dec}$ and is not so highly nonhomologous as in the 3D contraction. We shall survey the causes for these differences in the following.

4.1 The 1D Contraction of Disks with Horizontal Magnetic Fields

A disk in equilibrium has a pressure at the midplane given by $P_c = \pi G\Sigma^2/2$, where $\Sigma = \int_{-\infty}^{\infty} \rho dz \simeq 2\rho_c H$ is the surface density of the disk, ρ_c and H being the density at the midplane and the effective half-thickness of the disk, respectively. The magnetic flux of the disk can also be given by $\Phi = \int_{-\infty}^{\infty} B dz \simeq 2B_c H$, where B_c is the field strength at the midplane. When the disk is supported by the gas pressure and magnetic force, or $P_c = C_s^2\rho_c + B_c^2/8\pi$, where C_s is the isothermal sound velocity, we have

$$\frac{\Phi^2}{32\pi H^2} + \frac{C_s^2\Sigma}{2H} \simeq \frac{\pi}{2}G\Sigma^2. \tag{12}$$

From this equation we find that an equilibrium state exists for any non-zero Φ even if the gas pressure is negligible. This means that there is *no* critical magnetic flux for such disks. Because $\rho_c \simeq 2\pi G^{1/2}\Sigma^2/\Phi$ when the gas pressure is minor, we have for the contraction time

$$t_{\rm cont} \equiv \left(\frac{1}{\rho_c}\frac{d\rho_c}{dt}\right)^{-1} \simeq -\left(\frac{1}{\Phi}\frac{d\Phi}{dt}\right)^{-1} \equiv t_B. \tag{13}$$

Because the magnetic flux loss time t_B for the disk is nearly the same as that for the oblate cloud investigated in §3 if the mean density is the same and the magnetic force nearly balances with the gravity, we have $t_{\rm cont} > t_{\rm f}$ at $n_H < n_{dec}$. Therefore as long as the initial magnetic flux is sufficiently large, contraction of the disk is quasistatic up to $n_H \simeq n_{dec}$ and dynamical only at $n_H \gtrsim n_{dec}$. Because $\Phi \propto \rho_c^{-1}$, the magnetic flux may decrease with contraction by several orders of magnitude even at $n_H \ll n_{dec}$. This is the process followed by the 1D simulations[19)].

However, the disks with horizontal magnetic fields are gravitationally unstable and break into fragments in a free-fall time $t_{\rm f}$[22), 23)], which is much shorter than $t_B \simeq t_{\rm cont}$ at $n_H \ll n_{dec}$. This means that the gas motion along field lines, which was inhibited in the 1D simulations[19)], actually proceeds much faster than the motion across field lines and the disk changes its configuration into a quite different one before significant magnetic flux loss occurs as pointed out by Nakano[24]. Finally each fragment must establish pressure equilibrium along field lines like the clouds studied in the 3D simulations.

4.2 The 2D Contraction of Cylinders with Longitudinal Magnetic Fields

A cylinder in equilibrium has a pressure on the symmetry axis given by $P_c \simeq G\Lambda\rho_c/2$, where ρ_c is the density on the axis and $\Lambda = \int_0^\infty 2\pi r\rho dr \simeq \pi R^2\rho_c$ is the line density (mass per unit length) of the cylinder and R is the effective cylinder radius. The magnetic flux of the cylinder is given by $\Phi = \int_0^\infty 2\pi rBdr \simeq \pi R^2 B_c$, where B_c is the field strength on the axis. When the cylinder is supported by gas pressure and magnetic fields, we have

$$\frac{\Phi^2}{8\pi^3 R^4} \simeq \frac{G\Lambda}{2\pi R^2}\left(\Lambda - \frac{2C_s^2}{G}\right). \tag{14}$$

As seen from this equation, the cylinder can take an equilibrium state for any non-zero Φ even if the gas pressure is negligible. This means that there is no critical magnetic flux for such cylinders. When the gas pressure is negligible, we find $\rho_c \simeq 4\pi G\Lambda^3/\Phi^2$ and then the contraction time

$$t_{\rm cont} \equiv \left(\frac{1}{\rho_c}\frac{d\rho_c}{dt}\right)^{-1} \simeq -\left(\frac{2}{\Phi}\frac{d\Phi}{dt}\right)^{-1} \equiv \frac{1}{2}t_B. \tag{15}$$

Because t_B is nearly the same for the cylinder and the oblate cloud in §3 for the same mean density as long as the magnetic force balances with the gravity, we again have $t_{\rm cont} \gg t_{\rm f}$ at $n_{\rm H} \ll n_{\rm dec}$. Therefore as long as the initial magnetic flux is sufficiently large, the contraction is quasistatic up to $n_{\rm H} \simeq n_{\rm dec}$ and the cloud contracts dynamically only at $n_{\rm H} \gtrsim n_{\rm dec}$. Because $\Phi \propto \rho_c^{-1/2}$ the magnetic flux decreases with contraction by orders of magnitude even at $n_{\rm H} \ll n_{\rm dec}$.

However, such a cylinder is gravitationally unstable and breaks into fragments in a growth time nearly equal to the free-fall time $t_{\rm f}$[25], which is much shorter than $t_{\rm cont}$ at $n_{\rm H} \ll n_{\rm dec}$. This means that the gas motion along field lines, which was inhibited in the 2D simulations[20, 21], actually proceeds much faster than the motion across field lines and the disk changes its configuration into a quite different one before significant magnetic flux loss occurs. Finally each fragment must establish pressure equilibrium along field lines and contract three-dimensionally as numerically simulated by Nakano[15, 16, 17].

4.3 The 3D Contraction of Magnetized Clouds

The essence of the 3D contraction has been derived by Nakano[26] which can be summarized as follows. Let us consider a cloud core with mass M, radius R, and mean field strength B embedded in a medium with field strength B_0. The magnetic tube penetrating the core has a radius $R_0 = R(B/B_0)^{1/2}$ far from the core. When the core is mainly supported by magnetic force, the virial theorem for this core[5], $GM^2/R \simeq (B^2R^3 - B_0^2R_0^3)/4\pi^2$, can be rewritten as

$$\frac{R}{R_0} \simeq 1 - f^2, \tag{16}$$

where $f = \Phi_{\rm cr}/\Phi$ is the ratio of the critical flux $\Phi_{\rm cr} \simeq 2\pi G^{1/2}M$ to the flux $\Phi = \pi R^2 B$ of the core. The pressure equilibrium along field lines gives the central density of the core

$$\rho_c \simeq \frac{\pi G\Sigma^2}{2C_s^2} \simeq \frac{B_0^2}{2\pi C_s^2}\frac{f^2}{(1-f^2)^4}. \tag{17}$$

As seen from equations (16) and (17), R decreases and ρ_c increases indefinitely as Φ approaches Φ_{cr} ($f \rightarrow 1$) as long as the gas pressure is negligible. From equation (17) the quasistatic contraction time is obtained as

$$t_{cont} \equiv \left(\frac{1}{\rho_c}\frac{d\rho_c}{dt}\right)^{-1} \simeq \frac{1-f^2}{2(1+3f^2)}t_B, \tag{18}$$

where $t_B = -\Phi/(d\Phi/dt) = f/(df/dt)$ is the flux loss time of the core. As f approaches 1, t_{cont} decreases indefinitely. This means that the contraction shifts from quasistatic to dynamical one at some stage before Φ decreases to Φ_{cr}. By setting $t_{cont} \simeq t_f$ in equation (18) we find that this shift occurs at the stage of $f \simeq (1 + t_f/t_B)^{-1}$, or

$$\frac{\Phi}{\Phi_{cr}} \simeq 1 + \frac{t_f}{t_B}, \tag{19}$$

assuming $t_f/t_B \ll 1$. Thus the 3D cloud can contract dynamically when Φ is smaller than that given by equation (19) even at $n_H \ll n_{dec}$.

Roughly speaking t_B is a decreasing function of n_H as seen from Fig. 2. Because t_{cont} is nearly equal to t_B for the 1D and 2D systems [see equations (13) and (15)] and then a denser cloud contracts faster, we can expect that the central region with higher density contracts faster than the outer region. Increase of the central density further accelerates contraction of the central region. Thus we can expect some nonhomology in the 1D and 2D contraction. In the 3D system in addition to this effect t_{cont} is proportional to $1 - f^2$. The central region must have f closer to 1 than the outer region and f is generally not very far from 1. Therefore the contrast in $1 - f^2$ between the central and outer regions must be much more conspicuous than the contrast in t_B. Thus the 3D quasistatic contraction is much more nonhomologous than the 1D and 2D contractions.

4.4 Summary on Flux Loss and Contraction

We have confirmed that the 1D and 2D contractions are quite different in some essential points from the realistic 3D contraction. This difference is caused by the (non-)existence of the critical magnetic flux which comes from the dependence of the forces on the length scales of the clouds. Table 1 shows the dependence of some quantities on the length scales of the clouds for 1D, 2D, and 3D systems. The strength of the magnetic force can be given by $|(\nabla \times \mathbf{B}) \times \mathbf{B}|/4\pi \simeq B^2/4\pi l$, where l is the smallest length scale of magnetic configuration in the cloud. For the 3D system l is nearly equal to the length scale of the cloud along field lines, Z. As seen from Table 1, for 1D and 2D systems the dependence of the magnetic force on the length scale is different from that of the gravity. Therefore for non-zero Φ the cloud can settle down in an equilibrium state by adjusting the length scale H or R even if the gas pressure is negligible. For the 3D system the magnetic force and the gravity have the same dependence on R (radius of the cloud across field lines) and Z, and then the cloud can settle down in an equilibrium state only when Φ takes some special value which is proportional to the cloud mass M. This is nothing but the critical magnetic flux given by equation (1).

The magnetic flux loss time, t_B, or the instantaneous rate of magnetic field dissipation, is nearly the same for the 1D, 2D, and 3D systems as long as the magnetic force balances with the gravity and the mean density is the same. On the other hand, because the length scales of the cloud change with contraction and the dependence of the magnetic and gravitational forces on the length scales is different among the three systems, the fundamental nature of the contraction is inevitably different among them. This is another explanation on the difference in the contraction described above. Because the gas motion along field lines, which

Table 1. Dependence of some physical quantities on the length scales of the clouds for 1D, 2D, and 3D systems

	1D	2D	3D
l (smallest length scale)	H	R	Z
Φ	BH	BR^2	BR^2
ρ	Σ/H	Λ/R^2	M/R^2Z
magnetic force.........	$B^2/4\pi H \propto \Phi^2/H^3$	$B^2/4\pi R \propto \Phi^2/R^5$	$B^2/4\pi Z \propto \Phi^2/R^4Z$
gravitational force.....	$G\Sigma\rho \propto \Sigma^2/H$	$G\Lambda\rho/R \propto \Lambda^2/R^3$	$GM\rho/R^2 \propto M^2/R^4Z$

is inhibited in the 1D and 2D simulations, proceeds in reality much faster than the motion across them in these systems, and the force laws are quite different from those in the 3D system, we can learn little from the 1D and 2D simulations.

REFERENCES

1) Mestel, L. 1965, *Quarterly J. Roy. Astron. Soc.*, **6**, 265.
2) Mestel, L. 1966, *Monthly Notices Roy. Astron. Soc.*, **133**, 265.
3) Strittmatter, P. A. 1966, *Monthly Notices Roy. Astron. Soc.*, **132**, 359.
4) Nakano, T. 1983, *Publ. Astron. Soc. Japan*, **35**, 87.
5) Nakano, T. 1984, *Fundament. Cosmic Phys.*, **9**, 139.
6) Mouschovias, T. Ch. 1991, in *The Physics of Star Formation and Early Stellar Evolution*, ed. C. J. Lada and N. D. Kylafis (Kluwer Academic Publishers), p. 61.
7) Paleologou, E. V., and Mouschovias, T. Ch. 1983, *Astrophys. J.*, **275**, 838.
8) Whitworth, A. 1992, *Observatory*, **112**, 236.
9) Mouschovias, T. Ch. 1991, *Astrophys. J.*, **373**, 169.
10) Mestel, L., and Spitzer, L., Jr. 1956, *Monthly Notices Roy. Astron. Soc.*, **116**, 503.
11) Nakano, T., and Umebayashi, T. 1986, *Monthly Notices Roy. Astron. Soc.*, **218**, 663.
12) Umebayashi, T., and Nakano, T. 1990, *Monthly Notices Roy. Astron. Soc.*, **243**, 103.
13) Nishi, R., Nakano, T., and Umebayashi, T. 1991, *Astrophys. J.*, **368**, 181.
14) Mathis, J. S., Rumpl, W., and Nordsieck, K. H. 1977, *Astrophys. J.*, **217**, 425.
15) Nakano, T. 1979, *Publ. Astron. Soc. Japan*, **31**, 697.
16) Nakano, T. 1982, *Publ. Astron. Soc. Japan*, **34**, 337.
17) Nakano, T. 1983, *Publ. Astron. Soc. Japan*, **35**, 209.
18) Hayashi, C., and Nakano, T. 1965, *Prog. Theor. Phys.*, **34**, 754.
19) Mouschovias, T. Ch., Paleologou, E. V., and Fiedler, R. A. 1985, *Astrophys. J.*, **291**, 772.
20) Mouschovias, T. Ch., and Morton, S. A. 1992, *Astrophys. J.*, **390**, 144.
21) Mouschovias, T. Ch., and Morton, S. A. 1992, *Astrophys. J.*, **390**, 166.
22) Nakano, T. 1988, *Publ. Astron. Soc. Japan*, **40**, 593.
23) Nakamura, F., Hanawa, T., and Nakano, T. 1991, *Publ. Astron. Soc. Japan*, **43**, 685.
24) Nakano, T. 1988, in *Galactic and Extragalactic Star Formation*, ed. R. E. Pudritz and M. Fich (Kluwer Academic Publishers), p. 111.
25) Nakamura, F., Hanawa, T., and Nakano, T. 1993, *Publ. Astron. Soc. Japan*, **45**, No. 4, in press.
26) Nakano, T. 1990, *Monthly Notices Roy. Astron. Soc.*, **242**, 535.

DYNAMICS AND OUT OF EQUILIBRIUM CHEMISTRY IN MOLECULAR CLOUD ENVELOPES

Constance de BOISANGER and Jean-Pierre CHIEZE

Centre d'Etudes de Bruyères-le-Châtel, Service PTN
91680 Bruyères-le-Châtel, France

ABSTRACT

In this work, we emphasize the importance of the coupling between the thermal, chemical and dynamical interstellar gas evolution. We suggest that, at scales of 1 pc or less, part of the molecular gas turbulence and condensation is due to variations of the UV field intensity. Using 2D hydrodynamical simulations and 1D chemico-hydrodynamical models, we show that these variations are efficient in triggering both gas condensation and fluid motions. Moreover, this process provides a natural background for out of equilibrium chemical abundances.

1. INTRODUCTION

In regions not strongly affected by shocks or outflows from young stellar objects, the origin of turbulence and gas condensation in the cold interstellar medium is always unclear. Moreover, observed abundances of different atomic or molecular chemical species are not compatible with those predicted by pseudo-time dependent models, so that out of equilibrium models have been proposed[1)].

Since it is likely that, due to the mutual shading of moving clumps, the distribution of UV field in fragmented molecular clouds is non uniform, we propose a new process in which the energy required to drive turbulence and condensation is extracted from the thermal energy of the gas, by variations of the ultraviolet radiation field. In Section 1, we present 2D hydrodynamical simulations of molecular cloud envelopes, in which the microscopic processes which govern the heating and cooling of the gas have been taken into account. They show that, in gas of initial density up to a few 100 cm^{-3}, variations of the ultraviolet field intensity by a factor of ten (or, equivalentely, variations by 1 *mag* of the visual extinction) generate a sonic velocity field, along with the formation of discrete transient blobs of condensed gas[2),3)].

In Section 2, we present preliminary results, obtained with a 1D chemico-hydrodynamical model of a molecular cloud envelope exposed to a varying UV field, which show that the process proposed above, gives out of equilibrium abundances, in particular high fractions of CI, in good agreement with the observed values. Furthermore, we show that out of equilibrium effects push back the chemical transition between regions of high and low electronic abundances[4)] into the dense part of the cloud.

2. THERMAL AND DYNAMICAL EVOLUTION OF THE INTERSTELLAR GAS

Assuming an initial slab geometry, we calculate the response of a molecular cloud envelope exposed to a varying UV interstellar radiation field. The perturbation of the UV flux moves parallel to the x-axis, with an absolute velocity 0.2 km s^{-1}, and consists in reducing the incident UV field intensity over a limited region of the cloud surface by at most a factor of ten. The cloud surface is free, in pressure equilibrium with a virtual medium of constant pressure. Periodic boundary conditions are imposed along the x-axis.

The initial density and temperature profiles correspond to thermal, chemical and hydrostatic equilibrium in a uniform gravitational field (parallel to the z-axis) : from the surface to the bottom, the initial gas density, temperature and internal extinction vary from: $n_H \sim 40$ cm^{-3}, $T \sim 80$ K and $A_v \sim 0.1$ mag to $n_H \sim 10^5 - 10^6$ cm^{-3}, $T \sim 15$ K and $A_v \sim 40$ mag.

The gas heating and cooling rates[2)] are calculated at each time step and at each mesh point in the envelope. In order to get reasonable computer time, the chemical abundances are determined assuming, throughout these 2D simulations, chemical equilibrium for the

instantaneous local density, temperature and UV intensity.
The perturbation induces a strong decrease in the dominant heating rates. Shielded gas cools down and condenses by a factor of 5 to 10. In steady state, velocities are in the range 0.3 km s^{-1} to 0.7 km s^{-1} (Figure 1).

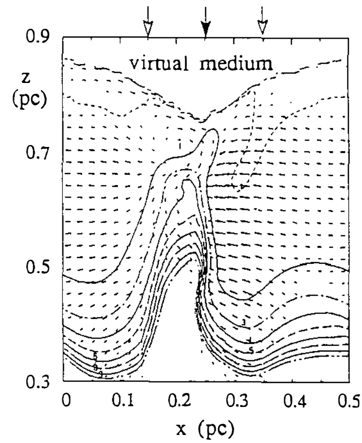

Figure 1 : 2D simulation of a cloud envelope : isodensity contours (between n_H = 50 and 850 cm^{-3}) and velocity field (v_{max} = 0.7 km s^{-1}). The arrows indicate the center and the total width of the UV perturbation.

3. OUT OF EQUILIBRIUM CHEMICAL EVOLUTION

In order to study the coupling between dynamics and out of equilibrium thermal and chemical gas evolution, we have developed a 1D chemico-hydrodynamical model. The kinetic chemical equations, coupled to the hydrodynamical ones, are solved in each zone of the model and at each time step using an implicit scheme, which would be described in a forthcoming paper. The chemical network is a modified and updated version of the dark cloud chemistry described by Pineau des Forêts et al.[5] : the major change concerns the rate for the dissociative recombination of H_3^+, which has been taken to be 1.5 10^{-7} $(T/300)^{-0.5}$ cm^3s^{-1} [6]. The original network has been reduced from 50 to 32 species - and 165 reactions: we have checked that this reduced network gives the same abundances, for the dominant species, than the larger one. The heating and cooling processes are the same than in the preceding simulations.

As a first application, we examine, once again, the effects of a varying UV field on molecular gas. Initially the plane parallel cloud model, exposed to the standard UV field, is at chemical, thermal and isobaric equilibrium (gravity has not been taken into account in this study). We mimick the effect of the external shielding clump by adding to the internal visual extinction (originally equal to zero at the surface) a perturbation $\Delta A_v \sim$ 1 mag. The external pressure is maintained to the initial equilibrium one. As discussed in the preceding section, the gas cools and condenses due to the shielding (Figure 2). But now the chemical abundances evolve with their own time scales. Since the formation of CO is a slow process, high abundances of CI are obtained during the evolution. At a given

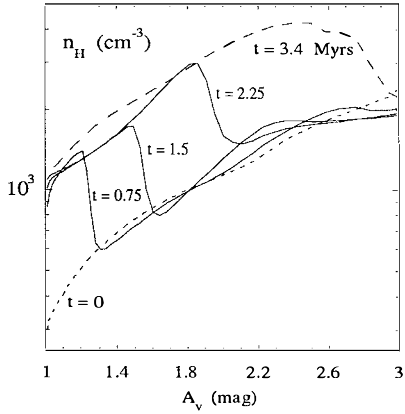

Figure 2 : hydrogen nuclei density versus total visual extinction at different times.

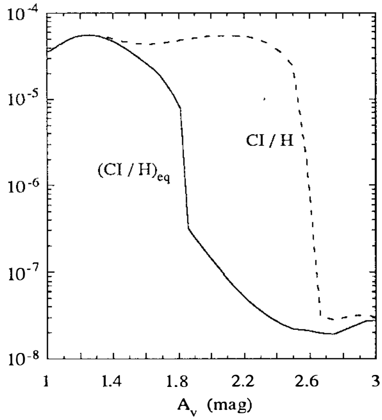

Figure 3 : fraction of atomic carbon, at t = 3.4 Myrs (dashed line) and at chemical equilibrium for the same density profile (solid line).

time, comparison with equilibrium abundances, which would be derived from equilibrium calculations for the same density profile, show large differences (Figure 3) and the location of the steep chemical transition[7] is displaced.

4. CONCLUSION

Illumination of intermediate density atomic and molecular gas, by a non uniform UV radiation field, generates gas condensation and fluid motions in the range 0.3 - 0.7 km s^{-1}, which can contribute to the observed turbulence. Furthermore, preliminary results of 1D chemico-hydrodynamical cloud models, show that this process goes with important out of equilibrium chemical effects : in particular, high atomic carbon abundances are obtained during gas condensation.

REFERENCES

[1] Chièze, J. P., Pineau des Forêts, G. & Herbst, E.,1991, Ap. J., 373,110

[2] de Boisanger, C., & Chièze, J.P.,1991, A & A,241, 581

[3] Bréart de Boisanger, C., Chièze, J.P. & Meltz, B.,1992, Ap. J., 401,182

[4] Pineau des Forêts, G., Roueff, E. & Flower, D. R., 1992, M.N.R.A.S., 258, 45p

[5] Pineau des Forêts, G., Flower, D.R., Dalgarno, A.: 1988, M.N.R.A.S., 235, 621.

[6] Canosa, A., Gomet, J.C., Rowe B., Mitchell J.B.A., Queffelec J.L.,1992, J. Chem. Phys., in presss.

[7] Flower, D. R., Le Bourlot, J., Pineau des Forêts, G. & Roueff, E., 1993, submitted to A & A

A CHEMICAL STUDY OF THE PHOTODISSOCIATION REGION NGC 7023

A. Fuente, J. Martín-Pintado, J. Cernicharo, R. Bachiller
Centro Astronómico de Yebes (IGN), Spain

ABSTRACT

To investigate the effects of the UV radiation on the chemistry of nitrogenated molecules, we have carried out an observational study of the reflection nebula NGC 7023. We have mapped a region of 3′×3′ over the photodissociation region (PDR) in millimeter transitions of ^{12}CO, ^{13}CO, $C^{18}O$, HCO^+, HCN, HNC and N_2H^+. Spectra of CS, CN and C_2H and of the rarer isotopic species $H^{13}CO^+$, $H^{13}CN$, and $HN^{13}C$, were also obtained at selected positions. We find evidences of selective photodissociation in the estimated $^{13}CO/C^{18}O$ ratio. Futhermore, all molecular abundances, except those of CN and perhaps C_2H, decrease towards the star, and significant gradients in the values of some molecular abundance ratios (the HNC/HCN ratio decreases by a factor of 5, the N_2H^+/HCO^+ ratio decreases by a factor of 12, the CN/HCN ratio increases by a factor of 8 and the (CN+HCN+HNC)/NH_3 ratio increases by a factor of 30 towards the star position) reveal the existence of important chemical changes towards the star. Chemical equilibrium model calculations have been carried out in order to interpret the observed behavior. Our results show that the variations found in molecular abundances cannot be explained by the kinetic temperature and/or the hydrogen density gradients measured in the nebula, but they are well explained by the influence of the stellar UV radiation on the chemistry of the molecular gas if the emission arises in a region at a visual extinction between 6 and 10 mag from the star. Molecular destruction in this region ($A_v \sim$ 6 mag) is due mainly to reactions with H^+, C, H, C^+, O, and to electronic recombination.

1 INTRODUCTION

One expects that newly formed stars alter chemically the clumps surrounding them. We have chosen the reflection nebula NGC 7023 to carry out a detailed study of the influence of UV radiation on the nitrogenated molecules chemistry. The results of previous works[1),2)] show that NGC 7023 has a favorable geometry for this kind of project. Futhermore, although a bipolar outflow[6),2)] is likely to be associated with HD 200775 (the star illuminating NGC 7023), the relative narrowness of the CO and NH_3 lines[1),2)] suggest that shock fronts are not the dominant process in this nebula.

2 OBSERVATIONAL RESULTS

All the observations were carried out with the IRAM 30m telescope on Pico de Veleta (Granada, Spain). Our observational results can be summarized as follows:

1. The abundances of ^{13}CO, $C^{18}O$, HCO^+, HCN, HNC, and CS decrease towards the star. Table 1 shows the estimated fractional molecular abundances of HCN, HNC, N_2H^+ and HCO^+ towards some selected positions in the nebula. Offsets are relative to the star position. Note that all the molecular abundances, except those of CN and perhaps C_2H decrease towards the star. Some of them, like HCO^+ and HNC abundances, decrease by a factor >30 (See R_{ph} in Table 1).

2. The behavior of the $^{13}CO/C^{18}O$ ratio suggests the existence of selective photodissociation effects in these isotopes. Fig. 1 shows the ^{13}CO and $C^{18}O$ column densities, and the $^{13}CO/C^{18}O$ column density ratio as a function of the distance from the star for a strip in declination at a constant offset in right ascension of 0″. This ratio takes values of $\sim$ 10 close to the star, increases up to values of $\sim$ 20 - 30 at a distance of 60″ - 80″ from the star and then decreases again to values $\sim$ 10 further away. This enhancement of the $^{13}CO/C^{18}O$ ratio can be explained in terms of selective photodissociation (isotopic fractionation can also contribute to enhance the $^{13}CO/C^{18}O$ ratio for kinetic temperatures T_k<36K).

3. Significant variations in the values of the abundance ratios when approaching to the star prove the existence of chemical changes in this direction. These changes can be summarize as follows:

   - The HNC/HCN ratio decreases by a factor of $\sim$ 5 (see Fig. 2).
   - The CN/HCN ratio increases by a factor of $\sim$ 8 and the $(CN+HCN+HNC)/NH_3$ increases by a factor $\geq$ 35 (see Fig. 2).
   - The N_2H^+/HCO^+ ratio decreases at least by a factor of 12.

Table 1. Fractional molecular abundances[1]

Offsets (″)	$C^{18}O$ (10^{-8})	HCO^+ (10^{-9})	HCN (10^{-10})	HNC (10^{-10})	CN (10^{-10})	CS (10^{-10})	NH_3^2 (10^{-9})	N_2H^+ (10^{-10})	C_2H (10^{-9})
(0,0)	1.2						≤0.1		
(-10,20)	2.4	0.02	0.3	0.2	2.5	0.3		≤1.0	≤0.8
(-30,50)	7.6	0.4	1.4	0.7	6.2	0.8	0.1	≤0.7	0.6
(-50,40)	7.4		4.2	2.3		1.3	0.3		
(-30,80)	4.7	1.3	1.1	6.7	5.7	3.0	2.1	1.8	0.9
(-20,100)	10.4	0.9	1.3	3.1	1.6	1.8	3.4	1.5	0.7
(20,130)		0.6	4.7	4.6			1.6	0.6	0.4
(-40,120)	6.7	0.4	3.7	2.8			0.7		
R^3_{ph}	9	65	15	33	2	10	≥34	≥2	≥1

[1] Defined as N(X)/N(H) where N(H) is the total hydrogen nuclei column density

[2] Data taken from[1)]

[3] R_{ph} is the ratio between the largest estimated abundance and the abundance at (-10″,20″)

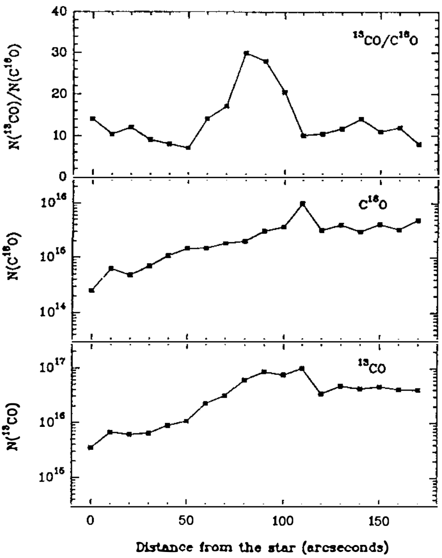

Fig. 1: ^{13}CO column density, $C^{18}O$ column density and $^{13}CO/C^{18}O$ column density ratio as a function of the distance from the star for a strip in declination for a constant offset in right ascension of 0″.

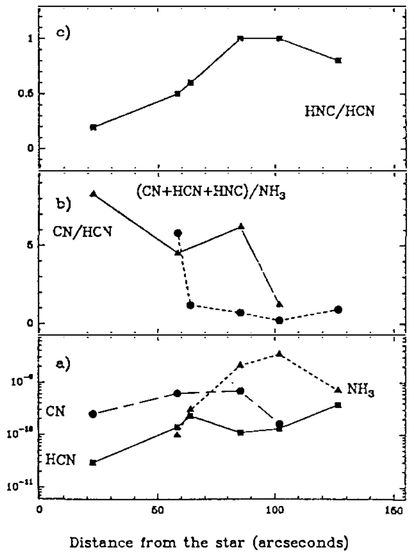

Fig. 2: Indicated fractional abundances and abundance ratios as a function of the distance from the star for the strip formed by the offsets (-10″,20″), (-30″,50″), (-30″,80″), (-20″,100″) and (-40″,120″).

3 CHEMICAL MODEL

In order to interpret the behavior of the chemical abundances found towards NGC 7023 we have carried out some chemical equilibrium calculations assuming different kinetic temperatures, hydrogen densities and visual extinctions from the star. The set of reactions used in our calculations is essentially the scheme of[4),5)] excluding the reactions involving PAHs, but including photodissociation and photoionization reactions. (See[3)] for more details.) The results can be summarized as follows:

- **We can explain the changes observed in the HNC/HCN abundance ratio as the effect of the increasing kinetic temperature and/or the effect of the increasing UV flux towards the star. However, the behavior observed in the CN/HCN and (CN+HCN+HNC)/NH_3 ratios can only be explained by the influence of the stellar UV radiation on the chemistry.**

- All the observed abundances except that of C_2H, and all the studied abundance ratios except the N_2H^+/HCO^+ one, are **consistent with those calculated theoretically for a region located at a visual extinction between 10 and 6 mag from the star,** and with the kinetic temperatures and hydrogen densities estimated from observational data. To account for the C_2H abundance and the N_2H^+/HCO^+ abundance ratio, we have to suppose that C_2H emission arise mainly in the low density envelope/interclump medium and that the N_2H^+ and HCO^+ emission come from regions with different density.

- Reactions with H, H^+, C, C^+, O, N and electronic recombination are the most important molecular destruction mechanisms for a visual extinction larger than 6 mag from the star (i.e., where the nitrogenated molecules emission is expected to arise).

The results of model calculations and the detailed comparison of theoretical predictions with observations are presented in[3)].

References

(1) Fuente A., Martín-Pintado J., Cernicharo J., Bachiller R., 1990, A & A 237, 471

(2) Fuente A., Martín-Pintado J., Cernicharo J., Brouillet N., Duvert G., 1992, A & A 260, 341

(3) Fuente A., Martín-Pintado J., Cernicharo J., Bachiller R., 1993, A & A, in press

(4) Pineau des Forets G., Flower D.R., Dalgarno A., 1988, MNRAS 235, 621

(5) Pineau des Forets G., Roueff E., Flower D.R., 1990, MNRAS 244, 668

(6) Watt G.D., Burton W.B., Choe S.-U., Liszt H.S., 1986, A & A 163, 194

(7) Whitcomb S.E., Gatley I., Hildebrand, R.H., Keene J., Sellgren K., Werner W., 1981, ApJ 246, 416

INTERACTING H_2O MASERS IN STAR-FORMING REGIONS

NIKOLAOS D. KYLAFIS
University of Crete, Physics Department
714 09 Heraklion, Crete, Greece
and
Foundation for Research and Technology-Hellas
P.O. Box 1527, 711 10 Heraklion, Crete, Greece

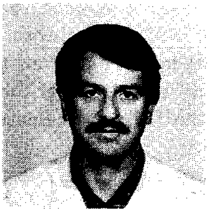

ABSTRACT

We (i.e., my student K. Pavlakis and I) have studied the interaction of H_2O masers in star forming regions as a physical mechanism for the explanation of the very strong H_2O maser sourses. We have carried out detailed numerical calculations for both saturated and unsaturated masers and have derived approximate analytic expressions for the expected brightness temperature from interacting masers. We have found that the interaction of two low or medium power masers can in principle lead to the appearance of a very strong one.

1. INTRODUCTION

An interesting idea regarding the powerful Galactic H_2O masers was proposed by Deguchi & Watson (1989). They demonstrated that two medium power masers, separated by distances characteristic of the size of star-forming regions and aligned to within the angular size of the beam of one maser, can result in reduced beam size and therefore enhanced brightness temperature. Elitzur, McKee, & Hollenbach (1991) extended the work of Deguchi & Watson and proposed that the two giant bursts of H_2O maser emission in W49 and Orion were the result of interacting masers.

In this paper we present a qualitative discussion of interacting (both saturated and unsaturated) masers. The results of our numerical calculations appear in a lengthier publication (Kylafis & Pavlakis 1992).

2. QUALITATIVE DISCUSSION

Consider a maser region in the form of a cylinder of diameter d and length l (see Figure 1). Its maser radiation is emitted mainly through the bases of the cylinder and into solid angles Ω along the axis of the cylinder. Let the brightness temperature of the maser along the axis of the cylinder be T_{b0}. Now consider in addition a background source (in Figure 1 it is shown as a similar maser) at a distance $D >> l$ from the maser and an observer on the other side of it. When the radiation of the background source enters the maser, and if its intensity is high, it causes the maser radiation to be emitted in the solid angle $\Omega_s \approx (d/D)^2 << \Omega$ (Deguchi & Watson 1989; for the case of dissimilar sources see Elitzur, McKee, & Hollenbach 1991). The observer on the right, who detects this radiation and does not know its origin, calculates an *isotropic* luminosity which is orders of magnitude larger than what would be inferred if the maser were alone. In what follows we explain qualitatively and quantitatively the effects of the background source on the observed intensity.

Let ϕ_i be the net rate (i.e., stimulated emission minus absorption) of maser photon production per unit volume due to the internal radiation of the maser and ϕ_s the corresponding rate due to the radiation of the background source. The photons produced with rate ϕ_i are emitted on either side of the maser and into solid angle 2Ω, while those produced with rate ϕ_s are emitted toward the observer and into solid angle $\Omega_s \approx (d/D)^2 << \Omega$.

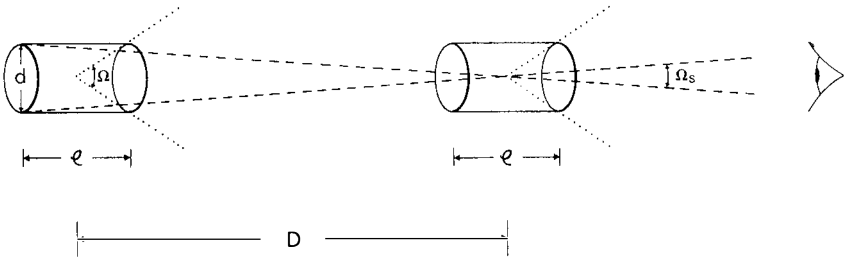

Fig. 1. Schematic representation of two similar masers interacting with each other.

The brightness temperature or the intensity seen by the observer can be written as

$$T_{obs} \approx (|T_x| + T_s)\exp(|\tau|) \qquad \text{or} \qquad I_{obs} \approx \frac{\phi_i}{2\Omega} + \frac{\phi_s}{\Omega_s}, \tag{1}$$

where T_x is the excitation temerature of the maser line, T_s is the brightness temperature of the background source and τ is the optical depth of the maser line.

For the sake of this qualitative discussion let us treat the intensity of the background source as a parameter. When the mean intensity of the photons that are produced with rate ϕ_s is much smaller than the mean intensity of those produced with rate ϕ_i, then clearly the effect of the source on the maser is negligible. An equivalent condition is $T_s << |T_x|$.

For collisionally pumped H_2O masers the excitation temperature is typically in the range $10^2 \lesssim |T_x| \lesssim 10^3$ K and $|\tau| \lesssim 25$ (Kylafis and Norman 1991).

As T_s increases, a point is reached where $T_s \approx |T_x|$ or $\phi_s/\Omega_s \approx \phi_i/2\Omega$. At this point, the effect of the background source on the observed intensity begins to become important. Note however that the equation $T_s \approx |T_x|$ implies $\phi_s << \phi_i$. That is, the radiation from the background source has a significant contribution to the observed intensity *despite the fact that it causes the production of a negligible number of photons.*

As T_s increases further, the observed intensity grows essentially linearly with T_s (see eq. [1]). This is because with $\phi_s << \phi_i$, the background radiation has a negligible effect on the populations N_1 and N_2 and therefore on τ and T_x.

The linear increase of T_b will continue until $\phi_s \approx \phi_i$. This occurs when $T_s \approx (2\Omega/\Omega_s)|T_x|$. At this point, equal number of photons are emitted into solid angles 2Ω and Ω_s. A further increase of T_s can have different effects on the observed intensity depending on whether the maser is saturated or unsaturated.

2.1. Saturated Masers

If the maser is saturated, then the photon production rate per unit volume ϕ_i has essentially its maximum possible value. That is, for every pumping event a photon is emitted. As T_s increases, ϕ_s increases, but only at the expense of ϕ_i. Thus, more and more photons that would be emitted into solid angle 2Ω are emitted into Ω_s and this last increase of T_s can at most increase the observed brightness temperature by a factor of two.

In summary, to within a factor of two, the brightness temperature T_b^f of a saturated maser *in the direction of the observer* as a function of the brightness temperature T_s of the background source is given by

$$T_b^f \approx \begin{cases} T_{b0}, & \text{if } T_s \lesssim |T_x|; \\ (T_{b0}/|T_x|)T_s, & \text{if } |T_x| \lesssim T_s \lesssim |T_x|(2\Omega/\Omega_s); \\ T_{b0}(2\Omega/\Omega_s), & \text{if } |T_x|(2\Omega/\Omega_s) \lesssim T_s \,. \end{cases} \tag{2}$$

The background source affects not only the forward brightness temperature T_b^f, but also the brightness temperature T_b^b of the maser *in the direction of the source.* It is straightforward to show (Kylafis & Pavlakis 1992) that the background brightness temperature T_b^b of the maser is given by

$$T_b^b \approx \begin{cases} T_{b0}, & \text{if } T_s \lesssim |T_x|(2\Omega/\Omega_s); \\ T_{b0}(|T_x|/T_s)(2\Omega/\Omega_s), & \text{otherwise}\,. \end{cases} \tag{3}$$

If the background source is a maser (call it 2) identical to the one under study (call it 1), then T_s cannot be arbitrary. The radiation of maser 2 affects maser 1, but also the radiation of maser 1 affects maser 2. Self-consistency is obtained when the output of maser 2 is the input to maser 1 and visa versa (Deguchi & Watson 1989). This means $T_s = T_b^b$. Equating T_s with expression (3) we find that self-consistency requires

$$T_s = T_b^b \approx \left(T_{b0}|T_x|\frac{2\Omega}{\Omega_s}\right)^{1/2} \tag{4}$$

2.2. Unsaturated Masers

If the maser is unsaturated, then the photon production rate per unit volume ϕ_i is not the maximum possible. Therefore ϕ_s and consequently T_b^f can continue increasing linearly with T_s, while ϕ_i remains constant. This linear increase will stop when the maser saturates. For a collisionally pumped maser, saturation occurs roughly when the radiative rate becomes comparable to the typical collision rate $C_{ji} \approx 10^{-2}(n_{H_2}/10^9 \mathrm{cm}^{-3})\ \mathrm{s}^{-1}$ (Palma *et al.* 1988). From then on ϕ_s can increase only at the expense of ϕ_i and only a small increase in T_b^f can occur with increasing T_s.

According to the above discussion, one can write approximate analytic expressions similar to those for saturated masers. Thus, for the forward brightness temperature we have

$$T_b^f \approx \begin{cases} T_{b0}, & \text{if } T_s \lesssim |T_x|; \\ (T_{b0}/|T_x|)T_s, & \text{if } |T_x| \lesssim T_s \lesssim T_s^*; \\ (T_{b0}/|T_x|)T_s^*, & \text{if } T_s^* \lesssim T_s\ , \end{cases} \tag{5}$$

where T_s^* is a brightness temperature of the background source at which the net radiative rate becomes comparable to the typical collision rate. For the backward brightness temperature we have

$$T_b^b \approx \begin{cases} T_{b0}, & \text{if } T_s \lesssim T_s^*; \\ T_{b0}(T_s^*/T_s), & \text{otherwise}\ . \end{cases} \tag{6}$$

3. SUMMARY AND CONCLUSIONS

In agreement with previous work on interacting H_2O masers, we have found that the interaction of two low or medium power masers can in principle lead to the appearance of a very strong one.

The interaction of a very weak and a medium power maser can also lead to a very strong one.

We find it tempting to suggest that probably all H_2O masers in star-forming regions with observed brightness temperature $T_b \gtrsim 10^{13}$ K are the result of interacting masers. The reason for this is the following: To obtain brightness temperatures $T_b > 10^{13}$ K one needs aspect ratios (i.e., ratio of length to width) $a > 10$ if the maser region is static (Elitzur, Hollenbach, & McKee 1989) and $a \gtrsim 100$ if the maser region has velocity gradients (Kylafis & Norman 1991). Since velocity gradients are probably present in star-forming regions, it makes more sense to think of the masers with $T_b \gtrsim 10^{13}$ K as interacting masers rather than as very long cylinders.

REFERENCES

Deguchi, S., & Watson W. D. 1989, ApJ, 340, L17
Elitzur, M., Hollenbach, D. J., & McKee, C. F. 1989, ApJ, 346, 983
Elitzur, M., McKee, C. F., & Hollenbach, D. J. 1991, ApJ, 367, 333
Kylafis, N. D., & Norman, C. 1991, ApJ, 373, 525
Kylafis, N. D., & Pavlakis, K. G. 1992, ApJ, 400, 344
Palma, A., Green, S., DeFrees, D. J., & McLean, A. D. 1988, ApJS, 68, 287

HOT IN COLD : *ROSAT* X-RAY SOURCES IN MOLECULAR CLOUDS

Thierry Montmerle
Service d'Astrophysique, Centre d'etudes de Saclay
91191 Gif-sur-Yvette Cedex, France

ABSTRACT. Based on data collected by the "Einstein" satellite in the early 80's, the study of star-forming regions in soft X-rays had a strong impact on the understanding of the pre-main sequence evolution of low-mass stars (T Tauri stars), but little on molecular clouds and star formation *per se*. The newly available data from the ROSAT satellite, with an order-of-magnitude improvement in sensitivity and angular resolution over "Einstein", allows to address not only stellar problems like PMS evolution, dynamo-related magnetic activity, star-forming efficiencies, etc., but also problems related to molecular clouds. This is because X-rays have been found to be associated with deeply embedded objects, and therefore to provide an intense source of ionization in the dense regions of molecular clouds. In particular, these stellar X-rays may provide a feedback mechanism on star formation.

[Photograph courtesy of Serge Brunier©, *Ciel & Espace* magazine]

1. INTRODUCTION

One of the early discoveries of the "Einstein" satellite, around 1980, was that soft X-ray emission was ubiquitous throughout the H-R diagram. In addition, it was soon recognized that pre-main sequence (PMS) stars were among the brightest of the cool stars. Also, many X-ray sources near molecular clouds were found to be associated with previously unnoticed stars, which subsequent optical spectroscopy revealed to be very similar to "T Tauri stars" (~ solar mass PMS stars), but lacking their characteristic emission lines. The new PMS stars were therefore called "weak" T Tauri stars (or "WTTS"), in contrast with the previously known "classical" T Tauri stars ("CTTS"). This discovery was important for the understanding of early stellar evolution, since there were 2 to 3 times as many WTTS as there were CTTS: the known population of low-mass PMS stars had suddenly at least tripled. (It is now believed that, in rough terms, CTTS are WTTS surrounded by an optically thick circumstellar accretion disk; for a review, see, e.g., Bertout 1989).

Several nearby molecular clouds were observed with "Einstein", typically in a few exposures only thanks to the large field-of-view (~ 1 sq. degree) of the IPC instrument (see Giacconi et al. 1981): Orion (~ 450 pc), Taurus-Auriga, Ophiuchus, and Chamaeleon (~ 150 pc).

At the distance of the nearest clouds, the detectable X-ray luminosity was ~ 10^{29} erg.s^{-1} at minimum, and reached ~ 10^{32} erg.s^{-1} in flaring events, i.e., 10^2 to 10^5 times the quiescent solar X-ray luminosity. The X-ray emission mechanism is bremsstrahlung from a ~ 10^7 K plasma (kT ~ 1 keV), trapped in large magnetic loops. Most of the emission characteristics (timescales, temperature, densities, etc.) are basically solar in nature; given the observed levels of luminosity, one can speak of a "supersolar" activity (for reviews, see, e.g., Feigelson, Giampapa, & Vrba 1991, and Montmerle et al. 1993).

Most of the "Einstein" PMS sources were however found in the vicinity, or at best in the periphery, of molecular clouds, with a moderate extinction (A_V < a few units at most). As a result, the problems addressed by "Einstein" were entirely of a stellar nature: evolution of low-mass PMS stars, dispersal of the accretion disk of CTTS, which then evolve into WTTS, dependence of activity on age, rotation or other stellar parameters as a test of the dynamo mechanism (see, e.g., Montmerle et al. 1994), etc.

The advent of the ROSAT X-ray satellite (launched in 1990 and still operating; see, e.g., Trümper 1983), with an order-of-magnitude increase in sensitivity and angular resolution over "Einstein", has brought significant changes and improvements in the field of early stellar evolution: as we shall see, the number of PMS sources is severalfold larger than with "Einstein", allowing a much more statistically significant database (which is especially useful for stellar studies), and making it possible to probe deeply into molecular clouds, with potentially important implications on molecular cloud structure and star formation.

In this paper, we will concentrate on this last aspect, discussing the two first available cases of ROSAT observations of molecular clouds: Chamaeleon I and Ophiuchus.

2. THE CHAMAELEON I CLOUD

In a recent paper, Feigelson et al. (1993) discuss ROSAT observations of the Chamaeleon I dark cloud. In two overlapping ~ 6,000 sec. exposures, they find 70 X-ray sources with a good S/N ratio, and up to 19 more less reliable sources, which is a factor 3-4 more than earlier "Einstein" data (Feigelson & Kriss 1989). A deeper (~ 30,000 sec.) exposure (Krautter et al. 1994) yields only a handful more sources, indicating that the Feigelson et al. sample is essentially complete at a typical ROSAT level of sensivity. About 1/3 of these sources are new WTTS, and most of the others are CTTS and previously known WTTS, studied in the optical by Gauvin & Strom (1992). All the Cha I ROSAT sources have optical counterparts on photographic plates ($m_V \lesssim 18$), and their extinction is generally weak ($< A_V > \sim 1$). The X-ray luminosities range from ~ 6×10^{28} to ~ 2×10^{31} erg s^{-1}. Fig. 1 shows the location of these sources in relation with an IRAS contour map of the cloud. The H-R diagram of the optically studied sources indicates an average age of ~ 10^7 yrs.

One of the most striking results is a previously unknown (and still unexplained) tight correlation, in the form of a proportionality, between the X-ray luminosity L_X and the stellar mass M_*. This allows the use the X-rays to estimate the star formation efficiency (SFE): from the X-ray luminosity function, one can derive a mass function, yielding an estimate of ~ 200 low-mass ($0.1 < M_*/M_\odot < 5$) young stars present in the cloud (half of them being too faint to be detected by ROSAT even in long exposures), with a combined mass of ~ 150 $M_\odot$. On the other hand, the molecular content of the cloud is poorly known: its large angular size has up to now prevented a complete CO survey with a good angular resolution using the SEST. From the IRAS map (see Fig. 1), two dense cores may be seen, with a mass of ≈ 300 - 500 $M_\odot$ estimated from CO data. This yields an SFE ≲ 20 %.

IR studies (e.g., Prusti, Whittet, & Wesselius 1992) show a small number of "Class I" sources (evolved protostars), with respect to "Class II" and "Class III" sources (embedded CTTS and WTTS, respectively; for details on the classification of IR sources, see André & Montmerle 1994, and André, this volume, and ref's. therein). Combined with the small mass of the molecular cores and the relatively large age of the TTS, this indicates that star formation activity in Cha I is low at present, although the relatively high SFE suggests that it must have been higher in the past.

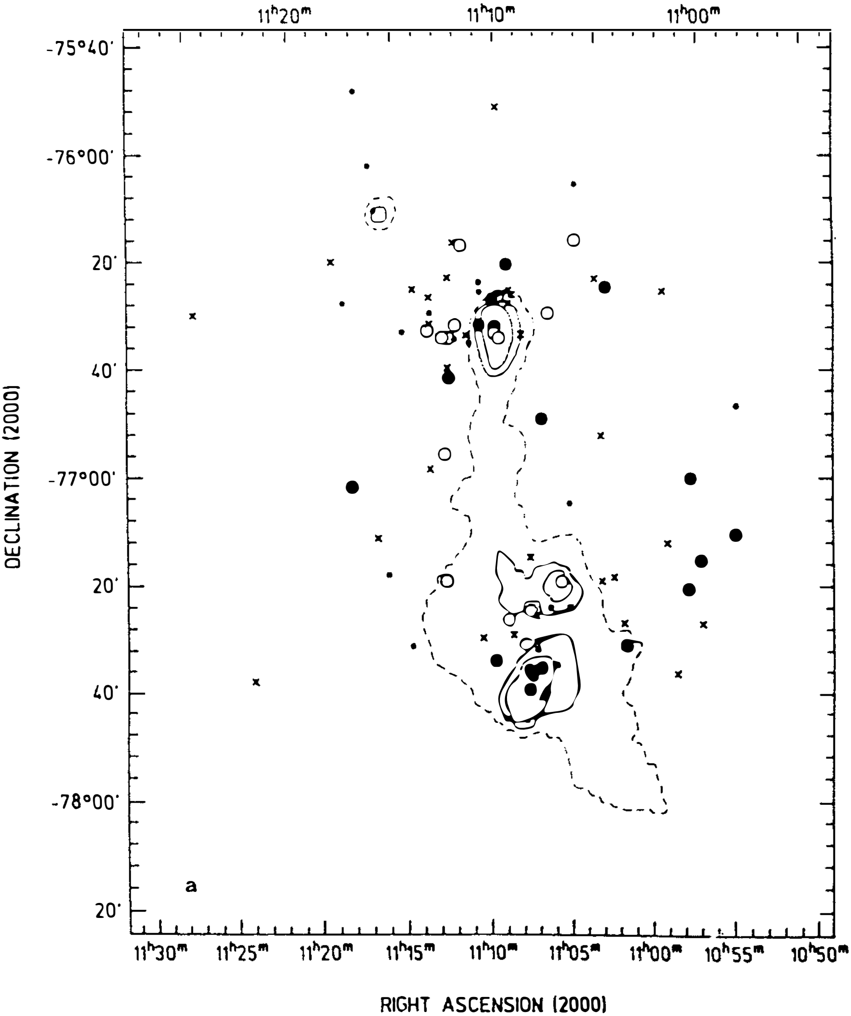

Fig. 1. Spatial distribution of the 89 ROSAT X-ray sources in the Cha I cloud. Symbols: *filled circle,* CTTS; *open circle,* WTTS; *cross,* new source; *dot,* source unrelated to the cloud. The contours are from the IRAS 100μm map: *dashed line,* outer boundary; *solid lines,* cloud cores. (From Feigelson et al. 1993.)

3. THE ρ OPH CLOUD

The recently obtained ROSAT results on the ρ Oph cloud are in sharp contrast with those on the Cha I cloud outlined above. Having obtained a deep (33,000 sec.) exposure of the ρ Oph cloud core region, Casanova et al. (1993) concentrated on the most sensitive central ~ 1/4 sq. deg. of the ROSAT image (as opposed to the ~ 4 sq. deg. total image of the Cha I cloud). In this area, 55 sources were detected with a good S/N ratio, and up to 50 more may be present. In addition, 1/3 of the reliable sources are invisible on photographic plates, whereas all the sources previously discovered with "Einstein" (Montmerle et al. 1983) had optically visible counterparts.

On the other hand, the ρ Oph cloud core has been the target of many IR observations over the past years, which have yielded almost 100 IR sources definitely associated with the cloud, at various stages of evolution (e.g., Wilking, Lada, & Young 1989, Greene & Young 1992, Comeron et al. 1993). Casanova et al. find that over 70 % of the ROSAT sources have cloud member counterparts, with the tentative detection of a few Class I sources. Many of the remaining ROSAT sources have IR counterparts which are not yet confirmed, but likely to be, cloud members. So contrary to the Cha I cloud, where a large fraction of the ROSAT sources are associated with as yet unidentified optically visible stars, it is found that the ρ Oph X-ray sources are almost all identified with IR sources, only 2/3 of them being also optically visible. The majority of the X-ray sources are therefore closely associated with the cloud (with corresponding likely ages $< 10^6$ - 10^7 yrs), which is confirmed on two grounds: (i) the ROSAT sources tend to cluster around dense regions (Fig. 2); (ii) the visual extinction A_V, determined from optical or IR photometry, reaches 40 or more (Fig. 3), showing that the X-ray sources are truly embedded in the cloud. The resulting X-ray luminosity function ranges from ~ 10^{28} to ≳ 10^{31} erg s^{-1}, and is statistically indistinguishable from that of the optically visible X-ray detected TTS; the total X-ray luminosity in the cloud is ≈ 5 x 10^{32} erg s^{-1}. Assuming that an extrapolation of the X-ray luminosity function down to solar X-ray luminosity levels (~ 10^{27} erg s^{-1}) is valid, implies a total number of X-ray emitting stars ~ 300.

This number is much larger than the one found in the Cha I cloud (when normalizing to the same area), testifying again to the well-known intense star-forming activity of the ρ Oph cloud, but perhaps more importantly indicating an intense irradiation of the dense parts of the cloud by embedded X-ray sources. While this had been suspected after the "Einstein" results on ρ Oph and Orion (Silk & Norman 1983, Krolik & Kallman 1983), the ROSAT results not only prove the presence of X-ray sources deep within molecular clouds, but also suggest they have a close link with the densest regions.

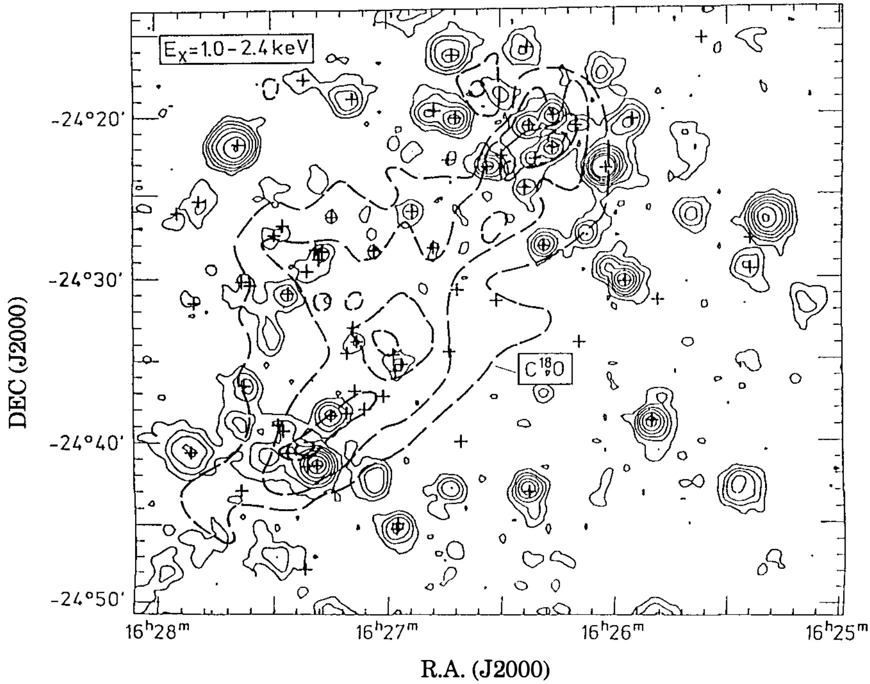

Fig. 2. ROSAT X-ray sources in the ρ Oph cloud core. *Continuous lines,* X-ray contours; *crosses,* confirmed cloud members (IR sources); *dashed lines,* $C^{18}O$ ($1 \rightarrow 0$) column densities, corresponding to visual extinctions $A_V \sim 30$ - 100. (From Casanova et al. 1993.)

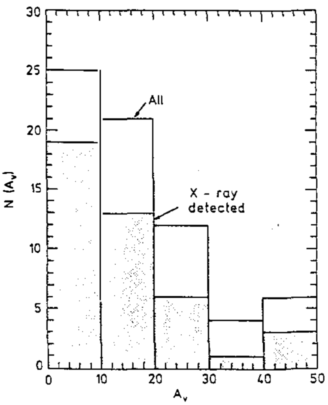

Fig. 3. Histogram of the number of ρ Oph cloud members as a function of visual extinction A_V, for the X-ray detected sources (shaded area), and for all member IR sources. (From Casanova et al. 1993.)

4. X-RAY IONIZATION IN MOLECULAR CLOUDS

The immediate consequence is that in *active* star-forming regions there must be important sources of *in situ* ionization. (The main ionization source is Auger electrons from X-ray absorbing atoms, see Krolik & Kallman 1983.) Indeed, Casanova et al. show that the dense regions of ρ Oph are sufficiently opaque to X-rays of energy $\gtrsim$ 1 keV for the average ionization rate to be $\langle\zeta\rangle \gtrsim 10^{-17}$ s^{-1}, which is comparable to (or greater than, near the X-ray sources) the usual ionization rate inferred from the observed chemical states (radicals, etc...) in molecular clouds, and generally attributed to low-energy cosmic rays. Since these cosmic rays have a very uncertain spectrum because they have not been observed, ionization by embedded X-ray sources therefore provides an attractive, measurable alternative ionization source in molecular clouds. We note, however, that this would not be the case in less dense regions like in the Cha I cloud, for which the X-ray luminosity and opacity are too small to result in a significant ionization by this process.

Although the average ionization fraction in molecular clouds is very small ($\langle x\rangle \approx 10^{-7}$), ionization effects are crucial for many aspects of their structure and evolution:

- they control the chemical states of the gas and dust, and the abundance of molecules, especially radicals;
- they govern the way gas and dust are tied to the magnetic field (ambipolar diffusion);
- because of this, they have a direct impact on gravitational collapse and star formation (more ionization means less ease for collapse, in other words less star formation).

As emphasized by Silk & Norman (1983), this last point is especially interesting in that, contrary to low-energy cosmic rays, it provides a *feedback effect* : since X-ray emission apparently starts very early during PMS stellar evolution, it prevents, or at least regulates, further star formation in the vicinity of the already formed stars. We note that, unfortunately, current star formation models (e.g., Shu, Adams, & Lizano 1987, McKee 1989) do not take this effect into account.

5. CONCLUSIONS

After the sensitive ROSAT observations of low-mass PMS stars spanning a wide age range (> 10^7 yrs for T Tauri stars to < 10^6 yrs for embedded sources, or even < 10^5 yrs if the dectection of Class I sources is confirmed), soft X-rays appear perhaps surprisingly as a unique and verstatile tool to find and identify young stars, and thus to study the earliest stages of stellar evolution. Also, in regions where active star formation is going on, X-rays from embedded young stars may provide via ionization effects an important feedback mechanism which should be taken into account in star formation models.

REFERENCES

André, P., & Montmerle, T. 1994, *Ap. J.* **420**, 837.

Bertout C., 1989, *Ann. Rev. Astr. Ap.,* **27**, 351.

Casanova, S., Montmerle, T., Feigelson, E.D., & André, P. 1993, *Ap. J.,* submitted.

Comeron, F., Rieke, G.H., Burrows, A., & Rieke, M.J. 1993, *Ap. J.* **416**, 185.

Feigelson, E.D., Casanova, S., Montmerle, T., & Guibert, J. 1993, *Ap. J.* **416**, 623.

Feigelson, E.D., Giampapa, M.S., & Vrba, F.J. 1991, in *The Sun in time,* ed. C.P. Sonnett et al. (Tucson: U. of Arizona Press), p. 658.

Feigelson, E.D., & Kriss, G.A. 1989, *Ap. J.* **338**, 262.

Gauvin, L.S., & Strom, K.M. 1992, *Ap. J.* **385**, 217.

Giacconi R., et al. 1981, in*Telescopes for the 1980s,* ed. G. Burbidge & A. Hewitt, (Palo Alto: Annual Reviews).

Greene, T.P., & Young, E.T. 1992, *Ap. J.* **395**, 516.

Krautter, J., Alcalá, J.M., Wichmann, R., Neuhäuser, R., & Schmitt, J.H.M.M. 1994, *Rev. Mex. Astr. Ap.,* in press.

Montmerle, T. André, P., Casanova, S., & Feigelson, E.D., 1993, in *Cosmical Magnetism,* Cambridge (GB), in press.

Montmerle, T., Feigelson, E.D., Bouvier, J., & André P. 1993, in *Protostars and Planets III,* ed. E.H. Levy and J.I. Lunine (Tucson : U. of Arizona Press), p. 689.

Montmerle, T., Koch-Miramond, L., Falgarone, E., & Grindlay, J.E. 1983, *Ap. J.* **269**, 182.

Prusti, T., Whittet, D.C., & Wesselius, P.R. 1992, *M.N.R.A.S.* **254**, 361.

Trümper, J. 1983, *Adv. Sp. Res.* **2**, 241.

Wilking, B.A., Lada, C.J., & Young, E.T. 1989, *Ap. J.* **340**, 823.

dense regions where active star formation is going on, X-rays from embedded young stars may provide via ionization effects an important feedback mechanism which should be taken into account in star formation models.

Our group has undertaken a large program with ROSAT to observe a number of molecular clouds at various distances, which may reveal yet other aspects of the interactions between young stellar X-ray sources and interstellar matter.

Acknowledgements. I thank Philippe André, Sophie Casanova, and Eric Feigelson for their efficient and friendly collaboration on this project, and Jean Guibert for his help in the optical identification of the ROSAT sources with the MAMA automatic digital measuring engine at the Observatoire de Paris.

REFERENCES

André, P., & Montmerle, T. 1994, *Ap. J.* **420**, 837.

Bertout C., 1989, *Ann. Rev. Astr. Ap.,* **27**, 351.

Casanova, S., Montmerle, T., Feigelson, E.D., & André, P. 1993, *Ap. J.*, submitted.

Comeron, F., Rieke, G.H., Burrows, A., & Rieke, M.J. 1993, *Ap. J.* **416**, 185.

Feigelson, E.D., Casanova, S., Montmerle, T., & Guibert, J. 1993, *Ap. J.* **416**, 623.

Feigelson, E.D., Giampapa, M.S., & Vrba, F.J. 1991, in *The Sun in time,* ed. C.P. Sonnett et al. (Tucson: U. of Arizona Press), p. 658.

Feigelson, E.D., & Kriss, G.A. 1989, *Ap. J.* **338**, 262.

Gauvin, L.S., & Strom, K.M. 1992, *Ap. J.* **385**, 217.

Giacconi R., et al. 1981, in*Telescopes for the 1980s,* ed. G. Burbidge & A. Hewitt, (Palo Alto: Annual Reviews).

Greene, T.P., & Young, E.T. 1992, *Ap. J.* **395**, 516.

Krautter, J., Alcalá, J.M., Wichmann, R., Neuhäuser, R., & Schmitt, J.H.M.M. 1994, *Rev. Mex. Astr. Ap.,* in press.

McKee, C. 1989, *Ap. J.* **345**, 782.

Montmerle, T. André, P., Casanova, S., & Feigelson, E.D., 1993, in *Cosmical Magnetism,* Cambridge (GB), in press.

Montmerle, T., Feigelson, E.D., Bouvier, J., & André P. 1993, in *Protostars and Planets III,* ed. E.H. Levy and J.I. Lunine (Tucson : U. of Arizona Press), p. 689.

Montmerle, T., Koch-Miramond, L., Falgarone, E., & Grindlay, J.E. 1983, *Ap. J.* **269**, 182.

Prusti, T., Whittet, D.C., & Wesselius, P.R. 1992, *M.N.R.A.S.* **254**, 361.

Shu, F.H., Adams, F.C., & Lizano, S. 1987, *Ann. Rev. Astr. Ap.* **25**, 53.

Trümper, J. 1983, *Adv. Sp. Res.* **2**, 241.

Wilking, B.A., Lada, C.J., & Young, E.T. 1989, *Ap. J.* **340**, 823.

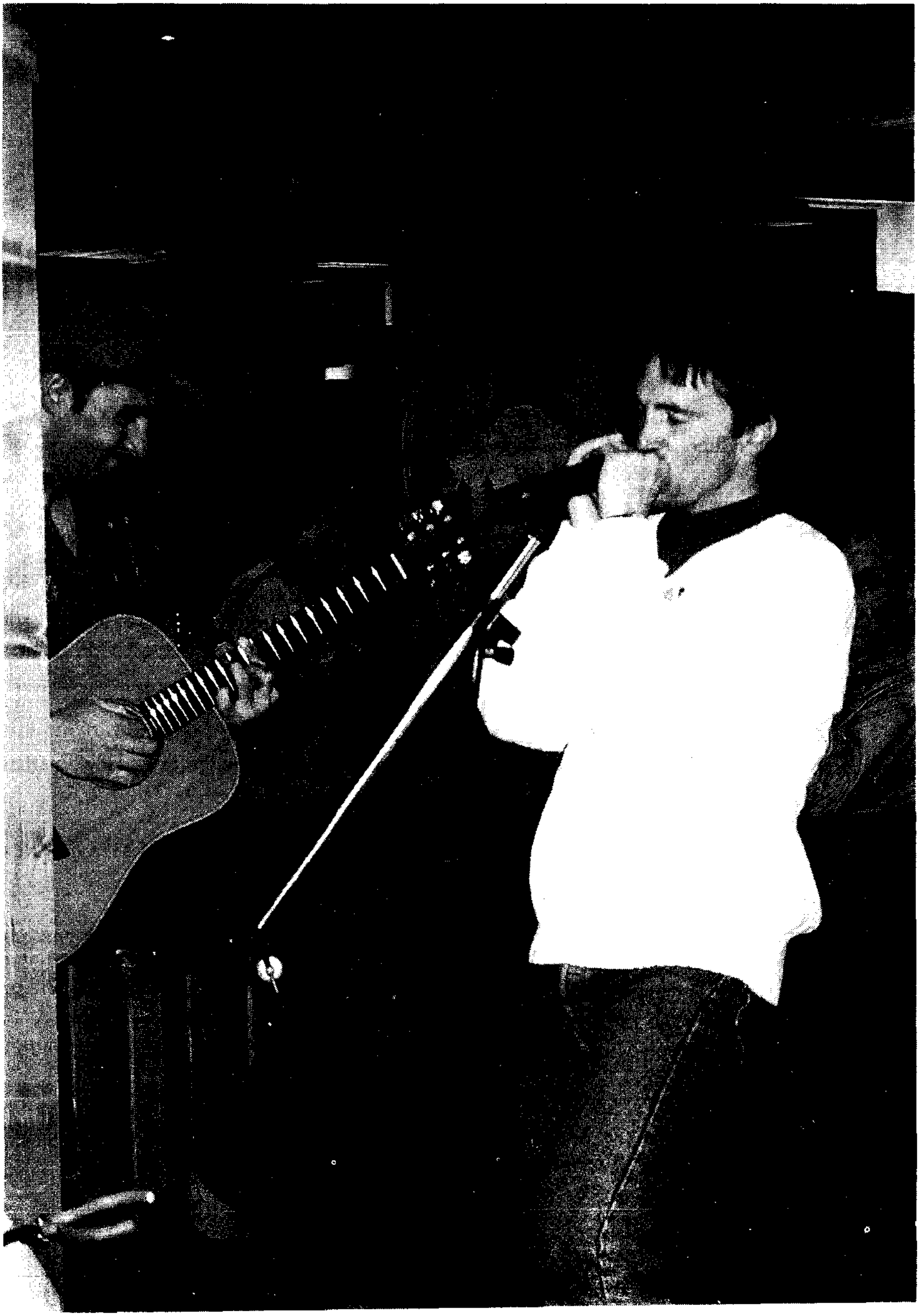

Pat Hartigan : blowin'in the (stellar) wind...

THE QUEST FOR PROTOSTARS

UNBIASED SURVEYS FOR DENSE CLOUD CORES

Yasuo FUKUI, Akira MIZUNO, Hideo OGAWA, Kazuhito DOBASHI,
Tomoo NAGAHAMA, Jean-Philippe BERNARD, Takashi TSUBOI,
Toshikazu ONISHI, &Yoshinori YONEKURA
Department of Astrophysics, Nagoya University
Nagoya 464-01, Japan

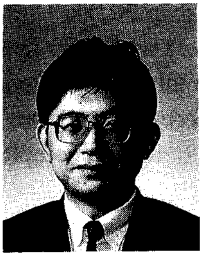

Yasuo Fukui

ABSTRACT

Dense cloud cores are sites of star formation, having density greater than 10^4 cm^{-3}. Molecular observations at radio wavelength so far were rather slow is searching for dense cores since radiation from them is fairly weak, making it difficult to carry out an extensive search in a reasonably short time scale. The recent advent of sensitive receivers reaching the quantum detection limit are overcoming this difficulty, providing an unbiased sample of dense cores. This paper describes one of the most recent efforts to search for dense cores that are directly connected to stellar birth.

1. INTRODUCTION

Star formation is one of the most basic issues of keen interests in modern astrophysics. Dense cloud cores are believed to be the site of star formation. Our knowledge on dense cores however is far from complete due to limited observational data on these cold objects in interstellar space. This is because millimeter-wave radiation from dense cores are generally too weak to be mapped in a reasonably short time. The recent advent of extremely sensitive superconducting receivers are now beginning to overcome such a difficulty. In particular, one of the most sensitive receivers developed at Nagoya University is extending studies of dense cores significantly over the last two years[1, 2, 3]. This receiver having receiver noise temperature of 20 K in double side band is installed on the highly efficient two 4m millimeter telescopes in Nagoya. The survey already obtained more than 20,000 $C^{18}O$(J=1-0) and CS(J=2-1) spectra at 3 millimeter wavelength. These molecular spectra can trace dense gas with density of 10^4 - 10^5 cm^{-3}. In this contribution we will describe high density cores in three low mass star formation regions; i.e., Orion(L1641 and Ori KL), Taurus, and Ophiuchus on the basis of a complete dataset of dense gas on a size scale of 0.1 pc.

We will in particular discuss the following three questions; 1. What molecular spectrum is best to probe dense cores, 2. What is required for a dense core to form stars, and 3. Can we witness the very early stage of the gravitational collapse of a dense core.

2. PROBES FOR DENSE GAS; CS vs $C^{18}O$

Two of the most frequently observed spectra to probe dense gas are CS and $C^{18}O$. CS J=1-0 and 2-1 transitions are collisionally excited at density greater than 10^4 cm^{-3}. The $C^{18}O$ J=1-0 transition can probe density similar to or a little lower than CS because of its smaller optical depth on a size scale of 0.1 pc, although this transition has lower critical density than CS. It is however not well confirmed how these two spectra are consistent with each other in terms of the intensity distribution. If the two are equally good tracers, their distribution should be reasonably similar to each other. Except for a few works of limited angular extents[4,5], observational efforts to compare distributions of different molecules have not been made systematically.

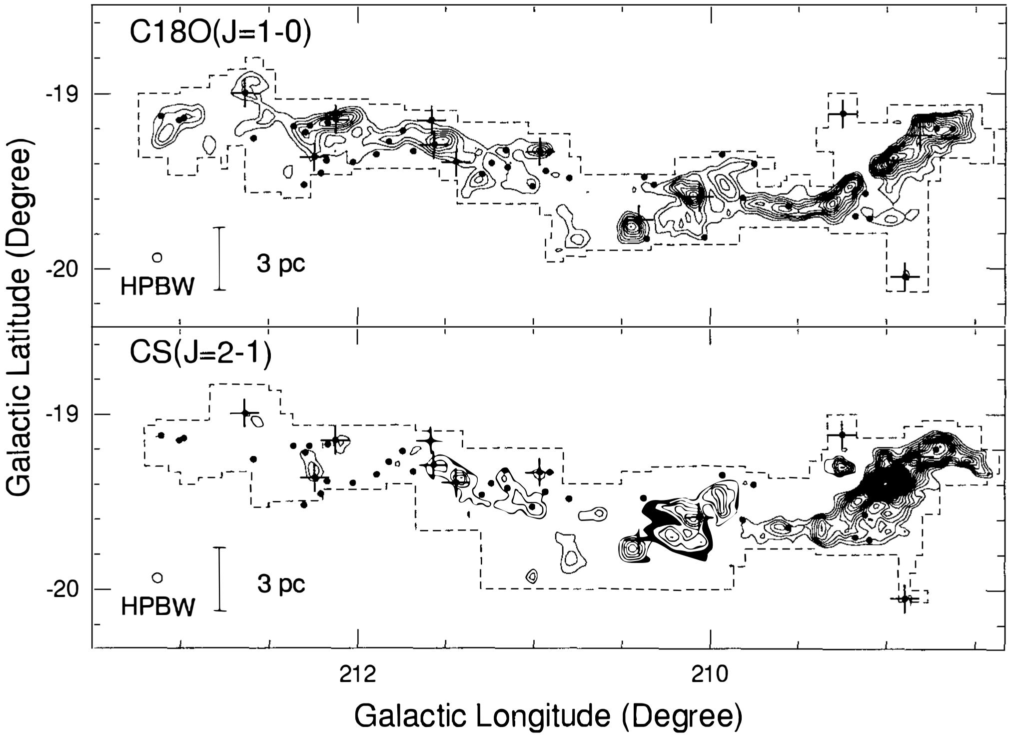

Figure 1 Total intensity maps in $C^{18}O$ (J=1-0) (upper) and CS (J=2-1) (lower) for the Orion A molecular cloud including the L1641 cloud. They are obtained with the Nagoya 4-m millimeter-wave telescope with a 2' grid spacing. Mapping area is surrounded with a dashed line. Filled circles and crosses indicate the locations of the protostar-like IRAS sources and the molecular outflows, respectively. Contours are from 0.6 K km/s with a 0.2 K km/s step.

We made a coordinated $C^{18}O$ and CS survey of the Orion A molecular cloud that includes Ori KL region and the L1641 dark cloud. Figure 1 shows the two distributions with 3 arc min resolution. They look generally similar to each other, while a closer look indicates that they are considerably different particularly at galactic longitude greater than 211 degrees. The difference is most clearly shown in Figure 2, a close up of the CS and $C^{18}O$ distributions. The $C^{18}O$ distribution shows a ridge elongated roughly along the galactic plane, being associated with several far infrared compact sources detected by the IRAS (the Infrared Astronomical Satellite). These IRAS sources show rising spectra toward the longer wavelength typical to a protostellar object. The IRAS sources coincide in position with the $C^{18}O$ ridge remarkably well.

We interpret this difference indicates nonuniform CS abundance. It is well established that CO abundance is uniform, basically determined by atomic carbon abundance in the gas phase, although CS abundance may be affected by environmental conditions. We infer that the $C^{18}O$ abundance represents the true gas distribution. The remarkable agreement of the protostellar IRAS sources and the $C^{18}O$ ridge in Figure 2 is a natural consequence of recent star formation in an elongated dense gas distribution. There are two CS peaks in Figure 2, and each of them is associated with molecular outflows[6], suggesting that CS abundance may be enhanced due to some dynamical effect of the outflow.

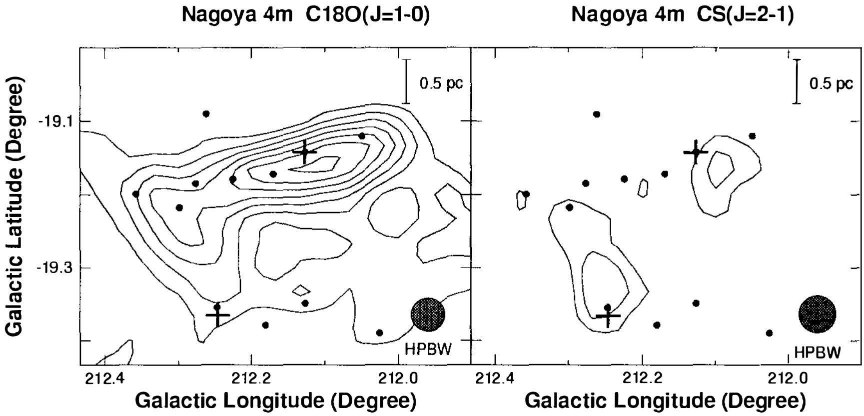

Figure 2 Close-up views of a dense core in the left side part of the L1641 cloud. Protostar-like IRAS sources are displayed as filled circles. Crosses mark the locations of molecular outflows. Contours are from 0.6 K km/s with a 0.2 K km/s step.

CS enhancements by a factor of 10 due to shocks are suggested in high velocity wings in CO outflow sources[7, 8]. Theoretical works also predict enhancement of sulfur bearing molecules in shocked molecular gas[9].

We note that the CS distribution does not show a detailed agreement with that of the high velocity CO wings. This is explained as a result of different time scales of formation and destruction of CS. The time scale of CS formation is determined by the dynamical time scale of shocks, while the destruction time scale is determined by the ion-molecule chemistry, an order of magnitude larger than the formation time scale. In other words the CS enrichment can freeze a recent record of a shock passage, and may last longer than the shock itself.

In the north of the cloud (at smaller galactic longitude), difference between CS and $C^{18}O$ is generally less clear, except for the Orion KL region containing a most spectacular outflow from a young star at l=210 degree. The Ori KL is most prominent in CS. The total molecular column density in the north region is by a factor of 3 greater than that in the south region on the average. This tends to make molecular emission optically thicker than in the south, and may explain the similar distribution of CS and $C^{18}O$ in the north at least qualitatively.

The above data indicate that CS is considerably different from $C^{18}O$ particularly in regions of smaller molecular column density, suggesting that CS is not a good tracer of dense gas. It seems that CS abundance is affected by shock or some local physical conditions. Thus, we shall use $C^{18}O$ data in the following in order to describe dense gas distribution.

3. CONDITIONS FOR STAR FORMATION

In order to address conditions for star formation we shall compare two nearby regions of low mass star formation in the Ophiuchus north and Taurus regions at distance of ~140-160 pc. The Taurus dark cloud complex has total molecular mass of 3000 $M_\odot$ as estimated from the ^{13}CO data[10], and is known as an active site of star formation. The Ophiuchus north region[11] is a more extended complex of smaller clouds in the north of the ρ Oph main cloud. The total molecular mass of the Ophiuchus north region is also 3000 $M_\odot$ as estimated from the ^{13}CO data.

The ^{13}CO distribution of the Taurus dark cloud is shown in Figure 3. We observed $C^{18}O$ emission towards most of the ^{13}CO peaks with the 4m telescope.

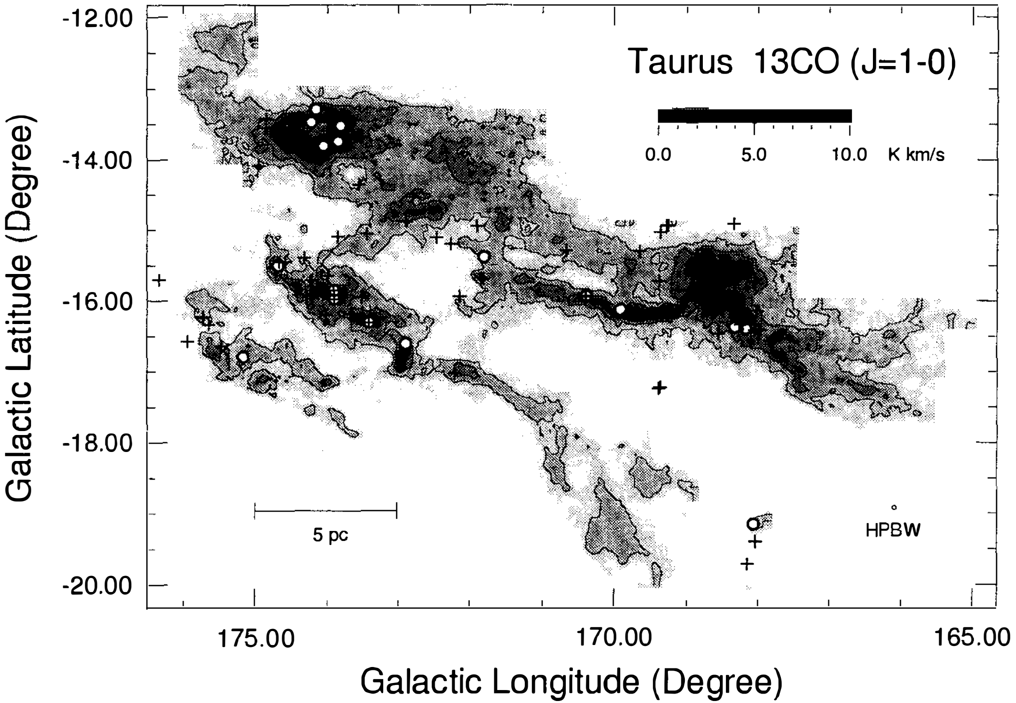

Figure 3 Contour map of ^{13}CO (J=1-0) total intensity toward the Taurus molecular cloud complex obtained with the Nagoya 4-m millimeter-wave telescope. The mapping grid is 2', and the beam size is 2.'7. Crosses mark the position of visible T Tauri stars cataloged by Herbig and Bell (1988). Contours are from 1.5 K km/s with a 1.5 K km/s step. Open circles indicate the protostar-like IRAS point sources selected by the following criteria: (1) detected in more than 3 bands, (2) correlation coefficient is better than 99%, (3) color index of 12μm and 25μm, $\log[F(12)/F(25)] \leq -0.4$.

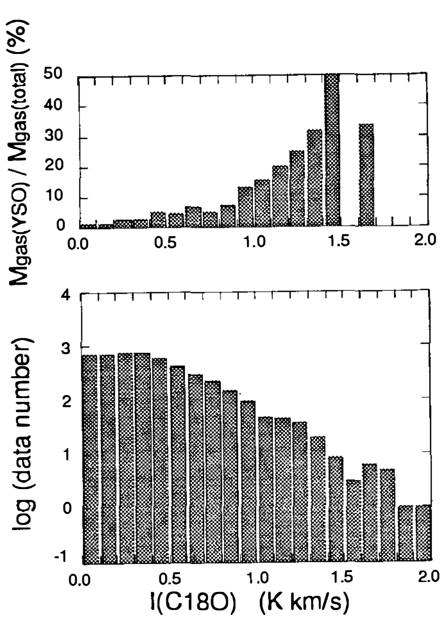

Figure 4 a) (bottom) Intensity histogram of ~ 5,000 $C^{18}O$ (J=1-0) spectra toward the dense part of the Taurus. Vertical axis denotes the number of the spectra included in each $C^{18}O$ intensity range in logarithmic scale. b) (top) Histogram of the mass fraction of the gas associated with the young stellar objects as a function of $C^{18}O$ intensity.

The angular coverage is complete for the gas having molecular column density greater than 2×10^{21} cm^{-2}. In stead of showing individual $C^{18}O$ maps, we show only a histogram of $C^{18}O$ intensity for the whole data set of 5,000 $C^{18}O$ spectra in Figure 4. We have identified $C^{18}O$ gas that is associated with young stars or protostars by comparing the dataset with lists of IRAS point sources and T Tauri stars[12, 13]. The result shown in the upper part in Figure 4 illustrates that young stars are preferentially located in regions of high $C^{18}O$ integrated intensity greater than 1.0 K km s^{-1}, corresponding to large molecular column density above ~ 8×10^{21} cm^{-2}. This suggests that stars are formed in dense molecular gas at a higher rate; we estimate star formation efficiency to be 2 - 3 % by dividing the stellar mass by the molecular mass as estimated from the $C^{18}O$ data.

It is a little curious that the sign of star formation is not so strong at the densest gas the $C^{18}O$ emission can probe, i.e., with $C^{18}O$ integrated intensity greater than 1.5 K km s^{-1}. This may be partly due to the limit of sampling (only 20 points are included), or may actually indicate the lower fraction of densest gas is associated with a protostar. If the latter is the case, the lifetime of the densest gas in $C^{18}O$ may be fairly short, suggesting a rapid dispersal of the dense gas after stellar birth.

The Ophuichus region is a huge complex of dark clouds including not only the ρ Oph main cloud but also more than 20 smaller cloudlets in the north as revealed by ^{13}CO observations[11]. These dense molecular clouds are enveloped by a less dense ^{12}CO clouds[14]. This north region has been completely surveyed for $C^{18}O$ cores with the 4m telescope. 26 $C^{18}O$ cloud cores are now identified, seven of which are shown in Figure 5. For these seven cores, the intensity distribution of $C^{18}O$ was modelled by a power-law distribution, resulting an average power index of -0.5 for the column density distribution. This corresponds to a power-law density distribution with an index of -1.5, nearly consistent with that of an isothermal spherical cloud in dynamical equilibrium.

A remarkable fact for these cores in the Ophiuchus north region is that only a few of them are associated with a star or IRAS source, suggesting that star formation is considerably inefficient in the region. This marks a significant difference in star formation activity from the Taurus cloud described above. Although cloud properties of the two regions are quite similar in total mass and density as inferred from similar $C^{18}O$ column density, the Taurus cloud appears significantly more active than the Ophiuchus north region, by about a factor of ten in star formation efficiency. It seems that cloud collapse is significantly slower in Ophiuchus than in Taurus. Nozawa et al. (1991)[11] suggests that

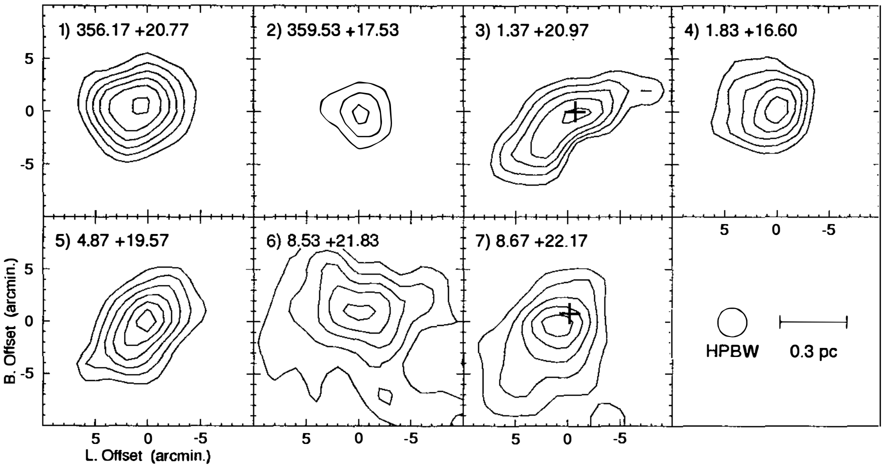

Figure 5 Typical dense cores in the northern part of the Ophiuchus region. $C^{18}O$ (J=1-0) total intensity maps. Contours are from 0.36 K km/s with a 0.18 K km/s step. Crosses mark the positions of the IRAS point sources. The number represents the central position of a core in l and b.

ultraviolet radiation from the Sco OB2 association may make the ionization degree higher in Ophiuchus than in the general interstellar space. In fact, according to a calculation by Nozawa et al. the average UV radiation may be about 10 times higher. This higher ionization degree tends to make stronger the coupling between the magnetic field and the molecular gas, and thereby, to slow down the gravitational collapse in Ophiuchus north. In Taurus, there is no strong source of ultraviolet radiation like Sco OB2.

4. SEARCH FOR COMPACT CORES

Dense cores are the ultimate site of star formation in molecular clouds. Searches for dense cores however are far from complete. This can be particularly a serious problem for starless cores, since most of the searches for dense cores are made toward IRAS point sources or optical young stellar objects. In order to overcome this difficulty we have carried out a new search for dense cores at a high angular resolution of 20 arc sec. with the 45 m telescope at Nobeyama on the basis of a fully sampled $C^{18}O$ map taken with a 3 arc min beam in Taurus.

The $C^{18}O$ data at Nagoya covers about 30% of the area of detectable ^{13}CO emission corresponding to a molecular column density of 10^{21} cm^{-2} with 3 arc min resolution. The $C^{18}O$ distribution was used to select regions for the higher

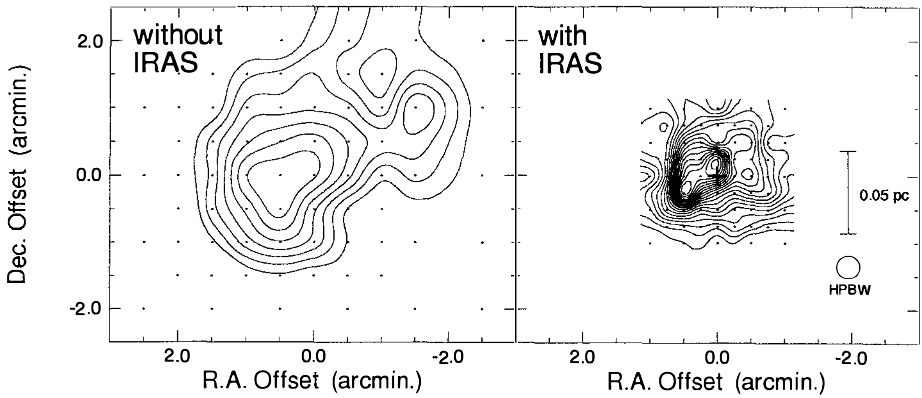

Figure 6 Typical examples of the "star-less" core (left) and the dense core with IRAS source (right) in the Taurus region. Contour maps of $H^{13}CO^+$ (J=1-0) total intensity obtained with the Nobeyama 45-m radio telescope. Contours are from 0.14 K km/s with a 0.07 K km/s step. The positions of the infrared sources are indicated as a cross mark.

resolution study. The spectra observed are C_3H_2 (2_{20}-2_{11}) and $H^{13}CO^+$ (J=1-0), since at such an angular scale even $C^{18}O$ (J=1-0) emission is saturated. The two spectra are collisionally excited at density of 10^5 cm^{-3}, while their uniformity in abundance remains to be checked by further observations. 2,000 points were observed with 20 arc sec beam, more than 20 dense cores were detected and mapped (a set of cores with and without stars is shown in Figure 6). About a half of them are dense cores discovered in the present study. Figure 7 shows histograms of the core diameter and line width. A core radius of a starless core is systematically larger than that of a core with a star. The average radius of the starless cores is by a factor of three larger than that of cores with stars. In addition, the linewidth of starless cores is larger by 40% than that of cores with stars .

The present result suggests that there is a significant difference in physical properties between cores with and without stars although statistics is still to be improved. If this trend is real, the difference may represent the dynamical collapse of a cloud core as modelled by numerical simulations[15)]. These simulations indicate that the cloud radius at a certain density decreases with the collapse. The observed trend that stars are always found in most compact cores is consistent with the predicted decrease of a core radius in time. The increase of the linewidith in cores with stars is another notable aspect. This may be due to outflow from a protostellar core, or may represent dynamical mass accretion. The linewidth, 0.7 km s^{-1}, is consistent with the gravitational accretion if we adopt 0.5 solar mass as a mass of the stellar core.

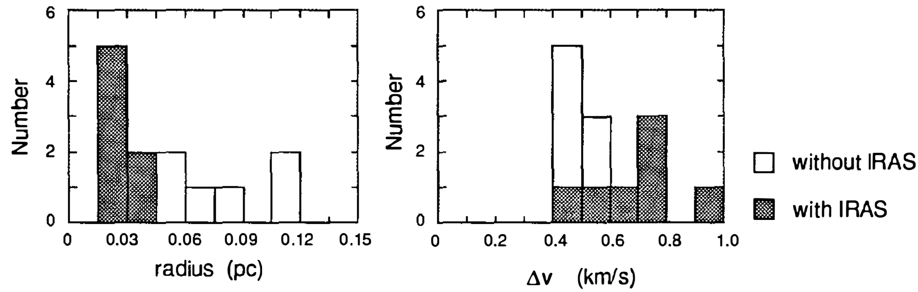

Figure 7 A histogram of the size(left) and velocity width(right) of dense cores in Taurus observed with the Nobeyama 45-m telescope in $H^{13}CO^+$. Shading indicates the dense cores with the protostar-like IRAS sources, and non-shading indicates the "star-less" cores.

5. SUMMARY

We summarize this contribution as follows;

1.$C^{18}O$ is a tracer better than CS at a size scale down to 0.1pc

2.The collapse time scale differs from region to region. The radiation field may play a role in retarding the collapse in Ophiuchus north.

3. Compact cores with 0.01pc radius, probable candidates for the earliest phase of collapse have been detected in Taurus.

The high resolution study at Nobeyama was made under a collaboration with Tetsuo Hasegawa, Masahiko Hayashi, Kazuyoshi Sunada, and Nagoyashi Ohashi. This research was supported by the Specially-Promoted-Research Grant of the Ministry of Education, Culture and Science (No. 01065002).

References

1) Ogawa, H., Mizuno, A., Hoko, H., Ishikawa, H., and Fukui, Y., 1990, Int. J. Infrared and Millimeter Waves, 11, 717.

2) Fukui, Y., Mizuno, A., Nagahama, T., Imaoka, K., and Ogawa, H., 1992, Memorie della Societa Astronomica Italiana, 62, 801.

3) Fukui, Y., and Mizuno, A., 1993, in Proc. of the 5th Asian Pacific Physics Conference, in press.

4) Goldsmith, P., Margulis, M., Snell, R., and Fukui, Y., 1992, Astrophys. J., 385, 522.

5) Swade, D. A., 1989, Astrophys. J., 345, 828.

6) Fukui, Y., Iwata, T., Takaba, H., Mizuno, A., Ogawa, H., Kawabata, K., and Sugitani, K., 1989, Nature, 342, 161.
and unpublished results.

7) Thronson, Jr., H. A., and Lada, C. J., 1984, Ap. J., 284, 135.

8) Takano, T., 1986, Ap. J. (Letters), 300, L85.

9) Hartquist, T. W., Oppenheimer, M., and Dalgarno, A., 1980, Ap. J., 236, 182.

10) Fukui, Y., and Mizuno, A., 1990, in IAU 147 Fragmentation of molecular clouds and star formation, eds. E. Falgarone et al., (Reidel, Dordrecht), 275.

11) Nozawa, S., Mizuno, A., Teshima, Y., Ogawa, H., and Fukui, Y., 1991, Astrophys. J. Suppl., 77, 647.

12) IRAS Catalogs and Atlases, Explanatory Suppl.,Beichman, C. A., Neugebauer, G., Habing, H. J., Clegg, P.E., and Chester, T. J., eds. (U.S. Government Printing Office, Washington D.C.,1984).

13) Herbig, G. H., Bell, K. R., 1988, Lick Obs. Bull. No. 1111.

14) de Geus, E. J., Bronfman, L., and Thaddeus, P., 1990, Astron. Astrophys., 231, 137.

15) Nakano, T., 1979, PASJ., 31, 697.

PROTOSTELLAR CONDENSATIONS

Rolf Güsten
Max-Planck-Institut für Radioastronomie
Auf dem Hügel 69, 53121 Bonn, F.R.G.

ABSTRACT

I summarize the expected signatures of protostellar condensations, defined as ultra-dense compact pre-stellar cloud cores undergoing collapse. The question addressed is why, while there should be hundreds of $\mathcal{PSC}$s potentially detectable with current technology, have there only been a few convincing cases presented so far. The choice of suitable observing tools and appropriate search strategies is discussed. Observational evidence for low-mass candidate objects and their physical characteristics is reviewed.

1 Introduction

The physical nature and structure of dense molecular clouds is directly related to our understanding of the late star formation process. Despite major efforts over the last decade, our knowledge about that decisive phase when a compact ultra-dense cloud core finally evolves into a protostar, and about the physical environment controlling this process, is still rather incomplete. Answers to the questions of what ultimately triggers the star formation process, at what critical density a cloud core decouples from the ambient cloud and starts collapsing into the stellar phase, and on what time scales, are observationally barely constrained. For a better definition of the late star formation process, the *gas density and temperature*, the *magnetic field* and the *velocity field* need to be determined - on all relevant scales and, at best, before the structure is affected by the (so-formed) stellar object.
In the following, a protostellar condensation is defined as an **ultra-dense compact prestellar cloud core undergoing collapse**. For an unambiguous identification, it has to be demonstrated that

- o towards the core the gas density and column density is steeply rising,
- o the kinematic pattern characteristic of collapse is observed (in form of eg. local red-shifted self-absorption), and
- o in the earliest evolutionary phases, the IR luminosity is due mainly to accretion.

In Section 3, I will briefly summarize the "expected" characteristics of a protostellar condensation ($\mathcal{PSC}$ hereafter). The number density of $\mathcal{PSC}$s in the solar neighborhood will be estimated and possible search strategies (together with their limitations) will be addressed. Finally, some new pieces of evidence for $\mathcal{PSC}$ candidates will be discussed. For excellent, more thorough reviews on the subject I refer to the articles by eg. Evans[2)] and Shu et al.[21)].

2 Statistics & Search Strategies

Widely used and rather straightforwardly interpreted tracers of mass column density are the mm continuum emission of interstellar dust and the optically thin line emission of the ubiquitous, easily excited $C^{18}O$ molecule[1]. Amazingly, in the parameter range discussed here and with current single-detector technology, the sensitivity of both tools to a given H_2 column density are quite comparable (see Fig.1) - although clearly towards narrow-line cold targets (like dark cloud cores) line measurements are more advantageous. However, because large sensitive bolometer arrays will become available soon at the large mm/submm telescopes, while the

[1]The equivalent transitions of the more abundant CO isotopomers, ^{12}CO and ^{13}CO, are - due to their increased fractional abundance - sensible to lower H_2 column densities, but in consequence, towards the cloud cores become easily saturated, thus sensitive to details of the radiative transfer. Because $\mathcal{PSC}$s are typically found embedded in a more extended and often massive ambient cloud structure, studies based on these species are of limited dynamical range.

development of powerful heterodyne arrays will still take some time, in the near future the most efficient way to search for protostellar condensations will be via their mm dust continuum emission (particularly for the nearby and hence somewhat extended objects).

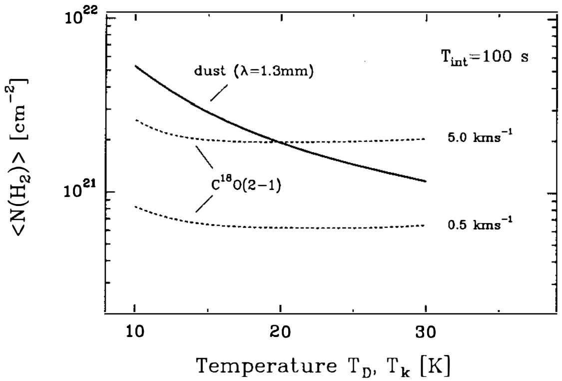

Figure 1: Point source response of single-element coherent and incoherent receivers to the λ=1.3mm dust continuum and the $C^{18}O$(2-1) molecular line emission, respectively. For an on-source integration time of 100 s, and observational and technical constraints characteristic for observations with the IRAM 30m-telescope, the detectable (rms) H_2 column density versus temperature is calculated (for two sets of linewidths ΔV). The sensitivity adopted for the bolometer is 50 mJy/$\sqrt{s}$ (Eq.1); for the 1.3mm SIS receiver I used T_{Sys}^{SSB} ~500 K and a spectral resolution of 4 channels/FWHP.

Next, an estimate is given for the number of protostellar condensations that will be potentially detectable with these state-of-the-art facilities (see also Mezger[11]). For optically thin emission (at λ=1300μm, H_2 column densities of $\sim 10^{25.5}$cm^{-3} are required for τ=1), and for standard submm dust absorption cross-sections[15], $\sigma_\lambda^H \simeq 2.4\ 10^{-20} \cdot \lambda_{\mu m}^{-2}$, the (total) flux density S_t observed towards an object at distance D relates directly to the mass column density, and thus to the clump mass M_{cl} by,

$$M_{cl}[M_\odot] \simeq 30(\pm.3) \cdot \left[\frac{S_t}{Jy}\right] \left[\frac{D}{kpc}\right]^2 \left[\frac{20K}{T_D}\right] , \qquad (1)$$

for dust temperatures $15 \leq T_D \leq 30$ K (see e.g., Mezger et al.[15] for the relevant formulae). For a given (local) star formation rate, $\Psi'_\odot$ [$M_\odot yr^{-1} pc^{-2}$], and an initial stellar mass spectrum, Φ(m), the number of detectable $\mathcal{PSC}$s in the mass interval (m,m′) is

$$N(m,m') = \frac{\pi}{2} \Psi'_\odot \int_m^{m'} dm \int_0^{R_h(m)} dR \cdot R \cdot \Phi(m) \times \tau_{PSC} , \qquad (2)$$

where the 'horizon' R_h(m) [=D] describes the distance up to which for a given detection threshold S_ν, cores of a given mass will be detectable (Eq.1). τ_{PSC} denotes the 'lifetime' of the protostellar phase ($\sim 10^5$ yrs). In Eq.2 it is assumed that the mass of the (isothermal) protostellar clump equals the mass of the so-formed stellar object ($M_* = M_{cl}$) – a rather unlikely, conservative approach. In Table I, for representative mass bins, N(m,m′) is calculated for the classical Miller-Scalo IMF and a local SFR $\Psi'_\odot \sim 5 \cdot 10^{-9}$ $M_\odot yr^{-1} pc^{-2}$ (Miller & Scalo[16]), assuming a detection threshold in mapping mode of ~50 mJy – a number deduced from this year's experience with the MPIfR 7-element bolometer array[8] attached to the IRAM 30m-telescope.

Mass bin [$M_\odot$]	Horizon R_h [kpc]	$N_{\mathcal{PSC}}$
0.1 – 1.0	0.3 - 0.9	600
1.0 – 10.	0.9 - 3.0	660
10. – 50.	3.0 - 6.6	>100

Table 1: The number of protostellar condensations, $N_{\mathcal{PSC}}$, is calculated from Eq.2, for a detection threshold of S_ν = 50 mJy and the *local* formation rate $\Psi'_\odot$. Because the galactic SFR is sharply increasing towards the galactic center, massive $\mathcal{PSC}$s will be found at a ~3 times higher probability than based on the (comparatively low) local rate.

In summary, there should be many hundreds of protostellar condensations detectable with current technology, and thus the question to be addressed is, why there are only so surprisingly few claims of detection in the literature? The answer is twofold. First, the technological progress has been quite dramatic only over the last few years, and thus until recently, even prominent dark cloud cores in the nearby Taurus Molecular Cloud have been difficult to detect[13)]. Second, and more relevant for future perspectives, little observing time has been allocated for systematic search projects. So far much of the work has been directed towards sites already well known for ongoing star formation activity, thus often lacking a clear-cut l-o-s geometry and often suffering from quite confusing physical interaction between the embedded/associated YSOs and potential $\mathcal{PSC}$s ([14),1)]). More unbiased activities have been started by several groups now[5),6),14)], and encouraging first results have been presented.

3 Characteristics of Protostellar Condensations

The detection of a strong dust emission peak[2] may be indicative of, but is definitively not sufficient evidence for, the presence of a dense core undergoing collapse. Independent complementary molecular excitation studies of the density (and temperature) profile across the core, and in particular of the velocity field have to be performed. To quantify the observational expectations, in this section I sketch the signature of a low-mass protostellar condensation as deduced within the theoretical framework of the so-called *inside-out collapse* scenario developed by F.Shu and collaborators[20),21),9)]. The discussion is restricted to the physical characteristics of low-mass $\mathcal{PSC}$ – not only because they clearly outnumber the more massive protostars, but also because the theoretical framework of low-mass star formation is more advanced and the observational constraints are better established.

The basic starting point is the observational finding[17)] that the typical low-mass (~ solar mass)

[2]The (optically thin) mm dust emission scales as $S_\nu \propto N \cdot T_D$. Broadband submm photometry is required to derive independently the temperature of the dust, T_D – thus excluding that the observed flux enhancement is due to internal heating by an embedded YSO ("hot spot"). Similar arguments hold for a proper analysis of the molecular line emission.

dense core is cold and isothermal ($T_k \leq 10$ K), displays little rotation, and evolves in approximate equilibrium between gravity and (mainly) thermal pressure (Table 2).

L1498: Energy densities		
Gravity	$\epsilon_G = \frac{4\pi}{5} G\,\rho^2 R^2$	29
Magnetic Pressure	$\epsilon_B = \frac{B^2}{8\pi}$	<19
Thermal Pressure	$\epsilon_{th} = \frac{3}{2}\,\rho\,\sigma_{th}^2$	22
Non-thermal Pressure	$\epsilon_{nth} = \frac{3}{2}\,\rho\,\sigma_{nth}^2$	0.7
Rotation	$\epsilon_{rot} = \frac{1}{5}\,\rho R^2 \Omega^2$	0.3

Table 2: The physical conditions in the L1498 dark cloud core (according to Fiebig & Güsten [4]) suggest that the core is thermally supported against gravity. Energy densities, ϵ, are given in $[10^{-11}\mathrm{erg\ cm^{-3}}]$. A 3-sigma upper limit on the magnetic field strength $B_{\|}$ <70μG is deduced from Zeeman observations in the $CCS(J_N{=}1_0{-}0_1)$ transition with the MPIfR 100m-telescope. Excitation studies of NH_3 and C_3H_2 imply a H_2 density, $n(H_2) \sim 10^5$ cm^{-3}, and a core mass of ~1-1.5 $M_\odot$. The thermal and non-thermal velocity dispersion has been separated in a multi-molecular line study, probing the variation of linewidth as function of molecular mass. Notably, the so-derived "kinematic" temperature is totally consistent with the kinetic temperature of the gas, $T_k = 9.7(\pm 0.2)$ K, derived from the NH_3 excitation.

Shu[20] suggested that cores following these properties finally develop the (unstable) equilibrium density distribution of a *singular isothermal sphere* with,

$$\rho(r) = \frac{a^2}{2\pi G} \cdot \mathcal{R}^{-2}\,, \qquad n(\mathcal{R}) = 6.3 \cdot 10^5 cm^{-3} \cdot a^2 \cdot \mathcal{R}_{17}^{-2}\,, \tag{3}$$

and where a is the effective 'sound' speed [3]. The right-hand equation is expressed in convenient units, measuring a in [kms^{-1}], the core radius $\mathcal{R}$ in [10^{17} cm], for a mean molecular mass μ=2.3. The collapse of a singular isothermal sphere proceeds in a self-similar manner (from *inside-out*), with the central core collapsing first (essentially in free-fall, $V(\mathcal{R}) \propto \mathcal{R}^{-\frac{1}{2}}$) and an expansion wave propagating outward at speed a (at $R_{in}(t)$). The density profile inside R_{in} flattens, approaching

$$\rho(r) = \frac{0.975 \cdot a^3}{4\pi(2G^3M)^{\frac{1}{2}}} \cdot \mathcal{R}^{-\frac{3}{2}} \qquad and \qquad n(\mathcal{R}) = 6.5 \cdot 10^5 cm^{-3} \cdot a^3 \cdot \mathcal{R}_{17}^{-\frac{3}{2}} \cdot M^{-\frac{1}{2}}\,. \tag{4}$$

M [$M_\odot$] is the mass of the central protostellar core, increasing with time, $M = \dot{M}\cdot t$. The mass accretion rate ($\doteq$ the infall rate), which is a function only of the sound speed, is given by,

$$\dot{M} = \frac{.975 \cdot a^3}{G} \qquad \dot{M}[M_\odot yr^{-1}] = 2.2 \cdot 10^{-4} \cdot a^3\,. \tag{5}$$

Thus with only two parameters – the effective sound speed a and the core mass M(t) – the overall scenario is determined (compare with Fig.2). Strong predictions are made both on

[3]In the original approach[20] a was the isothermal sound speed $(k\cdot T/m)^{\frac{1}{2}}$. Later a 'turbulent' pressure term was added[9] to account for the finding that – outside the densest cores – purely thermally broadened lines are rarely observed, and in fact, on larger scales, non-thermal 'turbulent' broadening dominates[7] ($V_{tur} \propto r^{0.7\pm.1}$).

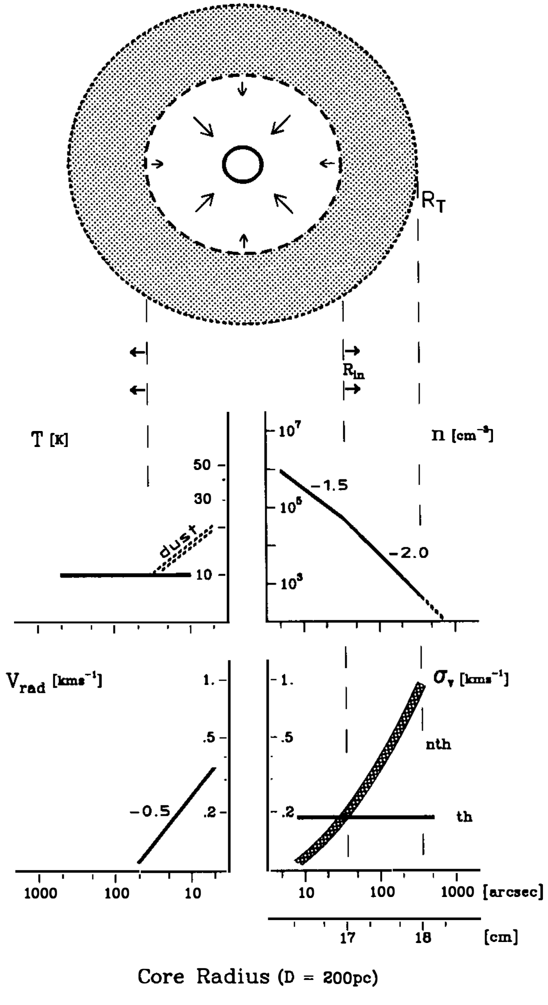

Figure 2: Characteristics of a low-mass protostellar condensation as predicted in the framework of the *inside-out collapse* scenario developed by F.Shu and coworkers[20),21)]: the core, undergoing free-fall collapse, is embedded in a static envelope described as a singular isothermal sphere. An expansion wave travels outwards at radius R_{in}. The physical parameters determining the pattern, the effective sound speed a (=0.28 kms^{-1}) and the grown-up central core mass M(t) (~0.1 $M_\odot$), have been adjusted to fit the suspected protostellar object GF9-2 (Sect.4). The mass presently undergoing collapse, $M(R \leq R_{in})$, is ~ 0.8 $M_\odot$, the mass of dense gas amounts to $M(n \geq 10^4 cm^{-3})$ ~2 $M_\odot$.

the amplitude of the physical parameters and their spatial gradients. Their observational verification however, turns out to be difficult (for an evaluation of the predicted IR spectrum of the object, I refer to the contributions by Stahler and André):

- o low-mass protostellar condensations are cold and compact, and thus are of low intrinsic brightness. For example, the expected line temperatures of the dense gas tracing CS and NH_3 molecules are only a few K T_{mb};
- o lines emitted in the collapsing sphere are narrow (ΔV_{CS} ~0.2-0.3 kms^{-1} only), and the volume of interest itself is spatially very confined ($R < R_{in}$). Therefore highest angular (Θ_{mb} $\leq$10-20") and spectral (a few 10 kHz channel width at most) resolution is required to resolve and thus identify the kinematic footprint (i.e., local red-shifted self-absorption) of ongoing collapse. It seems worth pointing out, that while this absorption feature is best imprinted on optically thick transitions arising from the collapsing layers, optically thin transitions (being unaffected by radiative transfer effects) trace best the *intrinsic* velocity field and density distribution of the core. Appropriate tools, like the mm-transitions of CS or HCN and their rare isotope substituted species, need to be studied complementarily.

To conclude, observational verification of a protostellar object undergoing collapse requires dedicated experiments, with state-of-the-art detectors installed at the largest mm/submm facilities, in order to achieve present sensitivity limits. This explains the failure of earlier lower resolution studies to detect any such object. Clearly, the velocity pattern would be best resolved by means of mm-interferometry (providing arcsec angular resolution), but with most facilities the expectedly weak, narrow line signals are unaccessible.

4 Candidates of Protostellar Condensations

The discovery of quite a number of "so-defined" protostars has been reported during the recent years, most of them being identified via their excess dust continuum emission (see references in [1),11)]. However, the very nature of these objects is yet a topic of controversy (the dispute about NGC2024 represents an outstanding example [12),19)]), generally because observationally it is difficult to constrain the state of evolution of the heavily obscured central energy source (YSO versus protostar). The question to be answered is, from where does the observed IR luminosity originate, from nuclear burning or from the accretion of infalling matter? For only three of the objects has kinematic evidence[4] for ongoing collapse been claimed:
The morphology of **IRAS 1629** [22] is complex (the core is rapidly rotating, and harbors a close binary), and the local origin of the absorption has been questioned[10)]. The isolated globule **B335** represents a more clear-cut example. Zhou et al.[25)] state that the density and the velocity field as derived from their high-resolution CS and H_2CO data, is generally consistent with the inside-out collapse model (Sect.3). Studying globular filaments[18)] as potential sites of

[4] Although obviously, from the absence of this evidence, an object's protostellar nature cannot necessarily be ruled out – it is just that *the* most convincing piece of evidence is lacking.

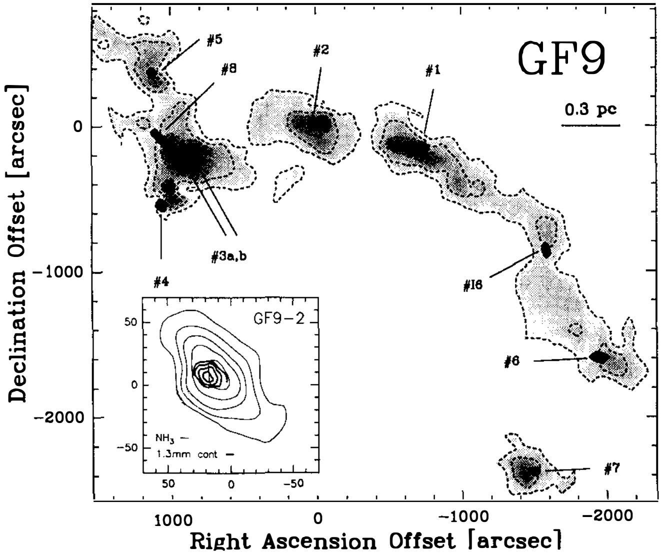

Figure 3: Greyscale representation of the $H_2CO(1_{01}\text{-}1_{11})$ absorption towards globular filament GF9[5]. Embedded dense NH_3 cores are superposed. The distribution of the 1.3mm dust continuum and NH_3 emission towards GF9-2, the suspected low-mass protostellar object, is shown in the insert.

low-mass star formation, Fiebig et al.[5] report the detection of a protostellar core undergoing collapse in its earliest evolutionary phases towards filament No.9 (Fig.3). This well-organized filament fragments into a series of quite regularly spaced globules containing a few 10 $M_\odot$ each. A total mass of $\sim$500 $M_\odot$ is derived, the full length is $\sim$5.9 pc with an axial ratio as small as 1:30. A search for higher-density cores (using NH_3 and CS) led to the identification of a total of 10 compact ($<n> \sim 10^5$ cm^{-3}) solar-mass clumps, with sizes as small as 0.02 pc. Most of the cores seem in approximate equilibrium evolution($\epsilon_G \sim \epsilon_{th+nth}$); but three contain very-low luminosity IR objects (a few 0.1 $L_\odot$ only), their cold IR spectra classify them as young 'Extreme Class I' objects (interpreted as *IR-protostars*, which luminosity L_{IR} derives entirely from accretion of infalling material onto the central core).

Clump no.2 has attracted special attention (see insert in Fig.3). High-resolution spectroscopy with the IRAM-30m telescope presents direct kinematic evidence that *the clump is collapsing*: CS spectra show deep red-shifted self-absorption which is spatially confined and most prominent towards the core's center (Fig.4). No associated IRAS source or CO outflow is detected (different to the previous two candidates), and the core is isothermally cold (the limit T_D <15 K deduced from the 1.3mm dust continuum, is consistent with the NH_3 rotation temperature of $\sim$10 K). Model fits to the molecular line data again show quantitative agreement with the low-mass star formation scenario developed in Sect.3 (Fig.2), making **GF9-2** a very likely candidate of **a protostellar condensation in its earliest evolutionary phase.** A high-resolution study

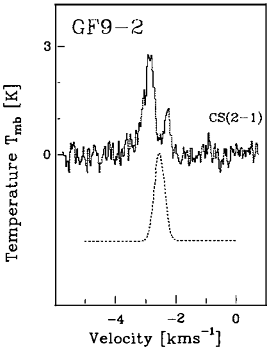

Figure 4: The CS(2-1) line towards the core of GF9-2, showing deep red-shifted self-absorption – the footprint of ongoing collapse. For reference, the intrinsic velocity profile, as derived from transitions unaffected by radiative transfer effects (e.g. the optically thin $C^{34}S$ line or the satellites of the NH_3 1.3cm inversion transitions), is given.

of the velocity field with the Plateau-de-Bure mm-interferometer is presently being carried out, from which a final confirmation about the evolutionary state of the object is expected.

References

1) André P., Ward-Thompson D., Barsony M. 1993, Ap.J. in press
2) Evans N.J. 1990, in *Frontiers of Stellar Evolution*, ed. D.L.Lambert
3) Fiebig D. 1990, Doctoral Dissertation, Univ. Bonn
4) Fiebig D., Güsten R. 1993, in preparation
5) Fiebig D., Güsten R., Ungerechts H. 1993, in preparation
6) Fukui Y. 1993, this volume
7) Fuller G.A., Myers P.C. 1992, Ap.J. 384,523
8) Kreysa E., Haslam C.G.T., Lemke R., Sievers A.W. 1993, in press
9) Lizano S., Shu F.H. 1989, Ap.J. 342,834
10) Menten K.M., Serabyn E., Güsten R., Wilson T.L. 1987, A&A 177,L57
11) Mezger P.G. 1993, in *1st Intl.Conf. on Planetary Systems*, Padadena
12) Mezger P.G., Chini R., Kreysa E., Wink J.E., Salter C.J. 1988, A&A 191,44
13) Mezger P.G., Sievers A., Zylka R. 1991, IAU Symp.147, *Fragmentation of Molecular Clouds and Star Formation*, eds. Falgarone et al., p.245
14) Mezger P.G., Sievers A., Zylka R., Haslam C.G.T., Kreysa E., Lemke R. 1992, A&A 265,743
15) Mezger P.G., Wink J., Zylka R. 1990, A&A 228,95
16) Miller G.E., Scalo J.M. 1979, Ap.J.Suppl. 41,513
17) Myers P.C., Benson P.J. 1983, Ap.J. 266,309
18) Schneider S., Elmegreen B.G. 1979, Ap.J.Suppl. 41,87
19) Schulz A., Güsten R., Zylka R., Serabyn E. 1991, A&A 246,570
20) Shu F.H. 1977, Ap.J. 214,488
21) Shu F.H., Adams F.C., Lizano S. 1987, Ann.Rev.Astron.Astrophys. 25,23
22) Walker C.K., Lada C.J., Young E.T., Maloney P.R., Wilking B.A. 1986, Ap.J. 309,L47
23) Wilson T.L., Walmsley C.M. 1989, The Astron. & Astrophys.Review 1,141
24) Zhou S. 1992, Ap.J. 394,204
25) Zhou S., Evans N.J., Kömpe C., Walmsley C.M. 1993, Ap.J. 404,232

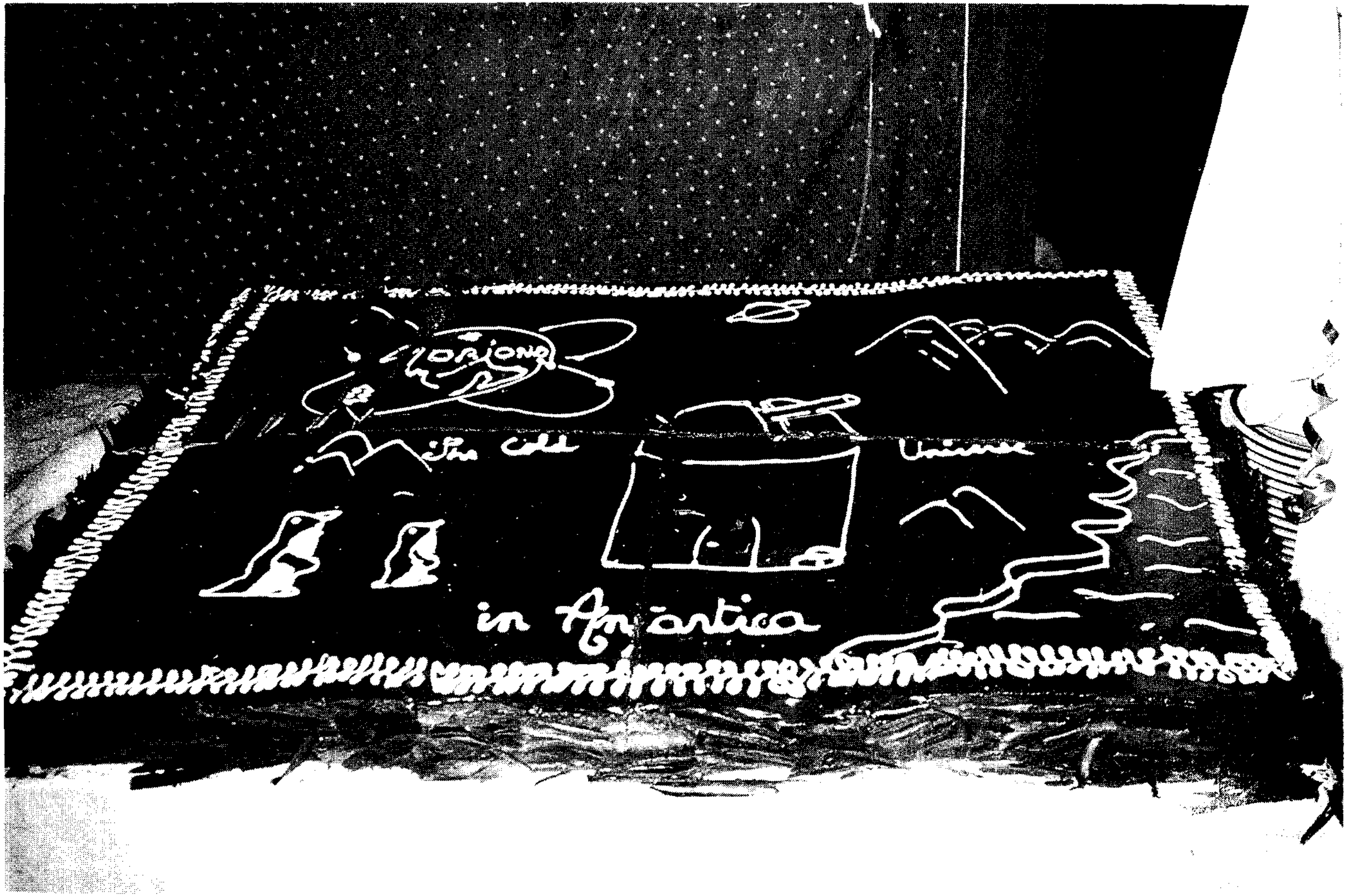

Cold cake at the banquet...

OBSERVATIONS OF PROTOSTARS AND PROTOSTELLAR STAGES

Philippe ANDRÉ
Service d'Astrophysique, Centre d'Etudes de Saclay
F-91191 Gif-sur-Yvette Cedex, France

ABSTRACT. Our observational understanding of star formation and early stellar evolution is closely linked with our capability to directly measure the basic characteristics (e.g., mass, size, density, temperature) of the circumstellar matter surrounding young stellar objects (YSOs). The advent of sensitive bolometers (including arrays in some cases) on large ground-based radiotelescopes such as the IRAM 30 m or the JCMT has recently yielded significant progress in this field, by providing a very sensitive way to detect and study the dust component of the circumstellar material. In particular, it is now possible to estimate the evolutionary states of all YSOs through systematic measurements of their circumstellar dust masses. In this way, a new type of extremely obscured YSOs (designated "Class 0") characterized by virtually no near-IR/mid-IR emission but strong submillimeter emission have been identified. Class 0 "protostars", of which the jet-like outflow source VLA 1623 in ρ Ophiuchi is the prototype, are surrounded by significantly larger amounts of circumstellar material ($M_{c\star} \gtrsim 0.5\ M_{\odot}$) than the Class I YSOs observed in the near-infrared (which typically have $M_{c\star} \lesssim 0.1\ M_{\odot}$). They are also rarer and correspond to the youngest protostellar stage known to date (probable age $\sim 10^4$ yr).

1. Introduction: Protostars, Prestellar clumps, and Pre-main Sequence Stars

Stars are thought to form from the inside-out collapse of dense cloud cores (e.g., Shu et al. 1993; Stahler in this volume). After a probably very short isothermal phase, during which the liberated gravitational energy is freely radiated away (e.g., Henriksen in this volume), an opaque stellar object or *protostar* forms at the center and starts heating up, while continuing to build up its mass from a surrounding infalling envelope or cocoon. The youngest protostars are thus surrounded by large masses of circumstellar material ($M_{c\star}$) compared with their own, growing stellar mass ($M_\star$), i.e., they have $M_{c\star} >> M_\star$. Their luminosity is well approximated by the infall luminosity $L_{inf} \approx GM_\star \dot{M}/R_\star$, where $\dot{M}$ is the infall rate (cf. Stahler and Henriksen in this volume). When protostars have accumulated most of their final, main sequence mass, they become pre-main sequence (PMS) stars which evolve approximately at fixed mass (although accretion of residual amounts of material may still occur through an accretion disk). Therefore, independently of the details of any protostellar theory, and in a statistical sense at least, larger amounts of circumstellar material are expected to surround younger stellar objects .

Observationally, distinguishing the youngest protostars from pre-protostellar condensations which have not started collapsing on the one hand, and from PMS stars still embedded in their parent clouds on the other hand, is very difficult. Because dust emission remains optically thin at $\lambda \sim 1$ mm up to extremely high column densities ($N_{H_2} \lesssim 10^{26}\ cm^{-2}$), submillimeter continuum observations with large single-dish radiotelescopes equipped with sensitive bolometers provide a very sensitive way to detect both high density prestellar clumps on the verge of collapse and circumstellar structures (envelopes and/or disks) around young stellar objects (YSOs) at any evolutionary stage (e.g., protostars, embedded PMS stars, post T Tauri stars). Once circumstellar structures have been distinguished from prestellar condensations by other means (e.g., evidence for a central YSO at infrared or centimeter radio wavelengths), it is possible to use the circumstellar mass inferred from millimeter continum observations as a tracer of YSO evolutionary state. The effectiveness of this method is illustrated in § 2 by the results of an extensive 1.3 mm continuum survey of the ρ Ophiuchi IR cluster. In § 3, the basic properties of a new class of very cold YSOs recently recognized in the submillimeter band and designated "Class 0" are described, with particular emphasis on the ρ Ophiuchi source VLA 1623. Finally, § 4 proposes a revised observational scenario of early stellar evolution.

2. Evolutionary Status of the near-IR sources of the ρ Ophiuchi cluster

2.1 Millimeter continuum observations

In an effort to sample the evolution of the mass and spatial distribution of the circumstellar material as a function of time, André & Montmerle (1994; hereafter AM) have used the IRAM 30-m telescope equipped with the MPIfR bolometer to conduct a 1.3-mm continuum survey of more than a hundred YSOs located in the ρ Ophiuchi cloud and nearby related regions. In particular, single-point photometry was obtained for each of the 78 members of the ρ Oph near-IR cluster discussed by Wilking, Lada, & Young (1989; hereafter WLY), which comprise a large number of Class I ("infrared protostars"), Class II ("embedded T Tauri stars"), and Class III sources ("naked T Tauri stars") (cf. Lada 1987). With an overall (3-σ) sensitivity of $\sim$ 20 mJy/beam, the detection rate of these systematic "ON-OFF" observations was high, on the order of 40 %. In addition, mapping observations were performed around a total of 19 YSOs (see AM for other details).

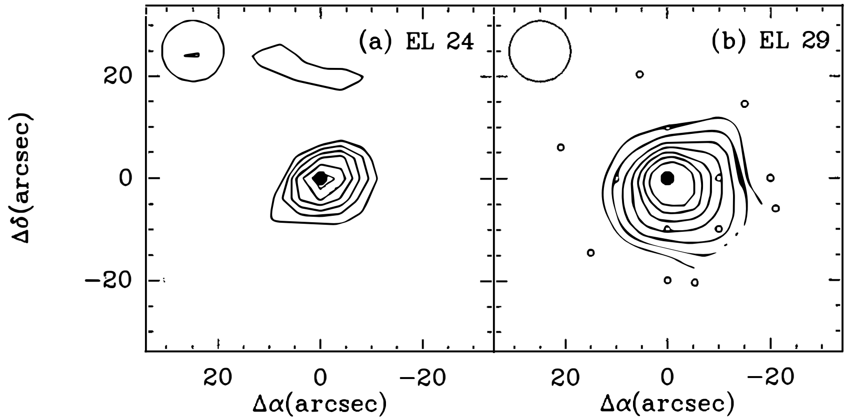

Figure 1. IRAM 30-m bolometer maps of the Class II IR source EL 24 (a) and of the Class I IR source EL 29 (b) (from André & Montmerle 1994).

2.2 Circumstellar nature of the millimeter emission

The millimeter continuum detections most likely correspond to thermal emission from cold dust around the young stars. In most of the bolometer maps (e.g., Fig. 1), the emission is centrally peaked at the nominal YSO position and well contrasted from the surrounding medium, almost independently of IR Class or strength. This is a clear indication that the emission arises from *circumstellar* dust associated with the YSOs themselves rather than from *interstellar* dust clumps related to cloud structure in regions of high column densities. In contrast, the various molecular-line maps that we have obtained so far with the *same* telescope toward the *same* sources show very little structure at the positions of the YSOs and most likely trace larger-scale emission from the ambient cloud itself (e.g., Despois et al. 1994). The single-dish continuum technique therefore appears particularly powerful to probe circumstellar material (although line observations with millimeter interferometers can also discriminate against large-scale cloud emission).

In addition, the maps show that, when detected, the millimeter emission of Class II IR sources is unresolved within the 12" beam of the telescope, consistent with the presence around these sources of circumstellar dust disks with radii significantly smaller than 1,000 AU. This supports the hypothesis of WLY that Class II sources are classical T Tauri stars (sometimes) embedded in (interstellar) cloud material. In contrast, the Class I IR sources, almost always detected at 1.3 mm, are resolved, but display a concentrated structure (FWHM $\lesssim$ 25", i.e., radii $\lesssim$ a few 10^3 AU at 160 pc). This is qualitatively consistent with Class I YSOs being protostellar sources "self-embedded" in spheroidal circumstellar envelopes, although the sizes of these envelopes appear to be $\gtrsim 5$ times smaller than predicted by the "standard" Adams, Lada, & Shu (1987; hereafter ALS) model.

2.3 Circumstellar masses

In order to make meaningful evolutionary comparisons, one needs to estimate the *total* (i.e., integrated) circumstellar fluxes $S^{int}_{1.3mm}$ from the various YSOs. We have done so on the basis of our mapping results and various extrapolation methods. In particular, because the outer parts of circumstellar envelopes may not be dense enough to emit significant dust continuum emission at 1.3 mm, we have used the standard model of protostellar envelopes (e.g., Terebey, Shu, & Cassen 1984; ALS) to infer an "effective" upper limit to $S^{int}_{1.3mm}$ based on the emission mapped in the inner regions (see AM and Terebey, Chandler & André 1993 for details).

Assuming an optically thin, isothermal dust source, $S^{int}_{1.3mm}$ is readily converted into a total (dust + gas) circumstellar mass $M_{c\star}$ by a relation of the type: $M_{c\star} = [\,S^{int}_{1.3mm}\, d^2\,] \,/\, [\,\kappa_{1.3}\, B_{1.3}(T_{dust})\,]$, where $B_{1.3}$ is the Planck function $\lambda = 1.3$ mm.

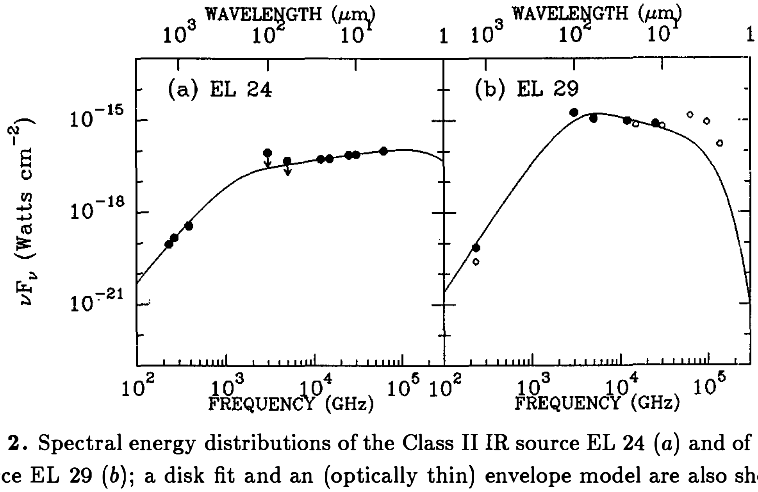

Figure 2. Spectral energy distributions of the Class II IR source EL 24 (*a*) and of the Class I IR source EL 29 (*b*); a disk fit and an (optically thin) envelope model are also shown in (*a*) and (*b*), respectively (adapted from André & Montmerle 1994).

In order to assess the influence of temperature effects on the mass estimates, we used disk models similar to those of Beckwith et al. (1990) for Class II sources and simple (optically thin) power-law envelope models for Class I sources (see examples in Fig. 2 and AM for details). This modeling study shows that the volume-averaged temperature of the emitting circumstellar material is generally well constrained by the spectral energy distributions

(SEDs) to be $< T_{dust} > \approx 30$ K.

The largest uncertainty in the mass determinations arises from the only approximately known value of the dust opacity per unit mass column density $\kappa_{1.3}$, which implicitly contains the dust-to-gas ratio. For the extended circumstellar matter seen around Class I sources which is probably quite similar to the material of dense cores, we use $\kappa_{1.3} \simeq 0.01$ cm^2 g^{-1}, as this value seems appropriate (within a factor ~ 2) for dense ($n \gtrsim 10^6$ cm^{-3}) cloud regions (e.g., Mezger 1990; André, Ward-Thompson, & Barsony 1993, hereafter AWB). In the circumstellar disks of Class II sources, the dust opacity is more uncertain since particle growth, possibly in the form of fractal aggregates, may occur prior to planet formation, which will enhance κ_ν over the value applying to dense cores (e.g., Beckwith & Sargent 1991; Ossenkopf 1991). To facilitate comparisons, we adopt the same value $\kappa_{1.3} \simeq 0.02$ cm^2 g^{-1} for Class II and Class III sources as Beckwith et al. (1990) in their related mm continuum study of T Tauri stars in Taurus.

Converting $S_{1.3}^{int}$ into $M_{c\star}$ in this way, we find that the circumstellar masses of Class III, Class II *and* (contrary to expectation) Class I near-IR sources are *small* compared to stellar masses (i.e., are $<< 1\ M_\odot$). They are also smaller than the masses (typically 0.5–3 $M_\odot$) found by Ward-Thompson et al. (1994) for *pre-protostellar* condensations, using a similar dust continuum technique. More precisely, the large majority of Class III sources are undetected at 1.3 mm, implying that their circumstellar masses are lower than our detection threshold: $M_{c\star} < 3 \times 10^{-3}$ M$_\odot$. The median value for detected Class II sources is $\sim 0.01\ M_\odot$, i.e., on the order of the mass of the "minimum solar nebula" only (but 70 % of all Class II sources have a circumstellar mass *below* this value). The median mass for Class I sources is only 6 times larger, and their maximum mass is comparable with that of Class II sources ($\sim 0.1\ M_\odot$).

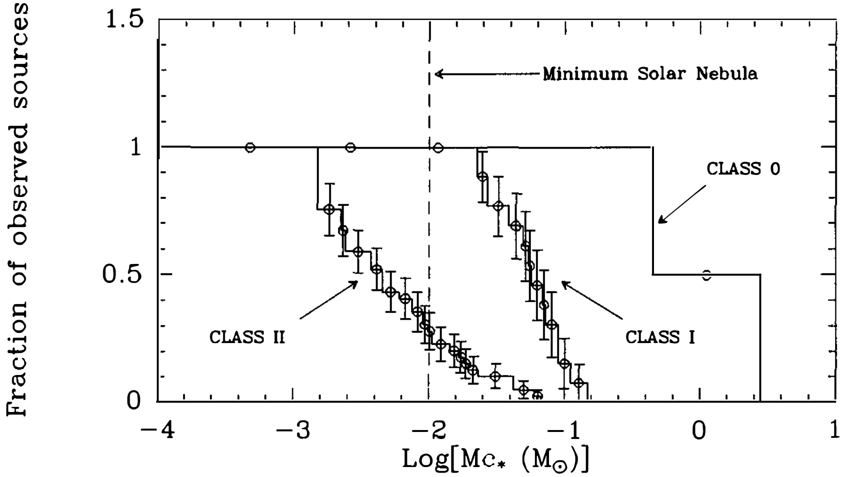

Figure 3. Cumulative distributions of the circumstellar mass $M_{c\star}$ for the ρ Oph Class II, Class I sources, and "Class 0" sources (see § 3) (from André & Montmerle 1994).

These results are illustrated in Figure 3. They confirm the evolutionary sequence Class I → Class II → Class III inferred from IR studies (Lada 1987). However, the small values of the circumstellar masses measured around the near-IR sources of ρ Ophiuchi suggest that, *as early as the Class I stage, YSOs have already accumulated most of their final stellar mass, and thus are no longer in the main accretion phase* (here defined by $M_{c\star} > M_\star$).

3. A New Class of YSOs: The "Class 0" protostars

A posteriori, the failure to find an object in the early protostellar stage when $M_{c\star} > M_\star$ among near-IR sources is perhaps not too surprising since detailed numerical calculations of protostellar collapse suggest that the spectral appearance of the youngest protostars should more closely resemble that of a blackbody at 10–30 K (cf. Boss & Yorke 1990) than that of a relatively broad Class I SED (as in ALS). The youngest stellar objects are thus likely to be found among strong (sub)millimeter continuum sources so highly obscured by their own circumstellar material that they are virtually undetectable at near-IR wavelengths.

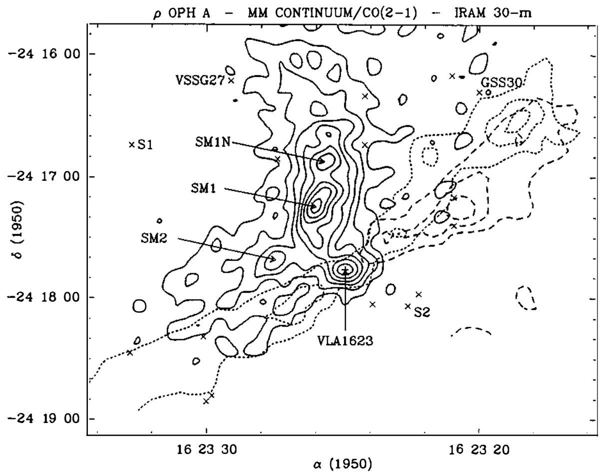

Figure 4. Millimeter continuum map of ρ Oph A obtained with the IRAM 30 m telescope and MPIfR bolometer (cf. AWB). The jet-like CO outflow driven by the candidate low-mass protostar VLA 1623 is superposed (cf. André et al. 1990).

3.1 Protostellar and/or prestellar condensations in ρ Oph A

It was recently recognized that the source VLA 1623 in the ρ Ophiuchi cloud core A is very likely a stellar object with such characteristics (AWB). VLA 1623 was first discovered with the VLA at 6 cm as part of a radio continuum study of the B3 star S1 and its surroundings (André et al. 1988; Leous et al. 1991). It was subsequently identified as the driving source of a jet-like CO outflow by André et al. (1990). Follow-up continuum mapping of ρ Oph A at 1.3 mm with the IRAM 30 m telescope (see Fig. 4) and 800, 450, and 350 μm with the JCMT showed that VLA 1623 coincides with a compact, roughly spherical clump of radius $\sim$ 1000 AU, total mass $\sim$ 0.6 $M_{\odot}$, average density $\sim 2 \times 10^7$ cm^{-3}, luminosity $\sim 1\ L_{\odot}$, and outer temperature $T_d \lesssim 20$ K (AWB; see also Fig. 5). This clump is thus a candidate protostellar condensation reminiscent of those described by Güsten in this volume (see also Mezger 1993). In fact, our submilimeter mapping of ρ Oph A reveals at least three more compact clumps (labeled SM1, SM1N, and SM2 in Fig. 4) which have apparent characteristics (e.g., M $\lesssim$ 1 M$_{\odot}$) very similar to VLA 1623 and are also invisible at infrared wavelengths.

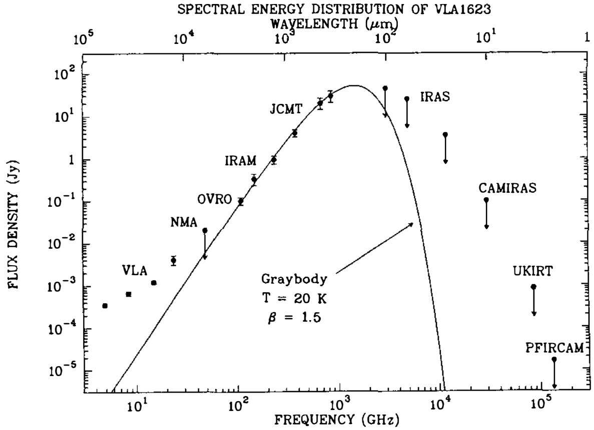

Figure 5. Spectral energy distribution of VLA 1623 along with a graybody fit (adapted from André, Ward-Thompson, & Barsony 1993).

Mezger et al. (1992) independently mapped the same region at IRAM with very similar results, and interpreted all these clumps as low-mass, "isothermal protostars". However, based only on dust continuum observations, it is very difficult to distinguish true *protostellar* condensations from *pre-protostellar* condensations similar to those found by Ward-Thompson et al. (1994) in their JCMT continuum mapping survey of "Myers" dense cores with no embedded sources. The reason is that these condensations are expected to form relatively slowly through a quasi-static phase of ambipolar diffusion during which they remain approximately in virial equilibrium. Since the collapse is expected to proceed from the inside-out (see Stahler in this volume), most of the material in the youngest protostellar condensations (those which have just started collapsing) is still in equilibrium, making them virtually indistinguishable from pre-protostellar condensations. (Spectroscopic signatures of collapse are often ambiguous, although claims have been made in the case of some "Class 0" objects such as B335 – Zhou et al. 1993; see also Güsten in this volume.)

In ρ Oph A, all four submillimeter clumps are within a factor of 2 of virial equilibrium (see AWB). In the case of VLA 1623, the compact VLA continuum emission (which most likely traces the existence of shock-ionized gas at $T \sim 10^4$ K), together with the presence of the bipolar flow, strongly suggest that the brief isothermal phase has been passed and that a *stellar* object has already formed at the center. On this basis, AWB interpreted VLA 1623 as a *protostar* in the main accretion phase (see also *3.2* below). In contrast, none of the other submillimeter condensations of ρ Oph A are associated with a molecular outflow or a compact radio continuum source. Furthermore, closer inspection reveals that these other clumps are more amorphous in shape than VLA 1623 (for instance, their peak positions tend to depend on the wavelength of observation), suggesting the absence of any central attracting and/or heating source inside them. On these grounds, AWB hypothesized that SM1, SM1N, and SM2 are *pre-protostellar* in nature and have *not yet* entered the isothermal collapse phase.

3.2 VLA 1623 as the prototype of a new class of YSOs

Independently of any model, the cold temperature, low bolometric luminosity, relatively massive circumstellar structure, and high internal obscuration ($A_V \gtrsim 1000$) of VLA 1623 all point to an extremely young object, perhaps a true protostar. For instance, the location of VLA 1623 in various theoretical evolutionary diagrams for (low-mass) protostars (e.g., Appenzeller & Tscharnuter 1975; Adams 1990) suggests an age ranging from $\sim 10^3$ yr to 3×10^4 yr (this "age" has to be understood as the time elapsed since the formation of a central, opaque protostellar core, i.e., since the end of the isothermal phase).

AWB suggested that VLA 1623 and a few other low-luminosity YSOs, all characterized by unusually high values of the ratio L_{submm}/L_{bol} and undetected in the near-IR, make up *an entirely new class of YSOs* (the "Class 0"), corresponding to the "theoretical" concept of a protostar in the main accretion phase (defined by $M_{c\star}/M_\star > 1$; cf. § 1). Indeed, while the submillimeter luminosity L_{submm} (or almost equivalently $L_{1.3mm}$) of a protostellar source provides a relative measure of its *circumstellar* mass $M_{c\star}$, the bolometric luminosity L_{bol} may be used to infer the central *stellar* mass $M_\star$ on the basis of various plausible mass–luminosity relations for protostars (e.g., Fig. 6). In the youngest (accreting) sources at least, the measurable ratio $L_{1.3mm}/L_{bol}$ should thus tend to reproduce the variations of the mass ratio $M_{c\star}/M_\star$. The boundary between the Class I and the Class 0 is by definition set at the critical luminosity ratio corresponding to $M_{c\star}/M_\star = 1$ (see AWB for explicit values). However, because of uncertainties in the relations between L_{bol} and $M_\star$ on the one hand and between $L_{1.3mm}$ and $M_{c\star}$ on the other hand, the actual boundary is necessarily somewhat vague. In practice, the two classes are best distinguished in diagrams plotting $S^{int}_{1.3mm}$ (or equivalently $M_{c\star}$) against L_{bol} (cf. Fig. 6). When studying highly obscured protostellar objects, such diagrams appear to be more appropriate equivalents of the H–R diagram than the L–A_V diagram of Adams (1990) (cf. Saraceno et al. 1994).

As Figure 6 shows, there is continuity between Class I and Class 0 sources. However, while objects still well in the main accretion phase are dominated by the effects of their circumstellar cocoon ($M_{c\star} >> M_\star$) and are likely to retain detailed information about their genesis, those with $M_{c\star} << M_\star$ are at the end of their accretion phase and are probably already dominated by stellar rather than protostellar processes. In that sense, Class 0 sources, which provide good observational candidates for being in the former stage, cannot just be considered as "extreme Class I" sources.

It is important to point out that Class 0 sources are statistically very young. For instance, in the ρ Oph central region where the IRAM 30 m mapping study of Mezger et al. (1992) provides an essentially complete survey for Class 0 sources down to $M_{c\star} \approx 0.1\ M_\odot$, VLA 1623 is the *only* good candidate while there are between 11 and 24 near-IR Class I sources known with $L_{bol} \gtrsim 1\ L_\odot$ (cf. WLY and AM). This suggests that the lifetime of Class 0 sources is at least an order of magnitude shorter (i.e., $\lesssim 10^4$ yr) than the estimated lifetime of Class I sources ($\lesssim 10^5$ yr; cf. WLY and Kenyon et al. 1990).

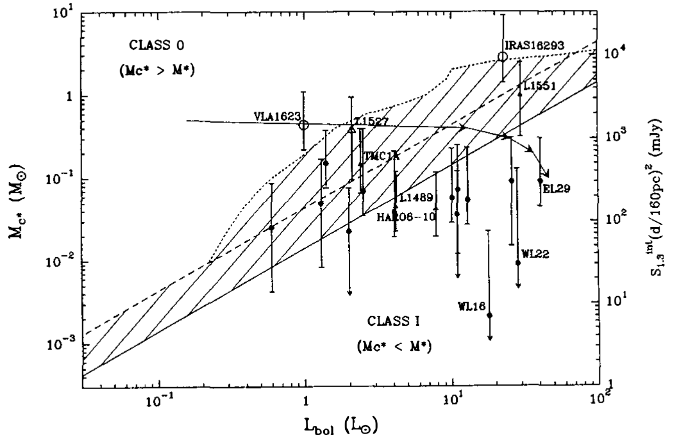

Figure 6. Circumstellar mass $M_{c\star}$ against bolometric luminosity L_{bol} for the ρ Oph Class I and Class 0 sources (filled and open circles). The hatched area represents the border zone between Class I and Class 0 (see AM for details). The locations of the Taurus infrared protostellar candidates modeled by ALS are shown (as triangles) for comparison. An indicative protostellar evolutionary track for an initial cloud core mass $\sim 0.5\ M_\odot$ and a mass infall rate $\sim 10^{-5}\ M_\odot\,\mathrm{yr}^{-1}$ is superposed.

3.3 Jet-like outflows from class 0 protostars

One of the most outstanding features of the newly recognized Class 0 sources is that virtually all of them drive spectacular CO molecular outflows. These outflows are highly collimated or "jet-like" (with length-to-width ratios exceeding 10 and opening angles smaller than 30°; see, e.g., Fig. 4), relatively fast (with typical characteristic velocities $V_{char} \gtrsim 50\ \mathrm{km\,s^{-1}}$), apparently very young (with dynamical timescales $t_{dyn} << 10^4$ yr), and powerful (with mechanical powers $L_{CO} = 1/2\,\dot{M}_{CO}\,V_{char}^2$ approaching ~ 50 % of the bolometric luminosity of the central sources). Two of the most remarkable of these jet-like CO outflows are those driven by the Class 0 sources L1448-C (Bachiller et al. 1990) and VLA 1623 (André et al. 1990). In contrast, while there is growing evidence that some outflow activity exists throughout the embedded phase (e.g., Terebey et al. 1989; Parker et al. 1991), the CO outflows from Class I sources tend to be poorly collimated, slower, and much less energetic than those from Class 0 sources. In an effort to characterize the evolution of molecular outflows during the protostellar phase, Bontemps et al. (1994) have recently obtained and analyzed a homogeneous set of CO(2–1) data around a large sample of low-luminosity ($L_{bol} < 100\ L_{\odot}$) embedded YSOs, including 28 Class I sources and 5 Class 0 sources. Their results shows that Class 0 sources are distinguished from Class I sources not only by stronger submillimeter continuum emission (which is the criterion defining the Class 0), but also by more collimated and *more powerful CO outflows* (see Fig. 7). This clear evolution of outflow characteristics from Class 0 to Class I is consistent with the most recent theoretical views on the structure of molecular outflows (e.g., Stahler 1993), according to which the observed CO outflows represent ambient gas that has been progressively entrained (in a turbulent fashion) by an underlying jet directly originating in the central star and/or circumstellar structure. In this picture, the youngest CO outflows are indeed expected to be the fastest and most highly collimated flows, i.e., to appear " jet–like". Evidence for the driving jet has very recently been found toward some Class 0 sources in the form of shock-excited molecular hydrogen emission (Bally et al. 1993; Davis et al. 1993) or Herbig-Haro objects (Eiroa et al. 1993).

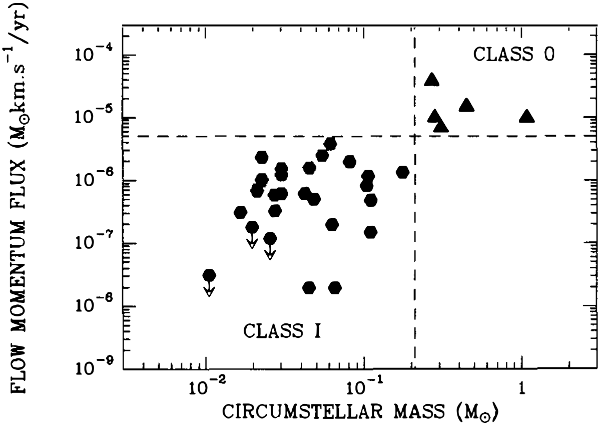

Figure 7. Outflow momentum flux against circumstellar mass of the driving source for a sample of nearby, low-luminosity Class I and Class 0 YSOs (from Bontemps et al. 1994).

4. Conclusions: A Revised Observational Scenario of Early Stellar Evolution

The recent (sub)millimeter continuum results obtained on low-mass YSOs (e.g., AM) confirm the usefulness of SEDs to infer the evolutionary states of YSOs, as first pointed out by Lada (1987) in the infrared range. However, it is now apparent that observing the SEDs at wavelengths significantly longer than 100 μm (e.g., at 1.3 mm) is of prime importance to get at a complete evolutionary picture. In particular, the strength and spatial distribution of the millimeter continuum emission of YSOs may be used as *quantitative* tracers of the progressive

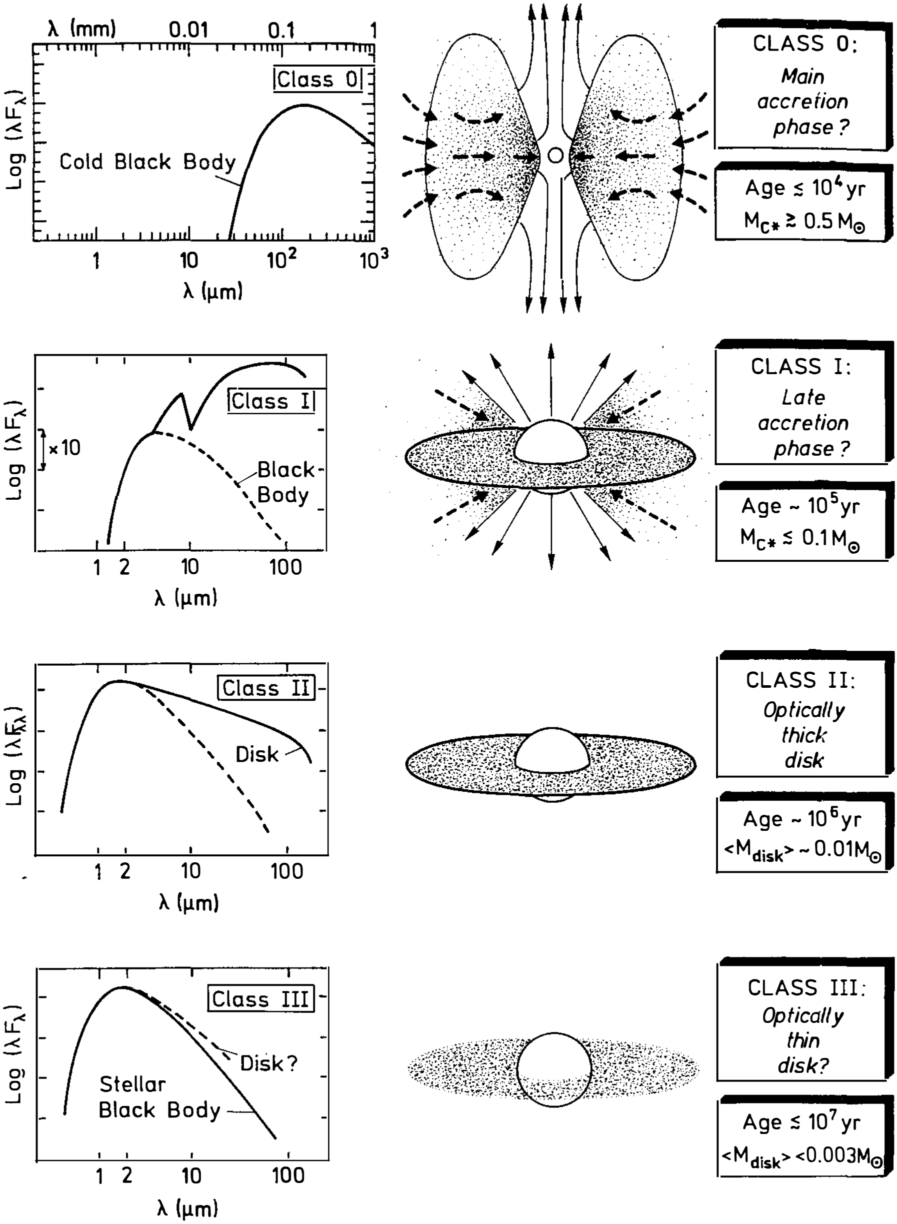

Figure 8. Our revised, quasi-continuous evolutionary sequence of SEDs for low-mass YSOs.

decrease and condensation of the circumstellar material as early stellar evolution proceeds. We thus propose a revised evolutionary scenario from Class 0 to Class III (see Fig. 8).

In this scheme, the Class 0 sources are the youngest stellar objects, probably true protostars at the beginning of the main accretion phase. They are virtually *undetectable in the near-IR* ($\lambda < 10\mu$m) and their SEDs closely resemble that of a *single temperature blackbody* at T $\sim$ 10–30 K. These objects are in the process of assembling the bulk of their final stellar mass which is still in the form of an "apple–like" circumstellar structure. Although they probably have not developed a significant disk yet, they are already driving jet–like outflows (see Henriksen & Valls-Gabaud 1993 and Henriksen in this volume for a possible mechanism). Present observations are indeed consistent with the outflow phase starting *as soon as a protostellar core forms* at the center of a collapsing dense cloud fragment. Inflow and outflow must therefore occur *simultaneously* (see also Lada & Shu 1990). Virtually all Class 0 sources known to date are associated with VLA radio continuum emission, which probably traces free-free radiation from shock-ionized material in the associated wind and/or the accretion shock at the surface of the central object (this VLA emission is one of the least understood observed characteristics of this stage).

The next stage is that of the near-IR Class I sources or "infrared protostars" of Lada (1987), which have much broader spectra than Class 0 sources, clearly implying a wide range of temperatures. Based on their millimeter continuum properties, these objects are confirmed to be *self–embedded* in spheroidal envelopes, but the new result is that these envelopes contain only *residual (i.e., substellar) amounts of circumstellar material.* In that sense, Class I sources have passed the main accretion phase and probably are in a late (and perhaps slower) accretion phase, affecting the highest angular momentum material of the parent cloud core. For this reason, they are likely to have developed a significant disk (with radius up to $\lesssim$ 100 AU; e.g., Terebey et al. 1984), although millimeter interferometric observations show that this disk cannot be very massive (Terebey et al. 1993). Class I sources also drive CO outflows, but these outflows are much broader, slower, and less "penetrating" than those of Class 0 sources (e.g., Bontemps et al. 1994).

The last two stages in our revised scenario correspond to the near-IR Class II and Class III sources, and are virtually unchanged with respect to Lada's scenario (see AM for details). These two classes group PMS stars which have passed the self-embedded phase but are in some cases still obscured by *interstellar* material from their parent clouds.

Although this evolutionary progression of SEDs is in fact continuous and may be parameterized by a "mean frequency" or a "bolometric temperature" (Myers & Ladd 1993), the break down of YSOs into of four distinct classes is justified by the fact they correspond to conceptually different stages of evolution.

Acknowledgements. I am grateful to Catherine Cesarsky and Thierry Montmerle for their encouragement about this work, and to Sylvain Bontemps for providing Figure 7 prior to publication.

References

Adams, F.C. 1990, ApJ, 363, 578

Adams, F.C., Lada, C.J., & Shu, F.H. 1987, ApJ, 312, 788 (ALS)

André, P., Martín-Pintado, J., Despois, D., & Montmerle, T. 1990, A&A, 236, 180

André, P., & Montmerle, T. 1994, ApJ, 420, 837 (AM)

André, P., Montmerle, T., Feigelson, E. D., Stine, P. C., & Klein, K. L. 1988, ApJ, 335, 940

André, P. Ward-Thompson, D. & Barsony, M. 1993, ApJ, 406, 122 (AWB)

Appenzeller, I., & Tscharnuter, W.M. 1975, A&A, 40, 397

Bachiller, R., Cernicharo, J., Martín-Pintado, J., Tafalla, M., Lazareff, B. 1990, A&A, 231, 174

Bally, J., Lada, E.A., & Lane, A.P. 1993, ApJ, 418, 322

Beckwith, S.V.W. & Sargent, A.I. 1991, ApJ, 381, 250

Beckwith, S.V.W., Sargent, A.I., Chini, R.S., & Güsten, R. 1990, AJ, 99, 924

Bontemps, S., André, P., Terebey, S., & Cabrit, S. 1994, in preparation

Boss, A.P., & Yorke, H.W. 1990, ApJ, 353, 236

Davis, C.J., Dent, W.R.F., Matthews, H.E., Aspin, C., & Lightfoot, J.F. 1993, MNRAS, in press

Despois, D., André, P., & Martín-Pintado, J. 1994, in preparation

Eiroa, C., Miranda, L.F., Anglada, G., Estalella, R., & Torrelles, J.M. 1993, A&A, in press

Henriksen, R.N., & Valls-Gabaud, D, 1993, MNRAS, in press

Kenyon, S.J., Hartmann, L.W., Strom, K.M., & Strom, S.E. 1990, AJ, 99, 869

Lada, C.J. 1987, in Star Forming Regions, Proc. IAU Symp. 115, eds. M. Peimbert and J. Jugaku (Dordrecht : Kluwer), p.1

Lada, C.J., & Shu, F.H. 1990, Science, 248, 564

Leous, J.A., Feigelson, E.D., André, P., & Montmerle, T. 1991, ApJ, 379, 683

Mezger, P.G. 1990, in Physics and Composition of Interstellar Matter, eds. J. Krelowski & J. Papaj (Institute of Astronomy, Nicolaus Copernicus University, Torun), p. 97

Mezger, P.G. 1993, in Proc. of 1st Intl. Conference on Planetary Systems (Pasadena), in press

Mezger, P.G., Sievers, A.W., Zylka, R., Haslam, C.G.T., Kreysa, E., & Lemke, R. 1992, A&A, 265, 743

Myers, P.C., & Ladd, E.F. 1993, ApJ, 413, L47

Ossenkopf, V. 1991, A&A, 251, 210

Parker, N.D., Padman, R., & Scott, P.F. 1991, MNRAS, 252, 442

Saraceno, P., André, P., Ceccarelli, C., Griffin, M., Molinari, S., & Russell, S. 1994, A&A, in preparation

Shu, F.H., Najita, D., Galli, D., Ostriker, E., & Lizano, S. 1993, in Protostars and Planets III, ed. E.H. Levy & J.I. Lunine, (Tucson : University of Arizona Press), p.3

Stahler, S.W. 1993, in Astrophysical Jets, eds. M. Livio, C. O'Dea, & D. Burgarella (New York: Cambridge U. Press), in press

Terebey, S., Chandler, C.J., & André, P. 1993, ApJ, 414, 759

Terebey, S., Shu, F.H., & Cassen, P. 1984, ApJ, 286, 529

Terebey, S., Vogel, S.N., & Myers, P.C. 1989, ApJ, 340, 472

Ward-Thompson, D., Scott, P.F., Hills, R.E., & André, P. 1994, MNRAS, in press

Wilking, B. A., Lada, C. J., & Young, E.T. 1989, ApJ, 340, 823 (WLY)

Zhou, S., Evans II, N.J., Kömpe, C., & Walmsley, C.M. 1993, ApJ, 404, 232

Philippe André at 2 μm. Picture taken with the ALICE IR array for UKIRT (ROE).

PROTOSTELLAR CONDENSATIONS IN THE SERPENS CORE

Mark M. Casali
Royal Observatory, Blackford Hill, Edinburgh EH9 3HJ
Carlos Eiroa
Fisica Teorica, Universitad Autonoma de Madrid, Cantoblanco 28049 Madrid
Glenn White
Queen Mary and Westfield College, London

ABSTRACT

MM/submm continuum maps made with the JCMT reveal at least 6 discrete objects in the Serpens cloud core, four of which have no NIR counterparts. Comparison with a $C^{18}O$ map shows that the submm objects are associated with the densest molecular gas in the core. It is clear that these represent the youngest population in the cloud core. CO(J=2-1) maps in the line wings reveal multiple outflows from the 50+ young stars known from the NIR and submm. The majority of NIR sources were not detected in the submm, a result consistent with other recent results showing that Class I sources are not particularly brighter in the submm than Class II. The brightest source in the core is FIRS1, a bright submm object similar to IRAS 16293. A near IR reflected continuum jet emerging from its obscured centre points to the presence of hot (>500K) material.

1. INTRODUCTION

The Serpens cloud core forms the densest part of a large 1°x2° molecular cloud at a distance of 300 pc. The core itself is some 30 sq. arcminutes in size and a well known site of low mass star formation[3]. A combination of UKIRT NIR, and JCMT mm/submm continuum and heterodyne maps has been used to study the young cluster population as well as its interaction with the gas.

2. PROTOSTELLAR CONDENSATIONS IN THE CORE

An 1100 μm contour map is shown in Fig.1 overlaid on a 2 μm (K) image of the core from Eiroa and Casali [5]. The K image shows approximately 50 YSOs reaching a density of 10^4-10^5 Mo pc^{-3} in the Southern subcluster. Yet of the 6 identified peaks in the mm, only sources 5 and 6 are associated with NIR point sources. This was confirmed with deeper maps at 800 and 1100 μm centred on the Southern part of the cluster. This lack of correlation is at first somewhat surprising, given the large masses of circumstellar material expected to surround these embedded phase (many are probably Class I) objects, but is actually consistent with recent findings which suggest that Class I sources are not significantly stronger mm continuum emitters than Class II TT-like objects[2].

The most luminous source in the core is FIRS1 with a flux density of 8 Jy at 800 μm. Integrating its spectrum gives a bolometric luminosity of 80 L_O. Of interest is a short jet seen at 2 μm emerging from the geometric centre of the mm peak.

3. MOLECULAR GAS AND MULTIPLE OUTFLOWS IN THE CORE

It is important to know where the dense molecular gas is in the core. In Fig.2a we see that the dense material as traced by $C^{18}O$(J=2-1) is generally associated with the mm continuum peaks, though the correspondence is not perfect in that the $C^{18}O$ peaks do precisely match those in the mm, an effect which may be related to heavy element depletion onto grains[6]. Further the dense gas is not well associated with the NIR sources. A picture naturally

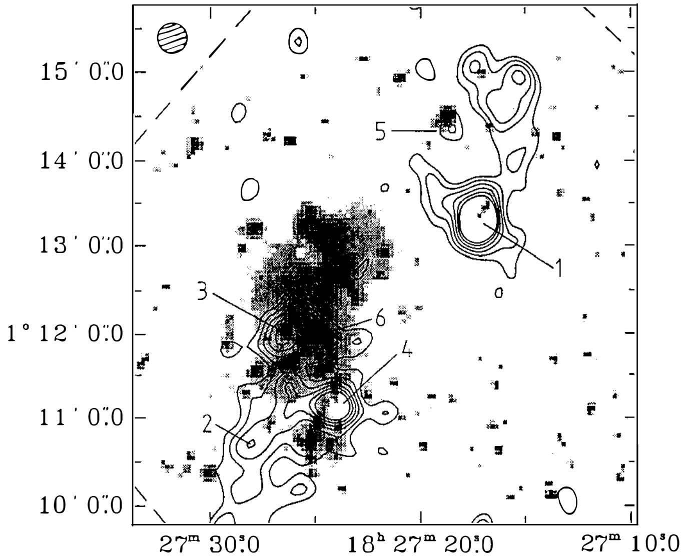

Figure 1 JCMT contour map at 1100μm overlaid on a greyscale 2μm image. FIRS1 is labelled as source 1.

emerges, then, in which the NIR sources are the oldest objects having dissipated surrounding material, while the remaining dense gas is forming new protostars - the mm peaks.

With so many young stars in the core, a large number of outflows would be expected and this is indeed the case as shown in Fig.2b where maps of the blue and red line wings of CO(2-1) are shown. Assigning sources to particular outflows is difficult, except for FIRS1 where a blue lobe seems associated with the near IR jet which must therefore be emerging from the cloud *towards* us.

4. FIRS1

The ratio of bolometric to submm luminosity for this object is a factor of 10 higher than the very coldest protostellar sources such as NGC1333-IRAS4 or VLA1623[1] and is in fact more like that of IRAS16293-2422. As with IRAS16293, there is substantial evidence for hot material in the core. In particular Eiroa and Casali[4] have shown that the tip of the NIR jet nearest the centre is probably reflected continuum. Assuming this to be thermal (extending the cm emission to the NIR results in negligible flux), considering the angle subtended by the

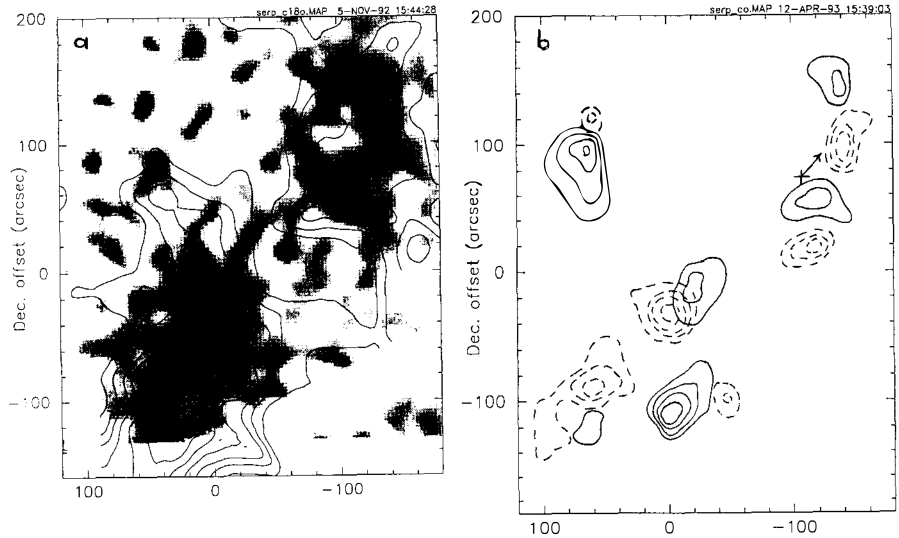

Figure 2 (a) JCMT $C^{18}O$ (J=2-1) contour map on greyscale 1100μm continuum image. (b) Contour of CO(J=2-1) line wings. Solid contours are integrated 10-20 km/s, and dashed contours -20 to -10 km/s.

reflection, and constraining the total luminosity to be 80 L_O, a temperature >500 K is required in the centre of FIRS1. Clearly a hot core has already formed in this young object.

REFERENCES

1. Andre P., Ward-Thompson D., Barsony M., 1993, Ap.J. In press.
2. Barsony M. and Kenyon S., 1992, Ap.J. **384**, L53
3. Eiroa C., 1991, in Low Mass Star Formation in Southern Molecular Clouds, ed Bo Reipurth, ESO report no. 11 p.197
4. Eiroa C. and Casali M.M., 1989, A&A **223**, L17
5. Eiroa C. and Casali M.M., 1992, A&A **262**, 468
6. Mauersberger R. et al , 1992, A&A, **256**, 640

COLD INTERSTELLAR DUST DETECTED AT MM WAVELENGTHS

P. Merluzzi
Istituto di Ingegneria Aerospaziale
Napoli, Italy

ABSTRACT

Recently several observations of the emission spectrum of the Galaxy at IR, submm and mm wavelengths have shown unexpected strong emission in various regions of the sky. In order to account for these results, the emitting dust must be characterized both by a wide range of dimensions (a few Å to about $1\mu m$) and of temperatures (10-50 K), at least for the inner part of the Galaxy.

Taking into account that the IRAS FIR measurements evidence the presence of hotter particles and are not completely adequate to estimate the total dust mass fraction, we should emphatize the importance of mm and submm observations. Actually Pajot et al.[1] find that about 90% of the dust is expected to have a temperature lower than 20 K so that it radiates only 10% of the energy at FIR wavelengths.

For a better understanding of the interstellar dust nature we have analysed previous observations performed in Antarctica and extended from $b \sim -6.5°$, $l \sim 305°$ to $b \sim -9°$, $l \sim 312°$ which are compared with new 3mm data by Piccirillo[2]. These data have been used to determine the spectral behaviour of the emission detected in this region of the sky. In addition, laboratory measured optical properties of cosmic grain analogs[3],[4] have been used to discuss the astronomical data.

1. EXPERIMENTAL

The scanning of the galactic plane ($\lambda = 2$ mm) was performed at the Italian Base in Antarctica using 1m instrument with a field of view (FOV) of $\sim 1°$. The observations were taken with the drift scan technique at the declination of $\sim -69°$. We have detected the flux coming from two galactic structures respectively at $\sim 13.75h$ and $\sim 14.50h$ of right ascension.

The 3mm fluxes of the same sources were measured with another experiment carried out at Terra Nova Bay with a FOV of 15 arcmin[2]. The brightness of each region of the sky is determined at 2mm by averaging the data every time-length lasting about 14 minutes. This procedure allows to smooth any high frequency atmospheric noise down to the frequency corresponding to half of the FOV width. Further analysis[5] allow us to achieve a signal to noise ratio of about 4 for the galactic regions.

3. RESULTS AND DISCUSSION

Figure 1(a,b) reports our data at 2mm, derived for the sky region at $\sim 14.50h$ of right ascension, and 3mm together with IRAS fluxes at 60 and 100 μm (we obtain a similar result for the adjacent region). We tend to interpret the observations as essentially due to thermal dust emission, we note that all data shown in fig. 1(a,b) may be fitted by appropriate thermal emission curves once the spectral index α is known. For the wavelength region covered by IRAS observations we have assumed the usual λ^{-2} emissivity[6]. The corresponding gray body temperature is found to be $T \simeq 24K$, in good agreement with the results obtained by various authors. Beyond approximately 400μm the experimental data can not be accounted for by the same thermal curve. Actually, two different couples of values for both the spectral index and the temperature are able to match the submm and mm observations.

We remind that several grain models suggest that at least three components are needed to reproduce the interstellar extinction curve[7] and IRAS fluxes.

We have, then, considered some laboratory studies about different materials believed to simulate interstellar dust grains and, in particular, data concerning different kinds of silicates and carbonaceus materials which have been investigated determining both the morphological properties and the optical characteristics from VUV to FIR and mm wavelengths.

The laboratory results show that, regardless of their specific composition, silicates present a spectral trend which follows a λ^{-2} law[4),8] in the FIR. The same spectral index is found for graphite[9]. On the contrary, amorphous/disordered carbon is characterized by an extinction efficiency $\lambda^{-\alpha}$ with α varying from 0.9 to 1.1 according to the actual structure of the carbon and the hydrogen content of the grains [3]. In particular, slightly hydrogenated amorphous carbon which contains randomly oriented small graphitic islands shows a $\lambda^{-1.1}$ spectrum[3].

The results of the fits reported in Figure 1(a,b) indicate that both silicates and amorphous/disordered carbon are able to account for the observational data that we are considering. However, the choice of one material respect to the other implies a different equilibrium temperature for the emitting material, respectively 7K and 16K.

The optical constants determined in laboratory for the two materials above mentioned (silicates[4] and amorphous/disordered carbon[3]) have been used to estimate grain equilibrium temperatures in two cases: (a) diffuse medium, (b) giant molecular cloud (characterized by $A_v \geq 5mag$). In the first case we have considered the usual interstellar radiation field as given by Mathis, Mezger and Panagia[10]; in the second one we have also taken into account the correction proposed by Bollea & Cavaliere[11]. The resulting equilibrium temperature values are reported in Table 1.

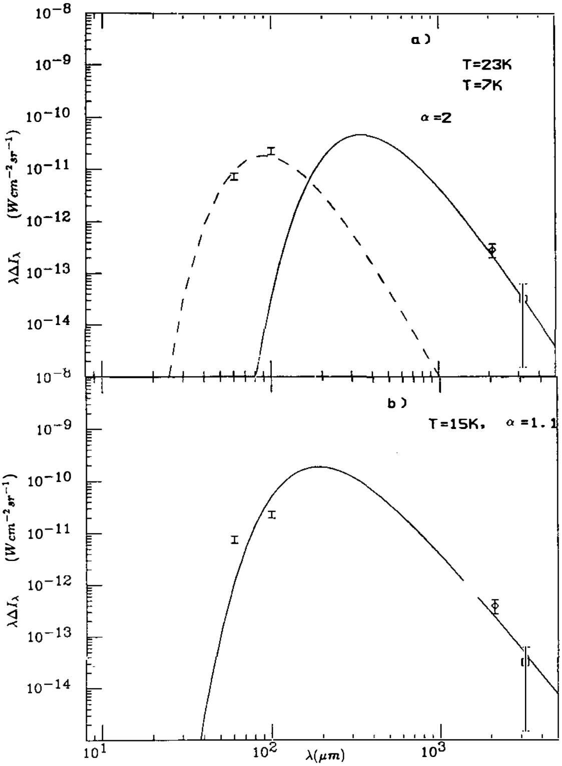

Fig. 1(a,b) Present work data for the galactic structure at r.a. 14.50h and $\delta \simeq -69.1°$ (◇) compared with 60 and 100 μm) IRAS data (I) and 3mm data (□).

If we compare the results reported in Table 1 with the fits shown in Figure 1(a,b) we note that, apparently, it is possible to account for the mm observations by considering two different grain components: a) cold particles with a λ^{-2} spectral trend; b) hotter particles with a $\lambda^{-1.1}$ spectral trend. In the case of the cold particles the observed fluxes should be prodaced by silicates sitting in giant molecular clouds. On the contrary, the wormer particles should be amorphous/disordered carbon grains present in the diffuse interstellar medium.

In order to verify if the long wavelength fluxes derive from giant molecular clouds or from molecular cirrus clouds we have considered two different catalogues[12),13)]. In neither catalogues we can identify any source located in the same direction of the galactic regions we have observed (i.e. $l \simeq 305° - 312°$, $b \simeq -6.5° - -9°$). This negative result seems to suggest that the submm and mm fluxes reported in Figure 1 have to be explained as due to thermal emission by dust sitting in the diffuse interstellar medium and characterized by a $\lambda^{-1.1}$ spectral trend.

We note, in this case, that the IRAS $100\mu m$ flux should be due to the same particles which produce the mm emission. This is particular interesting as agrees well with the model by Désert, Boulanger and Puget[7] which indicates that large grains dominated by silicates with additional dark refractory mantle do account for about 90% of the $100\mu m$ IRAS emission and the total submm emission. All these evidences imply that silicates emission prevails at intermediate and FIR wavelengths while at longer wavelengths it is dominant the amorphous/disordered carbon mantles emission with a $\lambda - 1.1$ spectral trend.

At the end it is interesting to note that, very recently, Meinhold & Lubin[14] have pointed out that their 3.3mm observations of dust emission at very high galactic latitudes seem to suggest an emissivity close to one.

Table 1
Equilibrium temperatures computed for silicate and amorphous/disordered carbon grains both in the interstellar medium and inside a molecular cloud.

Source	Silicate T (K)	Amorphous/disordered carbon T (K)
Diffuse medium	10	16
Giant Molecular Cloud	7	11

REFERENCES

1) F. Pajot, R. Gispert, J.M. Lamarre, R. Peyturaux, M.A. Pomeratz, J.L. Puget, G. Serra, C. Maurel, R. Pfeiffer, and J.C. Renault 1989, *Astron.Astrophys.*, 223, 107.
2) L. Piccirillo, in preparation.
3) E. Bussoletti, L. Colangeli, A. Borghesi, and V. Orofino 1987, *Astron.Astrophys. Suppl. Ser.*, 70, 257.
4) J. Dorschner, C. Friedemann, J. Gürtler, and Th. Henning 1988, in *Experiments on Cosmic Dust Analogues*, E. Bussoletti et al. eds. (Kluwer Academic Publishers, 1988), p. 209.
5) P. Andreani, G. Dall'Oglio, L. Martinis, L. Piccirillo, L. Pizzo, L. Rossi, and C. Venturino 1991a, *Astrophys.J.*, 375, 148.
6) P. Cox and P.G. Mezger 1989, *Astron.Astrophys.Rev.*, 1, 49.
7) F.-X. Désert, F. Boulanger, and J.L. Puget 1990, *Astron.Astrophys.*, 237, 215.
8) C. Koike, H. Hasegawa, and T. Hattori 1982, *Astrophys. Space Sci.*, 88, 89.
9) T. Tanabé, Y. Nakada, F. Kamijo, and A. Sakata 1983, *Publ. Astron. Soc. Jpn.*, 35, 397.
10) J.S. Mathis, P.G. Mezger, and N. Panagia 1983, *Astron.Astrophys.*, 128, 212.
11) D. Bollea, and A. Cavaliere 1976, *Astron.Astrophys.*, 49, 313.
12) T.M. Dame, H. Ungerechts, R.S. Cohen, E.J. De Geus, I.A. Grenier, J. May, D.C. Murphy, L.-Å. Nyman, and P. Thaddeus 1987, *Astrophys.J.*, 322, 706.
13) F.-X. Désert, F. Bazell, and F. Boulanger 1988, *Astrophys.J.*, 334, 815.
14) P. Meinhold and P. Lubin 1991, *Astrophys.J.*, 370, L11.

STAR FORMATION AND EARLY STELLAR EVOLUTION

Steven W. Stahler
Astronomy Department, U. of California, Berkeley, CA 94720
and NASA-Ames Research Center, Moffett Field, CA 94035

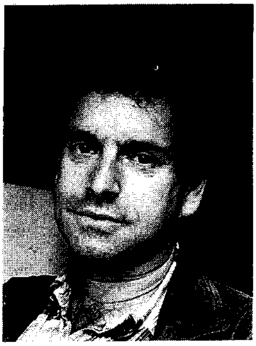

ABSTRACT

Stars form during the gravitational collapse of molecular cloud fragments known as dense cores. These cores grow slowly within a giant cloud complex, until they become gravitationally unstable. This "bottom-up" picture is very different from the traditional "top-down" scheme of heirarchical fragmentation first proposed by Hoyle. The structure and evolution of accreting protostars is well understood, but their predicted luminosities are higher than those of most deeply embedded stellar sources.

Protostars disperse their parent cores to become pre-main-sequence stars through the action of a powerful wind. Empirically, this wind is channeled into a bipolar nozzle configuration that gives rise to the optical jets and broad molecular outflows observed near young stars. Neither the cause of the wind nor the mechanism for nozzle formation is yet understood. Among optically revealed young stars, many have spectroscopic and photometric properties that indicate the continued presence of circumstellar disks, but a large fraction is curiously lacking these properties. Finally, the basic tenets of star formation theory could be tested in the near future, once observers obtain bolometric luminosity functions for populous clusters of embedded objects.

1. INTRODUCTION: THE PROBLEM OF STAR FORMATION

The basic question confronting a theoretical account of star formation can be readily framed. How is it that the vast, ragged structures known as giant molecular clouds, each measuring some 10^{20} cm in total extent, can produce the tiny, compact spheres we call stars, of typical size 10^{11} cm? The mean number density in a giant molecular cloud is 10^3 cm^{-3}, some 20 orders of magnitude less than the density of a solar-type star. Clouds are so different from stars that the path leading from one to the other must be long and complex. Nevertheless, star formation theory attempts to trace the main connecting thread, by isolating those few processes of paramount importance.

It is easy to see that the self-gravity of the cold ($T \approx 10\ K$) and massive ($M \sim 10^5\ M_\odot$) clouds must play a leading role. It is then also natural to suppose that some form of fragmentation, possibly in successive stages, might be the key to reducing clouds to stellar dimensions. Such a view was articulated 40 years ago by Hoyle[1)], in a paper which effectively guided thinking in the field for over two decades. Hoyle's scheme, which came to be known as *heirarchical fragmentation*, was an attempt to see how stellar masses might emerge naturally from the collapse of a diffuse parent body. The logic of Hoyle's argument is worth reviewing, despite the fact that, in his day, molecular clouds themselves had not yet been discovered through millimeter observations.

Hoyle reasoned essentially as follows. No cloud can undergo a sustained collapse unless it somehow radiates away most of the kinetic energy developed during the process. Otherwise, the cloud would "bounce," *i.e.*, its kinetic energy would be converted back into gravitational potential energy, and it would re-expand to its original size. Consider now a cloud so massive that its self-gravity greatly overwhelms its internal support from thermal pressure. During collapse, typical fluid elements will attain speeds that are highly supersonic. Even if the cloud were to remain perfectly isothermal, so that each element radiated away all of the work done by internal pressure, the total energy loss would still be much smaller than the increase in bulk kinetic energy.

There exists, however, another efficient means of energy loss, as Hoyle was quick to point out. Colliding supersonic streams will shock, and thereby attain temperatures that lead to copious radiation. In such a violent collapse, the cloud can be expected to break apart into smaller subunits before its average density has increased greatly. In some of these fragments, the thermal pressure gradient may actually exceed self-gravity; these bodies expand until hydrostatic equilibrium is reached. In other pieces, gravity might still dominate; these quickly break apart as before. It remains, therefore, to consider those fragments with only a slight excess of gravity over the pressure gradient.

In such marginally unstable bodies, Hoyle argued, the collapse must proceed subsonically, *i.e.*, without the generation of shocks. As the cloud fragment undergoes slow contraction, the gravitational force gradually overwhelms pressure, provided any internal energy increase is promptly lost through radiation. Hoyle showed that an initially spherical cloud of uniform density can contract by about a factor of 10 in volume before the increase in its kinetic energy exceeds radiative losses. At this point, he reasoned, the cloud fragments again. Some of the resultant pieces will again be marginally unstable to collapse, so that the cycle of condensation and breakup can continue through a number of generations. As the cloud density at every step steadily rises, the time between successive fragmentations drops.

The process ends with the production of a fragment so dense that it cannot radiate away sufficient energy during its brief contraction time scale. Such a piece achieves hydrostatic equilibrium as a star. In later versions of the model, the endpoint was identified as the time when the fragment becomes optically thick to its own cooling radiation[2)].

The idea of heirarchical fragmentation was appealing for its simplicity and internal consistency, but two subsequent developments, one theoretical and the other observational, served to undermine it. Hoyle was correct that only clouds with a slight predominance of gravity over pressure are viable candidates for star formation, but he was wrong about their mode of collapse. As the cloud begins its subsonic contraction, it has time to establish a centrally peaked pressure and density distribution, just as it would in true hydrostatic balance. Now the contraction time scale is shorter in the denser, inner region than farther out. Hence, the initial density gradient steepens with time. Eventually, the central region goes into true free-fall collapse, while the outside remains relatively static[3)]. During this *inside-out collapse*, the boundary of the falling material is a rarefaction wave that moves outward at the local isothermal sound speed[4)]. Three-dimensional numerical simulations[5)] indicate that this mode of collapse is actually stable against fragmentation, presumably because incipient perturbations are torn apart once they enter the region of collapse.

The observational development was the discovery, within giant molecular clouds, of the localized sites of low-mass star formation. Stars of approximately solar mass or less are believed to form within cloud condensations known as *dense cores*[6)]. These cores have typical diameters of 10^{17} cm, number densities of 10^5 cm^{-3}, and are frequently observed to contain young stars, *i.e.*, unresolved infrared sources of luminosity[7)]. To date, the cores have failed to show any convincing evidence for collapse motion. Indeed, with their internal temperatures of about 20 K, cores both with and without stars appear to be in hydrostatic balance.

It is natural, then, to suppose, that dense cores form stars through the process of inside-out collapse. The failure to observe free-fall motion reflects the small amount of interior gas that actually attains high speeds. If this view, now widely accepted, is indeed correct, then the heirarchical fragmentation picture fails, since no subsonic contraction is occurring at densities in excess of those observed in star-forming cores.

The fact that there exist dense cores *without* stars, and that these, too, are apparently in hydrostatic balance, suggests that Hoyle's "top-down" scenario for star formation be replaced by a "bottom-up" one. Dense cores begin as unobservably small "seeds," embedded within the background gas of a giant molecular cloud. These seeds grow by slowly drawing in, through their gravity, ambient matter. It is currently believed that this accumulation process is mediated through a magnetic field that threads the core and its environs. The dominant, neutral component of the gas can slip past the field and be pulled in by the core's gravitational field, while the ions gyrate about the field lines, retarding the neutrals through collisions[8),9)]. At any time during its growth, the dense core will appear to be in hydrostatic balance, as the observations indicate.[1]

Why do the cores ultimately go into collapse? It has long been known, through analytical studies, that hydrostatic, isothermal objects embedded in a uniform background

---

[1] The magnetic field also enters into the hydrostatic balance, but the associated force is of the same magnitude as both gravity and the thermal pressure gradient[9)].

pressure have a maximum stable mass[10),11)]. Numerical work has established a similar upper bound for magnetically supported configurations[12)]. The limit exists because heavier bodies need greater central pressures for hydrostatic support. Isothermal clouds, therefore, require higher densities, which eventually create a gravitational force near the center that cannot be resisted. Thus, dense cores are predicted to begin collapsing, from the inside out, once their central density exceeds the volume average by about a factor of 10.

2. PROTOSTARS

The primitive star, or *protostar*, that forms at the center of a collapsing dense core builds up its mass from the cloud material raining down upon it. As Hoyle surmised, this highly supersonic material must release its kinetic energy through a radiative shock in order for the collapse to continue. Early on, the cloud envelope can fall directly onto the stellar surface, which is bounded by a strong accretion shock front (*see Fig. 1*).

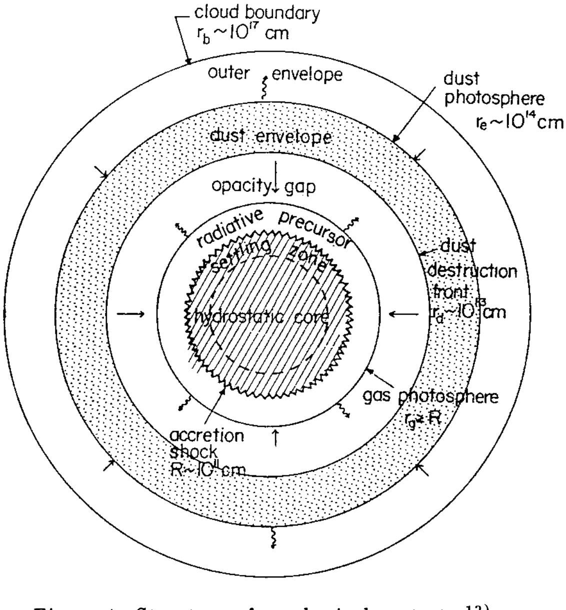

Figure 1. Structure of a spherical protostar[13)].

The protostar's luminosity is mostly from accretion, and is equal to

$$L_{acc} = \frac{G\dot{M}M}{R} , \tag{1}$$

for a star of mass M and radius R. Here, $\dot{M}$ is the accretion rate, *i.e.*, the mass per unit time falling from the overlying envelope. In a parent cloud with isothermal sound speed a_T, this rate can be found from the approximate equality

$$\dot{M} \approx a_T^3/G , \tag{2}$$

which holds with a numerical coefficient of order unity[4]. For a realistic cloud temperature range of 10 to 30 K, equation (2) predicts accretion rates between 2×10^{-6} and $1 \times 10^{-5}\, M_\odot$ yr^{-1}.

The radiation produced at the shock front still needs to make its way out of the cloud envelope. A photon produced near the stellar surface must traverse a large column density of gas and dust, which could, in principle, trap the radiant energy. In practice, however, the major source of opacity is the interstellar dust. The dust grains can only absorb a small fraction of the accretion luminosity before they sublimate. This sublimation occurs in a relatively thin layer at the *dust destruction front* in Figure 1. Inside the front is an optically-thin *opacity gap*, in which the incoming matter is entirely in the gaseous phase.

Once photons from the star reach the dust destruction front, they are quickly absorbed in the surrounding dusty envelope. The total luminosity crossing any sphere in this region remains constant, but the color temperature of the radiation field steadily falls as the photons are absorbed and reradiated many times. Finally, at the radius marked *dust photosphere* in Figure 1, the opacity is so low that the radiation can fly unimpeded through the rest of the dense core. By this point, the color temperature has fallen to several hundred degrees, corresponding to wavelengths in the mid-infrared regime.

The fact that protostars are infrared objects is, of course, troublesome from an observational perspective. In particular, their broadband spectra are influenced as much by the composition and spatial distribution of the grains in their cloud envelopes as by the nature of the underlying sources of radiation. Nevertheless, Adams, Lada and Shu[14] have proposed an empirical evolutionary sequence of infrared sources, using ı from both groundbased instruments and IRAS. In their scheme, objects which exhibit, longer wavelengths, the greatest departure from a blackbody spectrum are deemed to be protostars. Such "Class I" sources are relatively common. They constitute, for example, about 10 percent of all objects in the Taurus-Auriga molecular cloud complex[15),16], and about 30 percent in the ρ Ophiuchus region[17]. Unfortunately, the fraction of protostars in a forming cluster is expected, from general theoretical considerations, to be much lower[18]. In addition, the observed bolometric luminosities of typical Class I sources are frequently below that predicted by equation (1)[15].

To appreciate the latter point, we must establish the protostar's radius as a function of its mass. This mass-radius relation was a focus of controversy throughout the 1970's, as various researchers attempted to follow numerically the collapse process[3),19]. The controversy was finally resolved through careful treatment of the energy losses at the accretion shock[13),20]. It was found, for example, that the radius of a $1\, M_\odot$ protostar is about $5\, R_\odot$, far lower than had been predicted earlier from more qualitative arguments[21]. Thus, equation (1) can be rewritten

$$L_{acc} = 62\, L_\odot \left(\frac{\dot{M}}{10^{-5} M_\odot\, \mathrm{yr}^{-1}}\right) \left(\frac{M}{1\, M_\odot}\right) \left(\frac{R}{5\, R_\odot}\right)^{-1} \tag{3}$$

Although the mean protostar mass is expected to be less than $1\, M_\odot$, the average radius is also smaller than $5\, R_\odot$, and the luminosity strongly peaks at a value between 10 and $50\, L_\odot$[18]. Empirically, Class I sources are sometimes found with luminosities this high, but many are considerably dimmer[17]. Thus, the identification of such sources with protostars cannot be considered secure.

3. PRE-MAIN-SEQUENCE STARS

Young stars which are no longer surrounded by infalling cloud envelopes, but have not yet started burning central hydrogen, are said to be in the *pre-main-sequence* phase. Because they are optically visible, these objects are much easier to identify than the infrared protostars. Pre-main-sequence stars of roughly $2\,M_\odot$ or less are known as T Tauri stars[22)], while those of higher mass are called Herbig Ae/Be stars[23)]. The T Tauri class is more populous, and so its properties have been more firmly established [24)]. It is the infrared excess exhibited by many of these stars, for example, that is most often cited as evidence for circumstellar disks[25)].

A central issue in star formation theory is the nature of the transition between the protostar and pre-main-sequence phases. How does accretion end, and what disperses the remnants of the parent dense core? Complete answers to these questions are not yet available, but important observational clues exist. The most deeply embedded young stars are frequently seen to be driving *molecular outflows.* These are broad regions of cloud gas observed to be moving away in a bipolar fashion from the central stars, with typical speeds of 5 km s^{-1}. Several hundred outflows have now been detected, and their characteristics are well documented[26)].

It is generally accepted that molecular outflows are responsible for clearing away the remnant clouds, but the mechanics of the dispersal process has not been elucidated. Nor has the relationship between the outflows and another bipolar phenomenon associated with young stars, the *Herbig-Haro jets* [27)]. These are sinuous strands of hot ($T \sim 10^4$ K) gas, moving at high speed ($v \sim 300$ km s^{-1}) from the driving stars. The jets are intrinsically faint, and easily obscured by intervening cloud matter. Not surprisingly, few of them have been seen together with well defined molecular outflows, although there are some noteworthy exceptions[28)]. Nevertheless, there is growing evidence that every outflow represents turbulent cloud material that has been entrained by a central jet[29)]. The jet itself consists of a stellar wind which has somehow been constrained into a bipolar nozzle configuration.

Once the jet and outflow clear away the rest of the dense core, the exposed pre-main-sequence star gradually shrinks under the influence of its own gravity. During this phase of *quasi-static contraction*, the star's central temperature climbs until hydrogen ignites in the central region. In the case of T Tauri stars, the stellar interior contracts *homologously*, in a manner similar to what Hoyle envisioned for marginally unstable clouds. These low-mass objects are fully convective as a result of surface cooling, which draws out more heat than can be transported by radiation alone[30)]. The Herbig Ae/Be stars, on the other hand, have lower interior opacities, and are stable against convection. Most of these stars begin contracting *nonhomologously*, *i.e.*, their outer layers actually expand while their deeper interior shrinks[31)].

Since pre-main-sequence stars are optically visible, their evolution can be followed in a conventional H-R diagram. The evolutionary tracks of stars ranging in mass from 0.6 to $6\,M_\odot$ are shown in Figure 2. The dotted curve is the *birthline*, *i.e.*, the locus of stars immediately following the termination of protostellar accretion[33),34)]. The modest radii of accreting protostars imply that the set of pre-main-sequence tracks is severely truncated compared to older calculations that ignored the protostar phase[35)]. Most tracks depart smoothly from the birthline, but stars from about 2 to 4 $M_\odot$ first jump upward in luminosity, as a consequence of their nonhomologous contraction[31)].

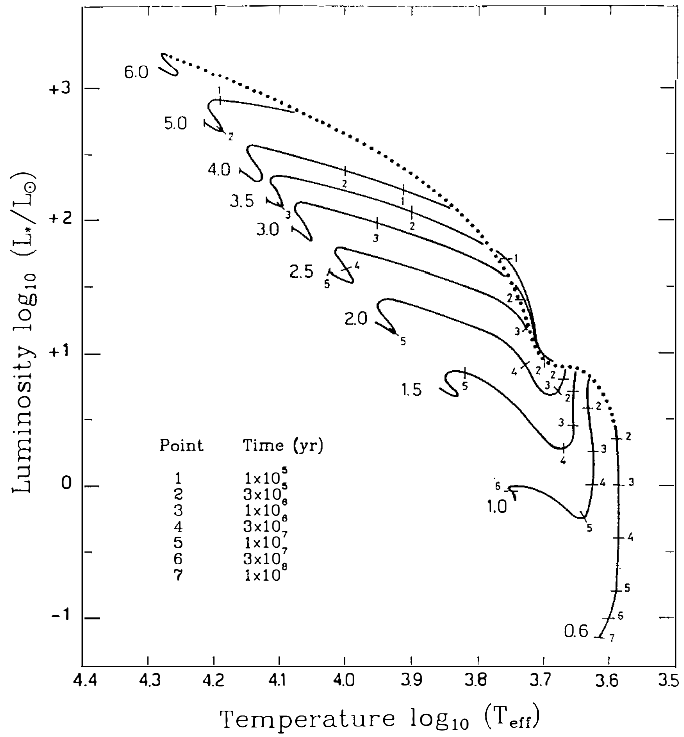

Figure 2. Theoretical pre-main-sequence evolutionary tracks (solid curves) and birthline (dotted curve) in the H-R diagram[32]. Each track is labeled by the stellar mass in solar units.

The theory outlined here makes definite predictions concerning the distribution of pre-main-sequence stars in the H-R diagram. No star in this class should be situated above the birthline, while the youngest stars should be located close to the line, but below it. Finally, the theory predicts a rather modest upper mass limit, about 8 $M_\odot$, to the pre-main-sequence phase. Stars which continue to add mass above this limit are burning hydrogen, and should appear on the ZAMS once they are optically revealed. In Figure 2, the limit corresponds to the intersection of the birthline and the main sequence.

Figure 3 shows that the observed stars appear to lie in the proper region of the H-R diagram. In addition, those young stars with mass more than about 8 $M_\odot$ do appear to be on the ZAMS, but the available sample is small[36]. Levreault[37] has studied about a dozen stars which are optically visible pre-main-sequence objects, but are still associated with molecular outflows, and therefore presumed to be especially young. It is gratifying that this sample indeed lies close to the theoretical birthline [34].

Many T Tauri stars exhibit a constellation of photometric and spectroscopic properties that set them apart from more mature objects of similar mass. These "classical" properties include the previously mentioned infrared excess, as well as an ultraviolet excess, and emission

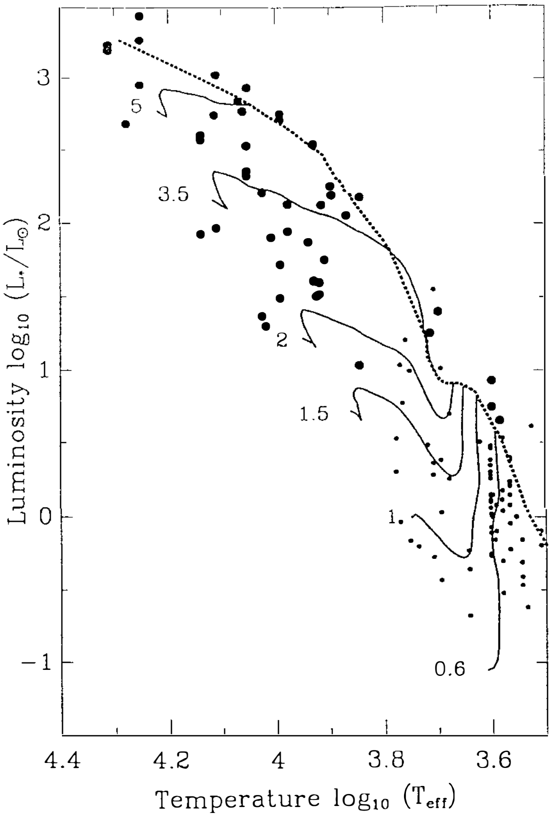

Figure 3. Observed pre-main-sequence stars in the H-R diagram[32].

lines whose profiles are indicative of strong winds. However, a large fraction of the T Tauri class, perhaps half of the total, does *not* have these properties[38]. These "naked" stars appear throughout the allowed region in the H-R diagram, including near the birthline[24,39]. Now many researchers have sought to explain the classical properties by the presence of circumstellar disks[40]. Furthermore, the theory of disk formation makes it clear that disks are a natural outcome of the collapse of *rotating* dense cores[41]. Thus, it appears that the naked T Tauri disks must have drained onto their central stars, or perhaps have been dispersed by these stars, early on. Given the inadequacy of our present knowledge of disk evolution, both alternatives remain viable.

4. CONCLUSION

It should be clear from this brief overview that significant gaps remain in our understanding of young stars. Nevertheless, a consensus has emerged over the past decade that the main outline of a more complete account of star formation is now secure. In some areas, such as the phenomenology of T Tauri stars, our knowledge is highly detailed. In others, such as the origin of protostellar winds, basic theoretical issues are still being debated. It is unlikely, however, that future observations, such as the first confirmed detection of protostellar collapse, will force a major alteration of the basic scheme.

The situation is entirely different regarding the formation of stellar *groups*. Most mature stars are in binary pairs[42)], and the current high rate of discovery of pre-main-sequence pairs makes it clear that binarity is common up to the birthline[43)]. Are such pairs born from the same dense core, or were they once more distant companions? Over larger scales, stars tend to form in clusters, usually gravitationally unbound. The existence of clusters *per se* is no mystery, given the large masses and sizes of giant molecular clouds, but what causes a giant cloud to begin producing stars? Finally, the distribution of stellar masses within such groups (the "Initial Mass Function") is heavily weighted toward low-mass stars. What is this important fact telling us about star formation?

The most basic properties of extremely young, embedded clusters are just now being learned. A key technological breakthrough has been the advent of the CCD infrared array camera[44)]. Researchers can, in a relatively brief time, construct high-resolution maps of extended, visibly obscured regions of star formation[45)]. Once array detectors are available at the mid- and far-infrared wavelengths where many young stars peak in intensity, astronomers will have at their disposal the basic tool for understanding stellar clusters - their bolometric *luminosity functions.*

Naturally, a complete theory of luminosity functions is not available, but important steps are being taken toward providing observers with a conceptual framework for the interpretation of their results. Only recently has it been emphasized that the luminosity functions of very young clusters should be qualitatively different from those of older systems[46),47)]. Fletcher and Stahler[18)] have calculated the evolution of the luminosity function by utilizing a simple stochastic model of cluster formation. Here, protostars have a certain probability per unit time of dispersing their cloud envelopes to become visible pre-main-sequence stars. This probability is determined by assuming that the cluster's mass distribution approaches a pre-assigned Initial Mass Function after long times. Once the data is available, it will be interesting to compare the actual luminosity functions of populous clusters with the predictions of this model.

Throughout this project, the author was supported principally by NSF Grant AST-9296096. He received additional support from the Center for Star Formation Studies, a consortium of U. C. Berkeley, U. C. Santa Cruz, and NASA-Ames Research Center funded through a special NASA astrophysics theory grant.

REFERENCES

1. Hoyle, F. 1953, 118, 513
2. Lowe & Lynden-Bell 1976, MNRAS, 176, 367
3. Larson, R. B. 1969, MNRAS, 145, 271
4. Shu, F. H. 1977, ApJ, 214, 488
5. Boss, A. P. 1985, Icarus, 61, 3
6. Myers, P. C. & Benson, P. J. 1983, ApJ, 266, 309
7. Beichman, C. A., Myers, P. C., Emerson, J. P., Harris, S., Mathieu, R., Benson, P. J., & Jennings, R. E. 1986, ApJ, 307, 337
8. Mestel, L. & Spitzer, L. 1956, MNRAS, 116, 505

9. Scott, E. H. 1984, ApJ, 278, 396
10. Ebert, R. 1955, Z.f.Ap, 37, 299
11. Bonnor, W. B. 1956, MNRAS, 116, 351
12. Mouschovias, T. Ch. & Spitzer, L. 1976, ApJ, 210, 326
13. Stahler, S. W., Shu, F. H., & Taam, R. E. 1980, ApJ, 241, 637
14. Adams, F. C., Lada, C. J., & Shu, F. H. 1987, ApJ, 312, 788
15. Kenyon, S. J., Hartmann, L. W., Strom, K. M., & Strom, S. E. 1990, AJ, 99, 869
16. Beichman, C. A., Boulanger, F., & Moshir, M. 1992, ApJ, 386, 248
17. Wilking, B. A., Lada, C. J., & Young, E. T. 1989. ApJ, 340, 823
18. Fletcher, A. B. & Stahler, S. W. 1993, ApJ, in press
19. Westbrook C. K. & Tarter C. B. 1975, ApJ, 200, 48
20. Winkler, K.-H. & Newman, M. J. 1980, ApJ, 236, 201
21. Hayashi, C. 1966, ARAA, 4, 171
22. Joy, A. H. 1945, ApJ, 102, 168
23. Herbig, G. H. 1960, ApJS, 4, 337
24. Stahler, S. W. & Walter, F. M. 1993, in Protostars and Planets III, ed. E. H. Levy, J. Lunine, & M S. Matthews (Tucson: U. of Arizona), in press
25. Adams, F. C. & Shu, F. H. 1986, ApJ, 308, 836
26. Fukui, Y., Iwata, T., Mizuno, A., Bally, J., & Lane, A. P. 1992, in Protostars and Planets III, ed. E. H. Levy, J. Lunine, & M. S. Matthews (Tucson: U. of Arizona Press), in press
27. Reipurth, B. 1991, in Physics of Star Formation and Early Stellar Evolution, ed. C. J. Lada & N. Kylafis (Dordrecht: Kluwer Academic), p. 497
28. Chernin, L. M. & Masson, C. R. 1991, ApJ, 382, L93
29. Stahler, S. W. 1993, in Astrophysical Jets, ed. M. Livio, C. O'Dea, & D. Burgarella (Cambridge: Cambridge U. Press), in press
30. Hayashi, C. 1961, PASJ, 13, 450
31. Stahler, S. W. 1989, ApJ, 347, 950
32. Palla, F. & Stahler, S. W. 1993, ApJ, in press
33. Stahler, S. W. 1983, ApJ, 274, 822
34. Palla, F. & Stahler, S. W. 1990, ApJ, 360, L47
35. Ezer, D. & Cameron, A. G. W. 1967, Can.J.Phys, 45, 3429
36. Thé, P. S., de Winter, D., Feinstein, A., & Westerlund, B. E. 1990, A&AS, 82, 319
37. Levreault, R. M. 1988, ApJS, 67, 283
38. Walter, F. M. 1987, PASP, 99, 31
39. Stahler, S. W. 1988, ApJ, 332, 804
40. Bertout, C., Basri, G. & Bouvier, J. 1988, ApJ, 330, 350
41. Cassen, P. & Moosman, A. 1981, Icarus, 48, 353
42. Abt, H. A. 1983, ARAA, 21, 343
43. Simon, M., Ghez, A. M., & Leinert, Ch. 1993, ApJ, 408, L33
44. Gatley, I., Depoy, D. L., & Fowler, A. M. 1988, Science, 242, 1264
45. Barsony, M., Schombert, J. M., & Kis-Halas, K. 1991, ApJ, 379, 221
46. Lada, C. J. 1991, in Physics of Star Formation and Early Stellar Evolution, ed. C. J. Lada & N. Kylafis (Dordrecht: Kluwer Academic), p. 329
47. Zinnecker, H., McCaughrean, M. J., & Wilking, B. A. 1993, in Protostars and Planets III, ed. E. H. Levy, J. Lunine, & M S. Matthews (Tucson: U. of Arizona), in press

INFRARED LUMINOSITY FUNCTIONS OF VERY YOUNG CLUSTERS

Charles J. Lada
Smithsonian Astrophysical Observatory
60 Garden Street, Cambridge, MA 02138 USA

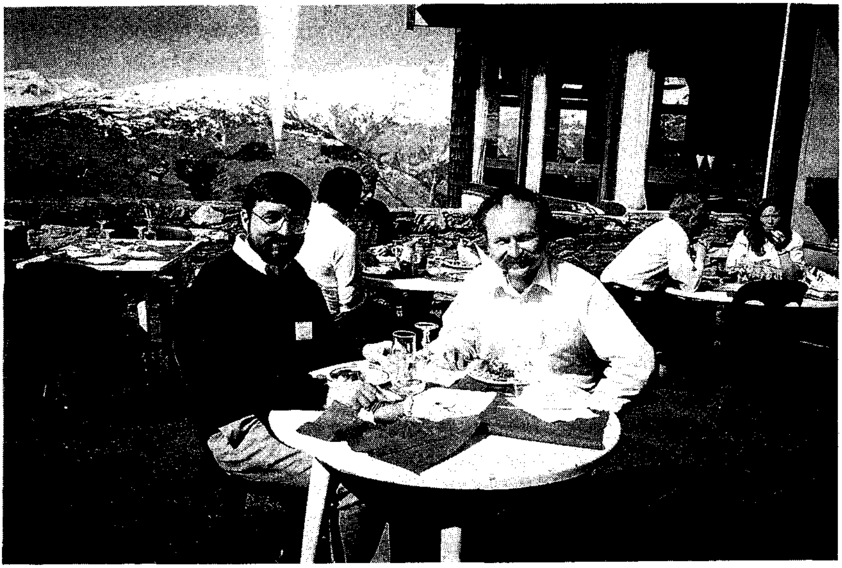

ABSTRACT

Young star clusters are important laboratories for studies of star formation and early stellar evolution. In particular, with sizes between 0.5-3 parsecs, rich young clusters, especially those embedded or partially embedded in molecular clouds, provide the smallest spatial scales for which a significant determination of the Initial Mass Function (IMF) can be made. Consequently, observations of such clusters enable tests of the universality of the IMF in both space and time. Infrared imaging observations have now been obtained for a small but growing number of young clusters in nearby molecular clouds. Infrared luminosity functions have been constructed for many of these clusters. In this contribution observations of two rich and relatively nearby clusters (IC 348 and NGC 2264) are discussed and compared. The infrared luminosity functions of these clusters are found to be surprisingly similar in shape. Moreover, their slopes are much steeper than that expected for a population of ZAMS stars whose distribution of masses is given by the field star IMF. However, with approximate adjustments for the effects of pre-main sequence evolution, the slopes of the luminosity functions of these clusters are found to be consistent with that expected if the underlying distribution of stellar masses in the clusters is identical to that of the IMF of present day field stars. In addition, in both cases the luminosity functions are found to flatten and turn over at K band magnitudes corresponding to masses (0.5–0.75 $M_{\odot}$) which are considerably above the hydrogen burning limit but roughly consistent with the peak in the present day field star IMF. To date, observations of these and other young embedded clusters have not yet provided any compelling evidence to refute the notion of a universal IMF.

1. INTRODUCTION

A fundamental consequence of the theory of stellar evolution is that the life history of a star is almost entirely pre-determined by its initial mass. Consequently, to understand star formation and the consequent luminosity evolution of the galaxy requires a detailed knowledge of both the initial distribution of stellar masses at birth and how this quantity varies through space and time within the galaxy. Unfortunately, stellar evolution theory is not able to predict the Initial Mass Function (IMF) of stars. This quantity must be derived from observations. However, to do so is not straightforward because stellar mass is not itself an observable quantity. Stellar radiant flux or luminosity is the most readily observed property of a star. According to stellar evolution theory there is a unique mass-luminosity relation for main sequence stars and in a classic paper nearly 40 years ago Salpeter (1955) used this fact and knowledge of post-main sequence stellar evolution to determine the IMF for present day field stars in the solar neighborhood. He found that the IMF was well represented by a simple power-law: $\xi(log m_*) \sim m_*^{-1.35}$ for stars with masses in the range between 1-10 $M_\odot$. The derived sign and slope of the Salpeter IMF indicates that most stars which form in the galaxy are of low mass and moreover that most of the stellar mass in our galaxy is contained in such stars. Subsequent studies, particularly by Scalo (1978, 1986) extended knowledge of the field star IMF to sub-solar masses and found that the IMF has a peak at about 0.3 $M_\odot$ and therefore turns over and departs from the Salpeter power-law well above the hydrogen burning limit.

The field star IMF, by itself, however may not necessarily provide a strong constraint for star formation theory. This is because the field star IMF is a globally averaged IMF, averaged over both the lifetime of the galaxy and a over a specific volume of space (i.e, the solar neighborhood). Although it is often assumed that the IMF is universal in both time and space, this has never been demonstrated in a completely satisfactory way. However, in order to develop comprehensive theories for star formation and galactic evolution it is crucial to know whether the detailed form of the IMF is universal. Are there spatial and/or temporal variations in the initial conditions and other important astrophysical parameters that can alter the process of star formation and the form of the IMF? Or is star formation such a robust process that the outcome is always an IMF of the same form?

In principle, observation of large enough groups of young or newly forming stars in different parts of the galaxy should be able to provide fundamental constraints on these questions. The smallest spatial size scale over which a meaningful determination of a luminosity function can be made is that characteristic of an open cluster. Clusters are important laboratories for studying the initial luminosity function because they consist of statistically significant groups of stars who share the common heritage of forming from the same parental cloud at the same epoch in time. Young embedded clusters are particularly useful since they are not old enough to have lost significant numbers of members due to stellar evolution or dynamical effects such as evaporation or violent relaxation (e.g., Lada Margulis and Dearborn 1984, Lada and Lada 1991). However, only in the last few years have advances in infrared detectors enabled the direct observation of such embedded and often obscured clusters. In particular, the development of large format infrared array cameras has made it possible to image in reasonable amounts of telescope time the relatively large regions of sky which contain entire clusters and embedded stellar populations (e.g., E. Lada *et al.* 1991, C. Lada *et al.* 1991, Gatley *et al.* 1991, Barsony, Shombert and Kis Halas 1991; Greene and Young 1992, Eiroa and Casali 1992, Carpenter *et al.* 1993). In this contribution I will discuss recent observations of two young clusters, NGC 2264 and IC 348, made with infrared array imaging cameras and the constaints such observations place on the question of the universality of the IMF.

2. INFRARED IMAGING OF NGC 2264 AND IC 348

NGC 2264 is a rich and relatively large ($\sim$ 6 parsecs in extent) young cluster located at a distance of about 800 parsecs from the sun. This cluster has been extensively studied at optical, infrared and millimeter wavelengths (e.g., Herbig 1954a, Walker 1956, Warner, Strom and Strom 1977, Blitz 1979, Adams, Strom and Strom 1983, Margulis, Lada and Young 1989, Margulis, Lada and Snell 1988). It has an age of roughly 5 x 10^6 years and is partially embedded in but largely foreground to a massive molecular cloud. We (Lada, Young and Greene 1993) recently completed an extensive near infrared imaging survey of this cluster with a 128 x 128 HgCdTe NICMOS array camera attached to the 1.55 meter reflector of the University of Arizona Observatories located on Mt. Bigelow near Tucson, Arizona. Images were obtained in three standard infrared colors: J (1.25 μm), H (1.65 μm) and K (2.2 μm). The present discussion will deal primarily with the K-band observations which are less sensitive to the effects of extinction than the two shorter wavelength bands. However, it should be noted that analysis of the J and H band data produces the same overall results. The K band survey consisted of 450 individual frames and covered an area of roughly 540 square arc minutes in size. From analysis of these images we were able to extract 1656 sources in the K band. Additional observations of the cluster and a large control field situated well off the cluster and its associated molecular cloud were obtained with the SQIID infrared array camera of NOAO attached to the 1.2 meter telescope on Kitt Peak. SQIID consists of 4 256 x 256 PtSi detector arrays mounted to permit simultaneous observations at four infrared bands: J, H, K and L. The control field covered an area roughly 225 square arc minutes in size or roughly half the area of the K band survey of NGC 2264. After accounting for the difference in surveyed areas, the control field was found to contain only 230 fewer K band sources above the completeness limit than the cluster field. The surface density of sources in the cluster is about 25% higher than that of the control field indicating that field star contamination is relatively severe for NGC 2264.

IC 348 is a relatively rich and young cluster in the nearby Perseus molecular cloud complex. At a distance of 380 parsecs it is considerably closer than NGC 2264 and in a direction that is less likely to be contaminated by background and forground stars. With a diameter of roughly 1.5 parsecs it is also significantly more compact than NGC 2264. Its age is estimated to be 0.5-1.2 x 10^7 years (Strom, Strom and Carrasco 1974) and is therefore somewhat (perhaps a factor of 2) older than NGC 2264. Like NGC 2264, however, IC 348 is situated in front of a relatively massive dark cloud and at least some of its members appear partially embedded within the cloud (Herbig 1954b). We (Lada and

Lada 1993) have recently performed an extensive near-infrared imaging survey of this cluster using SQIID on the NOAO 1.2 meter telescope. We imaged an area roughly 385 square arc minutes in size centered on the cluster as well as a region roughly 365 square arc minutes in size located well off the cluster and its associated molecular cloud. We extracted 505 K band sources above the completeness limit in the on field and roughly 160 sources in the equal size off field region. Clearly the issue of field star contamination is much less of a concern for IC 348 than for NGC 2264.

3. INFRARED LUMINOSITY FUNCTIONS

Figure 1a shows the K-band luminosty function (KLF) constructed for those stars observed toward NGC 2264 as well as the luminosity function constructed for the stars in the control fields. The latter KLF has been scaled by a factor of 2.4 to account for the difference in the observed areas of the cluster and control fields. In addition, the KLF of the control field has been adjusted to account for extinction due to the molecular cloud behind the cluster. Millimeter-wave spectral line observations of CO and NH_3 (Blitz 1979, Crutcher, Hartkoph and Giguere 1978, Margulis and Lada 1986; Krugel *et al.* 1987) show that the cluster lies projected onto a massive, dense molecular cloud core. The molecular gas is clumpy and we estimate the visual extinction to vary between roughly 2-15 magnitudes through this region. The effect of extinction is to decrease the number of ***background*** field stars that would otherwise be observed toward the cluster. To account for this effect quantitatively, we shifted the luminosity function of the control fields by 0.5 magnitudes to simulate a uniform extinction of 0.5 magnitudes at K (i.e., $A_v \approx 4.5$ magnitudes) caused by the background molecular cloud. With this correction for extinction there is an excess of 485 sources above the completeness limit (14.5 magnitudes) toward the cluster. Even with this adjustment, Figure 1a shows that for the faintest sources, the number of stars in the control fields is essentially the same as that observed toward the cluster. This indicates that at low luminosities the number of stars observed toward the cluster is consistent with that expected for line-of-sight field stars. This in turn suggests that the cluster luminosity function likely turns over at faint magnitudes. Figure 1b shows the KLF resulting from the subtraction of the luminosity functions of the cluster and extincted control fields for K magnitudes between 9 and 14. This should represent the luminosity function for the cluster members. The luminosity function is observed to rise until a K magnitude of roughly 12.5 after which it flattens out and turns over. A linear, least-squares fit to the data between 9 and 12.5 magnitudes gives a slope for the luminosity function of 0.32 ± 0.04 and is illustrated in the figure.

Figure 2a shows the KLFs constructed from our (Lada and Lada 1993) observations of the IC 348 cluster and its equal sized control field. The control field stars were each artifically extincted by 0.5 magnitudes at K to approximately account for the extinction due to the associated molecular cloud. The amount of extinction was estimated from comparison of the JHK color-color diagrams of the cluster and control fields. Given that most of the stars observed toward the cluster cannot be field stars, this estimate likely refers more to the average extinction toward the cluster members themselves rather than toward the background field stars and probably underestimates the extinction

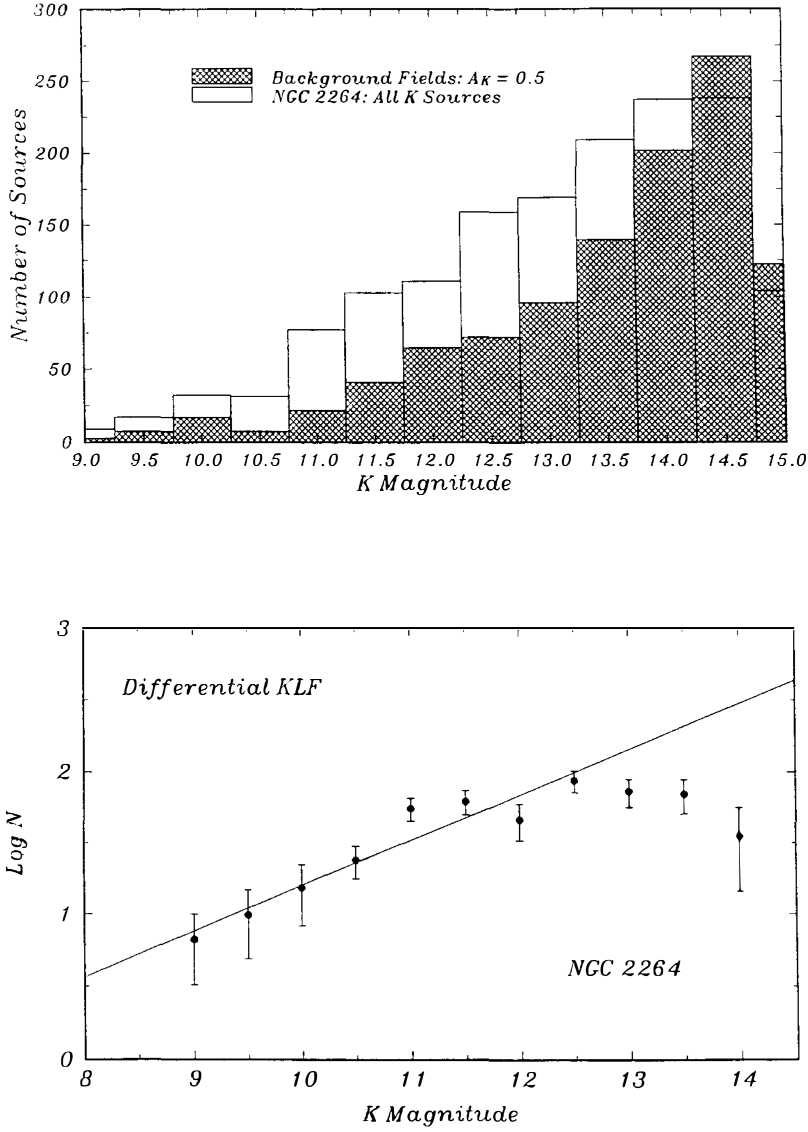

Figure 1. a)–Top: The K luminosity function of sources observed toward NGC 2264 along with the corresponding luminosity function for the eight control fields observed off the cluster. b)–Bottom: The difference between the cluster and control field luminosity functions. This should be representative of the luminosity function of the cluster.

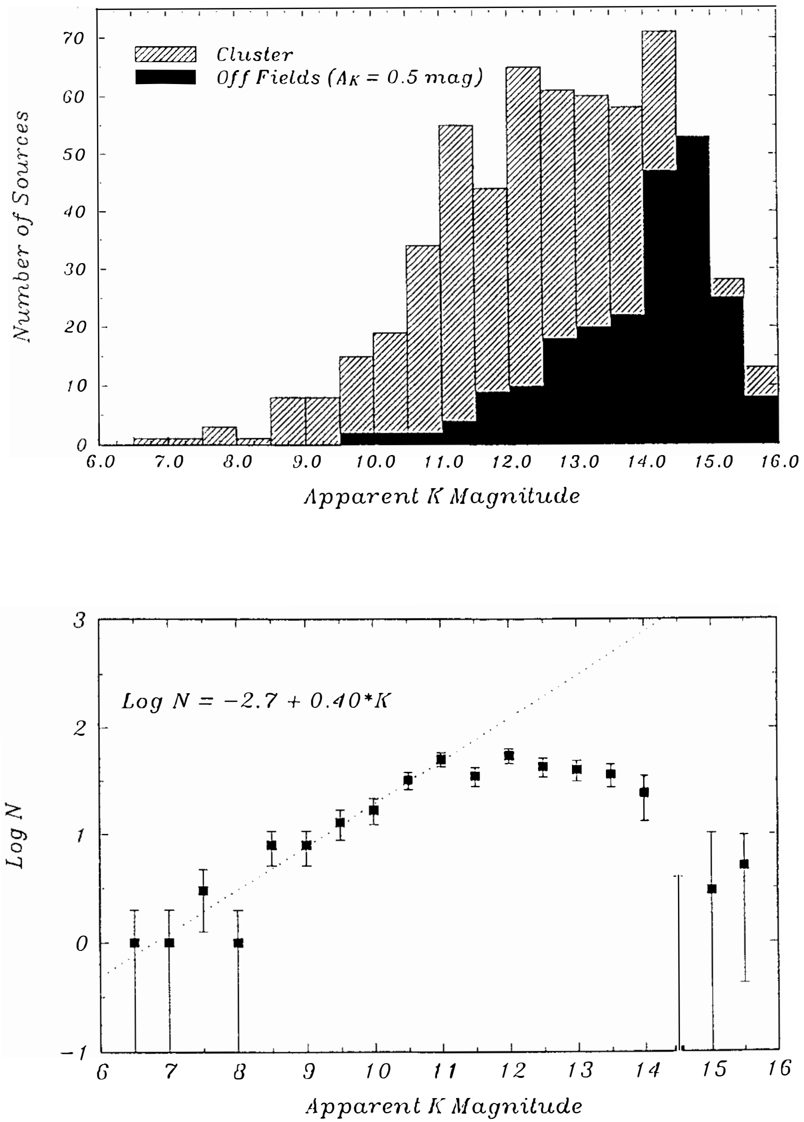

Figure 2. a)–Top: The K luminosity function of sources observed toward IC 348 along with the corresponding luminosity function for the control fields observed off the cluster b)–Bottom: The difference between the cluster and control field luminosity functions. This should be representative of the luminosity function of the cluster.

to the background stars. Even with this correction an excess of 369 K-band stars is found in the direction of the cluster and. except at the faintest magnitudes, field star contamination is minimal. As with NGC 2264, near the completeness limit (14.5 magnitudes) the number of stars observed toward the cluster is comparable to that expected from background/forground field star contamination. Figure 2b shows the KLF for the cluster resulting from the subtraction of the luminosity functions of the cluster and extincted control fields. The luminosity function rises until a K magnitude of about 11, then flattens and appears to turn over near the completeness limit. This behavior is evident even in the raw KLF (Figure 2a) uncorrected for field stars. A linear least-squares fit to the data between 6 and 11 magnitudes indicates that this KLF is well described by a single slope of 0.40$\pm$ 0.03 in this range.

4. DISCUSSION AND CONCLUSIONS

The KLFs of NGC 2264 and IC 348 share two important characteristics. First, both KLFs appear to be power-law in form for the brighest stars and second, their shape departs from a power-law form at large (faint) magnitudes, consistent with a flattening or turn over at the lowest stellar luminosities. Both these characteristics are also evident in the IMF for field stars (Scalo 1986). The slope of IC 348 (0.40) is just barely significantly steeper than that of NGC 2264 (0.32). However, as we show below, both slopes are considerably steeper than that expected for a young cluster of ZAMS stars whose underlying mass function is given by the field star IMF.

In principle, the luminosity function of a very young cluster is closely related to its initial mass function. For a stellar system for which the mass function and mass–luminosity relation are power law in form (i.e., $dN(log m_*) \propto m_*^{-\gamma} dlog m_*; L_K \propto m_*^{\beta}$), the slope of the K luminosity function can be shown to be:

$$\alpha = \frac{\gamma}{2.5\beta}$$

Here γ and β are the spectral indices of the stellar mass function and the K luminosity–stellar mass relation, respectively. For early-type (O-F) main sequence stars which are sufficiently hot that their infrared emission is in the Rayleigh-Jeans regime, one can show that the K luminosity–mass relation is approximately a power law with $\beta = 2.0$ and consequently $\alpha = \frac{\gamma}{5}$ (e.g., Lada 1991). For an underlying mass function similar to that derived for local field stars by Salpeter (1955), $\gamma = 1.35$. and $\alpha = 0.26$. This is appears to be significantly flatter than the slopes derived for NGC 2264 and IC 348.

This value is identical, however, to the slope of the K-band luminosity function derived from similar infrared observations obtained by Lada *et al.* (1991) for the luminous and rich cluster associated with M17. The agreement of the observed KLF for M17 and the predicted slope likely reflects the fact that the stellar population of M17 is dominated by massive OB stars. Not only are such stars likely to be on the main sequence in even the youngest clusters, but in addition, the IMF for massive stars is well represented by the Salpeter slope. On the other hand, both IC 348 and NGC 2264 consist mainly of later-type, low mass stars. Moreover, these clusters are young enough that most of their low mass stars (spectral types F and later) have not yet arrived on the main sequence. Predicting the form of the KLF for these clusters is a more challenging task since: 1)- it is well known that a single power-law shape is not consistent with the functional form of the field star IMF at all stellar masses and 2)- there is not a unique mass-luminosity relation for pre-main sequence stars as there is for main sequence stars.

The field IMF appears to flatten or even turn over at masses below about 0.3 $M_\odot$(e.g., Scalo 1978, 1986; Miller and Scalo 1979). For example, Scalo (1978) shows that if a log normal function is fit to the field star IMF, the slope of the IMF is variable and given by: $\gamma = 0.94 + 0.94\log(m_*)$. For a 1 $M_\odot$ star, which would be representative of the stellar populations in NGC 2264 and IC 348, we expect $\gamma = 0.94$. For a coeval cluster of stars one might guess that the mass-luminosity relation can be represented as a simple function of time, i.e., $\beta = \beta(t)$. However, to determine $\beta(t)$ either requires modelling of the luminosity evolution of a young cluster of pre-main-sequence stars (including the unknown effects of circumstellar disks and disk accretion) or observations of groups of such stars with known masses but of differing ages. Recently, Simon *et al.* (1992) have been able to calculate the M_K–mass relation for 10^6 year old PMS stars in Taurus using published pre-main sequence models. From their derived relation we find $\beta_{pms} \approx 1.0$. With this value of β, appropriate for one million year old low mass pre-main sequence stars, and $\gamma = 0.94$, we derive $\alpha = 0.38$. Within the uncertainties this is in good agreement with the observed KLFs for both IC 348 and NGC 2264 despite the fact that both clusters are considerably older than a million years. Recently, Zinnecker, McCaughrean and Wilking (1992) have modelled the luminosity evolution of a coeval cluster of diskless stars. Their models also predict slopes of the KLF that are steeper that those expected for ZAMS clusters. For a standard IMF, they predict that $\alpha = \alpha(t)$ as expected for a time varying mass luminosity relation and they also find that $\beta \approx 1.0$ for million year old stars. We have analyzed the results of their models and found in addition that α is not a single valued function of time. In fact the predicted slopes for KLFs of both 10^6 and 5 x 10^6 year old clusters are nearly identical. Apparently, the slopes of the KLFs of NGC 2264 and IC 348 are not different from those expected for young clusters whose underlying distribution of stellar masses is similar to the field star IMF.

The K luminosity functions of IC 348 and NGC 2264 also both appear to flatten and turn over at large magnitudes. For NGC 2264 the KLF departs from the power-law fit at a K magnitude of roughly 13.0 while for IC 348 the KLF begins to turn over at a magnitude of about 11.5. The distance moduli of the clusters differ by 1.6 magnitudes and thus the KLFs of both clusters appear to turn over at the same *intrinsic* brightness. This brightness corresponds to the luminosity of a main sequence star of early G spectral type (i.e., $M_* \approx 1$ $M_\odot$) as well as to the brightness of a 0.75 $M_\odot$ diskless pre–main sequence star of roughly the same age as the clusters (5 x 10^6 yrs.). This turnover appears to occur at a slightly higher mass than that (0.3 $M_\odot$) at which the local field star IMF is believed to peak (Scalo 1978). However, it does approximately correspond to a mass roughly consistent with that (0.6 $M_\odot$) at which the local field star IMF begins to flatten out. Consequently, it appears that both the overall slope of the observed luminosity functions at intermediate magnitudes and their apparent turnovers at relatively large magnitudes are consistent with the assumption that the underlying cluster mass function is well described by the IMF for local field stars.

Finally, we note that the nearly identical slopes (i.e., 0.37-0.38) derived for the luminosity functions of NGC 2071, NGC 2068, and NGC 2024, three rich embedded clusters in Orion, (E. Lada *et al.* 1991) further suggest that the mass functions of these clusters are also all consistent with the local field star IMF. Moreover, in another recent study, Carpenter *et al.* (1993) constructed differential H band lumninosity functions (HLFs) for 12 relatively distant clusters in the second and third quadrants of the galaxy and found the average of the HLF slopes for this sample to be 0.37 ± 0.12. A result which is again consistent with the idea of an underlying IMF similar to that of the field. Yet, the striking similarity of the slopes of the luminosity functions of so many young clusters is suprising and somewhat disconcerting. In particular, for young clusters of low mass stars the variation in β, the mass luminosity relation, is expected to be much larger than the variation actually observed in α, the slope of the KLF. Moreover, unlike model clusters, the observed clusters are not coeval on time scales comparable to their ages and they contain many stars with infrared excess emission. In this case a single mass-luminosity relation may not be appropriate for all members of a cluster. Evidently, any differences in either the ages of these various clusters, or in the natures of infrared stars within them are not manifest in the slopes of their infrared luminosity functions. Nonetheless, despite these problems, the observations are still consistent with the notion that all these clusters are characterized by the same underlying mass function. Within the framework of present understanding, there is therefore as yet no compelling evidence from infrared observations of young clusters to suggest that the IMF varies significantly through either time or space within the galaxy.

ACKNOWLEDGEMENTS

The work reported here has been partially supported by NSF Grant AST 8815753 awarded to the University of Arizona.

References

Adams, M. T., Strom K. M. and Strom S. E. 1983 *Astrophys. J. Suppl. Ser.*, **53**, 893.

Barsony, M., Shombert, J. M. and Kis Halas, K. 1991 *Astrophys. J.*, **379**, 221.

Blitz L. 1979 PhD Dissertation, Columbia University.

Carpenter, J., Snell, R. L., Schloerb, P. F. and Skrutskie, M. F. 1993 *Astrophys. J.*, in press.

Crutcher, R. M., Hartkopf, W. I. and Giguere P. T. 1978 *Astrophys. J.*, **226**, 839

Eiora C. and Casali M. M. 1992 *Astron. Astrophys.*, **262**, 468.

Gatley, I., Merrill, K. M., Fowler, A. M. and Tamura, M. 1991 in *Astrophysics with Infrared Arrays: A.S.P. Conference Series*, **14**, p. 230.

Greene, T. P. and Young E. T. 1992 *Astrophys. J.*, in press

Herbig, G. H. 1954a *Astrophys. J.*, **119**, 483.

Herbig, G. H. 1954b *Publ. Astron. Soc. Pacific*, **66**, 19.

Krugel, E., Gusten, R., Schulz, A. and Thum C. 1987 *Astron. Astrophys.*, **185**, 283.

Lada, C. J. 1991 in *The Physics of Star Formation and Early Stellar Evolution*, eds. C.J. Lada and N.D. Kylafis, (Kluwer Academic Publishers: Dordrecht), p. 329.

Lada, C. J., DePoy, D. L., Merrill, M. and Gatley, I. 1991 *Astrophys. J.*, **374**, 533.

Lada, C. J. and Lada E. A. 1991 in *The Formation and Evolution of Star Clusters*, ed. K. Janes, A.S.P. Conference Series **13**, 3.

Lada, C. J., Young, E. T. and Greene, T. P. 1993 *Astrophys. J.*, **408**, 471.

Lada, E. A., DePoy, D. L., Evans, N. J. and Gatley, I. 1991 *Astrophys. J.*, **371**, 171.

Lada, E. A. and Lada C. J. 1993 preprint.

Margulis, M. and Lada, C.J. 1986 *Astrophys. J. Letters*. **309**, 87.

Margulis, M., Lada, C. J. and Snell, R. N. 1988 *Astrophys. J.*, **333**, 316.

Margulis, M., Lada, C. J. and Young, E. T. 1989 *Astrophys. J.*, **345**, 906.

Miller, G. E. and Scalo J. M., 1979 *Astrophys. J. Suppl. Ser.*, **41**, 513.

Salpeter, E. E. 1955 *Astrophys. J.*, **121**, 161.

Scalo J. M. 1978 in *Protostars and Planets*, ed T. Gehrels. University of Arizona Press: Tucson, p. 265.

Scalo J. M. 1986 *Fund. Cosmic Phys.*, **11**, 1.

Simon, M., Chen, W.P., Howell, R.R., Benson, J. A., and Slowik D. 1992 *Astrophys. J.*, **384**, 212.

Strom, S. E., Strom K. M. and Carrasco L. 1974 *Publ. Astron. Soc. Pacific*, **86**, 798.

Walker, M. F. 1956 *Astrophys. J. Suppl. Ser.*, **2**, 365.

Warner, J. W., Strom, S. E. and Strom K. M. 1977 *Astrophys. J.*, **213**, 427.

Zinnecker, H., McCaughrean M. and Wilking B.A. 1992 in *Protostars and Planets III*, eds. G. Levy and J. Lunine, University of Arizona Press: Tucson, in press.

Luminous Radio-Quiet Sources in the W3(Main) Cloud Core

E. F. Ladd, J. R. Deane, D. B. Sanders, and C. G. Wynn-Williams
Institute for Astronomy, University of Hawaii, 2680 Woodlawn Dr., Honolulu, HI 96822

ABSTRACT

We have resolved the 450–800 μm emission from the W3(Main) star forming region into three major peaks, using an 8″ beam on the James Clerk Maxwell Telescope (JCMT). One of the submillimeter sources is identified with W3-IRS 5, a well-known candidate protostar. However, to our surprise, we find that none of the submillimeter peaks coincides with any of the prominent compact HII regions in the area. We estimate that the three submillimeter sources together contribute 35–50% of the total bolometric luminosity of the region and speculate that the contribution of luminous radio-quiet sources to the total luminosity of HII region/molecular cloud complexes may be larger than is often assumed.

The spectral energy distributions of HII region/molecular cloud complexes indicate that the bulk of their luminosity is emitted in the far infrared and that this far infrared and submillimeter emission is generated by cool (T = 30–60 K) dust (see, e.g. [1),2)]). Because of the large beam sizes typically used for far-infrared and submillimeter continuum observations, it has been difficult to determine whether the OB stars ionizing the HII regions are the sources of the luminosity, or whether this luminosity is generated independently within the nearby molecular material.

Submillimeter observations of the W3(Main) region were made with the 15 m JCMT in 1992 November. The continuum maps were obtained using the facility UKT-14 bolometer system with passbands centered at approximately 450 μm and 800 μm and beam sizes of 8″ and 14″, respectively. Our results are shown in Figure 1, along with maps of 20 μm[3)] and a 5 GHz radio continuum emission.[4)] The submillimeter continuum emission breaks up into three main emission centers—one in the east, and two in the west. We designate the sources SMS 1, 2, and 3 from E to W in order of decreasing right ascension.

SMS 1 is resolved and nearly circular at half power, with low flux level extensions to the east in the direction of IRS 3/W3B and north in the direction of IRS 1/W3A. The 450 μm and 800 μm centroid positions are consistent with the 20 μm position of IRS 5,[3)] several H_2O maser groupings,[5)] and the radio continuum source W3(M).[6)]

SMS 2 lies close to the 20 μm source IRS 4,[3)] and near to the compact HII region W3(C)[7)]. We find that the position of SMS 2 lies 7.5″ from the center of W3(C). The size of the positional discrepancy is sufficiently large that we are confident that SMS 2 is not associated with W3(C). IRS 4 lies 4″ from the centers of both W3(C) and SMS 2, nearly on a line between these two sources. Therefore we conclude that there are are least two distinct major sources of emission in this area (W3(C) and SMS 2), and quite likely an additional unrelated infrared source (IRS 4).

SMS 3 is more extended than the other two submillimeter sources. Cuts in right ascension and declination indicate that this source has a FWHM size of 30″ $\times$ 16″. No 20 μm emission was detected in this region to a point source detection threshold of 150 Jy,[3)] nor was radio continuum emission detected greater than 6 mJy/2″ beam.[6)]

Combining our data with infrared results,[3),8)] we have estimated the 20–800 μm luminosities for these three sources, as well as for IRS 1 (which was not detected as a distinct source in our submillimeter maps) and the entire region. The total luminosity for the region is estimated to be 5.2 $\times$ 10^5 $L_\odot$. IRS 1 and IRS 5 each account for about 30% of the total. SMS 1 and SMS 2 account for an additional 6% each. However, it should be noted that the luminosity of SMS 2 may contain some additional contribution from either IRS 4 or the source associated with W3(C), and therefore this luminosity should be regarded as an upper limit to the luminosity of SMS 2.

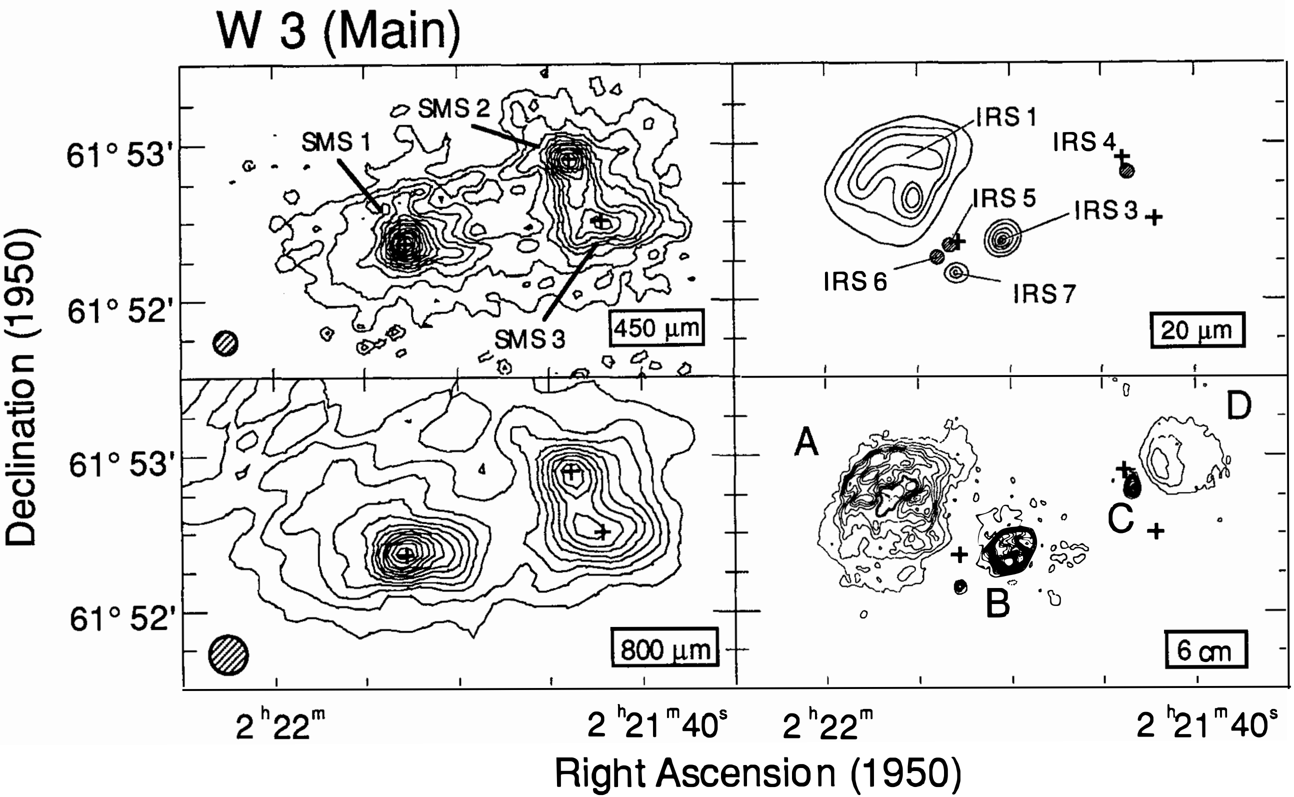

Fig. 1 Submillimeter images of the W3(Main) region at 450 μm (**top left**) and 800 μm (**bottom left**) compared with the 20 μm map from Wynn-Williams et al. (1972; **top right**) and the 5 GHz contours from Harris & Wynn-Williams (1976; **bottom right**). The submillimeter beam sizes are shown in the lower left of each relevant panel. Contours for the 450 μm map begin at 15 Jy/8″ beam and increment by 15 Jy/8″ beam. Contours for the 800 μm map begin at 1 Jy/14″ beam and increment by 1 Jy/14″ beam.

IRS 5 has long been recognized as a candidate high-mass protostar, based on its high luminosity, infrared energy distribution, and relatively weak radio continuum emission (see, e.g., [3),8),9),10)] We have found two more sources in the W3(Main) cloud that exhibit behavior similar to that of IRS 5. While both have luminosities about a factor of 5 lower than that of IRS 5, they are not associated with detected radio continuum emission.

These radio-quiet sources account for at least 35% (SMS 1/IRS 5 + SMS 3) and up to 50% (SMS 1/IRS 5 + SMS 2 + SMS 3) of the total luminosity generated in the W3(Main) core. With the addition of extended emission probably generated by lower-luminosity, non-ionizing sources, the luminosity from W3(Main) could be roughly equally divided between sources associated with HII regions and sources which have little or no ionized environs.

Based on these results, we suggest that the submillimeter continuum emission is a better tracer of the spatial distribution of luminosity in high mass star formation region than is the radio continuum emission.

On galactic scales, several authors have tried to determine the fraction of our galaxy's total luminosity that is generated by HII region stars. Sodrowski *et al.* found that roughly half of the total infrared luminosity in the galaxy is generated in or near HII regions,[11)] while Scoville & Good claim stars that ionize hydrogen can account for 25% of the total.[12)] However, these investigations used data with large beam sizes and therefore could not distinguish between luminosity generated by HII region sources and luminosity generated by nearby companions such as the sources examined in this work. With the large beams used in these surveys, all of the luminosity from the W3(Main) core would appear to be coincident with all of the radio continuum flux. If our result for W3(Main) can be generalized to all embedded HII regions, then the total galactic luminosity due radio-quiet and non-ionizing sources may be greater than that found by these authors.

1) Wynn-Williams, C. G., & Becklin, E. E. 1974, PASP, 86,5
2) Chini, R., Krugel, E., & Wargau, W. 1987, A&A, 181,378
3) Wynn-Williams, C. G., Becklin, E. E., & Neugebauer, G. 1972, MNRAS, 160,1
4) Harris, S., & Wynn-Williams, C. G. 1976, MNRAS, 174,649
5) Genzel, R. Downes, D., Moran, J. M., Johnston, K. J., Spencer, J. H., Walker, R. C., Haschick, A., Matveyenko, L. I., Kogan, L. R., Kostenko, V. I., Rönnäng, B., Rydbeck, O. E. H., & Moiseev, I. G. 1978, A&A, 66,13
6) Colley, D. 1980, MNRAS, 193,495
7) Wynn-Williams, C. G. 1971, MNRAS, 151,397
8) Werner, M. W., Becklin, E. E., Gatley, I., Neugebauer, G., Sellgren, K., Thronson, H. A., Harper, D. A., Loewenstein, R., & Moseley, S. H. 1980, ApJ, 242,601
9) Hackwell, J. A., Gehrz, R. D., Smith, J. R., & Briotta, D. A. 1978, ApJ, 221,797
10) Wynn-Williams, C. G. 1982, ARA&A, 20,587
11) Sodrowski, T. J., Dwek, E., Hauser, M. G., & Kerr, F. J. 1987, ApJ, 322,101
12) Scoville, N. Z., & Good, J. C. 1989, ApJ, 339,149

NUMERICAL SIMULATIONS OF MULTIPLE STAR FORMATION

Turner, J.A, Bhattal, A, Chapman, S.J, Disney, M.J, Whitworth, A.P., University of Wales College of Cardiff, U.K.

Abstract

From the growing observational evidence that binary/multiple star formation occurs prior to the pre-main sequence[1]), it is clear that any theory of star formation MUST also explain binary formation.

This paper details two formation mechanisms for binary/multiple stars, which occur simultaneously with protostar formation. The protostellar discs we form have masses $5 \rightarrow 30 M_{\odot}$, diameters $200 \rightarrow 4000$ AU. The binaries/multiples have separations $400 \rightarrow 7500$ AU. The formation mechanisms were found by conducting numerical simulations of star forming scenarios[2]).

The numerical modelling of star formation involves extreme changes in density (21 orders of magnitude), but by using Smoothed Particle Hydrodynamics [2,3]) with a spatially varying scale-length, we have obtained density changes of 10 orders of magnitude, which is about a million times greater than previous workers.

To minimize computational expense we use a hierarchical tree data structure, which reduces the gravity and hydrodynamic calculations from order N^2 to $N \log N$. This reduction allows us to use up to 200,000 particles in each calculation, thus enabling very detailed structure to be modelled. The temperature of the gas is prescribed to be isothermal at 100K and 10K for low and high densities respectively, with a continuous power-law dependance $T \propto n^{-\frac{2}{3}}$ inbetween. The particular scenario we are investigating is collisions between two identical clouds, which are isothermal, in detailed hydrostatic balance and confined by a hot, rarefied medium.

Binary and Multiple Protostar Formation

Each cloud is parameterised by its mass M, and radius R. The collision is characterised by its Mach number $\mathcal{M}$, and impact parameter b. The clouds are made of molecular hydrogen at 100K. These parameters have been systematically surveyed with $M = 150, 375, 750\ M_{\bullet}$; $b = 0, 0.1, 0.2, 0.3, 0.4, 0.5, 0.6$; $\mathcal{M} = 3, 5$, with R being chosen so that the clouds are Jeans-stable, $M = 0.3\ M_J$.

The collisions proceed with a layer of dense shocked gas forming between the clouds. When the layer is massive enough it becomes Jeans unstable and fragments into one or more condensations, which then collapse and interact with one another to form protostars.

All of these collisions form massive protostar(s) and the majority form binary/multiple systems. Those which only produce single protostars have small amounts of angular momentum i.e. $b \approx 0.0$. Increasing M or $\mathcal{M}$ means binary systems form at smaller impact parameters due to the increased angular momentum in the system. The two modes of binary formation which occur in our simulations are accretion induced rotational fragmentation (ARF), and shock induced thermal fragmentation (STF)[3].

ARF is a complicated formation mechanism, and begins with the layer fragmenting into one condensation (Figure 1). The gas flowing along the shock layer develops into two streams, which accrete onto the condensation, increasing its angular momentum because the gas flowing along the shock layer has larger and larger specific angular momentum the further along the shock layer it has to travel. This continues until the condensation goes rotational unstable and has to lose angular momentum. It does this in two ways. It can form a bar which then splits into two, or spiral arms can be excited (Figure 2). These arms detach and then condense (Figures 3). The new condensations orbit around the original condensation, and grow by accreting material from the accretion flows. They cause spiral arms to be re-excited in the original condensation. The surrounding condensation(s) then accrete these spiral arms as they detach and therefore grow at the expense of the original condensation. This process of accretion onto the smaller condensations, causes them to grow and form multiple systems with the original condensation (Figure 4).

STF occurs when the layer fragments into two or more condensations (Figure 5), which fall towards the centre of the layer and therefore towards each other (Figure 6), whilst collapsing to form individual protostars. At the centre of the layer they interact (Figure 7), and form binary/multiple systems by capture (Figure 8).

Summary

By conducting realistic simulations of cloud-cloud collisions, we have identified two formation mechanisms for binary/multiple protostar systems. ARF : a single condensation forms, the gas in the shock layer develops into two accretion streams onto this condensation, spinning it up. The condensation becomes unstable and smaller condensations break off it. These condensations then grow to become companions, thereby forming binary/multiple systems. STF : the fragments in the shock layer condense to form protostars, which fall towards each other and form binary/multiple systems by capture.

References

[1]) Mathieu, R. D., 1992. Disks in the pre-main sequence enviroment, In: *Evolutionary processes in interacting binary stars*, p.21, eds Kondo, Y., Sistero, R. F. & Polidan, R. S., Kluwer Academic Publishers, Dordrecht.

[2]) Lucy, L. B., 1977 A Numerical approach to the testing of the fission hypothesis/ *Astron. J.*, **82**, 1013.

[3]) Gingold, R. A. & Monaghan, J. J., 1977 Smoothed particle Hydrodynamics: theory and application to non-spherical stars. *Mon. Not. R. astr. Soc.*, **181**, 375.

[4]) Chapman, S. J., 1992 Multiple Protostar Formation from Cloud-Cloud Collisions, *PhD. Thesis* University of Walse, College of Cardiff.

[5]) Chapman, S. J. *et al*, 1992 The formation of binary and multiple star systems. *Nature*, **359**, 207.

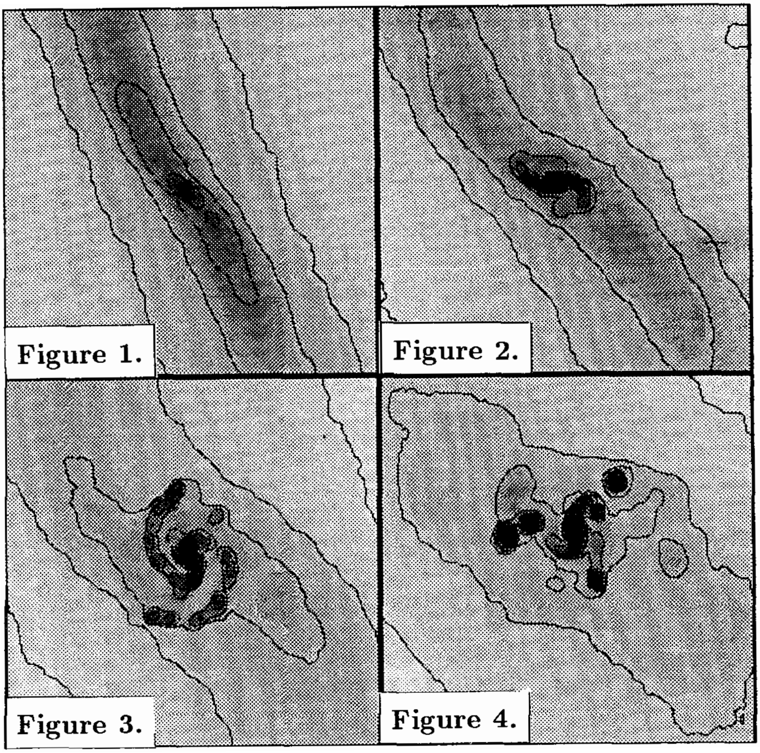

Figure 0.1: An example of ARF. The colours represent the column density through the shock layer and are logarithmically scaled, from white representing $6 \times 10^{23}\, cm^{-2}$ to blue $2.1 \times 10^{18}\, cm^{-2}$.

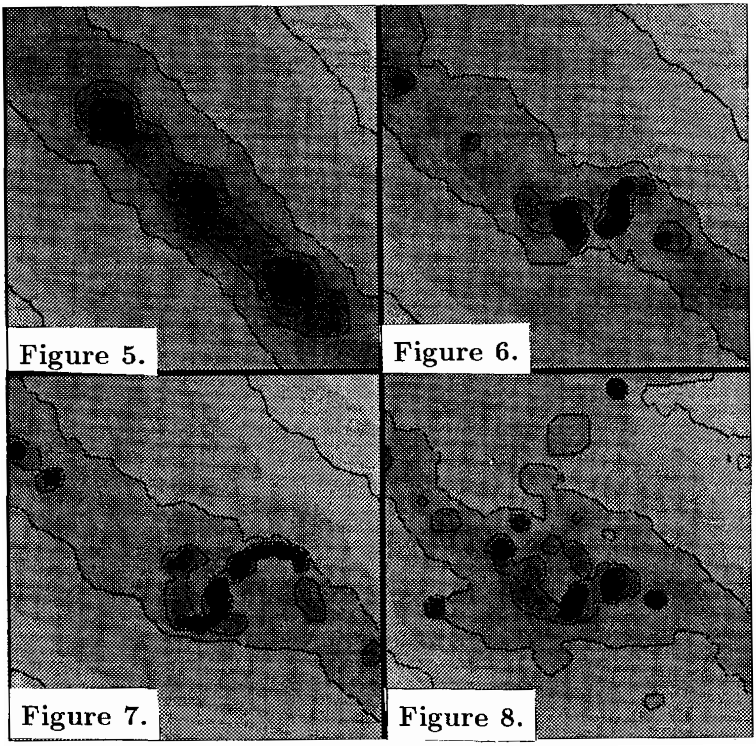

Figure 0.2: An example of STF. The colours represent the column density through the shock layer and are logarithmically scaled, from white representing $4 \times 10^{23}\, cm^{-2}$ to blue $2.1 \times 10^{18}\, cm^{-2}$

YOUNG STELLAR OBJECTS AND THEIR ENVIRONMENT

BIPOLAR FLOWS, WINDS AND JETS

A. C. Raga

Astrophysics Group, Mathematics Department

UMIST, P. O. Box 88, Manchester M60 1QD, U. K.

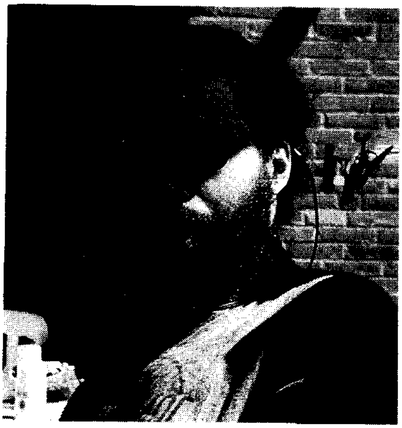

ABSTRACT. Young stellar objects many times eject high velocity, collimated, bipolar outflows. The optically detected Herbig-Haro (HH) objects show a rather wide range of characteristics, ranging from the more simple, "jet-like" HH objects to objects with highly chaotic structures. This paper presents a review of the mechanisms that have been suggested in the past for explaining these structures, with a particular emphasis on new models of outflows from variable sources. These "variable source" models are at this time quite attractive, since they seem to provide a unified framework for understanding the striking differences between the structures of the observed HH objects.

1. INTRODUCTION

Many young stars produce collimated outflows, which present many interesting observational properties, and produce detectable emission in a large wavelength range. Ultraviolet (IUE[1]), optical[2], infrared[3] and radio continuum[4] observations show the presence of highly collimated, high velocity (~ 100-400 km s^{-1}) stellar outflows, some of which have "jet-like" morphologies, and others showing considerably more chaotic structures.

Probably the most striking property of these outflows is that the emitting knots observed in Herbig-Haro (HH) objects (the name given to the optical manifestations of the outflows from young stars) have high proper motions directed approximately away from the central sources. This effect was discovered in HH 1 and 2 by Herbig and Jones[5], and has since been observed in several objects. Proper motion measurements have now also been carried out with radio continuum observations[6,7]. It is observed that both proper motion and radial velocities of HH objects generally lie in the 50-400 km s^{-1} velocity range.

A very interesting recent discovery has been that in the so called "HH jets" (=the HH objects with clear jet-like morphologies), the chains of well aligned knots along the body of the jet also show high (~ 300-400 km s^{-1}) proper motions directed away from the source[8,9,10]. A similar effect has also been detected in radio continuum observations[11]. As will be discussed later in this paper, this observation seems to be fundamental for discerning between different theoretical models.

As the HH jets appear to have the most simple, organized structure, a large part of the past theoretical effort has gone into modelling these objects. In this review, a critical discussion of the stellar jet models which have been proposed in the past is presented (§2). Finally, a more detailed discussion of recent models of jets from variable sources is carried out (§3).

2. MODELS OF HH JETS

Some HH objects (the "HH jets") show a chain of well aligned knots extending radially away from the source to distances of a few times $\sim 10^{17}$ cm, sometimes pointing to a brighter, bow shaped HH object (the best example of this morphology possibly being HH 34[12]). These bow shaped structures have been modeled quite successfully as the emission from a bowshock formed by the "head" of the jet [13,14,15,16] (though this is by far not a comprehensive list of the relevant literature, for which we refer the reader to the review of Reipurth[17]).

While (as discussed above) there is somewhat of a consensus regarding the interpretation of the "heads" of HH jets, the situation is much less satisfactory for the structures of aligned knots observed close to the outflow sources. The apparently most straightforward interpretation of these knots is that they correspond to the emission produced by stationary, recollimation "crossing shocks". Such shocks are always observed in over- or underexpanded (*i. e.* , initially under- or overpressured) laboratory jets.

The theory of stationary crossing shocks was first presented by Prandtl[18], who studied the linearized problem. In the context of astrophysical jets, extensive numerical simulations of such shocks have been carried out[19,20], some of them incorporating the physical processes relevant for stellar jets[21,22]. An analitic theory for the fully nonlinear regime has also been developed[23], and it is found to be in good quantitative agreement with the numerical simulations[24].

Predictions of intensity maps and position-velocity diagrams from these models[25] show structures that are reminiscent of HH jets. In qualitative agreement with observations, a structure of low excitation, more or less regularly spaced knots is predicted. Also in agreement with the observations, narrow emission line profiles centred at the projected jet velocity are predicted.

However, these models have two important problems :

- the predicted knot separation to jet diameter ratio agrees with the values observed in HH jets only if the Mach number of the flow is low ($M \sim$ 2-5, which is too low by a factor of ~ 5 compared to the empirically determined Mach numbers of $M \sim$ 10-30 for HH jets),
- the theoretically predicted knot structures are stationary (*i. e.* , the knots are always at the same distance from the jet source), in disagreement with the fact that (at least in some

cases, see §1) the knots of HH jets are observed to have high proper motions directed away from the jet source.

This second problem clearly elliminates the recollimation shock model, at least for the HH jets with observed high knot proper motions.

A second possibility that has received a lot of attention in the astrophysical literature is that the observed knots might correspond to "Kelvin-Helmholtz modes[26]" which could produce travelling crossing shocks inside the jet beam. This idea has been studied in detail for extragalactic jets, in particular in the context of linear analyses[27,28]. Also, numerical simulations show that if a direct forcing at the right frequency is applied, a "travelling crossing shock" pattern does arise in slab jets[29,30].

These travelling crossing shocks appear to be quite attractive in that they indeed can reproduce the observed proper motions of HH jets, though they still have somewhat of a problem for explaining the correct knot length to separation ratio. To reproduce the observed values, it is necessary for the Mach number of the jet with respect to the environmental sound speed to be $\sim$ 2-5, which seems to be somewhat unlikely since this would imply a temperature of $\sim 10^5$ K for the environment surrounding the jet beam. How such a temperature can be maintained for a substantial amount of time is unclear.

There are other lingering questions about the reality of the "Kelvin-Helmholtz mode" interpretation of knots in HH jets. For example, all simulations of jets which show such travelling crossing shock structures[31] are made for the case of beams which are in exact pressure balance with the surrounding environment (so as to elliminate the presence of the dominant "stationary mode" of Prandtl[18]). Such a pressure balance condition is unlikely to be present in HH jets, which are thought to be moving in strongly stratified environments.

It is also interesting to note that in high Reynolds number laboratory jets, the effect of the Kelvin-Helmholtz instability at the jet/environment boundary generally is not to drive long wavelength, organized "travelling crossing shock" modes, but to generate a turbulent boundary layer. This result is consistent to some extent with the fact that the growth rate of the Kelvin-Helmholtz modes is highest for modes with very large number of nodes, and that such modes are spatially confined to the region close to the jet beam/environment boundary[27]. This boundary layer grows both into the surrounding environment and into the jet, so that at large enough distances from the source the jet becomes fully turbulent[32] (and references therein).

The turbulent dissipation in the boundary layer results in the production of a diffuse emission, which might be observed in some HH jets[32,33,34] but does not explain the existence of organized knot structures. Birkinshaw[35] discusses the fact that organized shock structures can survive inside the turbulent region. However, these organized shock structures actually are the stationary crossing shocks, so that the problem of explaining the observed proper motions remains.

To finalize the discussion of the Kelvin-Helmholtz modes, one should mention the results of Blondin, Fryxell and Königl[36]. These authors (who studied the case of pressure matched jets). find that the passage of the head of the jet strongly disturbs the surrounding environment. These disturbances (possibly associated with vortex shedding from the head of the jet) excite internal shocks in the beam of the jet. The numerical simulations clearly show two "crossing shock cells" trailing the head of the jet. These shocks do have high proper motions, in qualitative agreement with observations of knots in HH jets. However, in the numerical simulations[36], the knots always trail the jet head by only a few jet diameters, in clear qualitative disagreement with HH jets (where the knots are observed to be close to the outflow source, far upstream of the head of the jet). These travelling knots following the leading working surface can also be seen in numerical simulations of jets out of pressure equilibrium with the surrounding environment37). Also interesting is the analytic model of Silvestro and collaborators[38] in which it is suggested that Kelvin-Helmholtz instabilities in the jet/environment interface might result in the formation of more or less "flat" shocks across the beam of the jet. However, it is unclear that such an effect could occur in a high Mach number flow.

3. JETS FROM VARIABLE SOURCES

An alternative explanation for the structures of aligned knots in HH jets is that they are the result of a time-variability of the ejection velocity. Rees[39] pointed out that even smooth variations in the source velocity would steepen into discontinuities, resulting in the production of shock waves travelling away from the source along the beam of the jet. Raga *et al.* [40] noted that if the amplitude of the velocity variability is supersonic, the resulting discontinuities actually correspond to two-shock "internal working surfaces". These internal working surfaces are qualitatively similar to the "leading working surface" (at the head of the jet), but instead of travelling into the undisturbed environment, they travel into the material ejected from the source in the previous "ejection episode" of the source variability.

Wilson[41] carried out numerical simulations of an adiabatic "variable velocity jet", in which he followed the formation of two working surfaces (the leading working surface, and one internal working surface). This simulation was intended for modelling extragalactic jets with two aligned lobes on one side of the outflow source.

A similar explanation was proposed by Raga *et al.* [40] for explaining the "two-headed structure" (the two heads being HH 47A and D) of the blueshifted-shifted lobe of the HH 46/47 outflow. Also, in the position-velocity diagrams (obtained by placing a slit along the HH 46/47 outflow axis[12,42]) the regions between the source and HH 47A and between HH 47A and HH 47D both correspond to "ramps" of increasing radial velocity (actually, increasing modulus, as the radial velocities are negative) away from the source. As pointed out by Raga *et al.* [40], this is exactly the right signature expected from models of jets from variable velocity sources (for an alternative interpretation of these "velocity vs. position ramps", see Hartigan, Raymond and Meaburn[43]).

Another example of such behaviour is HH 34, in which a velocity monotonically increasing away from the source is observed both in radial velocity[12] and proper motion[8,9] measurements. The most likely explanation of such velocity vs. position ramps is that they are the result of a "velocity sorting" of material ejected from the source in a time-dependent way[40]

Evidence for a time-variability of the outflow velocity is also seen in objects such as

HH 111[44,10]. This object shows three blueshifted and two redshifted bow-shaped structures, which can be straightforwarldy interpreted as working surfaces formed by a number of "ejection episodes" of the central source.

Raga *et al.* [40] also suggested that the aligned knots observed along most HH jets possibly could correspond to more or less unresolved "internal working surfaces" travelling away from the central source. This idea was pursued with analytic techniques[45,46] and also with numerical simulations[47,48,49,50]. Non-periodic variabilities result in the production of knots moving away from the source at different velocities, resulting in "catching up" processes between fast and slow knots[51]. It will be interesting to see if such events might be "caught" in the future by observers !

Even though there is substantial evidence that some of the characteristics of HH jets (such as the "multiple bowshock structures" and "velocity vs. position ramps" observed in some objects, see above) might be the result of a time-variability of the outflow velocity, there is still some scepticism whether or not the same explanation is valid for the almost unresolved, aligned knots close to the outflow source. Eislöffel and Mundt[8,52] claim that once a correction for the orientation angle of the outflow has been carried out, the deprojected proper motion velocity v_p of the knots (which Eislöffel and Mundt call the "pattern speed") is lower than the spatial velocity v_s of the emitting material (obtained from the de-projected radial velocity measurements).

If correct, this result appears to be in disagreement with the "internal working surface model"[53], as in such a model one would expect to have $v_p \approx v_s$ (as most of the emission is produced by the material "trapped" in the two-shock internal working surfaces, the radial velocity and the proper motion correspond to different projections of the motion of this trapped gas). However, from an analysis of similar data other authors[2,54] obtain $v_p \approx v_s$ (due to the fact that they use different methods for determining the orientation angle of the outflows). The question of whether or not the "internal working surface" model is applicable for the unresolved condensations of HH jets is thus still unanswered.

It has also been suggested that some of the features observed in HH objects might be the result of direction variabilities of the source[55,56]. This idea is particularly attractive for modelling objects which show "sinuous" structures (such as HH 46/47[42]) or HH 83[57]).

New models of jets from sources with a general velocity+direction variability also show interesting characteristics. For appropriate parameters such models result in a breakup of the jet beam into a series of discrete "interstellar bullets" travelling in different directions away from the source[58]). Such models might be attractive for explaining the more "bullet-like" HH objects (such as HH 32[59])). Detailed comparisons of these models with observations of HH objects should be made in the future.

4. CONCLUSIONS

We have presented a discussion of models of jet-like HH objects. Quite a large amount of work has been done in modelling the "heads" of these jets, and there is now an at least partial consensus that some of the observed HH objects do indeed correspond to the heads of jets.

There is substantially more controversy about the models for the structures of aligned knots close to the outflow sources. These models fall roughly into three categories :

- steady recollimation shocks, which seem to be ruled out at least in some objects (due to the observation of high proper motions for the emitting knots),
- Kelvin-Helmholtz travelling shock models, which can produce knots with high proper motions, but are in a still somewhat uncertain theoretical footing,
- models of jets from time-dependent sources.

This last category of models is very rich, opening up a range of possible analytic and numerical calculations. Both analytic and theoretical models clearly show that supersonic variabilities in the outflow velocity lead to the formation of "internal working surfaces" that travel down the beam of the jet. In such a model, all of the knots along a jet can be interpreted as being similar but smaller versions of the leading head of the jet.

More general variabilities of the source, involving direction as well as velocity time-changes, lead to rather complex flows. It is still unclear whether or not these more complex flows could explain the properties of the more chaotic, "bullet-like" HH objects. However, this question might be resolved in the near future through detailed comparisons between model predictions and observations.

REFERENCES

1. Brugel, E. W. 1989, in ESO Workshop on *Low Mass Star Formation and Pre-Main Sequence Objects*, ed. Bo Reipurth (ESO), p. 311.
2. Reipurth, B., and Heathcote, S. 1993, in STScI Symposium on "Astrophysical Jets", Eds. M. Fall, C. O'Dea, M. Livio, D. Burgarella (Cambridge Univ. Press), in press.
3. Lane, A. P. 1989, in ESO Workshop on *Low Mass Star Formation and Pre-Main Sequence Objects*, ed. Bo Reipurth (ESO), p. 331.
4. Torrelles, J. M. 1991, in *Atoms, Ions and Molecules : New Results in Spectral Line Astrophysics*, Eds. A. D. Haschick and P. T. P. Ho (*Publ. A. S. P.* Conference Series), p. 257.
5. Herbig, G. H., and Jones, B. F. 1981, *A. J.* **86**, 1232.
6. Rodríguez, L. F., Curiel, S., Moran, J. M., Mirabel, I. F., Roth, M., and Garay, G. 1989, *Ap. J. (Letters)* **346**, L85.
7. Rodríguez, L. F., Ho, P. T. P., Torrelles, J. M., Curiel, S., and Cantó, J. 1990, *Ap. J.* **352**, 645.
8. Eislöffel, J., and Mundt, R. 1992, *Astron. Astroph.* **263**, 292.
9. Heathcote, S., and Reipurth, B. 1992, *A. J.* **104**, 2193.
10. Reipurth, B., Raga, A. C., and Heathcote, S. 1992, *Ap. J.* **392**, 145.
11. Curiel, S., Rodríguez, L. F., Moran, J. M. and Cantó, J. 1993, *Ap. J.* (in press).
12. Reipurth, B. 1989, in ESO Workshop on *Low Mass Star Formation and Pre-Main Sequence Objects*, ed. Bo Reipurth (ESO), p. 247.
13. Hartigan, P., Raymond, J. C., and Hartmann, L. 1987, *Ap. J.* **316**, 323.
14. Raga, A. C., Mateo, M., Böhm, K. H., and Solf, J. 1988, *A. J.* **95**, 1783.
15. Blondin, J., Königl, A., and Fryxell, A. 1989, *Ap. J.* **337**, L37.
16. Wolfire, M. G., and Königl, A. 1991, *Ap. J.* **382**, 205.
17. Reipurth, B. 1991, in *The Physics of Star Formation and Early Stellar Evolution*, eds. C. J. Lada and N. D. Kylafis, NATO ASI Series (Kluwer), p. 497.
18. Prandtl, L. 1907, *Zs. Phys.* **8**, 23.
19. Falle, S. A. E. G., and Wilson, M. J. 1985, *M. N. R. A. S.* **216**, 79.
20. Wilson, M. J., and Falle, S. A. E. G. 1985, *M. N. R. A. S.* **216**, 971.
21. Falle, S. A. E. G., Innes, D. E., and Wilson, M. J. 1987, *M. N. R. A. S.* **225**, 741.
22. Raga, A. C., Binette, L., and Cantó, J. 1990, *Ap. J.* **360**, 612.
23. Cantó, J., Raga, A. C., and Binette, L. 1989, *Rev. Mexicana Astron. Astrof.* **17**, 65.
24. Biro, S., Cantó, J., Raga, A. C., and Binette, L. 1993, *Rev. Mexicana Astron. Astrof.* (in press).

25. Raga, A. C., Biro, S., Cantó, J., and Binette, L. 1991, *Rev. Mexicana Astron. Astrof.* **22**, 243.
26. Bührke, T., Mundt, R., and Ray, T. P. 1988, *Astron. Astroph.* **200**, 99.
27. Payne, D. G., and Cohn, H. 1985, *Ap. J.* **291**, 655.
28. Ferrari, A., Trussoni, E., and Zaninetti, L. 1981, *M. N. R. A. S.* **196**, 1051.
29. Norman, M. L., and Hardee, P. E. 1989, *Ap. J.* **334**, 80.
30. Hardee, P. E., and Norman, M. L. 1989, *Ap. J.* **342**, 680.
31. Norman, M. L., Smarr, L., and Winkler, K. H. 1985, in *Numerical Astrophysics*, eds. J. M. Centrella, J. M. LeBlanc, R. L. Bowers, and J. A. Wheeler (Jones and Bartlett), p. 88.
32. Cantó, J., and Raga, A. C. 1991, *Ap. J.* **372**, 646.
33. Solf, J. 1987, *Astron. Astroph.* **184**, 322.
34. Meaburn, J., and Dyson, J. 1987, *M. N. R. A. S.* **225**, 863.
35. Birkinshaw, M. 1991, in *Beams and Jets in Astrophysics*, ed. P. A. Hughes (Cambridge Univ. Press), p. 279.
36. Blondin, J., Fryxell, B. A., and Königl, A. 1990, *Ap. J.* **360**, 370.
37. Tenorio-Tagle, G. 1989, in *Structure and Dynamics of the Interstellar Medium*, eds. G. Tenorio-Tagle, M. Moles and J. Melnick (Srpinger-Verlag), p. 265.
38. Sivestro, G., Ferrari, A. Rosner, R., Trussoni, E., and Tsinganos, K. 1987, *Nature* **325**, 228.
39. Rees, M. J. 1978, *M. N. R. A. S.* **184**, 61p.
40. Raga, A. C., Cantó, J., Binette, L., and Calvet, N. 1990, *Ap. J.* **364**, 601.
41. Wilson, M. J. 1984, *M. N. R. A. S.* **209**, 923.
42. Reipurth, B., and Heathcote, S. 1991, *Astron. Astroph.* **246**, 511.
43. Hartigan, P., Raymond, J. C., and Meaburn, J. 1990, *Ap. J.* **362**, 624.
44. Reipurth, B. 1989, *Nature* **340**, 42.
45. Kofman, L., and Raga, A. C. 1992, *Ap. J.* **390**, 359.
46. Raga, A. C., and Kofman, L. 1992, *Ap. J.* **386**, 222.
47. Falle, S. A. E. G., and Raga, A. C. 1993, *M. N. R. A. S.* (in press).
48. Hartigan, P., and Raymond, J. C. 1993, *Ap. J.* (in press).
49. Stone, J., and Norman, M. L. 1993, *Ap. J.* (in press).
50. Biro, S., and Raga, A. C. 1993, *M. N. R. A. S.* (submitted).
51. Raga, A. C. 1992, *M. N. R. A. S.* **258**, 301.
52. Eislöffel, J. 1992, Ph. D. Thesis, University of Heidelberg.
53. Ray, T. P., and Mundt, R. 1993, in STScI Symposium on *Astrophysical Jets*, Eds. M. Fall, C. O'Dea, M. Livio, D. Burgarella (Cambridge Univ. Press), in press.
54. Morse, J. A., Hartigan, P. Cecil, G., Raymond, J. C., and Heathcote, S. 1992, *Ap. J.* **339**, 231.
55. Lightfoot, J. F., and Glencross, W. M. 1986, *M. N. R. A. S.* **221**, 47p.
56. Raga, A. C., Cantó, J., and Biro, S. 1993, *M. N. R. A. S.* **260**, 163.
57. Reipurth, B. 1989, *Astron. Astroph.* **220**, 249.
58. Raga, A. C., and Biro, S. 1993, *M. N. R. A. S.* (in press).
59. Solf, J., Böhm, K. H., and Raga, A. C. 1986, *Ap. J.* **305**, 795.

Theory of Bipolar Outflows

R.N. Henriksen
Department of Physics
Queen's University at Kingston Ontario Canada

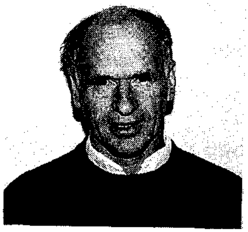

Abstract

I discuss briefly but completely the implications of time dependent accretion for the history of bipolar outflows in section 1. It is shown that the standard Shu estimate is good initially, but that either a 'bang' or 'whimper' mode may develop subsequently. In the case of a whimper mode the current outflow luminosity may not reflect the current infra-red luminosity. Section 2 discusses various outflow driving mechanisms. A general argument is given to explain observed correlations in terms of radiative driving. Recent wind and magneto-disc models are briefly summarized and criticized. Finally in section 3 a new type of outflow model is introduced in its 'toy', analytic form.

1. What Goes Up Must Have Come Down
Inflow, Outflow and Luminosity

In this section I wish to review certain subtleties of the accretion phase which may not be sufficiently well known. Such a study may help us to answer questions of the type: Is inflow/outflow occurring simultaneously? Is the bipolar phenomenon part of the actual star building process or is it rather an early secondary phase? Has the initial cloud been used up? If not, then out to what radius has it been disturbed? What are the possible histories of the luminosity due to accretion?

Now there is a commonly used estimate of the spherically symmetric accretion rate in an isothermal cloud due to Shu[1),2)] . But such a single value can only either be some average estimate or can only apply at some special epoch in what is more generally a time dependent flow . Let us first examine under what conditions this is a valid order of magnitude estimate.

If a is the isothermal sound speed in a spherically symmetric self- gravitating medium, and if the mass inside a sphere of interest is not changing rapidly in a dynamical time, then the accretion zone extends to the Bondi-Parker type critical point at the sonic or 'virial' radius r_s, where $r_s = Gm_s/(2a^2)$, and m_s refers to mass enclosed by the sonic radius[3)] . Since at this point the radial velocity is the sound speed (that is the radius moves outward relative to the material with the speed a), we see that an estimate of the accretion rate per unit solid angle *at this stage* is given by $A \approx r_s^2\rho_s a$. Here ρ_s is the density at the sonic point. If in addition we suppose that in order of magnitude $\rho_s \approx 3m_s/(4\pi r_s^3)$ (see below for a justification), then simple manipulation gives $A \approx (3/2\pi)\left(\frac{a^3}{G}\right)$, and $m_s^2 \approx (6/\pi)\left(\frac{a^6}{G^3\rho_s}\right)$. The latter expression gives essentially the "Bonnor-Ebert" mass [31)], which is the maximum mass of a spherical, isothermal, self- gravitating, cloud in hydrostatic equilibrium. Our estimate is in fact slightly larger by a numerical factor ≈ 1.17, and estimates the minimum mass required for transonic, steady inflow. For an observed density it may give the best estimate of the mass in the protostellar condensation in terms of a measured density.

I now turn briefly to an exact solution, which permits one to see when the Shu estimate needs to be generalized. We examine self-gravitating, zero temperature accretion of a cloud that has at $t = 0$ a power law density distribution[4)]. One can only expect this solution to be applicable out to an initial radius $r = r_s$ where we will assume that the collapsing region detaches from its surroundings. We shall therefore use the virial radius as our fiducial scale r_o, which is arbitrary without such physical considerations. In addition, for simplicity, we study here only the case of virialized or zero energy radial shells .

One measures time in units of $(2Gm_s/r_s^3)^{-1/2}$, space in units of r_s, hence velocity in units of $\sqrt{2Gm_s/r_s}$, and density in units of $m_s/(4\pi r_s^3)$. Throughout, m_s is the mass initially inside r_s and is the unit of mass. Then the initial density and mass distributions are $\rho_o(r) = (3-2/D)r^{-(2/D)}$, and $m_o(r) = r^{(3-2/D)}$.

The location of a shell initially at r namely $R(r,t)$ is found from the formulae[5),6)] $R = rS(\xi)$, where $S(\xi) = (1-3\xi/2)^{2/3}$, and $\xi = t/r^{(1/D)}$.

In these formulae D is any real number $\geq 2/3$ or < 0 so that they describe a considerable range of power law initial states of zero temperature. We observe that every shell finds itself at the centre when $\xi = 2/3$, so that the time to enter the singularity is simply $(2/3)r^{(1/D)}$ for the shell initially at r.

It is frequently necessary to invert $R(r,t)$ for $r(R,t)$, which one achieves by writing the equations for R, S and ξ together as

$$x^3 + (3/2)\varsigma x^{(2/D)} - 1 = 0, \tag{1}$$

where $x^2 \equiv S = R/r$, and $\varsigma \equiv t/R^{(1/D)} = \xi/x^{(2/D)}$. Fortunately this is readily solved for interesting choices of D. Note that ξ and ς are two equally good choices of self-similar variables since $\varsigma = \varsigma(\xi)$ by (1) and the definitions.

The radial velocity is given as a function of R, t, by the formula

$$U(R,t) = -\frac{R^{(1-1/D)}}{x^{(3-2/D)}}, \tag{2}$$

and the density by the expression (remembering that $r \equiv R/x^2$)

$$\rho(R,t) = \left(\frac{\rho_o(R/x^2)}{x^3(x^2(1-2/(3D)) + 2/(3D))}\right). \tag{3}$$

The most important result from this treatment then follows as an expression for the accretion rate per unit solid angle $A(R,t) \equiv \dot{m}/4\pi$ in units of $r_s^2(m_s/(4\pi r_s^3)\sqrt{2Gm_s/r_s} \equiv a^3/(\pi G)$ as

$$A(R,t) = \left(\frac{R^{(3-1/D)}\rho_o(R/x^2)}{x^{(6-2/D)}(x^2(1-2/(3D)) + 2/(3D))}\right). \tag{4}$$

The first example is to choose $D = 1$ which corresponds to the 'isothermal' density law[7),8)] and makes $\varsigma = t/R$. Equation (1) is now a cubic equation and the one positive real root is; for $\varsigma^3 \leq 2$ $x = -\varsigma/2 + \varsigma^2/(2\Delta) + \Delta/2$, where $\Delta \equiv (4-\varsigma^3 + \sqrt{8(2-\varsigma^3)})^{(1/3)}$, and for $\varsigma^3 > 2$ $x = -\varsigma/2 + \varsigma\cos(\phi/3)$, where $\cos\phi \equiv (4-\varsigma^3)/\varsigma^3$. We observe that $x = 1$ at $\varsigma = 0$ and that $x \to 0$ as $\varsigma \to \infty$ as is required to maintain $x^2\varsigma = \xi \leq 2/3$.

The striking behaviour in this case is that (see equation (4)) A varies from 1 when $x = 1$ to 3/2 as $x \to 0$, according to $A(R,t) = (3/2)/(x^2/2+1)$. One sees that the accretion flow is strictly self-similar in this case with the same spatial profile at all times and the same temporal variability at each point in space. On remembering the units of A and taking $r_o \equiv r_s$, this gives the asymptotic accretion rate *at all* R as $(3/2\pi)a^3/G$, precisely as in our estimate of the Shu mode above.

Equation (3) reveals that the density is asymptotically $\propto 1/(t^{1/2}R^{3/2})$, so that this region has the free-fall density profile, as have all cases in fact. The outer density variation continues however to reflect the transition from the initial law to the free-fall profile, for which equation (1) is needed.

However this behaviour is *critically* dependent on the initial density power law D. For example if $D = 3/4$ then equation (1) is no longer analytic, but $x^{8/3}\varsigma \leq 2/3$ plus this equation suffices to show that $x \to (3\varsigma/2)^{-3/8}$ as $\varsigma \to \infty$. Equation (4) yields $A(R,t) = (3x)^2/(x^2+8)R^{-1}$ and so (note that now $\varsigma = t/R^{4/3}$) one finds asymptotically that $A \to (9/8)x^2/R$ or $\propto t^{-3/4}$ for all R. The density is asymptotically $\propto 1/(t^{7/8}R^{3/2})$. I refer to this mode that occurs for $2/3 < D < 1$ as a 'whimper' mode since the accretion inevitably declines in time, although it increases with decreasing R. In this sense it is a true 'inside out' mode and is not strictly self-similar. This applies mostly at small R for physical reasons since the outer boundary falls in at $t = 2/3$ and abruptly ends the accretion. The mode with $D = 1$, appropriately referred to as the 'Shu' or 'stationary' mode, will end also with the falling in of the initial outer boundary, assuming a discontinuous density decrease beyond this surface.

The cases with $D > 1$ furnish us with another mode of considerable interest. We choose $D = 2$ so that we accrete an intially virialized zero temperature cloud whose density is proportional to r^{-1}. Equation (1) is now a cubic in standard form and gives $x = -\varsigma/\Delta' + \Delta'/2$, where $\Delta' \equiv (4+2\sqrt{4+2\varsigma^3})^{1/3}$ for the real root, and we note that $\varsigma = t/R^{(1/2)}$. Equation (4) now shows that $A(R,t) = 3/(x^3(x^2+1/2))\,R^{3/2}$, which is not strictly self- similar. However in the asymptotic limit $x\varsigma \to 2/3$ suffices to show with equations (3) and (4) that $\rho \to 9t/R^{(3/2)}$ and $A \to (81/4)t^3$! Thus this initial distribution yields a 'bang' mode. In fact one sees from the form of $A(R,t)$ that initially ($x \leq 1$) the mass flow decreases towards the center ('outside in' mode in this sense), while at every R it ultimately increases without limit as $t \to \infty$. But this latter phase is probably terminated by the infall of the initial surface r_s.

The apparently zero density special case when $D = 2/3$ corresponds in fact to accretion of nonself- gravitating virialized matter onto a central point mass m_s. The above formulae apply, except that the expression for the initial self- gravitating density must be replaced by an equation for the initial test particle density of the same form, but wherein $(3-2/D)$ is replaced by an arbitrary constant λ, and the power law dependence also becomes arbitrary in the form $r^{-(2/\delta)}$. One then finds that the bang and whimper modes exist respectively for $\delta = 2$ and $\delta = 1$ respectively, although as emphasized below the non self-gravitating phase may generally be considered a whimper mode relative to the self-gravitating phase since λ will be much smaller than one. Thus the different time dependences in this mode are perhaps best named as 'whimper-bang' and 'whimper-whimper' modes.

In essence the arguments of this section manage to extend the discussion of isothermal accretion to more general initial mass distributions, by using this device of neglecting the pressure in the inner collapsing core region. This region has presumably become unstable due to the outward diffusion of magnetic flux, heat and angular momentum[2),9)] . But what have these simple models got to dc with the questions raised at the beginning of this section? Most directly we see that *the protostellar accretion should be strongly time dependent* in general. This means that in the whimper mode for example, an earlier phase of rapid accretion might have launched an energetic bipolar outflow, but that the currently observed low IR luminosity might reflect rather the tail of the accretion phase.

If this latter idea were to be correct it would imply that a bipolar phenomenon is already launched in the protostellar collapse. The characteristic time for this phase is 2/3 or $Gm_s/(6a^3)$ in regular units ($r_o = r_s$) or $1.6 \times 10^5 \times m_s\, T_{10}^{-(3/2)}$ years, where in this paragraph the core mass is in units of $2m_\odot$ and a mean molecular mass of 2 amu is used. The outer cloud temperature is given in units of $10K$. This time is near the upper end of the range of dynamical life-times of bipolar outflows so that they may indeed be sensitive to variations in the protostellar flow . Note also that in this period the cloud has been disturbed out to a radius of r_s, which is $0.1 \times m_s/T_{10}$ *pc*. Interestingly enough, for plausible ranges of core mass and cloud temperature, this scale encompasses that of the observed bipolar outflows.

To illustrate the possible luminosity history of a proto-stellar object (PSO) that is first condensing under the influence of its own self-gravity, and subsequently becomes a young stellar object (YSO) that accretes essentially massless surrounding material, let us follow in detail a plausible special case.

There is a very early proto-stellar phase during which the cold cloud is contracting but has not yet formed a substantial opaque core. There will be nevertheless a thermal luminosity due to the efficient radiation of the work done by the force of gravity on the collapsing cloud. Assuming that the gas remains isothermal throughout, it is easy to calculate this luminosity thermodynamically as

$$L_{th} = -a^2 \int \rho \nabla . \mathbf{v}\, dV, \tag{6}$$

or in our standard units for the case $D = 1$ as

$$L_{th} = 9\frac{a^5}{G} \ln \frac{r_s}{R_o}.$$

Here $R_o(t)$ is an inner cutoff radius that coincides with the small but growing opaque core of the cloud. If one supposes that $a \approx 0.2\ km\ s^{-1}$ as below then this luminosity is only $\approx 2 \times 10^{-3} L_\odot$ if $R_o/R_s = 10^{-8}$, and it decreases slightly as the opaque core grows. It increases rapidly with the ambient temperature however and it will be somewhat larger for the flatter density profiles, as may be calculated from the formulae above.

During the later proto-stellar phase the thermal luminosity due to the isothermal compression is generally dominated by the accretion shock luminosity released at the radius of the opaque core R_o, where $\tau \equiv \kappa\rho(R_o,t)R_o \approx 1$. This may be estimated as

$$L_{sh} = (4\pi f)Gm_o/R_o \times A_o(R_o,t),$$

which becomes, on expressing the various quantities in terms of our standard units,

$$L_{sh} = (4\pi f)(2a^5/\pi G)\frac{m_o(t)}{R_o(t)}A_o(R_o,t). \tag{5}$$

We will take the efficiency factor $4\pi f$ as essentially unity in this illustration to allow for a net accretion efficiency of $\approx 10\%$ due to geometrical effects (see e.g. section 3 and references therein). The dependence of m_o on time follows from $\dot{m}_o = (4\pi f)A_o$ with A_o given by equation (4) above and thus, besides the efficiency, only the time dependence of the opaque core is not calculated consistently in this estimate.

Now if we suppose that the PSO is in the Shu isothermal sphere mode, then $D = 1$ and at small radii $A_o \approx 3/2$ by equation (4) so that $m_o \approx (3/2)t$, whence by (5)

$$L_{sh} \approx \left(\frac{9}{2\pi}\right)\frac{a^5}{G}\frac{t}{R_o}.$$

This becomes on putting $R_o = 10^{-6}$ (essentially several times the eventual stellar dimension), and $a \approx 0.2\ km\ s^{-1}$

$$L_{sh} \approx 6.9 \times 10^{34}t\ ergs\ s^{-1},$$

that is of order 10 solar luminosities when the surface initially at r_s falls in $(t = 2/3)$.

On the other hand if the protostar is still primarily a virialized turbulent cloud[32] so that the initial density profile is with $D = 2$, then the same considerations as above yield

$$L_{sh} \approx 1.02 \times 10^2\frac{t^4}{R_o}\left(\frac{2a^5}{\pi G}\right) \approx 3.2 \times 10^{30}\frac{t^4}{R_o}\ ergs\ s^{-1}.$$

Thus choosing once again $R_o \approx 10^{-6}$ and $t = 2/3$, one finds $L_{sh} \approx 160L_\odot$. The onset of the bright period is however rather abrupt compared to the isothermal case above, being a real bang mode near the end of the protostellar phase.

If as above the initial cloud boundary is taken to be rather close to r_s, then it is reasonable to assume that there is a discontinuous decrease in the density beyond this radius and that the mass already accreted in the protostellar phase now dominates that in the surroundings. In this case we may continue to follow the luminous history of what is now a YSO by switching to the appropriate formulae for the accretion of test particle matter with an initial density $\rho_o(r) = (4\pi r_s^2 \rho_{os}/m_s) r^{-2/\delta} \equiv \lambda r^{-2/\delta}$ and $D = 2/3$. Supposing further that $\delta = 1$ gives by equations (4) and (5) with $m_o = 1$

$$L_{sh} = (4\pi f)\lambda R_o^{1/2} \left(1 + \frac{3t}{2R_o^{3/2}}\right)^{1/3} \times \frac{2a^5}{\pi G}.$$

This result shows clearly that in comparison with the protostellar luminosities above this continuing accretion is a 'whimper-bang' mode since the 'whimper factor' $\lambda = 4\pi r_s^2 \rho_{os}/m_s$ should be small when the self-gravity of the surroundings is negligible, and nevertheless the luminosity increases slightly with time. This 'after birth' phase might continue until the supply of surrounding material is exhausted; but since the accreting material originates beyond r_s and hence beyond the direct gravitational domination of the star, the luminosity is rather sensitive to fluctuations of the density, specific angular momentum, and comoving magnetic flux in the surroundings. Such perturbations may provoke the anisotropic instabilities such as discussed in section 3.

All of this discussion ignores in fact the inevitable anisotropy that must be present if inflow and outflow are to coexist. Such anisotropy is likely to come from the increasing effects of angular momentum in the outer core-cloud material, and ultimately perhaps also the magnetic field. The effect of angular momentum added to an initial Bondi flow has been studied numerically[10),11)] . The results show core accretion and the formation of *thick* discs with maximum scales of order r_s, which are maintained dynamically in a sort o f convective circulation of the cloud material. The eventual accretion of such 'storage discs' is likely to be the second, longer lived phase of young stellar activity. Section three discusses the existence of a sort of 'bipolar instability' provoked by the same effects.

2. Outflow Mechanisms

(i) Radiation Driving

The radiation force per unit mass in an opaque spherically symmetric medium driven by a central luminosity L_* is $\kappa L_*/(4\pi r^2 c)$, where κ is the Rosseland mean opacity. The luminosity may be taken to be constant in a steady state. We equate this specific force to the acceleration in a radially accelerating outflow $v(dv/dr)$, and then integrate this equation times the constant mass flux $4\pi r^2 \rho v$ from zero to a radial optical depth τ to obtain the radial component of momentum flux imparted to the layer of optical thickness τ as $F_\tau = \frac{\tau L_*}{c}$. Taking into account that the photons will not all be moving purely radially in an opaque medium, reduces this estimate by about a factor of 3. This is of course the basic way in which the envelope of a star supports itself.

All of this is fine, but the essential question is rather how quickly are the photons diffused in frequency into gaping spectral holes? If for example the initial photons are absorbed by cool dust grains after very few scatterings or high temperature absorptions and reemitted to escape directly in the IR (the Rosseland mean is dominated by the most transparent spectral regions), then the mechanism is defeated . Thus we infer that such a momentum flux must be established in a region where the 'scattering' plus thermal absoption opacity is greater than the dust opacity by the requisite factor τ . Such a region is likely to be close to the star, depending among other things on the radius of grain formation. *It may in the limit be the source of the high velocity wind that is frequently invoked* to explain the outflows.

The requirements on the optical depth are most severe for the low luminosity sources where factors of 10^4 or so are necessary[12]. This can only be true rather close to the 'stellar' photosphere. It may be rather that we have to invoke a 'whimper' accretion mode wherein the current outflows were driven by an earlier more vigorous luminosity and larger opacity. If so then in figure 1[12] , the low luminosity sources (say $L_* < 10^{2.5} L_\odot$) have to be shifted horizontally by some step (roughly constant?) to meet the true radiation driven line presumably delineated by the high luminosity sources.

But what is this 'radiation driven line'? If we could deduce it a priori, then the shift introduced above might provide a direct measure of the accretion age according to the theory of section 1. It turns out that the slope at least may be simply calculable.

Much can be learned simply by placing a point source of constant luminosity L_* inside an opaque (at least in the inne r regions we assume LTE) self-gravitating medium. The angular dependence of the flow and such questions as the asymptotic velocity will be discussed elsewhere, but it is instructive to carry out a dimensional analysis. From L_*, G, and the radiation constants one can construct more or less uniquely:

A characteristic mass[13]; $m_o \equiv \sqrt{3k^4/(a\mu^4 G^3)}$, which is almost exactly $1 m_\odot$ for a mean molecular mass μ of 2 amu (this might more appropriately be 1 in this phase), and which amusingly is also expressible as $\sqrt{45/\pi^2}\, m^3_{planck}/\mu^2$. It is really a kind of self-gravitating 'Eddington' mass, given L_* and the diffusion limit.

A characteristic scale; $r_o^2 \equiv (3k^4/a\mu^4 G^{9/5}) L_*^{-4/5}$, which is numerically $r_o = 3.7 \times 10^{15} (L_*/L_\odot)^{-2/5}$ cm and is probably an estimate of the scale over which the outflow attains its characteristic velocity.

A characteristic velocity; $V_o \equiv (GL_*)^{(1/5)}$, which is numerically $2(L_*/L_\odot)^{1/5}$ km s^{-1}. This must be distinguished from the maximum velocity in the outflow which must be calculated asymptotically.

A characteristic density follows as $\rho_o \equiv m_o/r_o^3$, or numerically $4 \times 10^{-14} (L_*/L_\odot)^{6/5}$ gm cm^{-3}.

These scales allow us to calculate the characteristic momentum flux in the flow $r_o^2 \rho_o V_o^2$ as $\propto L_*^{4/5}$, the characteristic mass flux $r_o^2 \rho_o V_o$ as $\propto L_*^{3/5}$, and of course the characteristic energy flux $r_o^2 \rho_o V_o^3$ as $\propto L_*$.

These last proportionalities are then a relatively general estimate of the slopes of 'radiation driving' lines in the three planes of interest. The observational measures are a slope of 0.6 in the mass flux- luminosity plane[14], which is as expected (ignoring error!), and more recently[12] 0.69 ± .05 in the momentum flux - luminosity plane, and 0.8 ± .06 in the energy flux-luminosity plane. These latter two measures are rather flatter than expected above. However in each case an interpretation of the data wherein the sources with luminosity greater than $\approx 10^{2.5} L_{\odot}$ define the radiation driving lines with slopes close to the predicted values, while the low luminosity sources define a second line with the same slope but shifted horizontally to higher luminosities, is possible. It is particularly compelling in the energy flux luminosity plane[12].

I conclude then that although the case is not proven, since no working detailed models yet exist, there is some support for radiation driving.

(ii) Stellar Winds

Snow plough or thin shell models[15],[16] have led to a clear discussion of the wind-ambient medium interface in terms of energy-driven or momentum-driven outflows. This picture has been tested against the observed 6cm radio emission and the observed correlations between L_*, and the two mechanical fluxes in the CO outflows[12]. It is concluded that all constraints are met by fast ($500 - 1000 km\ s^{-1}$) mostly ionized winds whether the ultimate interaction be energy or momentum driven, and by low velocity ($300 km\ s^{-1}$) mostly neutral, momentum driven winds that are subsequently shock ionized. The energy driven case is the most efficient relative to the observed bolometric luminosity in the IR. However it requires delayed cooling, which seems problematical in a dense expanding wind. A similar problem is posed by the remark[12] that ionizing photons at the Balmer limit lead to predicted 6 cm emission that is close to that observed. This suggests that high temperatures must be maintained in the wind region so as to populate the Balmer ground state and that the wind is optically thick. Thus radiative driving may play a role and in fact the observed[12] correlation between the 6 cm emission and L_{CO} is reminiscent of that found[17] for extra-galactic bipolar outflows, between the mechanical lumino sity of the outflow and the nuclear narrow line luminosity.

Another model[18] treats both the temperature and opacity problems for the high luminosity sources. The radiation from a polar accretion shock heats a 10 au cavity in a thick accretion disc that intermittenly 'backfires' along the polar axis. It predicts outflows to be associated with soft x-ray sources however, at least when one is looking down the polar axis in an outburst phase. Admittedly this phase is only thought to last a few years, and the moving object found recently[19] in Cepheus A bears some ressemblence to the type of ejected object that is predicted .

(iii) Magneto-Disc Driven Outflow

These are wind generation models[20],[21] wherein a centrifugally driven outflow is launched from the open magnetosphere of a Keplerian disc. The equatorial disc material is dense and dominates the magnetic field (super Alfvénic) but, just as is the case for the Sun, there is a gradual transition with height to a magnetically dominated (sub Alfvénic) 'corona' (of relatively low temperature). The interesting idea is that the angular momentum carried off by the spun up material permits in turn the steady inflow of material in the disc. Thus the wind mass flux becomes related to the desired accretion rate onto the central object. There seems to be no clear opinion as to the phase in which this disc phenomenon occurs, but it may of course operate at various times on different scales.

The most detailed ideal MHD model[20] is that of a 2D steady flow. Each flux tube is defined by the cylindrical radius of its foot point in the disc, r_{fp}, and boundary conditions at the disc are fixed simply by means of conservation laws. Although a family of non-self-similar models is found, there is no real matching to the boundary conditions either at infinity (in cylindrical radius) or at the protostellar boundary layer. However the authors do select a model with an axial current flow that is constant with disc radius as the one that avoids both central and surrounding singularities. In their preferred example the asymptotic outflow velocity $v_\infty \propto r_{fp}^{-1}$, where the value is around 41 km s^{-1} at 1 au. Thus this is really a kind of jet model where the high velocities are produced on rather small scales. The mass outflow in the wind is very small compared to the mass flow through the disc, by the square of the lever arm ratio r_{fp}/r_A (r_A is the distance of the Alfvén point on each flux tube from the axis) since this is the ratio of the specific angular momentum carried by a mass element at each end of the 'lever'.

The preceding treatment ignores the necessary disc structure and internal dissipation. Assuming ambipolar diffusion in a weakly ionized disc, one finds[22] a consistent vertical structure that can eventually be matched onto the centrifugal type models, and which is correctly sub-Keplerian in the disc mid-plane. It should be noted however that they believe that this applies on much larger scales than the inner few au. This latter region they expect to be dominated by Ohmic diffusion and is really the beginning of the boundary layer. At 100 au, they suggest a mid-plane density of $10^{10} cm^{-3}$. The thermal structure of the disc as a function of radius has also been calculated[23]. It is found that the ambipolar heating in such a weakly ionized disc can maintain temperatures near $10^4 K$ out to distances approaching 1000 au. This has the virtue of explaining the forbidden line emission in the disc, although it has also been argued[24] that the recollimation of the centrifugal winds will produce these lines in an oblique shock structure. Such large discs are virtually identical in location to the 'storage' discs discussed previously, except that they are Keplerian. They might be the next evolutionary phase after extensive internal dissipation and cooling of the thick discs.

These models are not without their difficulties. The most worrying of these may be the boundary condition at infinity which must serve to hold the disc magnetosphere open. For unlike solar wind type models where the open field is 'combed' out by an organized differential flow, it is rather the open field here that must create the large scale flow and so it must be otherwise created. Such fields are subject to various instabilities, of which the pinching or recollimation mode and the kink and helical instabilities are just a few examples. The non-linear relaxation of dominant magnetic fields to either a force free or an equipartition configuration is another. Moreover the open field is necessarily anchored both at the Keplerian disc and at infinity and so it is subject to strong 'twisting'. It is not clear that the open field structure can be maintained in the presence of such effects, even in the mean.

There is a variant[25),26)] of these models that was also suggested previousl y in the context of extra-galactic sources[27)]. Here a magnetic field is wound up in the disc near an Alfvénic point until a magnetic explosion is driven vertically in both directions along the axis. Angular momentum is extracted during this process so that material falls onto the star simultaneously. Unlike the centrifugal models, the mass flux is equally balanced between the accretion and the outflow. The asymptotic velocity is limited however to about twice the Keplerian velocity at the ejection radius. The model produces a time dependent (bursting) jet model. The scales at which high velocities are produced are comparable to the stellar radius so that this is a near boundary layer phenomenon in contrast to the disc models discussed above. Nevertheless this model avoids having to maintain the globally ordered magnetic field.

Overall I feel that it is not very satisfying that a Keplerian disc should be inserted as an ad hoc component, separate from both the surrounding outflow and the distant accretion. In effect the study of the vertical velocity structure of the disc suggests that we seek to integrate it into the combined inflow/outflow. We turn to such a model in the final section.

3. Bipolar Circulation Models

An analytic example of a new class of model has recently been described[28)]. The essential characteristic of the class is to represent the central point in centrally symmetric accretion flow as a saddle singularity rather than as a node. That is, the spherically symmetric nodal 'Bondi' type accretion meridional stream lines are parametrically unstable to the development of hyperbolic circulation under the addition of rotation and/or a magnetic field. In the steady state, the magnetic field is parallel to the stream lines. Since the flow is super-Alfvénic everywhere the stability of the global structure is maintained by the familiar 'combing' of the magnetic field due to the differential motion. The self-similar structure of the stream -field lines does not strictly match an arbitrary boundary condition at infinity, but this symmetry seems to be a natural small scale limit of a more general self-gravitating circulation or 'convection' flow. I call it a circulation flow since the material is not accreted unless it lies on those relatively few stream lines that physically intersect the stellar disc. It is in this way that these models minimize the luminosity associated with a massive outflow/inflow, in contrast to the low efficiency disc wind models. One expects that they should be mainly relevant in an early post protostellar formation phase as the more distant, high specific angular momentum, material falls in.

In addition to the meridional behaviour, each stream-field line in the bipolar outflow version of these models makes a spiraling approach to the axis roughly parallel to the equatorial plane and then emerges in the form of a conical helix wrapped about the axis of symmetry. Interestingly enough, there is an alternate mode wherein the sense of the motion is reversed.

In order to produce realistic models of bipolar outflows including the asymptotically fast velocities, it seems that the models must be worked out with self-gravity and radiative heating included. However the discovery of sources such as VLA 1623[29] with large relatively uniformly distributed external masses stimulated[28] a reassessment of an analytic solution previously discussed[30]. This 'toy' model is incompressible, viscous and does not produce the requisite velocities at large distances, but it does illustrate nicely the behaviour characteristic of this class of model. Figure 1 shows on the left the meridional stream-field lines for a typical case, while on the right it shows the pressure contours and the pressure in a gray scale representation with the lighter shades representing the higher pressure. One sees that a thick pressure disc forms as a result of the inflow and as a cause of the outflow. In effect the material falls in and rebounds into a bipolar pattern rather than attain the star radially . Most material 'misses' the target as it were. If as it turns the corner some free energy is added, then reasonable velocities at infinity may be attained. The bottom image of Figure 1 shows the path in space of one of the self-similar family of stream-field lines.

Acknowledgements

I am grateful to Thierry Montmerle for his invitation and for realizing the importance of mountains to a cold universe, and to Philippe André for discussion. The work was supported by the Canadian NSERC.

Figure 1

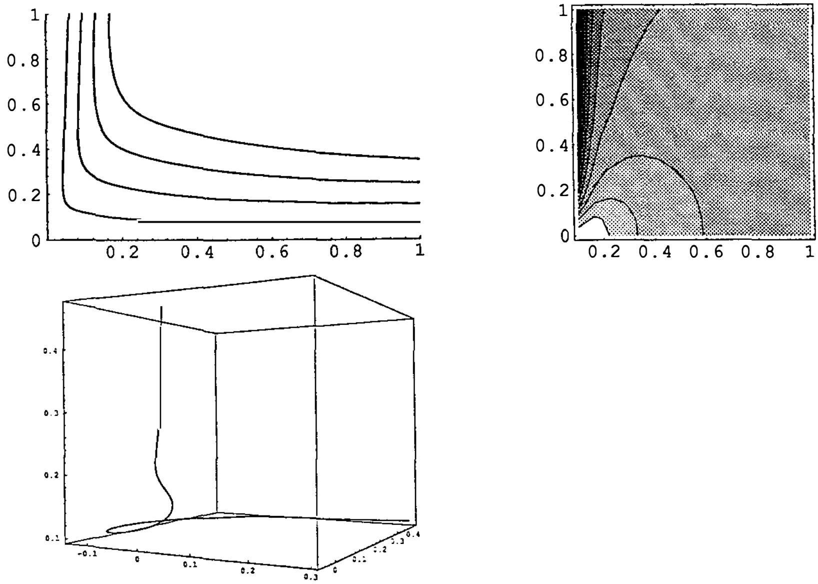

References

1. Shu,F.H. 1977. Ap.J.214:488.

2. Shu,F.H.,Adams,F.C.,Lizano,S.1987. Ann.Rev.Astron.Astrophys.25:23.

3. Chia.T.T.1978. MNRAS. 185:561.

4. Lynden-Bell,D.,Lemos,J.P.S.1988. MNRAS.233:197.

5. Henriksen,R.N.1989. MNRAS.240:917.

6. Carter,B.,Henriksen,R.N.1989. Annales de Physique. 14:47.

7. Penston,M.V.1969. MNRAS.144:425.

8. Larson,R.B.1969. MNRAS.145:271.

9. Henriksen,R.N.1986. Ap.J.310:189.

10.Clarke,D.,Karpik,S.Henriksen,R.N.1985.Ap.J.(supp.)58:81.

11.Loken,C.1986.MSc.thesis, Queen's University at Kingston,Ontario.

12.Cabrit,S.,Bertout,C.1992.Astron.and Astrophys.261:274.

13.Chandrasekhar,S.1984.Science 226:497.

14.Levreault,R.M. 1988.Ap.J.330:897.

15.Kwok,S.,Volk,K.1985.Ap.J.299:191.

16.Dyson,J.E.1984.Ap&Sp.Sci.106:181.

17.Rawlings,S.,Saunders.R.1991.Nature 349:138.

18.Choe,S.-U.,Henriksen,R.N.1986. Ap.J.305:131.

19.Hughes,V.A. 1993.Astron.J.105:331.

20.Pelletier,G.,Pudritz,R.E.1992.Ap.J.394:117.

21.Blandford,R.D.,Payne,D.G.1982. MNRAS.199:883.

22.Wardle,M.,Königl,A.1993.Ap.J. June 10.

23.Safier,P.N.1993.Ap.J.May 1.

24.Gomez de Castro,A.I.,Pudritz,R.E.1992.Ap.J.397:L107.

25.Lovelace,R.V.E.,Berk,H.L.,Contopoulos,J.1991.Ap.J.379:696.

26.Lovelace,R.V.E.,Romanova,M.M.,Contopoulos,J.1993.Ap.J.403:158.

27.Henriksen,R.N.,Reinhardt,M.1977.Ap.&Sp.Sci.49:3.

28.Henriksen,R.N.,Valls-Gabaud,D.1993. MNRAS, December.

29.André,P.,Ward-Thompson,D.,Barsony,M.1993.Ap.J.406:122.

30.Henriksen,R.N.1987.Ap.J.314:33.

31.Bonnor,W.B.1956. MNRAS.116:351;Ebert,R.1957,Z.Ap.42:263.

32.Henriksen,R.N.,Turner,B.E.1984.Ap.J.287:200.

EVIDENCE FOR DISKS AROUND HERBIG AE/BE STARS

T.P. Ray
School of Cosmic Physics
Dublin Institute for Advanced Studies, Ireland

ABSTRACT

The Herbig Ae/Be stars are thought to be the intermediate mass counterparts of the T Tauri stars. It is now clear that these two groups share a lot of properties in common and it would seem that a significant fraction are surrounded by circumstellar disks. The presence of such disks manifests itself in a number of ways not only by their expected infrared excess but also from optical spectroscopy. For example, we see not only "veiling" of absorption lines but the occulting effect of these disks on the forbidden line emission. The most heavily enshrouded stars appear to be the most active as determined for example by their degree of outflow activity. The "activity level" of their disks, however, could be overrated due to underestimates of A_V, this may account in part for their seemingly large values of $\dot{M}_{acc}$.

Although a lot of effort has gone into understanding low mass formation, relatively little is known about how intermediate mass stars ($2M_\odot < M_* < 10M_\odot$) form as emphasised for example by Palla[1]. This situation is beginning to change. Herbig [2] was the first to identify a group of spectral type B-A stars which he thought might be the higher mass counterparts of the T Tauri stars. They showed similar spectroscopic properties such as strong Hα emission (often with P Cygni profiles) and Ca II K and NaI D lines, et cetera. In addition, Herbig stipulated that to be a member of this group, the star had to be associated with a dark cloud and reflection nebulosity. These conditions virtually ensured that the"Herbig Ae/Be stars" were young stellar objects (YSOs) although this conclusion has been challenged up to relatively recently , see for example the review by Catala[3].

Within the past few years it has become clear that Herbig Ae/Be stars share a large number of other properties in common with T Tauri stars such as infrared excesses in their spectral energy distribution (SEDs), Herbig Haro (HH) outflows, a high degree of polarisation, radio continuum emission indicative of a wind, as well as other features usually associated with higher mass star formation such as the presence of water masers[4]. The reader is referred to several reviews of the properties for details[1),3),5]. Here we wish only to concentrate on one facet of their physics: the evidence that they are surrounded by disks.

Most of this evidence is indirect, for example optical studies of Herbig Ae/Be stars have shown us that they are associated with HH emission. Occasionally this is in the form of highly collimated jets such as LkHα 198[6] or LkHα 234[7] but often the emission is much more poorly collimated as for example in MWC 1080[8]. Either way, there is a clear association between such emission and the presence of a disk[9]. An alternative approach is to examine their SED[10]. Here we see the infrared excess expected of such disks (see Fig. 1) but in addition a feature pointed out by Hillenbrand et al.[10] i.e. a dip or inflection around 2-3 microns. The origin of this feature remains uncertain but it has been variously attributed to the sublimation of dust as well as magnetospheric accretion[10]. The SEDs of Herbig Ae/Be stars can be broadly classified into 3 classes[10], Group I have a $\lambda F_\lambda \propto \lambda^{-\frac{4}{3}}$, Group II have a flat or rising spectrum (at least between 10-100 μm, while Group III have virtually a blackbody spectrum. Group III may be the Herbig Ae/Be star equivalent of the weak-line T Tauri stars although this is far from certain. There does appear to be at least a small number of stars classified as Herbig Ae/Be stars that are not young and may in some cases be "ordinary" Be type stars. A $\lambda F_\lambda \propto \lambda^{-\frac{4}{3}}$ spectrum can be equally attributed to a "reprocessing" disk or to one that this actively accreting[12]. It is impossible to distinguish between these two possibilities on the basis of the SED alone in the mid to far infrared. Obviously a pure reprocessing disk cannot reprocess more energy than is incident upon it from the star. This limit, in the thin disk approximation, is $L_*/4$ so the clear way to distinguish between these possibilities is to measure L_* by determining the photospheric contribution.
This method is however fraught with difficulties. The usual thing that is done is to measure E(B-V) and, given the spectral type, one can determine the visual extinction A_V and hence derive the true apparent photospheric luminosity. For many of these stars, however, particularly those that are heavily enshrouded in dust, the spectral type is either unknown or is thought to lie within a wide range of spectral classes. Moreover E(B-V) values may be a poor gauge of the extinction, broadband photometry measures

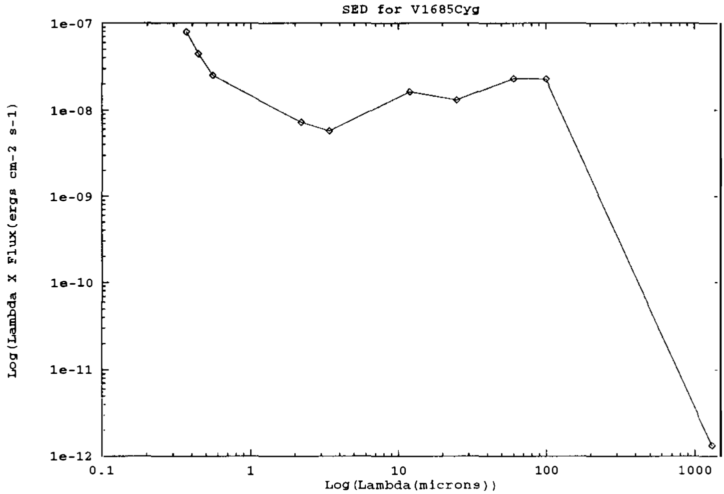

Figure 1: The spectral energy distribution for V1685 Cyg[12]. Note the inflection in the spectrum at about 3 μm and the sharp drop in λF_λ at mm wavelengths. This is a Group II object (see text)

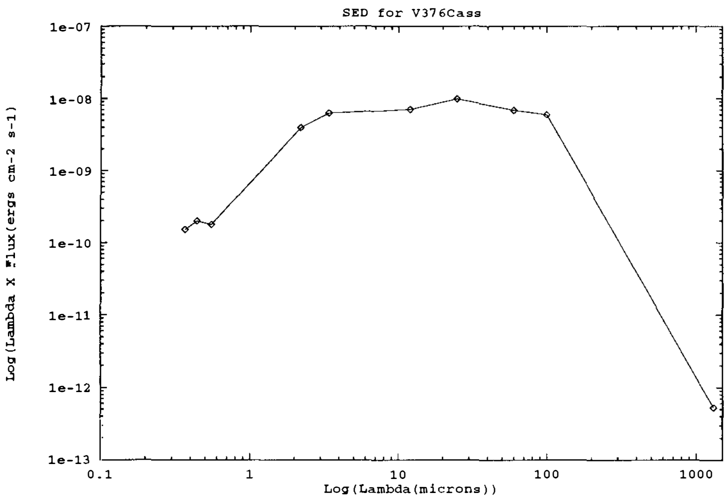

Figure 2: The spectral energy distribution for V376 Cass between the optical to mm regimes[11]. This type of SED would be classified as belonging to that of a Group II star. The extinction however towards this YSO could be grossly underestimated (see text) so that the photospheric contribution might be much larger.

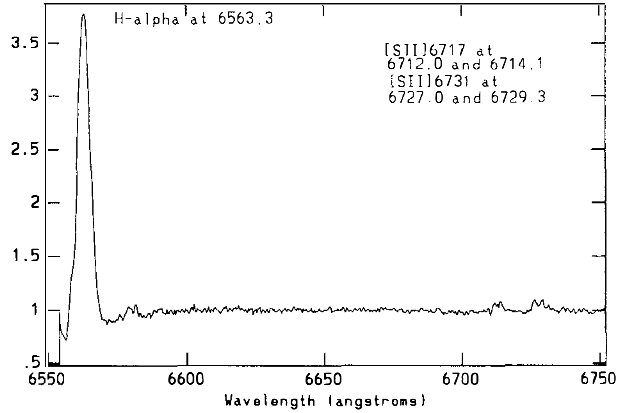

Figure 3: The spectrum of LkHα 233 between Hα and the red [SII] doublet[11]. Note only blueshifted [SII] emission is observed. When seen forbidden line emission is either highly blueshifted or at a velocity close to the systemic velocity.

not only the contribution of the photosphere but any "continuum " component due to the disk. That such a component is present, and is important, is clear from the strength of optical veiling in Herbig Ae/Be stars which is only now beginning to be explored[11]. Since, as in the case of the T Tauri stars, there is a "blue continuum", attributable for example to the boundary layer between the disk and the star or , for example, accretion columns, this would lead to an underestimate of A_V. We note also that the that the relationship between E(B-V) and A_V depends on assuming that the grains around Herbig Ae/Be stars are similar to those in the interstellar medium. In fact recent observations[11] suggests that this is not the case. Thus SEDs such as the one illustrated in Fig. 2 for V376 Cass are highly uncertain in the optical regime. It could be the case that the photospheric contribution is much larger and the SED even disk-like in the near to far-infrared. Group II SEDs have been attributed to a combination of star+disk+envelope[10),13)]. Whether some Herbig Ae/Be stars are truly Group II might be questioned in at least a number of cases. Finally we mention one other effect that should caution us against using E(B-V) values. For some stars, like R Mon, it is apparent that we do not observe the star directly but instead scattered emission; again this will make the star look bluer than it truly is and hence contribute to an underestimation of A_V. All of these effects will clearly be most evident in the heavily enshrouded stars i.e. the Group IIs which are presumably still in the early stages of formation. That they are still surrounded by relatively large quantities of dust and gas and presumably accreting is evidenced not by the very high A_V (even if underestimated) and their high polarisation but the greater chance of finding optical outflows amongst this group[11]. Note also that underestimates of the true luminosities of these stars (hence their masses and, more importantly, their true contribution to the disk luminosity via reprocessed radiation) could be responsible for what appears to be anomalously high estimates of mass accretion rates[13].

Recently we have undertaken a spectroscopic study of Herbig Ae/Be stars not only to quantify the effects of veiling and determine their photospheric class more precisely but to examine their forbidden line emission[11]. Forbidden line emission is only seen in a relatively small number of cases (about 20%) of the stars surveyed i.e. somewhat less frequently than with classical T Tauri stars. In part this can be attributed to the luminosity of the forbidden line emission growing much more slowly with mass than that of the star itself. Thus there is increasingly a contrast problem as the mass of the YSO increases. What is interesting though is that forbidden line emission is very common amongst Group II sources and that, when seen, this emission is either at, or close to, the systemic velocity or is blueshifted i.e. we see the Appenzeller-Jankovics-Östreicher effect[14] in Herbig Ae/Be stars. This effect is generally attributed to the presence of a disk obscuring the redshifted emission (see Fig. 3).

It is now evident that Herbig Ae/Be stars are, as Herbig originally claimed, the higher mass counterparts to the T Tauri stars. Close analogies can be drawn between the two groups. These stars, however, may in time provide a vital link in our understanding of how high mass and low mass stars form.

References

1) Palla, F.: 1991, in *Fragmentation of Molecular Clouds and Star Formation*, eds. E. Falgarone et al., (IAU), p.331

2) Herbig, G.: 1960, ApJS, 4, 337

3) Catala, C.: 1989, in *Low Mass Star Formation and Pre-Main-Sequence Evolution*, ed. B. Reipurth, (ESO, Garching), p.471

4) Palla, F., and Prusti, T.:1993, A&A, 272, 249

5) Ray, T.P.: 1993, in *Kinematics and Dynamics of Diffuse Astrophysical Media*, ed. J. Dyson, (Kluwer), in press

6) Corcoran, D., Ray, T.P., and Bastien, P.: 1993, in preparation

7) Ray, T.P., Poetzel, R., Solf, J., and Mundt, R.: 1990, ApJ, 357, L45

8) Poetzel, R., Mundt, R., and Ray, T.P.: 1992, A&A, 262, 229

9) Edwards, S., Ray, T.P., and Mundt, R.: 1993, in *Protostars and Planets III*, eds. E.H. Levy and J. Lunine, (University of Arizona press), p.

10) Hillenbrand, L.A., Strom, S.E., Vrba, F.J., and Keene, J.: 1992, ApJ, 397, 613

11) Corcoran, M., Ray, T.P., Sargent, A.I., Beckwith, S.V.W., and Koresko, C.D.: 1993, in preparation

12) Adams, F.C., Emerson, J.P., and Fuller, G.A. (and references therein): 1990, ApJ, 357, 606

13) Natta, A., Palla, F., Butner, H.M., Evans, N.J., and Harvey, P.M.: 1993, Arcetri Astrophysics Preprint n. 19/92

14) Appenzeller, I., Jankovics, I., and Östreicher, R.: 1984, A&A, 141, 108

Geneviève peers at a weird hat.

CIRCUMSTELLAR MATTER IN HERBIG AeBe STARS

Antonella Natta

Osservatorio di Arcetri

Largo Fermi 5

50125 Firenze, Italy

ABSTRACT

The observational evidence for large envelopes and disks in the immediate environment of Herbig AeBe stars are reviewed. In particular, I firstly summarize the results of far infrared observations, then discuss the capability of very small grains (VSG) and policyclic aromatic hydrocarbons (PAHs) to account for the observed mid-infrared fluxes. Finally, I briefly discuss the possibility that the disk properties are deeply affected by the surrounding matter, and suggest that, at least for large number of these stars, accretion may play a less relevant role than previously thought.

1. INTRODUCTION

Herbig Ae/Be stars are early-type emission-line stars associated to optical nebulosities. As first shown by Herbig [1], they are pre-main-sequence stars of intermediate mass and luminosity.

The presence of large amount of circumstellar matter around Herbig Ae/Be stars is shown by a variety of observations. According to the selection criterium first defined by Herbig [1], they are associated to extended optical nebulosities. The average extinction, derived from the reddening of the stellar spectrum, is of the order of 2-3 mag, significantly larger than the values found, for example, in T Tauri stars in Taurus. The spectral energy distributions are characterized by the presence of large infrared excesses. Polarization maps [2][3][4] reveal the existence of extended clouds of dust. Molecular observations show that dense gas is associated to several Herbig Ae/Be stars [5][6][7][8]. On smaller scales, speckle interferometry results indicate that matter exists very near the central stars, with complex geometrical configurations [3][9]. Finally, there is ample spectroscopic evidence of high velocity winds [10], CO outflows [11] and HH objects [12] associated to Herbig Ae/Be stars.

In spite of the large and growing body of observations, up to now most of the information on the circumstellar matter around these stars has been obtained through studies of their spectral energy distributions. Observations in the far infrared [13] and detection of the silicate feature [14] indicate that the infrared excess of Herbig Ae/Be stars is likely due to dust. However, attempts to model it with spherically symmetric dust shells have failed (see, for example, [15][16][17]). Hillenbrand et al.[18] have divided Herbig Ae/Be stars in three groups. Group I includes 29 stars (out of 51) with large infrared excess and spectral energy distribution decreasing with increasing λ in the range 2.2-20 μm. Group II includes 13 objects with flat or raising infrared spectra. Group III is formed by 9 stars with small infrared excess, probably arising from free-free emission. Hillenbrand et al. propose that in Group I stars the infrared excess is due to a geometrically flat, optically thick circumstellar disk, similar to those advocated for T Tauri stars [19][20]. Natta et al.[16][17] have shown that the spectral energy distribution and the far infrared brightness profiles of some Group II objects can be fit by models where the star and its circumstellar disk are embedded in a large envelope of dust of moderate optical depth.

However, the accretion disk interpretation is not entirely satisfactory. The observed near infrared colours, in fact, are compatible with the disk hypothesis only if the disks have inner holes of several stellar radii [17][18][21]; these, in turn, are not consistent with the high accretion rates derived by various authors, as discussed by Hartmann et al.[22].

In this paper, I will present recent results on some aspects of the star+disk+envelope system. I will first summarize the results obtained from 50 and 100 μm brightness profiles, then discuss the possible role of very small grains and polyciclyc aromatic hydrocarbons. Finally, I will show that disk properties can be changed by the presence of surrounding matter, and how this may affect our estimates of the disk properties themselves.

2. THE FAR INFRARED PROPERTIES OF Herbig Ae/Be STARS

Observations at 50 and 100 μm from the Kuiper Airborne Observatory using a multi-channel scanning photometer have been obtained for a total of 14 Herbig Ae/Be stars [16][17][23]. The system compares a stable, well known point-source profile with a scan across the source; in good signal-to-noise observations, it can resolve objects with FWHM sizes of the order of 10 arcsec. Table 1 summarizes the results available so far. It gives in Column 1 the name of the source, in Column 2 the classification according to Hillenbrand et al.[18], in Column 3 the distance, in Column 4 the bolometric luminosity, in Column 5 the position angle of the scan on the plane of the sky, measured counter-clockwise from the declination axis, in Column 6 the

FWHM at 100 μm in pc, S_{100}, computed assuming that both the source and the point source have gaussian profiles. Typical uncertainties on S_{100} are of 10%.

TABLE 1

FAR–IR SIZES

Source	Group	D (pc)	L ($L_\odot$)	θ (deg)	S_{100} (pc)	Ref.
LkHα 198	II	600	250	60	0.1	17
				165	0.1	17
				258	0.1	17
AB Aur	I	160	80	130	<0.010	23
				220	<0.013	23
MWC 137	I	1300	750	170	0.36	23
				255	0.34	23
LkHα215	I	800	700	173	0 20	23
				262	0.37	23
R Mon	II	800	700	266	0.05	17
				176	<0.06	17
Z CMa	II	1150	8000	320	<0.07	17
CD -42° 11721	II	2000	28000	87	0.40	17
				177	0 30	17
MWC 297	I	450	2000	35	0.12	23
				115	0.15	23
R CrA	II	126	90	70	0.027	17
				160	0.026	17
V1686 Cyg	I	1000	1800	340	0.15	23
PV Cep	II	500	100	115	<0.04	17
				255	<0.05	17
V645 Cyg	II	3500	40000	350	0.37	17
LkHα234	I	1000	550	262	0.10	23
				348	0.18	23
MWC 1080	I	2500	30000	280	0.34	23
				15	0.16	23

Of the objects listed in Table 1, only three (AB Aur, Z CMa and PV Cep) are not resolved at 100 μm, and many are also resolved at 50 μm. S_{100} varies between 0.03 and 0.4 pc, and it is independent of the classification as Group I or Group II sources.

The width of the 100 μm brightness distribution can only be accounted for by a large dusty envelope heated by a central source of radiation. The five Group II resolved sources have been studied in detail by Natta et al.[16)17)], who compared the 50 and 100 μm sizes and fluxes to the predictions of radiation transfer models. The results indicate that the envelopes have moderate optical depth (about 5-10 mag in the visual), large inner holes (in the range 0.01 to 0.1 pc), and density profiles which vary from flat ($n \propto r^{-0.5}$) to steep ($n \propto r^{-2}$).

The scan results rule out the possibility that most of the 100 μm flux is emitted by a circumstellar disk. In this case, and regardless of the physical size of the disk, the 100 μm size would be very small (typically, less than 2 arcsec), and would appear unresolved with the KAO resolution. Note, however, that the data do not rule out the existence of disks, in addition to the envelopes, as long as the disk emission does not dominate over the envelope in the far infrared. Group I objects have been interpreted by Hillenbrand et al.[18)] as pure star+disk systems. However, all the Group I stars listed in Table 1 show a far infrared excess, with respect to the disk predictions, which can naturally be accounted for by the emission of dust in an envelope, more optically thin than those found in Group II objects, but otherwise similar.

Notably, the scan data also rule out the possibility that the fir flux is dominated by the emission of a very cold companion.

Model calculations show that star+envelope models account well for the far infrared, submillimetric and millimetric observations, but they fail to explain the large values of the near and mid-infrared fluxes observed in Herbig Ae/Be stars.

3. THE ROLE OF VSG AND PAH

Envelope models discussed so far include only large grains, such as in the ISM, which are in thermal equilibrium with the radiation field. The possibility that the near and mid-infrared missing flux is emitted by very small grains (VSGs) and polyciclic aromatic hydrocarbon particles (PAHs), mixed to larger grains in the envelope, has been mentioned by Natta et al.[16)17)] and Hartmann et al.[22)]. VSGs and PAHs do not achieve thermal equilibrium with the local radiation field, but are transiently heated by ultraviolet photons, so that they attain temperatures much higher than the larger grains in thermal equilibrium. In fact, they emit most of the absorbed radiation at near and mid-infrared wavelengths. VSGs and PAHs account for the extended near infrared emission in various reflection nebulae [24)]. Their presence in the environment of Herbig Ae/Be stars is suggested by the discrepancy of the 10 μm fluxes between large beam IRAS and small beam ground based observations in several young stars [25)26)], and by the detection of PAH features in some Herbig Ae/Be stars [27)].

Natta, Prusti and Krügel [28)] have examined the role of the VSGs and PAHs in the circumstellar environment of Herbig Ae/Be stars, by computing the spectral energy distribution and the brightness distribution of models where VSGs and PAHs are added to large grains. The envelopes have either A_V=5 mag, as appropriate to Group II stars, or A_V=0.1, appropriate to Group I stars. In all cases, an envelope inner radius of 0.01 pc has been adopted, so that the large grains contribution in the near and the mid-infrared is negligible. Some examples of the spectral energy distributions are shown in Fig.1. The spectra are all quite flat in the range 2-20 μm; the exact shape of the spectrum depends mostly on the amount and size of the VSGs and only little on the envelope parameters.

Two observational tests have been discussed by Natta et al.[28)]. First of all, they compute the ratio $L_{\rm mir}/L_{\rm bol}$, where $L_{\rm mir}$ is defined between 1.25 and 20 μm, as a function of the various model parameters, and compare it to the average observed values. They find that VSGs and

PAHs can provide a significant fraction of the observed luminosity in this range, but not all, unless there is an extremely large amount of very small VSGs. Secondly, they compute the near-infrared colours indexes J-H and H-K and show that the model predicted colours do not fit the observations significantly better than those of models where only large grains, in equilibrium with the local radiation field, are considered.

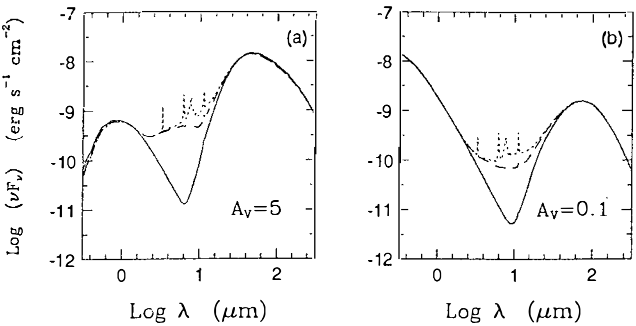

Fig. 1.— Spectral energy distribution for models where VSGs and PAHs are added to large grains. parameters are varied. Panel a: Models with A_V=5 mag. The solid curve is a model with only large grains, the dotted curve one where VSGs are included (relative abundance with respect to the large grains of 10%, minimum and maximum size of VSGs of 5 and 20 Å, respectively. The dotted curve is a model where also PAHs are added. The values of the other parameters are: R_i=0.01 pc, R_{out}=0.5 pc, $n \propto r^{-0.5}$, T_{rad}=15000 K and luminosity of 250 $L_\odot$. Panel b: same for A_V=0.1 mag.

A crucial test of the significance of VSGs and PASHs in the Herbig Ae/Be stars environment may come from studies of the spatial extent of the emission in the range 3 to 10 μm.

4. THE EFFECTS OF THE SURROUNDING MATTER ON DISKS

Good fits to the observed spectral energy distributions of both Group I [18] and Group II objects [16)17] are easily obtained when the emission of the circumstellar disk is taken into account [17].

When the disk parameters are constrained to fit the observations, it is found that the disks must dissipate accretion energy, not just reprocess stellar light [17)18]. This result relies on two different kinds of evidence. Hillenbrand et al.[18] compare the bolometric luminosity of the source, to the stellar luminosity. This last is, in turn, obtained from the observed spectral type and visual magnitude of the star, corrected for extinction, and suffers from severe uncertainties [28]. Natta et al.[17] derive the disk luminosity L_D from the observed value of $L_{\rm mir}$, and estimate the accretion luminosity as $L_{ac} \sim (4 \times L_D - L_{\rm bol})/3$. This procedure, which makes use of more reliable data, neglects the effects of the surrounding matter on the disk emission itself. In fact, a small amount of dust around the disk may contribute significantly to the heating of the outer parts of the disk, by scattering and re-emitting back onto the disk part of the stellar radiation [29]. The result is that the disk spectrum is significantly flatter than the $\nu F_\nu \propto \lambda^{-4/3}$, typical of both accretion and reprocessing disks, and that the disk luminosity may exceed significantly the value $1/4 L_{\rm bol}$ assumed in the derivation of L_{ac}. Fig. 2 shows the spectral energy distribution of a typical Herbig Ae/Be disk, embedded in a thin envelope of dust. The $L_{\rm mir}/L_{\rm bol}$ of such a model is 0.38. When we consider that VSG and PAH can easily absorb and reradiate in the mid-infrared about 20% of the stellar luminosity, the predicted values of $L_{\rm mir}/L_{\rm bol}$ come close to the observed average for Group II objects ($\sim$ 0.6).

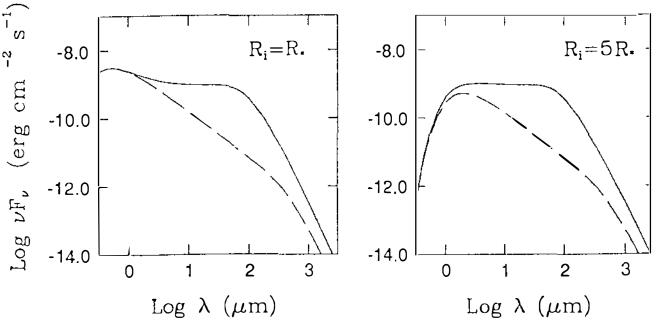

Fig. 2.— Spectral energy distribution for disk models. The dashed curve shows the spectral energy distribution of a disk heated only by direct stellar radiation, the solid curve that of a disk, with the same parameters, which is heated, in addition, by radiation scattered by the surrounding cloud of dust. The dusty envelope has optical depth τ=0.4, a density profile $n \propto r^{-1}$, inner radius of 8 $R_\star$, outer radius of 300 AU. The central star has luminosity $L_\star$=250 $L_\odot$, effective temperature of 15000 K. In Panel a the disk extends to the stellar surface, while in Panel b it has an inner hole of 5 $R_\star$.

Purely reprocessing disks, such as those just described, are not inconsistent with the presence of inner holes, as required to fit the observed near infrared colours. Table 2 compares the properties of two disk models, embedded in an envelope of optical depth 0.4, to those of "naked" disks with the same parameters. In one case the disks extend down to the stellar surface ($R_i=R_\star$), in the other $R_i=5R_\star$. As expected, the near infrared colours of the latter are much closer to the observed values than those of the former. More important, the disk luminosity, when the surrounding matter is taken into account, is much larger than that of "naked" disks, and is still as large as 18% of the stellar luminosity in models with $R_i=5\ R_\star$.

TABLE 2

DISK MODELS

$R_i/R_\star$	τ_{sc}	$L_D/L_\star$	J-H	H-K	K-L
1	0.0	0.25	0.57	0.51	0.73
5	0.0	0.04	1.10	0.90	1.08
1	0.4	0.39	0.68	0.68	1.01
5	0.4	0.18	1.21	1.03	1.39

5. CONCLUSIONS

The results summarized in the previous sections provide further evidence of the fact that there is a large amount of circumstellar matter surrounding Herbig Ae/Be stars, and that its geometrical configuration is quite complex.

We suggest that at least three components must be present, the central star, a circumstellar disk and an extended dusty envelope. Although the 50 and 100 μm scans indicate the existence of an inner cavity, where the dust optical depth is very small, some dust must exist inside this cavity, in the vicinity of the disk.

The resulting spectral energy distribution is deeply affected by the interaction between these various components. Detailed models of star+disk+envelope (including the effect of scattered and re-emitted radiation on the disk heating are taken into account and the emission of VSGs and PAHs in the envelope) need to be computed before conclusions, in particular on the frequency and rate of accretion in Herbig Ae/Be stars, can be reached.

References

1 Herbig, G.H. 1960, ApJS, 4, 337

2 Bastien, P., Ménard, F. 1990, ApJ, 364, 232

3 Leinert, Ch., Haas, M., Lenzen, R. 1991, A&A, 246, 180

4 Piirola, V., Scaltriti, F., Coyne, G.V. 1992, Nature, 359, 399

5 Fuente, A., Martin-Pintado, J., Chernicharo, J., Bachiller,R. 1990, A&A, 237, 471

6 Nakano, M., Kogure, T., Yoshida, S., Tatematsu, K. 1990, PASJ, 42, 567

7 Yoshida, S., Kogure, T., Nakano, M., Tatematsu, K., Wiramihardja, D. 1992, PASJ, 44, 77

8 Fuente, A., Martin-Pintado, J., Chernicharo, J., Brouillet, N., Duvert, G. 1992, A&A, 260, 341

9 Leinert, Ch., Haas, M., Weitzel, N. 1993, A&A, 271, 535

10 Catala, C. 1989, in Low Mass Star Formation and Pre-Main-Sequence Evolution, ed. B. Reipurth (Garching: ESO,), 471

11 Levreault R.M. 1988, ApJS, 67, 283

12 Mundt, R. 1992 in Stellar Jets and Bipolar Outflows, ed. L. Errico and A. Vittone (Kluwer: Dordrecht),

13 The, P.S., Wesselius, P.R., Tjin A Djie, H.R.E., Steenman, H. 1986, A&A, 155, 347

14 Cohen, M. 1980, MNRAS, 191, 499

15 Catala, C. 1983, A&A, 125, 213

16 Natta, A., Palla, F., Butner, H.M., Evans, N.J.II, Harvey, P.M. 1992, ApJ, 391, 805

17 Natta, A., Palla, F., Butner, H.M., Evans, N.J.II, Harvey, P.M. 1993, ApJ, 406, 674

18 Hillenbrand, L.A., Strom, S.E., Vrba, F.J., Keene, J. 1992, ApJ, 397, 613

19 Adams, F.C., Lada, C.J., Shu F.H. 1987, ApJ, 312, 788

20 Adams, F.C., Lada, C.J., Shu F.H. 1988, ApJ, 326, 865

21 Lada, C.J., Adams, F.C. 1992, ApJ, 393, 278

22 Hartmann, L., Kenyon, S.J., Calvet, N. 1993, ApJ, 407, 219

23 Di Francesco, J., Evans, N.J.II, Harvey, P.M., Mundy, L.G., Butner, H.M. 1993, in preparation

24 Sellgren, K. 1984, ApJ, 277, 623

25 Wilking, B.A., Lada, C.J., Young, E.T. 1989, ApJ, 340, 823

26 Prusti, T., Whittet, D.C.B., Wesselius, P.R. 1992, MNRAS, 254, 361

27 Whittet, D.C.B., Williams, P.M., Bode, M.F., Davies, J.K., Zealey, W.J. 1983, A&A, 123, 301

28 Natta, A., Prusti, T., Krügel, E. 1993, A&A, in press

29 Hamann, F., Persson, S.E. 1992, ApJS, 82, 285

30 Natta, A. 1993, ApJ, in press

FU ORIONIS OBJECTS AND MOLECULAR OUTFLOWS

Scott J. Kenyon
Harvard-Smithsonian Center for Astrophysics
60 Garden Street, Cambridge, MA 02138 USA

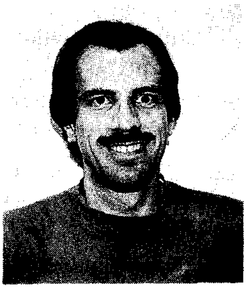

ABSTRACT

FU Orionis variables – FUors – are pre-main sequence stars in which the central star accretes mass from a circumstellar disk at a high rate. FUors also eject material in high velocity winds. The momentum in these winds is sufficient to power a typical molecular outflow providing a young star accretes most of its material through a circumstellar disk. Recent observations suggest FUors do mostly occur during early stages of the star formation process, when the central star-disk system lies deeply embedded within the collapsing circumstellar cloud. The FUor state also appears to last long enough for a young star to accrete a large fraction – perhaps all - of its mass from a circumstellar disk.

1. Introduction

The FU Orionis variables – FUors – are eruptive pre-main sequence stars (Hartmann 1991). Most FUors have undergone 3–6 mag optical eruptions and resemble rapidly-rotating F–G supergiants on optical spectra. These objects also show distinctive optical and/or near-infrared reflection nebulae; large ultraviolet and infrared excesses of radiation; wavelength dependent spectral types; broad, blueshifted Hα and Na I absorption lines; and "double-peaked" absorption line profiles at optical – and sometimes infrared – wavelengths.

We have interpreted observations of FUors with viscous accretion disk models (Hartmann 1991). A disk naturally accounts for the broadband spectral energy distribution (SED), the wavelength dependent spectral types, and the double-peaked absorption profiles. A disk wind explains the blueshifted absorption features; our models suggest this mass loss occurs close to the inner edge of the disk (Calvet *et al.* 1993). Finally, some type of circumstellar envelope – probably material still falling into the disk – produces the ubiquitous reflection nebulae and the large far-IR excess emission (Kenyon & Hartmann 1991).

The FUor state is an exciting time when a young star can accrete a large amount of mass *and* eject a fair amount of momentum and energy into the surrounding molecular cloud. For example, the central star in FU Ori itself has accreted ~ 0.01 $M_\odot$ and has lost material with a momentum of ~ 0.3 $M_\odot$ km s^{-1} since its eruption began in 1936. These values represent a modest fraction of typical stellar masses, $M_\star \sim 0.5$ $M_\odot$, and outflow momenta, $(Mv)_o \sim 1$–100 $M_\odot$ km s^{-1}, but a FUor event lasting several millenia – or a series of eruptions – could have a significant impact on the central star and the surrounding cloud. The goal of this paper is to estimate the importance of FUor events on stellar masses and molecular outflows.

2. Molecular Outflows and Class I Sources

Current arguments suggest a low mass star accretes most of its mass during an infall phase, when material from the cloud core collapses into a central star-disk system (Shu *et al.* 1987). The cloud is opaque at optical wavelengths and radiates most of the disk and stellar radiation at far-IR wavelengths. IRAS detected many of these class I sources in nearby molecular clouds, and they usually comprise $\sim$ 10% of the pre-main sequence stellar population. These objects appear closely associated with extended optical and near-IR reflection nebulae, lie at the centers of dense cloud cores, and often power low velocity molecular outflows and higher velocity optical jets and Herbig-Haro (HH) objects. They are also among the youngest stellar sources in nearby molecular clouds, with estimated ages of ~ 1–3×10^5 yr (Lada 1991).

The origin of the energetic outflows remains uncertain, although this activity likely begins during – or perhaps even before – the class I phase (e.g., André *et al.* 1993). The available observations show reasonable correlations between the outflow's mechanical luminosity and the central source luminosity, $L_\star$. The initial energy flux in the wind seems comparable to the total system luminosity, which appears to rule out models involving radiation pressure, thermal expansion of a hot corona, or dissipation of Alfvén waves (e.g., Cabrit 1989). Centrifugal winds or disk winds can account for the observed kinematics and luminosity correlations, and both mechanisms require accretion energy to drive the outflow. Indeed, observations of T Tauri stars and FUors suggest the mass loss rate in the wind is closely tied to the mass accretion rate through the disk: $\dot{M}_w \sim \alpha \dot{M}_a$, with $\alpha \sim 0.1$ (e.g., Natta & Giovanardi 1991; Hartmann 1991).

Can disk winds provide enough momentum for a typical outflow? To answer this question, assume that the mass loss rate in the disk wind scales with the accretion rate, as in the previous paragraph. The total momentum in the wind – over a time scale τ – is then $(Mv)_w \sim \dot{M}_w \, \tau \, v_w \sim 0.1 \, \dot{M}_a \, \tau \, v_w$, where v_w is the wind velocity. If the disk processes most of a typical stellar mass, then $M_\star \sim \dot{M}_a \tau$, so the outflow momentum is

$$(Mv)_w \sim 20 \, (M_\star/M_\odot) \, M_\odot \, \mathrm{km\,s^{-1}} \tag{1}$$

for a typical wind velocity of 200 $\mathrm{km\,s^{-1}}$. The observed range of outflow momenta – $(Mv)_o$ = 1–100 $M_\odot \, \mathrm{km\,s^{-1}}$ (Fukui 1989) – requires typical stellar masses of $M_\star \sim 0.1$–5 $M_\odot$ if the flows conserve momentum. Thus, *a young stellar system must eject ~ 10% of its final mass to produce a typical molecular outflow.* A disk wind can power the outflow if a young star accretes most of its material through the disk.

Current observations suggest some fraction of a typical stellar mass does flow through a circumstellar disk before landing on the central star. Several groups estimate accretion rates of $\sim 10^{-7} \, M_\odot \, \mathrm{yr^{-1}}$ for the pre-main sequence T Tauri stars (e.g., Hartigan *et al.* 1991). Source statistics suggests an age of $\sim 10^6$ yr for these objects, so a typical young star accretes ~ 0.1 $M_\odot$ during this optically visible phase of evolution. FUors represent the most active disk accretion phase of pre-main sequence evolution; both the accretion and mass loss rates are a factor of ~ 1000 larger than for T Tauri stars. Thus, a young star might accrete *all* of its mass from a disk if FUors preferentially occur during the class I phase – when the infall occurs – and if the FUor lifetime is a significant fraction of the class I lifetime of 1–3 $\times 10^5$ yr.

3. Age and Lifetime of FUors

As a group, FUors have many observed features in common with class I sources. All FUors possess very distinctive optical and near-IR reflection nebulae (e.g., Goodrich 1987). Nearly all FUors display large far-IR excesses and drive molecular outflows (Kenyon & Hartmann 1991; Evans *et al.* 1994). Finally, at least 1/3 are associated with jets or HH objects (Reipurth 1991). These properties suggest FUors are much younger than most T Tauri stars – which usually have none of these features – and more similar to class I sources. Thus, FU Ori objects generally occur during the main accretion (class I) phase and have typical ages of $\tau \sim$ a few $\times 10^5$ yr.

FUor statistics are very crude, because only 11 examples are known within ~ 1 kpc. If we have discovered all FUors that have occured since the discovery of FU Ori (~ 50 yr), the FUor frequency is 0.2 $\mathrm{yr^{-1}}$. The local star formation rate within 1 kpc is roughly 0.01 $\mathrm{yr^{-1}}$, so a typical young star must undergo at least 20 eruptions to reach the observed FUor frequency (e.g., Hartmann 1991). If a typical eruption lasts ~ 100 yr, a star accretes ~ 0.2 $M_\odot$ – almost half of a typical stellar mass – in FUor eruptions.

The FUor frequency needed to accrete *all* of a typical stellar mass can be estimated by assuming that a young star spends its class I lifetime either in the high accretion – FUor – state **or** in a state with $\dot{M} \sim 0$. The quiescent state lasts until the disk mass becomes high enough to trigger an outburst; the outburst continues until the disk empties of material. This cycle repeats until infall from the cloud ceases. The cause of this cycle may not be clear, but it is simple to estimate the fraction of time in the FUor state from the ratio of the infall rate to the FUor accretion rate: $f \sim \dot{M}_i/\dot{M}_{FU}$. FU Ori disk models suggest $\dot{M}_{FU} \sim 10^{-4}$ $M_{\odot}\,yr^{-1}$, so $f \sim 0.05$ for a typical infall rate of $\dot{M}_i \sim 5 \times 10^{-6}$ $M_{\odot}\,yr^{-1}$. Thus, a young star must spend $\sim$ 5% of its class I lifetime as a FUor to accrete all of its mass in this high $\dot{M}$ state.

The discussion in §2 established that a disk wind could power a typical molecular outflow if a young star accretes most of its mass from a circumstellar disk. Thus, FUor eruptions can power molecular outflows if 5% of class I sources are FUors. This possibility can be tested by deriving the FUor frequency among class I sources in many molecular clouds. For example, the Taurus dark cloud contains $\sim$ 20 class I sources and one object – L1551 IRS 5 – in the FUor state, which agrees with the simple prediction (perhaps fortuitously). Source statistics for class I sources in other clouds are not as good as in Taurus and the FUor population in these clouds is even less well-known. However, both of these numbers can be improved with sensitive photometric and spectroscopic surveys of nearby molecular clouds to identify class I sources and then determine which – if any – of these objects display the characteristic spectroscopic properties of FUors. If the FUor frequency among class I sources turns out to be more than a few per cent, then FUors may represent the main accretion phase of early stellar evolution.

4. References

Adams, F. C., Lada, C. J., & Shu, F. H. 1987, ApJ, 312, 788

André, P., Ward-Thompson, D., & Barsony, M. 1993, ApJ, 406, 122

Cabrit, S. 1989, in *ESO Workshop on Low-Mass Star Formation and Pre-Main Sequence Objects* ed. B. Reipurth (Garching, ESO) p. 365

Calvet, N., Hartmann, L., & Kenyon, S. J. 1993, ApJ, 402, 623

Evans, II, N. J., Balkum, S., Levreault, R. M., Hartmann, L., & Kenyon, S. J. 1994, ApJ, submitted

Fukui, Y. 1989, in *ESO Workshop on Low Mass Star Formation and Pre-Main Sequence Objects,* ed. B. Reipurth (Garching: ESO), p. 95

Goodrich, R. 1987, PASP, 99, 116

Hartigan, P., Kenyon, S.J., Hartmann, L., Strom, S.E., Edwards, S., Welty, A.D., & Stauffer, J. 1991, ApJ, 382, 617

Hartmann, L. 1991, in *Physics of Star Formation and Early Stellar Evolution*, NATO Adv. Study Inst., edited by C.J. Lada and N.D. Kylafis, p. 623

Kenyon, S. J., & Hartmann, L. 1991, ApJ, 383, 664

Lada, C. J. 1985, ARA&A, 23, 267

Lada, C. J. 1991, in *Physics of Star Formation and Early Stellar Evolution*, NATO Adv. Study Inst., edited by C.J. Lada and N.D. Kylafis, p. 329

Natta, A. & Giovanardi, C. 1991, in *Physics of Star Formation and Early Stellar Evolution*, NATO Adv. Study Inst., edited by C.J. Lada and N.D. Kylafis, p. 595

Reipurth, B. 199[illegible], in *Physics of Star Formation and Early Stellar Evolution*, NATO Adv. Study Inst., edited by C.J. Lada and N.D. Kylafis, p. 497

Shu, F. H., Adams, F. C., & Lizano, S. 1987, ARA&A, 25, 23

CIRCUMSTELLAR DISKS AND PLANET FORMATION

MOLECULAR EMISSION FROM CIRCUMSTELLAR DISKS

Steven V. W. Beckwith, David Koerner, and Anneila I. Sargent
Max-Planck-Institut für Astronomie
D-6900 Heidelberg, Germany
and
California Institute of Technology
Pasadena, California 91125, USA

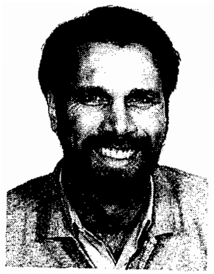

Abstract

The interpretation of millimeter-wave molecular line emission from circumstellar disks has been complicated by the high opacity of the lines, emission from the parent molecular clouds, and emission from molecular outflows. Observations of the disk around GM Auriga overcome the latter two of these problems and show that GM Auriga is another good example of a circumstellar gas disk in Keplerian rotation around a pre-main sequence star.

I. Introduction

Circumstellar disks begin as flattened clouds of hydrogen gas with miniscule amounts of the heavier elements that might later collect into planets and other large bodies. The gas can as yet only be observed in millimeter-wave emission lines from trace constituents such as CO. These long wavelengths require aperture synthesis arrays for adequate resolution of the disks, and the best resolution provided by existing arrays is still more than 100 AU at the distances to the nearest young stars, several times the size of the present Solar System. Fortunately, several objects have disks that appear to extend over several thousand AU making it possible to study the gas directly. The interpretation of these observations is controversial, however, largely because the emission is not easily distinguishable against that from the surrounding molecular cloud (*e.g.*, Beckwith and Sargent 1993a, and references therein).

The molecular line observations provide two important tools for the study of these disks: the direct images show the size and inclination angle, and they have sufficient velocity resolution to determine if the gas is, in fact, orbitting the stars. Furthermore, a direct image is persuasive support for the disk interpretation of infrared continuum observations (Adams, Lada, and Shu 1988, hereafter ALS; Strom *et al.* 1989; Beckwith *et al.* 1990, hereafter BSCG) that otherwise relies on indirect arguments to infer the distribution of the circumstellar material. (Although we note that in no case known to us does the emission imply a unique geometry which must be a disk.)

Between 100 and several thousand AU beyond the star, there should be some memory of cloud collapse, but there is as yet no reliable theoretical framework to guide our observational expectations for the cloud-disk boundary. The disks could be sharply bounded, or they might blend smoothly into the cloud as the Keplerian velocities decrease to the same levels as the cloud turbulence. Temperatures in this region are low; emission from very cold particles and molecular lines will be at far-infrared and millimeter wavelengths.

The first system detected in molecular lines was around the pre-main sequence star HL Tauri (Beckwith *et al.* 1986; Sargent and Beckwith, 1987, 1991). HL Tau is a classical T Tauri star with a strong bipolar jet. It is the brightest T Tauri star in millimeter-wave continuum emission in the Taurus cloud implying one of the most massive disks. Maps of the ^{13}CO line emission show an elongated, apparently flattened pancake, suggesting an almost edge-on disk.

Observations of the gas along the disk plane demonstrate that the highest velocities are close to the star ($\lesssim$200AU) with the red- and blue-shifted components on opposite sides; lower velocities are spread out to over several thousand AU. The "rotation" curve has the general appearance of Keplerian orbital motion and was thus interpreted by Sargent and Beckwith (1987). This interpretation is not unique, and it becomes more complicated at higher angular resolution (Sargent and Beckwith 1991; Guilloteau 1993). In particular, the low velocity gas no longer exhibits a regular pattern; there is substantial contamination by ambient cloud emission and by emission from a molecular outflow emerging perpendicular to the disk in maps at the lower relative velocities.

The few other observed systems have their own ambiguities. T Tauri is almost face-on making the rotation curve signature difficult to distinguish; the data are, nevertheless, consistent with Keplerian orbits (Weintraub, Masson, and Zuckerman 1989). DG Tauri shows considerable interference from its cloud and outflow (Sargent and Beckwith 1993). IRAS 16293–24 (Mundy *et al.* 1990) is a young, embedded binary in which disk structure has not clearly been resolved. Similarly, the structure around the obscured star L1551 IRS 5 is very difficult to interpret as disk-like (Sargent *et al.* 1988; Padin *et al.* 1989); there is much material from the surrounding cloud and molecular jet which adds to the molecular emission.

The molecular lines used for these observations probably have high optical depths in the disks ($\gtrsim$100) and appreciable opacity in the surrounding material, as well. Although interferometer measurements discriminate against relatively smooth, large-scale emission, it is difficult to distinguish the disk emission from clumpy cloud emission at scales of a few thousand AU, where the velocities are low (Sargent and Beckwith 1993). At the distance of the Taurus cloud, the best angular resolution to date, $1''.5$, is still inadequate to resolve the material at radii less than 100AU which produces the observed far infrared spectral energy distributions of the disks.

As part of a longer term programme to study the outer parts of these disks, we have carried out two new studies. The first is to calculate molecular line emission expected from disks, using as input parameters the best available interpretations to the spectral energy distributions (Beckwith and Sargent 1993b). The second is to search for disks in which some combination of fortuitous circumstances favors direct study of the disk itself without contamination by the background cloud (Koerner, Sargent, and Beckwith 1993).

II. Opacity of Disk Emission Lines

The appearance of a disk at specific velocities (*channel maps*) depends on the inclination to the line of sight, its size or outer radius, and the line emissivity within it. Here, we consider only disks with inclinations of order 45° and assume they are sharply bounded. The velocity profiles of emission lines integrated over the spatial extent of the disk will be characteristically double-peaked with maxima occurring at the orbital velocities at the edges (Horne and Marsh 1986). In each channel map, the emission traces out those portions of the disk whose velocity projected onto the line of sight matches the observing velocity. In general, maps of the disks at different velocities will show a series of arcs, such as those shown in Figure 1. The arcs are small and closed at high velocities and large and open at the low velocities. Arcs at velocities on opposite sides of the systemic velocity are mirror images of each other.

Disks viewed exactly edge on will also have this pattern of arcs, but they are not observed as such because of projection. Nearly face on disks should exhibit little discernible structure.

The optical depths at line center for the $J = 1 - 0$ line of ^{13}CO, are several hundred or more for disks such as that around HL Tau. Even for disks which are rather large ($R_d \gtrsim 1000$AU), the optical depths remain much greater than unity, the lower average surface density being compensated by lower temperatures which preferably increase the number of molecules in the low rotational states.

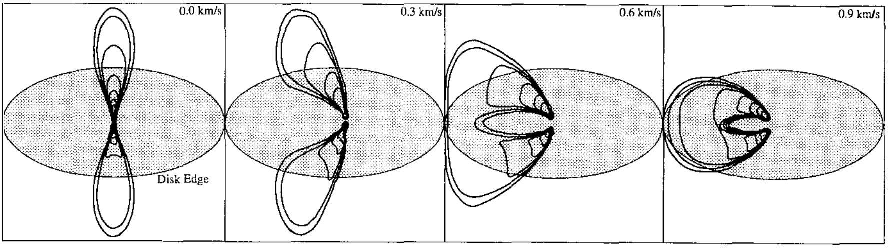

Figure 1: The appearance of a Keplerian disk at inclination 45° to the line of sight in four channel maps near a star of $1 M_\odot$ in the $J = 1 - 0$ line of ^{13}CO from Beckwith and Sargent (1993b). Only the redshifted emission is shown making only one half of the disk visible. The outline of the disk is the dashed line; the contours are brightness temperature in increments of 2 K starting at 2 K. The disk has a radial temperature gradient $T(r) \sim r^{-1/2}$. A slight flaring of the disk introduces the asymmetry in the vertical lobes.

Thus, although ^{13}CO maps can indicate the general morphology of T Tauri disks, the lower rotational transitions are probably too opaque to serve as useful probes of the physical conditions.

The disk emission in the outer parts of the arcs always dominates the total emission if the temperatures decrease more slowly than inversely with the radius, the usual case for T Tauri star disks (BSCG). Therefore, those arcs which have the largest apparent area on the sky are responsible for the most emission. This dominance of the outer parts of the disk in the line strengths means that the integrated line intensity is quite sensitive to the temperatures in the outer parts of the disk. Line strengths for the stars which have been mapped in ^{13}CO indicate that the outer disks are indeed quite warm (Sargent and Beckwith 1993), warmer, in fact than they would be if heated only passively by the stars or through the normal release of accretion energy (ALS; BSCG). In fact, the line strengths support the evidence from the far-infrared spectral energy distributions that the temperature in the disks decreases only as $T(r) \sim r^{-1/2}$.

III. GM Auriga

GM Auriga is an older T Tauri star, approximately 2×10^6yr, with a relatively low luminosity, $0.7 L_\odot$. The far infrared spectral energy distribution indicates an extensive disk with a relatively flat spectrum ($T(r) \sim r^{-0.55}$), while the relative paucity of near infrared radiation suggests clearing of the central regions (Strom, Edwards, and Skrutskie 1993; BSCG). Although it is a classical T Tauri star with Hα emission, there is little evidence of a wind from this star (Cabrit *et al.* 1993). The combination of no wind and a hole in the inner part suggests that the star is not actively accreting. GM Aur should, therefore, be relatively free from the confusing effects of outflow unlike the case of HL Tau as noted by Guilloteau (1993). It has had a longer time to establish orbital motion in the outer parts of disk. It is an ideal candidate to test against the calculations described in the previous section.

The left hand side of figure 2 is a series of maps of GM Aur in the $J = 2 - 1$ line of ^{13}CO at 1.3mm made with the Owens Valley millimeter-wave array (Koerner, Sargent, and Beckwith 1993). The resolution is $3''.5 \times 5''.8$ (525×870AU). There is a large-scale velocity gradient across the face of what we will interpret to be a disk. On the north-east side, the relative velocities are all positive (red shifts); on the south-west, they are negative (blue shifts). We interpret the emission to come from a disk whose axis has a position angle of about 50° on the sky and an inclination angle of 30° along the line of sight.

The right hand side of figure 2 is a series of synthesized maps for an inclined disk in Keplerian rotation. We assumed the emissivity falls with radius as a sum of two different exponential functions: a core which has a half width of 150AU and an extended part which has a radius of about 1000AU. The model calculations reproduce the gross features seen in the maps and several of the details, as well. The central velocity channels have distinct arc-shapes, the arcs exhibiting mirror symmetry about an axis at a position angle of 140°, perpendicular to the major axis of the disk ellipse. The model not only matches the overall shape of the emission but also the relative intensities. It is striking that in the central two channels around 14 km s^{-1} both observed and synthetic emission is weaker. This weakness is the result of relatively small areas in the disk for which the central velocities are in resonance, the decrease in area resulting in decreasing overall emission. The agreement between the models and the observations is not perfect - note for example the confusing blobs that are seen in the highest velocity maps. Again, these demonstrate the sensitivity of the interferometer to clumping in the ambient medium; they presumably have little or nothing to do with the disk. Nevertheless, the overall agreement between the calculations and the observations is quite good.

GM Aur is another example in which both the morphology and the dynamics of the molecular emission suggest a molecular disk around the star. The disk extends over many hundreds of astronomical units. The line intensities require the outer parts of the disk to be warmer than they would be under heating by accretion or direct illumination by the central star. This result is consistent with the strength of the 1.3mm continuum flux, 180mJy, and the relatively flat spectral energy distribution.

A stronger test of the disk model requires better spatial resolution and, perhaps, observation of molecules less abundant than ^{13}CO. Already, it seems likely that HCO^+ may be a good tracer of the dense parts of disks (Blake, van Dishoeck, and van Langevelde 1993). Although technically difficult, higher resolution (sub-second of arc) observations would match the observed scales with those responsible for the spectral energy distributions. There are rather strong expectations of disk structure based on the observations of the spectral energy distributions in the far infrared at scales of a few tens of AU. It is at that point that our observations will really begin to test current disk theory.

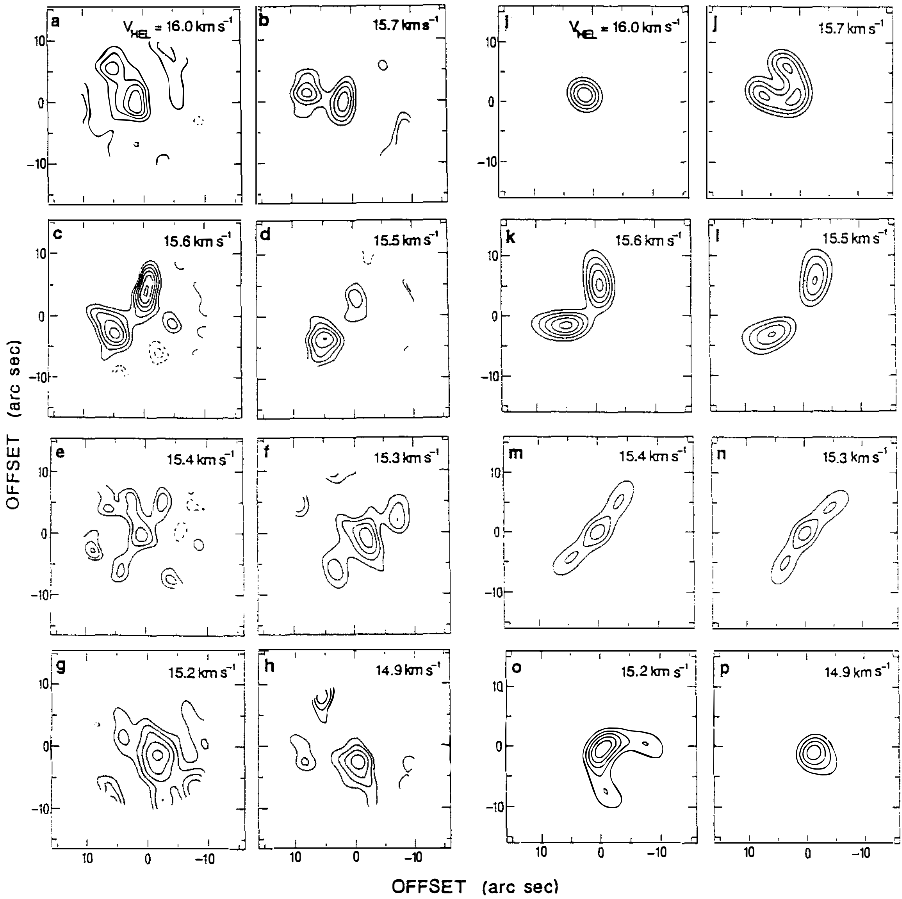

Figure 2: The two columns on the left show a series of channel maps of GM Auriga; the right hand columns are artificial maps calculated from a model of an inclined disk with the major axis at 140° (Koerner, Sargent, and Beckwith 1993).

REFERENCES

Adams, F. C., Lada, C. J., and Shu, F. H. 1988, *Ap. J.*, **326**, 865 (ALS).

Beckwith, S. V. W. and Sargent, A. I. 1993a, in *Protostars and Planets III*, ed. E. H. Levy and J. I. Lunine (Tucson:U. Arizona Press), p. 521.

Beckwith, S. V. W. and Sargent, A. I. 1993b, *Ap. J.*, **402**, 280.

Beckwith, S., Sargent, A. I., Scoville, N. Z., Masson, C. R., Zuckerman, B., and Phillips, T. G. 1986, *Ap. J.*, **309**, 755.

Beckwith, S. V. W., Sargent, A. I., Chini, R., and Güsten, R. 1990, *Astron. J.*, **99**, 924 (BSCG).

Blake, van Dishoeck, and van Langevelde 1993

Guilloteau, S. 1993, in *The Cold Universe*, ed. T. Montemerle, in press.

Horne, K. and Marsh, T. R. 1986, *MNRAS*, **218**, 761.

Koerner, D. W., Sargent, A. I., and Beckwith, S. V. W. 1993, *Icarus*, submitted.

Mundy, L. G., Wooten, H. A., and Wilking, B. A. 1990, *Ap. J.*, **352**, 159.

Padin, S., Sargent, A. I., Mundy, L. G., Scoville, N. Z., Woody, D. P., Leighton, R. B., Scott, S. L., Seling, T. V., Stapelfeldt, K. R., and Terebey, S. 1989, *Ap. J. Let.*, **337**, L45.

Sargent, A. I. and Beckwith, S. V. W. 1987, *Ap. J*, **323**, 294.

Sargent, A. I., Beckwith, S., Keene, J., and Masson, C. R. 1988, *Ap. J.*, **333**, 936.

Sargent, A. I. and Beckwith, S. V. W. 1991, *Ap. J. Lett.*, **382**, L31.

Sargent, A. I. and Beckwith, S. V. W. 1993, in *URSI/IAU Symposium 140: Interferometry with Millimeter and Submillimeter Arrays*, ed. M. Ishiguro and R. Kawabe (ASP conference Series, San Francisco: Bookcrafters), in press.

Strom, K. M., Strom, S. E., Edwards, S., Cabrit, S., and Skrutskie, M. F. 1989, *Astron. J.*, **97**, 1451.

Strom, S. E., Edwards, S., and Skrutskie, M. F. 1993, in *Protostars and Planets III*, ed. E. Levy and J. Lunine (U. Arizona Press: Tucson).

Weintraub, D. A., Masson, C. R., and Zuckerman, B. 1989, *Ap. J.*, **344**, 915.

Watch out for the sun, Dick !

THE STABILITY OF PROTOSTELLAR DISKS

Steven P. Ruden
Physics Department
University of California, Irvine, CA 92717

The gravitational, magnetic, and thermal stability of protostellar disks is reviewed. Large scale (global), one-armed gravitational instabilities can dominate the evolution of young, relatively high mass disks. If the instability is sufficiently violent, the disk may fragment into a binary companion to the central protostar. When the ratio of the disk mass to the stellar mass decreases via mass accretion below the critical value 0.314, global gravitational disturbances are stabilized, and the disk evolves due to small scale (local) instabilities. In cool, dusty, and nearly neutral protostellar disks, thermal convective instability is the dominant mechanism driving the evolution of disks.

I. Introduction

Protostellar disks form during the star formation process because collapsing molecular clouds rotate. During the collapse, each fluid parcel preserves its angular momentum and is prevented from falling directly into the center by a centrifugal barrier. By symmetry a geometrically thin disk of matter is built up around the central protostar. Collapse calculations indicate that a substantial fraction of the molecular gas falls onto the disk rather than directly onto the protostar and that the star gains much of its final mass through disk accretion[1,2]. The collapse phase, during which the disk is created, typically lasts less than about 10^5 years[3]. The size of the disk and the partitioning of mass between the star (of mass M_*) and the disk (of mass M_d) is determined by the mass and angular momentum distribution in the collapsing cloud. For a uniformly rotating molecular cloud core, Cassen and Summers[4] estimate that $M_d/M_* \approx 1$ after 80% of the molecular core mass is accreted.

The physical mechanism that drives the accretion of mass through the disk and onto the star is uncertain. We believe that different processes are responsible for disk accretion during different evolutionary epochs. Furthermore, different processes probably govern the accretion process in different parts of the disk at the same epoch. We will discuss some of these mechanisms in detail below. However, as Lynden-Bell and Pringle[5] elegantly demonstrated in 1974, *whatever* physical process responsible for the accretion must transport angular momentum *outwards* in the disk. This can be seen as follows. Consider a centrifugally supported disk with rotation rate $\Omega(r)$. Dynamical stability (to axisymmetric disturbances) requires the specific angular momentum $h = \Omega r^2$ to increase outwards: $dh/dr > 0$[6,7]. Although the total mass and angular momentum of the disk must be conserved, the total disk energy can be lowered because energy can be radiated. Any process then that allows mass to flow inwards, where it becomes more tightly bound in the gravitational potential well, will lower the energy of the disk. However, in order to flow inwards to smaller radii this mass must lose some of its orbital angular momentum (because $dh/dr > 0$). In order to conserve total angular momentum, the inward flow of mass (the accretion process) must be accompanied by an outward flow of angular momentum. The evolutionary timescale for the accretion is determined by the rate at which physical processes in the disk can transport angular momentum outwards. A signature of the accretion process is the radiation emitted by the disk, which has been observed and modeled in numerous young stellar objects[8,9,10].

The equations governing the evolution of an accretion disk can be derived from considerations of mass and angular momentum conservation[1,5,11]. The rotation rate is determined from

$$\Omega^2 r = \frac{\partial \Phi_*}{\partial r} + \frac{\partial \Phi_d}{\partial r} + \frac{\partial \eta}{\partial r}, \tag{1}$$

where Φ_* is the stellar gravitational potential, Φ_d is the disk self-gravitational potential, and η is the disk enthalpy. The surface density Σ is governed by

$$\frac{\partial \Sigma}{\partial t} + \frac{1}{r}\frac{\partial}{\partial r}(r\Sigma v_r) = 0, \tag{2}$$

where v_r is the (outward) radial velocity in the disk. All the torques acting on the disk matter produce radial flow according to

$$v_r = \left(\frac{dh}{dr}\right)^{-1}\left[-\frac{1}{r\Sigma}\frac{\partial}{\partial r}\left(r^3\Sigma\nu\frac{\partial\Omega}{\partial r}\right) - \frac{1}{2\pi r\Sigma}\frac{\partial\mathcal{F}}{\partial r} + \mathcal{T}\right]. \tag{3}$$

In this equation, the first term on the right-hand-side is the velocity caused by local viscous stresses (characterized by a shear viscosity ν), the second term is that caused by the local deposition of angular momentum carried by waves ($\mathcal{F}$ is the outward wave flux of angular momentum), and the third term is that caused by an external torque per unit mass $\mathcal{T}$ (which might represent the effects of an imposed external magnetic field or the back torque on the disk due to an outflowing wind). Given an equation of state to relate the enthalpy to the surface density and a prescription for the viscosity, the wave flux, and the external torque as a function of the variables r, t, and Σ, equations (1)-(3) can be integrated to yield the evolutionary behavior of an accretion disk. The primary difficulty is to deduce physically valid forms for ν, $\mathcal{F}$, and $\mathcal{T}$ in the appropriate regimes.

II. Eccentric Gravitational Instabilities

Disks are stable to short wavelength axisymmetric disturbances if the Toomre Q parameter exceeds unity everywhere[7]. In terms of the epicyclic frequency κ defined by $\kappa^2 = r^{-3}dh^2/dr$ and the sound speed c_s defined by $c_s^2 = \Sigma d\eta/d\Sigma$, the Toomre parameter is $Q = \kappa c_s/\pi G\Sigma$. In young stellar objects the disk mass is typically much less than the stellar mass except during the early stages (during and just after the formation of the disk) when the two may be comparable. The self-gravitational potential therefore does not dominate the stellar potential in equation (1), and the rotation curve is roughly Keplerian, $\Omega \propto r^{-3/2}$, and $\kappa \approx \Omega$.† If the Toomre condition is violated anywhere ($Q < 1$) dynamically growing localized instabilities can lead to local heating that will raise the temperature (and c_s) and return the disk to a marginally stable state ($Q \gtrsim 1$)[12]. We therefore consider only disks that are axisymmetrically stable to Toomre's criterion. In such disks, however, nonaxisymmetric propagating disturbances can still be unstable. These spiral density waves are characterized by a pattern speed, Ω_p, at which they rotate and an azimuthal wavenumber m, which gives the number of spiral arms. A characteristic radius for the wave is its corotation radius r_c where $\Omega(r_c) = \Omega_p$. From a consideration of the principal ranges of propagation of spiral density waves, it can be shown for $m \geq 2$ that a wave is localized around its corotation radius and cannot propagate globally throughout the disk[13,14]. A gravitational instability of $m \geq 2$ spiral modes will therefore be of a localized nature and can be treated like a viscosity (see below)[12].

Adams, Ruden, and Shu[14] (hereafter ARS) showed that one-armed ($m = 1$) instabilities do not suffer from this localization problem in nearly Keplerian disks such

† The enthalpy term is negligible in geometrically thin (cool) disks: $|\eta| \ll |\Phi_* + \Phi_d|$.

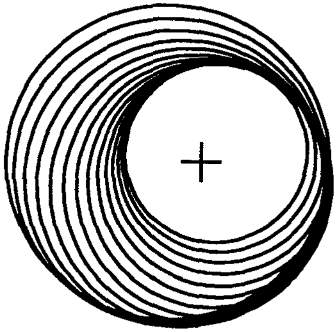

Fig. 1. A one-armed $m = 1$ global spiral density wave can be constructed from appropriately nested elliptical gas streamlines in Keplerian potentials. The cross marks the position of the protostar. Additional disk self-gravity is needed to make a one-armed mode in realistic protostellar potentials.

as those around protostars. The reason this mode is of primary importance is that an $m = 1$ disturbance perturbs initially circular gas streamlines into ellipses (*i.e.*, it generates a small eccentricity). In exactly Keplerian potentials elliptical orbits do not precess in space, therefore, a true *global* mode of oscillation (with $\Omega_p = 0$) can be constructed from nested ellipses (see Figure 1). In the nearly Keplerian potentials of protostellar disks, a small amount of self-gravity is needed to give the slight precession rates a single uniform value in order to make a global modal oscillation. Furthermore, it is important to note that the $m = 1$ instability concentrates mass towards one side of the disk (at the expense of the other side); hence, the protostar must be displaced away from the geometric center of the system to keep the center-of-mass fixed.

ARS found the $m = 1$ modes to be exponentially unstable with growth rates comparable to the orbital frequency at the outer edge of the disk as long as the Q value does not exceed about 3 in the outer disk regions. The growth time is less than a thousand years for typical protostellar disk systems making this a relatively violent instability. In an analytical study, Shu, Tremaine, Adams, and Ruden[15] (hereafter STAR) elucidated the nature of the instability. In an $m = 1$ disturbance the protostar is periodically displaced from the geometric center and it acts like a gravitational oscillator that generates waves in the outer disk regions beyond corotation. If these waves propagate in a manner that preserves their phase coherence with the oscillator (the protostar), a self-excited, growing disturbance is created. STAR named this instability mechanism by the acronym SLING: "Stimulation by the Long-range Interaction of Newtonian Gravity." For the instability mechanism to work, STAR showed the following conditions must be met.

1) The outer disk edge must be reasonably sharp in order to reflect waves back into a "resonant cavity" between corotation and the edge. Disks in which the surface density falls very gradually to zero will absorb waves, and one-armed disturbances will not grow. Fortunately, Ruden and Lin[16] have shown that viscous diffusion in protostellar disks, where the viscosity depends in a nonlinear fashion on the surface density, will naturally lead to sharp edges.
2) The disk must be cool enough for the Toomre Q parameter to be less than about 5 or pressure effects will stabilize $m = 1$ modes.
3) A finite threshold exists for SLING amplified modes. For $Q \gtrsim 1$, the ratio of the disk mass to the stellar mass must be *larger* than the critical value 0.314 for the $m = 1$ instability to occur. If the disk mass is less than this value and if Q exceeds unity everywhere, then the disk can at best only be weakly overstable to *any* m-armed instability.

In protostellar disks above the critical mass ratio, we can envisage two distinct types of evolution. In the first scenario, the one-armed instability never goes violently nonlinear, and the $m = 1$ wave transports mass, energy, and angular momentum globally through the disk[14,15]. The $m = 1$ wave angular momentum flux is $\mathcal{F} \approx \pi r^2 \Sigma\, \delta v_r\, \delta v_\theta$ with δv_r and δv_θ being the perturbed radial and tangential velocities, respectively. The linear theory used by ARS and STAR cannot estimate the magnitude of this wave flux, but if its value and radial form were known, then equations (2) and (3) would determine the disk evolution. We can estimate from equation (3) that the wave flux $\mathcal{F}$ will dominate the viscous diffusion of angular momentum when the wave amplitudes satisfy

$$\frac{\delta v_r}{c_s}\frac{\delta v_\theta}{c_s} \gtrsim \frac{\nu}{c_s^2/\Omega}. \tag{4}$$

Since the right-hand-side of this expression is typically much less than unity in protostellar disks[16,19] (see below) we see that even moderately "sonic" wave amplitudes will suffice for the one-armed modes to dominate the evolution of relatively massive disks. In the second scenario, the wave amplitude becomes so nonlinear that the one-armed instability causes the outer disk (the region between corotation and the edge) to fragment gravitationally into a companion body whose mass is roughly comparable to the disk mass. In this way, binary companions to stars can be formed. Their separations will be of order the disk sizes observed ($\sim 10 - 100$ AU), and their mass ratio will be of order $0.1 - 1$ (recall the instability will not work for very low mass disks).

III. Viscous Evolution

As a young stellar object evolves, mass is transferred from the disk to the star. Eventually the ratio M_d/M_* will drop below the critical value 0.314, and rapidly growing gravitational instabilities will shut off. The star/disk system enters the phase of purely viscous evolution driven by whatever local process can lead to efficient angular momentum transport. This phase of evolution has received extensive theoretical study[5,11,16,17,18,19,20,21]. The prime problem in accretion disk physics is to understand the origin and magnitude of the viscous torque in the disk, *i.e.*, the value of ν in equation (3). It is easily shown that ordinary atomic or molecular viscosities are too small by many orders of magnitude to lead to astrophysically interesting evolutionary timescales. Thus it is widely assumed that the fluid flow in the disk is turbulent and that angular momentum is transported when fluid elements carrying different amounts of specific angular momentum mix together in turbulent eddies. We must point out however that there is no proof that thin accretion disks are generically unstable to fluid turbulence.

In a turbulent disk, we expect the largest eddies to be responsible for the angular momentum transport because they couple together regions of the disk with the largest differences in specific angular momentum. If the largest eddy size is H_t (in the radial direction) and its turnover speed is v_t, the turbulent viscosity is of order

$$\nu \sim v_t H_t. \tag{5}$$

Since the eddy size is almost certainly less than the vertical scale height of the disk, which is easily shown to be $H \sim c_s/\Omega$ from the requirement of vertical hydrostatic equilibrium, and since the eddy velocity is less than the sound speed for subsonic turbulence, we can rewrite equation (5) as

$$\nu = \alpha c_s H = \alpha \frac{c_s^2}{\Omega}, \tag{6}$$

which is the famous "alpha" prescription of Shakura and Sunyaev[21] that lumps all the uncertainties about the turbulence into the unknown parameter $\alpha \approx (H_t/H)(v_t/c_s) \lesssim 1$. If a particular fluid dynamical mechanism or instability is proposed for the origin of the turbulent viscosity, the parameter α may be calibrated by comparing equations (5) and (6). In most treatments, α is simply treated as a constant parameter. We will consider next some of the physical mechanisms that may be responsible for viscosity in protostellar accretion disks. Although the qualitative nature of disk evolution is not particularly sensitive to the origin for the turbulence, the quantitative evolutionary timescales do depend on the magnitude of the viscosity.

III A. Magnetic Instabilities

Shakura and Sunyaev[21] pointed out that the Maxwell stresses associated with a tangled magnetic field in a disk will lead to an effective viscosity where $\alpha \approx v_A^2/c_s^2$, where v_A is the Alfven velocity. Since magnetic flux tubes are buoyant and can be lost from the disk[22], the magnetic pressure is most likely limited to be comparable in magnitude to the thermal pressure, which implies that $\alpha \lesssim 1$.

The most important recent idea on the origin for viscosity is the suggestion by Balbus and Hawley[23,24] (hereafter BH) that a disk threaded by a weak vertical magnetic field is unstable to axisymmetric shear instabilities. Based on a local analysis of the disk, they argue the instability grows at nearly dynamical rates ($\sim \Omega$), its maximum growth rate is *insensitive* to the strength of the magnetic field (for weak fields whose magnetic pressure is less than the thermal pressure), the instability is unaffected by small radial or toroidal fields, and the only requirement for instability is that the angular velocity decrease outwards ($d\Omega/dr < 0$). Keplerian disks clearly satisfy the latter condition and may be unstable provided a small poloidal seed field is present. The mechanism for the proposed instability is that as a fluid parcel, threaded by a small, frozen-in vertical magnetic field, is perturbed (outwards, say) the field lines stretch, and their tension tries to restore the parcel to its initial position (which is stabilizing). However, the field lines also resist azimuthal shearing and attempt to enforce rigid rotation of the parcel at its new, larger radius. This magnetic torque on the parcel gives it additional angular momentum, which drives the parcel still farther out (which is destabilizing). For sufficiently large wavelengths, the magnetic restoring forces are smaller than the (destabilizing) azimuthal stresses, and the instability proceeds with neighboring regions of high and low angular momentum interpenetrating and mixing. As the instability progresses and field lines are stretched, the magnetic field energy increases. BH suggest two mechanisms for saturation. In the first, the magnetic field increases until the critical unstable wavelength exceeds the disk height, at which time the shear instability should shut off; this corresponds to $\alpha \approx 1$. In the second, magnetic reconnection limits the maximum field strength, and α is probably significantly less than unity. In either case, the proposed magnetic instability provides an interesting origin for the angular momentum transport in Keplerian disks.†

However, in cool disks around protostars, the ionization fraction is so low[26] that the assumptions of field freezing break down, and the Lorentz forces, which act only on ions, are only weakly transferred to the dominant neutral component. Thus it is unlikely that this instability provides the dominant viscosity mechanism in the cool midplane regions of protostellar disks. The BH mechanism however may be the origin of viscosity in the disk regions within a few stellar radii of the protostar where the temperatures are high enough for there to be significant ionization and where there is a natural source for the poloidal magnetic field, namely, the protostar. Shu (personal communication, 1992) has suggested that farther from the star the topmost surface layers of the disk may be ionized sufficiently by cosmic rays for the ion-neutral coupling to be sufficient for this instability to provide some viscosity. In these regions one may have both a magnetic and convective (see §III B) origin for turbulence.

---

† However, see Dubrulle and Knobloch[25] for a dissenting view.

III B. Thermal Convective Instabilities

In nebular regions where the temperature is less than ~ 1500K, micron-sized dust grains will condense out of the gas. The dust will dominate the opacity, and its presence will be the key ingredient for determining the vertical thermal structure of the disk. In 1980 Lin and Papaloizou[27] demonstrated that the vertical temperature gradient in disks will be unstable to convection if the temperature dependence of the opacity is sufficiently large. In dusty, solar composition, molecular gas the opacity is found to be sufficiently temperature sensitive[28] for thermal convection to occur throughout most of the interior of the disk. Lin and Papaloizou proposed thermal convection as the origin for turbulent viscosity.

To estimate the magnitude of the convective viscosity Ruden and Lin[16] constructed detailed vertical structure models of cool nebular disks and using a mixing-length prescription for convection, determined that the convective viscosity could be well represented by a Shakura and Sunyaev alpha-law with $\alpha \approx 10^{-2}$. Using a different model for convective turbulence Cabot, et al.[20] found that α is in the range $10^{-3} - 10^{-2}$, while Ruden, Papaloizou, and Lin[29] estimated α to be in this same range from a linear perturbation analysis of axisymmetric convective modes.

Ryu and Goodman[30] have analyzed the behavior of linear, nonaxisymmetric, convective wavelets in a sheared disk and found that although there are exponentially growing solutions they seem to carry angular momentum the wrong way - inwards - which called into question the role of thermal convection for angular momentum transport. Recently however, Lin and Papaloizou[31] and Ruden and Korycansky[32] have used different techniques to analyze the angular momentum transport in linear, nonaxisymmetric convection. Both sets of authors find that there are indeed convective disturbances that carry angular momentum outwards. These disturbances grow at rates that depend on the degree of superadiabaticity of the vertical temperature gradient. Thus, as long as fully developed, nonlinear convection retains similar properties to the linear modes discussed here, the theoretical basis for a convective turbulence is back on firm footing (see Figure 2).

Using the above calibration for alpha and with a detailed opacity table, self-consistent simulations of the viscous evolution of protostellar disks can be made[16,19,20]. These calculations find that (1) actively accreting disk lifetimes are in the range $10^5 - 10^6$ years, (2) mass accretion rates decrease from 10^{-5} to 10^{-8} $M_\odot$/yr as the disk is depleted, (3) much of the final protostellar mass is accreted through the disk, (4) evolutionary models are insensitive to the initial conditions except for the values of the total disk mass and angular momentum, (5) self-gravity is unimportant ($Q \gg 1$) for disks with $M_d/M_* \lesssim 0.3$ except at the cool, outer edge of the disk, and (6) disk radii can spread by a factor $\lesssim 10$ during the lifetime of the disk. These conclusions are in good accord with the observational lifetimes and luminosities of protostellar disks[9,10].

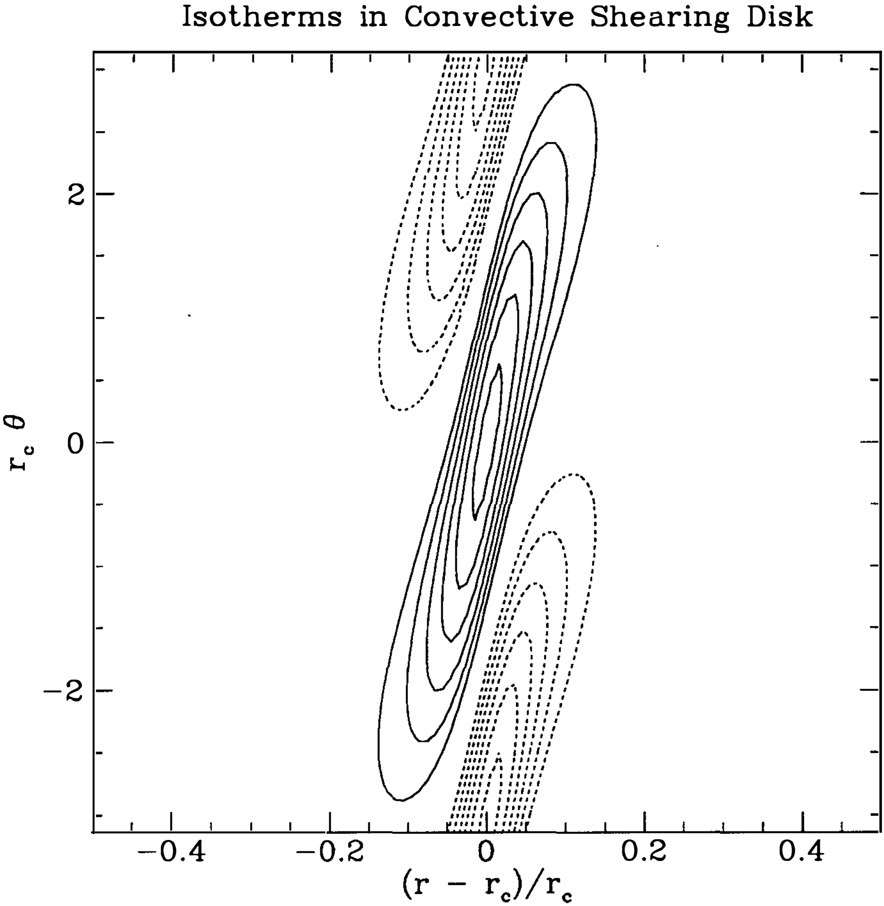

Fig. 2. Isothermal contours in the midplane of a convective disk for a modal disturbance centered at the corotation radius r_c. The view is in the frame rotating at the rate $\Omega(r_c)$ Hot, rising thermal plumes are shown with solid lines; cool, descending plumes with dotted lines. This figure illustrates a typical sheared convective mode that transports angular momentum outwards. From Ruden and Korycansky[32].

IV. Conclusions

The evolution of protostellar disks, from their formation to their dispersal, is governed by a variety of angular momentum transport mechanisms. The early stages, when the ratio of the disk mass to the stellar mass exceeds 0.314, are driven by global one-armed gravitational instabilities. Fragmentation into a binary stellar companion can occur during this epoch. As the disk becomes less massive relative to the star, large scale gravitational disturbances are stabilized, and the disk evolves due to localized turbulent viscosity. The most likely origin for the turbulence in cool, dusty disks is thermal convection, but a magnetic origin cannot be ruled out for the inner, ionized regions of the disk.

V. Acknowledgements

This work has been supported by NASA Grant NAGW-2260 and by NSF Grant AST-9157420.

VI. References

1. Cassen, P., and Moosman, A. 1981, *Icarus*, **48**, 353.
2. Terebey, S., Shu, F. H., and Cassen, P. 1984, *Ap. J.*, **286**, 529.
3. Shu, F. H., Adams, F. C., and Lizano, S. 1987, *Ann. Rev. Astron. Ap.*, **25**, 23.
4. Cassen, P., and Summers, A. 1983, *Icarus*, **53**, 26.
5. Lynden-Bell, D., and Pringle, J. E. 1974, *Mon. Not. Roy. Astron. Soc.*, **168**, 603.
6. Drazin, P. G., and Reid, W. H. 1981, *Hydrodynamic Stability* Cambridge: Cambridge University Press.
7. Toomre, A. 1964, *Ap. J.*, **139**, 1217.
8. Adams, F. C., Lada, C. J., and Shu, F. H. 1987, *Ap. J.*, **312**, 788.
9. Strom, K. M., Strom, S. E., Edwards, S., Cabrit, S., and Skrutskie, M. 1989, *Astron. J.*, **97**, 1451.
10. Beckwith, S. V. W., Sargent, A. I., Chini, R. S., and Gusten, R. 1990, *Astron. J.*, **99**, 924.
11. Pringle, J. E. 1981, *Ann. Rev. Astron. Ap.*, **19**, 137.
12. Lin, D. N. C., and Pringle, J. E. 1987, *Mon. Not. Roy. Astron. Soc.*, **225**, 607.
13. Lin, C. C., and Shu, F. H. 1964, *Ap. J.*, **140**, 646.
14. Adams, F. C., Ruden, S. P., and Shu, F. H. 1989, *Ap. J.*, **347**, 959 (ARS).
15. Shu, F. H., Tremaine, S., Adams, F. C., and Ruden, S. P., *Ap. J.*, **358**, 495 (STAR).
16. Ruden, S. P., and Lin, D. N. C. 1986, *Ap. J.*, **308**, 883.
17. Cameron, A. G. W. 1978, *Moon and Planets*, **18**, 5.
18. Lin, D. N. C., and Papaloizou, J. 1985, in *Protostars and Planets II*, eds. D. C. Black and M. S. Matthews, (Tucson: University of Arizona Press), 981.
19. Ruden, S. P. and Pollack, J. B. 1991, *Ap. J.*, **375**, 740.
20. Cabot, W., Canuto, V. M., Hubickyj, O., and Pollack, J. B. 1987, *Icarus*, **69**, 423.
21. Shakura, N. I., and Sunyaev, R. A. 1973, *Astronomy & Astrophysics*, **24**, 337.
22. Parker, E. N. 1979, *Cosmical Magnetic Fields: Their Origin and Their Activity*, (Oxford: Oxford University Press).
23. Balbus, S. A., and Hawley, J. F. 1991, *Ap. J.*, **376**, 214 (BH).
24. Balbus, S. A., and Hawley, J. F. 1992, *Ap. J.*, **400**, 595.
25. Dubrulle, B., and Knobloch, E. 1993, *Astr. Ap.*, in press.
26. Umebayashi, T., and Nakano, T. 1988, *Prog. Theor. Phys. Suppl.*, **96**, 151.
27. Lin, D. N. C., and Papaloizou, J. 1980, *Mon. Not. Roy. Astron. Soc.*, **191**, 37.
28. Pollack, J. B., McKay, C. P., and Christofferson, B. M. 1986, *Icarus*, **64**, 471.
29. Ruden, S. P., Papaloizou, J. C. B., and Lin, D. N. C. **1988**,*Ap. J.*, **329**, 739.
30. Ryu, D., and Goodman, J. 1992, *Ap. J.*, **388**, 438.
31. Lin, D. N. C., and Papaloizou, J. 1993, submitted to *Ap. J.*
32. Ruden, S. P., and Korycansky, D. G. 1993, submitted to *Ap. J.*

BIRTH AND EVOLUTION OF GIANT PLANETS

DANIEL GAUTIER
DEPARTMENT DESPA - OBSERVATOIRE DE MEUDON
92195 MEUDON Cédex (FRANCE)

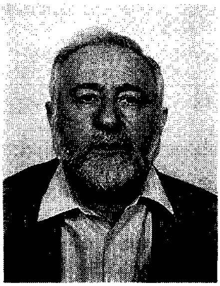

ABSTRACT

Present theories of the formation and of the subsequent evolution of Giant Planets are briefly reviewed, and compared to observational data.

Giant planets are characterized by the presence of a high density core surrounded by a fluid enveloppe mainly composed of hydrogen and helium. The mass and size of the cores of Jupiter and Saturn are small compared to those of the planets while in Uranus in Neptune the H2-He enveloppes have a small mass compared to that of the planet. These structures are inferred from moments of the external gravitational field accurately measured from the trajectography of the two spacecrafts of the Voyager mission. (Hubbard, 1989). The observable regions of all outer atmospheres are enriched in heavy elements relatively to the solar abundance, but those of Uranus and Neptune are much more enhanced in carbon at least, than Jupiter and Saturn (Gautier and Owen, 1989). The observed helium abundance seems to be protosolar in Uranus and Neptune, but not in Jupiter and Saturn. (Conrath et al., 1991, 1993). The outer atmospheres of Uranus and Neptune but not those of Jupiter and Saturn are also enhanced in deuterium relatively to the protosolar abundance (Gautier and Owen, 1989). Finally, Jupiter, Saturn and Neptune exhibit substantial sources of internal energy but not Uranus.

These observational data strongly constrain theories of planetary formation and of their subsequent evolution. The most favored scenario invokes a formation of the cores of giant planets from accretion of grains embedded in the nebula and composed of "rocks" of silicates and minerals and of ices of CNO compounds (H2O, CH4 or CO, NH3 of N2). Heating due to accretion presumably vaporizes a part of the ices which form a primary atmosphere of CNO compounds. The core grows and, when it reaches a critical size, the material of the surrounding nebula is gravitationally attracted and mix with the primary atmosphere, leading to a gaseous enveloppe mainly made of H2 and He in solar proportions but which is enriched in heavy elements relative to the solar abundance, in agreement with observations (Mizuno, 1980).

After the giant planets have completed the accretion, they contract to their present sizes over the age of the solar system. Initially, their contraction is fast and. thus their size decreases rapidly. During a second contraction period, an increasing fraction of the fluid enveloppe attains high densities at which the fluid is much more incompressible. Accordingly, their rate of contraction sloes down while their luminosity decreases rapidly. At least Saturn and probably Jupiter should have completely cooled and should not exhibit any internal heat, contrary to observations (Pollack and Bodenheimer, 1989). The explanation is that molecular hydrogen becomes metallic at pressures higher than 1.5 to 3 Mbar. When the planet is sufficiently cooled, helium does not mix anymore with metallic hydrogen and migrates towards the center of the planets, liberating gravitational energy which is the source of the observed internal energy. The helium abundance is then enriched in the deep interior relatively to the protosolar value and depleted in the outer atmosphere, in agreement with observations (Stevenson, 1982).

Since the H2-He enveloppe is relatively thin in Uranus and Neptune, the pressure never reaches the level where molecular hydrogen could undergo a transition to metallic phase. Therefore, no demixing of helium from hydrogen is expected. On the other hand, since Uranus and Neptune exhibit fairly similar masses and sizes, their evolution shoud have been similar. The absence of internal energy in Uranus, contrary to Neptune, is still an enigma. The interpretation of the enhancement of deuterium observed in Uranus and

Neptune (and Titan), relative to the protosolar value is controversial. The ices in grains could have been enriched in deuterium through ions-molecules reactions in the Interstellar Medium, prior to the formation of the Solar System, as currently advocated (Owen et al., 1986). In such a case, grains should have survived to the collapse of the protosolar cloud, and not to have been reprocessed during the subsequent mixing of elements in the nebula. Note that the question of the extent of the chemical homogeneity in the nebula is controversial (see for the two opposite scenarios : Prinn, (1990) who prefers a well mixed solar nebula and Stevenson (1990) who advocates an imperfect mixing). Recent calculations based on laboratory data suggest that the enrichment in deuterium with respect to the protosolar value could have occurred in the nebula through the condensation of water ice (Lecluse and Robert, 1994).

REFERENCES

Conrath, B.J., Gautier, D., Lindal, G.F., Samuelson, R.E., and Shaffer, W.A., J. Geophys. Res., 96, 18, 907, (1991).

Conrath, B.J., Gautier, D., Owen, T.C., and Samuelson, R.A., **Icarus, 101**, 168, (1993).

Gautier, D., and Owen, T., in **"Origin and Evolution of Planetary and Satellite Atmospheres"**, S.K. Atreya, J.B. Pollack, and M.S. Matthews, eds., The University of Arizona Press, Tucson, (Arizona), (1989), p. 487.

Hubbard, W.B., in **"Origin and Evolution of Planetary and Satellite Atmospheres"**, S.K. Atreya, J.B. Pollack, and M.S. Matthews, eds., The University of Arizona press, Tucson, (Arizona), (1989), p.539.

Lecluse, C., and Robert, F., **Geochem. Cosmochem. Acta**, (1994), in Press.

Mizuno, H., **Prog. Theor. Phys., 64**, 544, (1980).

Owen, T., Lutz, B.L., and de Bergh, C. **Nature, 277**, 640, (1972).

Pollack, J.B., and Bodenheimer, P. in **"Origin and Evolution of Planetary and Satellite Atmospheres"**, S.K. Atreya, J.B. Pollack, and M.S. Matthews, eds., The University of Arizona Press, Tucson, (Arizona), (1989), p. 564.

Prinn, R.G., **Astrophys.** J., 348, 725 (1990).

Stevenson, D.J., **Ann.** Rev. Earth **Planet. Sci.** 10, 257, (1982).

Stevenson, D.J., **Astrophys.** J., **348**, 730, (1990).

GAS AND DUST IN NEARBY GALAXIES

INTERGALACTIC HI

Elias Brinks
National Radio Astronomy Observatory[1]
P.O. Box O, Socorro, NM 87801, USA

ABSTRACT

According to popular belief, the early, hot Universe consisted of almost pure hydrogen with some 8% (by number) of helium thrown in and peppered with an almost negligible (but cosmologically very important) selection of light elements. At that time all matter was "Intergalactic" as no material had yet condensed into self-gravitating (proto-)galaxies, nor had any nuclear synthesis in stars enriched the primordial material. At look back times corresponding to redshifts between, say z=1 and z=4, most matter is found as part of larger systems. Part, though, is thought to be in the form of "Intergalactic Clouds", the Lyα forest.

In the local, cold Universe, no trace of Intergalactic HI (or Intergalactic Clouds for that matter) is seen, despite the many searches which have been conducted. All claimed detections of Intergalactic HI could, on subsequent inspection, be linked to optical counterparts, often low surface brightness dwarf galaxies. The only exception is the giant ring of HI in Leo within the M 96 group of galaxies.

I will summarise the latest searches for Intergalactic HI clouds. Also, I will spend some time on everything which has been called Intergalactic HI but which is either enriched (i.e. not primordial) material or gravitationally part of a larger system or both. An example of the former is HI gas seen in absorption in cooling flows in clusters; an example of the latter is material flung to large distances from a galaxy due to tidal interactions.

An exciting new result is the finding of HI companion clouds to actively star forming dwarf galaxies (also known as HII galaxies). Several of these objects have no obvious optical counterpart and might be of primordial composition. They just might be the remainders of the clouds which at larger redshifts cause the Lyα forest. They, with the HI ring in Leo, are the objects which come closest to the definition of "Intergalactic HI".

---

[1] The National Radio Astronomy Observatory is operated by Associated Universities, Inc., under contract with the National Science Foundation.

1. INTRODUCTION

Many searches have been performed over the past two decades for Intergalactic HI. Despite a lot of effort, there still is no clear answer to the question if there is any such material in the local Universe. Excellent reviews, summarising the often-times frustrating quests have been written by Roberts (1988) and Briggs (1990). To the question, do we want Intergalactic HI to be present, the answer is a resounding yes! Firstly, it seems highly improbable for the process of galaxy formation to have been 100% efficient. It is hard to believe that all material which at very early times was hot, gaseous, and virtually uniformly distributed has now been fully incorporated into galaxies. Secondly, there are many occasions where Intergalactic HI clouds are invoked to explain observations. For example, the proposed infall of gas clouds needed to explain some of the larger HI holes in nearby galaxies (Tenorio-Tagle & Bodenheimer 1988; van der Hulst & Sancisi 1988; Kamphuis & Briggs 1992) or the need to provide HI gas which circles galaxies in polar orbits (Briggs 1991) or which is found as counter-rotating material in elliptical galaxies (Bertola *et al.* 1990) or even spiral galaxies (Braun, Walterbos & Kennicutt 1992).

As the term "Intergalactic HI" has been used by many authors, each interpreting it differently, I think a clear definition is called for. A description which I particularly like was given by Mort Roberts in his 1988 review:

> *The concept, the possibility of intergalactic matter is not a new idea in astronomy. And, as we shall see, there is indeed matter between the galaxies, in special places and under special circumstances. What would be new and exciting would be the finding of an isolated cloud of such matter. One well separated from galaxies, having no stellar component, a cloud of gas alone. Such clouds appear to be frequent at high redshifts. They have yet to be found locally.*

Before one rushes to the nearest telescope to search for such clouds, it is wise to ask oneself what the typical masses and column densities are likely to be. This will largely be dealt with in the next section. After that I will review the various search strategies which have been employed, updating the reviews by Roberts (1988) and Briggs (1990). I will start with searches for Intergalactic HI at high redshift and gradually move to the local environment. In the last section I will present a new method which consists of searching for HI clouds near star forming dwarf galaxies. This might be a very efficient way of finding candidates for Intergalactic HI clouds.

2. EXPECTED CHARACTERISTICS OF INTERGALACTIC HI CLOUDS

What range of masses, temperatures or HI surface brightnesses can we actually expect? I assume that the reader is familiar with the basics of HI radiation transfer. A good summary is given by Kulkarni & Heiles (1988) whose notation I will follow. Their equation (3.2) shows that, using the Rayleigh-Jeans approximation for the Planck law, the equation of radiation transfer at radio wavelengths can be written as:

$$\frac{dT_B}{d\tau(\nu)} = T_s - T_B(\nu) \tag{1}$$

with T_s the spin temperature of the HI cloud, T_B the brightness temperature as seen by the receiver as a function of frequency and τ the optical depth. This equation can be solved in the case of a homogeneous isolated HI cloud embedded in a background radiation field with a brightness temperature of T_{bg}. Employing e^{τ} as an integrating factor, one finds the following relation:

$$T_B(\nu) = T_{bg}(\nu)e^{-\tau(\nu)} + T_s(1 - e^{-\tau(\nu)}) \tag{2}$$

When making a typical observation, one always measures the emission with respect to the background level. So, in general one measures a ΔT_B as follows:

$$\Delta T_B(\nu) = (T_S(\nu) - T_{bg}(\nu))(1 - e^{-\tau(\nu)}) \tag{3}$$

This has some interesting consequences for intergalactic atomic hydrogen gas. Suppose that the spin temperature of the HI cloud is of the same level as that of the background. In this case no emission can be detected; the only way to spot it would be through a measurement of HI in absorption against a suitably located and more distant background source. At the current epoch the temperature of the Cosmic Microwave Background according to the latest *COBE* results is $T_{bg} = 2.736\,K$. Do we expect Intergalactic HI clouds to be as cold as this, i.e., is there any sub–thermal HI? By the way, this would be about as cold as one can get in *The Cold Universe!* The answer is, probably not. In the relatively dense interstellar medium, such as in the Cold Neutral Medium in the Galaxy, collisional excitation will ensure that the spin temperature reflects the kinetic temperature of the gas. In more rarefied environments, Deguchi & Watson (1985, and references therein) have shown that most HI will achieve a spin temperature which is close to the kinetic temperature of the cloud due to Lyα-excitation (see also Kulkarni & Heiles 1988). Even the very diffuse HI cloud discovered by Schneider *et al.* (1983; see below for a more detailed discussion) is probably dense enough at a column density which is generally larger than 10^{18} atoms cm^{-2} for its HI to avoid becoming sub–thermal.

As a matter of fact, when HI clouds reach these low surface densities another effect will become important. This is ionisation by the extragalactic UV radiation field (Maloney 1993). Using his equation (2) and an ionising flux of 10^4 photons cm^{-2} s^{-1} one can calculate that HI clouds should have a column density larger than about 10^{19} atoms cm^{-2} in order to remain neutral. There is another interesting limit which is that, in order to avoid star formation, the column density of an HI cloud should remain below the empirical threshold for star formation which lies at around 10^{21} atoms cm^{-2} (Skillman 1987; Kennicutt 1989).

These considerations imply that one can only hope to find Intergalactic HI clouds with surface densities in the above range, i.e., between 10^{19} and 10^{21} atoms cm^{-2}. For clouds with dimensions of typically 1–10 kpc this translates to HI masses of between 10^6 and 10^9 M$_\odot$. Anyway, clouds smaller in mass than 10^6 M$_\odot$ are too fragile to have survived the much harsher environments at large redshift (Ostriker 1988).

3. SEARCHES FOR INTERGALACTIC HI

3.1 Searches for Intergalactic HI at High Redshift

Several groups are attempting to probe HI in the early Universe by searching for HI in absorption against the highest redshift objects such as QSOs and, at somewhat lower redshifts of $z \approx 3$, against radio galaxies. Briggs (1988) presents a summary of the many attempts and few successes to detect HI in absorption. All absorption to date can be traced to originating in metal rich, thus *not* primordial, systems. Womble (1992) confirms this picture. Her study of QSO–galaxy "pairs" shows that when HI absorption is seen, the intervening galaxy is often disturbed or undergoing an interaction. This increases the area on the sky over which matter is distributed, thus increasing the probability for a line of sight towards a more distant object to cut through this enriched material.

These results are really only the beginning. Many searches are at present restricted by the limited frequency range covered by today's receivers. For example, at the NRAO–Very Large Array the P–band receivers which operate from 300 to 340 MHz span a redshift range of $z = 3.2$ to 3.7. The new, frequency–agile front–ends of the 100–m Green Bank Telescope and the front–ends of the Giant Metre–wave Radio Telescope in India which are under construction, will open up this field. As an example of what can be achieved, a new result is the detection of HI in absorption at the redshift of the radio galaxy 0902+343 by Uson, Bagri & Cornwell (1991). The absorption is seen at the redshift of the radio galaxy and therefore is likely to originate within the galaxy, i.e., it is not intergalactic.

Searches for HI in emission at high redshift at present are inconclusive. Wieringa, de Bruyn & Katgert (1992), using the Westerbork Synthesis Radio Telescope, set interestingly low limits to the HI density at high redshift. The claimed detection by Uson *et al.* (1991) eagerly awaits confirmation.

3.2 Links with the Lyα Forest

One component in spectra to QSOs which is thought to be due to Intergalactic Clouds is the ubiquitous Lyα Forest. For recent reviews the reader is referred to Carswell (1988) and Weymann (1993). These clouds have very low neutral fractions of 10^{-4} to 10^{-5} and neutral column densities in the range of 10^{13} to 10^{16} atoms cm^{-2}, far too low to be detectable with current radio techniques and, as they are ionised clouds rather than atomic, outside the scope of my review. Still, I would like to spend a few words on them as it is interesting to note that if a Lyα forest cloud were to approach a neutral fraction of about one, its column density would fall in the range expected by Intergalactic HI clouds. The fact that quite nearby examples of Lyα clouds have been found (Morris *et al.* 1991, Bahcall *et al.* 1991) is especially exciting. Note, however, that some Lyα lines are linked to metal lines, i.e., enriched material, and that part of the absorption might occur in the ionised extension of the disks of spiral and irregular galaxies (Maloney 1992).

3.3 Cooling flows

More for completeness than anything else I will mention cooling flows briefly (see e.g. Fabian 1992). Large clusters of galaxies have been found to contain X–ray emitting gas. If the density near the centre of the cluster reaches high enough levels, cooling becomes efficient and the cooling time becomes short compared to a Hubble time. With the cooling, the pressure at the centre drops and gas starts moving inwards: a cooling flow is set up. Once gas cools, it is not clear at which temperature it will settle. Hα filaments, HI in absorption and in emission (see the review by Jaffe 1992) are all detected but, except for a CO detection towards NGC 1275, no molecular gas is seen (McNamara & Jaffe 1993). Obviously, we are dealing with gas which is bound to the dominating cluster member and which is enriched. So, although one might claim that a cooling flow moves between the galaxies of a cluster, one wouldn't consider this Intergalactic HI.

3.4 Searches for Intergalactic HI in clusters

Clusters have proved to be a rich hunting ground for Intergalactic HI candidates, especially the Virgo cluster. Sancisi, Thonnard & Ekers (1987) discovered an HI cloud which is located half–way between the elliptical NGC 4472 and the dwarf irregular galaxy UGC 7636. More recent observations by Patterson & Thuan (1992) and Henning, Sancisi & McNamara (1993) confirm the picture originally proposed by Sancisi *et al.* that the HI cloud consists of gas which had belonged to the dwarf galaxy but which has been stripped due to ram–pressure exerted by the X-ray halo surrounding NGC 4472. So, it is not a true Intergalactic HI cloud.

Another cloud in Virgo is the object discovered by Hoffman *et al.* (1992b). They show a large cloud of HI gas enveloping the galaxies NGC 4532 and DDO 137. The extended cloud moves at velocities which are lower by about 200 km s^{-1} compared to the systemic velocites of both galaxies. Hoffman *et al.* suggest that this material is gravitationally bound to the system and is therefore not classifiable as Intergalactic HI.

Again in Virgo, Giovanelli and Haynes (1989) described an object which they initially called an Intergalactic HI cloud. On closer inspection this cloud proved to be made up of two components, as shown in Figure 1 which is taken from their follow–up article (Giovanelli, Williams & Haynes 1991). The northern component coincides with what seems to be a dwarf galaxy whose characteristics have been summarised by Salzer *et al.* (1991). Interestingly, the southern component doesn't have an optical counterpart. Therefore, although the initial claim by Giovanelli and Haynes that they had discovered an Intergalactic HI cloud was mildly optimistic, subsequent study has shown that as far as the southern component is concerned, they might indeed have found such an object! I will come back to this in section 4.

There have been plenty of other searches for Intergalactic HI clouds. An important piece of work is that by Hoffman *et al.* (1989) in which they survey about 3% of the volume of the Virgo cluster. They set a limit to the number of Intergalactic Clouds with HI masses $\geq 3\times10^7$ M$_\odot$ of $\leq$ 100 for the entire volume. Hoffman, Lu & Salpeter (1992a) looked at the nearest void, i.e., perpendicular to the plane of the Local Supercluster. Again, no intergalactic gas

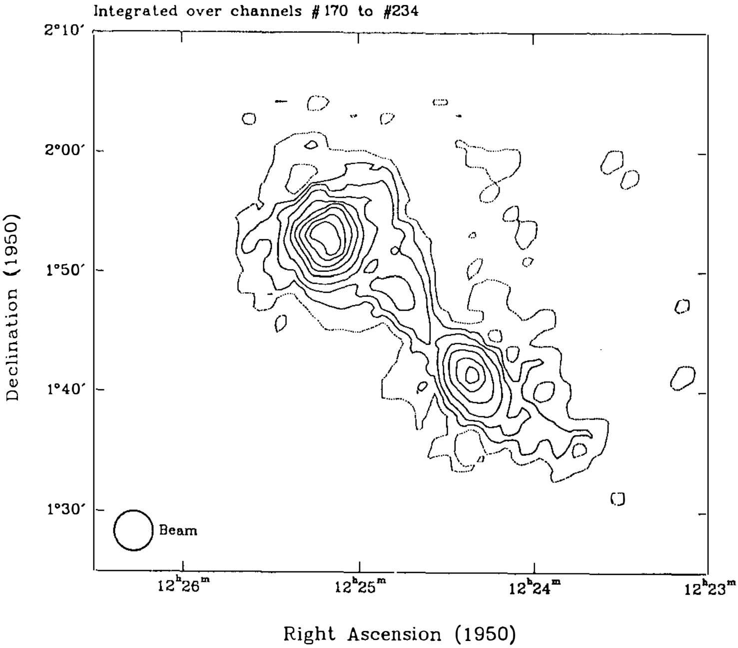

Fig. 1. Column density map of HI 1225 + 01 at a resolution of 3.3 arcmin (Giovanelli *et al.* 1991). Contour levels correspond to 2, 5, 10, 20, 30, 40, 50, 75, and 100 $\times$ 10^{18} atoms cm^{-2}.

is found by them and they put an upper limit of about 5% of the closure density in the form of clouds with $M_{HI} \geq 5 \times 10^6$ $M_\odot$.

Weinberg *et al.* (1991) performed a "blind" HI survey of the Perseus–Pisces supercluster and the foreground void. Again, no HI clouds with masses $\geq 10^8$ $M_\odot$were found in the void field, leaving no room for a substantial population of HI dwarfs or Intergalactic Clouds. They did find plenty of dwarf companion galaxies to the bright galaxies (see also the review by van Gorkom 1993). Simpson & Gottesman (1993) report on a search for HI in a void and in a cluster, finding three previously uncatalogued objects. Spitzak & Schneider (1992) claim to have completed the most definitive systematic survey to date, finding some 39 new objects. Further study will prove if any of the objects found by these groups is without an optical counterpart.

It should be stressed that all of these studies had more than sufficient sensitivity to find HI clouds in the expected mass range, i.e. from 10^6 to 10^9 $M_\odot$. Briggs (1990), compiling data from earlier searches, makes the point that current evidence doesn't support the increase in space density of such objects which was proposed by, e.g., Tyson & Scalo (1988). Intergalactic HI clouds seem either not to exist, or not to be where we expect them to be, or in a physical state which makes them hard to detect.

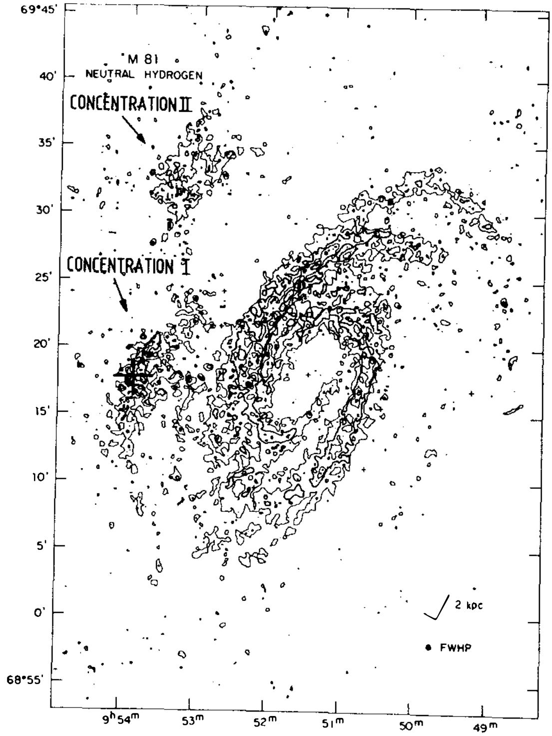

Fig. 2. Contour map of the HI column density distribution in M 81. The contour interval is 5×10^{20} atoms cm^{-2}. CO was detected at the eastern edge of Concentration I. This is marked with a cross (Brouillet *et al.* 1992).

3.5 Intergalactic HI and tidal interactions

Recently, several authors have claimed that tidal interactions can "spawn" dwarf galaxies. This has been discussed at this meeting by Mirabel (see also Mirabel, Lutz & Maza 1991; Mirabel, Dottori & Lutz 1992; Barnes & Hernquist 1992; Elmegreen, Kaufman & Thomasson 1993; Hibbard *et al.* 1993). Brouillet, Henkel & Baudry (1992) detected a CO(!) signal from what they consider to be an intergalactic molecular complex (see Figure 2). Fascinating as this detection may be, it doesn't fit the description of an Intergalactic HI cloud as, firstly, it contains enriched material, and secondly, it clearly is a result of the complex tidal interaction which is going on in the M 81–M 82–NGC 3077 group of galaxies. A nice presentation of the complexity of the interaction is given by Yun *et al.* (1993). Current models predict that the self-gravitating bodies produced by an interaction are composed of stars and gas. This would make it easy to discriminate them from Intergalactic HI clouds. However, if interactions can produce dwarf-like clumps from the outermost, gaseous, and presumably metal-poor regions of galaxies, then these clumps, once self-gravitating, would be hard to distinguish from primordial objects.

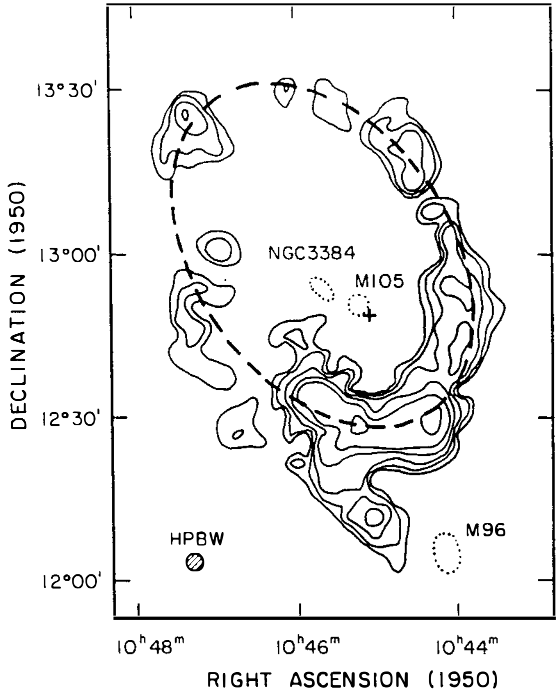

Fig. 3. Distribution of the Intergalactic HI in the M 96 group at a resolution of 3.3 arcmin. Contour levels correspond to 2, 4, 8, 16, 32, and 64 $\times$ 10^{18} atoms cm^{-2}. The optical dimensions of nearby galaxies are outlined with dots. Image taken from Schneider (1991).

3.6 The HI Cloud in Leo

There is one object which seems to be truly an Intergalactic HI cloud: the giant HI ring encircling NGC 3384 and M 105 in the M 96 group of galaxies in Leo. The discovery was reported by Schneider *et al.* (1983) and an updated description was given by Schneider (1991). The HI forms an inclined ring with a diameter of some 200 kpc, an estimated dynamical mass of 5.6×10^{11} $M_{\odot}$, and a rotation period of 4.1×10^{9} years. Figure 3 shows an HI column density map of the ring. HI clumps in the ring have peak column densities of 4×10^{20} atoms cm^{-2}, i.e., below the threshold for star formation. As reported by Schneider *et al.* (1989), the cloud has been detected only in HI and possibly in Hα. This strongly suggests a primordial composition and an intergalactic nature, especially in the light of the long timescale involved for rotation. Still, it can't be ruled out that the gas is due to tidal forces within the Leo group of galaxies.

4. DWARF GALAXIES AND INTERGALACTIC HI CLOUDS

As was mentioned above, one of the components of the object which was found by Giovanelli & Haynes seems devoid of any stars and might be primordial (Salzer *et al.* 1991). Another, somewhat similar object is II Zwicky 33, where a companion HI cloud is found

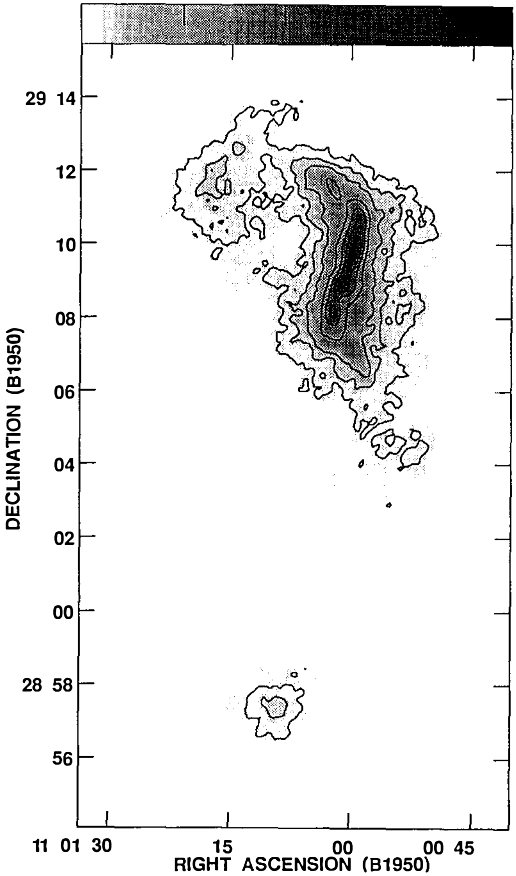

Fig. 4. Integrated HI column density map of Haro 26 showing its two companion cloudlets, one at its north-eastern tip and the other one 4 arcmin to the south. The resolution is about 19 arcsec. Contour levels correspond to 1.5, 3, 6, 20, 30, 45, and 60×10^{20} atoms cm^{-2} (Taylor *et al.*, in preparation).

which has almost the same size and mass as the star-forming dwarf, but without any clear presence of a stellar population and with only marginal star-forming activity (Brinks 1990). A third example might be II Zwicky 40, again a dwarf galaxy which is undergoing a burst of star formation and which is one of the prototypical "extragalactic HII regions" (also referred to as Blue Compact Dwarfs or HII galaxies). This object seems to consist of two HI clouds which are merging. Star formation is restricted to the northern cloud; no stellar component is seen in the southern part (Brinks & Klein 1988).

This suggests that it might pay off to search for companion HI clouds to star forming dwarf galaxies. The idea being that the star burst, which turns the dwarf galaxy into a beacon, is induced by the interaction, either with another dwarf or perhaps with an Intergalactic HI cloud. A pilot survey has been carried out by Taylor, Brinks & Skillman (1993) with an encouraging sucess rate. A statistically more complete follow-up survey of some twenty galaxies has resulted in a 75% detection rate thus far. Higher resolution observations, which might uncover some further companion clouds, remain to be done. Figure 4 shows, as an example, Haro 26 as observed with the VLA, combining C– and D–array observations. One companion is seen near the north–eastern tip of Haro 26, a second companion is seen 4 arcmin to the south. At present there are more questions than answers. A first priority will be to make optical follow–up observations of our HI detections. Preliminary work shows that some HI clouds have optical counterparts; others might be without stars, and perhaps primordial. Also, it is not known if the dwarf companions are merely ships passing in the night or if they are gravitationally bound to the HII galaxies. The general properties of these HI companion clouds match remarkably well those of the Lyα forest in terms of their size, velocity dispersion and HI column density (taking into account the high ionisation fraction, of course) and they might be, as speculated by Taylor *et al.*, the local counterparts. Our finding of dwarf companion clouds has gained significance by the detection of a population of faint blue galaxies at redshifts of z=0.2–0.6 (see Colless *et al.* 1993 and references therein) which might indicate merger–dominated galaxy evolution or bursts of star formation in dwarf galaxies. This would make these HI clouds even more interesting as they might be the remnants of the units from which galaxies were formed in the first place.

5. CONCLUSIONS

The current state of affairs regarding Intergalactic HI is embarrassing. Searches for HI in emission or in absorption at high ($z > 3$) redshift are still in their infancy. At lower redshifts, there seems to be plenty of intergalactic gas, the Lyα forest, but it is highly ionised. Some of it might be primordial. At low redshifts dedicated searches for Intergalactic HI have turned up plenty of dwarf galaxies and dwarf companions to larger galaxies, but no primordial HI clouds. The only Intergalactic HI cloud is the M96 cloud detected serendipitously by Schneider (1983). However, there is hope, as is shown by the Giovanelli & Haynes cloud in Virgo and the subsequent detection of HI companion clouds to HII galaxies (Taylor *et al.* 1993). But, there are still plenty of mysteries. The HI companions near HII galaxies show that there are objects which come tantalisingly close to Mort Roberts' description of an Intergalactic HI cloud. But then, why do we seem to find them *only* there? Plenty of searches for objects of similar mass have been fruitless, as aptly demonstrated by Briggs (1990). Are they perhaps so diffuse that they are ionised by the extragalactic UV radiation field (Maloney 1993) or are they sub-thermal? Do they need to be gravitationally disturbed by an interaction in order to enhance their density to make them detectable? Despite the low emission measures which are expected, it might be profitable to look for Intergalactic Hα clouds. Similarly, what about Schneider's cloud in the Leo group of galaxies? It would be disturbing if that would be a one of a kind, as, to date, it is the best example of Intergalactic HI of which we know. No doubt, the quest for Intergalactic HI will continue.

ACKNOWLEDGEMENTS

It is a pleasure to thank Thierry Montmerle and Felix Mirabel for inviting me to this stimulating meeting and for providing financial support. I am grateful to the NRAO for covering my travel expenses. Many colleagues shared their results with me or offered advice for which I am thankful. The following deserve a special word of thanks: Robert Braun, Chris Carilli, John Dickey, Dwarakanath, Bill Junor, Phil Maloney, Michael Rupen, Steven Schneider, Caroline Simpson, Evan Skillman, Chris Taylor, Thijs van der Hulst, Jacqueline van Gorkom and Donna Womble.

REFERENCES

Bahcall, J.N., Januzzi, B.T., Schneider, D.P., Hartig, G.F., Bohlin, R., & Junkkarinen, V. 1991, ApJ, 377, L5
Barnes, J.E., & Hernquist, L. 1992, Nature, 360, 715
Bertola, F., Bettoni, D., Buson, L.M., & Zeilinger, W.W. 1990, in *Dynamics and Interactions of Galaxies*, ed. R. Wielen (Springer Verlag: Heidelberg), 249
Braun, R., Walterbos, R.A.M., & Kennicutt, R.C., Jr. 1992, Nature, 360, 442
Briggs, F.H. 1988, in *QSO Absorption Lines: Probing the Universe*, eds. J.C. Blades, D.A. Turnshek & C.A. Norman (Cambridge University Press: Cambridge), 275
Briggs, F.H. 1990, AJ, 100, 999
Briggs, F.H. 1991, in *Warped Disks and Inclined Rings around Galaxies*, eds. S. Casertano, P.D. Sackett & F.H. Briggs (Cambridge Univ. Press: Cambridge), 1
Brinks, E. 1990 in *Dynamics and Interactions of Galaxies*, ed. R. Wielen (Springer Verlag: Heidelberg), 146
Brinks, E., & Klein, U. 1988, MNRAS, 231, 63p
Brouillet, N., Henkel, C., & Baudry, A. 1992, A&A, 262, L5
Carswell, R.F. 1988, in *QSO Absorption Lines: Probing the Universe*, eds. J.C. Blades, D.A. Turnshek & C.A. Norman (Cambridge University Press: Cambridge), 91
Colless, M., Ellis, R.S., Broadhurst, T.J., Taylor, K., & Peterson, B.A. 1993, MNRAS, 261, 19
Deguchi, S., & Watson, W.D. 1985, ApJ, 290, 578
Elmegreen, B.G., Kaufman, M., & Thomasson, M. 1993, ApJ, submitted
Fabian, A.C. 1992, in *Clusters and Superclusters of Galaxies*, ed. A.C. Fabian (Kluwer: Dordrecht), 151
Giovanelli, G., & Haynes, M.P. 1989, ApJ, 346, L5
Giovanelli, G., Williams, J.P., & Haynes, M.P. 1991, AJ, 101, 1242
Henning, P.A., Sancisi, R., & McNamara, B.R. 1993, A&A, 268, 536
Hibbard, J.E., van Gorkom, J.H., Kasow, S., & Westpfahl, D.J. 1993, in *The Evolution of Galaxies and their Environment: The Contributed Papers*, eds. D. Hollenbach, H. Thronson & J.M. Shull, NASA Conf. Publ., 3190, 367
Hoffman, G.L., Helou, G., Salpeter, E.E., & Lewis, B.M. 1989, ApJ, 339, 812
Hoffman, G.L., Lu, N.Y., & Salpeter, E.E. 1992a, AJ, 104, 2086
Hoffman, G.L., Salpeter, E.E., Lamphier, C., & Roos, T. 1992b, ApJ, 388, L5
Jaffe, W. 1992, in *Clusters and Superclusters of Galaxies*, ed. A.C. Fabian (Kluwer: Dordrecht), 109
Kamphuis, J., & Briggs, F. 1992, A&A, 253, 335
Kennicutt, R.C., Jr. 1989, ApJ, 344, 685
Kulkarni, S. R., & Heiles, C. 1988, in *Galactic and Extragalactic Radio Astronomy, 2nd edition*, eds. G.L. Verschuur & K.I. Kellermann, (Springer–Verlag: New York), 95
Maloney, P. 1992, ApJ, 398, L89

Maloney, P. 1993, ApJ, submitted
McNamara, B.R., & Jaffe, W. 1993, A&A, submitted
Mirabel, I.F., Dottori, H., & Lutz, D. 1992, A&A, 256, L19
Mirabel, I.F., Lutz, D., & Maza, J. 1991, A&A, 243, 367
Morris, S.L., Weymann, R.J., Savage, B.D., & Gilliland, R.L. 1991, ApJ, 377, L21
Ostriker, J.P. 1988, in *QSO Absorption Lines: Probing the Universe*, eds. J.C. Blades, D.A. Turnshek & C.A. Norman (Cambridge University Press: Cambridge), 319
Patterson, R.J., & Thuan, T.X. 1992, ApJ, 400, L55
Roberts, M.S. 1988, in *New Ideas in Astronomy*, eds. F. Bertola, J.D. Sulentic & B.F. Madore (Cambridge University Press: Cambridge), 65
Salzer, J.J, di Serego Alighieri, S., Matteucci, F., Giovanelli, R., & Haynes, M.P. 1991, AJ, 101, 1258
Sancisi, R., Thonnard, N., & Ekers, R.D. 1987, ApJ, 315, L39
Schneider, S.E. 1991, in *Warped Disks and Inclined Rings around Galaxies*, eds. S. Casertano, P.D. Sackett & F.H. Briggs (Cambridge University Press: Cambridge), 25
Schneider, S.E., Helou, G., Salpeter, E.E., & Terzian, Y. 1983, ApJ, 273, L1
Schneider, S.E., Skrutskie, M.F., Hacking, P.B., Young, J.S., Dickman, R.L., Claussen, M.J., Salpeter, E.E., Houck, J.R., Terzian, Y., Lewis, B.M., & Shure, M.A. 1989, AJ, 97, 666
Simpson, C., & Gottesman, S.T. 1993, in *The Evolution of Galaxies and their Environment: The Contributed Papers*, eds. D. Hollenbach, H. Thronson & J.M. Shull, NASA Conf. Publ., 3190, 181
Skillman, E.D. 1987, in *Star Formation in Galaxies*, ed. C.J. Lonsdale Persson, NASA Conf. Publ., 2466, 263
Spitzak, J.G., & Schneider, S.E. 1992, BAAS, 24, 1267
Taylor, C.L., Brinks, E., & Skillman, E.D. 1993, AJ, 105, 128
Tenorio-Tagle, G., & Bodenheimer, P. 1988, ARA&A, 26, 145
Tyson, N.D., & Scalo, J.M. 1988, ApJ, 329, 618
Uson, J.M., Bagri, D.S., & Cornwell, T.J. 1991, Phys. Rev. Lett., 67, 3328
van der Hulst, T., & Sancisi, R. 1988, AJ, 95, 1354
van Gorkom, J.H. 1993, in *The Evolution of Galaxies and their Environment*, eds. J.M. Shull & H.A. Thronson (Kluwer: Dordrecht), in press
Weinberg, D.H., Szomoru, A., Guhathakurta, P., & van Gorkom, J.H. 1991, ApJ, 372, L13
Weymann, R.J. 1993, in *The Evolution of Galaxies and their Environment*, eds. J.M. Shull & H.A. Thronson (Kluwer: Dordrecht), in press
Wieringa, M.H., de Bruyn, A.G., & Katgert, P. 1992, A&A, 256, 331
Womble, D.S. 1992, PhD Thesis, University of California at San Diego
Yun, M.S., Ho, P.T.P., Brouillet, N., & Lo, K.Y. 1993 in *The Evolution of Galaxies and their Environment: The Contributed Papers*, eds. D. Hollenbach, H. Thronson & J.M. Shull, NASA Conf. Publ., 3190, 253

EXTRAGALACTIC MASERS

Moshe Elitzur
Department of Physics and Astronomy
University of Kentucky, Lexington, KY 40506

ABSTRACT

Maser emission has been detected in numerous external galaxies in both OH and water transitions. Isotropic luminosities can be quite high and in some cases exceed those of typical Galactic sources by a factor of million, hence the name *megamasers*. Water masers appear to be directly associated with star forming regions and are generally similar to those observed in our own galaxy. OH megamasers, currently detected up to red-shift of $z = 0.265$, form a unique class of objects that marks a certain active phase in galaxy evolution. In spite of their spectacular luminosities, OH megamasers have modest brightness temperatures. They appear to be strongly correlated with the infrared signature of the host galaxy and are associated with either a Seyfert or a star burst phase. This review covers the properties of the maser emission, compares extragalactic to Galactic maser sources and attempts to deduce their meaning in terms of galactic evolution.

1. INTRODUCTION

A fascinating and most important development in astronomy is the detection of molecules in external galaxies. Thus far, extragalactic maser emission has been detected in three molecular species: OH, H_2O and H_2CO. The last one is unique in that currently, more extragalactic (five) than Galactic H_2CO maser sources have been detected. Most work on extragalactic masers has concentrated on studies of OH and H_2O, and these are the species that will be covered here. Additional material can be found in valuable reviews recently presented by Baan (1991, 1993).

2. EXTRAGALACTIC H_2O

2.1 *Galactic-Like H_2O Masers*

Extragalactic H_2O maser sources divide into two classes. The first one includes 14 masers that closely resemble masers in Galactic star-forming regions, located outside nuclei of nearby systems (distances less than ~ 3 Mpc). Detailed summaries and tabulations are provided by Moran, Greenhill and Reid (1991) and Greenhill et al. (1990). These masers reside in either irregular galaxies (LMC, SMC, IC10) or the spiral arms of spiral galaxies (M33, IC342). At a detection level of 0.1 Jy, M33 contains five H_2O masers, the strongest among them is the HII region IC 133 with an isotropic luminosity $L_{iso} \sim 0.2\ L_{\odot}$. By comparison, W49, the most powerful Galactic H_2O maser, reaches isotropic luminosity of $\sim 1\ L_{\odot}$ in its strongest phase while typical Galactic masers only have $L_{iso} \sim 10^{-4}\ L_{\odot}$. High-resolution observations by Greenhill et al. (1990) affirm the similarity of IC 133 to W49. A synthesized map of the W49 maser source shifted from its Galactic distance of 10 kpc to the distance of M33, 720 kpc, shows close resemblance to the actual map of IC 133.

In all likelihood, these masers are simply the counterparts of the Galactic H_2O masers abundant in star forming regions, which are generated in shocks driven by powerful winds around newly formed stars (Elitzur, Hollenbach and McKee 1989). The detection in other galaxies enables statistical studies of the properties of these masers. Combining the statistics of detected sources with lack of detections in 22 nearby galaxies (including M31 and M81), Greenhill et al. (1990) conclude that the number of masers N that have features more luminous than L is given by the relation

$$\log N = -0.6(1 + \log L),$$

where L is luminosity in units of $L_{\odot}$ and $-4 < \log L < 0$. Hence, if all the galaxies in the sample were similar to the Galaxy, each would host about four sources with features as luminous as $\sim$ 0.01 $L_{\odot}$ and one source with features as luminous as 0.1 $L_{\odot}$ (similar to W49).

An exciting recent development is the first epoch measurements of maser proper motions in M33 (Greenhill et al. 1993a). This promises to provide kinematic-geometric extragalactic distances, removing some of the uncertainties from the determination of the Hubble constant.

2.2 *H_2O Megamasers*

The other class of H_2O masers was discovered by Dos Santos and Lepine (1979) with the detection of strong 22 GHz emission from NGC 4945, a bright edge-on spiral galaxy. At an assumed distance of 4 Mpc, the isotropic luminosity is $\sim 85\ L_{\odot}$, almost two orders of magnitude more than W49 at its strongest phase. Subsequent discoveries brought the number of such extragalactic H_2O masers to nine, with isotropic luminosities ranging from ~ 0.2 — $520\ L_{\odot}$. Unlike the former class of extragalactic masers, these H_2O masers occur at the nuclei of distant galaxies (distances ranging to $\sim$ 16.5 Mpc). The linewidths of single features, $\gtrsim 5$ km s^{-1}, and the velocity extent of the emission, up to ~ 600 km s^{-1}, are larger than typical values for Galactic H_2O masers. VLA mapping by Claussen and Lo (1986) of the masers in NGC 4258 and NGC 1068 constrain their locations to regions with spatial extent less than 1.3 and 3.5 pc, respectively, at the center of each galaxy. Claussen and Lo conclude that the luminous maser emission originates in very dense molecular gas clumps in the immediate vicinity of a central source with mass outflow. The underlying assumption of this proposal is that in analogy with Galactic star-forming regions, the H_2O masers are generated by the interaction of a powerful outflow with the surrounding medium, only in this case the wind originates from the nucleus of a galaxy rather than a young star. Luminous H_2O masers are then associated with activity at the nuclei of galaxies.

A different interpretation was proposed by Ho et al. (1987), following observations toward NGC 253 and M51. Both sources are spiral galaxies with active nuclei, and Ho et al. detected also H_2O maser emission with moderate luminosities — 0.2 $L_\odot$ in NGC 253 and 0.8 $L_\odot$ in M51. These luminosities are comparable to those of active Galactic star-forming regions, leading Ho et al. to suggest that the high luminosities observed in other galaxies are simply the extreme end of a continuous distribution that includes the Galactic masers. The key then is the large sample rather than special gas properties in the nuclear environment; according to Ho et al., nuclei of galaxies are good places to find the most luminous masers simply because of the higher concentration of young stars.

Yet another interpretation was proposed by Haschick and Baan (1985) and Baan (1985). They suggest that, similar to OH megamasers (see sec. 3), luminous H_2O nuclear emission corresponds to low-gain maser amplification of the background continuum radio source. Since background amplification appears to play a significant role in extragalactic masers, a brief discussion is in order.

2.3 *Beaming, Isotropic Luminosity, etc.*

Because maser radiation is amplified, it is *always* highly beamed in all sources with an appreciable gain, no matter what the geometry; the larger the gain, the more pronounced the beaming (Elitzur 1990). Still, depending on the geometry, a maser can emit isotropically in all directions. An example is a spherical maser. Every point on the surface emits a sharply focused beam centered on the outward radial direction, and the maser appears the same in all directions. But in other geometries, only a fraction f of the sky is illuminated by the maser beam so the actual maser luminosity, L_m, is only a fraction f of the inferred isotropic luminosity:

$$\frac{L_m}{L_{iso}} = f.$$

In a sphere, $f = 1$ and the isotropic luminosity coincides with the actual luminosity. However, in a disk maser with thickness d and radius ℓ the radiation is effectively confined to the solid angle subtended by the rim of the disk and $f \sim d/\ell$. And a cylindrical maser with diameter d and half-length ℓ emits mostly through its caps, so $f \sim (d/\ell)^2$. In both cases, the inferred isotropic luminosity greatly exceeds the actual luminosity if the ratio d/ℓ is small.

The same reasoning applies to the radiation amplified by a maser with area A_m located at a distance D_m from a background source, which can be either a thermal source or itself a maser. Observers whose line of sight to the background source is intercepted by the maser cloud will detect enhanced intensity with inferred isotropic luminosity

$$\frac{L_m}{L_{iso}} = \frac{A_m}{4\pi D_m^2} .$$

Depending on the covering factor of the maser clouds, the inferred isotropic luminosity can greatly exceed the actual source luminosity, and if generated this way, extreme extragalactic maser luminosity need not necessarily imply unusual emission.

Detailed observations by Greenhill et al. (1993b) show that the H_2O masers in NGC 3079 cannot be explained with amplification of the nuclear radio continuum emission because the spatial coincidence is not perfect. Grennhill et al. find that a likely explanation for this source is amplification of a background maser by a foreground maser slab intercepting the line of sight face-on, a reasonably likely occurrence in active regions crossed by shock waves (Elitzur, McKee and Hollenbach 1991). An alternative explanation may be provided by the substantial magnetic field, ~ 3 G, that Grennhill et al. deduce for the nuclear region; Elitzur, Hollenbach and McKee (1989) point out that maser spot sizes and luminosities increase with magnetic field strength, although the brightness temperature stays the same.

3. EXTRAGALACTIC OH

The OH main lines at 1665 and 1667 MHz provided the first detection of interstellar molecular lines outside the Galaxy (Weliachew 1971). Narrow emission features superimposed on broad absorption lines were correctly identified as maser emission in NGC 253 by Whiteoak and Gardner (1973) and in M82 by Rieu et al. (1976). In both sources the 1667 MHz line is stronger than the 1665 MHz, similar to the situation in late-type stars and the opposite of that in HII/OH regions. Overall isotropic luminosities of these masers are between 10 — 100 times higher than those of the most luminous OH masers in the Galaxy. Maser background amplification has been suggested in both cases.

3.1 *OH Megamasers*

A new class of extragalactic OH sources was discovered with the detection of broad OH main-line maser emission from IC 4553 (Arp 220) with an unprecedented isotropic luminosity, ~ $10^3\ L_\odot$ (Baan, Wood and Haschick 1982). By comparison, the isotropic luminosity of W3(OH), the prototype Galactic HII/OH region, is only ~ $10^{-5}\ L_\odot$, that of the most luminous Galactic HII/OH region ~ $10^{-3}\ L_\odot$. Thus IC 4553 is almost a million times more luminous than any OH maser source observed in the Galaxy, hence the name *megamaser*. By now, more then fifty megamasers have been detected, ranging in luminosity and redshift all the way up to $L = 0.9\text{x}10^4\ L_\odot$, $z = 0.129$ for IRAS 20100-4156 (Staveley-Smith et al. 1989) and $L = 1.4\text{x}10^4\ L_\odot$, $z = 0.265$ for IRAS 14070+0525 (Baan et al. 1992). The existence of high red-shift sources with OH luminosities of order $10^4\ L_\odot$ was suggested by Burdyuzha and Kromberg (1990), who dubbed them *gigamasers*.

The prototype of this class is IC 4553, the site of the original detection. Optical photographs show that this source has a double nucleus, which may indicate a recent merger. A dark band divides the image in half and is interpreted as a dust lane whose appearance suggests a disk structure. Even though its visual appearance is relatively faint, IC 4553 is a remarkable infrared source whose far-IR luminosity, ~ $2\text{x}10^{12}\ L_\odot$, is comparable to that of the brightest Seyfert galaxies and many quasars. The ratio of IR to blue luminosity is ~ 80, an extremely high value. The IR spectrum is well fitted with thermal dust emission at a temperature of ~ 60 K. OH main lines stand out in single dish spectra as two prominent, broad emission features with full width at half maximum of 108 km s^{-1}. The line shape of the 1667 MHz line is reasonably well fitted with two components, corresponding to a solidly rotating disk superimposed on a Gaussian. Together with HI observations of 21 cm absorption, these data suggest that the main emission originates in a rotating disk, seen edge-on. The 1667 MHz line is stronger than the 1665 MHz, similar to the situation in late-type stars and the opposite of that in HII/OH regions. High-resolution mapping shows that the overall spatial distribution of OH emission closely follows the radio-continuum distribution. Even though the physical conditions in the central continuum component, the dominant core, probably differ substantially from those in the outer, weaker components, the maser emission is uniformly distributed across the entire continuum source. In spite of a spectacular 380 $L_\odot$ isotropic luminosity, the OH brightness temperature of IC 4553 is rather moderate, only ~ $10^6 - 10^7$ K, comparable to that of the radio continuum at the same wavelengths.

All of these properties were incorporated into a simple model by Baan and Haschick (1984) and Baan (1985) that provides the currently accepted standard model for the entire class: OH megamaser emission is low-gain ($\tau \sim 1$) unsaturated amplification of the galactic-nucleus radio continuum by intervening molecular material. The amplifying material resides in molecular clouds, ~ 50 — 300 pc from the nucleus. The clouds are similar to those found in our own galaxy and populate a nearly edge-on rotating disk around the nucleus. The required number of amplifying clouds is ~ 30 — 1000 with a continuum source covering factor of ~ 0.01 — 0.1 and a volume filling factor of ~ $10^{-4} - 10^{-3}$ pc^{-3} (Henkel and Wilson 1990; Baan 1993). Pumping is by far-IR, the only pumping agent that can plausibly permeate the large volume of space necessary for generation of the observed OH luminosities; indeed, all megamaser galaxies are copious infrared emitters with $L(\mathrm{IR}) > 10^{11}$ $L_\odot$! A quadratic relation between OH and IR luminosities of megamaser galaxies was first noted by Martin et al. (1988) and Baan (1989), and supported by subsequent observations (Baan et al. 1992). The IR luminosity distribution of all OH galaxies shows that those displaying absorption are clustered toward the lower luminosity end while megamasers occur at the higher end (Baan 1989, 1991). The distributions of the two groups are almost mutually exclusive, reflecting in all likelihood a separation between low and high effective dust temperatures. While detailed modeling of pumping in megamaser galaxies is not yet available, this trend is in agreement with modeling of OH main-line emission from late-type stars, whose line ratios appear similar to those of megamasers. Such modeling shows that the prerequisites for main-line inversion with $F(1667) > F(1665)$ are high dust temperature ($\gtrsim$ 60 K) and steep IR spectrum (Elitzur 1978).

All of these results indicate that the distribution of molecular clouds around the nucleus could be similar in all OH galaxies and that their different OH signatures arise from differences in dust properties. When the dust is not sufficiently warm to invert the main lines, absorption of the nuclear radio continuum produces OH absorption features. Warmer dust and a steep IR spectrum lead to inversion and background amplification, and the galaxy appears as a weak-gain, high-luminosity megamaser. Similar though much weaker emission may exist in our own Galaxy (Mirabel, Rodriguez and Ruiz, 1989), and this important possibility requires more study. Quite possibly, the key to the entire megamaser phenomenon could be the galactic IR, rather than OH properties.

What is the phase of galactic activity associated with OH megamaser emission? On the average, OH megamasers are more likely to contain Seyfert nuclei rather than star-burst nuclei as compared with the IRAS galaxy sample as a whole. Seyfert 2's are also far more numerous than Seyfert 1's among the megamasers. For megamaser activity to be triggered, the host galaxy must posses the following ingredients: (1) OH molecules, to enable amplification; (2) IR radiation with sufficiently high intensity and color temperature to provide the pump excitations; (3) a radio nucleus to provide the background radiation for amplification; and (4) if the amplifying clouds indeed reside in a disk around the nucleus as has been advocated in a number of studies, the disk orientation with respect to the Earth must allow interception of the nuclear emission. The last requirement is consistent with classification schemes where Syfert 2's have more edge-on inner disks then Syfert 1's.

There are a number of indications that mergers could play a significant role in triggering OH megamaser activity. Norris (1990) has recently proposed that Arp 220, the prototype OH megamaser galaxy, may contain two merging quasar cores and that the entire class of ultra-luminous far-infrared galaxies, which appears to be the parent population of megamaser galaxies, may be characterized by enhanced merger activity. Combined optical, IR and radio study of the megamaser galaxy III Zw 35 shows that it is a pair of galaxies, one of which is an early-type LINER or Seyfert with an active nuclear region — the megamaser location (Chapman et al. 1990).

An ambitious attempt to incorporate megamaser activity into a generalized scheme of galaxy formation has been made by Burdyuzha and Komberg (1990). In their scheme, small mass ($\leq 10^{10}\ M_{\odot}$), gas-rich protogalaxies form at $z \gtrsim 4$ from primeval fluctuations. As the protogalaxies themselves are in groups and clusters, they will experience tidal interactions which in due course can produce dissipative merging of several objects into single massive objects. With these tidal interactions, about ten small objects merge into a single one during $\sim 10^9$ years. This is followed by a brief ($< 10^8$ years) star formation and evolution phase which produces heavy elements (hence OH) and dust. According to this scenario, conditions are right for gigamasers at $z \sim 2$. Although this scheme is rather speculative, the discovery of gigamasers at moderate z's indicates that this phenomenon could be correlated with some early stage of galaxy evolution. If the steep relation between the OH and far-IR luminosities holds over another decade, OH megamaser amplification may be a better diagnostic tool for cosmological studies than the thermal line emission of CO.

Partial support by NSF grant AST-9016810 is gratefully acknowledged.

REFERENCES

Baan, W. A. 1985, *Nature* **315**, 26.

Baan, W. A. 1989, *Ap. J.* **338**, 804.

Baan, W. A. 1991, in *Skyline: Proc. 3rd Haystack Conf.*, eds. A. D. Haschick and P. T. P. Ho (San Francisco: Ast. Soc. Pac.) p. 45.

Baan, W. A. 1993, in *Astrophysical Masers*, eds. G. Nedoluha and A. W. Clegg (Springer Verlag), in press.

Baan, W. A. and Haschick, A. D. 1984, *Ap. J.* **279**, 541.

Baan, W. A., Rhoads, J., Fisher, K., Altschuler, D. R. and Haschick, A. 1992, *Ap. J.* **396**, L99.

Baan, W. A., Wood, P. A. D. and Haschick, A. D. 1982, *Ap. J. Lett.* **260**, L49.

Burdyuzha, V. V. and Komberg, B. V. 1990, *Astr. Ap.* **234**, 40.

Chapman, J. M., Staveley-Smith, L., Axon, D. J., Unger, S. W., Cohen, R. J., Pedlar, A. and Davies, R. D. 1990, *MNRAS* **244**, 281.

Claussen, M. J. and Lo, K. Y. 1986, *Ap. J.* **308**, 592.

Dos Santos, P. M. and Lepine, J. R. D. 1979, *Nature* **278**, 34.

Elitzur, M. 1978, *Astr. Ap.* **62**, 305.

Elitzur, M. 1990, *Ap. J.* **363**, 638.

Elitzur, M., Hollenbach, D. J. and McKee, C. F. 1989, *Ap. J.* **346**, 983.

Elitzur, M., McKee, C. F. and Hollenbach, D. J. 1991, *Ap. J.* **367**, 333.

Greenhill, L. J., Moran, J. M., Reid, M. J., Gwinn, C. R., Menten, K. M., Eckart, A. and Hirabayashi, H. 1990, *Ap. J.* **364**, 513.

Greenhill, L. J. Moran, J. M., Reid, M. J., Menten, K. M. and Hirabayashi, H. 1993a, *Ap. J.* **406**, 482.

Greenhill, L. J. Moran, J. M., Reid, M. J., Menten, K. M., Haschick, A. D., Hirabayashi, H. and Baan, W. A. 1993b, in preparation.

Haschick, A. D. and Baan, W. A. 1985, *Nature* **314**, 144.

Henkel, C. and Wilson, T. L. 1990, *Astr. Ap.* **229**, 431.

Ho, P. T. P., Martin, R. N., Henkel, C. and Turner, J. L. 1987, *Ap. J.* **320**, 663.

Martin, J. M., Bottinelli, L., Dennefeld, M., Gouguenheim, L. and Le Squeren, A. M. 1988, *Astr. Ap.* **201**, L13.

Mirabel, I. F., Rodriguez, L. F. and Ruiz, A. 1989, *Ap. J.* **346**, 180.

Moran, J. M., Greenhill, L. J. and Reid, M. J. 1991, in *Frontiers of VLBI*, eds. Hirabayashi, H., Inoue, M. and Kobayashi, H. (Universal Academic Press).

Norris, R. P. 1990, in *Paired and Interacting Galaxies, IAU colloq. 124*, eds. Sulentic, J. W., Keel, W. C. and Telesco, C. M. (NASA Conference Publication 3098), p 387.

Rieu, N. Q., Mebold, U., Winnberg, A., Guibert, J. and Booth, R. 1976, *Astr. Ap.* **52**, 467.

Staveley-Smith, L., Allen, D. A., Chapman, J. M., Norris, R. P., and Whiteoak, J. B. 1989, *Nature* **337**, 625.

Weliachew, L. 1971, *Ap. J. Lett.* **167**, L47.

Whiteoak, J. B. and Gardner, F. F. 1973, *Astroph. Lett.* **15**, 211.

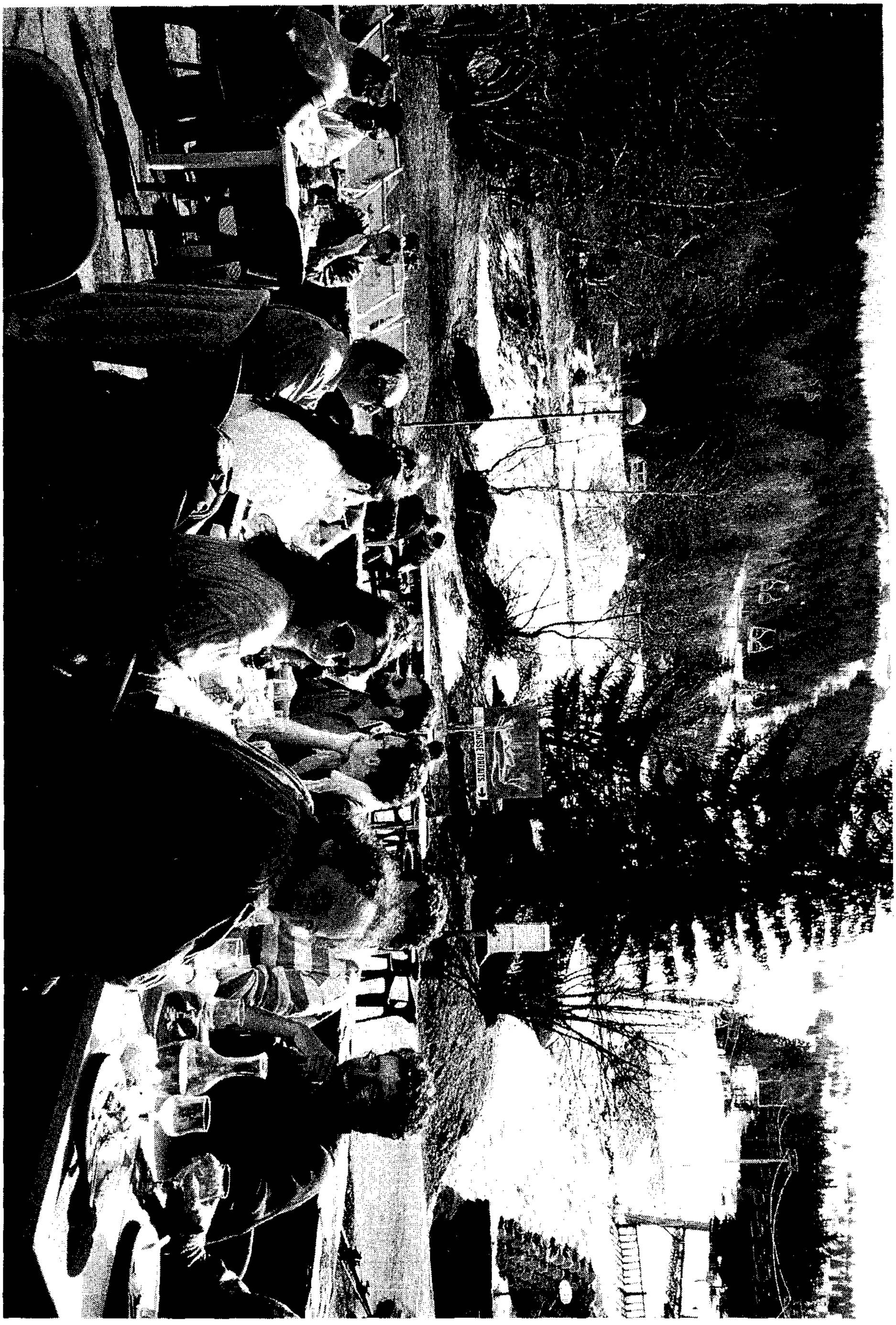

An IR lunch.

DENSE GAS IN NEARBY GALAXY NUCLEI

NGUYEN-QUANG-RIEU
Observatoire de Paris-Meudon,
Demirm-URA336, 92195 Meudon Principal Cedex

ABSTRACT

The study of the dense gas component of the interstellar medium in galaxies has been made possible thanks to large instruments operating at millimeter and submillimeter waves. Highly excited transitions of CO up to the rotational quantum number J = 6 are excellent tracers of the warm and dense gas. Molecular species much less abundant than CO such as CS, HCN and the ion HCO^+ whose excitation requirements are more stringent than those of CO have also been used through multi-transition analyses to probe the dense regions of star formation in the vicinity of galactic nuclei.
Aperture synthesis images of the molecular emission from the nuclear regions of nearby starburst galaxies reveal the presence of molecular cores of the size of giant molecular clouds observed in the centre of our Galaxy. Radio continuum and radio recombination lines are useful tools in studying the properties of the ionized gas near the nucleus.
Atomic fine-structure and molecular lines in the far infrared can be observed towards a large number of galaxies, using the spectrometers on board the ISO satellite. These observations spanning a wide infrared spectrum from 2 to 180 μm will provide valuable information on the physico-chemistry and the excitation of atomic and molecular lines.

1. INTRODUCTION

Over the last decade, the molecular component of the interstellar medium in galaxies has been investigated by means of the J = 1-0 and J = 2-1 CO lines at millimeter wavelengths. These low excitation lines, which are detected in interstellar clouds of gas densities and temperatures as low as ~ 10 cm^{-3} and ~ 5 K, respectively, have been used to study the large scale properties of galaxies. They trace not only the grand design spiral structure but also the more diffuse interarm regions.

Dense and highly excited molecular gas ($n_{H2} \geq 10^4$ cm^{-3} and $T_k \geq 15$ K) is rather confined in the nuclear region where intense star formation activity takes place. This dense and warm molecular component can be better probed by molecular transitions of large excitation energies or high dipole moments, as we shall see later.

The detection of the dense and warm clumps of the size of Giant Molecular Clouds (GMCs) observed in the centre of our Galaxy [1] requires high spatial resolution and sensitivity. A GMC of 50 pc which has an angular size of 2" at a distance of 5 Mpc is small compared to the ~ 10" resolution of large millimeter and submillimeter single dish telescopes currently in operation. In order to minimize the dilution in the telescope beam, the study of the distribution of the dense gas component has been restricted to nearby bright galaxies. Arcsecond interferometry is the most suitable for the observation of the clumpy environment of galactic nuclei.

High resolution observations of the radio continuum and radio recombination lines, give additional information on the ionized component in the nuclear region. The far infrared fine structure lines of atoms are also good tracers of star formation. In particular, the CII line at 158 μm observed with the Kuiper Airborne Observatory (KAO) has been found to be widespread and easily detected in galaxies [2]. The high sensitivity spectrometers of the ISO satellite will offer us a possibility of detecting other atomic and molecular lines over a wide spectral band from ~ 2 to ~ 180 μm in a large number of objects.

2. DENSE MOLECULAR GAS

2.1 High excitation CO lines

The importance to observe high rotational level transitions is twofold:
i) the critical density that is the minimum density for collisional excitation to operate increases with the rotational quantum number J as $(J^4)/(J+1)$. Therefore, high J transitions are more appropriate to probe dense gas.
ii) the observations of as many transitions as possible of the same molecular species provide useful constraints to models of line excitation, thereby leading to a better determination of the physical conditions inside the galaxy.

Furthermore, molecular line emission has an important role in the thermal balance of dense clouds. CO is the dominant coolant of the moderately dense ($n_{H2} \sim 10^4$ cm^{-3}) and warm ($T_K \sim$ 10-40 K) interstellar clouds [3]. In dense clouds, the most efficient cooling is produced by high J transitions, which are difficult to observe owing to the modest performance of the receivers and of the poor atmospheric transmission at submillimeter wavelengths. So far, submillimeter transitions of CO up to rotational quantum numbers as high as J = 6 (level energy = 117 K above the ground state) have been successfully detected at $\lambda \sim$ 0.4 mm (ν= 691.5 GHz) in some nearby starburst galaxies [4]. The infrared luminosity of these objects, ~ 10^{10}-10^{11} $L_{\odot}$, which measures the rate of star formation, is an order of magnitude higher than that of the Galactic Centre. The fact that high J transitions have been detected in the inner ~ 150 pc region of nearby galaxies indicates that the gas is significantly denser (~ 10^4 - 10^6 cm^{-3}) and warmer (~ 30 - 50 K) in galactic nuclei than in the disks.

2.2 Other extragalactic molecules

Although submillimeter CO lines have proven to be useful in investigating the dense gas component, they are not the only lines to trace the gas in regions where shocks and star formation activity take place. Other molecular species of dipole moments larger than that of CO are also suitable for this purpose. Because of their high critical density, which is proportional to the square of the dipole moment, they probe the molecular cloud core ($n_{H2} \geq 10^5$ cm^{-3}). Since the discovery of extragalactic OH and CO, more than twenty molecules have been detected, mostly around λ=3 mm (for details see [5]).

The abundance of most of these molecules is at least four orders of magnitude smaller than that of CO. Therefore, they have mostly been detected in nearby galaxies. At cloud densities higher than ~ 10^4 cm^{-3}, they can compete with CO in the cooling process [3]. Of particular interest are molecules like CS, HCN, and HCO^+, which have dipole moments, ~ 20-30 times that of CO [6],[7]. These molecular lines are among the strongest millimeter lines after CO. The radial distributions of CO, HCN, HCO^+ and CS have been determined for the nearby starburst galaxies, M 82 and NGC 253 observed with the Nobeyama 45 m telescope [6]. There are differences in the line ratios along the major axis of the galaxy. In particular, the CO/HCO^+ and CO/HCN line ratios increase outwards, suggesting that HCO^+ and HCN are more intimately associated with the nuclear star forming region.

Figure 1 shows the (J=1-0) and (J=4-3) spectra of HCO^+ and HCN in the direction of the centre of NGC 253 and M 82 [8]. The CO (J=3-2) line is also plotted for comparison. All these lines have been observed with a similar angular resolution of ~ 25". The millimeter (J=1-0) lines at 89 GHz and the submillimeter lines at 345-355 GHz were observed with the Nobeyama 45 m telescope [6] and with the Caltech Submillimeter telescope [8], respectively. The excitation of the (J=4-3) lines requires special physical conditions since their upper energy level and their critical density are ~ 43 K and ~ 10^7 cm^{-3}, respectively. It is interesting to note that the excited (J=4-3) lines of HCN and HCO^+ are much weaker in M82 than in NGC 253 (see Fig. 1), indicating that the molecular gas is denser and warmer in the latter galaxy, despite practically similar far infrared, ground state and excited CO luminosities.

The results of model calculations in the case of NGC 253 with non-LTE excitation and radiative trapping using both the HCN (J=4-3) and (J=1-0) data are shown in Figure 2 [8]. In this diagram, the solid curves represent the loci of densities and temperatures consistent with the observed HCN (J=4-3) brightness temperature, while the dashed curves correspond to the loci of the same parameters which fit the observed (J=4-3)/(J=1-0) line ratio. In both cases, the central curve represents the observed value, and the curves above and below represent error bars of 30%. Solutions which fit the observed data are at the intersections of the two sets of curves. The line excitation model shows that the solution is not unique and suggests that kinetic temperatures and densities larger than 20 K

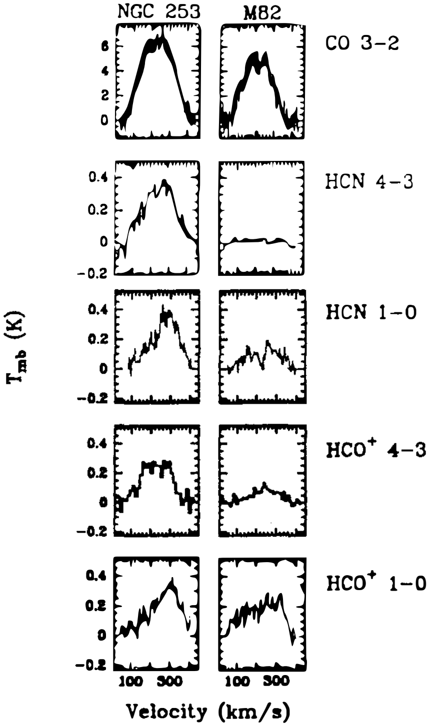

Fig. 1 Millimeter and submillimeter spectra of NGC 253 and M 82

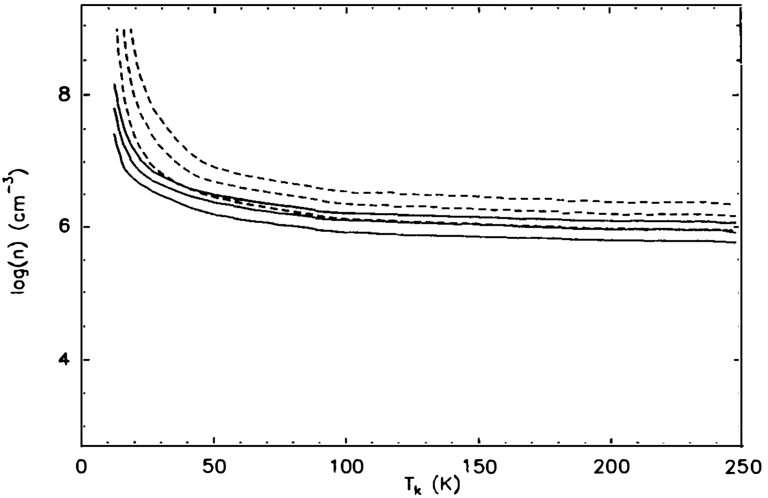

Fig. 2 Model calculations for HCN (J=1-0) and (J=4-3) emissions from NGC 253

and 10^6 cm^{-3}, respectively, are needed to explain the HCN line intensities observed in the nuclear region of NGC 253. The model indicates that the gas density is at least ten times lower in M 82 than in NGC 253. The difference in the gas density between the two galaxies may be explained in terms of an evolutionary model in which NGC 253 is in an early phase of starburst activity, while M 82 may have already dispersed part of its nuclear molecular gas [8]. In both galaxies the densest and warmest molecular gas is confined in a very inner region whose size is $\leq$ 500 pc.

3. INTERFEROMETRIC OBSERVATIONS

The determination of the physical parameters through a model of line excitation requires the knowledge of the detailed distribution of the emission inside the source. Current single dish observations suffer from the fact that the extragalactic interstellar medium is clumpy, leading to uncertain beam filling factors. Interferometric measurements are helpful in clarifying this situation. Arcsecond interferometry currently performed with the IRAM instrument is capable of resolving the inner 1 Kpc nuclear region of nearby galaxies into individual molecular clouds of the size of the GMCs observed in the Galactic Centre.

Figure 3 displays the map of HCO^+ (J=1-0) (89 GHz) emission (contours) overlaid on the CO (J=1-0) (115 GHz) image (grey scale) of the inner 60 arcsec (~ 550 pc at a distance of 1.8 Mpc) nuclear region of IC 342. This galaxy is a nearby spiral seen nearly face on. The CO image is constructed from the data observed with the Nobeyama interferometer at a resolution of 2.4 arcsec [9]. The HCO^+ map was obtained with the IRAM interferometer at a similar resolution [10]. The CO emission is extended and distributed along a S shaped tiny central bar. The inner bar is bent into a ring surrounding the nucleus. The HCO^+ emission is less widespread and more clumpy than the CO image. The three well defined HCO^+ clouds correspond to the densest CO complexes. These results are consistent with the fact that HCO^+ requires a high gas density, ~10^5 cm^{-3}, to be collisionally excited. However, the northern dense CO region has no HCO^+ counterpart. HCO^+ should arise from the cores of the molecular cloud complexes, and is not necessarily closely associated with CO. The HCN distribution is similar to that of HCO^+ [11].

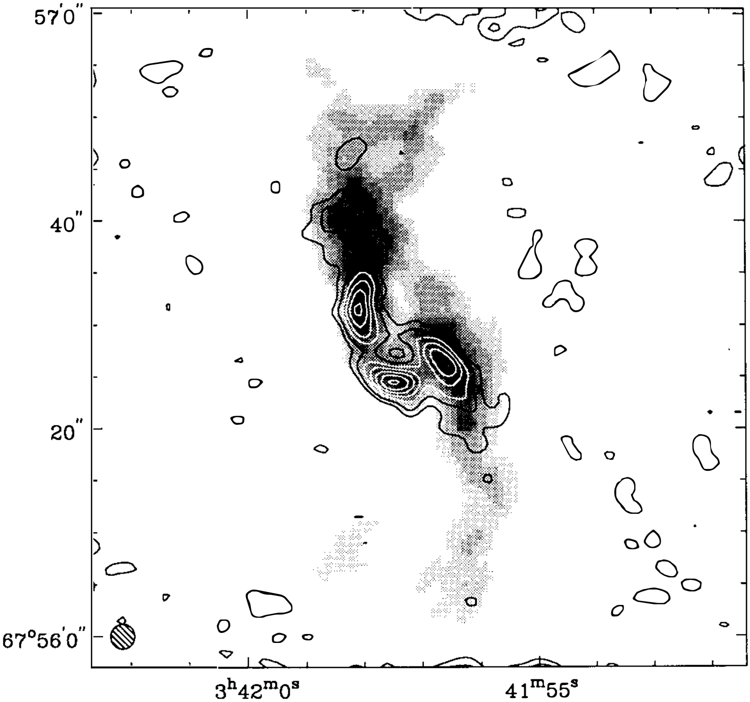

Fig.3 Emissions of CO (J=1-0) (grey scale) and HCO^+ (J=1-0) (contours) from IC 342

The detection of thermal radio continuum at 3 mm [10), 11)] arising from ionized gas suggests that IC 342 is a starburst galaxy undergoing massive star formation activities. Two of the three HCO^+ clouds are associated with the continuum peaks and are located in the CO ring. Such a ring may actually delineate the inner resonance region where gas accumulates before falling onto the nucleus.

4. THE IONIZED COMPONENT

VLA observations of radio recombination lines (RCLs) have been used to determine the distribution of the ionized nuclear component and its kinematics as well as its physical parameters namely the electron temperature and density. The observations of the RCL of hydrogen such as the H92α (8309 MHz) and the H166α (1424 MHz) lines from NGC 253 have shown that these lines arise in

regions of different electron densities [12]. The high frequency H92α line, which is mainly due to spontaneous emission and traces the high electron density regime ($n_e \sim 10^4$ cm^{-3}) is centred on the non-thermal continuum nuclear core. The highly excited CO, HCN and HCO^+ line emissions may originate from this region. The low frequency H166α line, which is dominated by stimulated emission and probes a region of lower density ($n_e \sim 10^2$ cm^{-3}) is shifted by ~ 30" south-east from the continuum peak [12]. These observations have also revealed the existence of peculiar motion of ionized gas along the minor axis near the nucleus.
VLA observations of the H92α line towards the starburst nucleus of NGC 3628 suggest that hundreds of HII regions of a few parsecs in size and thousands of O5 stars may be present in the nuclear region [13]. The detection of the H53α (43 GHz) and H40α (99 GHz) spontaneous emissions from M 82 at millimeter wavelengths provides a reliable estimate of the photoionization rate and electron temperature [14].
The nonthermal radio continuum at 20 cm, has proven to be also a good tracer of star formation [15]. It is expected that the synchrotron emission of the compact nuclear radio source (of size ≤20"), which is separated from the disk component by interferometric measurements, may be correlated with the HCO^+ emission. There is a correlation between the intrinsic luminosity of HCO^+ (Jy km s^{-1} Mpc^2) and that of the 20 cm radio continuum (Jy Mpc^2), especially for starburst and Seyfert galaxies [7]. The reason that the star forming regions of galaxies with active nuclei are rich in HCO^+ may be found in the fact that ionization by cosmic rays produced by supernova explosions is substantial near the nucleus.

5. INFRARED LINES

5.1 Atomic fine-structure lines

The observations with the Kuiper Airborne Observatory (KAO) have shown that the CII ($^2P_{3/2}$ - $^2P_{1/2}$) line at 158 μm is one of the brightest atomic fine structure lines in galaxies [2]. A good correlation is found between the CII and CO (J=1-0) intensities for galaxies with high dust temperatures larger than 40 K (starburst galaxies). The data points corresponding to star forming regions in our Galaxy fall also along the same correlation line, while those corresponding to normal galaxies with low dust temperature are scattered below this line [2]. This suggests that the physical properties of starburst nuclei are similar to those of galactic star forming regions. The CII and CO lines should probe the photodissociated gas at the periphery of warm and dense neutral molecular clouds exposed to a UV field. It is worth noticing that the CO (J=1-0) emission produced in star forming regions and in starburst nuclei arises from warm gas, as indicated by high brightness temperatures and by the detection of high-J rotational transitions. Like the ion C^+, neutral oxygen $\overset{o}{O}$ is also a photodissociation product of CO. The KAO observations of the bright OI ($^3P_1$-$^3P_2$) line at 63 μm are somewhat hindered by the high thermal background and the presence of an adjacent telluric water vapour feature. Therefore, the OI emission is more difficult to detect in galaxies than the CII emission, which seems to be widespread. Neutral carbon is also expected to arise from moderately dense photodissociation regions (critical density ~ 10^3 cm^{-3}). The detection of the neutral carbon CI ($^3P_1$-$^3P_0$) line at 0.6 mm in IC 342 has recently been reported [16]. These CI observations have been made using the ground-based telescope at the Caltech Submillimeter Observatory. Atomic lines corresponding to species with high ionization potentials like the OIII (52 and 88 μm), SIII (19 and 33 μm), and NII (122 μm) lines can be used to trace the bright HII regions near the nucleus. Some of these lines are not observable with the KAO because of the presence of telluric features.

The short and long wavelength spectrometers (SWS and LWS) on board the Infrared Space Observatory (ISO) satellite will offer us an opportunity to observe atomic fine structure lines with a sensitivity higher than that of the KAO and totally free from the terrestrial atmosphere.

5.2 Far infrared molecular lines

So far no extragalactic molecular transitions have been detected in the far infrared. This is due to the fact that the infrared transitions, which connect with high rotational levels necessitate higher densities and temperatures than the submillimeter transitions to be excited. For example, the upper level of the CO (J=15-14) line at 174 μm, which is observable with the LWS lies at 665 K above the ground. With a critical density ~ 10^5-10^6 cm^{-3}, this line is appropriate to investigate the very inner hot and dense nuclear region of galaxies. High J transitions of CO should be searched for in nearby starburst galaxies using the ISO instruments.

H_2O which is relatively abundant (fractional abundance ~ 10^{-5}) is also a good candidate. Since water is photodissociated into OH, the observations of both species are helpful in determining the physico-chemistry in the nuclear photodissociation region, which is a reservoir of UV photons and cosmic rays. Since water and OH exhibit strong maser emission in the microwave range, the observations of thermal infrared transitions of these molecules, which play a key role in the population transfer to lower energy levels will provide valuable constraints on the pumping mechanisms of extragalactic masers, whose case is still open.

REFERENCES

1) Bally, J., Stark, A.A., Wilson, R.W., & Henkel, C. 1987, Ap.J.S. 65, 13

2) Stacey, G.J., Geis, N., Genzel, R., Lugten, J.B., Poglitsch, A., Sternberg, A., & Townes, C.H. 1991, Ap.J. 373, 423

3) Goldsmith, P.F., & Langer, W.D. 1978, Ap.J. 222, 881

4) Harris, A.I., Hills, R.E., Stutzki, J., Graf, U.U., Russell, A.P.G., & Genzel, R. 1991, Ap.J. 382, L75

5) Henkel, C., Baan, W.A., & Mauersberger, R. 1991, A.&A. Rev. 3, 47

6) Nguyen-Q-Rieu, Nakai, N., & Jackson, J.M. 1989, A.&A. 220, 57

7) Nguyen-Q-Rieu, Jackson, J.M., Henkel, C., Truong-Bach & Mauersberger, R. 1992, Ap.J. 399, 521

8) Jackson, J.M., Paglione T.A., Carlstrom, J.E., & Nguyen-Q-Rieu 1992 (Ap.J. submitted)

9) Ishizuki, M., Kawabe, R., Ishiguro, M., Okumura, S.K., Morita, K-I., Chikada, Y., & Kasuga, T. 1990, Nature 344, 224

10) Nguyen-Q-Rieu, Viallefond, F., Combes, F., Jackson, J.M., Lequeux, J., Radford, S., & Truong-Bach 1992, IAU Coll. 140, Astronomy with Millimeter and Submillimeter Wave Interferometry 5-9 October 1992, Hakone, Japan

11) Downes, D., Radford, S.J.E., Guilloteau, S., Guélin, M., Greve, A., & Morris, D. 1992, A.&A. 262, 424

12) Anantharamaiah, K.R., and Goss, W.M. 1990, Radio Recombination lines: 25 Years of Investigation, M.A. Gordon & R.L. Sorochenko (eds), Kluwer Academic Pub, 267

13) Anantharamaiah, K.R., Jun-Hui Zhao, Goss, W.M., Van Gorkom, J.H., & Viallefond, F. 1993 in preparation

14) Puxley, P.J., Brand, P.W.J.L., Moore, T.J.T., Mountain, C.M., Nakai, N., and Yamashita, T. 1989, Ap.J. 345, 163

15) Braine, J. 1993, A.&A. in press

16) Buttgenbach, T.H., Keene, J., Phillips, T.G., & Walker, C.K. 1992, Ap.J. 397, L15

IMAGING OF THE EDGE-ON GALAXY N891 IN THE 3.3 μm PAH FEATURE

Daniel Rouan, P. Normand, F. Lacombe, D. Tiphène
Département Spatial, Observatoire de Paris-Meudon
92195 MEUDON Cedex, France

ABSTRACT
We present K and 3.3 μm images of the nearby, almost perfectly edge-on, spiral galaxy N891, taken at CFHT with the IR camera Circus. The line, whose emission was convincingly attributed to C-H bond in PAHs molecules of the diffuse ISM, is probably detected throughout the whole plane of the central region of this galaxy. The distribution, at a scale of 3 arc-sec (= 150 pc), exhibits features that are very reminiscent, in terms of thickness, smoothness and contrast of the line, of the distribution of the same component in the ISM of the Milky Way, as detected a few years ago by the baloon experiment AROME. The idea of a diffuse PAH component ubiquitously found in quiet spiral galaxies is thus strongly supported.

1- PAHs in the diffuse component of the ISM

A few years ago, Giard et al., using the baloon-borne experience AROME detected unambiguously the 3.3 μm emission band throughout the whole Galactic plane [6),7)]. This result showed that the carrier of this emission, presumably very small particles, was associated to the diffuse Insterstellar Medium on a large scale and was abundant. Since the 3.3 μm band corresponds to a vibrationnal mode of the C-H bond, it was proposed that large Polycyclic Aromatic Molecules (PAHs) [8),1)] were the actual carriers. Those particles emits IR radiation by fluorescence when transiently heated by a UV photon, so their emission should peak in UV-rich regions such the large complexes of star formation. On the other hand, it has been shown that the strong correlation between IRAS colour, specially the 12 μm band, and the presence of the IR features is a clue that PAHs are closely associated to, or even identified with, the very small grains responsible for the peculiar IRAS colours of all the ISM components (H^+, HI, H_2), which imply a component of high temperature grains [4)]. Despite their good stability, PAHs may be dissociated when the density of the UV field becomes larger than $\approx$ $5 - 10$ eV cm^{-3}: this would explain why the abundance of PAHs varies largely and why they are lacking in center of H^+ regions [3)], in AGN[5)], or even in the heart of starburst nuclei[10)].

Indeed the 3.3 μm feature was observed in several galaxies[9)], but generally starburst galaxies where young stars are responsible of a large UV density, heating efficiently PAHs. Detailed mapping at 3.3 μm of normal spiral galaxies, preferably edge-on to increase the column density, should then provide important pieces of information such as spatial distribution and clumpiness, heating, destruction/formation equilibrium, on this component of the ISM whose mass is comparable to that of the CO molecule [11)].

2- The edge-on galaxy N891

N891 is one of the most perfectly edge-on nearby spiral galaxy (inclination = 89^o) exhibiting in the visible a very well defined dust lane. This galaxy is specially interesting since it is an extrelemy close analogue of our Galaxy: for instance, it is one of the rare galaxies to show, as in the Milky Way, a CO molecular ring with a distinct gap between the intense nuclear peak and the ring [15),13)]. If the maps made by IRAS [14)] have too poor an angular resolution compared to the disk thickness to measure a disk brightness, on the other hand, the the ratio $\nu I_\nu(12\mu m)/(\nu I_\nu(60\mu m) + \nu I_\nu(100\mu m))$, a sensitive indicator of the abundance of small grains [3)] has a value (0.13) extremely close to the galactic one (0.14). For all those reasons, it was tempting to try to repeat on this galaxy the successful observations of the large scale emission of the 3.3 μm PAH feature made, in our Galaxy, by Giard et al.[6)]

3- Observation, data reduction

A search for the 3.3 μm feature in an edge-on quiet galaxy (NGC 4565) was already made by Adamson and Whittet [2)] who reported a probable detection; however their measurement was done using a spectro-photometer with 12 arc-sec diaphragm that did not give any spatial information. The results we present correponds likely to the first attempt done in a high angular resolution imaging mode.

The main difficulty of this observation comes from the extremely low brightness to be detected which is of the order of 60 $\mu Jy('')^{-2}$ in the line, while the instrumental and atmospheric background amounts to $\approx$ 1 $Jy('')^{-2}$: we thus restricted the long integration on the nuclear region, where Solomon[12)] showed that molecular hydrogen is largely dominating.

The observations were performed using the IR camera *Circus*, developped by the DESPA (Obs. de Paris-Meudon) to be essentially used at the f/36 IR focus of the Canada-France-Hawaii 3m60 telescope on the Mauna-Kea observatory (Hawaii). This instrument features a 128 $\times$ 128 - InSb detector from AMBER, standard filters in 1 - 5.2 μm plus two dedicated 3.3 μm filters (line and continuum); the plate scales used here is 0.50"/pixel (field 64"$\times$64"); the pixel full well storage capacity of $\approx 40\ 10^6\ e^-$ gurantees a sky noise limited regime.

The central region around the assumed position of the nucleus, hidden in the visible, was mapped at 3.3 μm (line and continuum) and in the K band. Sky and object frames were alternatively recorded,

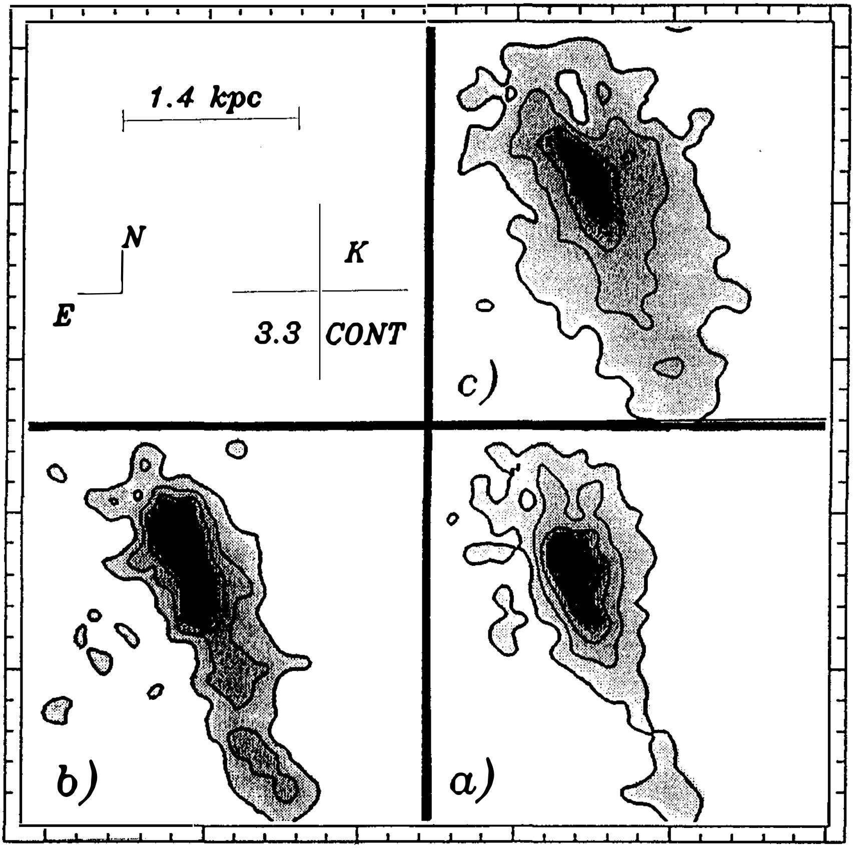

Figure 1: The edge-on galaxy N891 seen in three IR filters: 2.2 μm, narrow 3.3 μm (line) and broad 3.3 μm (continuum). The three maps have been scaled to the same dynamic range, with a low cut at 5 % of the maximum. The linear scale is given assuming a distance of 9.7 Mpc

by offseting the telescope rather than moving the secondary mirror, with elementary integration times of 6 and 9 seconds on the continuum and the line respectively. The integration was repeated two successive nights and gave a total of 3.5 hours on the line and 1 hour on the continuum after selection of periods not affected by cirrus.

A micro-scanning plus median filtering method was used to reduce the effects of bad pixels. Finally a 3 arc-sec FWHM gaussian was convolved to the image in order to increase the signal to noise at the price of a reduced angular resolution.

4- Probable detection of the large scale component of PAHs

At an assumed distance of 9.5 Mpc, the field of CIRCUS (64×64 $arc - sec^2$) corresponds only the to the inner 3 kpc diameter region. The three maps are presented in Fig. 1.

The continuum map (Fig. 1-a) reveals a distribution of the emission along the major axis which is much closer from the CO distribution than from the 2.2 μm image, assumed to trace the stellar component: the 2.2 μm map (Fig. 1-c) shows a narrow peak at the nucleus with a smooth falloff with increasing distance, while the 3.3 μm continuum exhibits a well defined nuclear disk of typically 1 kpc FWHM (the same size as mesured on the CO data from Scoville et al.[13]) and a local smaller peak at 1.8 kpc distance from the nucleus, probably indicating a giant $H^+/H2$ complexe of star formation that could be the counterpart of a small enhancement in the CO emissivity. This secondary peak is also present on the K and the line image.

Despite its lower signal to noise ratio, the map in the 3.3 μm line (Fig. 1-b) is of sufficient quality to give the following pieces of informations:

- The line is probably detected with a significant contrast: the histogram of the ratio of line to continuum peaks at 1.20, which is precisely the value measured by ARÔME in the inner ($8.5^o < l < 35^o$, $|b| < 1^o$) Milky Way [7]. Note that this rather small contrast results from two effects: an instrumental one, the line filter bandwidth which is not so narrow, and an astronomical one, the dilution of the line by the stellar light.
- The intensity distribution has grossly the same characteristics as the continuum map, with however a smaller contrast between the central peak and the outer parts: such a behaviour, observed in our Galaxy, is expected since the stellar emission at the nucleus is comparatively more important in the continuum, diluting the PAH emission, while in the line, the PAH emission from the diffuse medium is more uniformly distributed.
- The distribution of the line emission in the direction perpendicular to the plane of the galaxy is significantly narrower than in the continuum, a fact in agreement with the molecular disk thickness (FWHM = 160 to 280 pc = 3.6 - 6 arc-sec) found by Scoville et al. [13]: the 3.3 μm line map would reflect essentially the thin molecular content, while the more extended continuum is largely contaminated by the stellar light from the bulge.

Those observations deserve a more thoroughful analysis, but we can already put forward that they probably confirm and extend to other spiral galaxies the result obtained in our Galaxy by the baloon-borne experiment ARÔME, namely *the ubiquity of the component of PAH molecules in the diffuse interstellar medium of normal (quiet) spiral galaxies* and the similarity of the properties of this component in terms of spatial distribution along and perpendicular to the disk and in terms of line contrast.

References

1. Allamandola L.J., Tielens A.G., Barker J.R., 1985, ApJ 290, L25
2. Adamson, A.J. and Whittet, D.C.B., 1990, A&A 232, 27
3. Boulanger, F. et al., 1988, ApJ 332, 328
4. Désert, F.-X., Boulanger, F. and Puget, J.L., 1990, A&A 237, 215
5. Désert, F.-X. and Dennefeld, M., 1988, A&A 206, 227
6. Giard M. et al., 1988, A&A 201, L1
7. Giard M. et al., 1989, A&A 215, 92
8. Léger A. and Puget J.L., 1984, A&A 137, L5
9. Moorwood, A.F.M., 1986, A&A 166, 4
10. P. Normand, D. Rouan, F. Lacombe et D. Tiphène, 1992, in proc. of *Astronomical IR Spectroscopy Conference*, Kwok Ed
11. Puget J.L. and Léger A., 1989, ARA&A, 27 , 161
12. Solomon, P.M., 1983, in *Internal Kinematics and Dynamics of Galaxies*, Athanassoula Ed
13. Scoville N.Z. , et al., 1993, ApJ 404, L59
14. Wainscoat, R.J., deJong, T. and Wesselius, P.R., 1987, A&A 181, 225
15. Young J.S. and Scoville N.Z., 1991, ARA&A, 29, 581

SUBMILLIMETRE OBSERVATIONS OF GALAXIES

D.L. CLEMENTS
Oxford University Physics Department
P. ANDREANI
Dipartimento di Astronomia, Universita' di Padova

Abstract

We present the first results from a programme of millimetre and submillimetre observations of a sample of galaxies selected from the IRAS catalogue. We find that a single dust component with a $\nu^2 B_\nu$ emissivity law fits the data well. Dust temperatures range from 28 - 35 K. We also present new results on the distribution of mm/submm emission in the galaxy NGC 3597. In contrast with earlier results, which supported the assumption that the dust distribution is more compact than the stellar emission, NGC 3597 seems to have its mm/submm flux distributed on a larger scale. Extended dust distributions allow for a much greater range in dust properties, including the possibilities of extra cold components (T < 20 K). Future instruments, such as bolometer arrays, will be necessary to address these problems.

Introduction

The IRAS satellite survey has shown that many galaxies, particularly spirals, radiate significant fractions of their luminosity in the Far Infrared (FIR). This radiation is predominantly thermal in origin, and is thought to be produced by cool dust in giant molecular clouds, star formation regions and in the general interstellar medium. Determination of the overall properties of this dust is difficult, however, since the emission spectrum is still rising in most objects at wavelengths as long as 100 μm. We can thus set an upper limit to the dust temperature, of around 50 K, but a proper determination of the dust temperature, emissivity law, etc. requires observations at longer, millimetre and submillimetre (mm/submm) wavelengths (Mathis et al 1983). Once dust properties for a range of galaxies have been determined, it will be possible to look for systematic differences between different classes of objects, and to compare nearby galaxies with objects at large redshift such as 10214+4724 (Clements et al 1992). We here summarise results from mm/submm observations of a number of galaxies conducted at the JCMT, SEST and IRAM 30m telescopes.

Dust Temperature and Emissivity Law

There has been much debate as to whether the mm/submm emission from galaxies is dominated by one or two components (e.g. Chini 1986), and what the temperature and emissivity law of this dust might be. The emissivity laws favoured range from $\nu^1 B_\nu$ to $\nu^2 B_\nu$ (e.g. Draine & Lee 1984), where B_ν is a normal Black Body emission law, and include the possibility of breaks in the additional power law at various frequencies. Observational data, where available, has so far tended to favour the $\nu^2 B_\nu$ emission law (e.g. Eales et al 1989). The results of our observations are summarised in Table 1.

Object	Distance	60 μm (Jy)	100 μm (Jy)	450 μm (mJy)	800μm (mJy)	1.1/1.25* mm (mJy)
1454+24	136 Mpc	7.04 ± 0.8	16.7 ± 2	412±80	63 ±12	40 ±13
1312+24	52 Mpc	19.0 ± 2.3	19.1 ± 3	370±100	64 ±11	40±8.4*
1046+26	103 Mpc	2.32 ± 0.3	2.48 ± 0.3	247±70	< 41	3.5±1.4*
1234+24	92 Mpc	4.1 ± 0.2	5.7 ± 0.2	< 120	< 39	7.9 ±2.4*
0953+27	16 Mpc	3.8 ± 0.15	8.0 ± 0.3	< 760	< 73	9.3 ± 0.9 mJy*

Table 1: Results of Observations

Results of JCMT observations, together with distance data (assumes H_0=75) and IRAS data (Smith et al 1987). Fluxes marked * are 1.25 mm data from IRAM 30m observations (Andreani et al 1990). Error values are 1σ and include calibration uncertainties. All measured fluxes are > 3 σ detections with most > 4 σ whilst upper limits are at the 2 σ level.

The results of our fits show that:

(1) There is no indication of two dust components, one cold ($\approx$ 15K), one hot ($\approx$ 50K), as suggested by Chini et al 1986.

(2) We find that the $\nu^2 B_\nu$ model is a better fit to all the galaxies than a $\nu^1 B_\nu$ law. We do not have sufficient signal to noise or frequency coverage, to attempt to discuss any of the models with a break in the emissivity law.

(3) Several of the galaxies show excess 1.3 mm emission above that predicted by the $\nu^2 B_\nu$ model. This may be due to weak non-thermal emission.

An example of the observations and fits to the data using both $\nu^1 B_\nu$ and $\nu^2 B_\nu$ emission are shown in Figure 1.

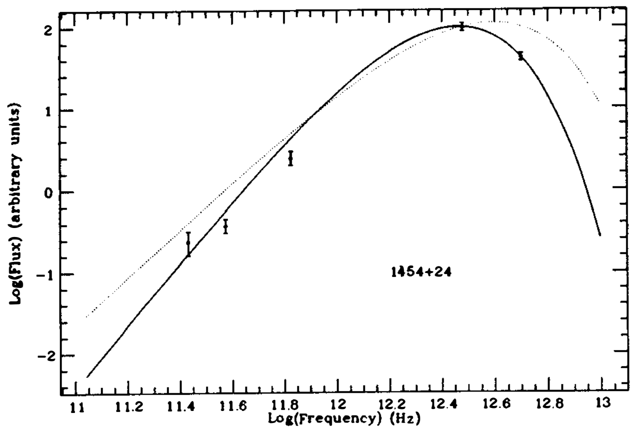

Figure 1: Comparison of observations with spectral fits for 1454+24
The solid line represents the ν^2 emissivity law, and the dotted line the ν^1 law. Data are from IRAS (60 and 100 μm points) and JCMT. Data and fits are normalised to 100 at 100 μm. Measured fluxes are shown as triangles with 1 σ error bars.

Dust Distribution

Unfortunately, we cannot be wholly confident that the IRAS and mm/submm observations are measuring emission from the same material. This is because there is a serious mismatch in the beamsizes of the mm/submm instruments (typical beamsize $\sim$ 20 arcseconds) and those of the IRAS 60 and 100 μm channels ($\sim$ 1.5 arcminutes). We would thus be underestimating the mm/submm emission relative to the IRAS fluxes if the dust in our target galaxies was distributed on arcminute scales. To cope with this problem the galaxies discussed above were all selected to have small optical sizes, $<$ 90 arcseconds, and we assume that the mm/submm emission is more compactly distributed than the optical emission. Initial mapping observations of NCG 992 suggested that this assumption was justified (Andreani & Franceschini 1992). However, more recent observations of an additional object imply that this assumption may not be as reliable as first thought, and that the details of the mm/submm emission, when compared to the optical emission, may vary significantly from object to object. Figure 2 shows these results, on the galaxy NGC 3597. The mm/submm emission is clearly extended on greater scales than the optical emission.

If the galaxies discussed above have mm/submm flux distributions similar to NGC 992, with an exponential scale length less than one third of the optical scale length, then our conclusions on the dust properties are unchanged. If their dust is distributed more like NGC 3597, then the total mm/submm fluxes are much greater than those measured

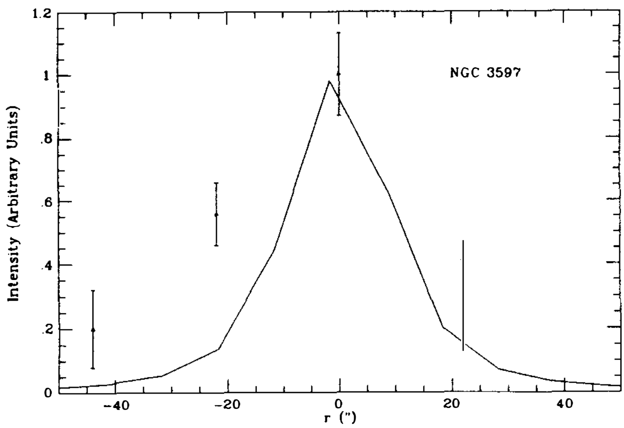

Figure 2: Comparison of optical and mm/submm flux distributions

in the $\sim$ 20" JCMT beam, and the far-IR to mm/submm spectrum is consequently much flatter. An additional component of cold dust or a flatter intrinsic dust spectrum may thus be permitted, and there will certainly be a greater total dust mass.

A more detailed study of the mm/submm flux distributions in a range of objects is thus needed to clarify this matter. Bolometer arrays and submillimetre interferometers are probably the optimum instruments for such studies. In the interim, we must take great care in the application of reasonable beam correction schemes and in the selection of objects.

References

Andreani, P., & Franceschini, A., 1992, *A. & A.*, **260**, 89.
Chini, R., Kreysa, E., Krugel, E., & Mezger, P.G., 1986, *A. & A.*, **166**, L8.
Clements, D.L., Rowan-Robinson, M., Lawrence, A., Broadhurst, T., & McMahon, R., 1992, *MNRAS*, **256**, 35p.
Draine, B.T., & Lee, H.M., 1984, *Ap. J.*, **285**, 89.
Eales, S.A., Wynn-Williams, G.G., & Duncan, W.D., 1989, *Ap. J.*, **339**, 859.
Mathis, J., Mezger, P.G., & Panagia, N., 1983, *A. & A.*, **128**, 212.

STARBURSTS AND COLLIDING GALAXIES

I. Felix MIRABEL and Pierre-Alain DUC

Service d'Astrophysique, CE-Saclay
91191 Gif sur Yvette cedex, France
e-mail: mirabel@sapvxg.saclay.cea.fr

ABSTRACT

Galaxy-galaxy collisions induce nuclear and extranuclear starbursts. The sudden reduction of angular momentum of the interstellar medium due to the gravitational impact of the encounter leads to the subsequent infall to the central regions of a large fraction of the overall interstellar gas. Starburst galaxies with bolometric luminosities $\geq 10^{11}$ $L_\odot$ have converted most of the HI into H_2 reaching extreme nuclear densities of molecular gas. We also discuss extranuclear starbursts in relation to the formation of dwarf galaxies in mergers. As a consequence of tidal interactions a fraction of the less gravitationally bound atomic hydrogen that populates the outskirsts of the pre-encounter disk galaxies may escape into intergalactic space. We find that the ejected gas may assemble again and collapse, leading to the formation of intergalactic starbursts, namely, tidal dwarf galaxies.

1 "STARBURST GALAXIES"

"Starburst" denotes star formation at higher rates than in normally, self-regulated processes. They are non-equilibrium episodes that last only a small fraction of the total life-time of the host stellar systems. "Starburst galaxies" are stellar systems where the overall energy output is dominated by recently formed stars. In the context of this definition we must distinguish the "extragalactic HII regions" (Searle and Sargent, 1972) from the "nuclear starburst galaxies" (Weedman et al. 1981). The first are small, irregular, and dust-poor galaxies where the starburst is encompassing most of the visible galaxy; the second are massive luminous galaxies where the most violent starburst takes place embedded in dust in the central regions. The extragalactic HII regions are identified optically either by the unusual ultraviolet continuum radiated by hot stars, or by the strong narrow emission lines that arise in the interstellar nebulae ionized by massive stars. A large sample of nuclear starburst galaxies were first identified by Balzano (1983) in the Markarian (1967) survey of extragalactic objects with strong ultraviolet continua.

The recent developments in infrared astronomy have permitted a new, less biased way to identify luminous starburst galaxies. Since the most violent nuclear star formation takes place within high optically thick clouds of dust and molecular gas that convert most of the visible and UV light into far-infrared radiation, the far-infrared luminosity has become the best indicator of the starburst bolometric luminosity. The optical absorption along the line of sight to the nuclear starbursts is often so high that a large fraction of the most extreme starburst galaxies had passed unnoticed in the optical surveys.

1.1 Luminous infrared galaxies

The Infrared Astronomical Satellite (IRAS) discovered a new class of luminous extragalactic sources of infrared radiation. These are galaxies that radiate a large fraction of their total energy in the far-infrared (FIR). The most extreme galaxies of this type, which radiate more than 10^{11} solar luminosities in the IRAS broad wavelength bands (12, 25, 60, 100μm) are named "luminous infrared galaxies". It is striking that the FIR luminosity of these galaxies can be equivalent to the bolometric luminosity of quasars, namely, about 10 times the optical luminosity of the first-ranked cD galaxies in rich clusters.

The study of luminous infrared galaxies has now become a key area in extragalactic research for two reasons: (1) We now realize that among objects with luminosities above 10^{11} $L_\odot$ the IRAS luminous galaxies are the dominant population of objects in the Universe; and (2) there is the increasing evidence that luminous infrared galaxies may represent an early phase in the evolution of galaxies. Their study may provide clues for our understanding of the genesis of some elliptical galaxies (e.g. Wright et al. 1990), quasars (Sanders et al. 1988), and radio galaxies (Mirabel, 1989).

Most of the FIR emission from galaxies is due to the absorption and re-emission of light by dust. In addition, from the IRAS colors we know that a large fraction of the FIR emission in luminous infrared galaxies is produced by warm dust. At present it is debated if the ultimate source of light that heats the dust consists solely of large amounts of recently formed stars, or if, in addition, the formation of massive compact objects with

X-ray emitting accretion disks is also required to explain the colossal amounts of thermal energy radiated in the FIR.

1.2 Historic background

Before the IRAS mission some of the ultraluminous Infrared galaxies had already attracted the attention of observational astronomers because of their peculiar properties in the optical, near infrared, and/or radio wavelengths. In fact, some of the prototypes of this class of objects (e.g. Arp 220) had enough unusual optical morphologies to warrant their inclusion in Arp's Atlas of Peculiar Galaxies (1966), and had been selected as prototypes of merger galaxies in the work by Joseph and Wright (1985). In addition, near infrared observations by Riecke and Low (1972) had shown that some of the objects that had been classified as quasars and/or active galaxies (e.g. Mrk 231, I Zw1) showed abnormally high near infrared luminosities.

Radio astronomers had also identified at centimeter wavelengths some of the ultraluminous infrared galaxies as members of a class of "bright radio-spiral galaxies" (Condon, 1980). These appeared as sources with radio-to-optical luminosity ratios more than an order of magnitude above the typical ratio for gas-rich galaxies. The radio spectral properties of these galaxies were somewhat perplexing. At λ21 cm they showed very broad atomic hydrogen absorption lines, indicating large amounts of unusually turbulent neutral gas (Mirabel, 1982). Another unexpected idiosycracy of these galaxies was the exceptionally bright hydroxyl maser emission comming from the nuclei (e.g. Baan, Wood, and Haschick, 1982).

1.3 Optical morphology: mergers of spiral galaxies

In the last two decades there has been an almost explosive growth of publications reporting evidences that interactions trigger starbursts in galaxies. After the seminal papers by Toomre and Toomre (1972) it was realized that interacting galaxies are more active in the UV (Larson and Tinsley, 1978), near infrared (Joseph and Wright, 1985), optical emission line strength (Kennicut and Keel, 1984), and radio emission (Stocke, 1978; Hummel, 1981).

However, the optical morphology of ultraluminous infrared galaxies has been a subject of recent controversy. From low resolution images of 10 ultraluminous infrared galaxies of the Bright IRAS galaxy sample obtained with the 1.5m Palomar telescope Sanders et al. (1988) concluded that nearly all ultraluminous infrared galaxies are strongly interacting merger systems. On the other hand, from images of a sample of luminous IRAS galaxies in the North Polar Cap obtained at La Palma, Lawrence et al. (1989) concluded that although galaxy interactions may be a common causal factor in luminous IR activity, it may not be an ubiquitous factor as had been suggested by Sanders et al. (1988).

In this context, Melnick and Mirabel (1990) obtained New Technology Telescope (NTT) images of the 16 nearest southern ultraluminous galaxies up to $z = 0.13$. The excellent quality of the NTT optics and the good seeing conditions on La Silla were fully exploited to reveal possible faint morphological features (e.g. Figure 1). Melnick and

Mirabel (1990) found that all the objects of this nearby sample of southern ultraluminous galaxies show the features that Toomre and Toomre (1972) had identified as resulting from gravity in disk-disk mergers. Tails, wisps and double nuclei are apparent in all galaxies at cz $\leq$ 25,000 km s^{-1}. However, the faint extended features that are characteristic of tidal interactions become less ostensible at cz $\geq$ 25,000 km s^{-1}, and only the brighter, distorted main bodies of the galaxies remain easily visible. From this imaging survey Melnick and Mirabel (1990) concluded that the faint extended features provoked by gravity during galaxy-galàxy collisions may become blurred at higher redshifts.

Rowan-Robinson (1990) and Sanders (1992) have in addition reviewed the results of optical imaging of larger samples of luminous galaxies. Sanders (1992) realized that the increase of luminosity is correlated with the degree of interaction as measured by the projected separation of galaxy nuclei. Rowan-Robinson (1990) noted that the percentage of interacting or merging galaxies increases steadily with increasing luminosity, concluding that the disagreements on the optical morphology between the different groups are now within the statistical uncertainties.

Melnick and Mirabel (1990) find a critical separation of 10 kpc between the nuclei of the colliding galaxies of their sample of ultraluminous galaxies. In other words, advanced merging seems to be a necessary condition for the greatly enhanced infrared luminosity. We point out that although merging is a necessary condition, it is not sufficient, since there are strongly interacting, and even merging systems that are not ultraluminous in the infrared. This is an indication that in order to bust the luminosity of the mergers, in addition to restricted sets of orbital parameters, the pre-encounter galaxies must be rich in interstellar gas.

2 NUCLEAR STARBURTS

The diverse forms of nuclear activity are likely to be fed by fresh gas. In particular, the most violent starbursts in the nuclei of luminous infrared galaxies appear to be the consequence of high concentrations of molecular gas in the central regions. It is found that the most efficient starbursts measured by the large $L_{fir}/M(H_2)$ ratios always have, as expected, the highest space densities of H_2.

The high concentrations of molecular gas in luminous IR galaxies must be a consequence of inward motions of the disk gas during collisions. To concentrate $\geq$ 50% of the overall interstellar gas in the nuclear region, gas from distances $\geq$ 10 kpc must be driven into the center in $\leq 10^9$ years. This implies mean infalling velocities of $\geq$ 10 km s^{-1}. When the systemic velocity of the galaxies are accurately known, observations of HI absorption at λ21 cm can be used to probe the kinematics of the cold gas along the line of sight to the nuclear radio continuum source. Since in colliding galaxies the HI absorption has typical half-widths $\geq$ 100 km s^{-1}, and the optical redshifts may have large errors, the analysis must be of statistical nature. Following this idea, Dickey (1986) and Mirabel and Sanders (1988) concluded, with some caveats, that in nuclear starburst galaxies there is infall of HI at a rate of $> 1\ M_{\odot}$/yr.

Large scale starbursts are expected to take place in stellar systems that readily form molecular gas out of atomic gas. Such high efficiencies of molecular cloud formation are

Fig. 1—CCD image of the "Superantennae", a prototype of ultraluminous infrared galaxy, obtained with the 2.2m telescope of ESO. This remarkable example of ultraluminous infrared galaxy at a distance of 250 Mpc is the product of the collision 10^9 years ago of two giant galaxies. From tip to tip, the tails extend across 350 kpc. The detailed study of this galaxy by Mirabel, Lutz and Maza (1991) showed that the tails emanate from a merger of giant gas-rich galaxies that harbor two nuclei (one Seyfert, one starburst) separated by 10 kpc. More than 80% of the energy radiated by this powerful infrared system comes from the deeply obscured Seyfert nucleus. On the left, a mosaic image of the whole system is shown, on the right the two nuclei embedded in the central part. The left scale bar corresponds to 1', the right one to 10" (= 10 kpc) in the central region.

likely to take place in merging spiral galaxies. When the mean densities become $\geq 10^2$ cm^{-3} most of the HI gas turns into molecular form. To study the overall faction of the interstellar gas that has been converted into molecular form, Mirabel and Sanders (1989) used the results from their HI and CO surveys of galaxies with FIR luminosities in the range of $2\ 10^{10}\ L_\odot$ to $2\ 10^{12}\ L_\odot$. In Figure 2 are shown the diagrams that resulted from this study. Figure 2a) shows that the CO(1→0) to HI global luminosity ratios of galaxies are proportional to the overall FIR excess. Of particular interest is the existence of extremely obscured galaxies like Arp 220 (IC 4553) and IRAS 10173-0828 where $\leq 15\%$ of the total mass of interstellar gas is in atomic form. Although there may be several factors implicated in the production of high $M(H_2)/M(HI)$ ratios, the relative depletion of HI is likely to be due to an enhancement of molecular cloud formation. Figure 2b shows that the galaxies with enhanced star formation are those that have more efficiently converted HI into H_2.

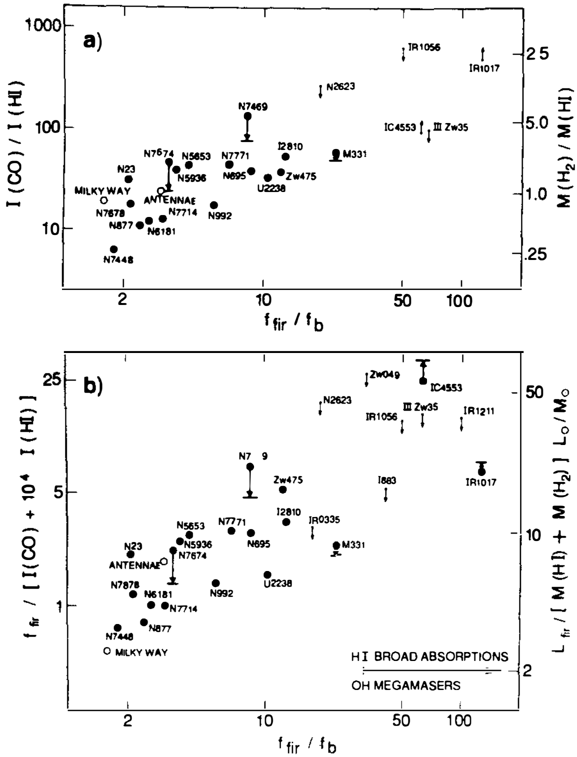

Fig. 2— a) CO(1-0)/HI flux ratio in Jy km s^{-1} measured at $\lambda 2.6$ mm and $\lambda 21$ cm, as a function of the FIR-to-blue flux ratios f_{fir}/f_b. b) Ratio of the FIR luminosity to the sum of the CO and HI spectral fluxes as a function of FIR excesses. These diagrams from Mirabel and Sanders (1989) show that in ultraluminous infrared mergers most of the atomic hydrogen is converted into molecular form.

3 EXTRANUCLEAR STARBURSTS: TIDAL DWARF GALAXIES

The idea that collisions between giant galaxies, in addition of driving matter inward, may eject stars and gas to intergalactic space, out of which star forming dwarf galaxies and star clusters may be formed, was first proposed by Zwicky (1956) and later followed up by Schweizer (1978). These recently formed dwarf galaxies and star clusters may be seen as patches of optically emitting material that usually appear along the tidal tails that emanate from merging disk galaxies. In the particular case of the system shown in Figure 1, the knots along the tails become bluer towards the far-ends. The condensations at the tip have colors (B-V) $\sim$ 0.4 and are likely to become detached systems, namely, star forming isolated dwarf galaxies or star clusters.

Kennicut and Chu (1988) have reviewed the question of the formation of young globular clusters and their possible association with giant HII complexes in nearby galaxies. They noted that young populous clusters with massive stars are invariably found in galaxies with widespread star formation bursts such as M82 and NGC 5253. Ashman and Zepf (1992) found the results by Kennicut and Chu (1988) consistent with the hypothesis that young globular clusters form preferentially in interacting galaxies. This hypothesis can provide clues to understand: (a) the high frequency of globular clusters around ellipticals; (b) the large number of globulars associated to the most massive galaxies at the centers of clusters of galaxies; (c) the evidence for higher mean metallicity in clusters around giant galaxies.

3.1 The Antennae

To further explore this hypothesis Mirabel, Dottori and Lutz (1992) made a spectrophotometric study of the condensation at the tip of the southern tail of the prototype merger NGC 4038/39 (The Antennae) that is shown in Figure 3. They found that this condensation is a dwarf galaxy formed out of the tidal remnants that were ejected to intergalactic space. The tidal dwarf consists of a chain of HII regions ionized by recently formed massive stars, which are embedded in an envelope of HI gas and low surface brightness optical emission. The metallicity of the HII regions is $\sim$ 1/3 solar, namely, similar to that of HII regions in the outskirsts of galactic disks. The spectrum shown in Figure 3 corresponds to an HII region with a luminosity equivalent to 300 Orion nebulae. Since the material at the tip of the tail was ejected $\sim$ 7 10^8 years ago, and the ionizing stars are younger than 2 10^6 years, these massive stars must have been borned well after the ejection. The time elapsed since the detachment of the material from the galactic disks is at least a factor of ten the internal crossing time, so this object will remain bound unless disrupted by stellar winds and supernovae from the massive stars being formed.

3.2 Arp 105: a multiple collision in a cluster

Arp 105 is one of the most remarkable instances of multiple collisions of galaxies. At a distance of $\sim$ 120 Mpc (Figure 4) it consists of several galaxies undergoing encounters near one of the centers of the X-ray cluster A1185. The elliptical is tearing apart a starburst

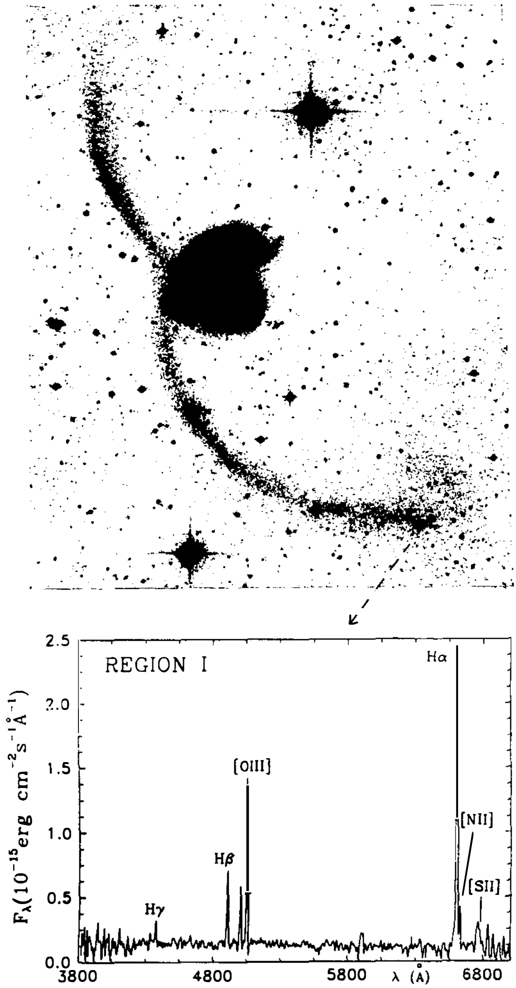

Fig. 3— Optical photograph of the interacting galaxies NGC 4038/39 (the Antennae). At the tip of the southern tail there is a chain of HII regions embedded in a diffuse low surface brightness envelope. The spectrum is from one of the HII regions at $\sim$ 100 kpc from the merging disks. The HII regions are being ionized by stars formed $\leq 2\ 10^6$ years ago. Mirabel, Dottori and Lutz (1992) proposed that the southern tip of the Antennae is a dwarf irregular galaxy of tidal origin.

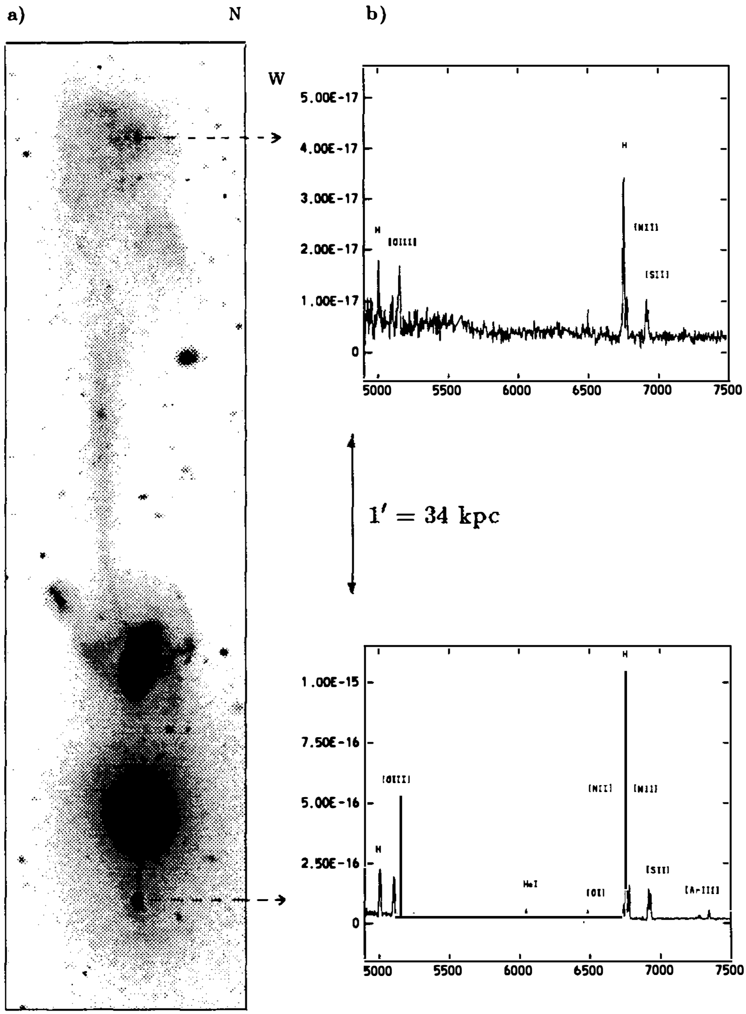

Fig. 4—a) V band image of Arp 105, a multiple collision in the cluster of galaxies Abell 1185. In this remarkable system it is observed the formation of a Magellanic irregular and a blue compact galaxy out of the debris of the collision. b) Spectra of the condensations detected in the forming galaxies. They are typical of star forming regions. From Duc and Mirabel (1993)

spiral galaxy that radiates 10^{11} $L_\odot$ in the far-infrared. From the spiral emanates a gigantic tail that at a distance of 100 kpc ends in an irregular system that is reminiscent of the Magellanic Clouds. Towards the South of the elliptical emanates a "jet-like" structure that ends in a blue compact object with strong optical emission lines. In addition, the victimed spiral appears to have been penetrated by an object flying by at a speed of 2,600 km s^{-1}.

The most striking result from our radio observations is that the spiral contains 10^{10} $M_\odot$ of molecular gas and $\leq 5\ 10^8$ $M_\odot$ of HI, namely, more than 95% of the cold interstellar gas in the spiral is in molecular form. On the contrary, the irregulars of Magellanic type at the end of the 90 kpc long tail contain as much as 6 10^8 $M_\odot$ of HI, but less than 10% of the gas is in molecular form. Therefore, Arp 105 is a striking case for the study of the segregation of interstellar gas during the collision of a spiral with an elliptical near the center of a cluster of galaxies. A more detailed description of our research on this system will be published by Duc and Mirabel (1993).

REFERENCES

Arp, H.: 1966, *ApJS* **14**, 1.

Ashman, K.M. and Zepf, S.E.: 1992, *ApJ* **384**, 50.

Baan, W.A., Wood, P.A.D. and Haschick, A.D.: 1982, *ApJ* **260**, L49.

Balzano, V.A.: 1983, *ApJ* **268**, 602.

Condon, J.J.: 1980, *ApJ* **242**, 894.

Dickey, J.M.: 1986, *ApJ* **300**, 190.

Duc P.A. and Mirabel I.F.: 1993, *A&A* to be submitted.

Hummel, E.: 1981, *A&A* **96**, 111.

Joseph, R.D. and Wright, G.S.: 1985, *MNRAS* **214**, 87.

Kennicut, R.C, and Keel, W.C.: 1984, *ApJ* **279**, L5.

Kennicut, R.C. and Chu, Y.: 1988, *AJ* **95**, 720.

Larson, R.B., and Tinsley, B.M.: 1978, *ApJ* **219**, 46.

Lawrence, A., Rowan-Robinson, M., Leech, K., Jones, D.H.P., Wall, J.V.: 1989, *MNRAS* **240**, 329.

Markarian, B.E.: 1967, *Afz* **3**, 55.

Melnick, J. and Mirabel, I.F.: 1990, *A&A* **231**, L19.

Mirabel, I.F.: 1982, *ApJ* **260**, 75.

Mirabel, I.F., and Sanders, D.B.: 1988, *ApJ* **335**, 104.

Mirabel, I.F. and Sanders, D.B. : 1989, *ApJ* **340**, L53.

Mirabel, I.F.: 1989, *ApJ* **340**, L13.

Mirabel, I.F., Lutz, D., and Maza, J.: 1991, *A&A* **243**, 367.

Mirabel, I.F., Dottori, H., and Lutz, D.: 1992, *A&A* **256**, L19.

Riecke, G.H. and Low, F.J.: 1972, *ApJ* **176**, L95.

Rowan-Robinson, M.: 1990, *Dynamics of Galaxies and their Molecular Cloud distributions, eds. F. Combes and F. Casoli*, 211.

Toomre, A., and Toomre, J.: 1972, *ApJ* **178**, 623.

Sanders, D.B., Soifer, B.T., Elias, J.H., Madore, B.F., Matthews, K., Neugebauer, G.,

Scoville, N.Z.: 1988a, *ApJ* **325**, 74.
Sanders, D.B.: 1992, *in Relationships between Active Galactic Nuclei and Starburst Galaxies, ed. A. Filippenko*, in press.
Schweizer, F.: 1978, *Structure and Properties of Nearby Galaxies, ed. E.M. Berkhuijsen and R. Wielebinski*, page 279.
Searle L. and Sargent, W.L.W.: 1972, *ApJ* **173**, 25.
Stocke, J.T.: 1978 *AJ* **83**, 348.
Weedman, D.W., Feldman, F.R., Balzano, V.A., Ramsey, L.W., Sramek, R.A., Chi-Chao Wu:1981, *ApJ* **248**, 105.
Wright, G.S., James, P.A., Joseph, R.D., McLean, I.S.: 1990 *Nat*, **344**, 417.
Zwicky, F.: 1956 *Ergebnisse der Exakten Naturwissenschaften* **29**, 34.

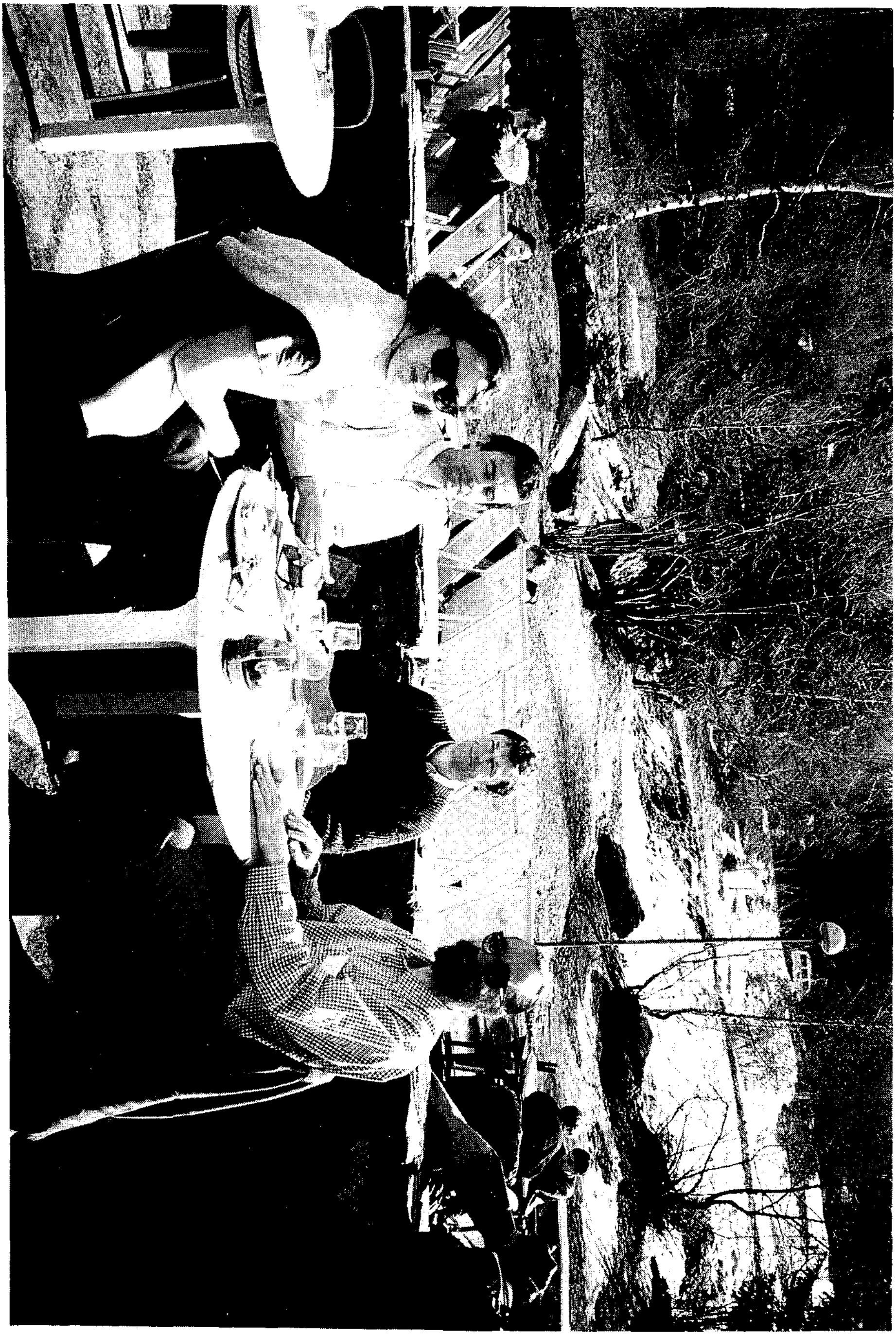

Isabelle & the boys.

MOLECULAR AND IONIZED GAS IN CIRCUMNUCLEAR STARBURST GALAXIES

Pere Planesas
Centro Astronómico de Yebes (IGN), Spain
Luis Colina, Diego Pérez-Olea
Dept. Física Teórica, Univ. Autónoma de Madrid
Jesús Martín-Pintado
Centro Astronómico de Yebes (IGN), Spain
Angeles I. Díaz
Dept. Física Teórica, Univ. Autónoma de Madrid

ABSTRACT

The present project intends to explore the causal physical connections between (a) the presence of high molecular gas surface densities in the nuclear and circumnuclear regions of galaxies, (b) the existence of a high star formation efficiency, i.e. presence of associated HII regions, and (c) the formation of an AGN, i.e. a central massive black hole, as the final product of this evolutionary path.

With regard to points (a) and (b), our results (Table 1) show that the amount of molecular gas in these galaxies is a factor of 10 smaller than in luminous IRAS galaxies. However, the global molecular gas surface brightness, $\Sigma(H_2)$, and the star formation efficiency (SFE), as measured by the usual L_{FIR}/M_{H_2} ratio, follows the correlation found for luminous IRAS galaxies extrapolated to lower surface brightness (Table 1).

If we calculate the same parameters locally, we find regions with a high (low) molecular gas surface brightness but a low (high) star formation efficiency. Examples of these situations are regions R2 and R4 (Fig. 1a) in NGC3351, and the 1480 km s^{-1} CO component in NGC3504 (Fig. 3b). It is not clear yet whether this result is a consequence of regions being in a different evolutionary phase.

In relation to points (b) and (c), we detect a galaxy, NGC3504, that could be an example of a galaxy in a starburst–AGN transient phase. This galaxy has a similar CO total mass and surface density as that observed in other Seyfert 1 galaxies for which high resolution CO maps have been obtained. It also shows a bright central radio, IR and [OIII] emission peak together with a more extended and diffuse structure. These characteristics are also similar to those of other Seyfert 1 galaxies like NGC3227 and NGC7469.

1. NGC 3351

The circumnuclear molecular gas distribution in this galaxy shows two almost equally bright emission peaks separated by about $10''$ (i.e. 500 parsecs) in the NNE–SSW direction, as illustrated in our CO(2→1) map (see Fig. 1b). These two CO peaks are also well separated in velocity by 140 km s^{-1}. The NNE peak has a velocity of V_{LSR}= 710 km s^{-1} while the SSW peak has a centroid velocity of V_{LSR}= 850 km s^{-1}.

The total amount of molecular gas has been calculated assuming a mean CO(2→1) to CO(1→0) ratio of 0.8 and the standard CO(1→0) to M_{H_2} conversion according to the expression $N_{H_2}[cm^{-2}] = 2.8 \times 10^{20}\ I_{CO}$ [K km s^{-1}]. The total mass of molecular gas within a region of $24''$ by $24''$ in size, corresponds to $M_{H_2} = 3.8 \times 10^8\ M_\odot$. The two CO peaks with comparable masses lay close to large complexes of HII regions.

The Hα map (Fig. 1a) shows a ring-like gas distribution where two of the brightest HII regions (R1 and R3 in Fig. 1a) seem to be spatially associated with the CO emission peaks. This hypothesis is also supported by the fact that the CO(2→1) over CO(1→0) ratio shows a positive gradient towards region R3 where a maximum value of 1.2 is measured. According to detailed radiative transfer models, this value indicates a fraction of the gas being optically thin, and, possibly, a high excitation temperature. These characteristics are found in M82 and may be common in starburst regions.

2. NGC 2903

This galaxy shows an elongated molecular gas distribution along the North-South direction (Fig. 2b). This elongation matches the morphology of the bright circumnuclear HII regions, as indicated by the Hα gas distribution (Fig. 2a). The total H_2 mass in a region of $24'' \times 24''$ is $1.9 \times 10^8\ M_\odot$.

The overall CO distribution is resolved in a $13''$ beam, but our observations do not show individual peaks, either spatially or kinematically resolved, in spite of the several HII regions detected in an $8'' \times 6''$ area (Fig. 2a).

3. NGC 3504

This galaxy shows a molecular gas distribution more compact than in the previous two galaxies (see Fig. 3b). This is in good agreement with the structure detected in our Hα image (Fig. 3a) where the HII regions are distributed in a circumnuclear ring-like structure $4''$ (i.e. 400 parsecs) in diameter.

The total molecular gas content over a size of $24''$ by $24''$ corresponds to $M_{H_2} \approx 2.3 \times 10^9\ M_\odot$ where it appears equally distributed in two emission peaks. The H_2 surface density quoted in Table 1 refers to the gas being uniformly distributed in a $24'' \times 24''$ area. If the deconvolved size of the two peaks is considered, the surface density increases by a factor of 3-4. The same applies to the molecular gas distribution in NGC 3351.

The two peaks are spatially separated by about $4''$ almost along the EW direction, and also kinematically separated by about 120 km s^{-1}. This velocity difference is consistent with the two [OIII]5007 velocity components detected within the first $4''$ around the nucleus. This

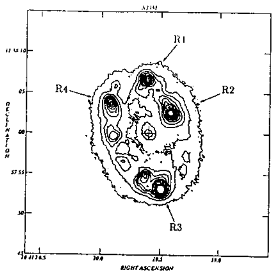

Figure 1(a): Hα image of NGC3351 obtained with the Nordic Telescope at La Palma Observatory. The pixel size corresponds to 0.196″ and the effective resolution is about 0.8″ in FWHM. The central cross indicates the emission peak in the broad R band filter. Labeled regions indicate circumnuclear HII complexes. The

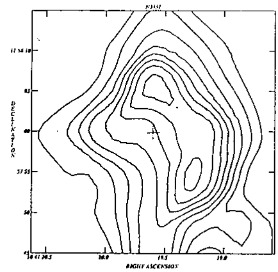

Levels = 16, 24, 32, ..., 72 K km/s
CO 1-1 integrated line intensity, measured with the IRAM-30m telescope.
Angular resolution was 13″. Units are in Tmb.

Figure 1(b)

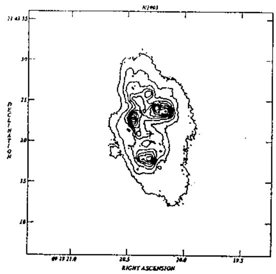

Figure 2(a): As figure 1(a) but for NGC2903. The linear scale corresponds to 36 pc arcsec^{-1}.

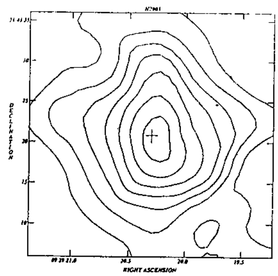

Levels = 20, 30, ..., 80 K km/s
CO 2-1 integrated line intensity, measured with the IRAM-30m telescope.
Angular resolution was 13″. Units are in Tmb.

Figure 2(b)

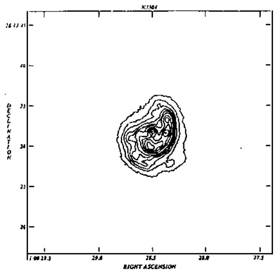

Figure3(a): As figure1(a) but for NGC3504. The linear scale corresponds to 100 pc arcsec^{-1}.

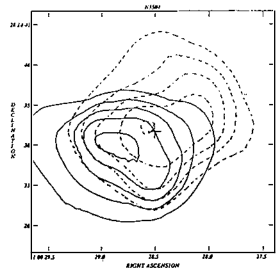

Levels = 24, 36, ..., 72 K km/s
CO 2-1 integrated line intensity, measured with the IRAM-30m telescope.
Full line for the 1480 km/s component; dashed line for the 1600 km/s component.
Angular resolution was 13″. Units are in Tmb.

Figure 3(b)

suggests that the motion of the cold molecular gas is also shared by the warm ionized gas. Consequently, it indicates a direct physical connection between the molecular clouds and the circumnuclear star forming regions.

Table 1: Properties of Circumnuclear Starburst Galaxies

Galaxy NGC#	$\alpha(1950)$ hh:mm:ss	$\delta(1950)$ ° ′ ″	$V_{LSR}^{(4)}$ km s^{-1}	P.A. °	i °	$D^{(5)}$ Mpc	L_{FIR} $10^9 L_\odot$	$M_{H_2}^{(6)}$ $10^8 M_\odot$	$\Sigma_{H_2}^{(7)}$ $M_\odot$ pc^{-2}	SFE $L_\odot$ $M_\odot^{-1}$
2903	09:29:20.3	21:43:21	543	17[1]	60[2]	7.2	3.6	1.9	140	19
3351	10:41:19.6	11:58:00	780	11[3]	46[3]	10.4	3.0	3.8	180	8
3504	11:00:28.5	28:14:32	1543	149[3]	22[3]	20.6	14.0	23.	380	6

REFERENCES

(1) de Vaucouleurs et al. 1991, Third Reference Catalog.
(2) Jackson, J.M. et al. 1989, Astrophys. J. **337**, 680.
(3) Grosbol, P., 1985, Astron. Astrophys. Suppl. **60**, 261.
(4) centroid of the CO emission.
(5) derived from the measured V_{LSR}, and assuming H_0=75 km s^{-1}.
(6) in a 24″ × 24″ region.
(7) H_2 mass assumed to be uniformly distributed in a 24″ × 24″ area.

ON THE GENERATION, STRUCTURE AND EVOLUTION OF THE MODONS IN THE ROTATING GASEOUS GRAVITATING SYSTEMS

M.G.ABRAMIAN
Yerevan State University. Yerevan. Armenia
A.M.FRIDMAN
Institute of Astronomy AS of Russia. Moscow. Russia
E.Ye.KHACHIKIAN
Byurakan Astrophysical Observatory. Armenia

ABSTRACT

The structure of a new type of objects - solitary dipole vortices (modons) - in solid-body rotating gaseous gravitating systems are investigated. The velocity field of modon has a dipolar structure. The isodenses coincide with stream lines in modons, the size a of which is much smaller than the Jeans critical size λ_J ($a<<\lambda_J$) and do not coincide with ones in the opposite case $a>>\lambda_J$. The generation mechanisms of modon, two differenet ways of their evolution and astrophysical applications are discussed.

INTRODUCTION

The structure of the solitary dipolar vortices (modons) were firstly described by [1] as dipolar Rossby vortices, propagating in a liquid layer on the Earth's surface (so-called β-plane [2]). The interior region of the modon is bounded by some separatrix and consists of the two vortices: cyclone and anticyclone. The anticyclone corresponds to a rize and the cyclone corresponds to a depression (the average level of the liquid in the dipolar Rossby vortex, which is the soliton, remains unchanged). In the interior region of the separatrix the stream lines are closed (this is the region where particles are trapped by the dipolar vortex), in the outer region the stream lines are open (Fig.1). The Larichev-Reznik's dipolar vortex differs fundamentally from the one that is described by [3] and [4] by its solitary nature: outside the separatrix from the center of the vortex the rotational velocity of modon decreases exponentially as a function of the distance, unlike the "classical" dipolar vortices, where the velocity profile corresponds to the r^{-2} law.

Analogic solitary dipolar vortices might be expected in a two-dimensional gaseous medium, for which the dynamical equations for an adiabatic index $\gamma = 2$ coincide identically with the dynamical equations of shallow water [5]. However, prior to their involvement in gaseous media, solitary dipolar vortices were theoretically predicted also for a nonuniform magnetized plasma [6].

Both in rotating shallow water [1] and in a nonuniform magnetized plasma [6] modons are described by the same type of nonlinear equation. In the hydrodynamics this equation is known as Charney-Obukhov's equation [7], [8] and in plasma physics - as Hasegawa-Mima equation [9]. This equation contains both vector and scalar nonlinearities.

MODONS IN ROTATING GRAVITATING MEDIA

For the first time the existence of modons in a rotating gravitating gas was hypothesized by [10] and a nonlinear equation was derived by [11], [12] to describe modons in this environment. The complication of this equation does not allow a solution in general case. But both in the case of short-wave perturbations (wavelenght λ much smaller than the Jeans wavelenght λ_J, i.e. $\lambda<<\lambda_J$) and in the opposite limiting case of long-wave perturbations ($\lambda>>\lambda_J$) the Dolotin-Fridman's equation reduces to the Charney-Obukhov's (or Hasegawa-Mima) equation.

The Dolotin-Fridman's equation has been received by assuming thr following assumptions: 1) uniform rotation of system with constant angular velocity Ω_0; 2) isentropic perturbations with arbitrary P(ρ), where P and ρ are pressure and density of gas; 3) epicyclic approximation (geostrophyc's approach): $\frac{1}{\Omega_0}\frac{d}{dt}<<1$, and in two limiting cases of long-wave and short-wave perturbations has the form [11], [12]:

$$\left\{\frac{\partial}{\partial t}+\frac{1}{2\Omega_0}[\nabla_\perp f,\nabla_\perp]_z\right\}\Delta_\perp f+2\Omega_0\beta\frac{1}{r}\frac{\partial f}{\partial\varphi}=0, \tag{1}$$

where

$$f=\begin{cases}W\\ \Phi\end{cases},\quad \beta=\begin{cases}\ln'\alpha & \text{for } \lambda_J>>\lambda\\ \ln'|\alpha-2| & \text{for } \lambda_J<<\lambda\end{cases} \tag{2}$$

$W=G^2\frac{\tilde{\rho}}{\rho_0}$ is the enthalpy of gas, G^2 is the sound velocity, $\tilde{\rho}$ is density perturbations, Φ is the gravitational potential, (r,φ) are rectangular coordinates, $\alpha=2\pi G\rho_0/\Omega_0^2$, by prime is denoted derivation with respect to r.

Transforming to a local Cartesian coordinate system

$$\frac{\partial}{\partial r}=\frac{\partial}{\partial x},\quad \frac{1}{r}\frac{\partial}{\partial\varphi}=\frac{\partial}{\partial y} \tag{3}$$

and introducing new varable $\eta=y-ut$, the equation (1) can be rewritten in the form

$$\left(\frac{\partial}{\partial\eta}-\frac{1}{U}[\nabla_\perp\xi,\nabla_\perp]_z\right)\Delta_\perp\xi=\Lambda\frac{\partial\xi}{\partial\eta}\quad, \tag{4}$$

where

$$U=2u\Omega_0;\quad \Lambda=\frac{4\Omega_0}{U}\beta \tag{5}$$

Equation (4) in a new polar coordinate system r,φ ($x=r\cos\varphi$, $\eta=r\sin\varphi$) has the following stationary solutions [11], [12]:

$$\xi(r,\varphi)=2\Omega_0 u a\begin{cases}\left[\left(1+\dfrac{s^2}{z^2}\right)\dfrac{r}{a}-\dfrac{s^2}{z^2}\dfrac{J_1(z\frac{r}{a})}{J_1(z)}\right]\cos\varphi, & r\le a\\ \dfrac{K_1(s\frac{r}{a})}{K_1(s)}\cos\varphi; & r\ge a\end{cases} \tag{6}$$

where J_1 and K_1 are Bessel and McDonald functions correspondingly; and z and $s^2 = a^2\Lambda$ satisfy the following transcendental equation:

$$J_1(z)K_3(s)+J_3(z)K_1(s)=0 \tag{7}$$

Solution (6) describes so-called modons with the following streamlines (Fig.1):

$$\frac{const}{\cos\varphi}=\begin{cases}\left(1+\dfrac{s^2}{z^2}\right)\dfrac{r}{a}-\dfrac{s^2}{z^2}\dfrac{J_1(z\frac{r}{a})}{J_1(z)}, & r\le a\\ \dfrac{K_1(s\frac{r}{a})}{K_1(s)}, & r\ge a\end{cases} \tag{8}$$

MAP OF ISODENSES

In the case of short-wave perturbations ($\lambda \ll \lambda_J$) the main role in perturbations plays pressure, so $f = W$, and the isodenses

$$\tilde{\sigma}\equiv\frac{\tilde{\rho}}{\rho_0}=\beta_{sw}\frac{f}{au\Omega_0}=const\,,\quad \beta_{sw}=\frac{au\Omega_0}{G^2} \tag{9}$$

coincide with the streamlines.

In the case of long-wave perturbations ($\lambda \gg \lambda_J$) the main role in perturbations plays gravitation, so $f = \Phi$, and the perturbed density is found by using the Poisson equation

$$\tilde{\sigma}=\beta_{lw}\begin{cases}\dfrac{J_1(s\frac{r}{a})}{J_1(z)}\cos\varphi; & r\le a\\ \dfrac{K_1(s\frac{r}{a})}{K_1(s)}\cos\varphi; & r\ge a\end{cases} \tag{10}$$

where

$$\beta_{lw}=\frac{a}{\alpha}(\ln|\alpha-2|)'\,. \tag{11}$$

Let us illustrate the perturbed density distribution (9) and (10) in the following solutions of the transcendental equation (7):

z = 4.0, s = 1.52
z = 4.2, s = 2.9

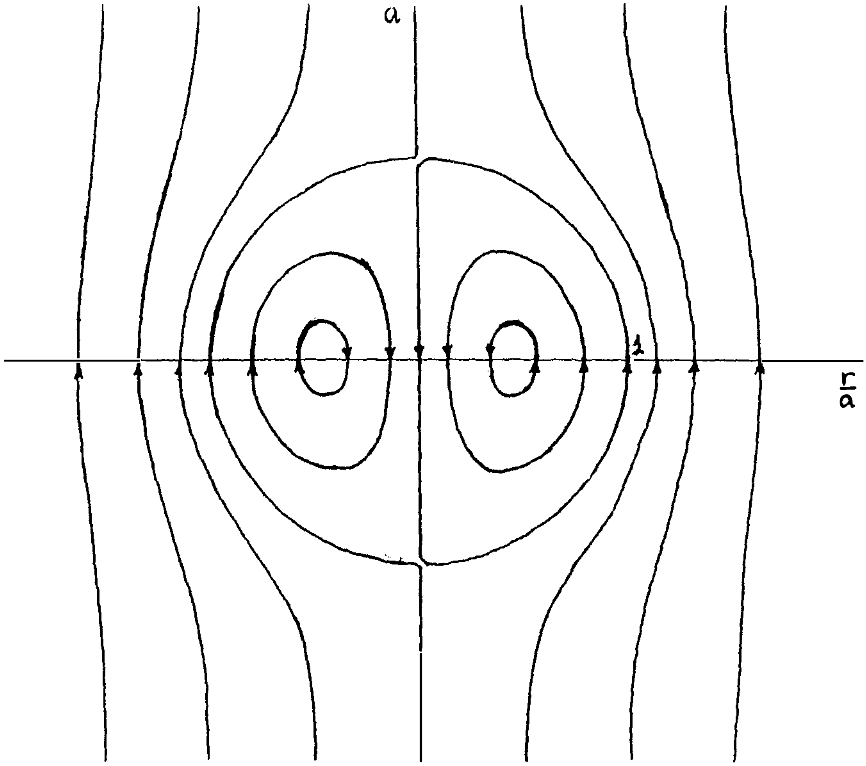

Fig. 1

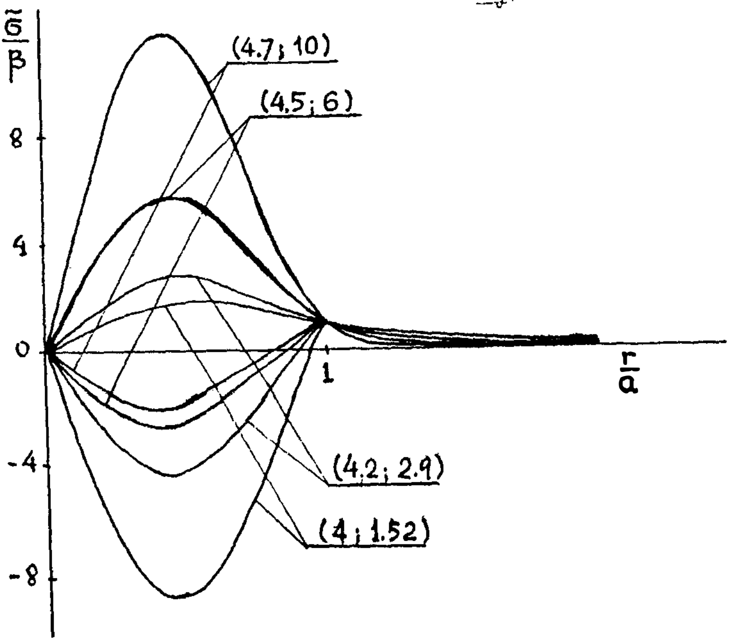

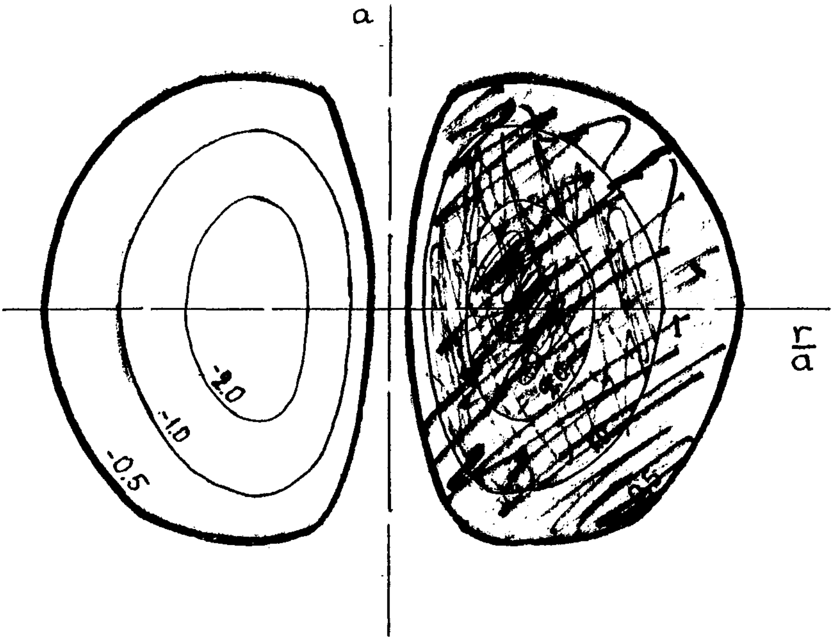

Fig. 3

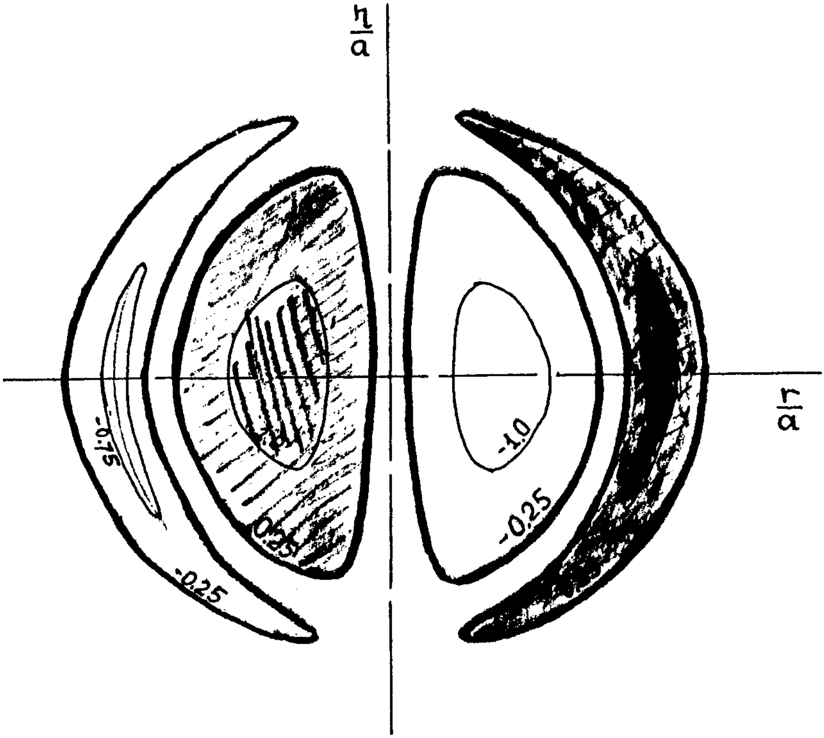

$z = 4.5, \quad s = 6.0$
$z = 4.7, \quad s = 10.0$

In the Fig.2 the curves represent dependencies of the perturbed density on the dimensionless distance from the modon center, r/a, in the short-wave approximation (growing in the cental regions curves) and in the long-wave one (decreasing in the central part curves).

It should be noted that the distribution of the perturbed density in the modon is antisymmetrical to the axis, where $\cos\varphi = 0$. If in some region of the right $(-\pi/2 < \varphi < \pi/2)$ half-plane a mass condensation takes place, in the symmetrical region a mass discharge takes place. The density distribution in long-wave perturbations (10) differs principally from the density distribution in short-wave case. If in the last case the matter is condensed in the tight half-plane and rarefied in the left one (Fig.3), then in the long-wave case a rarefying takes place in the right half-plane at a distance $r_1 < a$ from the modon center and condensation beyond; the same process holds true in the left half-plane (Fig.4). Hence, for long-wave perturbations, the modon is characterized by two mass condensations and two mass rarefications, unlike the case of a modon subject to short-wavelenght perturbations, which will result in one condensation and one rarefication of the density.

Let us estimate the perturbed mass in long-wave modon:

$$\tilde{m}_1 = \frac{2\pi h\rho_0}{J_1(z)}\beta_{lw}\int\limits_{\pi/2}^{3\pi/2}\cos\varphi d\varphi\int\limits_0^{r_1/a} J_1(z\tfrac{r}{a})rdr = \frac{4\pi a^2 h\rho_0}{J_1(z)}\beta_{lw}\frac{\pi x_1}{2z}J_0(zx_1)H_1(zx_1)\,, \qquad (12)$$

where $x \equiv r/a$. h is a gas disk thickness, $H_1(zx)$ is first order Struve function, x_1 is the Bessel function's first root: $J_1(zx_1) = 0$;

$$\tilde{m}_2 = \frac{2\pi h\rho_0 a^2}{J_1(z)}\beta_{lw}\int\limits_{-\pi/2}^{\pi/2}\cos\varphi d\varphi\int\limits_{x_1}^{1} J_1(zx)xdx + \frac{2\pi a^2 h\rho_0}{K_1(z)}\beta_{lw}\int\limits_{-\pi/2}^{\pi/2}\cos\varphi d\varphi\int\limits_1^{\infty} K_1(sx)xdx \quad (13)$$

The numerical estimation of the perturbed mass of both parts of the long-wave modon shows that they are same order quantities: $\tilde{m}_1/\tilde{m}_2 \cong 2$.

DISCUSSION

Hypothesis on double nuclei origin in galaxies

Here we would like to discuss the new scenario of the double nuclei origin in galaxies. According to the traditional point of view [13), 14), 15), 16), 17)] the double galactic nuclei are created as a result of gravitational attraction with further merging of two nearest galaxies with single nuclei.

Note that some of the observational data are difficult to reconcile with the hypothesis of gravitational merging*) such as:

a) the discovery of the Seyfert type double nuclei galaxies [18)] because of their most rarity between galaxies;

*) After the talk of one of coauthors (E.Ye. Kh.) on the conference "New Ideas in Astronomy" (Cambridge Univ. Press, 1988, pp.115-118) M. Burbidge noted, that "there are too many of these double nuclei to account them as a result of merging of previously separate galaxies"

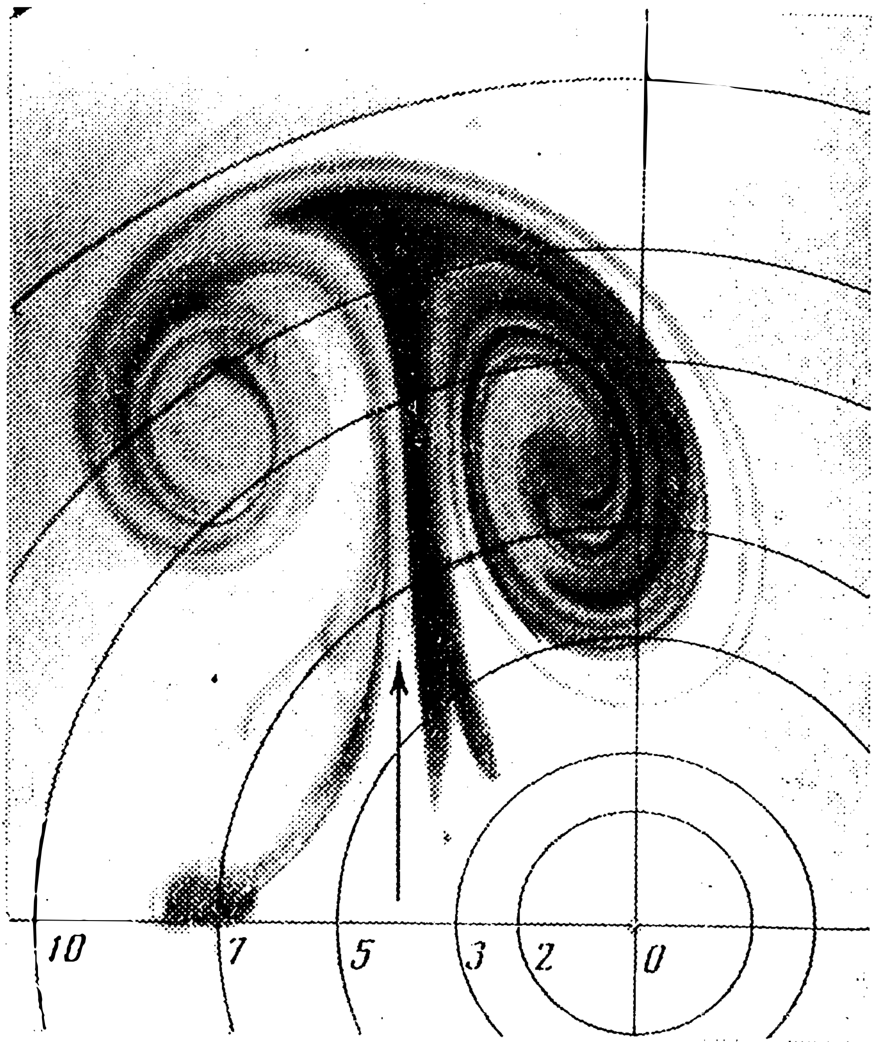
10
7
5
3
2
0

b) the discovery of the twin-objects with quite identical spectra and with morphology similar to two isolated superassociations (SA) being considered as one galaxy with double nuclei each of which is SA [19), 20)];

c) the discovery of numerous double nuclei galaxies (more than 100) among the UV excess galaxies only.

Perhaps there are two kinds of scenarios of double nuclei formation: either by means of double protonuclei creation or by means of merging. The probability of the latter can be easy estimated if one knows the density of singular objects, their average masses and peculiar velocities. We believe that the future estimation will confirm the Fridman's hypothesis [10)] of the formation of double nuclei from solitary dipole vortices (modons) in the central part of the protogalaxy which rotates as solid body. Let us advance some arguments in favor of this statement.

Two methods of modon generation.

The first way to generate a modon connects with the acceleration of the central part rotation of a galaxy. The process of short-scale modon generation ($a \ll \lambda_J$) can be modelled by rotating shallow water (Fig. 5).

An analog between two-dimensional hydrodynamical processes and ones on rotating shallow water is well known [5)], as was noted in the Introduction. Here we must distinguish two cases considered above: 1) $a \ll \lambda_J$, 2) $a \gg \lambda_J$. In a quickly rotating gravitating system where the centrifugal force plays an essential role in the equilibrium, the value λ_J and the epicyclic radius are of comparable sizes [21)]. The latter coincides with the Rossby radius R in the rotating shallow water. Hence the first case $a \ll \lambda_J$ corresponds to the following approximation for the rotating shallow water:

$$a \ll R \tag{14}$$

Experiments with rotating shallow water show [22)] that only double modons were generated under the condition (14). As follows from Fig. 3, two short-wave modons have two protonuclei. The role of the pumping disk in shallow water experiment for a protogalaxy may play its compressing central part, which increases its rotating velocity due of compression. The subsequent compression of two modon condensations can be caused by the thermal instability. The process of large-scale modon generation ($a \gg \lambda_J$) cannot be modelled by the rotating shallow water experiment, as this case does not satisfy to the necessary condition (14) of the modon creation on the shallow water. However, according to Fig.4, the generation of one large-scale modon ($a \gg \lambda_J$) in a central part of a protogalaxy is enough to form the double nuclei as a result of gravitational compression of two density condensations.

The second method of modon generation involves a jet from the central nucleus of a galaxy. The model of this process is shown in Fig.6. It is the generation of mushroom-like dipole vortices in a rotating basin of shallow water [23)]. It was proved [24)], that these structures are Larichev-Reznik modons.

REFERENCES

1. Larichev V.D., Reznik G.M., 1976, Dokl. AN SSSR, v.231, p.1077.
2. Pedlosky Y., 1982, "Geophysical Fluid Dynamics", Springer Verlag, N.-Y.
3. Lamb H., 1945, "Hydrodynamics", Dover Publ., N.-Y.

4. Batchelor G.K., 1967, "Introduction to Fluid Dynamics", Cambridge Univ. Press, N.-Y.
5. Landau L.D., Lifshitz E.M., 1959, "Fluid Mechanics", Pergamon Press, London.
6. Meiss J.D., Horton W., 1983, Phys.Fluids, v.26(4), p.990.
7. Charney J.G., 1948, Geophys.Publ. Kosjones. Vors. Vidershap. Acad. Oslo, v.17, p.3.
8. Obukhov A.M., 1949, Izv. AN SSSR, Geography and Geophys., v.13, p.281.
9. Hasegawa A., Mima K., 1978, Phys.Fluids, v.21, p.87.
10. Fridman A.M., 1988, Astron.Tsirk. No.1533, p.5.
11. Dolotin V.V., Fridman A.M., 1990, in: "Nonlinear Waves, Physics and Astrophysics" (ed. Gaponov-Grekhov A.V., Rabinovich M.I.), Springer Verlag, N.-Y.
12. Dolotin V.V., Fridman A.M., 1991, Sov.Phys. JETP, v.72(1), p.1.
13. Toomre A., Toomre J., 1972, Ap.J., v.178, p.623.
14. Toomre A., 1978, IAU Symp. No.79 (ed. Longair M.S., Einasto J.), p.109.
15. Joseph R., Wright G., 1985, MNRAS v.214, p.87.
16. Barnes J.E., 1990, Nature, v.344, p.379.
17. Wright G.S., James P.A., Joseph R.D., McLean I.S.,1990, Nature, v.344, p.417.
18. Petrosian A.P., Sahakian K.A., Khachikian E.Ye., 1990, Astrophysika, v.16, p.621.
19. Arp H., Heidmann J., Khachikian E.Ye., 1974, Astrophysika, v.10, p.298.
20. Khachikian E.Ye., 1979, "Stars and Star Systems", Uppsala, p.107.
21. Fridman A.M., Polyachenko V.L., 1984, "Physics of Gravitating System", Springer Verlag, N.-Y, Berlin.
22. Nezlin M.V., 1986, Sov.Phys. Uspekhi, v.29(9), p.807.
23. Ginzburg A.I., Kostianov A.G., Pavlov A.M., 1987, Izv. AN SSSR, Phys. of Atmosphere and Ocean, v.23, p.170.
24. Fridman A.M., 1989, Dokl. AN SSSR, v.301, p.200.

HIGH-REDSHIFT GALAXIES

DENSE MOLECULAR GAS IN ULTRALUMINOUS AND HIGH REDSHIFT GALAXIES

Simon J. E. RADFORD
Institut de Radio Astronomie Millimétrique, 38406 St. Martin d'Hères, France

Abstract

Molecular gas is the raw material for star formation and hence a crucial factor in galactic evolution. Ultraluminous infrared galaxies emit the bulk of their power in the far infrared, show disturbed morphologies indicative of recent mergers, and rival QSOs in their bolometric luminosities, but are more numerous in the local universe. Although they are as rich in molecular gas as the most gas rich normal spiral galaxies, they have elevated ratios of infrared luminosity to molecular mass that suggest they are undergoing bursts of very rapid and efficient star formation. A survey of HCN($1 \rightarrow 0$) emission from ten ultraluminous and normal galaxies shows far infrared emission correlates better with the amount of dense, $n(H_2) > 10^4\ cm^{-3}$, molecular gas than with the total amount of molecular gas. The star formation efficiency appears to depend on the fraction of the molecular gas reservoir at high density.
The galaxy IRAS 10214+4724 at $z = 2.286$ is perhaps the most luminous object in the universe. Observations of its CO($6 \rightarrow 5$), CO($4 \rightarrow 3$), and CO($3 \rightarrow 2$) lines indicate this galaxy has as much molecular gas as the total mass of the Milky Way. The molecular gas in 10214+4724 is both warmer and denser than that in the Galaxy and the normal gas to dust ratio suggests the abundances are nearly Solar. In the Milky Way, CO($6 \rightarrow 5$) is only observed in regions of high-mass star formation, so its presence in 10214+4724 implies the occurance of active star formation there. A map of the CO($3 \rightarrow 2$) emission with $2.3''$ resolution shows a small source slightly extended EW with a deconvolved size of $(10 \times 4) \pm 4h^{-1}$ kpc. The mass of molecular gas is comparable to the dynamical mass. This extraordinary primeval galaxy appears to have most of its mass in molecular gas and to be undergoing an extreme starburst that is generating metals with close to Solar abundances.

1 Dense Molecular Gas in Ultraluminous Galaxies

Rivalling QSOs in emitted power, ultraluminous infrared galaxies ($L_{FIR} > 5 \times 10^{11} h^{-2}\, L_\odot$; $H_0 = 100h\, \mathrm{km\,s^{-1}\,Mpc^{-1}}$, $q_0 = 0.5$) are three times more common in the local universe ($z < 0.3$).[16] Almost all show disturbed optical morpholgy: double nuclei, tidal bridges and tails, or other signs of mergers or interactions.[12] Rich in molecular gas, they typically contain[15] $> 5 \times 10^9 h^{-2}\, M_\odot$ of H_2. Although some normal spiral galaxies are equally gas rich, e.g. NGC 3147,[23] ultraluminous galaxies have L_{FIR}/L_{CO} ratios 30 times higher than do normal galaxies of the same mass.[15, 23] What powers ultraluminous galaxies, obscured black holes in active nuclei or rapid bursts of star formation?

Molecular gas is the raw material for star formation and hence a crucial factor in galactic evolution. The CO($1 \rightarrow 0$) line traces gas at $n(H_2) < 10^3\, \mathrm{cm^{-3}}$ and indicates the total H_2 mass in a galaxy. In ultraluminous galaxies, far IR radiation, emitted by dust warmed by UV radiation from O and B stars, indicates the formation rate of massive stars. The $L_{FIR}/M(H_2)$ ratio measures, then, the star formation rate per mass of gas, or the star formation efficiency. Why is this efficiency so much higher in ultraluminous galaxies than in normal gas rich spiral galaxies? Does another parameter besides the amount of fuel control star formation in galaxies? In the Milky Way most of the H_2 is in low density giant molecular cloud envelopes. Massive stars form, however, not in those envelopes, but in dense cloud cores, objects like M 17, W 51, etc. Although CO traces most of the H_2 mass, it does not necessarily trace the regions of active star formation where the gas density is more than ten times higher than average. Dense molecular gas is better indicated by the HCN($1 \rightarrow 0$) line, which traces gas at $n(H_2) \approx 10^4\, \mathrm{cm^{-3}}$.

In a sample of ten galaxies surveyed with the IRAM 30 m telescope,[19] ultraluminous galaxies have much stronger HCN($1 \rightarrow 0$) lines than normal galaxies (Figure 1). In absolute terms, Mrk 231, the most luminous galaxy in the local universe, has an HCN($1 \rightarrow 0$) line luminosity larger than the CO($1 \rightarrow 0$) luminosity of the Milky Way, while in relative terms, Mrk 231 has $L_{CO}/L_{HCN} \approx 4$ whereas $L_{CO}/L_{HCN} \approx 100$ in the Galaxy. For the whole sample, FIR luminosity correlates better with HCN($1 \rightarrow 0$) luminosity than with CO($1 \rightarrow 0$) luminosity. Over a range of 50 in L_{FIR}/L_{CO}, the range in L_{FIR}/L_{HCN} is only three. When normalized by the CO($1 \rightarrow 0$) luminosity, there is a very tight correlation between L_{HCN}/L_{CO} and L_{FIR}/L_{CO} (Figure 2). The L_{HCN}/L_{CO} ratio indicates the fraction of the total H_2 mass that has a density $\approx 10^4\, \mathrm{cm^{-3}}$, i.e. that has conditions necessary for formating massive stars. In any galaxy, ultraluminous or not, the star formation efficiency, measured by L_{FIR}/L_{CO}, depends on how much of the total molecular gas is in a dense phase.

In the most luminous galaxies in the sample, Mrk 231 and Arp 220, the mass of high density gas exceeds $5 \times 10^9 h^{-2}\, M_\odot$ and accounts for roughly half the total gas reservoir. In the Milky Way and other normal galaxies, on the other hand, only a small fraction of the gas is sufficiently dense to form high mass stars. The bulk of the molecular gas in the ultraluminous galaxies is, therefore, more similar to that in active star-forming cloud cores than that in the envelopes of GMCs. In our Galaxy, O stars form in massive cloud cores with high density gas and they will form under similar circumstances in ultraluminous galaxies as well. The large masses of high density gas implied by the strength of their HCN($1 \rightarrow 0$) lines indicate ultraluminous galaxies are extraordinary star forming environments and suggest star formation is their principal power source. These galaxies are evolving rapidly under conditions reminiscent of those when galaxies formed.

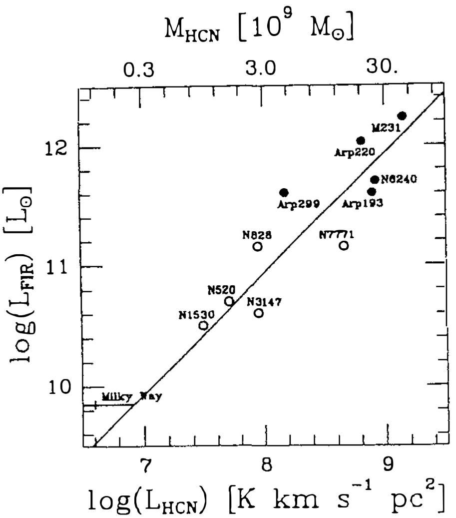

Figure 1: For both ultraluminous (*solid circles*) and more normal (*open circles*) galaxies, FIR and HCN(1→0) luminosity are well correlated.[19] The upper scale indicates the mass of high density molecular gas, $n(H_2) \approx 10^4\,\mathrm{cm}^{-3}$. In this Figure, $H_0 = 75\,\mathrm{km\,s^{-1}\,Mpc^{-1}}$.

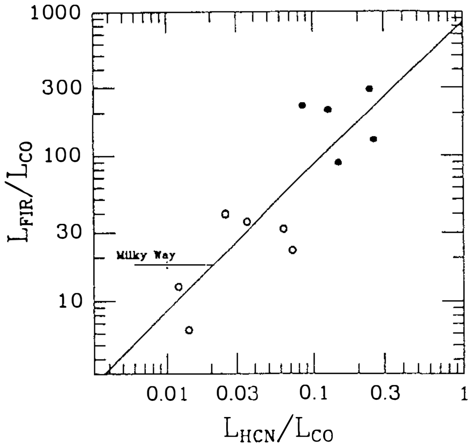

Figure 2: The tight correlation between $L_{\mathrm{FIR}}/L_{\mathrm{CO}}$ and $L_{\mathrm{HCN}}/L_{\mathrm{CO}}$ suggests the star formation efficiency of galaxies depends on the fraction of available molecular gas in a dense phase.[19] While $L_{\mathrm{HCN}}/L_{\mathrm{CO}}$ is dimensionless, $L_{\mathrm{FIR}}/L_{\mathrm{CO}}$ is measured in $\mathrm{L}_{\odot}\,(\mathrm{K\,km\,s^{-1}\,pc^2})^{-1}$.

2 Warm Molecular Gas in a High Redshift Galaxy

With a total luminosity near $10^{14}h^{-2}\,\mathrm{L}_{\odot}$, the faint IRAS galaxy 10214+4724 at $z = 2.286$ is as luminous as the strongest QSOs and 20 times more powerful than other known ultraluminous infrared galaxies.[14] It may be a primeval galaxy in an early evolutionary stage. Is this galaxy powered by star formation or by an active nucleus?

Submillimeter continuum emission from 10214+4724 was observed at 450 and 800 μm with the JCMT[5] and at 1.2 mm with the IRAM 30 m telescope.[7] The spectrum (Figure 3) shows the dust is optically thin longward of 175 μm (rest frame). For a ν^2 dust emissivity law, the dust temperature is 80 ± 10 K and the dust mass[7] is $2 \times 10^8 h^{-2}\,\mathrm{M}_{\odot}$.

The extraordinary detection[1] of CO(3→2) line emission from 10214+4724 indicates this galaxy has as much molecular gas as the total mass of a large spiral galaxy.[21] There has been, however, some uncertainty about the true line flux. While the original measurement[1] with the NRAO 12 m telescope was $26 \pm 6\,\mathrm{Jy\,km\,s^{-1}}$, all subsequent measurements with other instruments indicate a much weaker line (Figure 4). A flux of $4.1 \pm 0.9\,\mathrm{Jy\,km\,s^{-1}}$ was observed with the IRAM 30 m telescope,[3, 20] $4.4 \pm 0.7\,\mathrm{Jy\,km\,s^{-1}}$ with the Nobeyama 45 m telescope,[24] and $3.5 \pm 0.5\,\mathrm{Jy\,km\,s^{-1}}$ in a map made with the IRAM interferometer (that covers 85% of the total line width).[13] A higher flux, $7.5 \pm 2\,\mathrm{Jy\,km\,s^{-1}}$, was measured with the Nobeyama interferometer,[10, 17] but within the errors it is consistent with the others (the revised flux quoted for the amplitude calibrator is, moreover, 1.3 times that measured independently with the IRAM 30 m

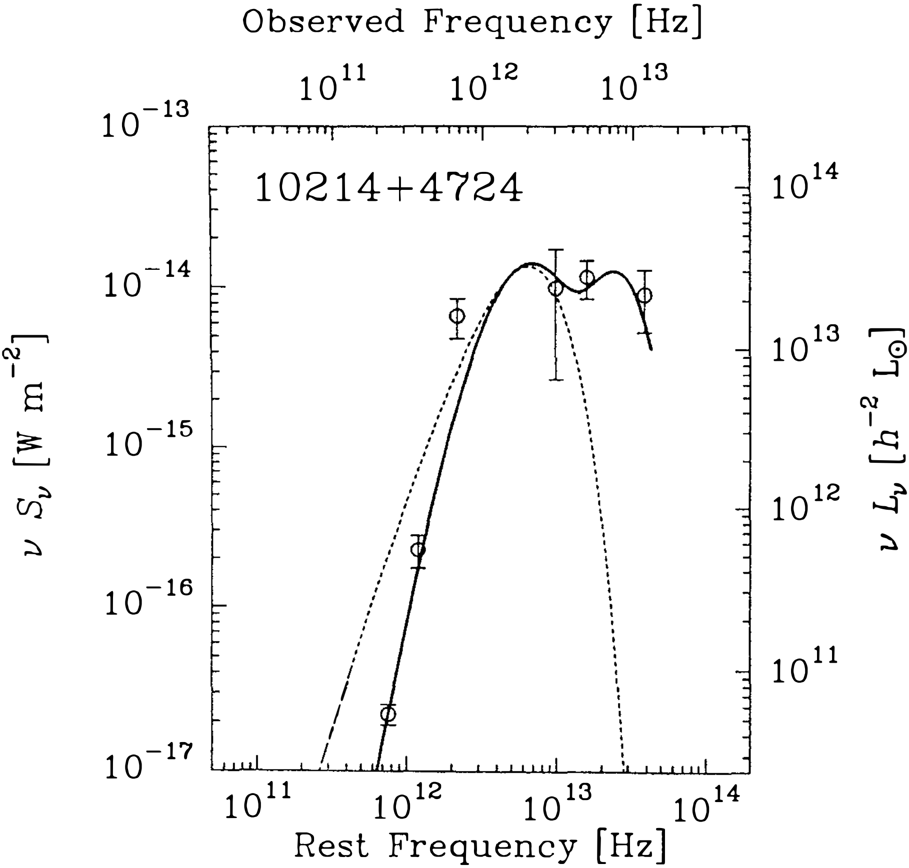

Figure 3: FIR and submm continuum spectrum of 10214+4724. The sum of an 80 K dust spectrum and a 300 K black body (*solid curve*) fits the measurements while an 80 K black body (*dashed curve*) would produce too much long wavelength radiation.[7)]

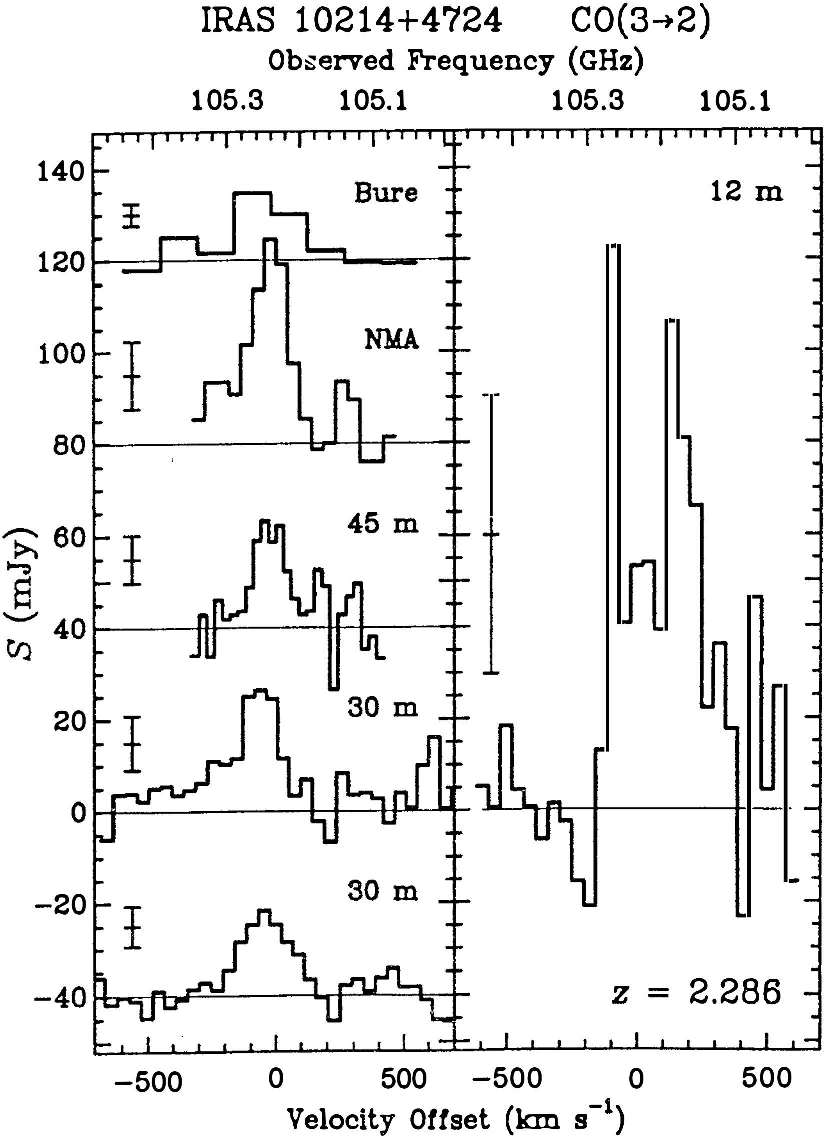

Figure 4: Spectra of CO($3 \rightarrow 2$) emission at z = 2.286 from IRAS 10214+4724 observed with the NRAO 12 m telescope at 16 MHz resolution,[1] the IRAM 30 m telescope at 16 MHz resolution (upper;[3] lower[20]), the Nobeyama 45 m telescope at 10.5 MHz resolution,[24] the Nobeyama Millimeter Array at 32.5 MHz resolution (note the spectrum is displayed with twice this resolution, but adjacent channels are not independent),[10, 17] and the IRAM interferometer (Bure) at 50 MHz resolution.[13] The $\pm 1\sigma$ error bars represent the per channel uncertainty in each spectrum.

telescope and interferometer). The weighted average of these measurements, $4 \pm 1\,\mathrm{Jy\,km\,s^{-1}}$, is six times less than originally reported. Proposed explanations for this discrepancy[3, 10, 17, 24] have invoked additional sources, not coincident with the optical and radio (cm) source, that are outside the primary beams of the 30 m and 45 m telescopes but within the primary beam of the 12 m telescope and hence *within the fields of view of the interferometers* and that emit five times more radiation than the central source yet are too extended to be detected by the interferometers. The only evidence for these extra sources, however, is the large flux seen in the original measurement, which also has the largest uncertainty.

Both CO($4 \rightarrow 3$)[3] and CO($6 \rightarrow 5$)[20] have been detected in 10214+4724 (Figure 5). In the Milky Way, the warm dense gas required for significant excitation of CO($J = 6$) is found only in molecular cloud cores near sites of massive star formation.[9] The measured line ratios in 10214+4724, CO($6 \rightarrow 5$)/CO($3 \rightarrow 2$) $= 0.6 \pm 0.2$ and CO($4 \rightarrow 3$)/CO($3 \rightarrow 2$) $= 0.8 \pm 0.2$, are considerably higher than overall values for the Milky Way. An LVG radiative transfer calculation shows these ratios are both consistent with $n(\mathrm{H_2}) \approx 5000\,\mathrm{cm^{-3}}$ and $T_{\mathrm{kin}} \approx 50\,\mathrm{K}$.[20] This calculation predicts CO($3 \rightarrow 2$)/CO($1 \rightarrow 0$) $= 0.9$ (this ratio is 0.24 in the Galaxy) and $M(\mathrm{H_2})/L_{\mathrm{CO}} = 4\,\mathrm{M_\odot}\,(\mathrm{K\,km\,s^{-1}\,pc^2})^{-1}$. Because the temperature of the Cosmic Background Radiation (CBR) should increase as $(1 + z)$, gas at $z \approx 2$ will always have CO($3 \rightarrow 2$)/CO($1 \rightarrow 0$) > 0.5, even if the density is quite low. The CO($3 \rightarrow 2$) line flux observed with the IRAM 30 m telescope then implies $M(\mathrm{H_2}) = 1 \times 10^{11}\,\mathrm{M_\odot}$ in 10214+4724. The gas to dust mass ratio, 500, is quite normal and suggests the metal abundance is already approximately Solar.[7]

The distribution of CO in 10214+4724 has been mapped with the Noybeyama,[10, 17] Owens Valley,[4] and IRAM[13] interferometers. The IRAM map (Figure 6), with 2.3″ resolution, shows a small source coincident with the Hα[6, 18] and extended 8.4 GHz continuum emission.[11] The ratio of the intrinsic CO($3 \rightarrow 2$) brightness temperature derived from the observed line ratios and a radiative transfer calculation, 40 K, and the peak rest frame brightness temperatures measured in the channel maps, 0.7 K, indicates about 1.7% of the synthesized beam area is occupied by radiating gas. A completely filled source of equivalent luminosity would be 0.3″ in diameter. Despite tnis low filling factor and the large apparent size of the CO($3 \rightarrow 2$) emission region, the average surface density, $2500\,\mathrm{M_\odot\,pc^{-2}}$, is ten times higher than for Galactic giant molecular clouds.[22] In two channels $143\,\mathrm{km\,s^{-1}}$ apart, there is a predominantly E-W shift of 1.4″ between the positions of maximum emission. After deconvolving the beam, the source size in the integrated map is $(2.5'' \times 1'') \pm 1''$ $[(10 \times 4) \pm 4h^{-1}\,\mathrm{kpc}]$. This size scale is characteristic of an entire galaxy, rather than just its nucleus. The velocity gradient implied by the E-W shift suggests the molecular gas is distributed in a rotating structure and the apparent dimensions and aspect ratio further suggest this structure is mostly edge on. For an edge on system with a velocity width of $240\,\mathrm{kms^{-1}}$ and a characteristic dimension of 6–$10h^{-1}$ kpc, the dynamical mass is 8–$13 \times 10^{10}h^{-1}\,\mathrm{M_\odot}$, which is consistent with the $\mathrm{H_2}$ mass determined from the line flux.

The outstanding property of 10214+4724 is its $L_{\mathrm{FIR}}/L_{\mathrm{CO}}$ ratio, $3000\,\mathrm{L_\odot}\,(\mathrm{K\,km\,s^{-1}\,pc^2})^{-1}$, which is ten times greater than that of other ultraluminous galaxies. If star formation powers this galaxy, then a short starburst of primarily high mass stars in required. The energy available from nuclear burning in $10^{11}\,\mathrm{M_\odot}$ of stars indicates star formation can only maintain the luminosity of 10214+4724 for $\approx 10^7$ yr. For a burst of formation of 10 to $100\,\mathrm{M_\odot}$ stars, the necessary formation rate is $\approx 3000\,h^{-2}\,\mathrm{M_\odot\,yr^{-1}}$, about 5000 times the rate in the Milky Way. A starburst of this magnitude will rapidly enrich the interstellar medium in heavy elements.

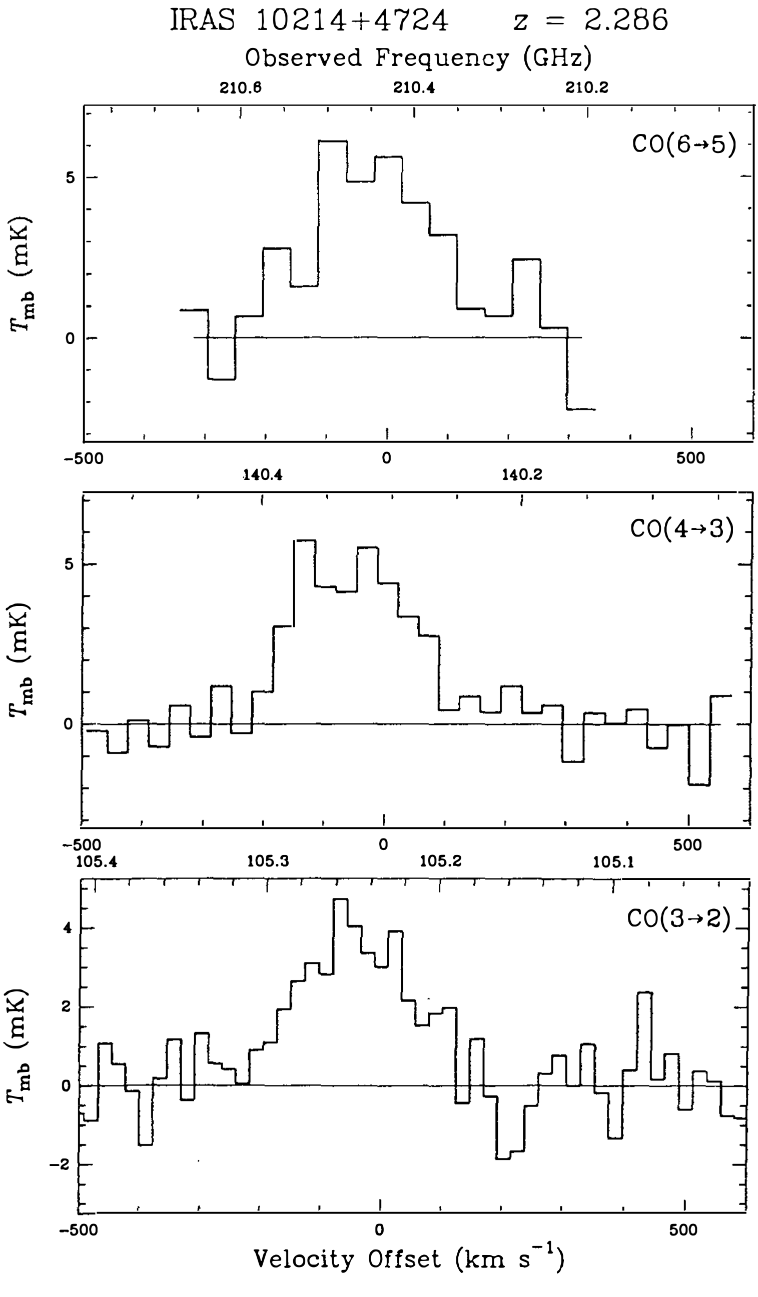

Figure 5: Spectra of CO(6→5), CO(4→3), and CO(3→2) emission at z = 2.286 from 10214+4724 observed with the IRAM 30 m telescope.[3, 20]

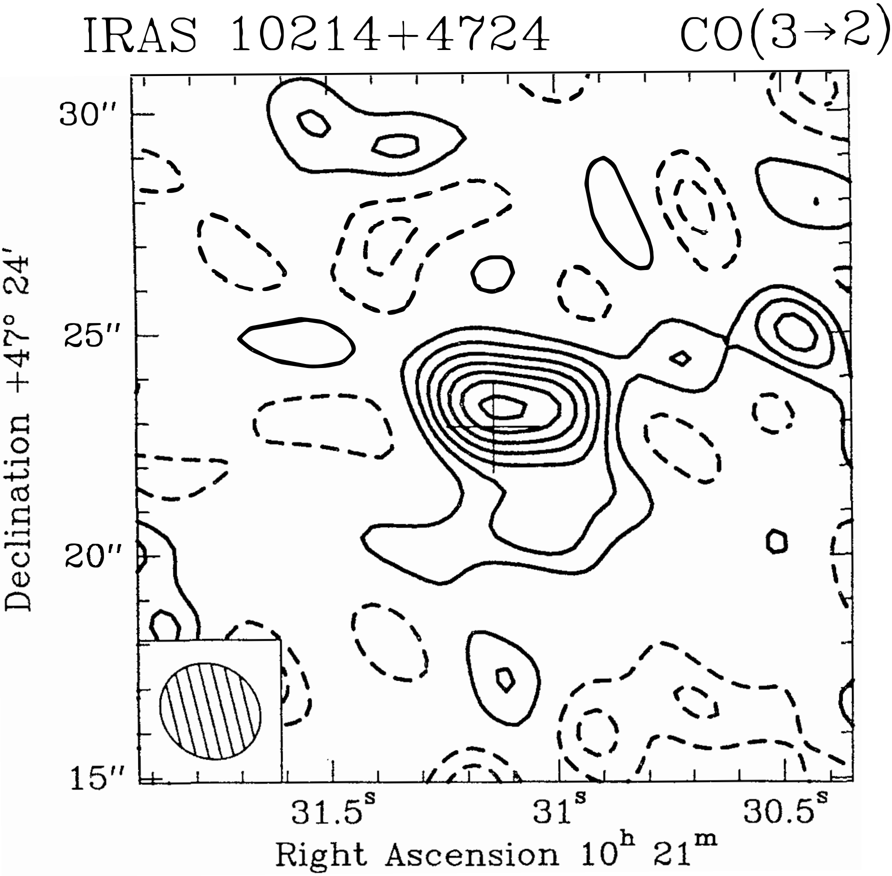

Figure 6: IRAM interferometer map of CO(3 → 2) emission from 10214+4724 at z = 2.2858 integrated over $\pm 143\,\mathrm{km\,s^{-1}}$. Contour interval is 1 mJy.[13)]

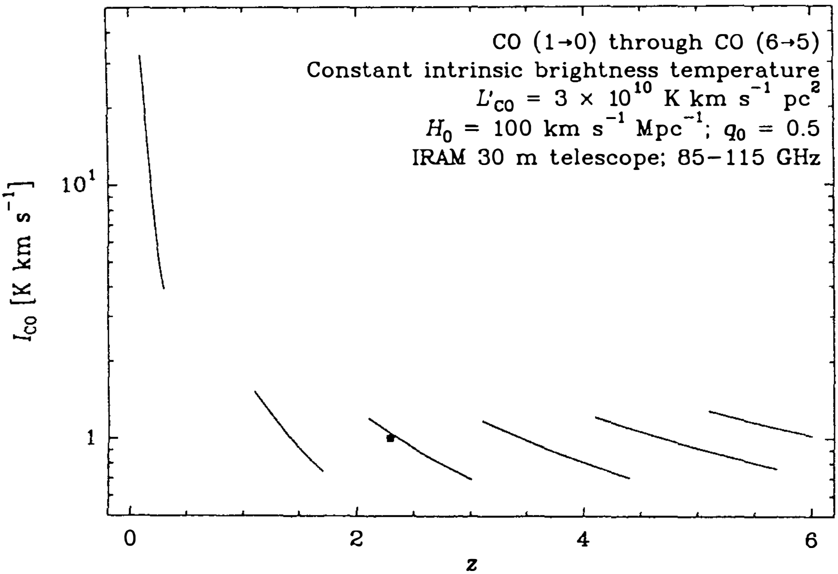

Figure 7: Predicted intensity of CO($1 \to 0$) through CO($6 \to 5$) line emission from sources of the same luminosity but different redshifts if observed with the IRAM 30 m telescope in the 3 mm atmospheric window (85–115 GHz). The square symbol indicates the observed CO($3 \to 2$) intensity of IRAS 10214+4724. Here $q_0 = 0.5$; if $q_0 = 0.05$ the results are, similiar, although somewhat less favorable for high redshifts. This assumes the intrinsic brightness temperatures are the same for all lines. If the high J lines are not thermalized, they will be, of course, weaker. For this telescope and wavelength, there are 4.5 Jy K^{-1}.

3 Further Prospects

Because of the large redshift of IRAS 10214+47624, it's possible to observe several submillimeter spectral lines from the ground that are normally impossible or at least very difficult. A tentative detection of the ($2_{1,1} \to 2_{0,2}$) line of para water has been made with the IRAM 30 m telescope.[8] Somewhat surprisingly, the ground state ($1_{1,0} \to 1_{0,1}$) transition of ortho water, which is presumably more abundant, was undetectable with similar sensitivity.

The $^3P_2 \to {}^3P_1$ and $^3P_1 \to {}^3P_0$ fine structure lines of neutral atomic carbon have been observed with the NRAO 12 m and IRAM 30 m telescopes.[2] In the published $^3P_2 \to {}^3P_1$ spectrum from the 12 m telescope, there is an apparent emission feature. The center of this feature is, however, displaced by -350 km s^{-1} from the CO lines. Furthermore, the emission feature coincides with the overlap between data taken with two receiver tunings that were combined without subtracting any baseline. Both transitions were observed with the 30 m telescope, but in neither spectrum are there features as strong as would be expected from the 12 m data if the source were small with respect to the telescope beams. Indeed at the velocities of the strongest feature in the 12 m spectrum, the $^3P_2 \to {}^3P_1$ spectrum from the 30 m telescope has a minimum. These measurements remain unconfirmed and controversial.

Because of the difference between angular size distance and luminosity distance,[25] spectral lines from high redshift objects are somewhat easier to observe than was first expected.[21, 20] Furthermore, for observations in a particular atmospheric window, the CO rotational ladder is convenient since the redshift where a line leaves the lower edge of the band is roughly the same redshift where the next higher transition enters the upper edge of the band. Both because of the increase in the temperature of the CBR with redshift and because we have detected CO($6 \rightarrow 5$) emission from 10214+4724, we expect CO lines up to $J = 6$ should have roughly the same intrinsic brightness temperatures. For objects with the same luminosity as 10214+4724 but at different redshifts, the predicted CO line intensities are almost constant for any $z > 1$ (Figure 7). Current millimeter wave telescopes can detect molecular gas in objects as distant as any known in the Universe.

Acknowledgements. The 30 m observations were done with Phil Solomon and Dennis Downes and the interferometery with Bob Brown and Paul Vanden Bout.

References

[1] Brown, R. L., & Vanden Bout, P. A. 1991. *Astron. J.* **102**, 1956
[2] Brown, R. L., & Vanden Bout, P. A. 1992. *Astrophys. J.* **397**, L11
[3] Brown, R. L., & Vanden Bout, P. A. 1992. *Astrophys. J.* **397**, L19
[4] Brown, R. L., Vanden Bout, P. A., & Wooten, H. A. 1993. *private communication*
[5] Clements, D. L., *et al.* 1992. *Mon. Not. R. astr. Soc.* **256**, 35P
[6] Clements, D. L., *et al.* 1993. *Mon. Not. R. astr. Soc. in press*
[7] Downes, D., *et al.* 1992. *Astrophys. J.* **398**, L25
[8] Encrenaz, P. J., *et al.* 1993. *Astr. Astrophys. in press*
[9] Jaffe, D. T., *et al.* 1989. *Astrophys. J.* **344**, 265
[10] Kawabe, R., Sakamoto, K., Ishizuki, S., & Ishiguro, M. 1992. *Astrophys. J.* **397**, L23
[11] Lawrence, A., *et al.* 1992. *Mon. Not. R. astr. Soc.* 260, 28
[12] Melnick, J., & Mirabel, I. F. 1990. *Astr. Astrophys.* **231**, L19
[13] Radford, S. J. E., Brown, R. L., & Vanden Bout, P. A. 1993. *Astr. Astrophys.* 271, L71
[14] Rowan-Robinson, M., *et al.* 1991. *Nature* **351**, 719
[15] Sanders, D. B., *et al.* 1986. *Astrophys. J.* **305**, L45
[16] Sanders, D. B., *et al.* 1988. *Astrophys. J.* **325**, 74
[17] Sakamoto, K., Ishizuki, S., Kawabe, R., & Ishiguro, M. 1992. *Astrophys. J.* **397**, L27
[18] Soifer, B. T., *et al.* 1992. *Astrophys. J.* 399, L55
[19] Solomon, P. M., Downes, D., & Radford, S. J. E. 1992. *Astrophys. J.* **387**, L55
[20] Solomon, P. M., Downes, D., & Radford, S. J. E. 1992. *Astrophys. J.* **398**, L29
[21] Solomon, P. M., Radford, S. J. E., & Downes, D. 1992. *Nature* **356**, 318
[22] Solomon, P. M., Rivolo, A. R., Barrett, J., & Yahil, A. 1987. *Astrophys. J.* **319**, 730
[23] Solomon, P. M., & Sage, L. J., 1988. *Astrophys. J.* **334**, 613
[24] Tsuboi, M., & Nakai, N., 1992. *Pub. Astron. Soc. Japan* 44, L241
[25] Weinberg, S., 1972. *Gravitation and Cosmology* (Wiley: New York)

DIFFUSE MATERIAL AT HIGH REDSHIFT FROM QSO ABSORPTION LINES

Patrick Boissé

Groupe de Radioastronomie/URA CNRS 336, Ecole Normale Supérieure
24, rue Lhomond 75231-PARIS Cedex 05

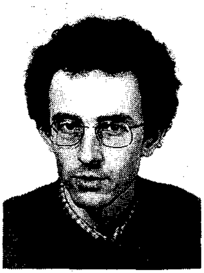

ABSTRACT

Spectroscopic observations of quasars in the visible and UV range is a powerfull means to reveal the presence of diffuse intervening material in the Universe. We summarize here some recent results in this field, in particular those which are the most relevant to high redshift galaxies.
The strongest of the metal line systems, the so-called "damped Lyman α systems", are thought to originate from galactic disks. We shall review which information can be extracted from detailed observations of these systems (number density, abundances, presence of dust and molecules, magnetic field) and how it can be used to infer the evolution that occured from $z > 2$ to $z \approx 0$ galaxies. Most of the other metal line systems seem to be caused by large envelopes of ionized gas surrounding galaxies. The characteristics of these halos will be briefly presented. Finally, the Lyman α forest lines will be considered.

1. INTRODUCTION

Let us first recall a few characteristics of quasar absorption line observations which are of interest here. Unlike most other studies, QSO absorption line data do not suffer from any bias favoring the objects closest to the observer. This is simply because the parameters which limits the detection of absorption lines are 1) the brightness of the background quasar and 2) the equivalent width (i.e. some combination of the column density of the ion considered and its velocity dispersion). One paradox in this field is that it is in fact often easier to study intermediate or high redshift systems than their low redshift analogs since the latter require space observations. This is especially true for the Lyα absorption lines which can be detected from the ground only at redshifts larger than about 2 (the same holds for high ionisation gas which is most efficiently probed by the CIV doublet at $\lambda \approx 1550$ Å). Therefore, while we may suspect that searches for high z galaxies just allow to pick up the most luminous "monsters", quasar absorption lines are of great interest if one wishes to investigate the properties of **normal** high z galaxies. The drawback is that the information extracted from absorption line studies involves some part or phase of the underlying galaxy that remains badly defined; as discussed further, it is relatively clear now that low z ($z \approx 0.4$) MgII absorption are due to extended ionized galaxy halos. The latter may be present as well around nearby and well-studied galaxies but presently we know very little about them (at $z \approx 0$, the only strong lines expected in the optical range - the CaII and NaI doublets - are not well suited to probe ionized gas).

Considering ground-based work only, it is solely in the redshift range $z \approx 0.3 - 0.7$ that one can at the same time obtain good images or spectra of the galaxy and see the absorption caused by its halo in the spectrum of the background quasar (the HST may bring in the future very usefull complementary data on absorption due to nearby $z \approx 0$ galaxies). It is worth noting in addition that there is nearly no overlap in space between the halo revealed by MgII absorption and the central parts of the galaxies seen in images or spectra. Therefore, the connection between the accessible characteristics of the halos (metal abundances or velocity distribution for instance) and the emission properties of the associated galaxy (morphology, star formation rate etc) may be loose and since it remains to be established, it is unfortunately not possible to infer much on the galaxy from quasar absorption data only. This is no longer true for the damped Lyα systems because several of their properties indicate that they are directly related to galaxy disks. For this reason, they are of special interest in our context and we shall consider them first.

2. THE DAMPED LYMAN α SYSTEMS

For N(HI) exceeding 2. 10^{20} cm^{-2}, the opacity far from the center of Lyα lines becomes noticeable and a new regime appears, the rest equivalent width increasing as W_{rest} α $(N(HI)^{0.5}$ (as in the optically thin case, a W measurement then provides a direct measure of N, whatever the velocity dispersion). Since the lines are relatively broad, they can be selected efficiently by using low resolution spectroscopy; confirmation of the candidate "damped lines" is then required to reject those features which turns out to be just random pairs or groups of Lyα forest lines [1]. Another method involves radio observations at the frequency expected for the redshifted 21 cm HI line. While searches for damped Lyα is restricted to z_{abs} larger than about 2 for ground-based observations, this latter method allows the selection of low redshift disks (four cases are known at $z_{abs} < 1$ of which two were found prior to optical observations [2]). Although the presence of a damped Lyα at the redshift of the 21cm feature has not yet been verified for the low redshift cases, it is natural to consider both Lyα and 21 cm absorption as signatures of galaxy disks since the lowest detectable column densities are comparable and well in the range expected for such interveners.

1.1 The heavy element abundances

This is a key point since inside galaxy disks, the gas is supposed to be significantly enriched (on the other hand, if truly intergalactic and primordial clouds were present, very low abundances should be observed). If data can be obtained over a large redshift range, one may then be able to follow the cosmic evolution of the metal abundances.

The damped Lyα systems are well suited for abundances determinations because the amount of hydrogen at least, is well known (the equivalent width already provides a good estimate of N(HI) and above 10^{20} cm^{-2}, the fraction of ionized hydrogen should be small). The situation is less favorable for the most abundant metals, C, O, N because in general their lines are heavily saturated. Further, they are spread over different ionization stages, not all of them being observable. Therefore, observers have focused toward less abundant elements and in particular Zn and

Cr[3),4)]. The $\lambda\lambda$ 2025, 2062 ZnII doublet can be identified easily and is expected to be optically thin. In addition, this element which should be mainly in the form of ZnII at large N(HI) is known to show little depletion onto interstellar grains (in our Galaxy) while the opposite is true for CrII (lines at 2055, 2061 and 2065Å near those of ZnII). The results obtained indicate typical relative abundances in the range 10^{-1} - 10^{-2} solar [4)]. Values as low as 10^{-3} solar have been observed in a N(HI) = 4 10^{20} cm^{-2} system [5)]. The scatter at a given redshift (up to two orders of magnitude and possibly more) is much too large to leave any noticeable trend with redshift. This suggests that the intervening objects observed are in very different states of chemical evolution. This may mean, if galaxies formed at some relatively well defined epoch, that evolution has proceeded at very different rates depending possibly on the mass or some other initial condition. Equivalently, a large abundance spread is expected if galaxy formation occured over a significant fraction of the age of the universe. Radial abundance gradients, if systematically present in remote galaxy disks as in nearby galaxies [6)] may contribute the observed scatter (which would in part reflect the spread in impact parameters of the lines of sight). Radial gradients will also tend to lower the observed abundances since most of the cross section is provided by the external parts where metals are rarer.

Concerning Cr, the Zn/Cr ratio observed implies little evidence for relative depletion which, by comparison with the local interstellar medium, is consistent with a dust to gas ratio below 1/10th of the Galactic one.

1.2 Number density of lines

Unbiased spectroscopic surveys [7)] yields a number density of lines per unit redshift interval, $dN/dz \approx 0.2$ at $\langle z \rangle \approx 2.5$. This is about five times the expected value assuming an unevolving population of spirals. The discrepancy implies a higher value of the product $n_{gal}\ \sigma_{gal}$ i.e. a larger comoving number density of spirals (n_{gal}) in the past (as expected if merging has affected the evolution of a significant fraction of galaxies) and/or a larger cross section for N(HI) > 2 10^{20} cm^{-2} (σ_{gal}) . A possible rapid increase in dN/dz above z = 3.5 has been announced [8)] but this result is based on few lines and requires confirmation from a larger sample.

1.3 The apparent lack of associated dust

Dust is a ubiquitous component of nearby gas-rich galaxies so we expect to find it in remote disks too. Several signatures can be searched for: reddening and bending of the spectra or presence of the 2175Å feature. Despite many searches, no clear evidence of dust has been found in any particular absorption system [9], [10]. Quasars which show a damped Lyα system in their spectrum are slightly redder than others, the inferred dust to gas ratio being about 1/10th of the galactic one [11]. This result is of a statistical nature since reddening cannot be considered as an unambiguous signature for a given object (there exists no unique intrinsic QSO spectrum). The third signature - the 2175Å feature - has been searched in 0215+015 at the redshift of a strong (but probably not damped) system[9]. Despite the remarkable smoothness of this BL Lac spectrum, no hint of a depression could be found in it. This signature is not easy to detect because, once redshifted at $z \approx 1$ or 2, it is very broad (up to 1000 to 1500Å). One objection often raised concerning its use is that it may not be universal. Indeed, this feature is much less pronounced in the LMC and is absent in the SMC - the only external galaxies for which detailed UV extinction curves have been obtained. However, Magellanic clouds are dwarf galaxies and we see no reason by which the extinction curve of our Galaxy should not be representative of those in other normal galaxies. Possibly, the feature may vary in strength from galaxy to galaxy (which includes the possibility that it may occasionnally be stronger !) as it does from one region to another inside the Galaxy; but it seems quite unlikely that it is systematically absent. Recently, an extinction curve has been obtained for M31 from HST spectroscopy of two OB stars [12] and although narrower, the 2175Å is present.

1.4 Searches for molecular absorption in damped systems

Two different techniques have been used. The first one involves absorption in the CO rotationnal lines (either J=0-->1, J=1-->2, etc). Only upper limits have been obtained [13]. Observations were also performed at the IRAM 30m telescope by our group with negative results (unpublished). Second, UV lines can be considered, either from H_2 (presumably the most abundant molecules) or CO. The latter is more easy to search for because some lines can occur outside the Lyα forest (depending on z_{em} and z_{abs}). Several stringent upper limits have been obtained with an implied fraction of gas in molecular form orders of magnitude lower than in the diffuse Galactic interstellar medium [10], [14]. The only detection (for H_2) has been obtained towards 0528-250 at $z_{abs} = 2.811$ [15], a quite peculiar system since z_{abs} is slightly larger than z_{em}. The absorbing material should then be located in the immediate vicinity of the active nucleus and falling onto it: this is not a very favorable environment for molecules and however, it is the only object in which H_2 has been detected !

The difficulty of the millimeter wave observations is that, because of a too low continuum flux level, detection could be expected only for a very small fraction of the potentially interesting sources; indeed, the upper limits obtained are less constraining than those obtained from the UV CO lines. However, radio observations remain of interest for low redshift systems because the CO and H_2 electronic transitions cannot be searched for from the ground. Further, if a detection were obtained in this range, several lines could be detected allowing to estimate the population of the various rotationnal levels (at high z, the cosmic background radiation should contribute to populate the J = 2, 3 ... levels since $T_{cbr}(z) \alpha (1+z)$).

1.5 Are the estimates of dust, molecules and metals biased ?

We now wonder to which extent the available sight lines can be used to get the true composition of the interstellar medium (ISM) in distant galaxies. For this purpose, let us estimate what quasars with damped systems would look like if the ISM were similar to that of our Galaxy and consider the case of PKS 0458-02 with N(HI) = 6 10^{21} cm^{-2} at z_{abs} = 2.04[16]. Using average Galactic dust to gas ratio and extinction curves, we get an attenuation induced by the intervener of 10 magnitudes at λ_{obs} = 4400Å (λ(B); corresponding λ_{rest} : 1450Å). Clearly, such an object would never have been recognized as a quasar. Further, even if N(HI) amounts to only 10^{21} cm^{-2}, the quasar will probably be considered too faint for a spectroscopic study at intermediate resolution. The brightest distant quasars have $m_B \approx$ 16-17 and below m $\approx$ 18, medium resolution spectroscopy becomes difficult; the range of detectable extinction is therefore very narrow. We conclude that the apparent lack of dust may be largely due to an observationnal selection effect. As dust must be present for molecules to form or survive, results concerning the latter may be biased in the same manner. One way to check this and to get firm evidence for associated dust and molecules in individual objects would be to search for damped Lyα lines in fainter quasars; objects which have already been noticed for their red colors are specially interesting in this regard. Very large telescopes will offer soon the opportunity to perform such observations.

Nevertheless, the available data at least proves that large HI column densities can exist with very little associated dust. This is not necessarily a distinctive feature of high z disks since the same may be true in the outer regions of nearby spirals. QSO absorption studies naturally lead to select lines of sight that cross the external parts of the interveners which dominate the cross section. If abundance gradients are already present in z $\approx$ 2 disks, then the measured heavy element abundances may also not be representative of the overall metallicity. We then conclude that the dust to gas ratio as well as the molecular fraction and metal abundance estimates are probably all lower bounds to the true values.

1.6 Magnetic field

It has been established that the presence of absorption systems in quasar spectra is statistically associated with an enhanced Faraday rotation [17]. The original study included a large variety of absorption systems and a stronger effect appear if only damped Lyα systems are considered [18]. VLA observations of PKS1229-021 performed recently [19] illustrates well how detailed information can be obtained in the radio range when the background source is extended. The high resolution polarisation maps show a complex pattern which is consistent with an intervening spiral (z_{abs} = 0.395) located at a few arcsec only of the QSO line of sight. The implied magnetic field is about 1 - 4 μG.

1.7 Emission from objects causing damped Lyα systems

One first technique consists in obtaining a high signal to noise spectrum of the damped Lyα profile since Lyα emission from the intervener is expected precisely where the QSO flux falls to zero. Controversial results have been obtained for the z = 2.466 Lyα system toward 0836+113 [20], [21]. Another method involves imaging in a narrow band where the QSO is completely absorbed, a technique which allows to reveal objects blended with the QSO image as well as neighbors. Broad band imaging with follow-up spectroscopy has also been used. Generally, the objects observed are not the damped absorber but neighbors [22], [20], [23]. These results led to conclude that clustering of galaxies around z $\approx$ 2.6 damped aborbers is strong [24]. Further, the objects are found to be of galactic size and show a star formation rate in the range 1-20M_{O}/yr.

Very recently, attempts have been made to detect the CO rotationnal lines in the millimeter range [25]. Considering that these observations have probably been stimulated by the detection of CO and CI emission from the 10214+4724 IRAS galaxy at z= 2.28 (see discussions in this volume), we wish to make two remarks. First, we stress that we have no reason to suspect that damped absorbers are characterized by a particularly large intrinsic luminosity or amount of interstellar material (the strength of the induced Lyα absorption being more likely just the result of a close alignment with the QSO). On the other hand, the galaxy 10214+4724 could be detected only because it is exceptionnal in its far infrared luminosity (indeed, normal galaxies become hard to detect in CO beyond z ≈ 0.03). Second, high frequency radio observations are characterized by a very narrow bandwidth which results in a small velocity coverage. The latter often do not exceed ≈ 1000km/s and it is not easy to judge the reality of a feature several hundreds of km/s wide. Repeating these observations at different telescopes and searching for several CO (or CI) lines from the same object is therefore crucial to establish the reality of any claimed detection.

All the data summarized above are consistent with a picture in which galactic disks are responsible for both the low z 21cm absorptions as well as the z > 2 damped Lyα systems (kinematical studies which have not been discussed here are also in good agreement with this view).

3. METAL LINE SYSTEMS AND GALACTIC HALOS

The absorption systems we consider now differ from the previous ones by their smaller N(HI) column density (N(HI) ≈ 10^{17} - 10^{20} cm^{-2}). Early after their discovery, the existence of large halos around galaxies was proposed as a likely explanation. About twenty years later, it became possible to test this assumption by direct observations and systematic searches reveal in nearly all cases a galaxy close to the quasar image with a redshift equal to that of the absorption system [26), 27)]. The consequence is that most bright galaxies ($L \geq 0.3\ L^*$) at z ≈ 0.5 should be surrounded by gaseous halos with radii as large as 80 h_{50}^{-1}kpc. The observations also indicate that the contribution of dwarf galaxies to the total cross-section is probably small [28)]. Our Galaxy does not possess such a halo (but just a "thick disk"); if it is considered to be representative of z≈0 galaxies (the HST will answer this question through observation of QSO/galaxy pairs), one must admit that strong evolution has occurred between z=0.5 and z=0. Unfortunately, halos are still very poorly understood and at present there is no model that could be used reliably to connect the absorption line data with the underlying galaxy properties.

4. THE LYMAN α FOREST LINES

We shall just summarize here a few properties of the so called "Lyα clouds", the hypothetical objects which give rise to the forest of lines blueward of the QSO Lyα emission line (for details, see recent reviews[29)]).

The large number density of lines together with the lack of clustering strongly suggest that a new and unknown population of objects is required to account for these absorptions. The metal abundance is quite low, less than $10^{-3.5}$ solar [30] . At high z, there is a strong cosmological evolution in the number density of lines since dN/dz α $(1+z)^{2.3}$ (therefore the comoving number density and/or the cross-section should decrease with cosmic time). Spectroscopic observations of the gravitationally lensed quasar UM 673 has allowed to establish that the clouds are of galactic size [31]. Regarding the temperature of the gas - a key parameter in physical models of the clouds - conflicting results have been obtained. A recent reanalysis of the data seem to indicate that the presence of very narrow lines ($b \approx 10$km/s which would imply a low temperature $T < 10^4$ K) as well as the existence of a velocity dispersion - column density correlation are artefacts due to a finite signal/noise ratio[32]. As shown by the HST [33], Lyα clouds still exist at $z \approx 0$ and are in fact more numerous than predicted from extrapolating the high z evolution law. The presence of nearby specimens allows detailed complementary optical or radio observations to be conducted [34] which will certainly help very much to establish the nature (possibly not unique) of these objects: primordial clouds, dwarf unevolved galaxies, gaseous clouds lying in the most external parts of galaxies and pulled out by past tidal interactions ?

References

1) Wolfe A.M.,Turnshek D.A., Smith H.E.,Cohen R.D.:1986,ApJS **61**, 249

2) Briggs F.H.: 1988, in QSO Absorption Lines: Probing the Universe, ed. J.C. Blades, D.A. Turnshek, C.A. Norman (Camb. Univ. Press), 275

3) Meyer D.M., Welty D.E., York D.G.: 1989, ApJ **343**, L37

4) Pettini M., Hunstead R.W.: 1990, Aust. J. Phys. **43**, 227

5) Rauch M., Carswell R.F., Robertson J.G., Shaver P.A., Webb J.K.: 1990, MNRAS **242**, 698

6) Pagel B.E.J.: 1992, in The Stellar Population of Galaxies, ed. Barbuy B. and Renzini A., IAU symposium N° 149, Kluwer, p133

7) Lanzetta K.M., Wolfe A.M., Turnshek D.A., Lu L., McMahon, R.G., Hazard, C.: 1991, ApJS **77**, 1

8) White R.L., Kinney A.L., Becker R.H.: 1993, ApJ **407**, 456

9) Boissé P., Bergeron J.: 1988, A&A **192**, 1
10) Lanzetta K.M., Wolfe A.M., Turnshek D.A.: 1989, ApJ **344**, 277
11) Pei Y.C., Fall S.M., Bechtold J.: 1991, ApJ **378**, 6
12) Hutchings J.B., Bianchi L., Lamers H.J., Massey P., Morris S.C.: 1992, ApJ **400**, L35
13) Takahara F., Nakai N., Briggs F.H., Wolfe A.M.: 1987, PASJ **39**, 933
14) Black J.H., Chaffee Jr. F.H., Foltz C.B.: 1987, ApJ **317**, 442
15) Foltz C.B., Chaffee Jr. F.H., Black J.H.: 1988, ApJ **324**, 267
16) Wolfe A.M., Briggs F.H., Turnshek D.A., Davis M.M., Smith H.E., Cohen R.D.: 1985, ApJ **294**, L67
17) Kronberg P.P., Perry J.J.: 1982, ApJ **263**, 518
18) Wolfe A.M., Lanzetta K.M., Oren A.L.: 1992, ApJ **388**, 17
19) Kronberg P.P., Perry J.J., Zukowski E.L.H.: 1992, ApJ **387**, 528
20) Wolfe A.M.,Turnshek D.A.,Lanzetta K.M.,Oke J.B.:1992, ApJ **385**, 151
21) Hunstead R.W., Pettini M., Fletcher A.B.: 1990, ApJ **365**, 23
22) Lowenthal J.D., Hogan C.J., Green R.F., Caulet A., Woodgate B.E., Brown L., Foltz C.B.: 1991, ApJ **377**, L73
23) Macchetto F., Lipari S., Gialvalisco M., Turnshek D.A., Sparks W.B.: 1993, ApJ **404**, 511
24) Wolfe A.M.: 1993, ApJ **402**, 411
25) Brown R.L., Vanden Bout P.A.: 1993, ApJ **412**, L21
26) Bergeron J., Boissé P.: 1991, A&A **243**, 344
27) Steidel C.C.: 1993, in The Evolution of Galaxies and their Environment, eds Shull J.M., Thronson H., Kluwer, in press
28) Le Brun V., Bergeron J., Boissé P., Christian C.: 1993, A&A in press
29) Carswell R.F.: 1988, in QSO Absorption Lines: Probing the Universe, ed.J.C. Blades, D.A. Turnshek, C.A. Norman (Camb. Univ. Press), 91
30) Chaffee F.H., Foltz C.B., Bechtold J., Weymann R.J.: 1986, ApJ **301**, 116
31) Smette A., Surdej J., Shaver P.A., Foltz C.B., Chaffee F.H., Weymann R.J., Williams R.E., Magain P.: 1992, ApJ **389**, 39
32) Rauch M., Carswell R.F., Webb J.K., Weymann R.J.: 1993, MNRAS **260**, 589
33) Bahcall J.N., Jannuzi B.T., Schneider D.P., Hartig G.F., Bohlin R., Junkkarinen V.: 1991, ApJ **377**, L5
34) Salzer J.J.: 1992, AJ **103**, 385

1.25mm DETECTION OF A RADIOQUIET QSO WITH z=4.69

A. OMONT[1], J. BERGERON[1], R.G. McMAHON[2],
E. KREYSA[3] and C.G.T. HASLAM[3]
[1]. Institut d'Astrophysique de Paris, CNRS,
98bis Boulevard Arago, F-75014, Paris, France
[2]. Institute of Astronomy, Madingley Road, Cambridge CB3 0HA, UK
[3]. Max-Planck-Institute fur Radioastronomie,
Auf dem Hugel 69, D-5300 Bonn, Germany

ABSTRACT

We report the results of 1.25mm continuum observations with the IRAM 30m telescope of five optically selected QSOs, and five radio selected, flat spectrum QSOs with high redshifts. One of the optically selected QSOs, BR1202−0725 with z=4.69, was detected. The observed flux of 10.5±1.5mJy is similar to that of the, z=2.29, high luminosity IRAS source F10214+4714 and under the assumption that the detected emission is due to thermal emission from dust with a single temperature, T_D=80K, the inferred dust mass $\sim 4 \times 10^8$ $M_\odot$ ($\Omega_0 = 1, H_0 = 50$). Three of the five radio selected QSOs with S_{6cm}>250mJy were detected with $S_{1.25mm}$ in the range ~20–50mJy.

IRAS has shown the importance of middle and far infrared (MFIR) emission of dust in starburst galaxies, radiogalaxies and QSO's, where it represents an important fraction of the total luminosity in all cases known. The MFIR emission of QSO's and other active galaxies at low z, is now relatively well documented from IRAS measurements (*e.g.* Sanders *et al.* 1989, Heckman *et al.* 1992), and complemented by mm and submm observations, especially with the 30m (*e.g.* Chini *et al.* 1989a,b). However, until recently no radio quiet QSO or AGN had been detected in the mm range beyond a z=0.107 (Chini *et al.* 1987). The situation has changed dramatically in the last 18 months with the detection of a few objects with z>2 in the mm range i.e. the ultraluminous IRAS galaxy, IRAS F10214+4724, at z=2.3, (Clements *et al.* 1992, Downes *et al.* 1992), and the gravitationally lensed QSO H1413+117 at z=2.5 (Barvainis *et al.* 1992). The submm-mm-IRAS spectrum of IRAS F10214+4724 appears to indicate a relatively high dust temperature (80K) and a surprisingly normal gas-to-dust ratio.

The MFIR emission of QSO's is a major issue. It is believed to be thermal in the majority of cases (Sanders *et al.* 1989, Heckman *et al.* 1992) and thus reflect the properties and the distribution of dust a large distance from the central source, up to several kpc. The knowledge of the total mass and temperature of dust gives information on its spatial distribution and on the star formation activity in the past (through the abundance of the heavy elements) and at the time of emission of the radiation (starburst).

Because of the steepness of the submillimetre and far IR emission of dust, the detection sensitivity of continuum radiation at mm and submm wavelengths is practically independent of the redshift z for large values of z and can even increase with z for q_o=0.5 (see *e.g.* Blain and Longair 1992, McMahon *et al.* 1993). This is in contrast to the IRAS bands where the fluxes are falling since they are on the other side of the blackbody peak. This is examplified by the quoted detections at z>2 of the galaxy IRAS F10214+4724 and the QSO H1413+117. While IRAS F10214+4724 is still unique, there is now a large sample of QSOs at larger z, and in particular more than 40 at z>4. Although the properties of these objects are still poorly known, there was a certain probability that they contain relatively important amounts of dust and that there are very powerful IR emitters. The presence of dust at large redshift is a fundamental question, both because it can be an important reservoir of heavy elements and because it can absorb visible and UV radiation, reprocessing the energy into the far infrared, thus making high redshift starforming galaxies very difficult to identify or study at optical or near IR wavelengths. Accordingly, we proposed to search for 1.25 mm emission among the bright QSOs with z>4 of the APM colour selected sample (Irwin, McMahon & Hazard,1991). We here report our initial observations and discuss the implications of our results for the amount of dust in one detected radio quiet QSO with z = 4.69 (a more complete discussion is given in McMahon *et al.* 1993 (MOBKH)).

The observations were performed in February 1993 with the IRAM 30m telescope. The detector used was the MPIfR 7-channel bolometer array with ^{3}He cooling (Kreysa 1993) which allows a good control of the sky noise. The observational procedure is described in MOBKH. Due to poor weather conditions, 80% of the allocated time was lost, so that only a very limited number of sources could be observed with a good sensitivity.

The results are reported in Table 1a. Three of the five radio selected QSOs with S_{6cm} >250mJy were detected with $S_{1.25mm}$ in the range ~20–50mJy. For these radio loud QSOs the 1.25mm observations indicate a steepening of the radio continuum from a median spectral index of +0.3 between 20cm and 6cm to ~−0.7 over the range 6cm to 1.25mm (see MOBKH for references of visible and cm fluxes).

Table 1. Observational results.

Table 1a – Present results at 1.25mm.

Source	z	mag	S_{6cm} (mJy)	α_{6cm}^{20cm}	$S_{1.25mm}$ (mJy)	$\alpha_{1.25mm}^{6cm}$
BR 1202−0725	4.69	18.7(R)	0.3 ± 0.2		10.5 ± 1.5	$> +0.70$
BRI1328−0433	4.20	19.0(R)			2.7 ± 1.6	
BR 2235−0301	4.25	18.2(R)	0.1 ± 0.2		0.6 ± 2.5	
HS 1700+6416	2.72	16.1(V)			1.5 ± 2.0	
BRI1050−0000	4.29	18.6(R)	10.6 ± 0.2	+0.02	1.5 ± 3.0	< -0.09
MC 1331+1704	2.08	16.7(V)	713 ± 97	+0.74	3.0 ± 1.5	< -1.21
MG 1500+0431	3.67	18.0(R)	169 ± 17	−0.19	5.0 ± 2.4	< -0.73
GB 1508+5714	4.30	18.9(R)	282 ± 29	+0.53	41.0 ± 4.0	−0.50
MG 1557+0313	3.90	19.8(R)	690 ± 19	+0.30	23.0 ± 4.5	−0.87
GB 1745+6227	3.89	18.3(R)	580 ± 55	−0.23	50.0 ± 7.0	−0.63

Table 1b. Results of Andreani, La Franca & Cristiani (1993)

Source	z	mag	S_{6cm} (mJy)	α_{6cm}^{20cm}	$S_{1.25mm}$ (mJy)	$\alpha_{1.25mm}^{6cm}$
PC2132+0126	3.19	19.8(R)	<0.2		11.5±1.7	
PC0344+0222	3.38	20.4(R)	<0.3		5.7±2.0	
PC0345+0130	3.64	19.9(R)	<0.2		6.1±2.0	
PC0307+0222	4.38	20.4(R)	<0.3		6.6±1.7	

Only one radio quiet QSO was detected, BR1202−0725 with z=4.69 and $S_{1.25mm}$=10.5± 1.5mJy. It was detected at a 4-5σ level on 3 different nights. 3σ upper limits of ~7 mJy, were obtained for the other three APM QSOs with z>4.0 and the luminous lower redshift QSO, HS1700+6461. At z=4.69, BR1202−0725 is the highest redshift QSO of the APM sample. Its 6cm flux was found smaller than 1 mJy by Irwin *et al.* (in preparation).

There is mounting evidence that the FIR emission in radio quiet QSOs (*e.g.* Sanders *et al.* 1989) is due to thermal emission from dust as originally proposed by Rees *et al.* (1969). Models of the 10–100μm emission (*e.g.* Barvainis 1990) show that no nonthermal source is necessary in radio quiet QSOs to explain the FIR emission. More importantly mm and sub-mm observations of low redshift radio quiet QSOs that have IRAS detections at 100μm (Chini, Kreysa & Biermann 1989, Hughes *et al.* 1993) have shown that a non-thermal synchrotron self-absorption origin for the turn-down in the FIR spectrum in radio quiet QSOs is highly unlikely. As discussed by Chini *et al.* (1989a), Andreani *et al.* (1993) and Hughes *et al.* (1993), whilst emission from the QSO nuclear region cannot completely be ruled out, it would require rather extreme cases of self-absorbed synchrotron emission (de Kool & Begelman 1989, Schlikeiser *et al.* 1991). Therefore we shall continue our discussion under the quite plausible assumption that the 1.25mm emision we have detected is due to thermal emission from dust.

If one assumes a mass of dust(M_d), which is optical thin at λ_{rest}~200 μm, with a single dust temperature (T_d), the relationship between the measured flux density $S_{(\nu_{obs})}$ at an observed frequency ν_{obs} for a source with redshift (z) is given by:

$$M_d \;=\; S_{(\nu_{obs})} D_L^2 \;/\; (1+z)\kappa_d(\nu_r) B(\nu_r, T_d) \qquad (1)$$

where ν_r is the rest-frame frequency, D_L is the luminosity distance:

$$D_L \;=\; \mathrm{cH}_o^{-1}\; q_o^{-2}\left(zq_o + (q_o - 1)[(2q_o z + 1)^{0.5} - 1]\right) \qquad (2)$$

and $B(\nu_r, T_d)$ is the Planck black body function. The dust absorption coefficient κ_d is quite uncertain for even local galactic dust. For quantitative estimates, we take, as Downes *et al.* (1992), $\kappa_d = 0.4(\nu_r/250\mathrm{GHz})^2 cm^2 gm^{-1}$ of dust (Krugel, Steppe & Chini 1990), noting that it is uncertain by at least a factor 3.

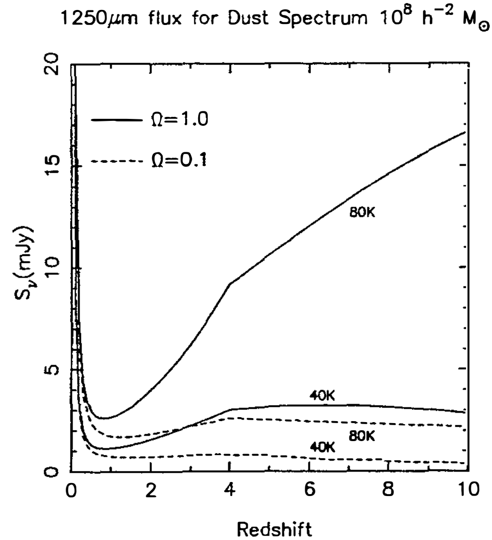

Figure 1 – The predicted 1.25mm flux as a function of redshift for a thermal dust spectrum (Hildebrand 1983). Two temperatures are shown, 40K and 80K.

Figure 1 illustrates quantitatively the behaviour of relation (1), and in particular the important increase of $S_{(\nu_{obs})}/M_d$ for q_o=0.5 and T_d=80 K. In all cases, the dust mass inferred from the observed flux density of BR1202−0725 at 1.25mm is large, with $M_d \sim 10^8\ h^{-2}\ M_\odot$ for q_o=0.5. (lower T_d and q_o mean higher dust masses). This value is comparable to that of IRAS F10214+4724 (Downes *et al.* 1992). The corresponding mass of gas assuming a typical gas to dust ratio of 500 (Downes *et al.* 1992) implies a gas mass $\sim 10^{11}\ M_\bullet$ *i.e.* a galactic scale mass. However, one must stress that, whilst mm/submm observations provide evidence for the presence of dust and the best estimate of the total mass, the uncertainty in the temperature means that the total FIR luminosity is quite uncertain since this varies as $\sim T^{4-6}$.

Recently Andreani *et al.* (1993) have reported a similar result ($S_{1.25mm} = 11.5 \pm 1.5$mJy) for a radio quiet QSO at z=3.19 (Table 1b). In addition they report observations of 3 other QSOs in the redshift range 3.4 to 4.4 with fluxes of ~6±2 mJy (~3σ) out of 16 radio quiet QSOs observed. Barvainis *et al.* (1992) report a comparable detection at 0.80mm of the gravitationally lensed QSO H1413+117 at z=2.5.

It is striking that in all these cases, including IRAS F10214+4724, the inferred masses of dust are comparable, in the range of $10^8\ h^{-2}\ M_\odot$. Altogether with the results of Andreani *et al.* (1993), our results show that such a large amount of dust is relatively common at z ~4, although the present number of observations with a good sensitivity is still too small to allow statistical conclusions.

It has been suggested that the extraordinary values of M_d and L_{FIR} in IRAS F10214+4724 could be explained by a large primeval galaxy undergoing at the scale of the whole galaxy an enormous starburst which could be an essential stage of elliptical galaxies (Elbaz *et al.* 1992). One could consider the same explanation for BR1202−0725, although there is no other proof of a starburst there, and the dust could as well be heated by the central radiation of the QSO (Sanders *et al.* 1989).

At such large redshifts the probability of strong gravitational lensing by intervening systems is relatively large (see *e.g.* Blandford and Narayan, 1992) so that the detected emission could be amplified considerably. All the above APM QSOs have been imaged in ~1" seeing and there is no evidence for faint stellar companions within 2–3 magnitudes or within a radius 0.5–10". Thus whilst we cannot exclude completely the possibility of lensing we consider it highly unlikely.

In conclusion the positive detection at 1.25mm of a radio quiet QSO at z=4.69, as well as those of Andreani *et al.* (1993), opens the possibility of systematic studies of the far infra-red emission in powerful QSOs at large redshift, together with further studies at shorter wavelengths (*e.g.* with JCMT and ISO). The results of these observations will be a new tool in attempts to understand the physics and the evolution of high z QSOs and their host galaxies and hopefully provide information about the star formation rate, heavy element production timescales and dust masses.

REFERENCES

Andreani P., La Franca F., Cristiani S., 1993, MNRAS **261**, L35.

Barvainis R., Antonucci R., Coleman P., 1992, Astrophys. J **353**, 416.

Barvainis R., 1990, Astrophys. J **353**, 419.

Blain A.W. and Longair M.S., 1993, MNRAS **264**, 509.

Blandford, R.D. and Narayan, R., 1992, Ann. Rev. Astron. Astrophys. **30**, 311.

Chini, R., Kreysa, E., Salter, C.J., 1987, Astron. Astrophys. **219**, 87.

Chini, R., Kreysa, E. and Bierman, P.L., 1989a, Astron. Astrophys. **219**, 87.

Chini, R., Bierman, P.L., Kreysa, E. and Gemund, H.P., 1989b, Astron. Astrophys. **221**, L3.

Clements, D.L., Rowan-Robinson, M., Lawrence, A., Broadhurst, T. McMahon, R., 1992, MNRAS **256**, 35p.

de Kool, M. and Begelman, M.C., 1989, Astrophys. J. **308**, 59.

Downes, D., Radford, S.J.E., Greve, A., Thum, C., Solomon, P.M. and Wink, J.E., 1992, Astrophys. J. **398**, L25.

Elbaz, D., Arnaud, M., Cassé, M., Mirabel, I.F., Prantzos, N. and Vangioni-Flam, E., 1992, Astron. Astrophys. **265**, L29.

Heckman, T.M., Chambers, K.C. and Postman, M., 1992 Astrophys. J. **393**, 68.

Hildebrand, R.H., 1983, QJRAS, **24**, 267.

Hughes, D.H, Robson, E.I., Dunlop, J.S., Gear, W.K., 1993, MNRAS **262**, 607.

Irwin, M.J., McMahon, R.G. and Hazard, C., 1991 In: *The Space Distribution of Quasars*, ASP Conference Series, Vol. 21, p.117 Ed. D. Crampton.

Kreysa, E., 1993, In: Proc.Int.Symp.on Photon Detectors for Space Instrumentation, edited by T.D.Guyenne, ESA/ESTEC Noordwijk, 1993.

Krügel, E., Steppe H. and Chini R., 1990, Astron. Astrophys. **229**, 17.

McMahon, R.G., Omont, A., Bergeron, J., Kreysa, E., Haslam, C.G.T., 1993, MNRAS in press (MOBKH).

Rees, M.J., Silk, J.I., Werner, M.W., Wickramasinghe, N.C., 1969, Nature **223**, 788.

Sanders, D., Phinney, E.S., Neugebauer, G., Soifer, B.T. and Matthews, K. , 1989, Astrophys. J. **347**, 29.

Schlikeiser, R., Biermann, P.L. and Crusius-Watzel, A., 1991, Astron. Astrophys. **247**, 283.

Inspection by Jean-Loup...

ABUNDANCE OF NUCLEAR PROCESSED MATERIAL AS A CONSTRAINT ON GALAXY PHOTOMETRIC EVOLUTION AND BACKGROUND RADIATION

B.E.J. Pagel, NORDITA, Blegdamsvej 17, Dk-2100 Copenhagen Ø, Denmark

ABSTRACT

Smoothed-out cosmic abundance of nuclear processed material is used as an additional constraint on past photometric evolution of galaxies, to supplement and refine constraints from extragalactic background light and make some predictions about the latter. In the solar neighbourhood, any exponential decline since the past in star formation rates needs an e-folding time of at least 5 Gyr, whereas in E-galaxies (early stages of which may be represented by luminous IRAS galaxies) much faster decline rates (or luminosity evolution with red-shift) are permitted in view of the likely high proportion of white dwarfs. Predicted diffuse backgrounds based on extrapolated galaxy counts agree well with those from plausible evolutionary synthesis models. The low red-shifts of faint blue galaxies, combined with current uv background limits, suggest that these are not major sources of cosmic metal production.

1. INTRODUCTION

In a classic paper, Partridge & Peebles [1] considered extragalactic background light intensity and cosmic abundance of nuclear processed material (mostly helium) resulting from photometric evolution of galaxies. PP model 1, with constant rate of star formation and nearly constant luminosity, was rejected by them because it made too little helium for ideas current at that time, but its background spectrum is quite near modern predictions in optical and near infra-red, e.g. Yoshii & Takahara [2] and Franceschini *et al.*[3]; the latter authors also point out that their model (see Fig. 1) actually leads to very reasonable fuel consumption. This fuel consumption constraint (satisfied in realistic models of photometric evolution) has otherwise been somewhat neglected in discussions of extragalactic background light, but Songaila, Cowie & Lilly (SCL) [4] have introduced an analogous though distinct constraint based on the relation between "metal" production from massive stars and the intensity of the nearly flat F_ν spectrum between 1000 and 2000 Å in the rest frame.

I try here to systematise the nuclear fuel consumption constraint in broad terms and draw some comments on galaxy evolution and extragalactic light that may be tested by future satellite missions.

2. LUMINOSITY EVOLUTION AND NUCLEAR FUEL CONSUMPTION

Galaxy evolution models should not lead to an excessive amount of nuclear processed material; this is partly in white dwarfs and partly in helium and "metals" ejected by dead stars. In the solar neighbourhood, about 10% of luminous matter may be in white dwarfs [5] and a similar amount of processed material in ISM and ordinary stars if $dY/dZ \simeq 4$ [6]. For luminosity decaying exponentially with time over 12 Gyr and M/L twice solar, one derives an e-folding time > 5 Gyr in agreement with other arguments [7]. For elliptical galaxies the white dwarf content could be much higher [8,9] allowing much higher past star formation rates [3] and luminosity evolution with red-shift of faint IRAS galaxies [10] if these are ellipticals in formation [9,11].

3. ABUNDANCE OF PROCESSED MATERIAL IN THE UNIVERSE

The smoothed-out cosmic density $<\rho(Z+\Delta Y)>$ of processed material is related to diffuse background light emitted at a red-shift z by

$$\int_0^\infty I_\nu d\nu = \frac{0.007 <\rho(Z+\Delta Y)> c^3}{4\pi(1+z)} \tag{1}$$

$$= 3.7\times 10^{-12} <\frac{4}{1+z}> \frac{<\rho(Z+\Delta Y)>}{10^{-32}\,\mathrm{gm\,cm^{-3}}}\ \mathrm{wt\,cm^{-2}\,ster^{-1}} \tag{2}$$

and I assume $<4/(1+z)> \simeq 1$. From visible matter densities estimated by Persic & Salucci [12] and assuming $<Z+\Delta Y>$ is 0.5 in ellipticals, $10^{32}<\rho(Z+\Delta Y)>$ is 0.6 to 2 gm cm^{-3} for Hubble constants of 50 to 100 km s^{-1}Mpc^{-1} respectively corresponding to total extragalactic background light levels between 2 and 7×10^{-12} wt cm^{-2} ster^{-1}. This can be compared with the total light from some representative models. PP [1] model 1 predicts 3 in these units, and the ORS [10] models give 1.0 and 2.6 respectively (acceptable), whereas PP model 5 gives 11 (unacceptable). This bears on tentative background light detections [13,14] which apparently agree with PP5 better than with the others (see Fig. 1). Extrapolated galaxy counts, on the other hand, like the estimate based on processed material, lead to backgrounds that agree within errors with the model predictions of Yoshii & Takahara [2], Franceschini *et al.*[3] or PP model 1. (I assume baryonic dark matter to be unprocessed beyond primordial abundances.)

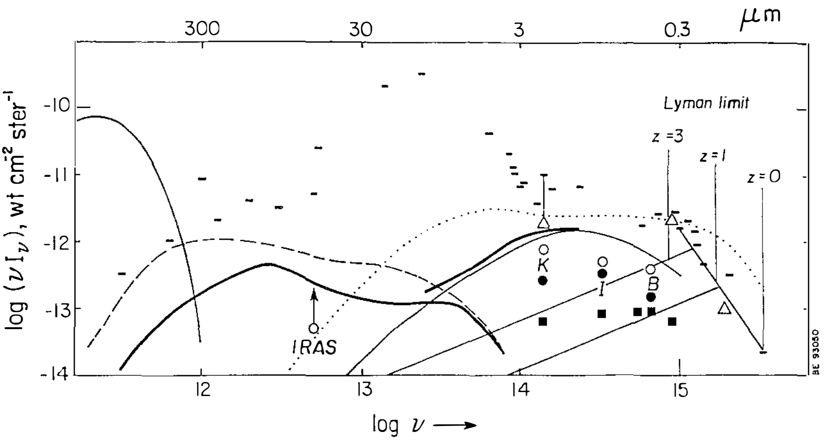

Fig. 1—Estimates of diffuse background light or limits thereto.

Horizontal dashes: obs. upper limits from Cowie [15], ORS [10], SCL [4] and references therein. Uv limits are joined by a downward sloping line fitted by eye.
Triangles: tentative detections at K [13], allowing for narrow bandwidth; at 3500 Å[14]; and at 1600 Å[16].
Open circles: my estimates of background expected from faint galaxy counts: IRAS (lower limit only) from ORS [1•], K from Cowie *et al.*[17] quoted by Colin & Schramm [18], and I and B from Lilly *et al.*[19].
Filled circles and squares: sky backgrounds contributed by galaxies with 19.5<I<24.5 and by faint "flat-spectrum" population after SCL [4].

Thin continuous curves: Cosmic microwave background and PP [1] Model 1.
Thick continuous curves: Time-exponential "Q" model for IRAS galaxy evolution by ORS [1•]; and model for near infra-red by Franceschini *et al.*[3].
Broken curve: IRAS galaxy evolution model by ORS [10] with $L \propto (1+z)^q$, q=3.15, $z \leq 5$.
Dotted curve: PP [1] Model 5.

Upward sloping parallel lines: SCL [4] metallicity limits for starbursts.

4. METAL PRODUCTION, FLAT F_ν SPECTRUM AND FAINT BLUE GALAXIES

SCL [4] point out that massive stars responsible for "metal" production radiate a fairly flat F_ν spectrum between 1000 and 2000 Å in the rest frame with $\epsilon_\nu \equiv L_\nu/(\dot{M}Z) \simeq (1 \pm 0.5) \times 5000$ ergs Hz^{-1} gm^{-1} leading with reasonable smoothed-out estimates $10^{32} < \rho_{lum+X-r\,gas} > \simeq 1.7 h_{50}^{1.65} \simeq 1.7$ gm cm^{-3} [12], $<Z> = 0.01$ to 0.02, to

$$\nu I_\nu = (c/4\pi)\, \nu\, \epsilon_\nu < \rho Z > \tag{3}$$

$$= \frac{3000}{\lambda} (1.2 \text{ to } 7) \times 10^{-13}\, \mathrm{wt\, cm^{-2}\, ster^{-1}} \tag{4}$$

(the same as found by SCL [4]) which is shown as the region between the pair of sloping straight lines in Fig 1; this should be occupied over a range of a factor of 2 or more in wavelength according to the spread in red-shifts. If this theory applies, and there is no significant reddening by dust, the red-shift at which the bulk of the metals was produced has to be > 1 in order for the drop at the Lyman limit to occur at a long enough wavelength to avoid violating uv extragalactic sky background limits. This raises difficulties for the suggestion [20] that the faint blue galaxy population revealed in recent surveys is responsible for a significant part of cosmic metal production, because down to B = 24, at any rate, most red-shifts are substantially below 1. Probably the small blue galaxies are not dominated by massive starbursts and they are more nearly of Magellanic type.

REFERENCES

1] Partridge, R.B. & Peebles, P.J.E. 1967, *Ap. J.*, **148**, 377.
2] Yoshii, Y. & Takahara, F. 1988, *Ap. J.*, **326**, 1.
3] Franceschini, A., Toffolatti, L. *et al.* 1991, *AA Suppl.*, **89**, 285.
4] Songaila, A., Cowie, L.L. & Lilly, S.J. 1991, *Ap. J.*, **348**, 371.
5] Fleming, T.A., Liebert, J. & Green, R.F. 1986, *Ap. J.*, **308**, 176.
6] Pagel, B.E.J. *et al.* 1992, *MNRAS*, **255**, 325.
7] Scalo, J.M. 1986, *Fund. Cosm. Phys.*, **11**, 1.
8] Yoshii, Y. & Arimoto, N. 1987, *AA*, **188**, 13.
9] Elbaz, D., Arnaud, M., Cassé, M. *et al.* 1992, *AA*, **265**, L29.
10] Oliver, S.J., Rowan-Robinson, M. & Saunders, W. 1992, *MNRAS*, **256**, 15P.
11] Kormendy, J. & Sanders, D.B. 1992, *Ap. J.*, **390**, L53.
12] Persic, M. & Salucci, P. 1992, *MNRAS*, **258**, 14P.
13] Matsumoto, T., Akiba, M. & Murakami, H. 1988, *Ap. J.*, **332**, 575.
14] Mattila, K., Leinert, Ch. & Schnur, G. 1991, *in* **The Early Observable Universe from Diffuse Backgrounds**, B. Rocca-Volmerange *et al.* (eds), Paris: Ed. Frontières, p. 133.
15] Cowie, L.L. 1991, *Phys. Scripta*, **T36**, 102.
16] Hurwitz, M., Bowyer, S. & Martin, C. 1991, *Ap. J.*, **372**, 167.
17] Cowie, L.L., Gardner, J.P., Hu, E.M. *et al.* 1992, Preprint.
18] Colin, P. & Schramm, D.N. 1992, *Fermilab Pub.*, 92/225A.
19] Lilly, S.J., Cowie, L.L. & Gardner, J.P. 1991, *Ap. J.*, **369**, 79.
20] Cowie, L.L., Songaila, A. & Hu, E.M. 1991, *Nature*, **354**, 460.

INSTRUMENTAL DEVELOPMENTS

DENIS : a Deep Near Infrared Survey of the southern sky

Nicolas Epchtein
Observatoire de Paris,
Département de Recherche Spatiale
F 92195 Meudon Principal Cedex
France

Abstract

DENIS is the first attempt to carry out an all southern sky digital survey in the near-infrared range. It will be undertaken with a dedicated three channel camera in the I, J and K' photometric bands installed at the ESO 1 meter telescope in Chile. Expected limiting magnitudes are 18, 16 and 14 in the IJK' bands, respectively and the spatial resolution will be 3" in JK' and 1" in I. Several areas of astrophysics will take advantage of this survey: the exploration of hidden stellar populations of our Galaxy, the improvement of the Initial Mass Function towards low mass stars, counts and statistics of evolved Galaxies leading to a better knowledge of the local structure of the Universe. The survey is planned to start early in '94 and to last for approximately 4 years. Data will be released in stages and will be made available to the community as soon as appropriate processings and calibrations will be achieved.

1. Objective of DENIS

Large scale K band surveys are of extreme importance to probe the stellar populations content of our Galaxy and evolved galaxies, in general. The 25-year-old *Two Micron Sky Survey (TMSS)* very limited in sensitivity ($m_K = 3$) and uncomplete in the southern sky is still the only available document in this range. A situation which is no longer satisfactory, whereas a gain of more than 4 orders of magnitudes in sensitivity can be achieved with modern array detectors, and while future very expensive space and ground based instruments partly aimed at near infrared wavelengths observations will badly need deep and complete catalogs and atlasses that would provide accurate source fluxes and positions.

DENIS, is the first accepted and funded project that will attempt to perform a digitized survey of the all southern sky in the near infrared. It will produce images in 3 photometric bands (I = 0.8, J = 1.25, K' = 2.15 μm) with a spatial resolution of 3" in the JK' band and 1" in the I band at the millijansky level (*i.e.*, [I] = 18, [J] = 16, [K'] = 14). The upper limit of the spectral domain is basically dictated by the very constraining effect of the thermal background emission of an uncooled telescope on the detector performances. Inclusion of a visible red band (I) was eventually chosen to provide a closer link with optical large scale surveys (Schmidt plates), and to allow a better spatial resolution than in the JK' bands. Hence, identification in real time of detected sources with objects in optical catalogs (e.g. the *Guide Star Catalog, Tycho Catalog* etc..) and separation of stars and galaxies should be greatly facilitated. The ultimate aim of *DENIS* is to build catalogs and databases of point-like sources and small extended sources and to open the access to the results through computer networks in the shortest delay compatible with the release of highly reliable data.

2. Scientific justifications

Several domains of astrophysics such as stellar and galactic populations statistics will clearly draw out a great benefit of a better knowledge of the sky at near-IR wavelengths. The two micron band is of extreme importance to probe the stellar content of evolved galaxies and, primarily, of our Galaxy, just because most of the stars in spiral and elliptical galaxies are K and M dwarf stars that radiate the bulk of their energy in the 1-2 micron range. Another well known advantage is the good transparency of the interstellar dust in the K band that will permit probing young stellar objects embedded inside their parental molecular clouds, and stars in highly reddened regions, such as the bulge of our Galaxy. In addition, stars surrounded by thick circumstellar dust shells will be also detected. It is estimated that all the supergiant stars and most of the stars of the Asymptotic Giant Branch in our Galaxy will be recorded in the survey. The combination of *IRAS* and near infrared colours will improve the classification of AGB stars and, in particular will permit a reliable break-up of carbon versus oxygen rich stars. Near infrared surveys such as *DENIS* will lead to significant improvements of the Initial Mass Function, and to better determinations of the scale heights of several poorly known species of stars such as *OH-IR* objects, extreme carbon stars, young planetary nebulae, etc....

DENIS will also produce the first complete digitized catalog of evolved spiral and elliptical galaxies up to a redshift limit of $z = 0.2$. Some 250 000 galaxies should be detected and recognized and notably in the obscured lane of our Galaxy. The near infrared emission is also a reliable tracer of the stellar mass contained in a galaxy and relatively independent of the evolution. This digitized catalog of galaxies will bring out new insights in the investigation of the local structure of the Universe.

3. The Instrument

The survey will be achieved with a specially designed and dedicated camera equipped with 3 array detectors working simultaneously in the 3 bands and attached at the cassegrain focus of the 1 meter telescope of the *European Southern Observatory* at La Silla (Chile). The telescope is granted to the survey during two consecutive months each trimester in the framework of an ESO keyprogram.

The infrared camera consists of a set of 3 dewars each equipped with one array. The J and K' channels houses one NICMOS 3 array (256 x 256) made by *Rockwell Int'l* and the I band one *Tektronix* CCD array (1024 x 1024). Both types of detectors are cooled to liquid nitrogen temperature. The f/15 beam that comes out of the telescope is split off into 3 separate beams thanks to 2 dichroic mirrors. The field of view of the camera is 12'. A microscanning device acting on the J and K' beams allows an improved sampling of the infrared images. The full coverage of one hemisphere requires about 1 million elementary images per colour taking into account some overlapping. The sky will be scanned in a step and stare mode at constant right ascension, near the meridian, along declination arcs of 30° amplitude, by steps of 10'. It is expected that, taking into account average meteorological conditions at La Silla, the coverage of the sky should be completed in less than 4 years of observation. Data are handled and processed in real time with three independent controllers based on *68040 Motorola* processors. The data flow will be approximately 130 kbytes/sec/channel that will yield an average of 8 Gbytes per night and a final amount of data of some 4 Tbytes, after completion. Raw data will be stored on digital audio tapes (DAT) after compression with no loss of informations. Sources brighter than approximately K = 8 will saturate the NICMOS arrays. To allow measurements of these sources, an additional filter, attenuated by 5 magnitudes, has been added on each channel. The main tasks that will be achieved in real time are flat fielding, sky subtraction, astrometric and photometric calibrations and identifications with entries of the Guide Star Catalog. A preliminary small source catalog will be produced in real time in order to allow the immediate follow up of newly discovered interesting sources, but the final data processing will be performed in two dedicated computing centers located at Leiden Observatory and Paris Institut d'Astrophysique.

4. Data processing and Analysis

It is out of the scope of the real time computers and of the operations team on the mountain to process properly such a stream of data. Moreover, special attention will be drawn to obtain an homogeneous set of measurements and data reduction methods will undoubtedly improve with the experience and time. The two analysis centers will achieve improved standard reductions, each one being in charge of a complementary task in the data reduction stream. The center in Paris will receive the raw image data on DAT, re-process them in an homogeneous way and to make them scientifically usable. Elementary images in three colours will be archived and made accessible in a databank. A copy will be forwarded to Leiden where the extraction of point like objects will be achieved in order to create a *small source database* that will eventually become the *small source catalog*. The Paris center will, in turn, identify and archive the extended sources and will create an extragalactic databank with the participation of Lyon Observatory. Other more specific databases will be implemented under the responsibility of the partners or users, but the normal access to the *DENIS* data, before final release will be through the 2 dedicated centers. Data will be delivered in stages in order to open an access of the community before the completion of the survey. However, the co-investigators of the project will have a priviledged access to the new data during one year.

5. Organisation, and planning

DENIS became an European project, after the initial plan of collaboration with the American *2MASS* project had failed. *DENIS* results of a collaboration between several Institutes pertaining to 7 European countries (Austria, France, Germany, Hungary, Italy, Netherlands and Spain) and a significant contribution of Brazil. The project involves about 60 scientists and engineers. The Space Department (DESPA) of Paris Observatory is leading the project and is responsible for the construction of the 3 channel camera with important technical and funding contributions of the partners. An operations team of 2 senior and 2 postdoctoral astronomers and one dedicated engineer, all resident in Chile will carry on the survey and take care of the continuity of the observations. Commissioning of the camera at the telescope is planned by the end of '93 and the survey should start early in '94. The total cost of the project, excluding salaries, but including 3 years of operations is approximately 12MFF (2.4 M$). The project is funded with the contributions of several National Institutions of the partners countries, and of the *SCIENCE* plan of the Commission of the European Community .

ADAPTIVE OPTICS IN THE NEAR-IR

Daniel Rouan
Département Spatial, Observatoire de Paris-Meudon
92195 MEUDON Cedex, France

ABSTRACT
After a review of the astrophysical programs that should take advantage of the advent of Adaptive Optics, two existing AO systems using different solutions are presented with their characteristics. The present performances, 0.1 arc-sec FWHM images currently obtained are illustrated by astrophysical results recently obtained. The limit in sky coverage of this technique, due to the scarcity of bright enough reference stars is shown, and prospects on present and future evolutions are mentioned.

1- Astronomy with Adaptive Optics

Among the various high angular resolution techniques, the adaptive optics approach, first proposed by Babcock [1], is gaining more and more support in the community since it represents one of the most desired improvement in astronomy [10] and appears now to be fully proven after the success of the first experiment ComeOn [14),7),12]. It will certainly become a standard facility on most of the large telescopes in the world [8),2].

Roughly speaking, Adaptive Optics opens the field of 0.1 arc-sec astronomy in the near-infrared and 0.2 arc-sec in the visible. Almost any area in Astrophysics should benefit from this instrumental breakthrough: here follows a few examples, from solar system to distant galaxies, of programs that should be adressed soon:

- Detection of the rings in Uranus and Great Brown Spot in Neptune, study of Titan
- Asteroïds: rotation (through thermal effects), shape, binarity
- Interstellar Medium: very small scale structure of molecular clouds (H_2, PAH etc.)
- Young Stellar Objects: disks around T Tauri, Ae/Be stars, binarity, dense very young clusters
- Proto Planetary Nebulae: disks and binarity in bipolar nebulae, grain condensation radius
- Missing mass: brown dwarfs in binary systems
- Globular clusters: mass in central region
- Nearby galaxies: galactic center, nuclear region, core of elliptic
- AGN and starburst nuclei: structure of the active region, Seyfert nucleus, BRL and NRL
- Gravitational lensing: multi-images mirages, arcs
- Primordial galaxies: small pixels increase the contrast against sky background

Fig.2-a gives an example of a recent result obtained with the ComeOn experiment on the post-AGB bipolar nebula *Frosty Leo.*

2 - Principles, advantages, existing systems

An adaptive optics (AO) system aims to correct in real-time the images distorded by atmosphere by sensing the wavefront from a nearby reference source - or in a few cases the source itself - and actionning, through a servo-loop, a deformable optics, generally a mirror (Fig. -a). An AO system working with a large number of corrected modes provides images that can be diffraction-limited (Fig. 2-b). In fact the number of cells to correct on the wavefront surface is typically the surface of the telescope divided by the surface of one coherent cell, i.e. $(D/r_o)^2$ where D is the telescope diameter and r_o the Fried parameter. Because r_o increases with wavelength (as $\lambda^{6/5}$), the number of sub-pupils to correct decreases and the characteristic time constant increases with wavelength, both conditions that make the situation much easier in the infrared than in the visible. Adaptive optics provides five definite advantages over other high angular resolution techniques: *i)* it restores a good approximation of the initial, unperturbed, transfer function of the optical system, whereas the transfer function for speckle interferometry is strongly attenuated in the middle to high spatial frequency range; *ii)* It allows long integration times in the imaging channel and hence extends the sensitivity of imaging towards the faint to very faint fluxes regime; *iii)* it provides a strongly enhanced contrast, so that the signal to noise ratio per pixel is largely increased, while background is proportionally reduced; *iv)* it allows real-time assessment of the data quality; *v)* it generates a small quantity of data as compared to short exposure methods.

Today, only two astronomy-dedicated instruments have reached a degree of maturity and performances that has lead to successful observations on large telescope: the ComeOn experiment from Meudon/ESO/ONERA and the IFA-Hawaii AO system:

• *Come-On* was the first successful astronomical adaptive optics experiment and, up to now, the one that produced published results of astrophysical interest [12),9),15]. This experiment was developed as a collaborative program of ESO and several french institutes (Observatoire de Paris, ONERA) and companies (Laserdot, LEP); it was recently upgraded to become *Come-On+*. The Come-On system [14] is installed at the f/8 focus of the ESO 3.60m telescope in La Silla (Chili). The deformable mirror

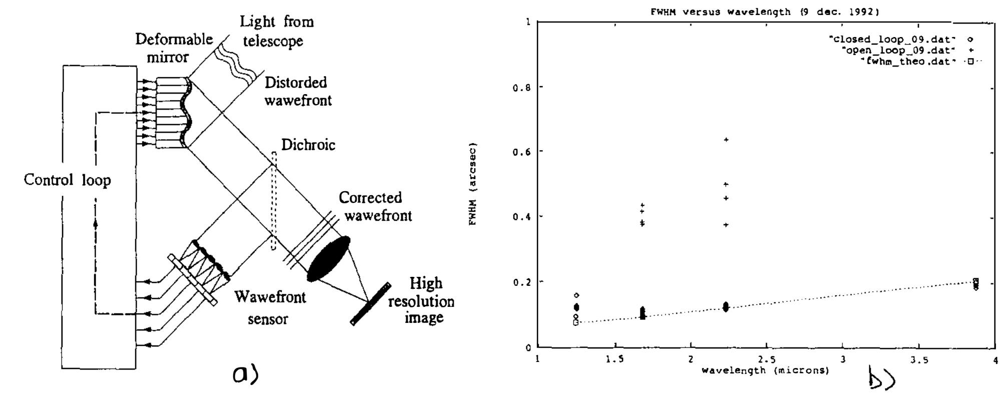

Figure 1: a) Principle of Adaptive Optics; b) FWHM of images obtained with ComeOn.

is a continuous facesheet mirror with 52 stacked piezoelectric actuators. A separate two-axis tip-tilt mirror compensates for the wavefront tilt. Both mirrors are driven by a digital control loop using fast computers. A Shack-Hartmann wavefront sensor (WFS) uses 52 subapertures on a 8×8 square grid to measure the slopes of the wavefront. The WFS, working in the visible, benefits from the high sensitivity of the detector, an Electron Bombarded CCD working essentially in a photon-noise limited regime. The corrected image is recorded on one of the two available IR cameras, one developed in Meudon (2.5-5μm) and one in MPE-Garching (1-2.5 μm) with a 0.05 arcsec pixel size on the sky. The present performances are such that the critical threshold of 0.1 arc sec is now currently crossed in normal seeing conditions (Fig.-b).

• The AO system developed at IFA-Hawaii by Roddier and co-workers, is based on the "curvature" appproach where the wavefront sensing is done by measuring its curvatures rather than the slopes and the correction achieved thanks to a bimorph mirror where curvatures are localy created through piezo effect [13)]. The main advantage of this approach is the excellent sensitivity of the wavefront sensor which uses fast, high quantum efficiency, photon-counting monodetectors (avalanche photo-diodes), the drawback is the degree of correction limited to $\approx$ 20 modes.

3 - Limits and prospects

The deformable mirror can no longer be considered as a hard technological point and systems with several hundred actuators have been successfully produced. Moreover, the number of actuators is not really the problem in astronomy where full correction represents a rare case because of the scarcity of bright reference stars that it supposes [13)].

Sensing the wavefront is the real problem, due to the requirement that a sufficiently bright and nearby reference star must lie in the vicinity of the studied object: *i)* sufficiently nearby because of the anisoplanetism (wavefront perturbations are less correlated at increasing angular distances, the turbulent layer being at a finite altitude), *ii)* sufficiently bright because the best correction implies a large number of sub-pupils and a large temporal bandpass (30-100 Hz) requiring a fast rate of wavefront sensing (typically 5 to 10 times the aimed bandpass).

With the present systems, one roughly evaluates as 10 %, the probability to find a star (mR < 17.5) at $b = 30^o$ when $\approx$ 15 modes are corrected. Hopefully, this drawback will be no longer actual once artificial laser sources are practically usable [4),5)], however severe difficulties, among which the impossibility to directly measure the wavefront tip-tilt [11)] and the light pollution by laser shot, make

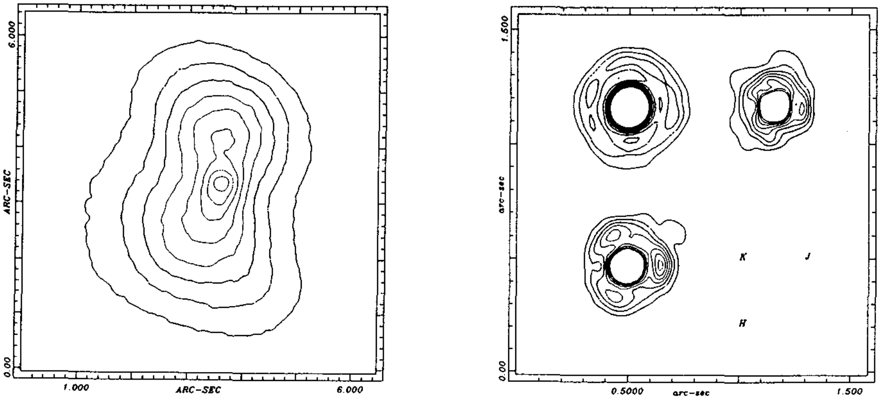

Figure 2: a) The Frosty Leo Nebulae at 2.2 μm is an envelope of gas and dust recently ejected by a post-AGB star; the off-center star location indicates that binarity is at the origin of the bipolarity; b) Stellar image in J, H and K showing distinctly the Airy pattern. All images from ComeOn.

this approach still far from routine.

In given circumstances, the AO system may not provide full correction, either because the reference source is too faint or too far or because one operates at too short a wavelength. It can be shown that the highest modes (or spatial frequencies) in the correction are the most affected by this situation and that even a degradation of the image can arise because of the noise introduced by those modes. The system may then be fine-tuned to provide the optimum, though limited, resolution: the highest spatial frequencies are attenuated by filtering the highest Zernike modes of the mirror. This method, known as the "modal control", has been shown to be very powerful[6)]. The complexity of this optimization procedure will require some artificial intelligence to be integrated in future AO systems [3)].

References:

1. Babcock H.W., 1953, P.A.S.P., 65, 229
2. Beckers J., 1987 in "Towards Understanding Galaxies at Large Redshift", Kron and Renzini Eds
3. Demailly, L., Gendron, E., 1992, in "AO for Large Telescopes...", Maui, Hawaii, Aug. 1992
4. Foy R. and Labeyrie A., 1985, A&A 152, L29
5. Fugate R.Q. et al., 1991, Nature, 353, 144
6. Gendron, E. et al., 1991, SPIE 1542
7. Kern P. et al., 1990, SPIE 1237, 345
8. Léna P., 1987, in "Ground-based Astronomical Observations with Infrared Array detectors", Wynn Williams and Becklin Eds
9. Malbet et al. , 1993, A&A, in press
10. Merkle F., 1989, in "Diffraction-Limited Imaging with Very Large Telescopes", Alloin and Mariotti Eds.
11. Rigaut F. and Gendron, E., 1992, A&A, 261, 677
12. Rigaut F. et al., 1991, A&A, 250, 280
13. Roddier F. et al., 1991, PASP 103, 131
14. Rousset G. et al., 1990, A&A 230, L29
15. Saint-Pé, O. et al., 1993, Icarus, in press

LONG BASELINE INTERFEROMETRY AT INFRARED WAVELENGTHS

Jean–Marie Mariotti
DESPA, Observatoire de Paris
Meudon, FRANCE

ABSTRACT

For many current astrophysical puzzles, infrared imaging at higher angular resolution is required: stellar astrophysics provides obvious cases of such situations (Young Stellar Objects, Circumstellar envelopes, detection of Brown Dwarfs in binary systems,...) but indeed examples can be found from Solar System bodies to Active Galactic Nuclei.

Recent progress, both in infrared instrumentation and in the application of long baseline interferometry in the optical range (visible and infrared), open the way to imaging and spectroscopy of infrared sources at an angular resolution of 10 milli–arcsecond or less.

This paper briefly reviews the main prospects offered by several projects of large ground-based interferometers. In particular the main characteristics of the VLT Interferometer (angular resolution, image restauration, sensitivity) are presented, as well as a list of prime astrophysical targets.

1. INTRODUCTION

The development of modern astronomical interferometry at optical wavelengths (visible and infrared) has started 20 years ago. In particular several interferometers have obtained results in the near infrared (2.2 μm) and in the thermal infrared (10 μm). These wavelengths correspond to maximum of emission of black bodies in the range 300 to 1300 K, so it might be more appropriate to speak of high angular resolution observations of the *cool universe*.

The reason why these techniques will play an increasingly important role for the next generation of earth-based facilities is that experience shows that many of the interesting astrophysical sources observed at these wavelengths with 4 m–class telescopes are barely resolved. This is in particular true for stellar objects (surface imaging of supergiants, circumstellar shells of evolved stars,...) for which only a few sources of each class, usually the brightests, are imaged with an adequate resolution by techniques like speckle interferometry or adaptive optics. Infrared astronomers have here to pay the price of the wavelength dependency of the diffraction limit λ/D. This calls for larger baselines, in the tens to hundreds of meters range.

2. INTERFEROMETERS AND PROJECTS

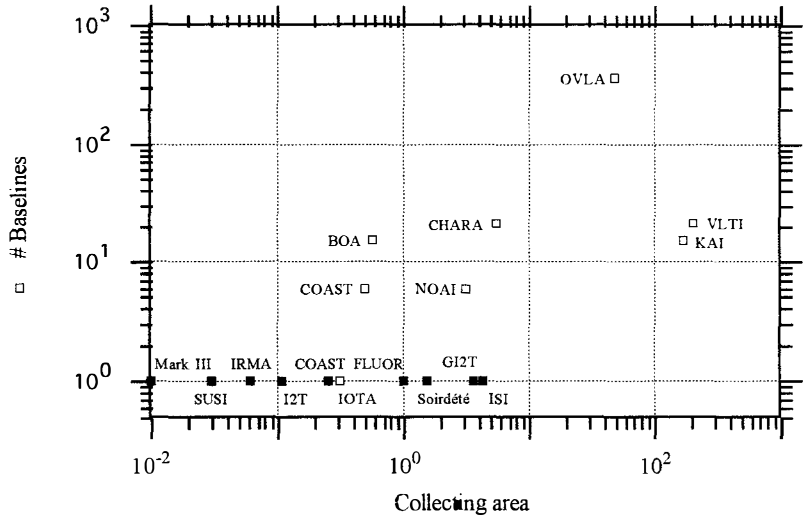

Figure 1: Number of baselines vs. the total collecting area (in square meters) for the interferometers in operation (filled squares) and in project (open squares)

It is of interest to place the various observing interferometers and projects on a graph (Fig. 1) giving the total collecting area of the array (i.e., a parameter related to its sensitivity) vs. the number of simultaneous baselines (related to the 'snapshot imaging' capability of the interferometer). A first fact is that all the observing interferometers are two-element arrays, while most of the projects offer at least six simultaneous baselines and up to 351. The

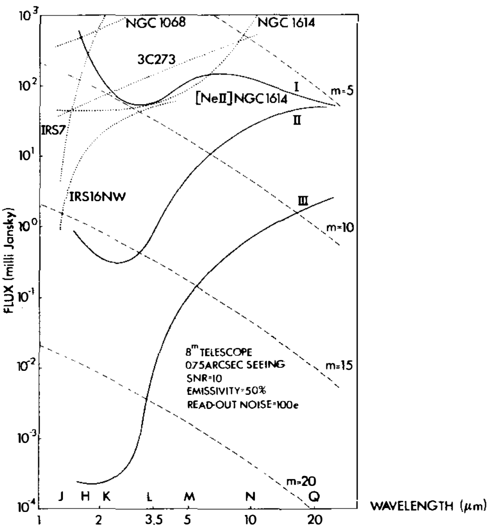

Figure 2: Limiting sensitivities of the VLTI Main Array for: I. on-source pupil phasing and co-phasing. II: off-source phasing and on-source co-phasing. III: off-source co-phasing and 10 minutes integration time (after [3])

emphasis is then clearly put on the imaging capabilities of the future earth-based systems. Among them, three stand out: OVLA, the Keck Interferometric Array, and the VLTI. The two latter show collecting areas of $\sim 200\,\mathrm{m}^2$ which will translate into impressive limiting magnitudes, at least in their phased mode of observation.

3. PERFORMANCES

As an example, we can consider the case of the interferometric mode of the VLT (VLTI). The imaging capabilties of the array of the four 8 m telescopes has been studied by Von der Lühe et al.[1]. Image reconstruction simulations have also been made in the case of seeing limited observations[2]. The configuration of the array provides a good Point Spread Function up to declinations of −20 deg approximately. Of course, a much better (u,v) plane coverage is obtained if the three movable auxiliary telescopes (VISA) are included in the array.

The sensitivy of the VLTI is illustrated on Fig. 2 (from Ref. [3]). In the near infrared the sensitivity in the interferometric mode is boosted by the use of Adaptive Optics, which restores the transverse coherence of the wavefronts on each aperture of the array: the limiting magnitude is hence no more limited by the atmospheric turbulence, but by the total collecting area of the telescopes in the array. In the thermal IR this situation persists but the performances become rapidly limited by the photon noise of the thermal background.

4. ASTROPHYSICAL PROGRAMS

Several papers present reviews of the astrophysical results obtained recently with earth-based interferometry. Such a work is beyond the scope of this paper and we refer the reader to the series of papers by Ridgway [4],[5] and the article by Shao and Colavita [6]. See also Gezari et al.[7] for a bibliography .

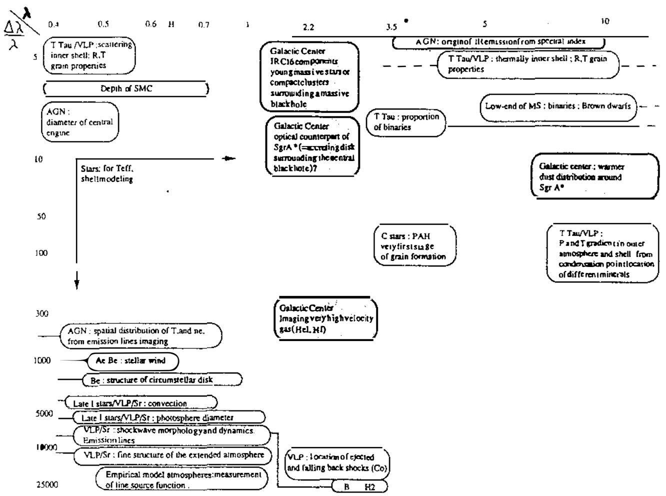

Figure 3: Prime targets for the VLTI in a diagram λ vs. spectral resolution. Bold boxes denote programs requiring an extented coherent field of view: 1" for light boxes and 8" for shaded boxes (after [8])

Concerning the astrophysical targets of the future large interferometric instruments, they include topics like study of the surface structure of asteroïds and satellites of giant planets, imaging of nearby super-giants and circumstellar shells of Long Period Variables and evolved objects, binaries at the very lower end of the main sequence, structures associated with Young Stellar Objects, detailled imaging of the Galactic Center and of the nuclei of the brightest AGNs[8]. The Keck Interferometric Array project emphasizes, as a prime target, detection of nearby exo-planets by narrow-angle astrometry[9]. Some of these topics are included in Fig. 3, which illustrates the requirements for the instrumentation in terms of wavelength range, spectral resolution and coherent field of view needed to adress these problems[8].

5. REFERENCES

1) Von der Lühe O, Beckers J M, Braun R, 1992, in ESO Conference on *High-resolution imaging by interferometry II*, J M Beckers & F Merkle eds., Garching (October 1991)

2) Reinheimer T., Hofmann K.-H., Weigelt G., 1992, in ESO Conference on *High-resolution imaging by interferometry II*, J M Beckers & F Merkle eds., Garching (October 1991)

3) ESO VLT Report No. 59, *The VLT Interferometer Implementation Plan* (1992)

4) Ridgway S T, 1988, in NOAO–ESO Conference on *High-Resolution imaging by Interferometry*, F Merkle ed., Garching (March 1988)

5) Ridgway S T, 1992, in ESO Conference on *High-resolution imaging by interferometry II*, J M Beckers & F Merkle eds., Garching (October 1991)

6) Shao M, Colavita M M, 1992, Ann. Rev. Astron. Astrophys. 30

7) Gezari D Y, Roddier F, Roddier C, 1990, *Spatial interferometry in optical astronomy*, NASA Reference Publication 1245 (September 1990)

8) ESO VLT Report No. 65, *Coherent combined instrumentation for the VLTI* (1992)

9) Report by the Solar System Exploration Division, *Toward Other Planetary Systems*, NASA

GROUND-BASED MID-INFRARED ARRAY IMAGING

Pierre-Olivier LAGAGE
Service d'Astrophysique, CE Saclay, Bat 709
F-91191 Gif-sur-Yvette Cédex, France
e-mail: 32779::LAGAGE

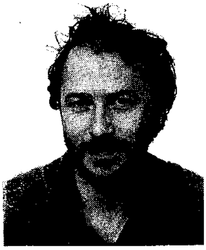

ABSTRACT

In this paper, I would like to draw the attention of the readers on a new type of instruments which will be soon widely available: infrared cameras for sub-arcsec imaging observations through the 10 and 20μm atmospheric windows. The possible impact of such instruments on the studies of young stellar objects, such as the finding of cold embedded companions or of spatial extensions, will be briefly discussed and illustrated by some results obtained with the Saclay 10μm CAMIRAS camera.

1. MID-INFRARED ARRAY IMAGING: A FIELD IN RAPID EXPANSION

Everybody has heard about the CCD's, which have revolutionized the optical observations. At least every infrared astronomer knows about such a revolution in the near-infrared domain (2-5μm). I am not sure that many people are aware that the mid-infrared (10-20μm) is now also concerned.

Indeed, after the pioneering 10μm cameras in the 80's by Arens, Gezari and collaborators[1-3], a dozen of cameras[4-14] have been mounted on various telescopes these last three years. Most of these cameras are team instruments, but the situation is rapidly evolving, and, for example, TIMMI, the ESO 10μm instrument built by SAp-Saclay[12,15], is now available as a common user instrument.

Such a growth is mainly due to the availability of two-dimension detector arrays, whose development has been powered by the space projects: ISO in Europe[16] and SIRTF in US[17]. There are several orders of magnitude between the photon background on ground (atmosphere and telescope) and in space (zodiacal light), so that space detectors are likely to be saturated when used on ground. To avoid this problem, various solutions have been worked out, but the best one consists in slightly modifying the space detectors by increasing their storage capacities. The first development of this kind was started in 1986 at the Laboratoire InfraRouge (LIR) at the Centre d'Etudes Nucléaires de Grenoble[18], as a by-product of the detector array developments undertaken in the framework of the ISOCAM project[16]. Thanks to these detectors, the first large format array images through a filter encompassing the entire atmospheric window were obtained in may 1990[19].

2. SPECIFIC INTEREST OF GROUND-BASED 10μm CAMERAS

By observing through the 10μm atmospheric window (8-13μm) with an array camera mounted on a 3-m class infrared telescope, a typical point source sensitivity of 0.3 Jy at the 10σ level can be achieved within an on-source integration time of 100 s. Such a sensitivity is comparable to the IRAS band1 point source sensitivity, but is two orders of magnitude worse than expected for ISOCAM. Then why not to wait for ISO, instead of building ground-based cameras?

The main reason is the high angular resolution achievable with the large ground-based telescopes (< 1" for a 3-m class telescope), much higher than the resolution of IRAS (several tens of arcsec), or the resolution achievable with the relatively small infrared telescopes to be embarked on satellites (60 cm for ISO). To take fully advantage of the angular resolution, array imaging observations are required. Indeed, although it is possible to obtain high angular resolution with monodetectors by the scanning technique[20], these observations are difficult and very time consuming, so that few images have been obtained by this technique.

A general aim for the ground-based thermal infrared cameras is therefore a high angular resolution follow up of the IRAS point sources. The gain in angular resolution will help in the identification of the IRAS sources, but will also certainly lead to new exciting findings, such as extensions at the arcsec scale or cluster of sources in the IRAS beam. Various classes of astronomical objects are concerned ranging from objects in our vicinity, such as planets or comets, up to objects located at the confine of the universe, such as quasars.

3. EXAMPLES OF IMPACT ON YSO's STUDIES

Young stellar objects are also good targets for 10μm cameras. First the extinction at 10μm is much lower than at 2μm, so that we can see deeper than at 2 μm. A good example is the observation of G35.2N, where the position observed at 10μm with the CAMIRAS camera[7] is 2" closer to the outflow source position inferred from polarization measurements than the 2μm position. Another example is the finding of cold embedded companions such as near LkHα234[21] (see Fig. below) or LkHα198[22]. Such a finding is important because the contribution of the companions at high wavelengths is probably important, so that models trying to deduce information on the environment of the YSO's by fitting the Spectral Energy Distribution could lead to erroneous conclusions.

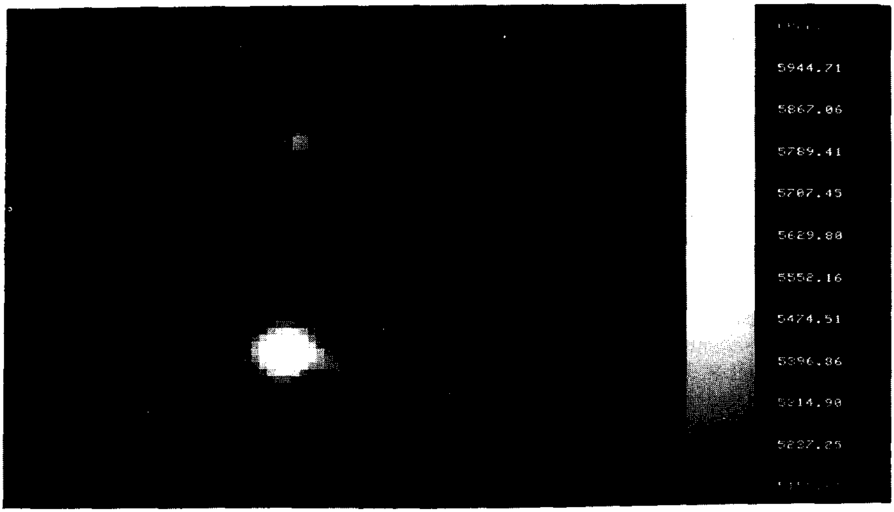

*Fig. 1: A typical example of a findingof an embedded companion: the LkHα234 region, observed in the N-band with the Saclay CAMIRAS camera mounted on the CFHT in 1991. North is bottom and east is left. The pixel field of viewis 0".4. Two new sources were found in the field of the instrument (25"*25"), an especially one at 3" to the west of Lkhα234[21]. Observing program conducted with S. Cabrit from the observatoire de Grenoble.*

Another important issue is the search for spatial extensions. At first glance, it seems unlikely to resolve, at 10μm, the thermal emission expected from normal dust disks associated with young stellar objects, because the temperature of the dusts heated by the central source decreases rapidly below the temperature range accessible at 10μm (80K). However, it could be possible to find extensions in the arcsec range, if very small grains stochastically heated by the UV and visible photons of the central source were present or if extra-sources of heating such as shocks were providing additional energy to dusts far from the central source. And, indeed an extension of 5" which cannot be explained by normal heating of standard circumstellar dusts, has been found around G35.2N[21].

REFERENCES

1. J.F. Arens, G.M. Lamb & M.C. Peck, 1981, SPIE, Paper 280-70, 1981
2. J.F. Arens, J.G. Jernigan, M.C. Peck, C.A. Dobson, E. Kilk, J. Lacy & S. Gaalem, 1987, Appl. Opt., **26**, 3846
3. D. Gezari, W. Folz & L. Wood, 1989, 3rd Ames Workshop on IR arrays
4. E. Keto, G. Jernican, R. Ball, J. Arens & M. Meixner, 1991, ApJ, **374**, L29
5. D. Gezari, C.F. Walter, A.W. Lawrence & F. Varosi, 1992, PASP, **104**, 191
6. S. Odenwald, K. Shivanandan & H. A. Toronson 1992, PASP,127
7. P.O. Lagage, R. Jouan, P. Masse, P. Mestreau & A. Tarrius, 1992, 42th ESO Conf., "Progress in Telescope and Instrumentation Technologies", M.H. Ulrich Ed., p. 601
8. M. Cameron et al., 1992, 42th ESO Conf., "Progress in Telescope and Instrumentation Technologies", M.H. Ulrich Ed., p. 705
9. P. Persi et al. 1992, Technical Report
10. D.M. Rank, P. Temi & J.D. Bregman,1993, SPIE, "Infrared Detectors and Instrumentation", Vol. 1946, in press
11. R.K. Pina, B. Jones & R.C. Puetter, 1993, SPIE, "Infrared Detectors and Instrumentation", Vol. 1946, in press
12. P.O. Lagage, R. Jouan, P. Masse, P. Mestreau, A. Tarrius & H.U. Käufl, 1993, SPIE, "Infrared Detectors and Instrumentation", Vol. 1946, p. 655, A.M. Fowler Ed.
13. T.L. Hayward, J.W. Miles, J.R. Houck, G.E. Gull & J. Schoenwald, 1993, SPIE, "Infrared Detectors and Instrumentation", Vol. 1946, in press
14. W.F. Hoffmann, G.C. Fazio, K. Shivanandan, J.L. Hora & L.K. Deutch, 1993, SPIE, "Infrared Detectors and Instrumentation", Vol. 1946, in press
15. H.U. Käufl, R. Jouan, P.O. Lagage, P. Masse, P. Mestreau & A. Tarrius, 1993, Infrared Physics Journal, special Issue on CIRP5, in press
16. C.J. Cesarsky, these proceedings
17. G.C. Fazio, these proceedings
18. P. Mottier et al., 1990, SPIE, Infrared Technology XVI, Vol. 1341, p. 368
19. P.O. Lagage, P. Merlin, S. Remy & F. Sibille, 1993, A&A, **275**, 345
20. G.L. Grasdalen, J.A. Hackwell & R.D. Gehrz, 1984, PASP, **96**, 1017
21. S. Cabrit, P.O. Lagage & E. Pantin, 1993, "Infrared Astronomy with arrays: the next generation", UCLA, journal Experimental Astronomy, special issue, in press
22. P.O. Lagage, G. Olofsson, S. Cabrit, C. Césarsky, L. Nordh & J.M. Rodriguez Espinosa, 1993, ApJ Letters

The Infrared Space Observatory Camera

Catherine J. Cesarsky
Service d'Astrophysique, DAPNIA
Centre d'Etudes de Saclay, 91191 Gif-sur-Yvette Cedex France

Abstract. At the focal plane of the ISO 60 cm telescope, ISOCAM will take images of the sky in the wavelength range 2.5 to 17 μm. It will make maps at various spatial and spectral resolutions, and at high sensitivity (at > 4 μm, < 1mJy/10 σ in 200 sec). It features two 32x32 infrared array detectors: an InSb CID for the 2.5-5.5 μm range, and a Si:Ga DVR for the 4-17 μm range. Four different pixel fields of view are available on each channel: 1,5, 3, 6 and 12". The spectral range can be selected in each channel by a set of about 10 fixed band-pass filters (resolution from 2 to 100) and continuous variable filters (resolution ≈45); polarisation measurements are possible as well.
A very wide range of astrophysical problems can be tackled with ISOCAM. We present a brief description of the programme planned by the ISOCAM team in its guaranteed time.

1. INTRODUCTION

In 1983, just as the first results of IRAS were presented to the European astronomical community, the decision was taken at the European Space Agency to fly a second generation infrared cryogenic satellite, ISO (the Infrared Space Observatory). While IRAS was scanning the whole sky in four colours, ISO was destined to perform detailed studies of selected regions, with better angular resolution, wider wavelength coverage, enhanced imaging and spectroscopic capabilities, and a higher sensitivity.

Four instruments will be placed in the focal plane of the ISO telescope: a camera (ISOCAM), a photometer (ISOPHOT), and two spectrometers (SWS and LWS), which, together, cover the range 2.5 to 200 μm. This paper is devoted to a description of ISOCAM, which will be the first astronomical space infrared camera using array detectors.

ISOCAM is a two-way camera, featuring two (32x32) array detectors, one for short wavelengths (SW, 2.5 to 5.5 μm), the other for long wavelengths (4 to 17 μm). On each channel, there are two wheels, one carrying four lenses, allowing four different pixels fields of view (1.5", 3", 6", 12"), and the other carrying 10 to 12 fixed filters and one or two CVF, allowing to reach a spectral resolution ~ 45. A wheel at the entrance has four positions: 3 polarizers and a hole. A selection wheel carries Fabry mirrors which can direct the light beam of the ISO telescope towards one or the other of the detectors, or illuminate them uniformly with an internal calibration source, for flat field purposes. The layout of ISOCAM is shown on Figure 1.

With exposures of a few minutes, the long wavelength detector will easily detect sources at the sub-mJy level, and the short wavelength channel sources at the mJy range. With longer exposures, the sensitivity of the long wavelength channel will be limited, in most filters, by the flat field accuracy achievable, given the presence of the zodiacal background; then it will be necessary, as in ground observations, to use beam switching or microscanning techniques.

The development of ISOCAM has lasted seven years, involving over one hundred and fifty scientists, engineers and technicians. Table I and II list the hardware responsibility share among the laboratories, the co-investigators and scientific associates, and some of the key people. About the co-investigators, it is worth mentioning also that D. Rouan is responsible for the short wavelength channel, and D. Cesarsky for the software ; M. Pérault, after S. Cazès, is in charge of the calibration and L. Nordh of the filters.

Today, the flight model of the camera, duly tested and calibrated, has been delivered to the European Space Agency and integrated in the Payload Module of the satellite (Figs. 2 and 3); the first tests at helium temperature have given excellent results. The expected launch date of the ISO satellite is September 1995. I summarize here the main characteristics of ISOCAM, and sketch the scientific programme that the ISOCAM consortium intends to cover in its guaranteed observing time (6.25% of the total observing time of the satellite).

2. *ISOCAM* CHARACTERISTICS.

I give here a brief description of the instrument. A more detailed presentation of ISOCAM, and of the results of the Flight Model Calibration can be found in Cesarsky et al. (1994) and in Pérault et al. (1994).

ISOCAM is composed of 4 units :

- a 9 kg opto-mechanical unit, to be implemented at 3 K in the focal plane of the cryogenic telescope,

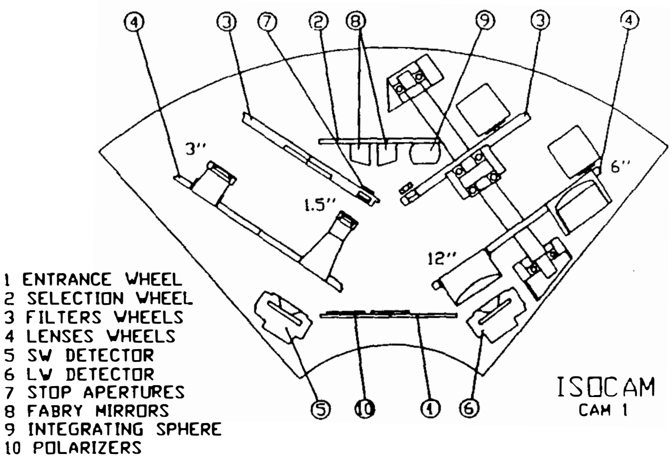

Figure 1. Schematic lay-out of the IR camera, ISOCAM. The optical beam enters in the camera through the entrance wheel and can be directed to a short or a long wavelength channel by field mirrors fixed on the selection wheel. Each channel includes a filter wheel and a lens wheel.

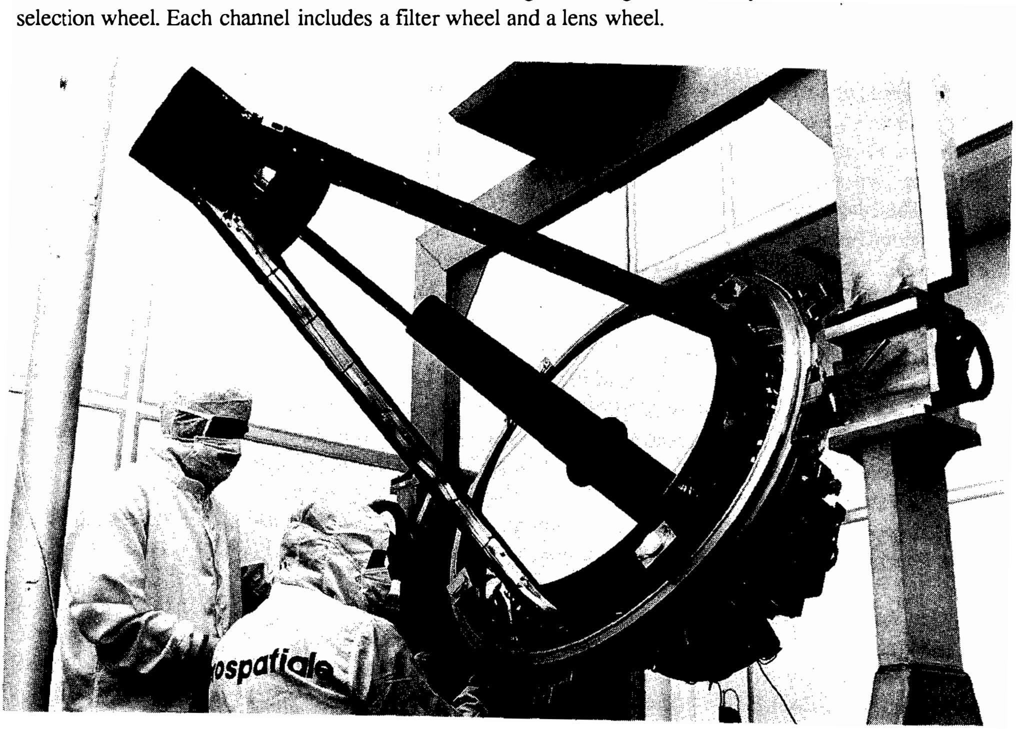

Figure 2. The Infrared Space Observatory telescope.

including 2 detectors and 6 wheels on which are mounted the optical components and the internal calibration device.

- a 2 kg pre-amplifier unit, fitted to the external wall of the cryostat as close as possible from the detectors, and working at 140K
- two 6 kg electrocnis units, implemented on the satellite service module, for instrument control and transmission to the ground of up to one 32x32 image every 2 seconds.

Much development work was necessary for the focal plane unit (Fig. 4), which has to satisfy stringent constraints: reliable operations at a temperature below 2.4 K, position accuracies of typically 100 microns, angular accuracy in the milliradian range, a mean thermal dissipation lower than 10 mW with peak dissipation below 50 mW. I briefly describe some of the solutions adopted.

a) *Cryomechanisms*

The ISOCAM mechanisms must whithstand difficult constraints, cryogenic temperature, high reliability, low dissipation, and good positioning accuracy. Of course, they must be designed to survive the high level of vibrations during launch. To save development time, we based the design of these mechanisms around a superconductor stepper motor developped by SAGEM which was already space qualified. The drawback of this solution was the small number of steps per turn, 24, and the high current required to drive the motor. A demultiplication gear train is required between the wheel and the motor to ensure the positioning of optical components. This is provided by a pinion on the motor axle driving the wheel through a gear on the edge of the wheel.

b) *Optics*

A very simple optical design has been adopted, where the beam intersects a Fabry mirror. The radius of the Fabry mirror (5.5 cm) is such that the pupil, 2.6 cm from the Fabry mirror, has a size of 1.7 mm. The filters or CVF are in the plane of the pupil, and the sky is then reimaged on the detector through one of the four relay lenses.

The filters have been manufactured by SPECTROGON, under the supervision of the Stockholm Observatory, which has verified that they adequately block the light out of their required range. Their transmissions have been .neasured in the ISOCAM test facility at ROE, after having been mounted in their holders by AEROSPATIALE. The filters are tilted by 5°, to avoid ghosts due to reflections between the filters and the detectors. The mounting of the CVF, which have very fragile substrates, was a particularly difficult task, and it was not possible to tilt them.

The overall optical performance of the optical bench of ISOCAM was tested at AEROSPATIALE, in a specific facility, using individual Si:Ga detectors arranged in the shape of a cross (Astruc et al. 1991). These tests also allowed to determine the position at which the array detectors had to be integrated. The fully integrated camera was only tested at Orsay, in the ISOCAL facility designed for this purpose.

Overall, the image quality results of the flight model (Vigroux et al. 1993, Pérault et al. 1994) showed good agreement with expectations, showing that AEROSPATIALE had succeeded in satisfying the tight wheel positioning specifications and that the opto-mechanical design of ISOCAM is robust.

c) *The long wavelength detector*

In 1984, at the time of the ESA Call for Proposals for the ISO satellite, there was no detector available in Europe for the long wavelength channel. A specific development was undertaken at the Laboratoire Infrarouge du CEA-LETI in Grenoble (Agnèse et al. 1989). It is a photoconductor array in Si:Ga hybridized by Indium bumps to a direct voltage readout circuit. It has 32x32 pixels, a 100 μm pitch with a thickness of 500 μm. The dopant concentration is 5 10^{16}cm^3, giving a resistivity of $10^{13}\Omega$ cm^{-2}. To

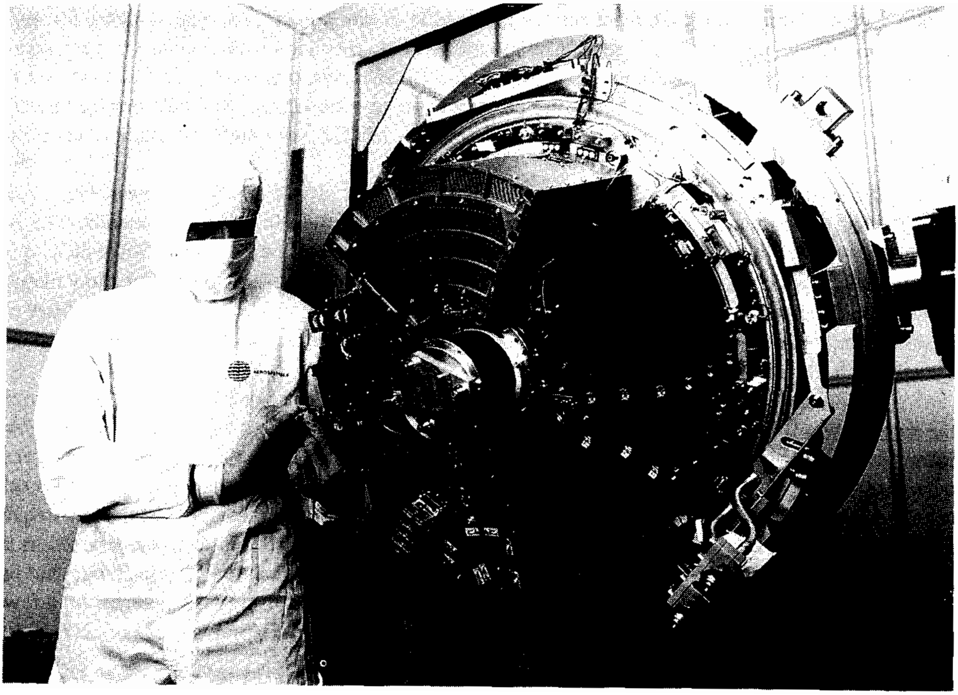

Figure 3. The four instruments mounted in the focal plane of the ISO telescope .

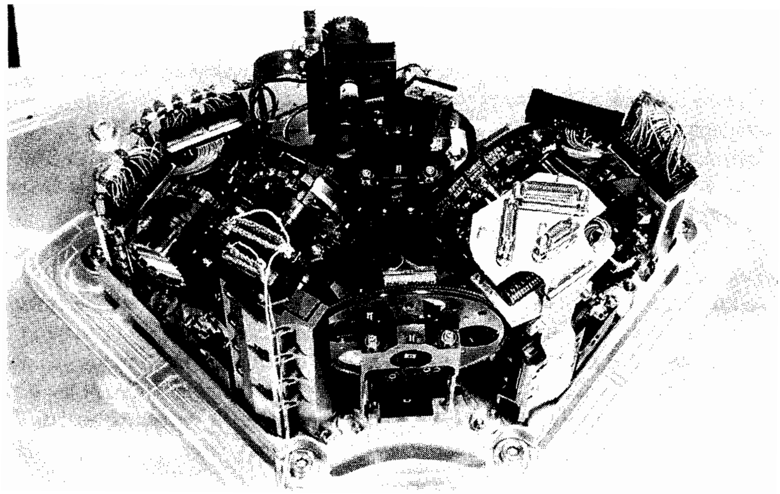

Figure 4. Focal plane unit of the ISOCAM flight model.

obtain a 100% filling factor, the front surface is doped to ensure a good electrical conductivity and the photoconductor voltage is applied to an Aluminium frame on the side of the optical sensitive area. An external guard, 3 pixel wide, has been added around the 32x32 arrays to prevent field line distortion at the edges. Despite the absence of a front grid, this detector has a very low optical crosstalk. For the fastest lens of the camera, the 12" lens which has a numerical aperture of f/0.6, the optical crosstalk remains below 1.5%.

The readout circuit has an integration capacitance of 0.12 pF and a MOS follower with a gain of 0.8. Typical individual integration times in flight will be between 0.2 and 20 seconds. The noise characteristics of this system present several components, a high frequency term which is well approximated by a constant readout noise of ~ 180 $e^{-}px^{-1}$ and photon shot noise , and a low frequency noise which becomes important after ~ 50 readouts. At high level, $>10^6 e^- px^{-1}$, an amplifier noise becomes preponderant and limits the Signal to Noise ratio to < 500 in a single image. The corresponding sensitivity, for twenty 10 sec exposures, is shown in fig. 5.

The flat fielding accuracy can be as good as $5\ 10^{-3}$ when the detector is stabilized. The flat field of the detector was found to be very stable all along the calibration ; this allows the use of a flat field library, instead of loosing observing time by making flat field calibration with the internal calibration device at each new observation. However, a limitation comes from the differential stabilization times between pixels in the array, which can be quite long. A good way to remove these small effects, as well as the low frequency noise mentioned earlier (which in fact may be related to these effects), is to use a beam switching procedure, switching the pointing from the source to an adjacent background, as is done on ground based telescopes. Alternatively, a microscanning procedure can be used, displacing the detector by a few arc seconds on the sky every few images ; this can be realized using the raster pointing mode of ISO.

d) *The short wavelength detector*

For the short wavelength channel, the basic device is a 32x32 pixels CID InSb array manufactured by the Société Anonyme de Télécommunications. At the time of ISOCAM selection, this detector was already qualified and presented the advantages of a low operating temperature and a large radiation tolerance, compatible with the ISO mission. Upgrades of the existing devices have been made along several tracks : increase of the pixel pitch up to 100 µm, increment of the surface filling factor to 89%, and a new design of the supporting ceramic to reduce electrical cross talk. A control and readout hybrid electronic was designed to work at 4 K close to the chip (Tiphène et al. 1989).

Measurements of the pixel charge can be done by sensing the voltages of the 32 output lines and sequentially injecting the pixel charges in the substrate through column voltage clocks. The analog chain uses an adaptive filter followeds by high gain preamplifiers. The sensitivity of this channel for point sources is displayed in Fig. 6.

e) *The internal calibration device*

The internal calibration device was designed to provide an internal flat field source, and a rough calibration reference. Calibration of the SW channel required sources near 350K which are difficult to fit in the low thermal dissipation allocation of ISO. The solution is a small resistor, 0.6 mm^2, mounted on a thin kapton film. These devices have been used all along the int'egration and calibration phases of the flight model, on a 1 year and a half time scale. During this period, a routine monitoring of the instrument has shown that the reproducibility of the calibration system is better than 10%, in all the configurations of ISOCAM, channels, filters and lenses.

f) ***Electrical design***
The electrical architecture is standard for a space experiment. It is organized around a 16 bit 80C86 microprocessor, powered by hybrid DC/DC converters using the satellite 28 volt power line. Redundancy is obtained by mounting two independent microprocessor units and DC/DC units which can be selected by external switches.

3. OBSERVING WITH *ISOCAM*

A very wide range of astrophysical problems can be tackled with ISOCAM. As the ISO satellite will be offered to the general astronomical community 2/3 of the time, I am sure that the readers of these proceedings already have their own ideas as to the problems they will wish to address; the ISO Call for Proposals will be issued in April 1994. As examples, I can give the outline of the programme that the ISOCAM team plans to perform in its guaranteed time. The rationale followed to establish this programme was to identify projects of a general or fundamental character, which take advantage of the specific capabilities of ISOCAM.

The ISOCAM Central Programme is divided into five sections.

The first section deals with solar system studies. There, we plan to investigate the structure of the zodiacal bands and of cometary trails, and to make spectral maps of comets. The goal is to study temperature distribution, sizes and albedos of grains, and the composition of the comet material.

The second section covers interstellar matter and star formation. We intend to obtain spectro-photometric data or CVF spectra of various components of the interstellar medium in various radiation environments. The aim is to ascertain that the 12 μm emission from the interstellar medium detected by IRAS is indeed due to "unidentified bands" emitted by small particles, and to understand the excitation conditions leading to this emission in various environments. We also want to map supernova remnants, old ones such as IC 443 and young ones such as Cas A, to study grain formation and destruction, and the interaction between supernovae and the interstellar medium. Finally, we plan to map large areas of nearby molecular clouds, to study the emission from dust and large molecules, and to search for protostellar objects and pre main sequence stars.

The third section, devoted to stars and circumstellar material, starts with specific observations of known young stellar objects as L1551, which are emitting strong winds. The goal is to combine ISOCAM and ISOPHOT observations to reduce the uncertainties in wind energetics, and better explain the collimation of the molecular outflow and its interaction with the interstellar medium. We also want to understand the nature of the extended 12 μm emission observed by IRAS around young stellar objects in the ρ Ophiuchi cloud. Our next proposal deals with observations of nearby stars, such as Vega, which have an excess infrared emission indicative of the presence of a dust disk around the star. We also plan to do spectral mapping of planetary and proto-planetary nebulae, in particular to study the faint, outer regions which cannot be detected by other instruments, and which are witnesses to the earlier phases of mass loss. All these studies will be complemented by polaro-imaging of different components of the interstellar and circumstellar dust, including the galactic centre region.

The fourth section deals with galaxies. A first part is devoted to nearby galaxies, where we will study star forming regions and compare the results with those obtained for galactic regions, with different

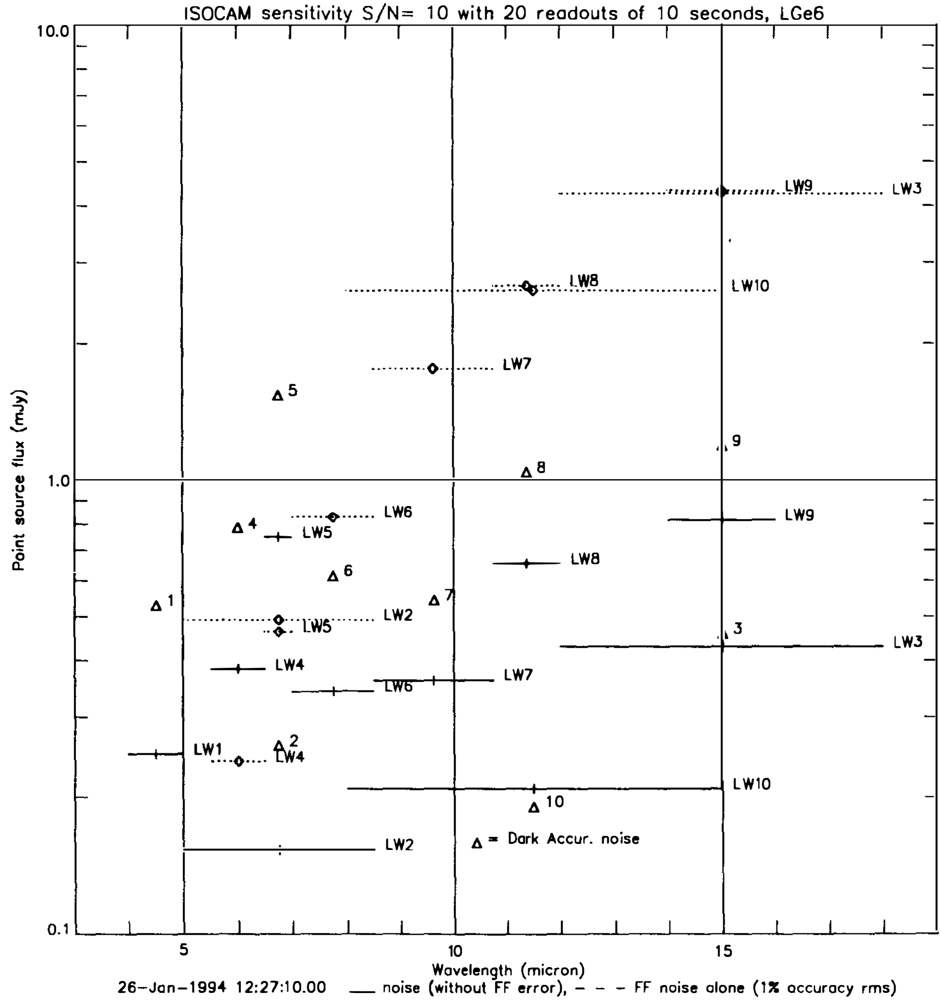

Figure 5. Point source flux giving a signal to noise ratio of 10, for all Long Wavelength filters, for 20 individual integrations of 10 s, and a 6" pixel field of view. The full line represents the sensitivity if the only limitation is the readout noise; the triangles represent the noise for standard dark frames (lower dark noises can be obtained, but at the expense of extra observing time), and the pointed lines the flat field noise for observations towards the ecliptic pole, with a 1% flat field accuracy (rms).

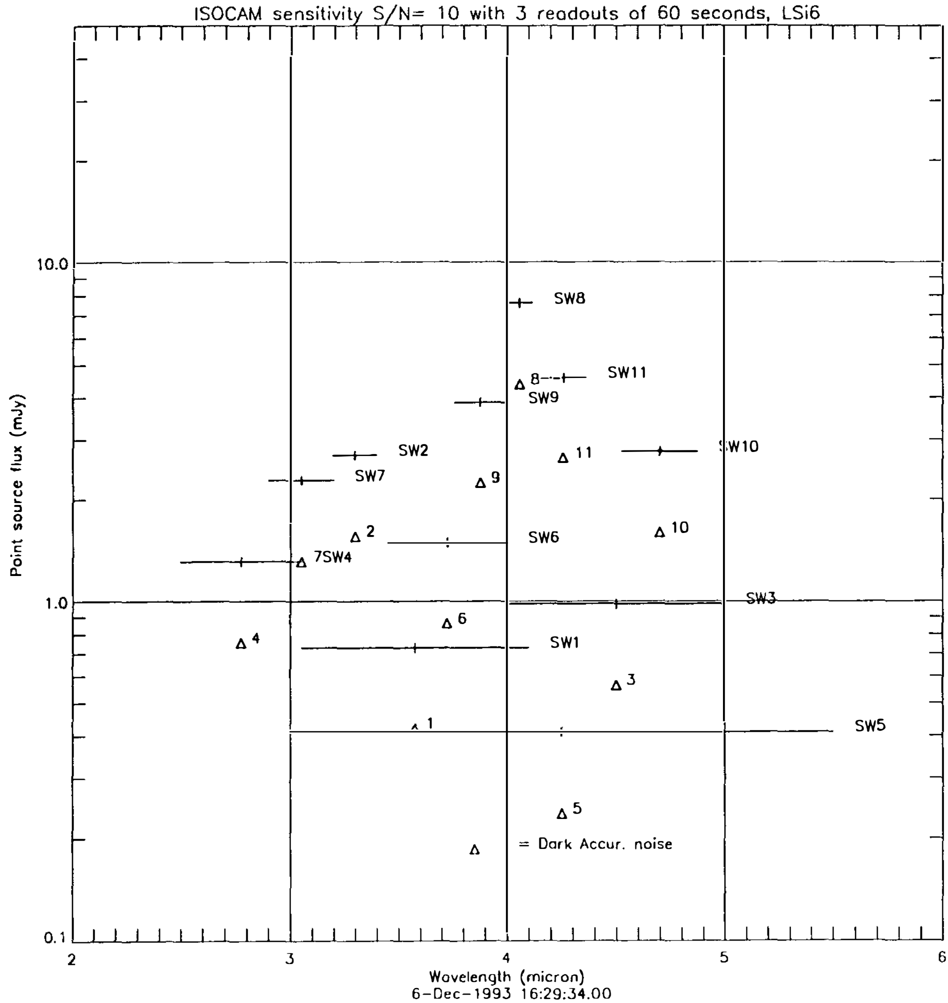

Figure 6. Point source flux giving a signal to noise ratio of 10, for all Short Wavelength filters, for 3 individual integrations of 60 minutes, and a 6" pixel field of view. At these wavelenghs, the flat field noise due to the zodiacal background is negligible. The triangles represent the standard dark noise.

chemical composition and stellar content. The second proposal, well co-ordinated with ISOPHOT, is devoted to a study of nearby normal galaxies: a variety of "typical" spirals and irregulars, spanning a large range of metallicities and physical conditions, will be mapped. The intention is to also observe a sample of galaxies in the Virgo cluster. The following proposals deal with barred galaxies which may be particularly prone to starbursts, and with early type galaxies, to study dust emission in cooling flows, and star formation in some elliptical galaxies. Several active and starburst galaxies will also be mapped; and an attempt will be made to detect an infrared halo, due to brown dwarfs, above or at the side of the disk of an edge on spiral galaxy.

The fifth section is devoted to cosmology. ISOCAM will carry out deep surveys in chosen regions of the sky, devoid of cirrus; the aim is to establish the luminosity function of galaxies and active nuclei in spectral intervals where it is unknown at present. The waveband of the ISOCAM long wavelength channel is particularly well suited for the study of faint active galactic nuclei; this mid-infrared range may be in fact the only one where it is possible to pick out the nuclear component, without being hampered by the stellar and dust emission from the galaxy. The deep surveys in empty fields will be complemented by deep surveys of clusters of galaxies at various distances, up to $z \sim 1$. The results will be useful for studies of galaxy evolution, and in particular for an assessment of the frequency of galaxy encounters and starbursts at various epochs in various environments. All these surveys will be supplemented with measurements in the far infrared with ISOPHOT.

Finally, ISOCAM may detect *brown dwarfs* in the solar neighbourhood and in star-forming regions, or, at least, set meaningful upper limits on their number.

4. CONCLUSION

ISOCAM is the first of a new generation of complex infrared instruments, featuring infrared arrays, to be used on a cryogenic spacecraft. The original scientific specifications were challenging in several domains, detector performance, cryomechanics, and optical design with regards to the severe constraints imposed by ISO. Most of the difficulties has been overcome during definition studies and during the testing of the qualification model. Minor modifications to improve stray light have been implemented after the first optical tests of the flight model. After the calibration of the flight model, we know that ISOCAM performances are within the expected range to carry out the scientific programs for which it has been designed, and hope that it will provide interesting results, not only to the ISOCAM team, but to the whole international astronomical community.

REFERENCES

Agnèse, P., Lucas, C., Maillart, P., Mottier, P., Le Pennec, Y., Masse, P., 1989, SPIE, 1070, 124

Astruc, P., Matthews, SRM, Auternaud, D., Vigroux, L., Rouan D., Sibille F., Perault, M., ICSO 1991, Toulouse, in press.

Cesarsky, C.J. et al. , 1994, to appear in Optical Engineering

Pérault, M. et al., 1994, to appear in Optical Engineering

Tiphène, D., Rouan, D., Lacombe, F., Combes, M., 1989, "Infrared Astronomy with Arrays", Univ. of Hawaii, G. Wynn Williams and E. Becklin eds.

Vigroux, L. et al., 1993, SPIE Orlando, in press.

Table 1

ISOCAM Hardware Responsibilities

SAp-Saclay	Principal Investigator:	C. Cesarsky
	Project Manager:	D. Imbault
	System Engineer:	L. Vigroux
Management Long wavelength detector Read out electronics Instrument command electronics		
Meudon Observatory		
Short wavelength detector Read out electronics On board calibration source		
I.A.S. Orsay		
Integration and calibration facility		
R.O.E. Edinburgh		
Optical concept Optical components		
Stockholm Observatory		
Filters		
Italian laboratories (TESRE, Padova Observatory)		
Equipment for ground support equipment and for observatory ground segment		
The optical bench was subcontracted to AEROSPATIALE. The SW detector was manufactured by the Société Anonyme de Télécommunications. The LW detector was manufactured by the LIR/LETI.		

Table 2

ISOCAM Scientific Team

Principal Investigator: C. Cesarsky (SAp, Saclay) **Co-Investigators**		**Scientific Associates**	
S. Cazes+	IAS Orsay	A. Abergel	IAS Orsay
D. Cesarsky	IAS Orsay	C. Bonoli	Padova Observatory
A. Chedin	L.M.D.	O. Boulade	SAp, Saclay
M. Combes	Meudon Observatory	F. Boulanger	IAS Orsay
M.S. Longair	ROE	M. Casali	ROE
A. Franceschini	Padova Observatory	L. Danese	Padova Observatory
M. Gorisse	SAp, Saclay	J.K. Davies	ROE
T. Hawarden	ROE	X. Desert	IAS Orsay
P. Lena	Meudon Observatory	F. Lacombe	Meudon Observatory
R. Mandolesi	TESRE Bologna	P.O. Lagage	SAp, Saclay
L. Nordh	Stockholm Observ.	J. Lequeux	ENS Paris
M. Perault	ENS Paris	G. Olofsson	Stockholm Observ.
P. Persi	IAS Frascati		
D. Rouan	Meudon Observatory		
A. Sargent	Caltech, USA		
F. Sibille (proj. sci.)	Lyon Observatory		
L. Vigroux	SAp, Saclay		
R. Wade	ROE		

FIRST - FAR INFRARED AND SUBMILLIMETRE SPACE TELESCOPE

Göran Pilbratt
Astrophysics Division/Space Science Department of the European Space Agency
ESTEC/SA, P.O. Box 299, NL-2200 AG Noordwijk, The Netherlands
Internet: GPilbratt@estsa2.estec.esa.nl

ABSTRACT

The present status of the ESA cornerstone mission FIRST is presented. The history of FIRST, including its place in the ESA science programme "Horizon 2000", is briefly reviewed as an introduction and background to the ongoing industrial study. Currently an industrial consortium is studying a FIRST concept with a 3 m telescope, employing mechanical cryo-coolers for payload thermal control. The model payload consists of a the Multi-Frequency Heterodyne receiver (MFH), a nine-channel heterodyne instrument covering selected bands in the range 500–1200 GHz (250–600 μm) for very high resolution spectroscopy, and the Far InfraRed instrument (FIR), a dual channel direct detection instrument emplyoing a photoconductor and a bolometer array, dual Fabry-Perots and filters for spectroscopy and photometry in the range 100–400 μm (0.75–3 THz) and an internal ^{3}He/^{4}He dilution sub-Kelvin refrigerator. With this payload FIRST will able to successfully address the great majority of the of the scientific objectives defined for the submillimetre cornerstone observatory from its 24-hour highly eccentric operational orbit, where observations can be conducted up to 17 hours per day. If selected for implementation as cornerstone number 3 later this year, FIRST could be launched in the year 2002/2003 timeframe.

1. INTRODUCTION

The Far InfraRed and Submillimetre Space Telescope (FIRST) is one of the cornerstone missions in the "Horizon 2000" long term ESA science programme plan. FIRST is intended to open up the submillimetre (submm) and far infrared (FIR) part of the electromagnetic spectrum, taken to be roughly 1–0.1 mm (or, equivalently, 300–3000 GHz), which is still mainly inaccessible for observational astronomers.

FIRST was originally proposed in 1982 and an assessment study[1)] was carried out in 1983. It was then reproposed in the context of a call for ideas for missions to be undertaken in the "Horizon 2000" long term science plan. Subsequently a submillimetre mission was incorporated in the plan as one of the four cornerstones, and was then identified with the FIRST concept.

The scientific objectives and mission requirements of the this cornerstone were discussed in 1986 in a workshop in Segovia[2)], and in 1987 a Science Advisory Group (SAG) was established, its terms of reference being to trade off scientific objectives, as defined in the Segovia meeting, against technical complexity and cost constraints.

In 1990–91 a System Definition Study (SDS) was carried out, which resulted in a spacecraft concept[3)] with a passively cooled non-deployable 4.5 m Cassegrain submillimetre telescope and a helium cryostat cooling the focal plane instrument assembly consisting of heterodyne receivers and direct detection imaging instruments for spectroscopy and photometry.

Since the total cost to completion of a mission with this spacecraft was found to be too high for ESA, a rescoped spacecraft employing mechanical coolers for payload cooling, a 3 m antenna, revised payload complement and less stringent pointing requirements is currently being studied, with a view to offer a less costly solution.

2. SCIENTIFIC OBJECTIVES OF FIRST

FIRST will open up the perhaps last major part of of the electromagnetic spectrum yet unobserved. In the "Horizon 2000" document[4)] the Space Astronomy Survey Panel lists 10 outstanding problems, 5 of which are described as directly depending on observations with a space mission for the submm/FIR. They are:

(i) formation and evolution of stars and planets, (ii) structure and dynamics of the interstellar medium, (iii) nature of the galactic centre, (iv) formation and evolution of galaxies, and (v) large scale structure and evolution of the universe.

These topics are still the essential goals, and FIRST will be the first submm/FIR observatory available to the whole scientific community to address them appropriately. Opening up a new part of the spectrum can be expected, as always, also to lead to serendipitous discoveries.

3. FIRST MODEL PAYLOAD

FIRST needs a complement of instruments for high and medium resolution spectroscopy, imaging and photometry covering as much a possible of the submm/FIR range. As presently defined the model payload is being used to define requirements, interfaces, operation and performance of the spacecraft for study purposes. The actual payload to be flown will be proposed by individual institutes or consortia as a response to an invitation issued by ESA; it could well differ from the model payload used in the course of this study.

The cryo-cooler design constrains the science payload to a maximum of two independent instruments. It is comprised of the MultiFrequency Heterodyne (MFH) receiver and the Far InfraRed (FIR) instrument.

The MFH receiver is a nine-channel instrument covering selected bands in the 500–1200 GHz regime. The design is fairly unsensitive to the exact allocation of bands for the individual mixers, and can be tailored in a number of ways. The mixers should ideally all be superconducting-insulator-superconductor (SIS) quasi-particle mixers, however, at the moment the demonstrated high frequency limit for SIS mixers is well below 1200 GHz. In the model payload design provision has been made (quite arbitrarily) to have one Schottky-mixer channel and eight SIS-mixer channels. The operating temperatures of the SIS and Schottky mixers are 4 K and about 25 K, respectively.

The local oscillator (LO) sources are phase-locked solid state oscillators followed by multipliers. A combination of digital autocorrelators and acousto-optic spectrometers will be used. LOs and spectrometers are operated at "room" temperature.

The FIR instrument employs a stressed Ge:Ga photoconductor array, as well as a bolometer array, to cover the range 100–400 μm. Two Fabry-Perot interferometer system wheels, and a filter wheel, are used for selecting the mode of the instrument, which can be high or medium/low resolution spectroscopy, or photometry.

The photoconductors must be operated at approximately 1.6 K and the bolometers at 0.15 K, necessitating further cooling from the 4 K provided by the spacecraft. A ^{3}He/^{4}He dilution cooler, internal to the instrument except for its helium tanks, will be used for this purpose.

4. FIRST SPACECRAFT AND MISSION

The cryo-cooler FIRST spacecraft concept (cf. Fig. 1) is split into a payload module (PLM) and a service module (SVM). The PLM is made up of the submillimetre telescope, the focal plane assembly with its associated cryo-cooler thermal control, attitude measurement sensors and thermal shield. The change from a cryostat to cryo-coolers has necessitated a total redesign of the PLM. The SVM provides the general infrastructure, e.g. power, attitude control, and telemetry.

The most challenging items on the spacecraft are probably the telescope and the cryo-coolers. The telescope is of Cassegrain design, protected from direct Sun- and Earth-shine by a fixed thermal shield, and has a non-deployable 3 m diameter main reflector. The baseline main reflector design concept is an all-CFRP sandwich monolithic "panel-only" construction, without a separate backing structure. A "shaped" subreflector may be used to further minimize the wave-front error.

The focal plane instruments will be provided with a 4 K environment by the spacecraft mechanical cryo-coolers. Three different but related types of coolers will be employed; single-stage and dual-stage Stirling cycle coolers ("65 K" and "20 K" coolers) and the dual-stage cooler with a Joule-Thomson (JT) stage added ("4 K" cooler). The "65 K" cooler has never failed in space and the other two are in various stages of space qualification.

The pointing accuracy is specified as 6″ (with a goal of 4″) absolute, with a stability of 3″ (goal 2″). After a shared launch by Ariane 5 to geo-stationary transfer orbit, FIRST will propel itself into its operational orbit, which is a highly eccentric (1000 x 70600 km) 24-hour (ISO-type) orbit with low (10 degrees) inclination, potentially offering 17 hours of observations per orbit. There will be no observations while in eclipse, and the operative mode will be near real-time with direct transmission of data to either of two ground stations.

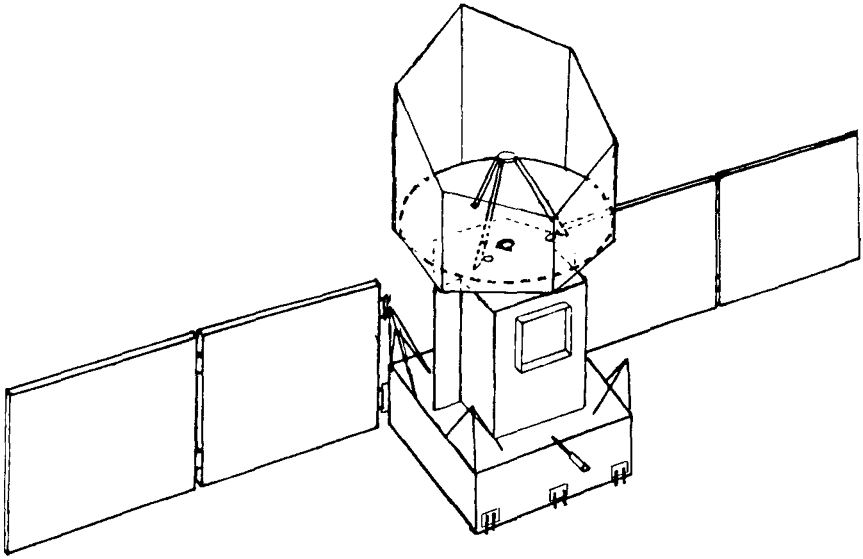

Fig. 1. Line drawing of the FIRST spacecraft, as of April 1993. It is approximately 7 m long and 14 m across, with a mass of roughly 2500 kg.

5. CURRENT AND FUTURE ACTIVITIES

The present study will be completed in the early summer of 1993. The future schedule depends on the outcome of the selection of the order of implementation of the two remaining cornerstones (FIRST and ROSETTA, an asteroid/cometary mission), due to be made by ESA in the second half of 1993.

The current approximate schedule for the third (the fourth four years later) cornerstone is: announcement of opportunity (AO) for experiments in 1994/95, invitation to tender (ITT) in 1996, start of phase B in 1997, followed by phase C/D leading to a launch in 2002/2003.

ACKNOWLEDGEMENTS

The work reported on in this talk is a collective effort involving a large number of individuals in the FIRST science teams, the European Space Agency, and the industrial contractors, all of whom deserve credit for their contributions.

REFERENCES

1). "FIRST - Far Infrared and Submillimeter Space Telescope", assessment study report, ESA SCI(83)1, September 1983
2). Proc. of an ESA Workshop on a "Space-Borne Sub-Millimetre Astronomy Mission", ESA SP–260, August 1986
3). Cf. e.g. "FIRST – Far Infrared and Submillimetre Space Telescope", Proc. of the European International Space Year Conference, ESA ISY–3, p.207, July 1992
4). "Space Science Horizon 2000", ESA SP–1070, December 1984

VERY LARGE ARRAY UPGRADE TO 7-mm

Luis F. Rodríguez
Instituto de Astronomía, UNAM
Apdo. Postal 70-264
México, DF 04510, México

ABSTRACT

A project to install 7-mm receivers in nine antennas of the Very Large Array is described. This project is a collaboration between the National Radio Astronomy Observatory (USA) and the Instituto de Astronomía, UNAM (with support from CONACyT, México). At present, the main scientific goal of this upgrade is to map at sub-arc second resolution the dust emission from protoplanetary disks around young stars. In objects like HL Tauri, this should be the dominant emission mechanism at 7-mm, present at typical levels of 10 mJy. Other interesting areas of research that will become feasible with this upgrade include SiO masers and photospheres from evolved stars, ultracompact H II regions, and the thermal continuum component from star-burst galaxies.

1. INTRODUCTION

The Very Large Array (VLA) is a radio interferometer formed by 27 antennas with a diameter of 25-meter each that is located in the plains of San Agustín, in New Mexico, USA. This instrument belongs to the National Radio Astronomy Observatory (NRAO) of the USA. In its most extended configuration, the so-called A configuration, the VLA has an angular resolution of $0\farcs05\ \lambda(cm)$. At present, the VLA is fully operational at six wavelengths: 90, 21, 6, 3.6, 2, and 1.3 centimeters. As a collaboration between NRAO and the Instituto de Astronomía of the National University of México (UNAM), a project to build and install 7-mm receivers in nine of the 27 antennas is now under way. The main responsibles of this project are Richard A. Sramek (NRAO) and Luis F. Rodríguez (UNAM).

Even when the VLA was originally planned to operate only up to 1.3-cm, the possibility of extending its range of operation to 7-mm was already considered in a 1984 memorandum authored by Ron Ekers and Miller Goss. In this paper I summarize some of the scientific possibilities and the present status of the project.

2. SCIENTIFIC POSSIBILITIES

The receivers being built for 7-mm operation are cooled HFETs that are expected to operate in the 41 to 49 GHz range. Several important projects are expected to be undertaken with these receivers. The main project of the UNAM group is to attempt to map at subarcsec resolution the dust emission from protoplanetary disks around young stars. This project is described in some detail in section 3.

At 43 GHz, the VLA will cover the important J=1-0, v=0,1, and 2 transitions of SiO. In particular, the J=1-0, v=1 transition emits as maser at the base of the winds of evolved, red giant and supergiant stars. The photospheric radius can be measured by observing the thermal (continuum) emission from the photosphere of red giant and supergiant stars using the SiO masers for self-calibration. This technique has been successfully applied to a few stars[1)] using simultaneous VLA observations of H_2O maser emission and continuum emission. At 43 GHz, this technique may be applied in the long run (with a fully equipped VLA at 7-mm) to a larger number of stars since the angular resolution will be two times higher and the thermal emission from the stellar photospheres is expected to be about four times stronger than at 1.3-cm.

Ultracompact H II regions surrounding young, massive stars provide information of the physical conditions of the gas from where the stars formed. Since these extremely dense and compact H II regions are always heavily obscured, most of our knowledge comes from radio observations of their radio recombination line and continuum emission. The continuum emission from some of the youngest objects[2)] has appreciable optical depth even at 1.3 cm and its adequate study requires going to higher frequencies. In Q band it will be possible to work with the H and He 53α lines and obtain information on the kinematics of the ionized gas with unprecedented angular resolution.

In general, the possibility of counting with a sensitive interferometer to measure the continuum at 43-GHz is very attractive, since this is not possible at present. In star-burst galaxies a good map at this frequency may be of value to disentangle the contributions of synchrotron, free-free, and dust emission in this type of objects.

Finally, with the 7-mm receivers the VLA will be able to participate in the Very Long Baseline Array (VLBA) as a most important station at that wavelength.

3. DUST EMISSION FROM DISKS

It is believed that when the Sun formed, 4.5 billion years ago, it was surrounded by a disk of gas and dust from where planets condensed. It is expected that young stars observable at present would be surrounded by similar, protoplanetary disks. In the last few years, the excess infrared and millimeter emission from young stars has been convincingly interpreted to arise from dust in protoplanetary disks[3,4] Other phenomena, such as the bipolar outflows and optical jets, can also find natural explanation with the presence of a disk.

These important observations lack, however, the angular resolution required to actually produce an image of the disks. The protoplanetary disks are expected to have dimensions of about 100 AU, about one arc second at the distance of Taurus. Then, an angular resolution of about 0.1 arc sec is needed to properly resolve the structures. Much larger ($\sim$1000 AU) disklike structures have been imaged in various molecular lines around some young stellar objects[5,6] but the relation of these structures to the much smaller protoplanetary disks is still unclear. Extrapolation of the available 1- and 3-mm data suggests that the optically thin dust emission from the disks of several young stars will be detectable at 7 mm (43 GHz) at levels of about 10 mJy (Figure 1). The flux density of this emission process goes approximately as frequency cubed, so the flux densities at 1- and 3-mm are much larger than at 7-mm. However, the mm arrays now at operation cannot reach the desired subarcsec angular resolution. On the other hand, the VLA at 1.3 cm has the angular resolution required but the total flux density expected is very small and at these wavelengths the contribution from another mechanism, namely free-free emission arising in the ionized outflow, becomes dominant.

4. PRESENT STATUS

At present (April 1993) construction and testing of the prototype receiver is underway. The first two receivers will be installed by August 1993 and then array testing will start. It is expected to have all nine receivers installed by April 1994. As all instrumentation from NRAO, the 7-mm receivers will be available to qualified world astronomers and proposals are being considered starting in the June 1, 1993 deadline.

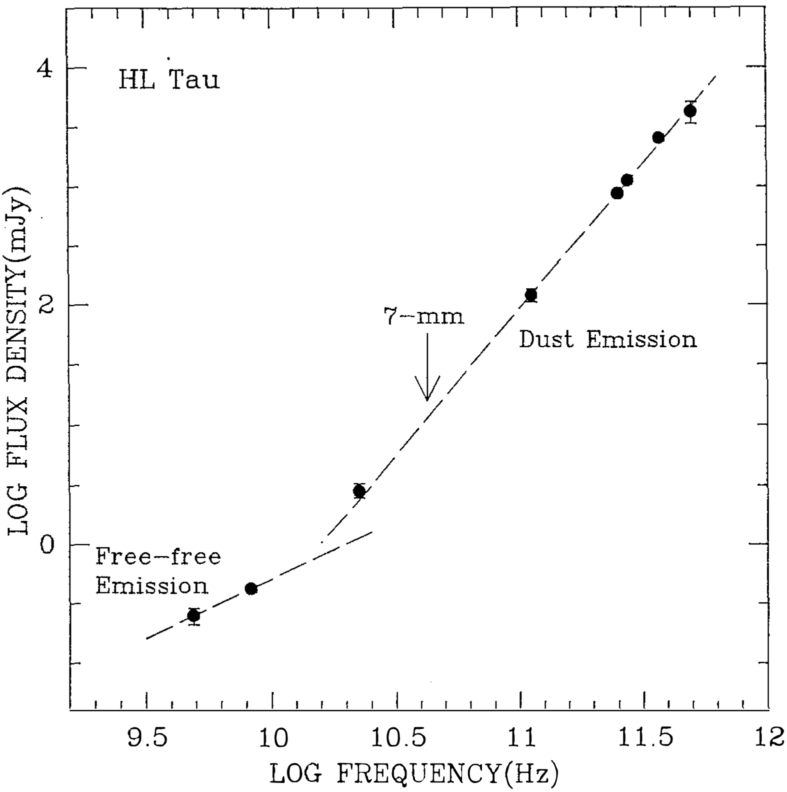

Figure 1. Continuum spectrum of the young star HL Tauri in the cm and mm wavelengths. The filled circles are measurements from various authors. The dashed lines are power law fits to the free-free emission from the ionized outflow (low frequency) and to the dust emission from the disk (high frequency). The arrow marks the wavelength of 7-mm, where the emission is expected to be dominated by dust emission from the protoplanetary disk.

REFERENCES

[1]Reid, M. J. and Menten, K. M. 1990, *Ap. J.*, **360**, L51.

[2]Garay, G., Rodríguez, L. F., and van Gorkom, J. H. 1986, *Ap. J.*, **309**, 553.

[3]Adams, F. C., Lada, C. J., and Shu, F. H. 1987, *Ap. J.*, **312**, 788.

[4]Beckwith, S. V. W., Sargent, A. I., Chini, R. S., and Gusten, R. 1990, *A. J.*, **99**, 924.

[5]Torrelles, J. M., Ho, P. T. P., Rodríguez, L. F., and Cantó, J. 1986, *Ap. J.*, **305**, 721.

[6]Sargent, A. I., Beckwith, S., Keene, J., and Masson, C. 1988, *Ap. J.*, **333**, 936.

Well done, Dick.

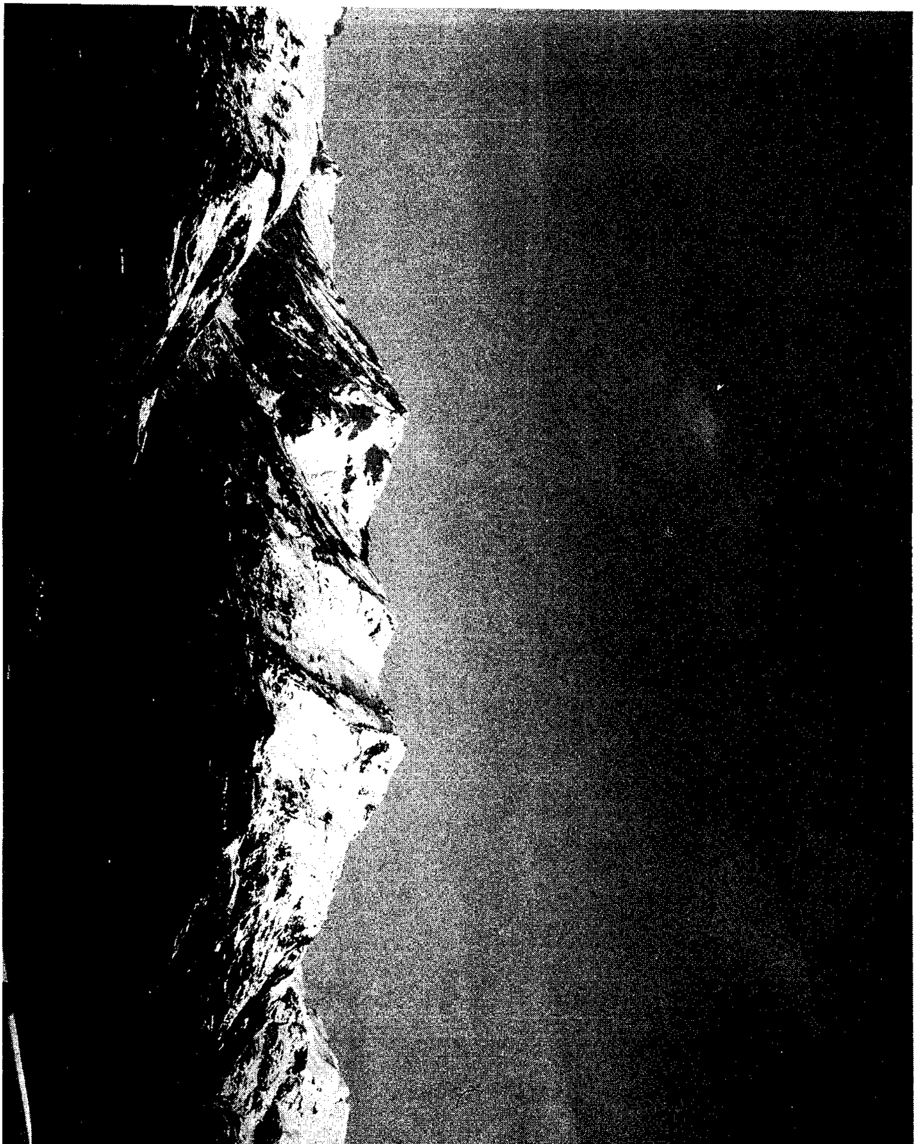

A piece of cold universe

THE COLD UNIVERSE: LIST OF PARTICIPANTS

ABERGEL Alain	Orsay	France
AGEORGES Nancy	Grenoble (Obs.)	France
ANDRÉ Philippe	Saclay	France
ARMAND Christiane	Marseille (LAS)	France
ASPIN Colin	Hawaii (JAC)	USA
BABEL Jacques	Saclay	France
BALLY John	Boulder	USA
BECKWITH Steve	Heidelberg	Germany
BENNETT Charles	Goddard	USA
BLITZ Leo	College Park	USA
De BOISANGER Constance	Bruyères-le-Châtel	France
BOISSÉ Patrick	Paris (ENS)	France
BONTEMPS Sylvain	Saclay	France
BOUVIER Jerome	Grenoble (Obs.)	France
BRINKS Elias	Socorro	USA
CABRIT Sylvie	Grenoble (Obs.)	France
CASALI Mark	Edinburgh	GB
CASANOVA Sophie	Saclay	France
CESARSKY Catherine	Saclay	France
CHIEZE Jean-Pierre	Bruyères-le-Châtel	France
CLEMENTS D.L.	Oxford	GB
CORREIA José	Lisbon	Portugal
DENT Bill	Hawaii (JAC)	USA
DOUGADOS Catherine	Amherst	USA
DUBRULLE Bérengère	Toulouse (Obs.)	France
DUTREY Anne	Grenoble (IRAM)	France
DUVERT Gilles	Grenoble (Obs.)	France
ELBAZ David	Saclay	France
ELITZUR Moshe	Lexington	USA
EPCHTEIN Nicolas	Meudon	France
FALGARONE Edith	Paris (ENS)	France
FAZIO Giovanni	Cambridge	USA
FERRARI-TONIOLO Marco	Frascati (IAS)	Italy
FOGLIZZO Thierry	Saclay	France
FORREST Bill	Rochester	USA
FUENTE Asunción	Yebes	Spain
FUKUI Yasuo	Nagoya	Japan
GALLAIS Pascal	Saclay	France
GALLI Daniele	Florence	Italy

GAUTIER Daniel	Meudon	France
GOMEZ Yolanda	Mexico City	Mexico
GOMEZ DE CASTRO Ana	Madrid	Spain
GRENIER Isabelle	Paris (University)	France
GUÉLIN Michel	Grenoble (IRAM)	France
GUILLOTEAU Stephane	Grenoble (IRAM)	France
GÜSTEN Rolf	Bonn	Germany
HARTIGAN Patrick	Amherst	USA
d'HENDÉCOURT Louis	Orsay	France
HENRIKSEN Richard	Kingston	Canada
HUGHES Victor	Kingston	Canada
JONCAS Gilles	Québec	Canada
JONES Anthony	Ames	USA
JOUBERT Martine	Marseille (LAS)	France
KENYON Scott	Cambridge	USA
KHACHIKIAN Edward	Erevan	Armenia
KYLAFIS Nikolaos	Heraklion	Greece
LADA Charles	Cambridge	USA
LADD Ned	Hawaii (IFA)	USA
LAGAGE Pierre-Olivier	Saclay	France
LÉGER Alain	Orsay	France
LEITHERER Claus	Baltimore	USA
LÉPINE Jacques	Grenoble (Obs.)	France
LIOURE Alain	Bruyères-le-Châtel	France
MARIOTTI Jean-Marie	Meudon	France
MÉNARD Francois	Grenoble (Obs.)	France
MERLUZZI Paola	Naples	Italy
MILLAR Tom	Manchester (UMIST)	GB
MINCHIN Nigel	London (QMW)	GB
MIRABEL Felix	Saclay	France
MITSKEVITCH Alexander	Florence	Italy
MOLINARI Sergio	Frascati (IAS)	Italy
MONTMERLE Thierry	Saclay	France
NAKANO Takenori	Nobeyama	Japan
NATTA Antonella	Florence	Italy
NENNER Irène	Saclay	France
OMONT Alain	Paris (IAP)	France
OSTERBERG Jürgen	Bonn	Germany
PAGEL Bernard	Copenhagen	Denmark
PERRIER Christian	Grenoble (Obs.)	France
PERSI Paolo	Frascati (IAS)	Italy
PIHLKUHN Hartmut	Karlsruhe	Germany

PILBRATT Göran	Noordwijk	Netherlands
PLANESAS Pere	Yebes	Spain
PUGET Jean-Loup	Orsay	France
RADFORD Simon	Grenoble (IRAM)	France
RAGA Alex	Manchester (Astro)	GB
RAY Tom	Dublin	Ireland
REMY Gilles	Meudon	France
RIEU Nguyen Quang	Meudon	France
RODRIGUEZ Luis	Mexico City	Mexico
ROELFSEMA Peter	Groningen	Netherlands
ROUAN Daniel	Meudon	France
RUDEN Steve	Los Angeles	USA
RUSSELL Stephen	Dublin	Ireland
SANDERS Dave	Hawaii (IFA)	USA
SARACENO Paolo	Frascati	Italy
SAUVAGE Marc	Hawaii (CFH)	USA
SERRA Guy	Toulouse	France
STAHLER Steven	Berkeley	USA
STECKLUM Bringfried	Jena	Germany
TACCONI Linda	Garching	Germany
TAGGER Michel	Saclay	France
TAPIA Mauricio	Mexico City	Mexico
TAUBER Jan	Noordwijk	Netherlands
TEREBEY Susan	Pasadena	USA
TERLEVITCH Roberto	Cambridge	GB
TURNER Jake	Cardiff	GB
VERSTRAETE Laurent	Bruyeres	France
WALMSLEY Malcolm	Bonn	Germany
WARD-THOMPSON Derek	Cambridge	GB
WHITE Simon	Cambridge	GB
YUN Joao Lin	Lisbon	Portugal
ZAGURY Frederic	Orsay	France

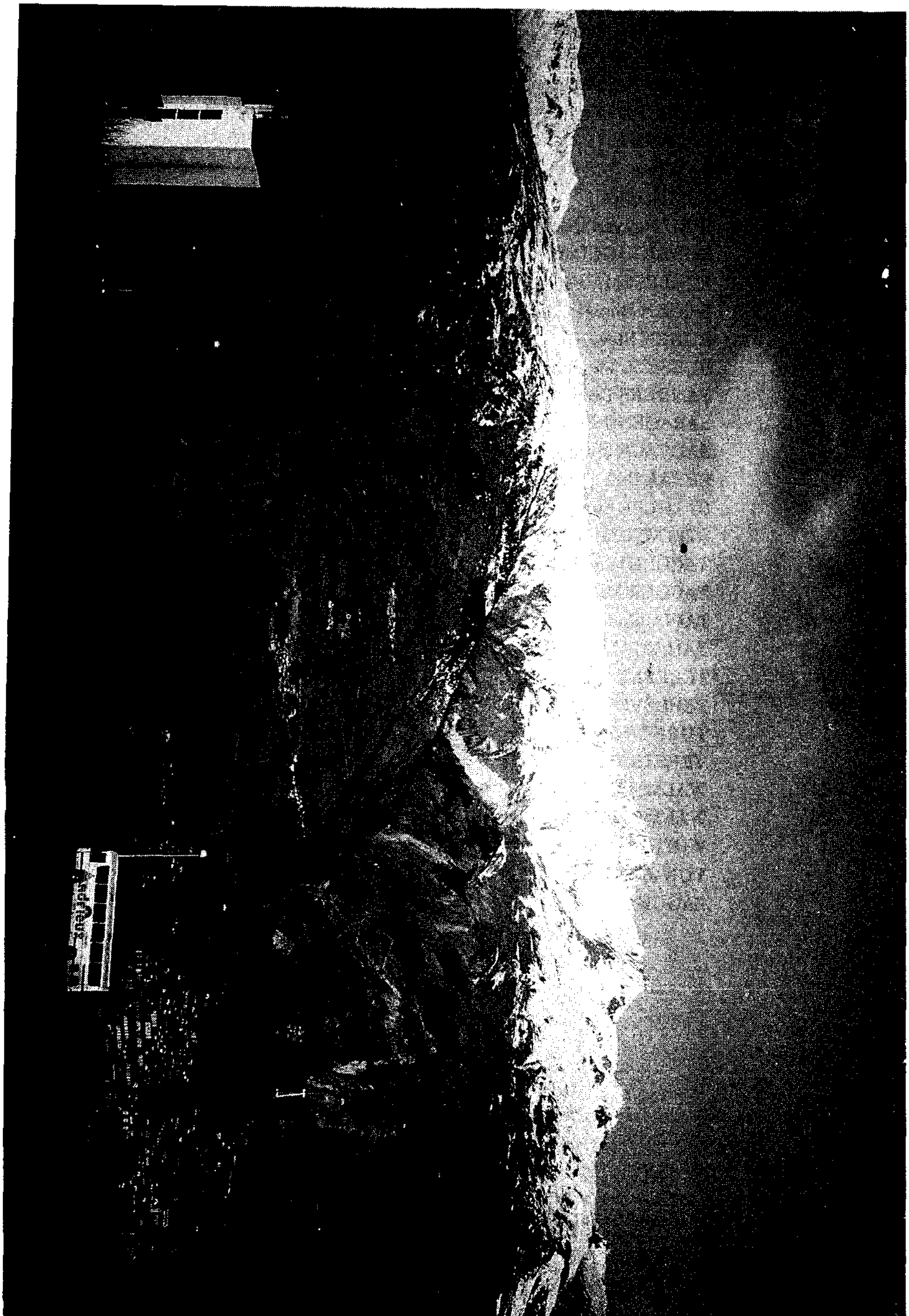

Saying good-bye....